OPTIMIZACIÓN DE LA INTERACCIÓN MICROTÚBULO-TAXOL: DISEÑO DE TAXANOS DE ALTA AFINIDAD.

TESIS DOCTORAL
U.A.M. Dpto. Biología Molecular.
Ruth Matesanz Rodríguez
Director: J. Fernando Díaz Pereira
Centro de Investigaciones Biológicas
(C.S.I.C.)

A Fla, abuelo y gata.
A todos "los del sexto".

Mucha gente amenaza con "odiarme" y retirarme el saludo si saco mi personalidad más autista y obvio este apartado, que no cunda el pánico que aquí viene, hay que ser formalitos...

Antes que nada agradecer a Fer, Isabel y J.M. que este trabajo haya podido llegar a buen puerto, sin ellos, imposible. También hubiera sido difícil sin los, no granitos, sino montones de arena respectivos de Wei, Jesús, Federico, Frances.

Y hasta aquí los nombres propios, ahora espero que cada cual se encuentre reflejado en el grupo que le corresponde porque enumerar se vuelve cansino. Y así por orden alfabético inverso quiero citar a los que han tenido arte y parte en mi esfuerzo de estos años, ya residan en Málaga, Madrid o Segovia (también en Pequín y otros destinos internacionales): novios, novias, familia, compañeros deportivos y laborales (los que conviven, los de enfrente, los de abajo, los de otras áreas), amigos, amigas y amantes. Cada cuál que se encuadre en el grupo o grupos que considere oportunos, todos sabemos los que corresponden, quién es quién e incluso quien no cabe en ninguno o merece otro para sí mismo.

Para terminar quería recordar a los ausentes, a los que no me van a oir agradecerles nada, pero a los que quiero ofrecer la letra impresa para prolongar su presencia siguiendo los argumentos de Jorge Manrique.
Y son: los que me regalaron mi primera bici, el que tantas cosas donó "a cuenta de herencia", aquellos cuya desaparición me hicieron sentir un tanto *Latrodectus mactans* y los "del sexto", en especial, no puedo evitarlo, de la que aprendí lo que era "encarnado".

- SUMMARY. 9

- INTRODUCCIÓN.

1. EL CÁNCER Y SUS TRATAMIENTOS. 13

1.1. Cirugía. 13

1.2. Radioterapia. 13

1.3. Quimioterapia. 14

2. DIANAS DE QUIMIOTERAPIA. 15

2.1. Interrupción del ciclo celular fuera de la mitosis. 15

2.1.1. Fármacos que interrumpen el ciclo fuera de la mitosis. 15

2.2. Interrupción del ciclo celular durante la mitosis. 17

2.2.1. Dianas de mitosis excepto tubulina. 18

3. TUBULINA Y MICROTÚBULOS. 19

3.1. Estructura de la tubulina. 19

3.2. Estructura de los microtúbulos. 20

3.3. Dinámica de los microtúbulos. 20

3.4. Agentes antimitóticos dirigidos contra tubulina. 22

3.4.1. Agentes desestabilizadores de microtúbulos. 24

3.4.1.1 ***Dominio vinca.*** 24

3.4.1.2. ***Sitio de colchicina.*** 25

3.4.2. Agentes estabilizadores de microtúbulos (MSA). 25

3.4.2.1. ***Sitio de laulimalida.*** 25

3.4.2.2. ***Sitio de taxol.*** 25

3.4.2.3. ***Sitio externo del taxol.*** 26

4. TAXANOS. 27

4.1. Unión del taxol a la tubulina. 27

4.2. Relación estructura-actividad. 29

4.3. Efectos celulares del tratamiento con taxanos. 29

5. LIMITACIONES EN EL TRATAMIENTO CON TAXANOS. 30

5.1. Resistencias múltiples a fármacos. 31

5.2. La glucoproteína P. 31

- OBJETIVOS. 35

- MÉTODOS.

1. LIGANDOS. 39

1.1. Métodos de análisis. 39

1.1.1. Análisis cromatográfico. 39

2. PROTEÍNAS. 39

2.1. Purificación de tubulina. 39

2.2. Preparación de microtúbulos estabilizados. 40

2.2.1. Medida de la concentración de sitios de unión de taxol en microtúbulos estabilizados. 40

3. EFECTO DE LOS LIGANDOS EN EL ENSAMBLAJE DE TUBULINA. ...41

3.1. Polimerización de microtúbulos. 41

3.1.1. Ensamblaje en fosfato. 41

3.1.2. Ensamblaje con glicerol. 41

3.2. Unión a tubulina dimérica. 42

3.3. Determinación del diámetro de los microtúbulos (SAXS). 42

4. UNIÓN DE LOS LIGANDOS A LOS MICROTÚBULOS. 43

4.1. Medida de las constantes de unión de los ligandos a microtúbulos estabilizados. 43

4.1.1. Desplazamiento de flutax-2. 43

4.1.2. Desplazamiento de epotilona B. 44

4.2. Reversibilidad de la unión. 46

5. CULTIVOS CELULARES. 46

5.1. Ensayos de citotoxicidad. 46

6. CONFORMACIÓN DE LOS LIGANDOS UNIDOS. 47

6.1. Medidas de Resonancia Magnético-Nuclear (RMN). 47

6.2. Modelado molecular. 47

7. UNIÓN A GLUCOPROTEÍNA-P. 48

- RESULTADOS.

1. CARACTERIZACIÓN QUÍMICA DE LOS TAXANOS. 51

1.1. Variabilidad química. 51

1.1.1. Taxoles. 53

1.1.2. Docetaxeles. 53

1.1.3. Cefalomaninas. 53

1.2. Pureza e identificación por HPLC. 55

1.3. Espectrofotometría. 55

2. EFECTO DE LOS LIGANDOS EN EL ENSAMBLAJE DE TUBULINA. ...56

2.1. Polimerización en tampón fosfato. 56

2.2. Polimerización en glicerol. 56

2.3. Requerimiento de Mg^{++}. 57

2.4. Unión a tubulina dimérica. 58

2.5. Estructura de los microtúbulos ensamblados. 58

3. TERMODINÁMICA DE UNIÓN A MICROTÚBULOS. 61

3.1. Constantes de unión. 61

3.1.1. Validación de las medidas de los compuestos con grupos potencialmente reactivos. 63

3.2. Energía libre de Gibbs. 64

3.3. Entalpía. 64

3.4. Entropía. 67

4. ESTRUCTURA DE LAS DROGAS UNIDAS AL SITIO DE TAXOL. 71

4.1. Modelado molecular de la conformación bioactiva de los taxanos. 71

4.2. Determinación por resonancia magnético-nuclear de la conformación bioactiva del docetaxel unido. 73

5. CITOTOXICIDAD Y RESISTENCIA A TAXANOS. 75

5.1. Citotoxicidad y resistencia en líneas celulares que sobreexpresan la glucoproteína P. 75

5.2. Citotoxicidad y resistencia en líneas celulares con mutaciones en tubulina. 78

6. UNIÓN A GLUCOPROTEÍNA-P. 80

- DISCUSIÓN.

1. INFLUENCIA DE LAS MODIFICACIONES EN LA AFINIDAD DE UNIÓN. 85

1.1. Efecto de los cambios en C-2. 85

1.2. Efecto de los cambios en C-13. 87

1.3. Efecto de los cambios en la "parte norte" del anillo de taxano (C-7 y C-10).. 88
2. DISEÑO DE UN TAXANO DE AFINIDAD OPTIMIZADA. 88

3. INTERPRETACIÓN ESTRUCTURAL DE LOS DATOS DE UNIÓN. 89

4. CONFORMACIÓN BIOACTIVA DEL TAXOL. 89

5. EFECTO DE LAS MODIFICACIONES EN LA ESTRUCTURA DE LOS MICROTÚBULOS. 91

6. RELACIÓN ENTRE AFINIDAD DE UNIÓN, CITOTOXICIDAD Y RESISTENCIA MÚLTIPLE A DROGAS CAUSADA POR LA GLUCOPROTEÍNA-P. 92

7. EFECTO DE LAS MODIFICACIONES EN LA CITOTOXICIDAD DE LOS COMPUESTOS EN CÉLULAS CON TUBULINAS MUTANTES. 96

- CONCLUSIONES. 103

- BIBLIOGRAFÍA. 107

- ANEXO. (publicaciones)

Nature Chemical Biology. 3(2) (2007) 117-25 125

ChemMedChem. 2(5) (2007) 691-701 135

Bioorganic & Medicinal Chemistry Letters. 17(11) (2007) 3191-4 147

Journal of Medicinal Chemistry. 50(12) (2007) 2865-74 151

Chemistry: An European Journal. 13(18) (2007) 5060-74 161

Chemistry: An European Journal. 14(25) (2008) 7557-69 177

Chemistry & Biology. 15(6) (2008) 573-85 191

Bioorganic & Medicinal Chemistry Letters. (en prensa) 205

SUMMARY.

Developed resistance to drugs is one of the causes of cancer chemotherapy failure. The effect of drug-site interaction optimization to fight against resistance have been studied in cells resistant to taxanes by two different mechanisms, P-glycoprotein mediated multidrug resistance and mutations in the taxane site.

To design drugs with high affinity for the taxane site microtubule binding affinities of a series of synthetic taxanes have been measured. From these measurements we could dissect individual group contributions and obtain a rationale for the design of novel compounds with the ability to overcome P-glycoprotein-mediated drug resistance. As previously observed for epothilones, contributions of the different substituents to the binding free energy are cumulative. Combination of the most favourable substitutions in one single analogue increased the binding affinity 500-fold over that of taxol.

Structural models built in this study assigned an important role to the interactions of C2 and C13 substituents with the protonated side chain of His229 in β-tubulin. The relative orientation of these groups was found to be in agreement with NMR data obtained for microtubules-bound docetaxel.

The cytotoxicities of the compounds in A2780 cells correlate with their affinities with an apparent cytotoxicity limit in the nanomolar range. Taxane resistance index plotted versus binding affinity fits a bell-shaped curve showing that the P-gp-overexpressing cells (A2780AD) are sensitive to the highest and lowest affinity compounds, whereas resistance indexes in the range of 100 to 1000 were obtained for those ligands whose binding affinities for tubulin and P-gp are similar. This finding strongly indicates that for a series of compounds with similar pharmacokinetic and bioavailability properties, optimization of the ligand-target interaction is a good strategy to overcome multidrug resistance mediated by efflux pumps. Moreover same high-affinity compounds seem to avoid resistance in cells with mutated tubulins as probed with their cytotoxicities in cells PTX10 and PTX22 when compared with the parental 1A9 cell line wich contains wild type tubulin.

INTRODUCCIÓN.

1. EL CÁNCER Y SUS TRATAMIENTOS.

Cáncer es un término con el que se denomina todo un amplio conjunto de enfermedades diferentes cuya característica común se encuentra en un crecimiento celular descontrolado (Southam, 1963). La división celular en un organismo sano está sujeta a un férreo control, pero la célula cancerosa escapa a ese control y comienza a dividirse desordenadamente y a un ritmo mucho mayor del habitual. Estas células suelen, además, adquirir la capacidad de invadir tejidos adyacentes e incluso de trasladarse e invadir órganos alejados.

El cáncer fue la causa del 13% de las muertes registradas en el mundo durante el año 2005 (datos de la organización mundial de la salud) siendo su principal causa etiológica el tabaco. Los cánceres con mayor contribución a la mortalidad son, por orden, los de pulmón, estómago, hígado, colon y mama.

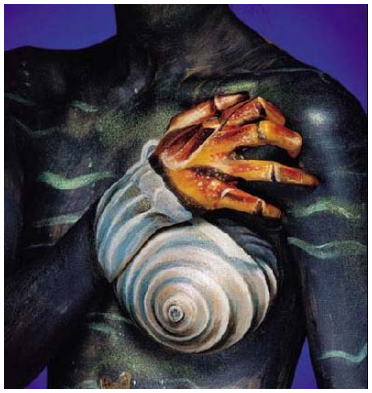

Figura 1. El cáncer ha sido desde antiguo representado como un cangrejo.

Dada la incidencia y gravedad de esta enfermedad se han hecho grandes esfuerzos para combatirla. En la actualidad los tratamientos más habituales son la cirugía, la radioterapia y la quimioterapia. Además existen algunos otros tratamientos, menos generales, utilizados en el caso de algunos tumores específicos, como la inmunoterapia o la hormonoterapia (por ejemplo aplicada en cánceres de mama o próstata).

1.1. Cirugía.

Hasta principios del siglo pasado, con la aparición en escena de la radiación, la cirugía era el único método conocido para luchar contra el cáncer. Aún en nuestros días este método juega un papel importante en el tratamiento de muchos tumores. La cirugía puede tener diversos objetivos en su uso: preventiva, diagnóstica, de estadiaje, curativa, citorreductora, paliativa o reparadora.

El desarrollo de la cirugía y la aparición de nuevas técnicas mucho menos agresivas hace que la aplicación de este tipo de tratamiento en estos momentos sea, en la mayoría de los casos, mucho menos traumática de lo que solía serlo hace unos años.

1.2. Radioterapia.

Desde el descubrimiento de la radiactividad a finales del siglo XIX se le buscaron aplicaciones médicas. El resultado de algunos de estos estudios nos lleva a la utilización de radiaciones ionizantes como terapia contra el cáncer

(Kaplan, 1970). Actualmente más de la mitad de los afectados con enfermedades tumorales reciben algún tipo de radioterapia. La radiación provoca daño en el ADN celular principalmente cuando la célula se está dividiendo. Por tanto la radiosensibilidad depende de la duración del ciclo de división celular de modo que las células cancerosas se verán más afectadas.

La radioterapia es un método local o loco-regional (cuando se incluyen los ganglios linfáticos en las cercanías del tumor). Al igual que la cirugía, la radioterapía puede llevar varios objetivos según cuándo sea administrada, así tendremos radioterapía neoadyuvante, radical, adyuvante, concomitante o intraoperatoria.

Aún cuando las células cancerosas presentan mayor radiosensibilidad y la radioterapia es un tratamiento local, hay que tener en cuenta que también las células sanas del área tratada se ven afectadas por esta radiación teniendo por tanto ciertos efectos secundarios que variarán dependiendo de la zona en la que apareció el tumor.

1.3. Quimioterapia.

La metástasis convierte el cáncer en una enfermedad sistémica y por tanto los tratamientos locales pueden no ser suficientes para atajarla, de ahí la necesidad de un tratamiento sistémico como la quimioterapia.

Encontrar fármacos efectivos contra una infección bacteriana es relativamente sencillo debido a la cantidad de dianas diferenciales que existen entre el patógeno y su hospedador, más difícil resulta cuando el patógeno es un protozoo, en el caso de células eucariotas no hay casi diferencias. En el caso del cáncer no existen diferencias químicas entre las células "patógenas" y las sanas puesto que ambos tipos proceden del propio organismo del paciente. Las drogas que se usan en estos tratamientos deben distinguir pues un comportamiento y no una diana exclusiva. Este comportamiento distinto es la diferencia en el ritmo de división.

En los años cincuenta aparece la quimioterapia como una nueva forma de combatir el cáncer (Scott, 1970). La idea de tratar esta enfermedad con algún tipo de droga surgió tras la observación de un grupo de personas que habían sido expuestas a gas mostaza durante la segunda guerra mundial; estas personas tenían un número de glóbulos blancos muy por debajo de lo habitual. Si esta droga dañaba así estas células de división rápida se supuso que podría actuar de manera similar ante células cancerosas. A principios de los años cuarenta a muchos pacientes con linfomas avanzados se les inyectó esta droga y, aunque solamente de forma temporal, mostraron notables mejorías. Estos datos propulsaron la búsqueda de otros fármacos que tuvieran efectos similares sobre las células cancerosas.

Evidentemente el objetivo de la quimioterapia es el de destruir células malignas pero su finalidad puede variar dependiendo de las circunstancias del

paciente pudiendo ser curativa o paliativa, además, a veces no se administra como tratamiento único sino asociado a otros pudiendo ser neoadyuvante, concomitante o adyuvante según el caso.

2. DIANAS DE QUIMIOTERAPIA.

A diferencia de los otros tratamientos anteriormente mencionados la quimioterapia es un tratamiento sistémico, lo que permite luchar contra la metástasis que se haya podido producir en el paciente. La mayoría de los medicamentos utilizados para esta terapia actúan sobre las células en división afectando principal, pero no exclusivamente, a las células cancerosas. Además los fármacos llegan a casi cualquier parte del organismo por lo que no es raro que este tipo de tratamiento tenga efectos secundarios. En estos momentos hay al menos cien drogas diferentes siendo utilizadas en la lucha contra el cáncer; estas drogas se agrupan en diferentes tipos según la fase del ciclo en la que interrumpen la reproducción celular. La decisión sobre cual usar dependerá principalmente del tipo de cáncer a tratar, su localización y otras particularidades del paciente.

Los fármacos más comúnmente utilizados en quimioterapia pueden dividirse en varios grupos según sus dianas de acción. Principalmente podemos distinguir entre drogas que inhiben la función del huso mitótico interrumpiendo la mitosis y drogas que afectan a otras fases del ciclo, fármacos que, principalmente, afectan al ADN bien interfiriendo en su síntesis, bien introduciendo daños en él.

2.1. Interrupción del ciclo celular fuera de la mitosis.

En su inmensa mayoría, la diana de las drogas que interrumpen el ciclo celular fuera de la mitosis es el ADN o enzimas necesarias en su síntesis. Ejemplos de drogas que interfieren en la síntesis y metabolismo del ADN son las tiopurinas, los inhibidores de la timidilato sintasa (análogos de folato o nucleótido) o los inhibidores de las topoisomerasas I (irinotecan) y II (antraciclinas). Fármacos que modifican el ADN son los agentes alquilantes y las drogas de platino.

2.1.1. Fármacos que interrumpen el ciclo fuera de la mitosis.

Tiopurinas.

El efecto final de las tiopurinas (6-mercaptopurina, azatioprina y 6-tioguanina) es la incorporación de 6-tioguanina en el ADN, esta base es mucho más reactiva que las canónicas y sufre metilaciones. La 6-tioguanina da lugar a apareamientos promiscuos (Rappaport, 1993) produciendo parejas aberrantes reconocidas por la maquinaria de corrección de errores. La consecuencia final

de la incorporación de esta base es un retraso en la entrada al paso de control de ciclo en G_2 (Yan *et al.*, 2003).

También hay evidencias que sugieren la capacidad de los metabolitos de la 6-mercaptopurina de inhibir la biosíntesis *de novo* de las purinas (Dervieux *et al.*, 2002; Tay *et al.*, 1969).

Inhibidores de la timidilato sintasa.

La timidilato sintasa es un enzima dependiente de folato que cataliza la metilación reductiva de 2'deoxiuridina-5'monofosfato (dUMP) a 2'deoxitimidina-5'monofosfato (dTMP). Este dTMP es fosforilado en dos pasos sucesivos para dar lugar a 2'deoxitimidina-5'trifosfato (dTTP), precursor esencial para la síntesis de ADN. Ésta es la única ruta intracelular de síntesis *de novo* de dTTP y la razón por la que la timidilato sintasa es una diana interesante para la terapia contra el cáncer (Chu *et al.*, 2003).

Hay dos grupos dentro de estos inhibidores: los análogos de folato (como el metotrexato, raltitrexed, pemetrexed, nolatrexed) y los de nucleótido (5-fluorouracil).

Inhibidores de topoisomerasas.

Las antraciclinas (ej. doxorubicina, daunorubicina) son drogas antitumorales muy efectivas entre cuyas características se encuentra la de ser inhibidores de la topoisomerasa II induciendo apoptosis en respuesta a esta inhibición (Gewirtz, 1999).

Los derivados semisintéticos de la camptotecina, topotecan e irinotecan son inhibidores de la topoisomerasa I utilizados en clínica (Cragg y Newman, 2004). La camptotecina es un alcaloide aislado de las hojas del árbol ornamental chino *Camptotheca acuminata* Decne al que se le encontró actividad antitumoral; tiempo después se descubrió su interacción con la topoisomerasa I (Hsiang *et al.*, 1985).

Sales de platino.

La actividad biológica de estos compuestos de platino fue descubierta accidentalmente en los años sesenta (Rosenberg *et al.*, 1965), desde entonces han tenido amplio uso en el tratamiento de cánceres de testículo y ovario.

Los primeros compuestos que se encontraron con esta actividad fueron dos complejos producto de electrolisis: el isómero cis [PtII $(NH_3)_2$ Cl_2] que fue denominado cisplatin y un análogo de platino(IV), cis-diaminotetracloro-platino(IV). El cisplatin presenta severos problemas renales por lo que se hizo un esfuerzo en encontrar análogos y pronto apareció carboplatin, igualmente efectivo pero con efectos secundarios algo menores (Kelland, 2007). También se han buscado compuestos entre los elementos vecinos en la tabla periódica (oro o paladio) con actividades similares.

El modo de acción de estas drogas implica una unión covalente a purinas del ADN que termina derivando en apoptosis celular. Estos aductos de ADN

activan varias rutas de transducción de señales entre las que se encuentran las involucradas en el reconocimiento y reparación de daños en el ADN, en la parada del ciclo celular y en la muerte celular programada (Siddik, 2003). Esta activación parece estar influida por las distorsiones en el ADN causadas por los aductos ADN-platino capaces de impedir procesos celulares esenciales, tales como la replicación o la transcripción que requieren la separación de las hebras de ADN, lo que produce una parada prolongada del ciclo en la fase G_2.

Agentes alquilantes.

Los agentes alquilantes adhieren grupos alquilos a las bases nitrogenadas del ADN. Los enzimas de reparación producen entonces excisiones en éste intentando reemplazar las bases alquiladas. Entre estos fármacos se encuentran las nitrosoureas y algunos derivados del gas mostaza como la ciclofosfamida (Matalon *et al.*, 2004).

La ciclofosfamida induce la apoptosis de las células tumorales (Schwartz y Waxman, 2001) y genera radicales libres (Sulkowska *et al.*, 1998).

2.2. Interrupción del ciclo celular durante la mitosis.

El objetivo de las drogas que interrumpen el ciclo celular en mitosis es el de interferir en la división celular para inhibir la proliferación desmesurada de las células tumorales, induciendo mitosis aberrantes que llevan a una parada en mitosis y la subsecuente muerte celular. Tradicionalmente la diana de estas drogas han sido los microtúbulos del huso mitótico (figura 2). Se conocen multitud de fármacos que alteran la dinámica de éstos (taxol, docetaxel, vinblastina, vincristina, colchicina) usados profusamente en clínica.

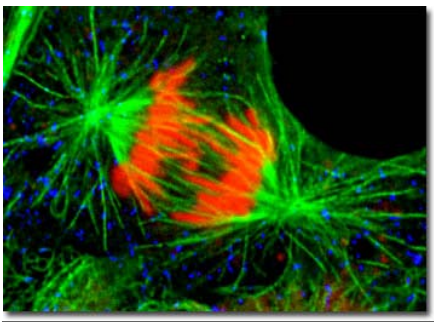

Figura 2. Célula en división. El huso mitótico está teñido en verde, los cromosomas en naranja y en azul se muestran los peroxisomas

Desde el descubrimiento de las drogas dirigidas a tubulina se ha venido observando cómo las células tumorales resultan sensibles a la parada en mitosis y cómo suelen morir en respuesta a aquellos agentes que perturban el huso mitótico, pero no hay una única explicación molecular de cómo mueren estas células como respuesta a la activación del punto de comprobación de mitosis (revisado en Jordan y Wilson, 2004; Zhou y Giannakakou, 2005).

En los estudios realizados con muchos de los fármacos antimitóticos conocidos se ha observado muerte apoptótica caracterizada por la activación de la caspasa 3, pero éste no es el único mecanismo por el que estas células mueren después de una mitosis fallida. Muchos estudios han definido una forma de muerte en estos casos denominada catástrofe mitótica. La catástrofe mitótica comparte muchas de las características morfológicas y bioquímicas de la apoptosis pero no precisa de las caspasas 9 ó 3 y sigue ocurriendo aún en

presencia de inhibidores de éstas, requiere la actividad de CDK1 (quinasa dependiente de ciclina), se distingue por la fragmentación del núcleo dando lugar a micronúcleos y se puede asociar a la activación de la caspasa 2, activación no necesaria en la ruta clásica de apoptosis (Castedo *et al.*, 2004). En cualquier caso no hay una explicación molecular clara de cómo se inicia o se regula la catástrofe mitótica.

2.2.1. Dianas de mitosis excepto tubulina.

En los últimos tiempos el conocimiento detallado de los efectores bioquímicos de los distintos pasos de la mitosis ha dado pie a la utilización de dianas adicionales para inducir su parada. La descripción de funciones adicionales durante la división celular de las quinesinas mitóticas, las quinasas Aurora y las quinasas tipo polo (PLKs: polo-like kinases) las han hecho objetivo del desarrollo de nuevas drogas quimioterapéuticas que inhiban sus funciones (Jackson *et al.*, 2007).

Las quinesinas mitóticas son un grupo de proteínas motoras que funcionan exclusivamente durante la mitosis. Diferentes proteínas pertenecientes a este grupo juegan papeles en aspectos particulares del ensamblaje y función del huso mitótico incluyendo la organización de sus polos, el alineamiento y segregación de los cromosomas y la regulación de la dinámica de los microtúbulos (Miki *et al.*, 2005). Entre éstas la KSP (kinesin spindle protein) es necesaria para establecer la bipolaridad del huso dirigiendo la separación de las cromátidas hermanas (Blangy *et al.*, 1995) y la proteína centromérica E (CENPE) es crucial para el encuentro correcto de los cromosomas durante la metafase (Wood *et al.*, 1997; Yao *et al.*, 2000). Para ambas proteínas se han encontrado inhibidores que inducen parada del ciclo en mitosis (Schmidt y Bastians, 2007).

Las quinasas Aurora y PLK también juegan papeles importantes durante la mitosis y han sido igualmente objeto de desarrollo de inhibidores con prometedores usos en quimioterapia. Aurora A es esencial para la maduración del centrosoma y su separación durante la profase temprana (Kinoshita *et al.*, 2005; Liu y Ruderman, 2006), mientras que Aurora B es un componente del CPC (chromosomal passenger complex) y está involucrada en la fosforilación de la histona H3 (Hsu *et al.*, 2000), en la condensación de los cromosomas, en su alineación en la placa metafásica, en la unión bipolar centrómero-microtúbulo, en el punto de comprobación del huso y en la citoquinesis (Ditchfield *et al.*, 2003; Hauf *et al.*, 2003; Terada *et al.*, 1998). PLK1, por su parte, está implicada en la maduración del centrosoma y la formación del huso mitótico, se necesita para la salida de mitosis y la separación de las cromátidas hermanas durante la anafase (van Vugt y Medema, 2005), además podría tener un papel durante la citoquinesis a través de la fosforilación de la proteína motora similar a quinesinas MKLP1.

Sin embargo la principal diana para la quimioterapia basada en la interrupción de la mitosis es la tubulina, proteína diana de los taxanos, fármacos objeto de esta tesis.

3. TUBULINA Y MICROTÚBULOS.

La tubulina es la proteína que forma los microtúbulos. Éstos son el componente principal del citoesqueleto y juegan un papel fundamental en el mantenimiento de la forma celular, en el transporte vesicular, en la señalización celular, forman las estructuras motiles cilios y flagelos y el huso mitótico durante la división celular. Éste es un paso crucial en la división, imprescindible para la correcta segregación de los cromosomas en las células hijas. A causa de su importante papel en la división celular es una de las dianas contra la que se dirigen un mayor número de fármacos.

3.1. Estructura de la tubulina.

El heterodímero de α/β tubulina es la unidad básica que compone los microtúbulos (figura 3). La tubulina es una proteína altamente conservada entre todos los organismos eucariotas. Las subunidades α y β tienen un 50% de homología de secuencia y una estructura tridimensional muy similar . Cada monómero de tubulina tiene unos 450 aminoácidos y un nucleótido de guanina; existen muchos isotipos de cada uno y ambos son susceptibles de sufrir multitud de modificaciones posttraduccionales.

La estructura de cada monómero consiste en un núcleo de dos láminas β rodeadas de hélices α y puede dividirse en tres dominios funcionales (Downing y Nogales, 1999; Nogales *et al.*, 1998):

el dominio amino terminal que contiene la región de unión a nucleótido tiene un plegamiento tipo Rossmann, común en las proteínas que unen nucleótido, formado por seis cadenas β palalelas alternando seis hélices α,

un dominio intermedio que comprende el sitio de unión a taxol y contiene cuatro cadenas β y tres hélices α y

un dominio carboxilo terminal que consta de dos hélices antiparalelas y forma parte de la cara externa del microtúbulo siendo, muy probablemente, la zona de unión de las proteínas motoras y las proteínas asociadas a microtúbulos.

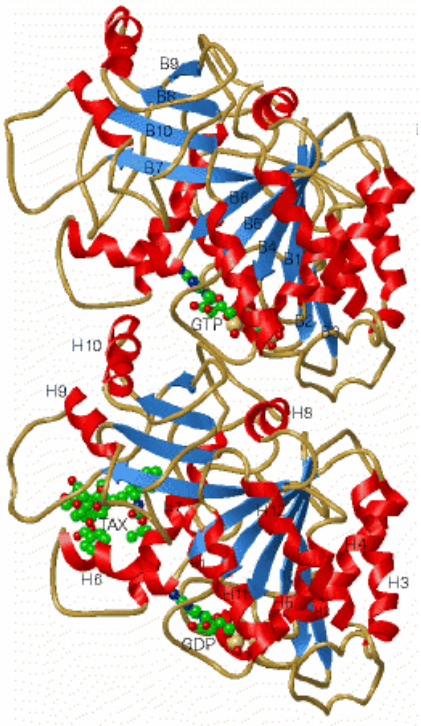

Figura 3. Estructura del dímero de tubulina. Diagrama de cintas mostrando una molécula de GTP unida en α tubulina (monómero superior) y GDP y taxol (señalado TAX) en β tubulina (monómero inferior). (Modificación de (Nogales *et al.*, 1998))

3.2. Estructura de los microtúbulos.

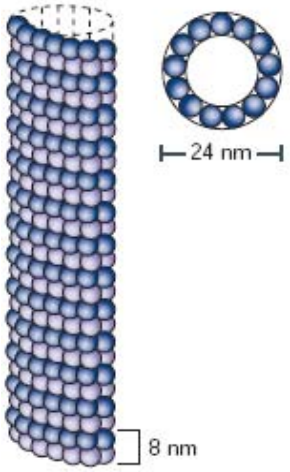

Figura 4. Estructura de un microtúbulo. (Adaptación de una figura de (Jordan y Wilson, 2004))

Los microtúbulos son estructuras cilíndricas huecas de 24 nanómetros de diámetro y una longitud que puede alcanzar varias micras (figura 4). Estos cilindros están formados por filamentos (entre diez y quince dependiendo de las condiciones; *in vivo* generalmente trece) de dímeros de tubulina ensamblada "cabeza con cola" (Amos y Klug, 1974; revisado en Valiron *et al.*, 2001; y Zhou y Giannakakou, 2005). Estos filamentos forman uniones laterales estando todos ellos paralelos entre sí y ligeramente desplazados, los dímeros de tubulina, respecto al filamento contiguo (alrededor de 0,9 nm.) de manera que describen hélices a lo largo del microtúbulo, dejando una "costura" en el eje longitudinal (Wade y Hyman, 1997). Esta disposición, en la que la molécula de tubulina se ordena, le confiere al microtúbulo una polaridad pues sus dos extremos no son idénticos: por un lado queda expuesta la subunidad alfa de la proteína, es el extremo menos dinámico (de crecimiento más lento, el extremo negativo) y por el otro la subunidad beta en el extremo más dinámico (el positivo). En la célula los microtúbulos están anclados por sus extremos negativos al centro organizador de microtúbulos y los extremos positivos se dirigen hacia la periferia; durante la formación del huso mitótico los extremos negativos se concentran en los polos del huso y los positivos se dirigen hacia su ecuador donde se alinearán los cromosomas antes de separarse (Honore *et al.*, 2005; Jordan y Wilson, 2004).

La polimerización de los microtúbulos ocurre por un mecanismo de nucleación-elongación en el que la formación, relativamente lenta, de un pequeño núcleo es seguida de un crecimiento rápido del microtúbulo, gracias a la adición reversible y no covalente de dímeros de tubulina en sus extremos. Las primeras estructuras son pequeñas láminas de protofilamentos que posteriormente se cierran para formar un microtúbulo (Erickson y Stoffler, 1996). Esto también es así cuando la nucleación está alimentada por porciones de microtúbulos estables.

3.3. Dinámica de los microtúbulos.

Los microtúbulos no son estructuras estáticas en absoluto sino polímeros intrínsecamente dinámicos que crecen y se acortan por la asociación y disociación reversible de los heterodímeros de α/β tubulina en sus dos extremos. Cada una de las subunidades de tubulina tiene un sitio de unión a nucleótido, el de la subunidad β se denomina sitio intercambiable mientras que el de la subunidad α es no intercambiable (Spiegelman *et al.*, 1977; Weisenberg *et al.*, 1968). Durante la asociación de un dímero de tubulina al extremo del

microtúbulo, la molécula de GTP contenida en la subunidad β se hidroliza, dejando el GDP resultante atrapado entre los dos dímeros e incapaz de intercambiarse hasta que el microtúbulo despolimeriza y los dímeros de tubulina se liberan (Chretien *et al.*, 1999; Panda *et al.*, 2002). La molécula de GTP unida al sitio no intercambiable (por tanto en la subunidad α) no puede ser hidrolizada durante la unión del heterodímero al extremo del microtúbulo. Esta propiedad característica de unión e hidrólisis de GTP en la tubulina confiere a los microtúbulos sus propiedades dinámicas (revisadas en Honore *et al.*, 2005; Jordan y Wilson, 2004; Valiron *et al.*, 2001; Zhou y Giannakakou, 2005) tan poco usuales y a la vez importantes para sus funciones: la inestabilidad dinámica y el flujo de subunidades.

La inestabilidad dinámica (figura 5) es el comportamiento dinámico durante el cual los extremos de cada microtúbulo pueden estar en fase de crecimiento o de acortamiento rápido con cambios repentinos de un estado al otro (Mitchison y Kirschner, 1984). Este comportamiento se caracteriza, principalmente, por cuatro variables: la relación de crecimiento, la de acortamiento, la frecuencia de transición entre el crecimiento o el estado estable al acortamiento (catástrofe) y la frecuencia de la transición opuesta (rescate) (Walker *et al.*, 1988).

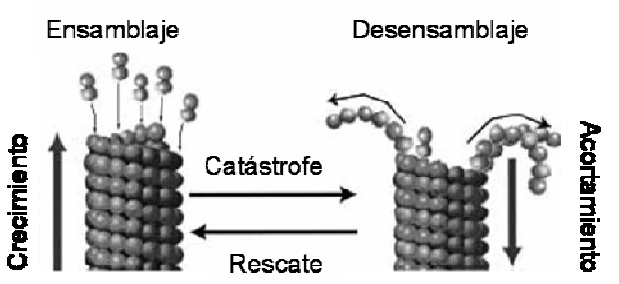

Figura 5. Inestabilidad dinámica de los microtúbulos. (Adaptación de una figura de (Valiron *et al.*, 2001))

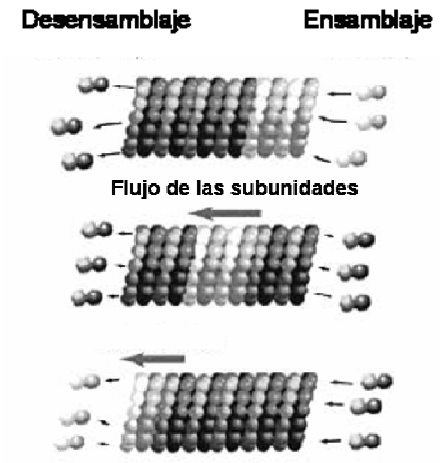

Figura 6. Flujo de subunidades. (Adaptación de una figura de (Valiron *et al.*, 2001))

El otro comportamiento dinámico de los microtúbulos (el flujo de subunidades, figura 6) consiste en el crecimiento neto de un extremo del microtúbulo y el acortamiento compensado en el extremo opuesto, esto conlleva un flujo de dímeros de tubulina del extremo positivo al negativo (Margolis y Wilson, 1978). Este tipo de comportamiento adquiere particular importancia durante la mitosis (Chen y Zhang, 2004).

Los dos tipos de comportamiento son compatibles en una población de microtúbulos pudiendo darse uno u otro o una mezcla de ambos. Se conocen muy vagamente los mecanismos de control que rigen en qué grado una población adopta un comportamiento o el otro pero parece que la proporción de los isotipos de tubulina que componen los

microtúbulos, el grado de modificaciones posttraduccionales de ésta y, sobre todo, la actuación de algunas proteínas reguladoras influyen en él (Wilson *et al.*, 1999).

Las propiedades dinámicas de los microtúbulos son de vital importancia para llevar a cabo correctamente diversas funciones celulares de las que son responsables; éste es especialmente el caso de la formación del huso mitótico durante la división celular. Los microtúbulos del huso mitótico son entre diez y cien veces más dinámicos que los interfásicos característica requerida durante todas las fases de la mitosis (Hayden *et al.*, 1990; Rusan *et al.*, 2001; Zhai *et al.*, 1996). En primer lugar, para el anclaje correcto de los cromosomas al huso a través de sus cinetocoros tras la ruptura de la membrana nuclear durante la prometafase (Hayden *et al.*, 1990), también para los complejos movimientos que los alinean en la placa metafásica y por último para su separación sincronizada durante la anafase y telofase una vez que se ha completado correctamente el punto de comprobación metafase-anafase (Jordan y Wilson, 2004). La alteración en la dinámica de los microtúbulos afecta a todas estas funciones, impidiendo que se lleven a cabo correctamente y, como consecuencia de ello, se bloquea la progresión normal del ciclo (Jordan *et al.*, 1993), provocando que la célula salga de mitosis de manera aberrante y entre en apoptosis (Jordan *et al.*, 1996).

3.4. Agentes antimitóticos dirigidos contra tubulina.

Los compuestos químicos cuya diana son los microtúbulos reciben su nombre (agentes antimitóticos) porque ejercen efectos inhibitorios sobre la proliferación celular bloqueando la mitosis, al alterar el exquisito control requerido de la dinámica microtubular durante este proceso. No obstante sus modos de acción sobre la estabilidad y la dinámica de los microtúbulos varían bastante entre unos y otros. A concentraciones relativamente altas estas drogas bien pueden inhibir la polimerización de los microtúbulos, desestabilizarlos y disminuir la masa de polímero o bien promover la polimerización, estabilizarlos y aumentar la masa de polímero (Checchi *et al.*, 2003). Según se comporten de uno de estos modos estas drogas se han dividido tradicionalmente en dos grupos: los agentes desestabilizadores de microtúbulos como son los alcaloides de vinca (vinblastina, vincristina) y la colchicina y los agentes estabilizadores de microtúbulos como los taxanos (taxol, docetaxel). Ambos grupos a concentraciones más bajas y clínicamente relevantes suprimen la dinámica de los microtúbulos sin afectar a la masa de polímero, manteniendo su capacidad de bloquear la progresión de la mitosis e inducir apoptosis (Jordan *et al.*, 1993).

A los agentes antimitóticos, aparte de su utilidad como antineoplásicos, se les descubrió la sorprendente capacidad de interferir en la aparición de nuevos vasos sanguíneos (Pasquier *et al.*, 2006). Esta particularidad, que se le ha encontrado tanto a drogas que se unen al dominio de vinca como a los sitios de taxol o colchicina, es muy interesante desde el punto de vista oncológico puesto que asociados a los tumores suele haber procesos angiogénicos. Un tumor al

que se le impida su vascularización no tendrá aporte de nutrientes y por tanto no progresará y sus células acabarán por morir. Esta propiedad antiangiogénica de los antimitóticos ha estado siendo estudiada y algunos de los compuestos que la poseen, como por ejemplo algunas combrestatinas, están ya en fase de ensayos clínicos.

La mayoría de los compuestos antimitóticos conocidos están dirigidos contra tres sitios de unión a drogas en β tubulina muy bien caracterizados (Jordan y Wilson, 2004; Zhou y Giannakakou, 2005): el dominio vinca y los sitios de taxol y colchicina (figura 7).

El dominio vinca se encuentra adyacente al sitio de unión intercambiable de GTP en β tubulina, en la interfase del extremo positivo (Jordan *et al.*, 1986; Rai y Wolff, 1996). El sitio de taxol se localiza en un bolsillo hidrofóbico en la unión lateral entre protofilamentos dentro del lumen del microtúbulo (Nogales *et al.*, 1998; Rao *et al.*, 1994; Rao *et al.*, 1995; Rao *et al.*, 1999) a este sitio la molécula accede tras su paso por un sitio externo cercano al poro de tipo I (Diaz *et al.*, 2003; Diaz *et al.*, 2005). El sitio de colchicina está en la región intradímero entre la β y la α tubulina (Bai *et al.*, 1996; Ravelli *et al.*, 2004; Uppuluri *et al.*, 1993). Además de estos cuatro sitios se conoce un quinto sitio de unión donde se dirige la laulimalida aunque su localización exacta no se conoce (Mooberry *et al.*, 1999; Pryor *et al.*, 2002); es el primer agente estabilizador de microtúbulos encontrado que se une a un sitio diferente del de taxol.

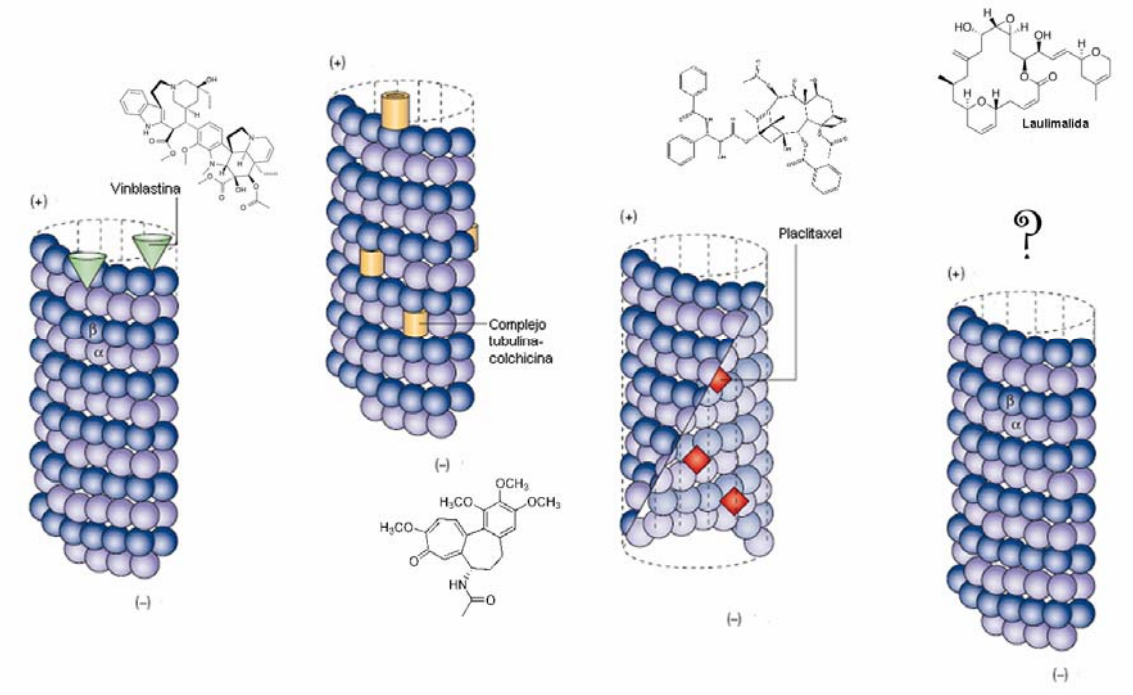

Figura 7. Sitios de unión de los agentes antimitóticos. (Modificación a partir de una figura de (Jordan y Wilson, 2004))

3.4.1. Agentes desestabilizadores de microtúbulos.

Este tipo de drogas se unen principalmente a dos sitios diferentes, el de vinca y el de colchicina:

3.4.1.1 *Dominio vinca.*

Figura 8. Flor de la vinca.

Los compuestos que encabezan la familia de los alcaloides de vinca, vinblastina y vincristina, fueron aislados en los años sesenta de una vinca de Madagascar (figura 8). La utilidad terapéutica de las hojas de vinca es conocida desde el siglo XVII. A finales de la década de los cincuenta se descubrieron sus efectos antimitóticos y, por ende, su potencial como agentes anticancerígenos (Cutts *et al.*, 1960; Johnson *et al.*, 1960). Seguidamente se empezó a usar en clínica para el tratamiento de leucemias, linfomas y algunos tumores sólidos. A partir de entonces su eficacia en combinación con otras terapias suscitó la aparición de varios análogos semisintéticos (vindesina, vinorelbina y vinflunina) (Duflos *et al.*, 2002). Además se han identificado muchos compuestos naturales de otras procedencias que también se unen al dominio de vinca: halicondrinas (aisladas de distintas esponjas marinas entre ellas *Halicondria okadai*) (Bai *et al.*, 1991), hemiasterlinas (sacadas de la esponja marina *Cymbastela sp.*) (Anderson *et al.*, 1997; Bai *et al.*, 1999), espongistatina (de la esponja *Spirastrella spinispirulifera*) (Bai *et al.*, 1993), dolastatinas (del gasterópodo *Dolabella auricularia*) (Bai *et al.*, 1990) y criptoficinas (aisladas del alga verde-azulada *Nostoc sp.*) (Kerksiek *et al.*, 1995); todos ellos bloquean igualmente la mitosis e inducen apoptosis en células cancerosas, cada uno se encuentra en distintas fases de desarrollo clínico para ser usados como agentes quimioterapéuticos en la lucha contra el cáncer (Duflos *et al.*, 2002; Hamel, 1992).

Todo este grupo de compuestos se unen tanto a tubulina como a microtúbulos y sus acciones dependen mucho de su concentración (Jordan *et al.*, 1991). A concentraciones relativamente altas provocan la despolimerización, hacen desaparecer los microtúbulos del huso mitótico y detienen las células en mitosis. A concentraciones aún mayores, del rango de micromolar, inducen la agregación de tubulina en estructuras paracristalinas (Jordan *et al.*, 1986). Sin embargo, a concentraciones bajas, estas drogas detienen la dinámica de los microtúbulos sin despolimerizar los que forman el huso pero siguen parando la mitosis e induciendo apoptosis (Jordan, 2002).

Los principales efectos secundarios que se han observado tras el tratamiento con estas drogas son neuropatías periféricas y mielosupresión reversible (Gidding *et al.*, 1999; Quasthoff y Hartung, 2002).

3.4.1.2. *Sitio de colchicina.*

Las drogas que se unen al sitio de colchicina tienen un comportamiento dependiente de su concentración similar al de los compuestos del dominio de vinca (Skoufias y Wilson, 1992). La colchicina fue aislada del azafrán *Colchicum autumnale* y fue uno de los primeros compuestos encontrados que se unía a microtúbulos (Borisy y Taylor, 1967a, b), tanto es así que la tubulina fue purificada por primera vez basándose en su gran afinidad por el compuesto e identificada como "la proteína que se une a colchicina" (Weisenberg *et al.*, 1968). La colchicina se usa para el tratamiento de la gota pero su utilización como antitumoral no ha tenido ningún éxito probablemente debido a su gran citotoxicidad en tejidos sanos. Sin embargo otras drogas que se unen al mismo sitio han cobrado interés en su desarrollo para estos tratamientos y se encuentran en ensayos clínicos, es el caso de las combrestatinas, aisladas de un sauce sudafricano (Hamel y Lin, 1983), o el 2-metoxi-estradiol, metabolito natural del estradiol (Mabjeesh *et al.*, 2003).

3.4.2. Agentes estabilizadores de microtúbulos (MSA).

Los agentes estabilizadores de microtúbulos (MSA: microtubule stabilizing agents) son drogas que se unen a microtúbulos provocando alteraciones en su dinámica, promoviendo su crecimiento y evitando el desensamblaje (Checchi *et al.*, 2003). La formación del huso mitótico es especialmente sensible a estas variaciones. En presencia de MSA la dinámica del huso se interrumpe provocando una parada de las células en mitosis bloqueando el ciclo celular en la transición de metafase a anafase; esta parada del ciclo induce la apoptosis celular (Jordan *et al.*, 1996). Aún cuando la actuación primaria de este tipo de drogas es bien conocida, sus consecuencias en las rutas de señalización que inducen la muerte celular continúan siendo objeto de estudio.

Se conocen tres sitios diferentes a los que se unen los MSA:

3.4.2.1. *Sitio de laulimalida.*

Poco se conoce de la localización de este sitio, la laulimalida ha sido el primer agente estabilizador de microtúbulos encontrado que, teniendo todas las características de éstos, se une a un sitio diferente del de taxol (Pryor *et al.*, 2002).

3.4.2.2. *Sitio de taxol.*

Los taxanos y sus biomiméticos (Buey *et al.*, 2005) son el segundo grupo conocido de agentes estabilizadores de microtúbulos, a concentraciones relativamente altas promueven la polimerización de microtúbulos y los estabilizan (Schiff y Horwitz, 1980), además concentraciones aún mayores provocan el agrupamiento de éstos en manojos (Schiff y Horwitz, 1980; Turner y Margolis, 1984). A concentraciones menores, al igual que las de los otros

grupos, estas drogas suprimen la dinámica de microtúbulos sin afectar la masa de polímero pero manteniendo su capacidad de bloquear la mitosis e inducir apoptosis (Jordan *et al.*, 1993; Jordan *et al.*, 1996; Yvon *et al.*, 1999). Los taxanos, aunque no se unen o se unen muy poco a la tubulina soluble, se unen con gran afinidad a la tubulina polimerizada en toda la extensión del microtúbulo. El primer compuesto de estas características que se conoció fue el taxol (paclitaxel) que fue aislado en 1967 de la corteza del tejo (Wani *et al.*, 1971), permaneció en el olvido hasta finales de los años setenta cuando se descubrió su acción sobre la dinámica de los microtúbulos (Schiff *et al.*, 1979). En 1995 fue aprobado su uso clínico y en la actualidad es comúnmente utilizado (junto con su análogo semisintético, docetaxel) en los tratamientos de los cánceres de mama, ovario y pulmón así como del sarcoma de Kaposi entre otros. Como principales efectos secundarios se encuentran, como en el caso de la colchicina, neurotoxicidad y mielosupresión (Markman, 2003). El gran éxito que ha tenido el uso clínico de estos compuestos ha llevado a la búsqueda de otras sustancias con propiedades similares, hallándose distintos compuestos de diferentes orígenes sobre los que se estudia su utilidad como agentes quimioterapéuticos, entre ellos se encuentran epotilonas (aisladas de la bacteria *Sorangium cellulosum*) (Bollag *et al.*, 1995), discodermolida (de la esponja *Discodermia dissoluta*) (Hung *et al.*, 1996; ter Haar *et al.*, 1996), eleuterobina (procedente del coral *Eleutherobia sp.*) (Long *et al.*, 1998), sarcodictinas (del coral *Sarcodictyon roseum*) (Nicolaou *et al.*, 1999), tacalonolidas (aisladas de la planta *Tacca chantrieri*) (Chen *et al.*, 1987), algunos derivados de esteroides (Verdier-Pinard *et al.*, 2000) y la cicloestreptina (aislada originalmente de *Streptomyces*) (Sato *et al.*, 2000a; 2000b).

3.4.2.3. ***Sitio externo del taxol.***

Los datos de la cinética de unión de los taxanos a los microtúbulos revelan una unión muy rápida (Diaz *et al.*, 2003) incompatible con la entrada por simple difusión a un sitio tan inaccesible como el descrito por Nogales *et al.* (1995) en el interior del lumen. En este trabajo se hipotetiza la presencia de un sitio externo cercano al poro de tipo I en la superficie del microtúbulo que debería contener el lazo entre las hélices H6 y 7 al que los taxanos se unirán primeramente para posteriormente traslocarse a su sitio en el lumen. Esta hipótesis explica el fácil acceso de los taxanos a su sitio, la ausencia del sitio de unión en tubulina no ensamblada y la influencia de la unión de los taxanos en el número de protofilamentos en los microtúbulos (Diaz *et al.*, 2005). Los datos obtenidos con un ligando que se une covalentemente al sitio de taxol, la cicloestreptina, en el trabajo de Buey *et al.* (2007) demuestran la existencia de este sitio. En este trabajo se detectan dos aminoácidos marcados por la unión de este compuesto: la treonina 220 y la asparagina 228. Este último residuo se encuentra en la luz del microtúbulo coincidiendo con el sitio luminal de taxol descrito y Thr220 es uno de los componentes del sitio externo propuesto en los trabajos anteriores. Esto además no parece algo propio y único de la cicloestreptina pues su unión a tubulina impide la unión de todos los ligandos del sitio de taxol probados en este estudio.

4. TAXANOS.

Los taxanos son diterpenoides provenientes de las plantas del género Taxus. La búsqueda de actividades anticancerosas dió lugar al descubrimiento del taxol, aislado de la corteza del tejo *Taxus brevifolia*, cuya estructura fue publicada en 1971 por Wani y sus colaboradores pero hasta 1979 ,(Schiff *et al.*, 1979) no se describe su modo de acción como estabilizador de microtúbulos. El compuesto entra rápidamente en fase clínica y su uso (junto al de su análogo semisintético, docetaxel (Guéritte-Voegelein, 1986)) es ahora habitual en el tratamiento de cáncer de ovario, mama y pulmón.

El tejo europeo (*Taxus baccata*) es conocido como venenoso desde la antigüedad, esta cualidad se debe a su alto contenido en alcaloides similares al taxol, las taxinas A y B.

El impacto del descubrimiento del taxol como antitumoral fue tal que en los años noventa se previeron problemas para su abastecimiento, la empresa farmacéutica que firmó los acuerdos de desarrollo y comercialización de la droga se responsabilizó del problema cuya solución vino con el hallazgo de la semisíntesis del taxol a partir de 10-deacetil bacatina III (Denis *et al.*, 1988).

4.1. Unión del taxol a la tubulina.

La determinación de la conformación del complejo microtúbulo-taxol se complica ante la imposibilidad de cristalizar microtúbulos. Aunque se ha determinado la estructura del dímero de α/β tubulina mediante difracción de rayos X a una resolución de 3,5 Å a partir de láminas de tubulina inducidas por zinc y estabilizadas con taxol (Lowe *et al.*, 2001), la resolución de estos datos no es suficiente para descifrar la conformación detallada del taxol unido en el polímero de tubulina y es necesario apoyarse en otros métodos indirectos adicionales. No obstante la cristalografía nos han enseñado la localización del sitio y los residuos implicados en los contactos con el ligando.

El sitio de taxol se encuentra en el monómero β cercano a los contactos entre protofilamentos adyacentes (Nogales *et al.*, 1995). El trabajo de Löwe *et al.* (2001) muestra los residuos directamente implicados en los contactos directos con la droga (figura 9), en el artículo se describen contactos hidrofóbicos de Val23 en la hélice 1 con los anillos fenilo en 3' y N' (Rao *et al.*, 1994) y que Asp26 está a distancia de puente de hidrógeno del nitrógeno de la cadena lateral en C-13. Se encuentran también interacciones hidrofóbicas entre el anillo fenilo en C-2 con las leucinas 217 y 219 del lazo entre las hélices 6 y 7 por un lado e His229 y Leu230 en el centro de la hélice 7 por otro (Rao *et al.*, 1995). El fenilo

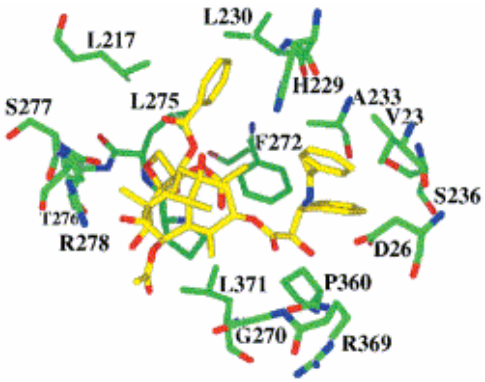

Figura 9. Sitio de taxol. En verde se muestran las cadenas laterales de los aminoácidos que interaccionan con la molécula de taxol (en amarillo). (Modificación de una figura de (Lowe *et al.*, 2001))

en 3' se localiza en un ambiente hidrofóbico proporcionado por los aminoácidos Ala233 y Ser236 en H7 y Phe272 en el final de la lámina B7. El lazo M es esencial para la unión del anillo taxano, en especial los residuos Pro274, Leu275, Thr276, Ser277 y Arg278. El bolsillo hidrofóbico que acoge la molécula de taxol se completa con los residuos Pro360, Arg369, Gly370 y Leu371 en el lazo entre las láminas B9 y B10.

Los estudios de los espectros de RMN del taxol en solución muestran que en solventes apolares la molécula adopta principalmente una conformación "no-polar" en la que los anillos N-benzoilo del carbono 3' y el benzoilo del carbono 2 están apilados (Dubois *et al.*, 1993; Williams *et al.*, 1994). En soluciones acuosas, sin embargo, aparecen una serie de conformaciones "polares" o "colapsadas hidrofóbicamente" en las que el grupo fenilo de C-3' está orientado hacia el benzoilo en C-2 (Vander Velde *et al.*, 1993). Snyder y sus colaboradores (2001) proponen una conformación de T-taxol en la que los dos fenilos de la cadena lateral de C-13 equidistan del grupo benzoilo en C-2, dándole un aspecto de "T" al que debe el nombre. Esta conformación se basa en los datos de la estructura cristalográfica del complejo tubulina-taxol, de dinámica molecular y en el análisis de flexibilidad molecular en solución por RMN del taxol (NAMFIS).

El panorama se completa con las predicciones de las interacciones y posiciones de otros sustituyentes del esqueleto taxano mostrados en el modelo de Snyder *et al.* 2001 donde la treonina 276 mantiene contacto electrostático con el oxetano entre C-4 y 5, el acetilo de C-4 encaja en una cavidad hidrofóbica compuesta por diez aminoácidos (Leu230 y Ala233 en H7; Phe272, Pro274, el metilo de Thr276, Leu286 y Leu291 en el lazo M; Pro360 y Leu371 en el lazo entre B9 y 10 y el -CH_2 de Ser374 en B10) la mayoría en el lazo M, el grupo hidroxilo en 2' forma un puente de hidrógeno con la arginina 369, el grupo metilo en C-12 se encuentra muy próximo a Leu371 y el de C-8 está orientado hacia el lazo M manteniendo interacciones de van der Waals con Thr276 y Gln281. Además los estudios de foto-marcaje de (Rao *et al.*, 1999) hacen preveer una interacción entre el hidroxilo de C-7 y Arg282.

La conjunción de todos estos datos apunta a un modelo en el que la molécula de taxol establece tres contactos principales: el del anillo de taxano con el lazo M (Nogales *et al.*, 1998), el del anillo en C-2 con el bosillo hidrofóbico formado por His229 y Asp226 y el del anillo en N' con los aminoácidos 1-31 del extremo amino; estos contactos con el benzoilo en C-2 y las cadenas laterales de C-13 deben anclar y reforzar la unión del anillo taxano (He *et al.*, 2000). El modelo de (He *et al.*, 2000) explica algunas de las observaciones de la relación estructura-actividad de la molécula de taxol en particular la introducción de grupos azida en el anillo de C-2.

4.2. Relación estructura-actividad.

La molécula de taxol ha sufrido multitud de modificaciones químicas a lo largo de su historia a fin de estudiar la relación entre su estructura y su actividad biológica. Las posiciones oxigenadas alrededor de su sistema de anillos (en los carbonos 1, 2, 4, 5, 7, 9, 10 y 13) han sido uno de los objetivos favoritos (Kingston, 2007).

Según los trabajos de Chaudhary *et al.* (1993) y Chen *et al.* (1993a) la pérdida del grupo hidroxilo en C-7 no tiene efectos sustanciales en la citotoxicidad de la droga. De igual forma la deacetilación en C-10 no supone una diferencia evidente en la toxicidad (Chaudhary y Kingston, 1993).

Sin embargo el cambio del acetilo en C-4 tanto por un hidroxilo (Neidigh *et al.*, 1994) como por un hidrógeno (Chordia *et al.*, 1994) da lugar a moléculas mucho menos activas.

El efecto de la inclusión de sustituyentes en el anillo benzoilo del carbono 2 depende de la posición en la que estos sustituyentes se encuentren de manera que, por ejemplo, el compuesto que presenta un grupo azida en posición para es prácticamente inactivo, mientras que esta sustitución en posición meta da lugar a una molécula unas seis veces más citotóxica que el taxol (Chaudhary *et al.*, 1994).

Al igual que la cadena lateral de C-2 la de C-13 admite ciertas modificaciones pero su presencia es esencial para la actividad biológica de la molécula (Kingston *et al.*, 2005)

4.3. Efectos celulares del tratamiento con taxanos.

La apoptosis inducida por el tratamiento con taxol requiere la activación del punto de comprobación del huso mitótico y la "escapada" de la parada en mitosis provocada por esta activación (Bergstralh y Ting, 2006). Para la función del punto de comprobación del huso y la parada en mitosis son necesarios una serie de componentes entre los que destacan la quinasa Aurora B, INCENP, Borealina y survivina todos ellos parte del CPC (chromosomal passenger complex). Esta última proteína, la survivina, ha sido reconocida como antiapoptótica durante la mitosis (Altieri, 2003) y su estabilidad se debe a una fosforilación específica durante la mitosis en su treonina 34 por la quinasa dependiente de ciclina CDK1 unida a ciclina B (O'Connor *et al.*, 2000). Durante la parada del ciclo provocada por este tipo de drogas parece que algunas de las proteínas del punto de comprobación del huso funcionan como reguladoras pro-apoptóticas mientras que otras podrían ser parte de rutas de supervivencia.

A la parada del ciclo en mitosis viene asociada la hiperfosforilación de bcl-2, proteína antiapoptótica que ejerce su acción evitando la actividad proapoptótica de bax ya que impide su activación conformacional al unirse a ella (Willis *et al.*, 2003).

En un proceso mitótico sin interferencias bcl-2 se encuentra hiperfosforilada y el CPC (que, recordemos, contiene survivina) está activo y localizado en los cinetocoros (Ling *et al.*, 1998). Parece que estos dos hechos son los protagonistas del mantenimiento de una ruta activa de supervivencia que

reprime una ruta apoptótica por defecto durante el proceso de la mitosis. Esto explicaría la eficacia de las drogas antimitóticas como agentes inductores de apoptosis.

Se ha sugerido que la iniciación de la apoptosis debida al tratamiento prolongado con este tipo de fármacos es consecuencia de la falta de proteínas antiapoptóticas causada por la inhibición de la transcripción durante la parada en mitosis (Blagosklonny, 2007).

Otra pieza clave en este escenario es la proteína bim, otro miembro de la familia de bcl-2. Durante el desarrollo de una mitosis inalterada, bim se encuentra asociada a microtúbulos; tras el tratamiento con taxol se disocia de ellos y se une ahora a bcl-2 inhibiendo su función antiapoptótica (Puthalakath *et al.*, 1999). No existen pruebas concluyentes de cómo se regulan las proteínas de la familia de bcl-2 durante la mitosis o los procesos de daño en el huso mitótico.

Aparte de los cambios mencionados muchas quinasas inducibles por stress (por ejemplo JNK o p38) se activan durante el daño mitótico pero sus papeles en este proceso no están aún muy claros (consultar Mollinedo y Gajate, 2003).

5. LIMITACIONES EN EL TRATAMIENTO CON TAXANOS.

Tras su aprobación para uso clínico, el taxol y el docetaxel han tenido una notoria importancia en el tratamiento contra el cáncer siendo fármacos de uso muy extendido en las terapias contra varios carcinomas y el sarcoma de Kaposi. A pesar del gran éxito obtenido, estas drogas están todavía lejos de ser la solución perfecta para la enfermedad y aún hay que soslayar problemas en su uso como por ejemplo su limitada solubilidad acuosa, sus efectos secundarios o la generación de resistencias tras un tratamiento prolongado.

Aparte de los efectos secundarios citados (neurotoxicidad, mielosupresión) debidos a la toxicidad en células sanas (Markman, 2003), se dan también una serie de reacciones alérgicas provocadas por el surfactante administrado junto a los fármacos, necesario a causa de la falta de solubilidad, para conseguir llegar a las dosis necesarias. Para poder obviar este problema se han desarrollado diversos taxoides sustancialmente más solubles en agua algunos de los cuales ya están en fase de ensayos preclínicos (Ganesh, 2007). Para evitar los efectos secundarios derivados de la inespecificidad de la diana se están haciendo toda clase de esfuerzos para encontrar un "vehículo" que "guíe" a estos fármacos hasta las células tumorales aprovechando las diferencias entre éstas y las normales; para ello se han ensayado algunas prodrogas y protocolos de "guía a la diana" (targeted delivery) (Skwarczynski *et al.*, 2006). Por último otro de los problemas que aparecen en el tratamiento con taxoides, que será recurrentemente mencionado a lo largo de esta memoria, es la aparición de resistencias.

5.1. Resistencias múltiples a fármacos.

Tras los tratamientos prolongados de quimioterapia es común que ésta deje de surtir efecto en los pacientes. Se han observado diversas modificaciones en células tumorales que las hacen resistentes al efecto de los taxanos (Jordan y Wilson, 2004; Zhou y Giannakakou, 2005): ciertas alteraciones en la dinámica de los microtúbulos, cambios en la regulación o expresión de proteínas asociadas a microtúbulos, diferencias en la expresión de los distintos isotipos de tubulina y mutaciones en el sitio de unión de los fármacos a tubulina, además de la aparición de resistencias múltiples a fármacos producidas por la sobreexpresión de proteínas transportadoras con motivo de unión a ATP ("ATP-binding cassette transporters"). Esta familia reúne un conjunto de proteínas de membrana que usan la energía de la hidrólisis de ATP para transportar sus ligandos a través de ella (Ozben, 2006). Se conocen muchos miembros de la familia, la mayoría de los cuales tienen un ligando específico pero algunas de ellas son capaces de transportar un amplio rango de moléculas hidrofóbicas. En este grupo de proteínas están clasificadas siete subfamilias nombradas como ABC (de ATP-binding cassette) seguidas de las letras de la A a la G. Las principales proteínas cuya sobreexpresión se ha encontrado asociada a resistencia múltiple a drogas en células tumorales son ABCB1, ABCC1, ABCC2 y ABCG2, entre ellas la ABCB1 (producto del gen humano mdr1, también conocida como glucoproteína P) es aparentemente la mayor causante de este fenómeno y también la mejor caracterizada.

5.2. La glucoproteína P.

La glucoproteína P humana (P-gp) tiene un peso molecular de unos 170 kD y está compuesta por una cadena polipeptídica de 1280 aminoácidos organizados en dos repeticiones en tándem de 610 aminoácidos cada una unidas entre sí por un segmento de unos 60. Cada una de estas "mitades" contiene un dominio intracelular de unión a nucleótido y un dominio transmembrana (Hennessy y Spiers, 2007). La proteína está glucosilada en su primer lazo extracelular, parece que la glucosilación influye en la estabilidad de la molécula, sin embargo su carencia no parece afectar al transporte de sus sustratos. Según los modelos más extendidos cada dominio transmembrana consiste en seis hélices α hidrofóbicas separadas

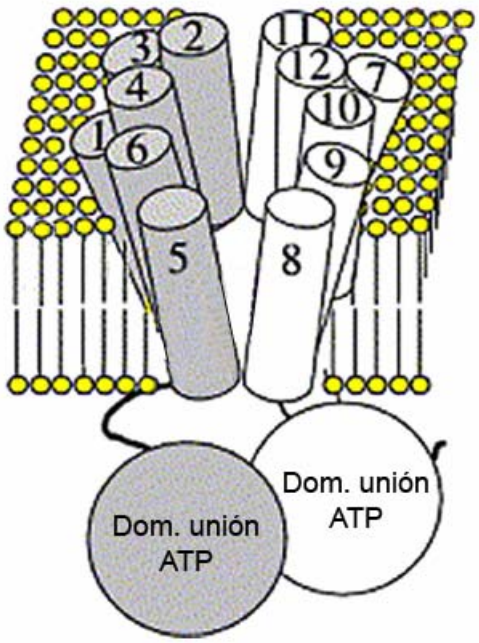

Figura 10. Esquema de la estructura de la P-gp insertada en la membrana plasmática, los dominios de unión a ATP quedan hacia el interior celular. (Modificada de (Hennessy y Spiers, 2007)

por lazos hidrofílicos (figura 10).

Los esfuerzos para evitar el problema que confiere la sobreexpresión de esta proteína en los tratamientos de quimioterapia han ido dirigidos, en su gran mayoría, a encontrar inhibidores que impidan su función y, por tanto, eviten la salida de la droga o a diseñar fármacos con una afinidad menor por ella para evitar su expulsión de la célula (Hennessy y Spiers, 2007; Modok *et al.*, 2006; Ozben, 2006; Shabbits *et al.*, 2001). En este trabajo mostraremos la posibilidad de superar la aparición de este tipo de resistencia múltiple a fármacos de una manera diferente.

OBJETIVOS.

Los taxanos son compuestos con una actividad antitumoral bien conocida y aceptada. Algunos miembros de la familia como el taxol y el docetaxel han sido muy utilizados en clínica para el tratamiento de diversos cánceres desde mediados de los años noventa con bastante eficacia. El principal problema de estos fármacos, aparte de ciertos efectos secundarios, es la aparición de resistencias tras un tratamiento prolongado.

En este trabajo introduciremos una serie de modificaciones sobre la molécula de taxol, tan efectiva en el tratamiento de esta enfermedad, con la pretensión de identificar los determinantes estructurales que pueden incrementar su afinidad y estudiar cómo la modulación de la afinidad influye en sus efectos citotóxicos en células tumorales sensibles y resistentes a taxanos.

Una vez localizadas las modificaciones estructurales que producen mayores incrementos de afinidad se combinarán en un solo compuesto que debe optimizar la interacción con la diana.

Se racionalizará la relación entre la afinidad de estas nuevas moléculas y sus modificaciones, modelando su estructura en el sitio de unión.

Se estudiará la relación entre las propiedades termodinámicas de la unión de los compuestos a su diana y su acción (su toxicidad en células cancerosas) con el fin último de ser capaces de diseñar un ligando optimizado en su afinidad, que debería ser activo en células tumorales que han desarrollado resistencias.

Por último, pretendemos, mediante estudios estructurales, incrementar nuestro conocimiento sobre la conformación de los ligandos y su sitio de unión, así como la influencia de su unión en la estructura de los microtúbulos que inducen.

MÉTODOS.

1. LIGANDOS.

Las diferentes modificaciones sobre la molécula de taxol fueron introducidas por síntesis química en el laboratorio del profesor Wei-Shuo Fang en el Instituto de Materia Médica en Pequín (China). Los detalles sobre la síntesis de cada ligando se encuentra en el material suplementario del trabajo (Matesanz *et al.*, 2008)

1.1. Métodos de análisis.

Todos los compuestos nos fueron suministrados en estado sólido, al recibirlos fueron disueltos en dimetilsulfóxido (DMSO) y su pureza comprobada mediante cromatografía líquida de alta resolución (HPLC), la de todos ellos resultó estar alrededor del 98% excepto para los chitax-3, 9, 19, 21, 26, 27, 28 y 41 que está en el 90%.

Asimismo se comprobó que su solubilidad en medio acuoso es al menos la concentración mayor utilizada en los ensayos, esto es 25 ó 50 µM.

1.1.1. <u>Análisis cromatográfico.</u>

La separación de los compuestos se realizó mediante cromatografía líquida a alta resolución en un aparato Agilent 1100 utilizando una columna de fase reversa C18 (Supercosil, LC18-DB, 250 x 4,6 mm) equilibrada en 50% de acetonitrilo en agua con un flujo de 1 ml/min creando un gradiente hasta el 80% de acetonitrilo en 30 minutos. La salida de los compuestos de la columna se siguió por absorbancia a 220 nm.

2. PROTEÍNAS.

2.1. Purificación de tubulina.

El material de partida para la purificación de tubulina fueron cerebros de bovino menor de 12 meses procedentes del Matadero Madrid Norte en San Agustín de Guadalix, Madrid. La purificación se hizo siguiendo el procedimiento de Weisenberg con algunas modificaciones (Andreu *et al.*, 1984; Andreu, 2007; Lee *et al.*, 1973; Weisenberg *et al.*, 1968). Se partió normalmente de 8 cerebros de vacuno obteniendo unos 400 mg de proteína. Para la obtención de tubulina se homogenizaron los cerebros con un homogenizador de aspas y se eliminaron las membranas por centrifugación. Después siguió un fraccionamiento con sulfato amónico (32%) y la precipitación de la proteína (43% sulfato amónico). Para la purificación de la tubulina se siguió con una cromatografía de intercambio iónico en DEAE-Sephadex A50, el eluido de esta separación se precipitó con sulfato amónico y se resuspendió en un volumen pequeño para ser cargado en una columna de cromatografía de filtración en gel Sephadex G25, las fracciones resultantes de la filtración se seleccionaron por su capacidad de precipitar con Mg^{++} (proteína activa, capaz de polimerizar). Tras

esta precipitación el exceso de Mg^{++} se eliminó mediante diálisis durante toda la noche en un tampón conteniendo 1 M Sacarosa que serviría como crioprotector. Esta proteína se almacenó en pequeñas alícuotas en nitrógeno líquido.

Para cada experimento la proteína fue descongelada rápidamente y equilibrada en el tampón apropiado mediante una cromatografía de filtración en gel (Sephadex G25). Las fracciones interesantes se seleccionaron por su elevada densidad óptica a 295 nm, se juntaron y se centrifugaron 10 minutos a 4 ^{o}C y 90.000g para eliminar posibles agregados.

2.2. Preparación de microtúbulos estabilizados.

Se partió de 40 mg de tubulina que fueron cargados en una columna de cromatografía de filtración en gel (Sephadex G25; 0.9 x 25 cm) equilibrada en un tampón 10 mM fosfato sódico, 1 mM EGTA, 0,1 mM GTP, 3,4 M glicerol, pH 6,8 (GAB: glicerol assembly buffer). Se seleccionaron las fracciones con una densidad óptica mayor de 1 a 295 nm, se juntaron y se centrifugaron 10 minutos a 4 ^{o}C y 90.000 g para eliminar posibles agregados. La concentración de proteína se midió espectrofotométricamente: la proteína diluida en tampón 10 mM fosfato sódico, 1% SDS, pH 7,0 tiene un coeficiente de extinción molar a 275 nm de 107.000 M^{-1}. Conociendo la concentración de tubulina se ajustó ésta a 50 µM y se ajustó la concentración de Mg^{++} y GTP a una concentración de 6 y 1 mM respectivamente en la solución y se comprobó que el pH era 6,5. La mezcla fue incubada a 37 ^{o}C para inducir la polimerización de tubulina, después de 30 minutos de incubación se añadió glutaraldehído hasta una concentración final de 20 mM y se mantuvo otros 10 minutos a 37 ^{o}C. El exceso de fijador fue eliminado con una incubación en 40 mM $NaBH_4$ durante 10 minutos en hielo y eliminando luego las burbujas producidas al vacío o por centrifugación suave. La muestra fue luego dializada durante toda la noche en un casete de diálisis Slide-A-Lyzer 10K (Pierce) frente a tampón GAB-0,1 mM GTP. Al día siguiente los microtúbulos fueron congelados gota a gota y almacenados en nitrógeno líquido.

2.2.1. Medida de la concentración de sitios de unión de taxol en microtúbulos estabilizados.

La concentración total de tubulina se midió espectrofotométricamente. Diluciones 2 µM de tubulina se incubaron a temperatura ambiente con 5 µM de flutax-2 en presencia o ausencia de 100 µM de docetaxel. Las mezclas se centrifugaron a 90.000 g durante 20 minutos a 25 ^{o}C para sedimentar los microtúbulos. Los sobrenadantes y los sedimentos se separaron cuidadosamente tras la centrifugación; los sedimentos fueron resuspendidos en una solución 10 mM fosfato sódico, 1% SDS, pH 7,0 y tanto éstos como los sobrenadantes se diluyeron cinco veces en la misma solución. La concentración de flutax-2 se mide espectrofluorimétricamente con la ayuda de una curva patrón. La cantidad de sitios de taxol en los microtúbulos se calcula restando la concentración de flutax-2 encontrado en el sedimento de las muestras tratadas

con docetaxel a la del hallado en las muestras sin docetaxel, esto nos dice la concentración de flutax-2 unido reversiblemente a los microtúbulos en condiciones de saturación que será la concentración de sitios de taxol que encontramos en los microtúbulos. Alrededor de un 95% de los dímeros de tubulina en las preparaciones de microtúbulos estabilizados son capaces de unir reversiblemente taxol. La concentración de sitios en estas muestras decae lentamente a 4 ºC y tienen una vida media de pocas semanas pero su almacenamiento en nitrógeno líquido permite mantenerla constante durante años.

3. EFECTO DE LOS LIGANDOS EN EL ENSAMBLAJE DE TUBULINA.

3.1. Polimerización de microtúbulos.

3.1.1. Ensamblaje en fosfato.

Para cuantificar el efecto de los ligandos en el ensamblaje de tubulina, se incubaron 30 µM de tubulina equilibrada en PEDTA (10 mM fostato sódico, 1 mM EDTA), 4 mM $MgCl_2$, 1 mM GTP con 35 µM del ligando estudiado, como controles se usaron taxol y docetaxel y blancos sin droga con el mismo volumen de DMSO. Las mezclas se incubaron a 37 ºC durante 30 minutos y los microtúbulos formados en este tiempo se sedimentaron por centrifugación durante 10 min. a 90.000 g en un rotor TLA 100 precalentado a 37 ºC. Los sobrenadantes fueron retirados cuidadosamente y los sedimentos resuspendidos en 10 mM fosfato sódico, 1% SDS y ambos diluidos cinco veces en la misma solución. La cantidad de tubulina se midió espectrofluorométricamente en estas diluciones (λ_{ex}=280 nm, λ_{em}=323 nm), en cada experimento se calculó la concentración extrapolando sobre una recta patrón confeccionada en paralelo.

Comprobamos el requerimiento de ión Mg^{++} para la polimerización de tubulina en presencia de aquellos ligandos que mejor inducen el ensamblaje en las condiciones anteriores. Para ello repetimos este ensayo pero en ausencia de $MgCl_2$.

3.1.2. Ensamblaje con glicerol.

Algunos compuestos de baja afinidad fueron incapaces de promover la formación de microtúbulos en fosfato, con estos ligandos se comprobó que al menos estabilizaban el ensamblaje en condiciones en que la proteína ensambla sin estabilizantes (p. ej. en buffer que contenga glicerol). En este tipo de ensayos se equilibró tubulina en GAB y se incubaron concentraciones diferentes de tubulina (15, 20 y 25 µM) con un 10% de exceso del ligando correspondiente durante 30 min. a 37 ºC y se procedió igual que en el caso anterior.

3.2. Unión a tubulina dimérica.

Para averiguar si los compuestos de más alta afinidad son capaces de unirse a tubulina dimérica la proteína fue equilibrada en buffer fosfato con GDP e incubada con los ligandos en condiciones en las que la polimerización está inhibida (10 mM fosfato sódico, 1 mM EDTA, 1 mM GDP) buffer con GDP y sin Mg^{++}. La tubulina en estas condiciones y a una concentración de 20 µM se incubó con 25 µM del ligando correspondiente durante 1 hora a 37 ºC. Tras la incubación, las muestras fueron centrifugadas en un rotor TLA 100 a 100.000 r.p.m. durante 1 hora a 37 ºC, separando posteriormente los 100 µl de la parte superior y los 100 µl inferiores y resuspendiendo el sedimento en 200 µl de tampón fosfato frío. En estas
condiciones de centrifugación la parte superior del sobrenadante no contendrá prácticamente proteína, sino únicamente ligando libre, en la parte inferior se encontrará tubulina sin polimerizar en equilibrio con el ligando libre, y en el fondo del tubo el sedimento será tubulina precipitada (Diaz *et al.*, 1993). Tomamos 100 µl del sedimento, las otras dos fracciones y 100 µl de buffer con la concentración inicial de compuesto (control de la extracción) y los extraemos con diclorometano. A cada fracción de cada reacción se le añade taxol como estándar interno a una concentración final de 5 µM. Se extraen los compuestos 3 veces con un volumen de diclorometano, se deja evaporar el solvente y una vez secos se resuspenden en 50 µl. de metanol. Luego se cargaron 20 µl. en una columna de HPLC C-18 y se cromatografiaron en un gradiente del 50 al 80 % de acetonitrilo:agua durante 30 minutos. La salida de la columna de cada compuesto se siguió midiendo la absorbancia a 220 nm. Las áreas bajo los picos de los compuestos en los cromatogramas permitieron calcular la concentración de los ligandos en cada fracción.

Con anterioridad a la extracción se toma un pequeño volumen de muestra (unos 15 µl) para determinar su contenido en proteína mediante el método de Bradford.

3.3. Determinación del diámetro de los microtúbulos (SAXS: small angle X-ray scattering).

Para tomar estas medidas la tubulina fue equilibrada en el buffer PEDTA 7 mM Cl_2Mg, cuya composición fue 10 mM fosfato sódico, 1 mM EDTA, 1 mM GTP, 7 mM $MgCl_2$ a pH 6,7, e incubada durante 20 min. a 37 ºC con un exceso de la droga correspondiente antes de registrar su patrón de dispersión.

Las medidas de dispersión de rayos X a bajo ángulo fueron tomadas en la estación bm26 (DUBBLE) en el ESRF en Grenoble (Francia) utilizando luz de sincrotrón de una longitud de onda de 1,24 Å. El patrón de dispersión se recogió con un detector de gases colocado a una distancia de 3,5 metros de la muestra. El detector fue calibrado con behenato de plata. La temperatura de la muestra se mantuvo a 37 ºC durante el registro de datos. Se acumuló la señal durante 10 minutos de registro. El análisis de los datos se realizó usando el software Fit2d para obtener el perfil de SAXS de la muestra en el espacio

recíproco.

El perfil de SAXS de los microtúbulos es característico de la función de Bessel para un cilindro cuyo máximo J_{01} es proporcional al diámetro del cilindro (D) en la relación

$$J_{01} = \frac{1,22}{D}$$

como se puede consultar en el manual Abramowitz (1965). En realidad si nos fijáramos en la disposición de las subunidades de tubulina en la superficie de los microtúbulos encontraríamos un entramado helicoidal (Amos y Klug, 1974), con los datos de los perfiles de SAXS éstas hélices se pueden modelar y hallar sus diámetros y número de protofilamentos de manera más aproximada (Andreu *et al.*, 1992; Andreu *et al.*, 1994). En este caso los diámetros y el número de protofilamentos de los microtúbulos producidos en presencia de nuestros taxanos se calcularon por interpolación usando los ya descritos en (Andreu *et al.*, 1992; Andreu *et al.*, 1994; Diaz *et al.*, 1994).

4. UNIÓN DE LOS LIGANDOS A LOS MICROTÚBULOS.

4.1. Medida de las constantes de unión de los ligandos a microtúbulos estabilizados

4.1.1. Desplazamiento de flutax-2.

Para calcular las constantes de unión en el equilibrio de los ligandos se midió el cambio de anisotropía de la molécula de flutax-2 al desplazarlo de su sitio de unión a microtúbulos (Buey *et al.*, 2004). Para ello se preparó una mezcla de flutax-2 50 nM y sitios de taxol en microtúbulos estabilizados 50 nM en GAB, se distribuyeron 200 µl de la mezcla en cada pocillo de una placa de 96 pocillos obviando los de los bordes. Sobre esta mezcla se añadieron concentraciones crecientes del ligando problema. Las mezclas de reacción se incubaron en un agitador orbital durante al menos 10 minutos y se midió la anisotropía de cada pocillo a distintas temperaturas después de incubar durante 20 minutos bajo cada condición utilizando un lector de placas POLARSTAR BMG.

En este ensayo el ligando de referencia es el flutax-2 cuya constante de unión a los microtúbulos conocemos. Con las medidas de anisotropía podemos calcular su saturación fraccional para cada punto del desplazamiento ($\upsilon = [\text{flutax-2}]_{unido} / [\text{sitios}]_{total}$). Al ser una propiedad aditiva la anisotropía de una mezcla será la suma de la anisotropía de cada uno de sus componentes ponderada por sus fracciones molares. Las anisotropías del flutax-2 en los dos estados de referencia (unido, r_{max} y libre, r_{min}) son conocidas y la unión del compuesto fluorescente en ausencia de competidor (υ_0) se puede calcular conocidos las concentraciones iniciales de los sitios de unión y de flutax-2 así como la constante de afinidad. Con los valores de anisotropía medidos se pueden calcular la saturación fraccional:

$$\upsilon=\upsilon_0 \frac{r - r_{min}}{r_{max} - r_{min}}$$

(esta relación es válida únicamente si no hay cambio de rendimiento cuántico, como es el caso de estas medidas (Lakowicz, 1999))

Conociendo que las constantes de equilibrio de unión de flutax-2 (K_{flutax}) y del ligando problema (K_x) son:

$$K_{flutax}=\frac{[SF]}{[sitios] \times [flutax]} \qquad K_x=\frac{[SX]}{[sitios] \times [X]}$$

donde [SF] y [SX] son las concentraciones de flutax y el ligando medido unidos al sitio de taxol y [flutax] [sitios] y [X] las concentraciones libres de flutax-2, sitios y ligando problema. La relación entre ambas constantes de equilibrio será:

$$\frac{K_x}{K_{flutax}} = \frac{[SX] \times [flutax]}{[SF] \times [X]}$$

además:

$$[flutax] = [flutax]_{total} - [SF]$$

$$[X] = [X]_{total} - [SX]$$

$$[sitios] = [sitios]_{total} - [SF] - [SX]$$

Sustituyendo en la relación de constantes tenemos:

$$\frac{K_x}{K_{flutax}} = \frac{[SX] \times ([flutax]_{total} - [sitios]_{total} - [sitios] - [SX])}{([sitios]_{total} - [sitios]-[SX]) \times ([X]_{total} - [SX])}$$

Sobre la representación de υ frente a $[X]_{total}$ calculamos el valor de la constante de unión del ligando competidor al sitio de taxol utilizando un programa desarrollado en el laboratorio (Equigra v5.0, Diaz y Buey, 2007) específicamente para ajustar por mínimos cuadrados esta función a partir de los valores conocidos $[flutax]_{total}$, $[sitios]_{total}$, $[X]_{total}$ y K_{flutax}.

4.1.2. Desplazamiento de epotilona B.

No es posible medir las constantes de unión de los compuestos de muy alta afinidad con el método anterior, ya que son muy diferentes de la constante de flutax-2 y el error es grande (Diaz y Buey, 2007). Por esta causa se diseñó una

forma alternativa de medirlas por desplazamiento de epotilona B que tiene una constante de unión al sitio de taxol mayor (Buey *et al.*, 2004).

Dado que el análisis de los datos en este tipo de ensayos de competición se basa en el desplazamiento estequiométrico del ligando de referencia (Diaz y Buey, 2007), todo compuesto que sobrepase en tres órdenes de magnitud la afinidad del ligando de referencia se comportará básicamente igual, no observándose diferencias entre ellos puesto que el ensayo se fundamenta en las cantidades del ligando de referencia libres y unidas a su sitio. Como supuesto clarificador podemos pensar en una mezcla que contenga una concentración 100 nM tanto de un ligando problema como de un compuesto de referencia (con una constante de unión, pongamos, 10^7 M^{-1}) y de sitios, la proporción de ligando de referencia libre dependerá de la afinidad del problema siguiendo estas pautas: si la constante problema es de 10^7 M^{-1} el porcentaje de ligando libre será el 76,6%, si es 10^8 M^{-1} entonces el ligando libre será el 81,9%, con 10^9 M^{-1} será el 92,8%, con 10^{10} M^{-1} llegará al 97,5 y para una constante de 10^{11} M^{-1} el ligando libre será el 99,2%. Así pues con un ligando de referencia de estas características se podrá medir con cierta precisión las afinidades de compuestos cuyas constantes de unión estén entre 10^7 y 10^9 M^{-1} pero será difícil distinguir entre dos ligandos de constantes en el orden de 10^{10} M^{-1}.

Para las medidas de las constantes de afinidad por desplazamiento de epotilona B se procedió como se explica en (Matesanz *et al.*, 2008): se distribuyó un mililitro de GAB con 1 µM de sitios en microtúbulos estabilizados y 1,1 µM de epotilona B en cada tubo, en cada uno se añadió 1,1 µM del compuesto problema o el correspondiente volumen de DMSO en el tubo control. Las mezclas se incubaron a 26, 35 ó 40 ^oC durante media hora y se centrifugaron durante 20 minutos a 90.000 g en un rotor TLA 120.2 a la temperatura correspondiente. Tras la centrifugación se separaron los sobrenadantes y se resuspendieron los pellets en 1 ml de buffer 10 mM fosfato sódico. A cada fracción de cada reacción se le añadió 1 µM de taxol como patrón interno en la extracción orgánica (en el caso del compuesto n^o 13 se usó docetaxel como patrón porque en el método cromatográfico empleado sale demasiado próximo al taxol). Se extrajeron los compuestos 3 veces con un volumen de diclorometano, se dejó evaporar el solvente y una vez secos se resuspendieron en 60 µl de metanol. Posteriormente se cargaron 20 µl en una columna de HPLC C-18 y se cromatografiaron en un gradiente del 50 al 80 % de acetonitrilo:agua durante 30 minutos. La salida de la columna de cada compuesto se siguió midiendo la absorbancia a 220 nm. Las áreas bajo los picos de los compuestos en los cromatogramas permitieron calcular la concentración de los ligandos en el sedimento (y por tanto unidos a microtúbulos) y en el sobrenadante (libre), la relación de las concentraciones del ligando problema y de epotilona B nos da la relación entre las constantes de unión de los dos compuestos de manera que podemos calcular así la constante de interés:

$$Mt + Epo \overset{K_{epo}}{\rightleftarrows} MtEpo$$

$$Mt + X \underset{}{\overset{K_x}{\rightleftarrows}} MtX$$

$$\frac{K_x}{K_{epo}} = \frac{[MtX] \times [Epo]}{[X] \times [MtEpo]} \qquad K_x = K_{epo} \frac{[MtX] \times [Epo]}{[X] \times [MtEpo]}$$

4.2. Reversibilidad de la unión.

La reversibilidad de la unión de los ligandos a los microtúbulos se comprobó incubando en 200 µl de volumen final 5 µM de los compuestos susceptibles de formar un enlace covalente con 10 µM de sitios a 25 ºC durante 30 minutos, centrifugándolos después en un rotor TLA 100 a 90000 g durante 10 minutos manteniendo la temperatura a 25 ºC. Después de la centrifugación las muestras fueron extraidas con diclorometano y analizadas por HPLC de igual forma que en el caso anterior.

5. CULTIVOS CELULARES.

Las líneas celulares de carcinoma ovárico A2780, A2780AD y 1A9 (clon de A2780) se cultivaron en medio RPMI-1640 complementado con un 10% de suero fetal bovino, 2mM L-glutamina, 40 µg/ml gentamicina, 100 IU/ml penicilina y 100 µg/ml estreptomicina, para las líneas A2780 y A2780AD el medio de cultivo se complementó además con 0,25 U/ml de insulina bovina.

Las líneas celulares LoVo y LoVo-Dox provenientes de carcinoma de colon se cultivaron en medio RPMI-1640 complementado de igual manera con suero, glutamina y antibióticos y además en presencia de 1 µg/ml de doxorubicina.

5.1. Ensayos de citotoxicidad.

Las células se sembraron en placas de 96 pocillos a una densidad de 12000 ó 16000 células por pocillo en 80 µl de medio de cultivo. Al día siguiente se añadieron otros 20 µl de medio con diluciones seriadas de ligando cubriendo el rango de concentraciones entre 5 pM y 40 µM y se incubaron durante otras 48 h, entonces se procedió a realizar un ensayo de MTT (Smith *et al.*, 1988) con alguna modificación: se añaden 20 µl de 2,5 mg/ml MTT (bromuro de 3-(4,5-dimetiltiazol-2-il)-2,5-difeniltetrazolio) a cada pocillo, se incuba durante 4 horas a 37 ºC , se añaden 100 µl de solubilizador de MTT (10% SDS, 45% dimetilformamida, pH 5,5) y se incuban las placas a 37 ºC durante toda la noche para disolver los precipitados de formazán antes de medir la absorbancia de cada pocillo a 595/690 nm en un lector de placas Multiscan MC. Pocillos sin células se usaron como blancos y células sin tratar como control del crecimiento. Las CI_{50} se calculan de la curva dosis-respuesta y se expresan como el promedio de al menos cuatro repeticiones independientes.

6. CONFORMACIÓN DE LOS LIGANDOS UNIDOS.

6.1. Medidas de Resonancia Magnético-Nuclear (RMN).

Los experimentos se realizaron a 37 ºC en D_2O en un espectrómetro Bruker Avance 500 MHz como se describe en el trabajo de Jiménez-Barbero *et al.* (2006) adaptándonos a nuestro caso particular.

Los tiempos de relajación para las medidas de Tr-NOESY se fijaron en 50 y 200 milisegundos. Para ajustar las intensidades experimentales de TR-NOE se probaron constantes de disociación entre 10 y 500 s^{-1}. El resultado óptimo se alcanza para unos valores de k_{off} en el rango de 15 a 150 s^{-1}.

Para ajustar los valores del efecto Overhauser nuclear (NOE) teóricos a los experimentales se utilizó el programa CORCEMA que tiene en cuenta una matriz completa de estados de relajación de los protones del ligando en el caso de intercambio entre las formas libre y unida. Por tanto se usaron diferentes tiempos promedios de correlación rotacional (entre 10 y 1000 nanosegundos) para ajustar los datos y se llegó a la conclusión de que 100 ns da el mejor ajuste entre los valores esperados y experimentales. Hay que tener en cuenta que este valor es de hecho un tiempo de correlación "efectivo" que contiene las contribuciones de los movimientos globales e internos.

6.2. Modelado molecular.

El modelado molecular y el acoplamiento del ligando se hicieron sobre la estructura refinada a 3,5 Å del dímero de α/β tubulina publicada en Löwe *et al.* 2001 (código del Protein Data Bank: 1JFF). Los átomos de hidrógeno no presentes se añadieron usando el servidor web H^{++} (Gordon *et al.*, 2005) basado en los parámetros del campo de fuerza AMBER (Cornell *et al.*, 1995) y en soluciones finitas diferenciales a la ecuación de Poisson-Boltzmann ; la computación del estado de protonación de los grupos ionizables en β tubulina a pH 6,5 se realizó en el mismo servidor. Para la visualización y representación molecular se empleó el programa gráfico PyMOL (DeLano Scientific). La distribución de cargas de los ligandos estudiados se obtuvo de la manera implementada en Gaussian 03 (Gaussian, Inc.): ajustando el potencial electrostático molecular calculado mediante un campo mecanocuántico (RHF 6-31G*\\3-21G*) a un modelo de carga puntual. Se asignaron por analogía o por interpolación entre aquellos ya descritos en la base de datos de AMBER (ff03), parámetros AMBER de enlace o no-enlace a los átomos de los taxanos.

Se utilizó el algoritmo genético lamarckiano implementado en AutoDock 3.0.5 (Garrett M. Morris, 1998) para generar conformaciones encajadas en su sitio de unión de las moléculas de taxol, docetaxel, chitax 13 y 40 cambiando al azar la orientación global y el ángulo de torsión del grupo benzoilo en C-2 de aquellas conformaciones representativas de las poblaciones mayoritarias entre las predichas por la dinámica molecular.

7. UNIÓN A GLUCOPROTEÍNA-P.

Las constantes de disociación de la unión de los ligandos a la glucoproteína-P se determinaron por el apagamiento de la fluorescencia intrínseca de un triptófano de ésta.

Para estos ensayos la P-gp se purificó a partir de células con fenotipo de resistencia múltiple a drogas siguiendo los métodos descritos (Sharom *et al.*, 1999).

El apagamiento de la fluorescencia se llevó a cabo como se describe en (Liu *et al.*, 2000) usando 50 µg/ml de proteína en un tampón 2 mM CHAPS, 20 mM HEPES, 100 mM NaCl, 5 mM $MgCl_2$, pH 7,5. Los distintos compuestos disueltos en DMSO en las soluciones stock se diluyeron en soluciones de trabajo con el buffer anterior (en diluciones entre 1,25 y 40 µg/ml). Para los experimentos de apagamiento se añadieron sucesivamente alícuotas de 5 µl de soluciones de trabajo de los ligandos sobre 500 µl de la solución de P-gp tal y como se describe en (Sharom *et al.*, 1999). Las concrentraciones finales de los compuestos añadidos están entre 0,0125 y 1,5 µg/ml. Después de cada adicción se midió la fluorescencia en estado estacionario a una $\lambda_{excitación}$ = 290 nm y una $\lambda_{emisión}$ = 330 nm con una apertura de las rendijas de 2 nm. Los taxanos no absorben significativamente a las longitudes de onda de excitación ni emisión por tanto las intensidades de fluorescencia registrada sólo se corrigieron por la dilución siguiendo esta ecuación:

$$F_{corregida} = (F_{medida} - F_{tampón}) \times \frac{Vol}{Vol_{inicial}}$$

donde la fluorescencia (F) es corregida restandole el blanco establecido con la fluorescencia de fondo del buffer sin proteína y la proporción del volumen (Vol) después de añadir los compuestos en cada momento de la titulación respecto al inicial. Los datos se analizaron ajustándolos a la siguiente ecuación:

$$\frac{\Delta F}{\Delta F_0} \times 100 = \frac{\left(\frac{\Delta F_{max}}{\Delta F_0} \times 100\right) \times [S]}{K_d + [S]}$$

donde $(\Delta F/F_0) \times 100$ es el tanto por ciento de apagamiento de la fluorescencia relativo al valor inicial (F_0) tras la adicción de una concentración de taxano ([S]). La representación de estos dos datos uno frente al otro nos permite calcular los valores de la constante de disociación (K_d) y el porcentaje máximo de apagamiento **(**$(\Delta F_{max}/F_0) \times 100$**)**.

RESULTADOS.

1. CARACTERIZACIÓN QUÍMICA DE LOS TAXANOS.

Para la realización de este estudio contamos con un grupo de cuarenta y siete compuestos con distintas modificaciones sobre el esqueleto de la molécula de taxol. Estas drogas fueron sintetizadas de acuerdo a nuestra colaboración con el laboratorio del profesor Weishuo Fang en el Instituto de Materia Médica en Pequín (China). Debido a su procedencia fueron nombrados como chitax seguido de un número identificativo. Sus fórmulas se pueden consultar en la figura 11.

1.1. Variabilidad química.

Los átomos de carbono de la molécula "patrón" (el taxol) se numeran de esta forma:

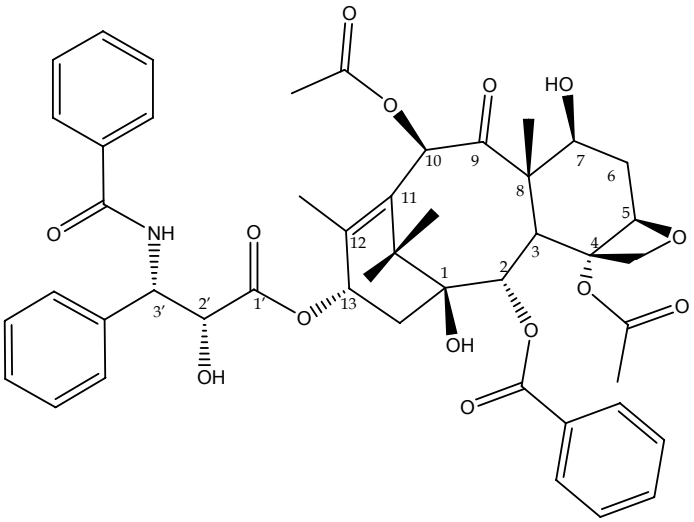

Todos los compuestos utilizados presentan modificaciones en al menos uno de estos sitios:

-en la cadena lateral del carbono trece (C-13)
-en C-7 y/o C-10
-en C-2

Según la cadena que encontremos en C-13 podremos dividir los compuestos en tres moléculas de partida: tendremos derivados de taxol, de docetaxel y de cefalomanina.

El docetaxel tiene un grupo terbutoxicarbonilo en C-13 en lugar del fenilo presente en la molécula de taxol (además está deacetilado en C-10 respecto al taxol). Como se describe en la introducción este compuesto es un producto semisintético.

Figura 11. Estructura química de los compuestos estudiados.

La única diferencia entre la molécula de cefalomanina y la de taxol está en C-13 donde presenta un grupo 2-metil, 2-butenoilo en lugar del fenilo. La cefalomanina fue aislada en los años setenta del tejo *Taxus walliana* por aquel entonces erróneamente clasificado como *Cephalotaxus manii*.

1.1.1. Taxoles.

En este grupo tenemos siete compuestos, en uno de ellos su única diferencia se encuentra en C-10 donde está deacetilado (chitax-15) y el resto (chitax-11, 12, 23, 25, 27 y 38) tienen distintas sustituciones en la cadena lateral de C-2.

Los chitax-11 y 12 se distinguen del taxol por la adicción de sendos sustituyentes en la posición meta del anillo aromático en C-2, un grupo metóxido en el caso de chitax-11 y una azida en el de chitax-12.

El resto de compuestos presentan sus diferencias en la unión del anillo bencénico en C-2 al esqueleto de taxol. El compuesto número 23 cambia el éster original por un tioéster. También el chitax-27 cambia este oxígeno por un azufre pero en este caso la unión del anillo se convierte en un tioéter. En el caso de chitax-25 el anillo se une mediante un enlace éter y en el chitax-38 el enlace resulta ser amino.

1.1.2. Docetaxeles.

Ocho de los nueve derivados del docetaxel usados en este trabajo están acetilados en C-10 (chitax-21, 22, 24, 26, 39, 42, 43 y 44), el noveno, el chitax-40, está propionilado en esta posición.

El resto de las diferencias entre unos y otros radicará nuevamente en los sustituyentes o la unión de la cadena lateral de C-2.

El chitax-40 además de estar propionilado en C-10 presenta la adicción de un grupo azida en la posición meta del anillo bencénico de C-2.

La única diferencia del chitax-21 respecto al docetaxel se encuentra en esa acetilación en C-10.

Los compuestos 42, 43 y 44 unen su anillos aromáticos en C-2 con un enlace amida en lugar del éster habitual, además los chitax-43 y 44 añaden un sustituyente en la posición meta del anillo, un grupo metóxido en el caso del primero y un átomo de cloro para el chitax-44.

Las diferencias entre los chitax-22, 24, 26 y 39 está en la unión del anillo de C-2. Nos encontramos con un éter para el chitax-24; un tioéster y un tioéter para los chitax-22 y 26 respectivamente y una amina para el chitax-39.

1.1.3. Cefalomaninas.

El grueso de los compuestos estudiados son derivados de cefalomanina. El único cambio en los chitax-17 y 18 es una deacetilación y una propionilación respectivamente en C-10. Los chitax-13, 14 y 16 tienen cambios sólo en C-2. Los chitax-19, 20 y 37 difieren del 18 en sus distintos sustituyentes en el grupo benzoilo de su cadena lateral en C-2.

De todos estos compuestos los chitax-13, 14, 19, 20 y 37 tienen un sustituyente en la posición meta del anillo bencénico en C-2. Se trata de un grupo metóxido en los compuestos 13 y 19, un grupo azida para los chitax-14 y 20 y un hidroxilo para el chitax-37.

En el caso del chitax-16 se pierde todo el grupo de C-2 y el hidroxilo de C-1 y aparece un carbonato entre estas dos posiciones.

El compuesto nombrado como **chitax-1** es una cefalomanina deacetilada en C-10 y propionilada en C-7. Sobre este esqueleto tenemos compuestos con distintos cambios en C-2: serán los compuestos del 2 al 10, del 28 al 36 y el 41.

Entre estos compuestos encontramos algunos en los que aparece la adición de distintos sustituyentes en distintas posiciones del benzoilo de C-2: las posiciones meta de los compuestos 4, 5, 6, 7, 8, 30, 33, 34 y 36 portan, por ese orden, una azida, un metóxido, un átomo de cloro, un grupo ciano, un metilo, un átomo de iodo, un formilo, un átomo de bromo y un hidroximetilo.

Los chitax-28, 29 y 35 sin embargo, tienen dos sustituciones. Éstas se encuentran en las posiciones para y orto en el caso de los compuestos 28 y 29 y se trata de sendos átomos de flúor (chitax-28) o de cloro (chitax-29). El compuesto 35, por su parte, tiene dos grupos metóxido en las posiciones meta y para.

Los compuestos 2, 3, 9 y 10 pierden el anillo benzoilo en C-2 por distintos grupos alquilo que serán respectivamente: 3-metil 2-butenoilo, 3-metil 3-butenoilo, 2-butenoilo y 3-metil butanoilo.

En el caso de los chitax-31, 32 y 41 el anillo bencilo en C-2 se intercambia por un anillo heterocíclico: 3-tiofeno (chitax-31), 2-tiofeno (chitax-32) o 2-piranona (chitax-41).

Tabla 1. Tiempos de retención de los compuestos a la columna C-18 en gradiente de acetonitrilo.

	tiempo de retención (min.)
Taxol	10,680
Docetaxel	9,225
Cefalomanina	9,710
Chitax-1	15,279
Chitax-2	14,511
Chitax-3	14,119
Chitax-4	18,491
Chitax-5	15,984
Chitax-6	18,915
Chitax-7	14,148
Chitax-8	18,043
Chitax-9	11,722
Chitax-10	15,955
Chitax-11	11,311
Chitax-12	13,577
Chitax-13	10,406
Chitax-14	12,715
Chitax-15	7,097
Chitax-16	7,583
Chitax-17	6,347
Chitax-18	11,769
Chitax-19	12,448
Chitax-20	14,654
Chitax-21	13,794
Chitax-22	15,490
Chitax-23	11,631
Chitax-24	18,267
Chitax-25	14,106
Chitax-26	20,148
Chitax-27	16,047
Chitax-28	16,275
Chitax-29	22,086
Chitax-30	20,824
Chitax-31	14,148
Chitax-32	13,720
Chitax-33	13,770
Chitax-34	19,819
Chitax-35	14,393
Chitax-36	9,798
Chitax-37	8,938
Chitax-38	10,180
Chitax-39	11,876
Chitax-40	18,680
Chitax-41	9,000
Chitax-42	10,751
Chitax-43	11,264
Chitax-44	13,314

1.2. Pureza e identificación por HPLC.

Todos los compuestos nos fueron suministrados en estado sólido, al recibirlos fueron disueltos en dimetilsulfóxido (DMSO) y su pureza comprobada mediante cromatografía líquida de alta resolución, la de todos ellos resultó estar alrededor del 98% excepto para los chitax-3, 9, 19, 21, 26, 27, 28 y 41 que está en el 90%. Sus tiempos de retención en el método descrito se listan en la tabla 1.

1.3. Espectrofotometría.

La caracterización de todos nuestros compuestos fue completada con la medida de sus espectros de absorción. Todos ellos pueden ser consultados en la figura 12.

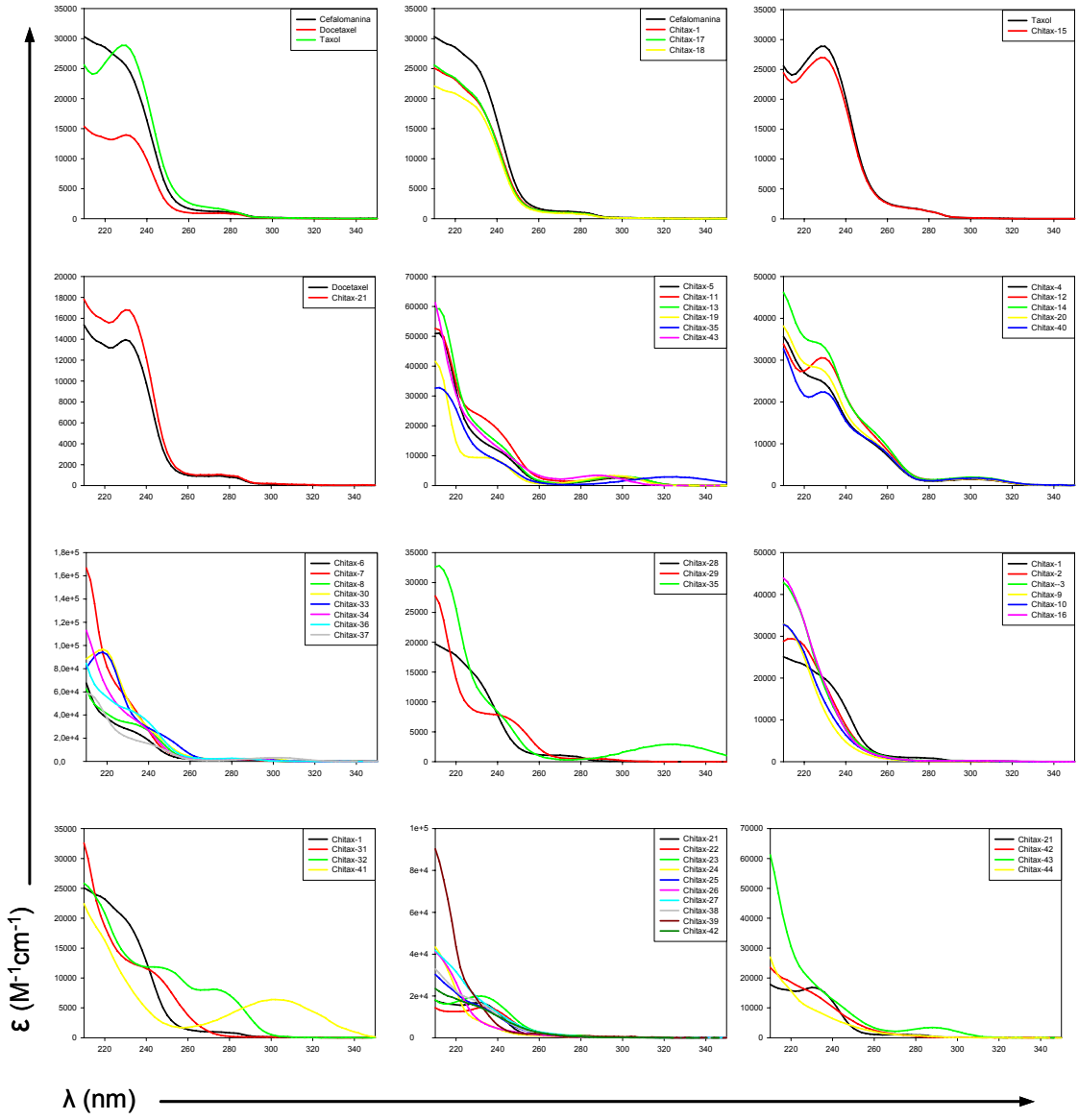

Figura 12. Espectros de absorción de los taxanos estudiados. Para mayor claridad de la figura los compuestos han sido agrupados según sus modificaciones.

2. EFECTO DE LOS LIGANDOS EN EL ENSAMBLAJE DE TUBULINA.

Como primer paso en este estudio comprobamos si nuestra colección de taxoides tiene un comportamiento típico como estabilizadores de microtúbulos en el ensamblaje de tubulina.

La formación de microtúbulos es una polimerización de tubulina por nucleación condensada no covalente; para que la polimerización tenga lugar necesita rebasarse el límite de una concentración crítica. La concentración crítica será la concentración de tubulina libre por debajo de la cual no se produce el ensamblaje (Oosawa y Asakura, 1975).

Los agentes estabilizadores de microtúbulos inducen la polimerización reduciendo esta concentración crítica (Buey *et al.*, 2004; Díaz *et al.*, 2008).

Se probó cómo influyen los compuestos en el ensamblaje de tubulina, midiendo la concentración crítica en tampón fosfato (10 mM fosfato sódico, 1 mM EDTA, 1 mM GTP, 4 mM $MgCl_2$, pH 6,7) en este tampón la proteína es incapaz de ensamblar (Diaz y Andreu, 1993) y/o estabilizando los microtúbulos formados en presencia de glicerol (Buey *et al.*, 2005); en este último caso se empleó el buffer GAB-1mM GTP (3,4 M glicerol, 10 mM fostato sódico, 1 mM EGTA, 1 mM GTP, 6 mM $MgCl_2$, pH 6,5).

2.1. Polimerización en tampón fosfato.

La tubulina equilibrada en el tampón se incuba con un 10% de exceso de la droga correspondiente y se centrifuga con objeto de sedimentar los microtúbulos polimerizados. Las cantidades de proteína presentes en sedimento y sobrenadante se miden espectrofluorimétricamente (λ_{exc} 280 nm; λ_{em} 320 nm.).

La concentración crítica es igual a la concentración de tubulina en el sobrenadante que debe ser igual a la concentración dada por la extrapolación y=0 de la representación $[tubulina]_{sedimentada}$ frente a $[tubulina]_{total}$.

Una vez determinada la concentración crítica de cada compuesto en estas condiciones (tabla 2) observamos que algunos de ellos no eran capaces de inducir el ensamblaje de tubulina: era el caso de los compuestos 9, 10, 16, 22, 23, 24, 25, 26, 27, 38 y 39. Todos estos compuestos presentan modificaciones en C-2 que bien cambian el grupo benzoilo por otro (chitax 9, 10, 16) o alteran el nexo de este grupo al esqueleto de la mólecula (chitax 22, 23, 24, 25, 26, 27, 38 y 39) cambiando el óxigeno del éster por otro átomo (azufre o nitrógeno, según el compuesto).

2.2. Polimerización en glicerol.

Medida igualmente la concentración crítica de cada compuesto en el tampón GAB-1mM GTP (tabla 2) queda claro que los ligandos que no eran capaces de ensamblar tubulina en el ensayo anterior eran capaces, al menos, de

estabilizar los microtúbulos ensamblados, como lo hacen otros compuestos de baja afinidad (Buey *et al.*, 2005), reduciendo las concentraciones críticas en este buffer, lo que nos indica que son agentes estabilizadores de microtúbulos.

Tabla 2. Concentraciones críticas (Cr) en las dos condiciones ensayadas.

	Cr (μM) en fosfato	Cr (μM) en glicerol
DMSO	N.P.	3,30±0,38d
Taxol	4,24±0,49c	0,63±0,06
Docetaxel	2,35±0,25	0,62±0,08
Cefalomanina	3,50±0,94	0,64±0,15
Chitax-1	3,68±0,81	0,67±0,04
Chitax-2	9,73±3,94	1,41±0,06
Chitax-3	11,38±2,83	2,60±0,19
Chitax-4	2,87±0,36	0,50±0,10
Chitax-5	2,81±0,08	0,95±0,10
Chitax-6	3,07±0,26	0,76±0,06
Chitax-7	3,81±0,23	1,12±0,18
Chitax-8	3,92±0,19	1,37±0,06
Chitax-9	N.P.	2,18±0,17
Chitax-10	N.P.	1,89±0,19
Chitax-11	3,52±1,52	0,72±0,04
Chitax-12	3,78±2,05	0,74±0,14
Chitax-13	4,03±1,15	0,48±0,13
Chitax-14	3,03±1,15	0,45±0,05
Chitax-15	4,27±0,30	0,48±0,04
Chitax-16	N.P.	4,00±0,70
Chitax-17	3,26±1,85	0,57±0,09
Chitax-18	3,96±2,18	0,47±0,07
Chitax-19	3,45±2,07	0,45±0,07
Chitax-20	3,38±1,62	0,44±0,06
Chitax-21	2,95±1,04	0,78±0,15
Chitax-22	N.P.	2,36±0,09
Chitax-23	N.P.	2,99±1,07
Chitax-24	N.P.	1,92±0,40
Chitax-25	N.P.	3,15±0,73
Chitax-26	N.P.	2,51±0,04
Chitax-27	N.P.	3,03±0,10
Chitax-28	5,78±1,18	0,80±0,17
Chitax-29	6,38±3,11	0,88±0,17
Chitax-30	5,98±1,01	1,19±0,31
Chitax-31	6,57±0,63	1,04±0,44
Chitax-32	6,27±2,59	1,58±0,38
Chitax-33	4,32±0,49	0,29±0,15
Chitax-34	3,89±1,16	0,69±0,28
Chitax-35	6,35±0,81	1,11±0,65
Chitax-36	7,88±1,50	1,22±0,08
Chitax-37	5,00±1,10	0,94±0,30
Chitax-38	N.P.	2,41±0,21
Chitax-39	N.P.	2,81±0,34
Chitax-40	3,62± 1,1	0,93±0,23
Chitax-41	9,22±2,42	1,50±0,42
Chitax-42	13,26±2,83	2,26±0,21
Chitax-43	12,84±2,29	2,33±0,43
Chitax-44	12,59±2,57	2,30±0,99

2.3. Requerimiento de Mg^{++}.

Como vemos algunos de los compuestos reducen muy significativamente la concentración crítica de tubulina necesaria para su ensamblaje en tampón fosfato (chitax-4, 11, 12, 13, 14, 19, 20, 21 y 40; tabla 2) además de tener este efecto en glicerol (tabla 2).

Nos preguntamos si el comportamiento de estos ligandos aparentemente tan potentes seguiría el patrón de comportamiento de los demás agentes estabilizadores de microtúbulos respecto a la dependencia del ión Mg^{++} para la polimerización (Buey *et al.*, 2004; Buey *et al.*, 2005; Diaz y Andreu, 1993).

En ensayos similares a los llevados a cabo para medir las concentraciones críticas en fosfato pero eliminando el $MgCl_2$ del tampón fuimos incapaces de detectar tubulina polimerizada en el fondo de los tubos después de centrifugar. Este hecho nos

señala que la presencia en el buffer de ión Mg^{++} sigue siendo imprescindible para el ensamblaje incluso en presencia de estos compuestos.

2.4. Unión a tubulina dimérica.

Otra característica de los agentes estabilizadores de microtúbulos es que se unen a microtúbulos pero no se ha encontrado evidencia directa de unión a tubulina dimérica hasta el momento.

La siguiente pregunta para la caracterización de nuestros compuestos fue si encontraríamos unión a proteína en solución con aquellos miembros de la colección que inducen fuertemente la polimerización de tubulina y cuyas contantes de afinidad deberían ser bastante altas (tal y como se muestra en el apartado siguiente; consultar la tabla 4).

Fuimos incapaces de detectar unión al incubar los ligandos y la tubulina en un tampón fosfato con GDP y sin iones Mg^{++}. En tales condiciones la proteína no polimeriza si no es en presencia de un inductor. Tras la incubación la mezcla se centrifugó de manera que pudimos separar microtúbulos y tubulina dimérica (Diaz *et al.*, 1993).

Llegamos a la conclusión de que efectivamente, toda nuestra colección de compuestos se comporta como agentes estabilizadores de microtúbulos clásicos (requieren Mg^{++} y se unen a la forma polimerizada de tubulina), la siguiente tarea consistiría en analizar su unión al sitio de taxol, sus afinidades y sus efectos citotóxicos.

2.5. Estructura de los microtúbulos ensamblados.

El número de protofilamentos que componen los microtúbulos cuando éstos se ensamblan *in vitro* oscila dependiendo de las condiciones experimentales (*in vivo* generalmente son trece). La presencia de taxanos es uno de los factores que puede modificar el número de protofilamentos -y por tanto su diámetro- (Andreu *et al.*, 1994). Al ensamblar microtúbulos en presencia de una de estas drogas no se obtiene una población homogénea y el número de protofilamentos que se calcula es un promedio, así el taxol forma microtúbulos de 12,1 protofilamentos y el docetaxel de 13,4 al igual que en ausencia de ligando.

Nuestra amplia colección de taxanos nos brinda la posibilidad de investigar cómo sucede éste cambio: si hay alguna relación entre la estructura del ligando, sus modificaciones químicas, su tamaño, su carga y la diferencia entre el número de protofilamentos de los microtúbulos que inducen.

A partir de los perfiles de dispersión de rayos X a bajo ángulo (SAXS) se pueden determinar el radio medio y el número de protofilamentos que componen los microtúbulos inducidos por los ligandos probados (Andreu *et al.*, 1992; 1994).

Para estas medidas seleccionamos un conjunto de moléculas con la pretensión de barrer una serie en la que hubiera modificaciones químicas sencillas entre un compuesto y otro y así entender qué grupo es responsable del engrosamiento o el adelgazamiento de los microtúbulos (figura 13).

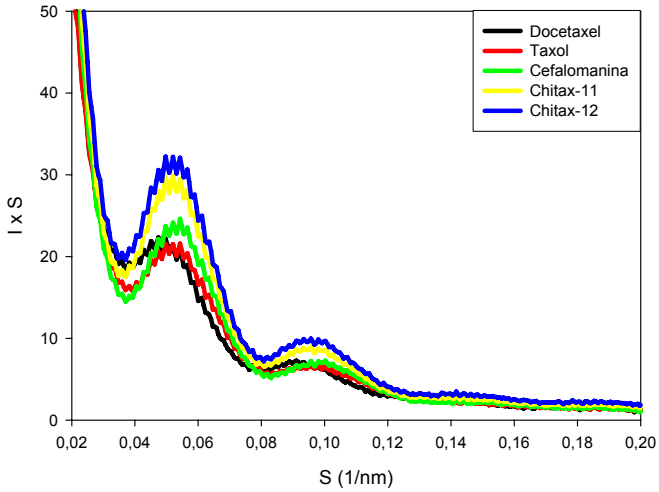

Figura 13. Perfiles de dispersión de rayos-X de los microtúbulos inducidos. Se muestran sólo algunos ejemplos de los ligandos medidos para mayor claridad en la figura. Los perfiles se generaron multiplicando las intensidades de la función de dispersión por su eje S para determinar con mayor facilidad la posición de los máximos.

En la tabla 3 se muestran los compuestos probados indicando sus modificaciones respecto a la molécula patrón (docetaxel, taxol o cefalomanina) y sus radios y número de protofilamentos normalizados respecto al docetaxel. La serie no está completa pues con algunas de las moléculas de la serie no obtuvimos datos suficientemente buenos como para calcular el diámetro de los microtúbulos ensamblados.

Los datos obtenidos nos indican que la cadena lateral de C-13 influye en el diámetro de los microtúbulos dependiendo de su complejidad, aumentando su grosor sobre los inducidos por bacatina por este orden: cefalomanina, docetaxel y taxol (nótese que para comparar la cadena lateral de docetaxel habrá que fijarse en los datos obtenidos con chitax-21 para que la acetilación en C-10 se mantenga respecto a las otras dos moléculas).

Nuestros resultados señalan que la acetilación en C-10 resulta en la desaparición de un protofilamento de media respecto a la hidroxilación en este sitio. Así los microtúbulos ensamblados en presencia de chitax-17 son más gruesos que los ensamblados con cefalomanina, de manera parecida los polimerizados con chitax-21 son más delgados que los que lo hicieron con docetaxel. Los datos indican que introduciendo un sustituyente mayor, en esta posición de C-10, que el hidroxilo los microtúbulos adelgazan pues, aun faltando los datos con el compuesto intermedio, además de lo que ocurre con la acetilación podemos observar un efecto similar con el propionilo que porta chitax-40 (tabla 3).

Siguiendo con la "parte norte" de la molécula, y al contrario de lo que observamos en C-10, la inclusión de un grupo mayor que el hidroxilo en C-7 parece implicar un engrosamiento de los microtúbulos que inducen estos ligandos. Un grupo tan grande como la fluoresceína sobre la molécula de taxol, (caso de flutax-1 y 2, -Diaz *et al.*, 2000) añade un par de protofilamentos a los microtúbulos así ensamblados y si a esto se le añade un separador de seis

átomos de carbono (hexaflutax) el diámetro de los microtúbulos aumentará aún más. Aunque nos vuelve a faltar un ligando intermedio para completar la serie, de los datos de chitax-4 podemos intuir que también un grupo más pequeño como un propionilo en este sitio supone un ensanchamiento en los microtúbulos.

La introducción de un grupo polar en la posición meta del benzoilo en C-2 parece conllevar un engrosamiento de los microtúbulos que aumentaría cuanto más polar sea el grupo añadido, al menos cuando esta modificación se realiza sobre la molécula de cefalomanina (ver en la tabla 3 las diferencias entre el grupo metóxido y la azida), pero estos datos no son concluyentes ya que la misma modificación introducida sobre la molécula de taxol no tiene ningún efecto.

Tabla 3. Radios y número de protofilamentos, calculados a partir de los datos de SAXS, de los microtúbulos ensamblados en presencia de cada compuesto.

	Modificación	R (nm)	protofilamentos
Docetaxel		12,1	13,4
chitax-21	acetilado en 10	11,0	12,2
chitax-40	propionilado en 10 -N3 en meta (C2)	10,9	12,1
Cefalomanina		10,4	11,5
chitax-13	-OCH3 en meta (C2)	11,0	12,1
chitax-14	-N3 en meta (C2)	12,2	13,5
chitax-17	deacetilado en 10	10,9	12,1
chitax-4	deacetilado en 10 propionilado en 7 -N3 en meta (C2)	13,1	14,5
Taxol		11,2	12,4
chitax-11	-OCH3 en meta (C2)	11,2	12,4
chitax-12	-N3 en meta (C2)	11,2	12,4
Flutax-1	fluoresceína en C-7	13,1	14,5
Flutax-2	di F, fluoresceína en C-7	13,1	14,5
Hexaflutax	fluoresceína + separador 6 carbonos en C-7	13,5	15,0
Bacatina	sin cadena lateral en C-13	10,1	11,2

3. TERMODINÁMICA DE UNIÓN A MICROTÚBULOS.

3.1. Constantes de unión.

Una vez constatada su naturaleza como agentes estabilizadores de microtúbulos analizamos cómo las distintas modificaciones en la molécula de taxol influyen en la afinidad de los ligandos por su diana, esta influencia se determinó midiendo sus constantes de unión a microtúbulos estabilizados.

Para medir estas constantes se utilizó el test de desplazamiento de flutax-2 (descrito en Buey *et al.*, 2004) a distintas temperaturas: 26, 27, 30, 32, 35, 37, 40 y 42 ºC. Estas medidas se tomaron al menos tres veces de manera independiente. Sus medias y desviaciones estándar están recogidas en la tablas 4 A y 4 B.

Rápidamente saltaron a la vista ciertos compuestos cuya afinidad era muy alta y la medida de la constante de unión poco precisa, encontrando desviaciones muy grandes respecto a las medias. Estas constantes se encuentran varios órdenes de magnitud por encima de la del flutax-2 y lo desplazan completamente a concentraciones equimolares, impidiendo la determinación correcta de la constante de afinidad (figura 14), por lo que se repitió la determinación utilizando otro método más apropiado para este caso. Para ello diseñamos una prueba de desplazamiento de epotilona B, compuesto que se une a los microtúbulos en el sitio de taxol con una afinidad mayor que la del flutax-2 (Buey *et al.*, 2004).

En este ensayo los microtúbulos estabilizados se incubaron en presencia de epotilona B y el compuesto del que debemos medir su afinidad; después la mezcla se centrifugó para sedimentar los microtúbulos. Al separar sobrenadante y sedimento separamos también ligandos unidos a su sitio y ligandos libres. Tras extraer los compuestos de la mezcla con diclorometano, y añadir taxol o docetaxel como estándar interno, los ligandos se separaron mediante HPLC y fueron cuantificados midiendo las áreas bajo sus picos en los cromatogramas.

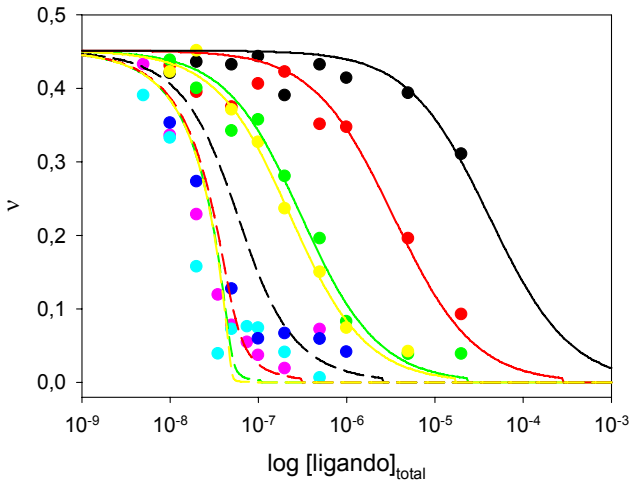

Figura 14. Desplazamiento de flutax-2 a 35 ºC. Las líneas continuas corresponden al ajuste de las constantes de unión de ligandos con afinidades menores de 10^7 M^{-1}. Las líneas a trazos representan los desplazamientos esperados para ligandos de constantes 10^8 (negro), 10^9 (rojo), 10^{10} (verde) y 10^{11} (amarillo). Los círculos señalan los datos de unión obtenidos con los ligandos cefalomanina (verde), chitax-2 (rojo), chitax-27 (negro), chitax-6 (amarillo), chitax-11 (azul oscuro), chitax-12 (rosa) y chitax-14 (azul claro).

Tabla 4 A. Constantes de unión a microtúbulos medidas por desplazamiento de flutax-2 a diferentes temperaturas (10^7 M^{-1}).

	26ºC	27ºC	30ºC	32ºC	35ºC	37ºC	40ºC	42ºC
Taxol[a]	2,64±0,17	2,19±0,05	1,83±0,09	1,81±0,21	1,43±0,17	1,07±0,11	0,96±0,14	0,94±0,23
Docetaxel[a]	6,95±0,42	6,57±0,52	5,42±0,42	4,89±0,38	3,93±0,27	3,09±0,22	2,89±0,17	2,38±0,11
Cefalomanina	S.D.	1,19±0,23	1,01±0,18	0,74±0,13	0,69±0,08	0,66±0,10	0,56±0,08	0,58±0,03
Chitax-1	0,8±0,23	0,91±0,26	0,37±0,07	0,57±0,07	0,49±0,12	0,29±0,09	0,28±0,02	0,27±0,03
Chitax-2	0,063±0,007	0,061±0,016	0,030±0,002	0,070±0,027	0,043±0,018	0,019±0,011	0,018±0,006	0,018±0,003
Chitax-3	S.D.	0,106±0,028	0,091±0,026	0,094±0,021	0,072±0,017	0,052±0,011	0,062±0,018	0,065±0,02
Chitax-4	S.D.	7,57±1,70	7,09±1,72	5,7±1,48	5,37±1,39	5,06±1,21	3,68±1,14	3,77±0,97
Chitax-5	S.D.	2,53±0,19	2,23±0,12	2,07±0,04	1,62±0,24	1,55±0,27	1,40±0,10	1,21±0,07
Chitax-6	S.D.	0,68±0,09	0,56±0,08	0,58±0,05	0,39±0,06	0,39±0,54	0,36±0,12	0,34±0,11
Chitax-7	0,732±0,011	0,770±0,155	0,629±0,281	0,595±0,092	0,492±0,073	0,470±0,197	0,467±0,066	0,441±0,114
Chitax-8	0,032±0,008	0,029±0,006	0,024±0,006	0,028±0,008	0,028±0,008	0,024±0,014	0,023±0,007	0,022±0,007
Chitax-9	0,048±0,004	0,040±0,005	0,034±0,006	0,038±0,009	0,042±0,008	0,033±0,010	0,036±0,001	0,032±0,001
Chitax-15	2,259±1,34	2,206±0,89	3,124±1,52	1,623±0,73	2,384±0,53	2,137±0,56	1,504±0,32	1,686±0,10
Chitax-16	0,044±0,007	0,043±0,006	0,057±0,030	0,051±0,012	0,050±0,030	0,043±0,024	0,029±0,008	0,035±0,025
Chitax-17	1,200±0,50	1,151±0,48	1,131±0,09	1,085±0,52	0,902±0,37	0,863±0,16	0,723±0,22	0,802±0,35
Chitax-18	1,401±0,46	1,430±0,44	1,326±0,11	1,436±0,59	1,281±0,27	1,115±0,26	1,050±0,33	0,863±0,20
Chitax-22	0,002±0,00	0,021±0,00	0,017±0,01	0,019±0,01	0,013±0,00	0,009±0,00	0,010±0,00	0,009±0,00
Chitax-23	0,009±0,00	0,010±0,00	0,008±0,00	0,010±0,00	0,007±0,00	0,005±0,00	0,006±0,00	0,005±0,00
Chitax-24	0,291±0,07	0,235±0,08	0,129±0,01	0,114±0,01	0,094±0,01	0,081±0,03	0,090±0,02	0,064±0,01
Chitax-25	0,014±0,00	0,011±0,00	0,010±0,01	0,011±0,01	0,008±0,00	0,006±0,00	0,007±0,00	0,004±0,00
Chitax-26	0,048±0,02	0,049±0,02	0,020±0,00	0,020±0,00	0,018±0,00	0,012±0,00	0,011±0,00	0,012±0,00
Chitax-27	0,011±0,00	0,012±0,00	0,011±0,00	0,009±0,00	0,007±0,00	0,005±0,00	0,007±0,00	0,005±0,00
Chitax-28	0,21±0,03	0,21±0,03	0,15±0,01	0,23±0,08	0,17±0,04	0,14±0,01	0,15±0,08	0,15±0,004
Chitax-29	0,33±0,02	0,40±0,06	0,39±0	0,37±0,18	0,25±0,08	0,17±0,05	0,16±0,08	0,15±0,07
Chitax-30	1,54±0,62	1,15±0,20	2,60±1,47	2,14±1,08	1,76±0,91	1,48±0,79	1,14±0,39	1,24±0,18
Chitax-31	0,12±0,04	0,13±0,02	0,10±0,02	0,15±0,05	0,10±0,04	0,06±0,01	0,06±0,03	0,06±0,001
Chitax-32	0,13±0,04	0,19±0,01	0,26±0,10	0,27±0,08	0,24±0,08	0,24±0,17	0,12±0,07	0,15±0,08
Chitax-33	0,16±0,07	0,23±0,06	0,19±0,04	0,14±0,06	0,07±0,01	0,07±0,0001	0,06±0,02	0,04±0,0004
Chitax-34	0,97±0,18	1,04±0,17	3,44±3,64	2,46±2,29	1,20±0,93	1,03±0,62	0,62±0,28	0,53±0,12
Chitax-35	0,62±0,44	0,66±0,54	3,64±5,38	1,54±1,75	0,88±0,77	0,67±0,28	0,47±0,12	0,50±0,11
Chitax-36	0,045±0,016	0,046±0,013	0,045±0,018	0,035±0,023	0,029±0,020	0,022±0,009	0,024±0,002	0,017±0,006
Chitax-37	0,11±0,03	0,10±0,03	0,077±0,029	0,049±0,018	0,035±0,010	0,023±0,009	0,018±0,001	0,019±0,019
Chitax-38	0,002±0,002	0,002±0,002	0,001±0,001	0,001±0,001	0,001±0,001	0,001±0,000	0,001±0,000	0,001±0,000
Chitax-39	0,019±0,004	0,017±0,004	0,011±0,004	0,007±0,001	0,003±0,001	0,001±0,000	0,001±0,000	0,001±0,000
Chitax-41	0,068±0,043	0,069±0,044	0,049±0,043	0,029±0,014	0,021±0,004	0,014±0,005	0,013±0,010	0,013±0,010
Chitax-42	0,026±0,003	0,025±0,014	0,021±0,015	0,010±0,003	0,008±0,003	0,004±0,002	0,003±0,002	0,004±0,005
Chitax-43	0,082±0,013	0,084±0,028	0,068±0,037	0,036±0,013	0,030±0,008	0,012±0,005	0,015±0,015	0,026±0,037
Chitax-44	0,011±0,017	0,008±0,012	0,005±0,006	0,001±0,001	0,001±0,001	0,0004±0,0004	0,0003±0,0003	0,0004±0,0005

Tabla 4 B. Constantes de unión a microtúbulos medidas por desplazamiento de epoB (10^7 M^{-1}). Comparación de las medidas por desplazamiento de flutax-2 a 35 ºC.

	26ºC	35ºC Flutax-2	35 ºC	40ºC
Chitax-4	124±39	S.D.	87±19	52±27
Chitax-11	34±19	33±24	38±10	25±2
Chitax-12	239±130	S.D.	151±3	147±43
Chitax-13	23±6	8±3	17±3	14±2
Chitax-14	126±50	S.D.	80±3	55±6
Chitax-19	27±2	13±5	14,8±0,2	12±2
Chitax-20	310±27	S.D.	81±5	63±20
Chitax-21	21±4	11±4	14±2	13±2
Chitax-40	612±228	S.D.	628±15	355±56

Gracias a este ensayo pudimos determinar las constantes de los compuestos 4, 11, 12, 13, 14, 19, 20, 21 y 40 a 26, 35 y 40 ºC.

Los resultados del ensayo de desplazamiento de epotilona B se validaron con medidas con el ensayo de flutax-2 de las afinidades de los compuestos cuyas constantes de unión están en el rango de 10^8 M^{-1} (chitax 11, 13, 19 y 21), se obtuvieron resultados similares siguiendo cualquiera de los dos métodos, radicando sus diferencias básicamente en la dispersión de las medidas (tabla 4 B).

Todos estos compuestos de afinidades más altas, excepto el chitax 21, tienen en común una sustitución en meta del benzoilo del C-2. Las sustituciones son: un grupo metóxido en el caso de los ligandos 11, 13 y 19 y un grupo azida en el de los compuestos 4, 12, 14, 20 y 40 (consultar la figura 11).

3.1.1. Validación de las medidas de los compuestos con grupos potencialmente reactivos.

Tras la experiencia con otros compuestos con muy alta afinidad aparente que resultaron unirse covalentemente a la tubulina (caso de la cicloestreptina aparecido en Buey *et al.*, 2007), comprobamos si éste podría ser el caso de algunos de nuestros compuestos con tan altas afinidades de unión cuyos sustituyentes eran grupos altamente reactivos como la azida.

Descartamos así que los chitax con un grupo azida como sustituyente en la cadena lateral de C-2 (chitax-4, 12, 14, 20 y 40) o aquéllos con una halogenación en el mismo lugar (chitax-6, 30, 34) o dihalogenados (chitax-28, 29) se unieran de forma covalente a los microtúbulos ya que somos capaces de recuperarlos (como ejemplo se muestra chitax-4 en la figura 15) después de extraer la solución con diclorometano (Buey *et al.*, 2007; Yang *et al.*, 2007).

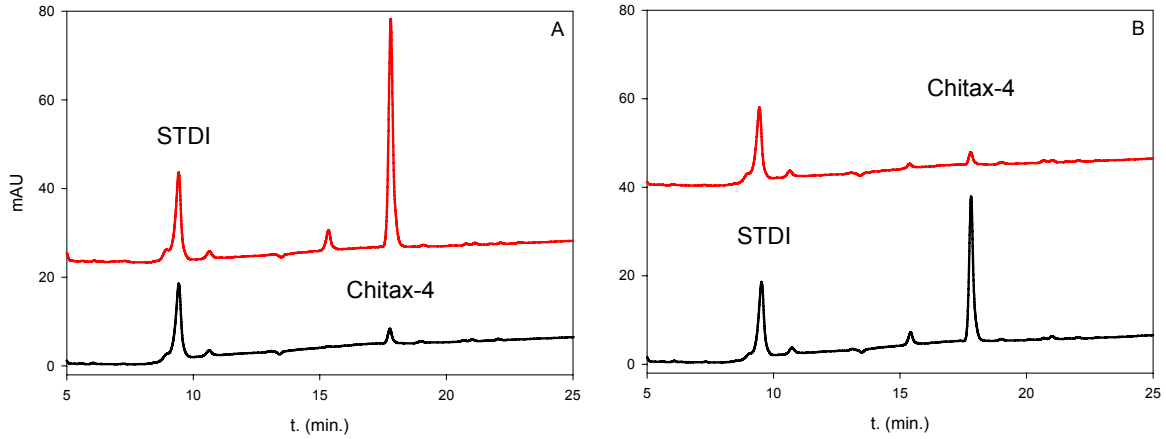

Figura 15. Unión no covalente de los chitax. Cromatogramas mostrando chitax-4 recuperado del fondo del tubo después de incubarlo con microtúbulos. Antes de la extracción orgánica se añadió docetaxel como estándar interno (STDI). Líneas rojas: sobrenadantes. Líneas negras: sedimentos. **A.** Chitax-4 incubado sin microtúbulos. **B.** Chitax-4 incubado en presencia de microtúbulos durante 30 min. a 25 ºC.

3.2. Energía libre de Gibbs.

Una vez conocidas las constantes de unión de los compuestos a su diana resulta fácil calcular las energías libres del proceso de unión aplicando:

$$\Delta G = -R\,T\,\ln K$$

Siendo R la constante de los gases, T la temperatura y K la constante de unión del ligando medida a la temperatura T. En la tabla 5 se pueden consultar las energías a 35 ºC calculadas para cada uno de nuestros compuestos.

3.3. Entalpía.

Además, obtenidas dichas constantes a distintas temperaturas, podemos calcular también la entalpía y entropía de la unión:

La entalpía será:

$$\Delta H = -m\,R$$

donde m es la pendiente calculada de la representación del inverso de la temperatura frente al logaritmo neperiano de la constante de afinidad.

La figura 16 muestra estas representaciones para cada compuesto y el ajuste de las rectas. La tabla 5 contiene los resultados obtenidos para cada compuesto.

Figura 16.. Representaciones de los logaritmos neperianos de las $K_{unión}$ de cada compuesto frente al inverso de sus temperaturas. La pendiente (m) de la recta calculada es proporcional a la entalpía de unión del compuesto en la relación $\Delta H = -m \times R$, donde R es la constante de los gases.

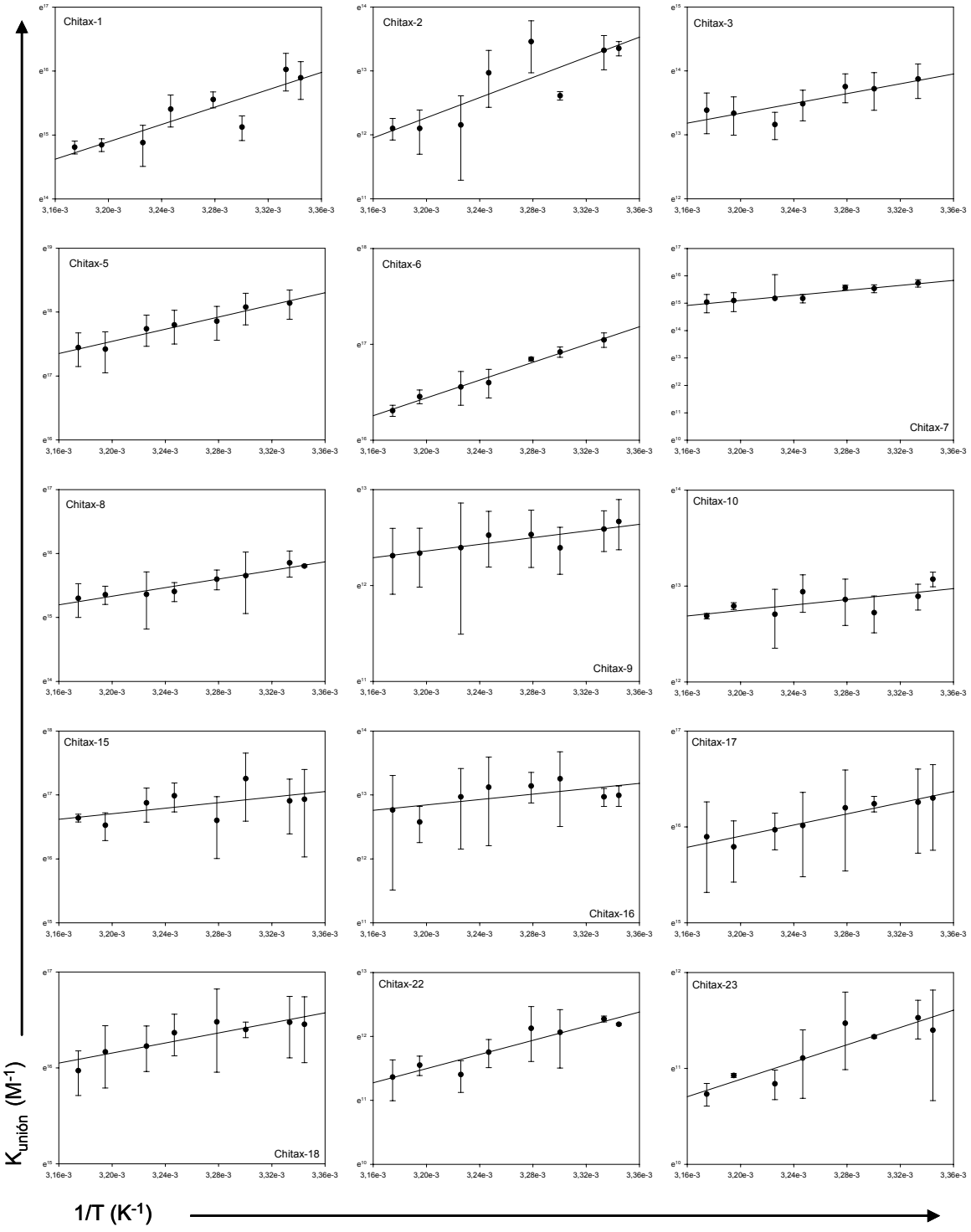

Figura 16. (II.Continuación)

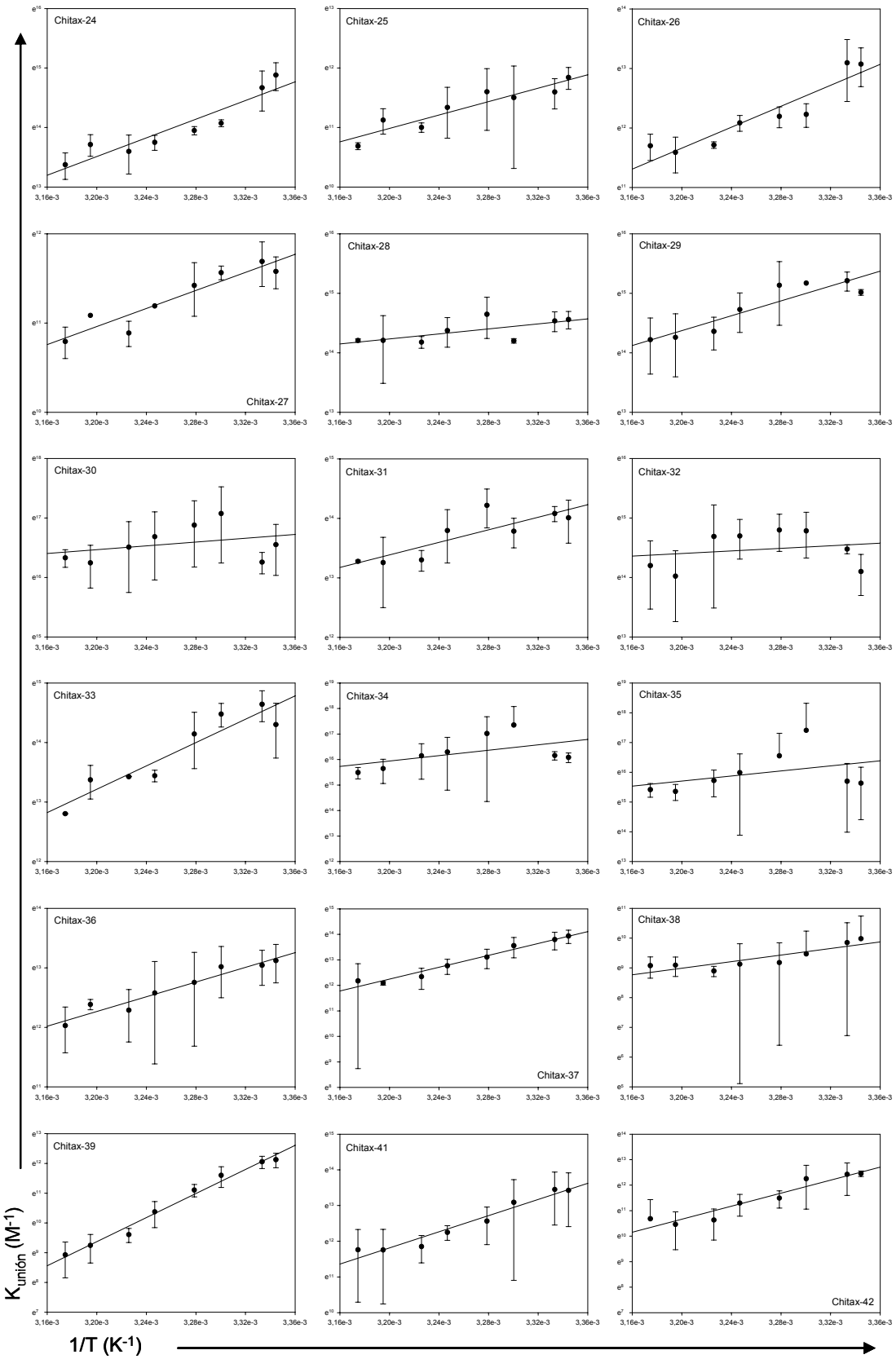

Figura 16. (y III.Continuación)

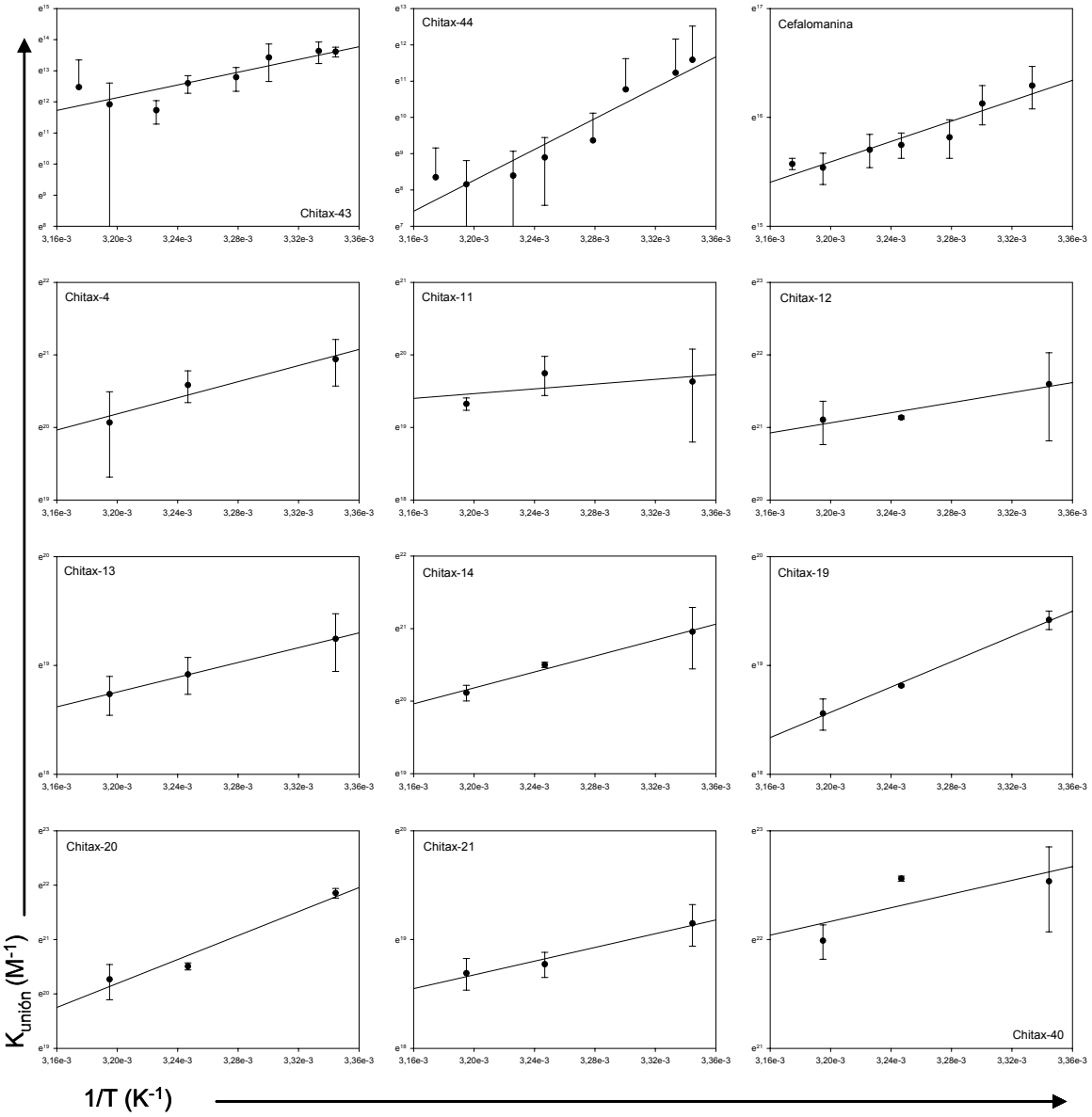

3.4. Entropía.

La entropía será exactamente el opuesto de la pendiente de la recta obtenida como consecuencia de representar la temperatura frente a la energía libre de Gibbs.

Todas estas representaciones las encontramos en la figura 17 y los datos para cada ligando en la tabla 5.

Tabla 5. Parámetros termodinámicos de la unión de los taxanos a su sitio en tubulina.
a. datos de (Buey *et al.*, 2004).
b. compuestos cuyas constantes de unión fueron medidas por desplazamiento de epoB.

	K_a 35 ºC (x 10^7 M^{-1})	ΔG 35 ºC (kJ/mol)	ΔH (kJ/mol)	ΔS (J/mol)
Taxol[a]	1,43 ± 0,17	-42,1 ± 0,3	-51 ± 4	-29 ± 13
Docetaxel[a]	3,93 ± 0,27	-44,8 ± 0,2	-53 ± 2	-26 ± 8
Cefalomanina	0,69 ± 0,08	-40,3 ± 0,3	-39 ± 6	-6 ± 18
Chitax-1	0,49 ± 0,12	-39,4 ± 0,6	-56 ± 12	-56 ± 39
Chitax-2	0,043 ± 0,018	-33,2 ± 0,9	-66 ± 18	-109 ± 38
Chitax-3	0,072 ± 0,017	-34,5 ± 0,5	-32 ± 9	10 ± 29
Chitax-4[b]	87 ± 19	-52,7 ± 0,5	-46 ± 13	19 ± 44
Chitax-5	5,37 ± 1,39	-45,6 ± 0,6	-40 ± 4	19 ± 14
Chitax-6	1,62 ± 0,24	-42,5 ± 0,4	-39 ± 2	13 ± 7
Chitax-7	0,39 ± 0,06	-38,8 ± 0,4	-38 ± 5	4 ± 17
Chitax-8	0,492 ± 0,073	-39,4 ± 0,3	-28 ± 3	39 ± 10
Chitax-9	0,028 ± 0,008	-32,1 ± 0,6	-15 ± 4	56 ± 12
Chitax-10	0,042 ± 0,008	-33,1 ± 0,4	-12 ± 5	68 ± 18
Chitax-11[b]	38 ± 10	-50,5 ± 0,6	-14 ± 20	117 ± 65
Chitax-12[b]	151 ± 3	-54,1 ± 0,1	-29 ± 9	84 ± 29
Chitax-13[b]	16,5 ± 2,8	-48,4 ± 0,4	-28 ± 1	66 ± 1
Chitax-14[b]	80,0 ± 2,9	-52,5 ± 0,1	-46 ± 6	21 ± 19
Chitax-15	2,384 ± 0,53	-43,5 ± 0,5	-18 ± 11	80 ± 35
Chitax-16	0,050 ± 0,030	-33,6 ± 1,2	-18 ± 9	49 ± 30
Chitax-17	0,902 ± 0,37	-41,0 ± 0,9	-24 ± 3	55 ± 10
Chitax-18	1,281 ± 0,27	-41,9 ± 0,5	-22 ± 4	64 ± 14
Chitax-19[b]	14,8 ± 0,2	-48,2 ± 0,1	-48 ± 3	0 ± 9
Chitax-20[b]	80,6 ± 5,1	-52,5 ± 0,2	-92 ± 19	-124 ± 64
Chitax-21[b]	14,2 ± 1,6	-48,0 ± 0,3	-26 ± 5	72 ± 16
Chitax-22	0,013 ± 0,00	-30,1 ± 0,0	-46 ± 7	-151 ± 23
Chitax-23	0,007 ± 0,00	-28,6 ± 0,0	-37 ± 7	-123 ± 22
Chitax-24	0,094 ± 0,01	-35,2 ± 0,3	-65 ± 10	-95 ± 33
Chitax-25	0,008 ± 0,00	-28,9 ± 0,0	-47 ± 7	-154 ± 24
Chitax-26	0,018 ± 0,00	-31,0 ± 0,0	-73 ± 11	-77 ± 137
Chitax-27	0,007 ± 0,00	-28,6 ± 0,0	-42 ± 6	-138 ± 21
Chitax-28	0,17 ± 0,04	-36,7 ± 0,5	-17 ± 8	62 ± 25
Chitax-29	0,25 ± 0,08	-37,7 ± 0,7	-52 ± 9	-48 ± 30
Chitax-30	1,76 ± 0,91	-42,7 ± 1,1	-11 ± 15	92 ± 49
Chitax-31	0,10 ± 0,04	-35,4 ± 0,9	-44 ± 11	-30 ± 36
Chitax-32	0,24 ± 0,08	-37,6 ± 0,7	-7 ± 16	87 ± 55
Chitax-33	0,07 ± 0,01	-34,4 ± 0,3	-81 ± 12	-152 ± 39
Chitax-34	1,20 ± 0,93	-41,7 ± 1,5	-38 ± 28	14 ± 94
Chitax-35	0,88 ± 0,77	-40,9 ± 1,6	-29 ± 33	13 ± 112
Chitax-36	0,029 ± 0,020	-32,2 ± 1,3	-48 ± 6	-63 ± 18
Chitax-37	0,035 ± 0,010	-32,7 ± 0,6	-91 ± 7	-207 ± 24
Chitax-38	0,001 ± 0,001	-23,6 ± 1,8	-44 ± 9	-70 ± 34
Chitax-39	0,003 ± 0,001	-26,4 ± 0,7	-157 ± 10	-461 ± 28
Chitax-40[b]	628 ± 15	-57,7 ± 0,1	-26 ± 24	99 ± 80
Chitax-41	0,021 ± 0,004	-31,4 ± 0,4	-94 ± 9	-202 ± 28
Chitax-42	0,008 ± 0,003	-28,9 ± 0,8	-106 ± 13	-250 ± 43
Chitax-43	0,030 ± 0,008	-32,3 ± 0,6	-85 ± 20	-169 ± 66
Chitax-44	0,001 ± 0,001	-23,6 ± 1,8	-177 ± 23	-493 ± 75

Figura 17. Representaciones de la energía libre de unión de cada compuesto frente a la temperatura. La entropía de unión es el opuesto de la pendiente de la recta calculada.

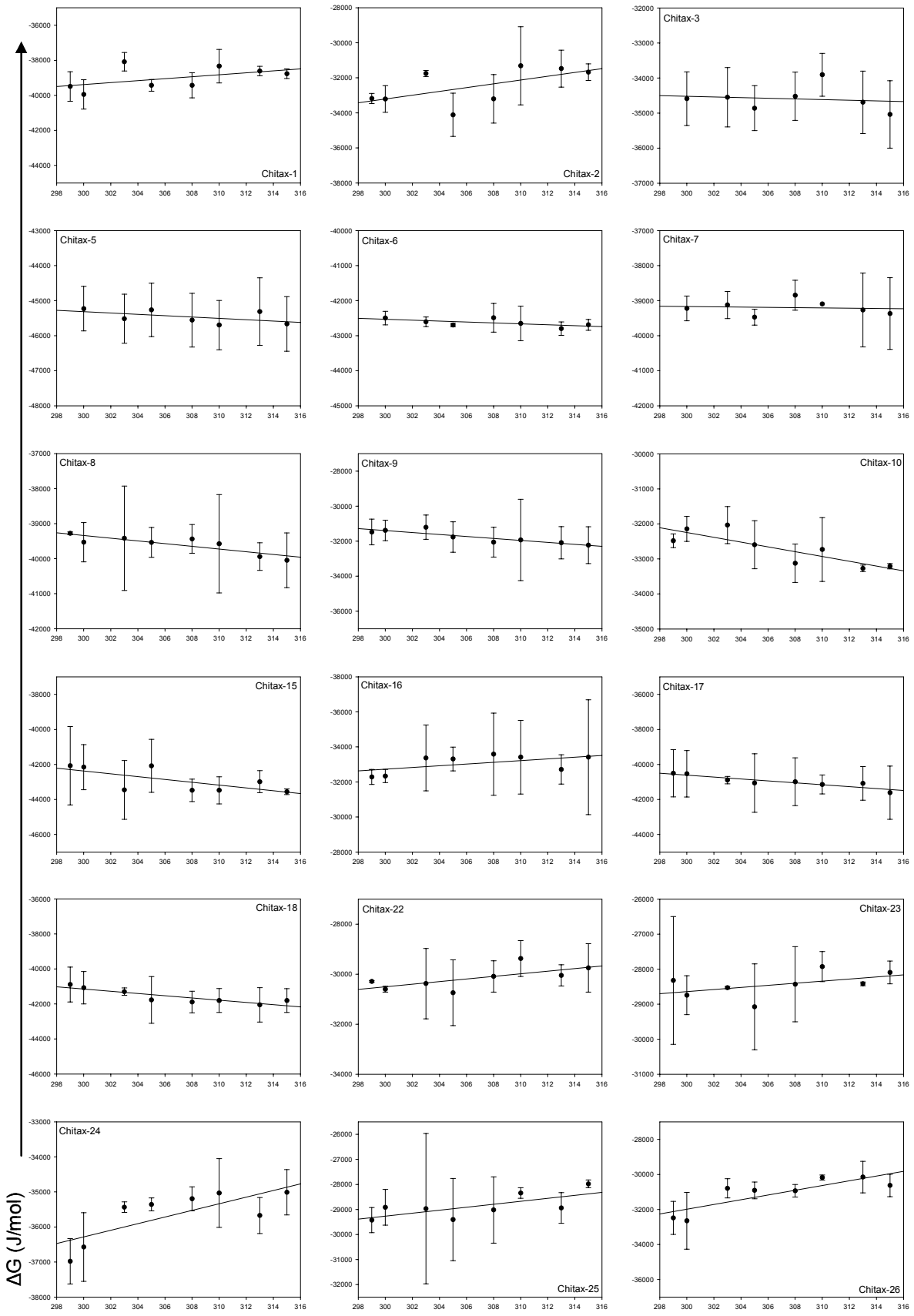

Figura 17. (II. Continuación).

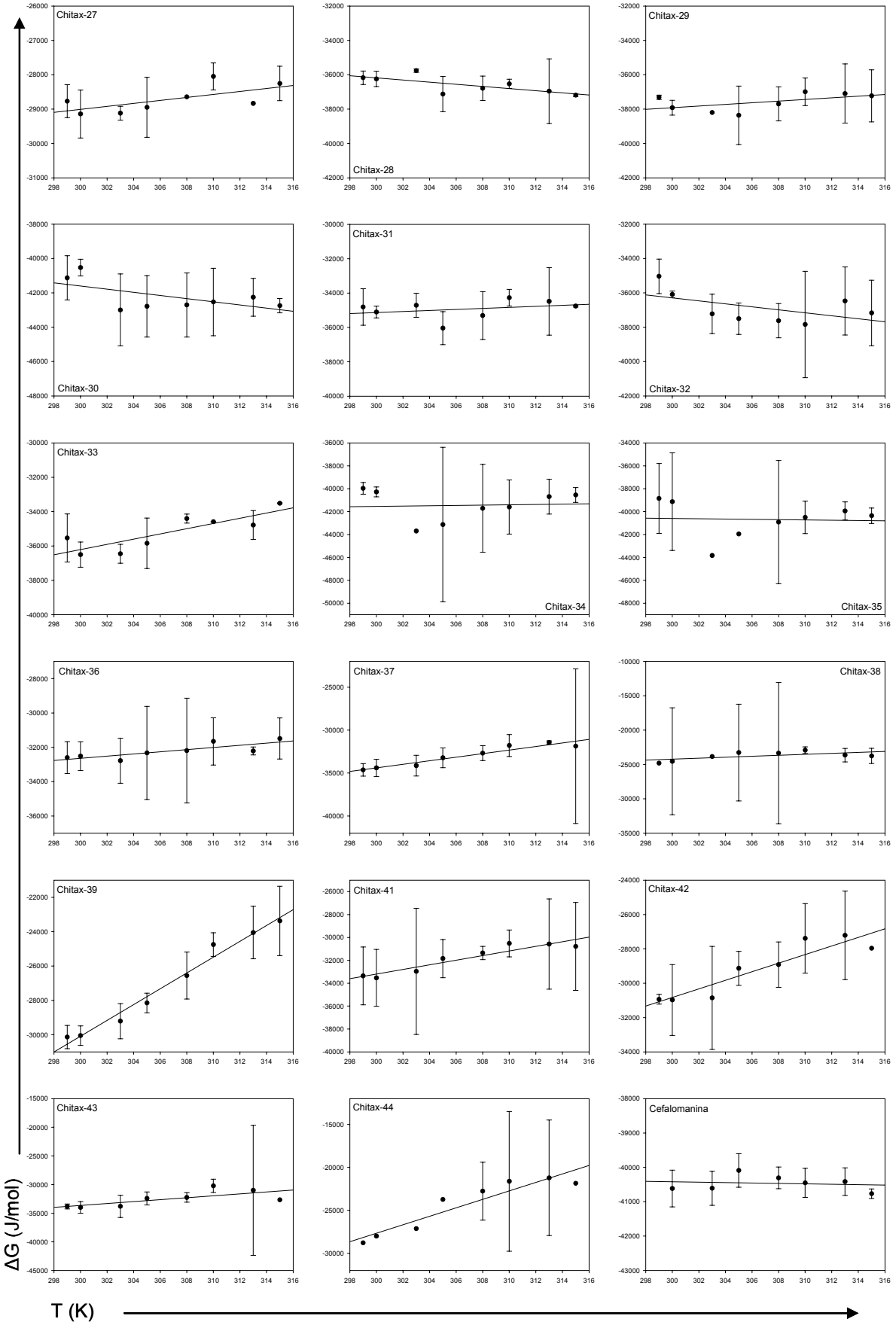

Figura 17. (y III. Continuación).

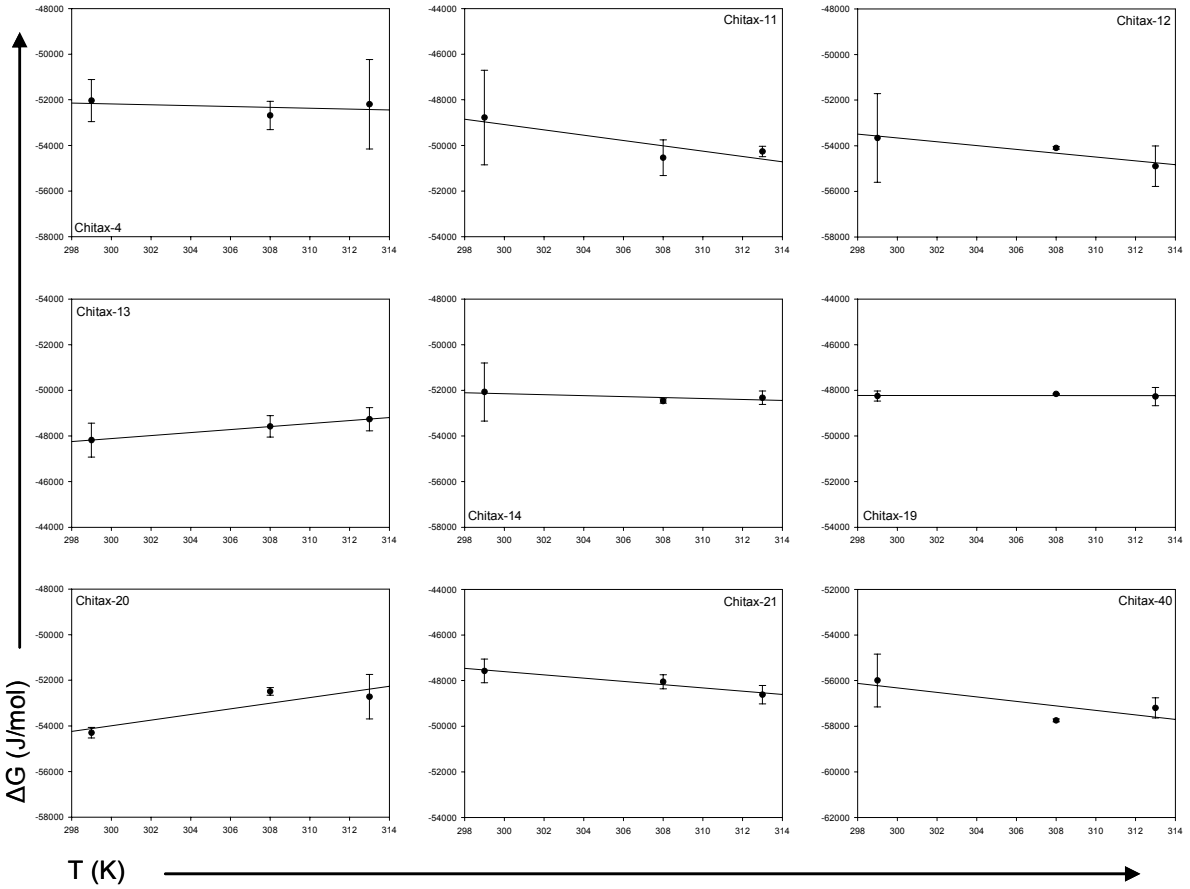

4. ESTRUCTURA DE LAS DROGAS UNIDAS AL SITIO DE TAXOL.

Para conocer cómo influyen o pueden influir las modificaciones introducidas en la molécula de taxol en su unión a su sitio en los microtúbulos contamos con la inestimable colaboración de los grupos de Federico Gago en la Universidad de Alcalá de Henares y Jesús Jiménez Barbero en el Centro de Investigaciones Biológicas con los que se determinó la estructura de la molécula unida gracias al modelado molecular y a medidas de resonancia magnético-nuclear. La deducción por ambos métodos de manera independiente nos lleva a los mismos resultados validándose mutuamente.

4.1. Modelado molecular de la conformación bioactiva de los taxanos.

Inicialmente se corrieron simulaciones de dinámica molecular con taxol, docetaxel y chitax-40 en solución. Para ello cada ligando se situó en un cubo de alrededor de 1350 moléculas de agua TIP3P en condiciones de límite periódico durante 50 nanosegundos. Las cinco estructuras más representadas en la población de conformaciones obtenidas se seleccionaron para su estudio

independiente de acoplamiento automático al sitio de taxol como cuerpos rígidos.

En el bolsillo al que se une el taxol lo más llamativo es la presencia de la histidina 229 sita en medio de la hélice 7; este aminoácido se encontró muy expuesto y separa el bolsillo en dos cavidades bien diferenciadas (consultar la estructura del sitio de taxol descrita en las láminas de tubulina estabilizadas con zinc en Lowe *et al.*, 2001).

El anillo de imidazol de la cadena lateral de esta histidina se predice doblemente protonado a pH por debajo de 7,2 según los cálculos electrostáticos realizados. Este estado protonado de la His229 se utilizó para todas las predicciones subsecuentes de nuestro modelado.

La distribución de cargas calculadas para la tubulina a pH 6,5 indica unos potenciales electrostáticos claramente diferentes a ambos lados de la His229 en el sitio de unión a taxol; esto se debe, principalmente, a la presencia de la arginina 278 en el lazo M y al ácido aspártico 26 en la hélice 1.

La conformación de taxol calculada con el programa AutoDock que mejor se ajusta a su sitio es la misma que se describió en el ajuste hecho utilizando DOCK (Lowe *et al.*, 2001) o FlexX (Snyder *et al.*, 2001), además encontramos conformaciones muy similares para docetaxel y chitax-40. Estas conformaciones no son las más representadas en solución acuosa aunque se observan esporádicamente durante las transiciones a estados más estables o a conformaciones "colapsadas hidrofóbicamente". La conformación de la molécula encajada en su sitio de unión (figura 18) coincide con la descrita para los cristales de 7-mesilpaclitaxel (Gao y Chen, 1996) justificada por interacciones específicas de la cadena lateral de C-13 con el solvente.

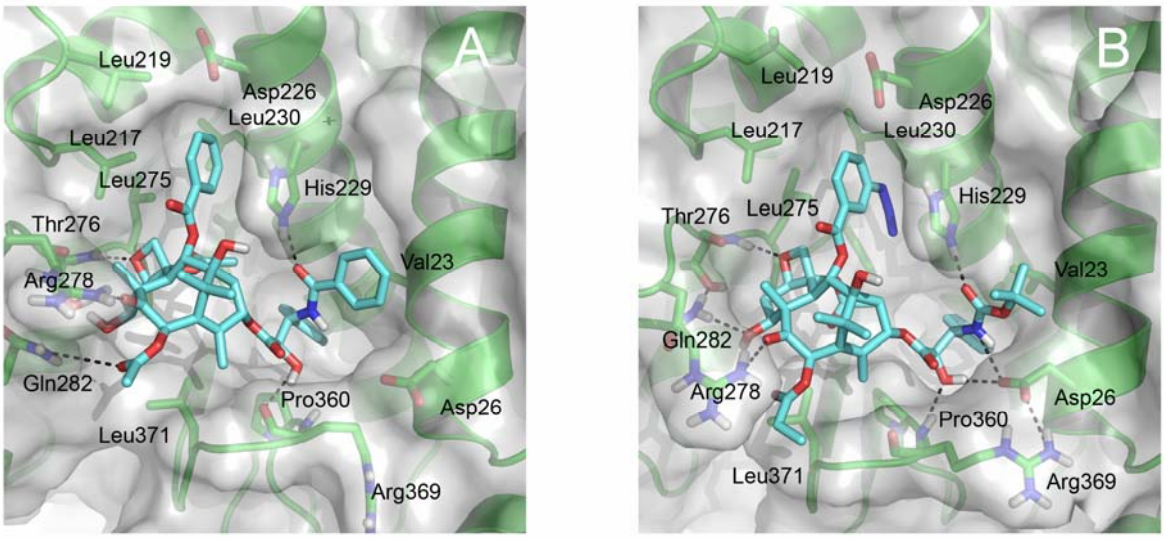

Figura 18. Modelo de los ligandos unidos al sitio de taxol. **A.** Taxol. **B.** Chitax-40

Una vez obtenidos los modelos de los complejos tubulina/ligando, se evaluó su viabilidad sometiendo a cada uno a una simulación de dinámica molecular de diez nanosegundos seguida de un procedimiento de atemperado simulado, que nos ofreció una serie de estructuras representativas del complejo con las que poder realizar análisis más profundos de descomposición de las energías implicadas.

En todas estas soluciones el ligando adopta una conformación en concordancia con la geometría de T-taxol (Snyder *et al.*, 2001) y está unido a su sitio gracias a una serie de interacciones comunes bien definidas.

En particular, el oxígeno del anillo oxetano puede establecer un puente de hidrógeno con el grupo -NH- del enlace peptídico en la treonina 276; otra interacción de este tipo se crea entre el nitrógeno ε de la histidina 229 y el sustituyente en C-13: el carbamato en el caso de docetaxel y chitax-40 o el oxígeno de la amida en el caso del taxol.

Por otra parte el anillo fenilo común en C-13 (en 3') de las tres moléculas (taxol, docetaxel y chitax-40) establece enlaces de van der Waals con las cadenas laterales hidrofóbicas de la valina 23 y la alanina 233 y al otro lado de la histidina 229, el anillo benzoilo de C-2 se introduce en una cavidad hidrofóbica construida por las cadenas laterales de las leucinas 217, 219 y 275.

Este anillo de C-2 apila con el imidazol de la histidina 229, esta interacción se ve reforzada con la inclusión de un sustituyente polar en la posición meta del anillo en C-2. El dipolo 1,3 en el caso de incluir un grupo azida (chitax-40) ó 1,2 en el caso de un grupo metóxido (chitax-13, complejo también modelado) aporta interacciones electrostáticas añadidas entre este dipolo y el que forma la amida del enlace peptídico entre His229 y Leu230.

Tres son los grupos hidroxilo comunes en las cuatro moléculas estudiadas: el sustituyente de C-1 se expone al solvente mientras que el de C-7 puede formar puentes de hidrógeno transitorios con el grupo carboxiamida de la glutamina 282 y el de C-13 (2' OH) está implicado en un puente de hidrógeno con el carboxilo del aspártico 26 en la hélice H1 y el nitrógeno del esqueleto de la arginina 369.

Las desviaciones cuadráticas medias de los átomos de la proteína en los cuatro complejos son muy pequeñas respecto a los de la estructura refinada β tubulina-taxol 1JFF (diferencias de unos 1,3 Å de promedio en 400 átomos). Las mayores diferencias con respecto a este complejo (1JFF) residen en la asunción de un estado rotamérico diferente para la histidina 229 (que nosotros proponemos protonada a pH fisiológico) y en el aumento de las interacciones de apilamiento y puentes de hidrógeno entre el ligando y la proteína como consecuencia de la adaptación mutua provocada por el procedimiento de atemperado simulado.

4.2. Determinación por resonancia magnético-nuclear de la conformación bioactiva del docetaxel unido.

De manera independiente al modelado molecular y con objeto de aportar soporte experimental a las conformaciones así encontradas, determinamos la

conformación bioactiva del docetaxel unido a microtúbulos bajo las condiciones experimentales en las que se midieron las constantes de unión. La molécula fue elegida porque se obtiene un buen espectro de RMN del estado unido y porque posee las características estructurales básicas para que la interacción tenga lugar.

Las conformaciones de otros ligandos unidos a su diana han sido previamente determinadas usando la técnica del efecto Overhauser nuclear transferido (ver Jimenez-Barbero *et al.*, 2006). Este método se ha mostrado adecuado para determinar la conformación de ligandos unidos a su diana en el caso de aquellos ligandos cuyo salto entre los estados unido y libre es razonablemente rápido. Para el trabajo que presentamos aquí se emplearon diferentes tiempos de relajación de la muestra (docetaxel:microtúbulos) que variaron entre 50 y 200 milisegundos.

La unión del ligando a los microtúbulos en nuestras preparaciones se muestra en los picos negativos cruzados que se observan claramente a 310 ^{o}K (figura 19), como era de esperar para una molécula que se une a microtúbulos ensamblados, en contraposición con lo observado para la droga libre donde no

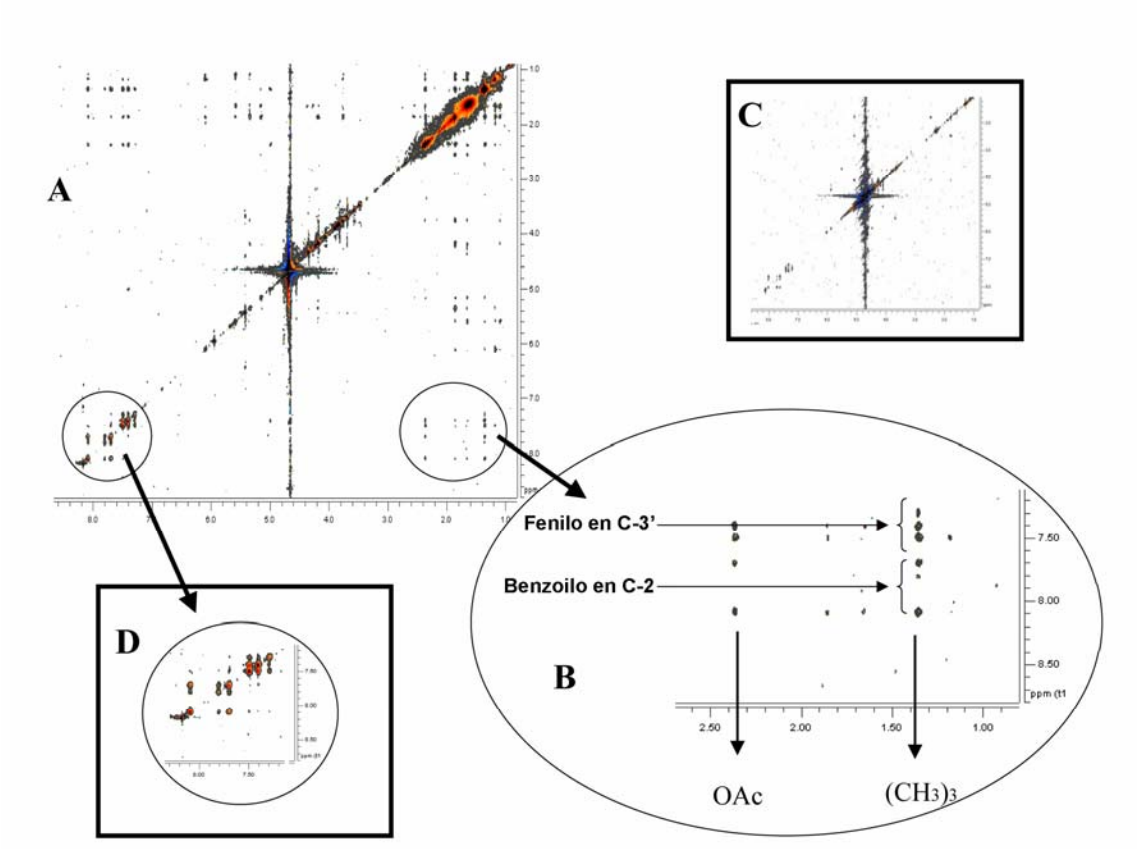

Figura 19. Caracterización por RMN de la conformación del docetaxel unido.
A. Espectro de TR-NOESY a 500 MHz del docetaxel en presencia de microtúbulos (en relación molar 20:1)
B. Detalle del espectro mostrando los contactos cercanos entre la cadena del tercbutilo y el anillo aromático en C-2 (además del los picos cruzados con el fenilo de 3' próximo)
C. El espectro del mismo ensayo en ausencia de microtúbulos no muestra ningún pico cruzado
D. En la región aromática del espectro de TR-NOESY no puede apreciar efecto Overhauser nuclear alguno entre los anillos de 3' y C-2.

se aprecia efecto Overhauser nuclear (NOE) alguno.

En estos ensayos se llevaron dos controles en paralelo, uno usando flutax-2 en lugar de docetaxel (la k_{off} efectiva de flutax-2 de liberación de los microtúbulos es 1,63 ± 0,18 s^{-1} (Diaz *et al.*, 2000)) y otro con discodermolida además de docetaxel a concentraciones equimolares. En el caso de flutax-2 no se observó ninguna señal de TR-NOESY indicando que la k_{off} efectiva del docetaxel es mayor que la de flutax-2. La señal de docetaxel se cancela con la presencia de discodermolida en el ensayo (cuya afinidad por el sitio de taxol es cien veces mayor) mostrando que el docetaxel está efectivamente unido al sitio de taxol (Buey *et al.*, 2005)

5. CITOTOXICIDAD Y RESISTENCIA A TAXANOS.

Gran parte del interés del estudio de toda esta colección de compuestos es su capacidad citotóxica en células en división y por tanto su actividad antitumoral.

Se realizaron los ensayos pertinentes para determinar la CI_{50} (concentración inhibitoria 50, concentración de droga a la que se observa una inhibición de la viabilidad celular del 50%) en líneas celulares tumorales sensibles y resistentes a taxol.

Las medidas de este parámetro nos enseñan cómo influyen las modificaciones introducidas en la molécula de taxol en su toxicidad y evalúa la utilidad de jugar con la afinidad de los compuestos como herramienta para la optimización de este tipo de drogas.

5.1. Citotoxicidad y resistencia en líneas celulares que sobreexpresan la glucoproteína P.

Todos los ligandos fueron ensayados en las líneas celulares humanas A2780 y A2780AD provenientes de carcinoma de ovario, la diferencia entre ambas radica en la sobreexpresión de la glucoproteína P (P-gp) en la segunda de ellas, hecho que le confiere resistencia múltiple a drogas (consultar la introducción).

Las CI_{50} de que cada uno de nuestros taxanos en cada tipo celular se muestra en la tabla 6.

Las citotoxicidades de los compuestos en las células sensibles a taxol (A2780) siguen una relación lineal con sus afinidades de unión a microtúbulos (figura 20) pero la linealidad se pierde para los compuestos cuyas energías libres a 35 ^{o}C son mayores de -50 kJ/mol (esto es, $K_{unión}$ por encima de $3x10^8$ M^{-1}); esto indica un límite en la toxicidad que se puede alcanzar con estas drogas. Aún cuando la diferencia de afinidad entre la cefalomanina y el chitax-40 alcanza los tres órdenes de magnitud, la CI_{50} se mantiene en el rango de nanomolar en ambos casos.

Tabla 6. Citotoxicidad de los taxanos en células de carcinoma ovárico sensibles y resistentes a taxol. R/S es el índice de resistencia; el cociente entre las CI_{50} en células resistentes y sensibles.

	CI_{50} (nM)		
	A2780	**A2780AD**	**R/S**
Taxol[a]	1,3 ± 0,4	980 ± 149	753
Docetaxel[a]	0,6 ± 0,2	290 ± 16	483
Cefalomanina	1,5 ± 0,2	910 ± 285	606
Chitax-1	13,2 ± 7	1222 ± 300	92,5
Chitax-2	950 ± 80	10200 ± 1900	10,7
Chitax-3	1250 ± 200	4000 ± 700	3,2
Chitax-4[b]	2,7 ± 0,6	14 ± 3,8	5,2
Chitax-5	6,6 ± 1,8	160 ± 19	24,2
Chitax-6	10 ± 2,4	274 ± 30	27,4
Chitax-7	14,5 ± 2,9	2100 ± 660	145
Chitax-8	22,5 ± 5	596 ± 105	26,4
Chitax-9	3900 ± 370	15000 ± 3500	3,8
Chitax-10	4900 ± 600	>20000	>4
Chitax-11[b]	1,36 ± 0,2	163 ± 37	120
Chitax-12[b]	2,8 ± 0,38	42 ± 13	15
Chitax-13[b]	1,3 ± 0,2	128 ± 17	98,4
Chitax-14[b]	1,6 ± 0,3	25 ± 10	15,6
Chitax-15	17,5 ± 2,7	5250 ± 1000	300
Chitax-16	740 ± 100	7360 ± 750	9,9
Chitax-17	18 ± 5,6	5412 ± 1200	301
Chitax-18	2,1 ± 0,8	452 ± 36	215,2
Chitax-19[b]	0,54 ± 0,07	39 ± 11	72,2
Chitax-20[b]	3,9 ± 1,2	27,4 ± 4	7
Chitax-21[b]	1,9 ± 0,3	41 ± 11	21,5
Chitax-22	2400 ± 1000	6960 ± 670	2,9
Chitax-23	11500 ± 1000	23800 ± 2200	2,1
Chitax-24	353 ± 19	8600 ± 3800	24,3
Chitax-25	6200 ± 2600	28500 ± 5300	4,6
Chitax-26	3500 ± 1400	8300 ± 2700	2,4
Chitax-27	10000 ± 740	9400 ± 1700	0,94
Chitax-28	82 ± 16	1880 ± 200	22,9
Chitax-29	102 ± 8,8	690 ± 60	6,8
Chitax-30	30 ± 0,5	246 ± 27	8,2
Chitax-31	106 ± 4,2	2950 ± 480	27,8
Chitax-32	62 ± 17	3200 ± 250	51,6
Chitax-33	69 ± 77	1500 ± 100	21,7
Chitax-34	28,7 ± 1,9	196 ± 14	6,8
Chitax-35	25 ± 2	153 ± 39	6,12
Chitax-36	1700 ± 120	>20000	>11,7
Chitax-37	86 ± 9,8	10000 ± 1000	116,2
Chitax-38	15400 ± 3200	20000 ± 3000	1,3
Chitax-39	4200 ± 100	5700 ± 300	1,3
Chitax-40[b]	7 ± 1	9,1 ± 0,45	1,3
Chitax-41	14000 ± 2000	>20000	1,4
Chitax-42	192 ± 20	2750 ± 430	14,3
Chitax-43	69,5 ± 3,8	331 ± 70	4,8
Chitax-44	>20000	>20000	

Frente a las células que sobreexpresan P-gp (A2780AD), sin embargo, la linealidad entre toxicidad y afinidad se conserva también en la franja de afinidades más altas lo que nos da un indicio de que, para estas células, la unión a tubulina podría ser la fuerza principal para competir contra la expulsión al medio a través de la glucoproteína-P.

Las regresiones lineales de ambos conjuntos de datos nos dan pendientes de 1,10 para la recta A2780 y 0,61 para la A2780AD lo que indica que la sobreexpresión de esta bomba de membrana está reduciendo la concentración intracelular de las drogas, como era de esperar, haciendo necesario por lo tanto aumentar la cantidad total de droga para conseguir el efecto citotóxico.

Observamos que los índices de resistencia para la pareja de células A2780AD/A2780 disminuyen con los taxanos de muy alta afinidad hasta el punto de llegar prácticamente a anular la resistencia a taxanos que confiere la P-gp (con índices que alcanzan el

valor de 1,3 en el caso del chitax-40). Esta disminución en el índice de resistencia también aparece en los compuestos poco citotóxicos con afinidades bajas para los que la CI_{50} en las células A2780AD se mantiene en altos valores similares a los que presentan para las células no resistentes.

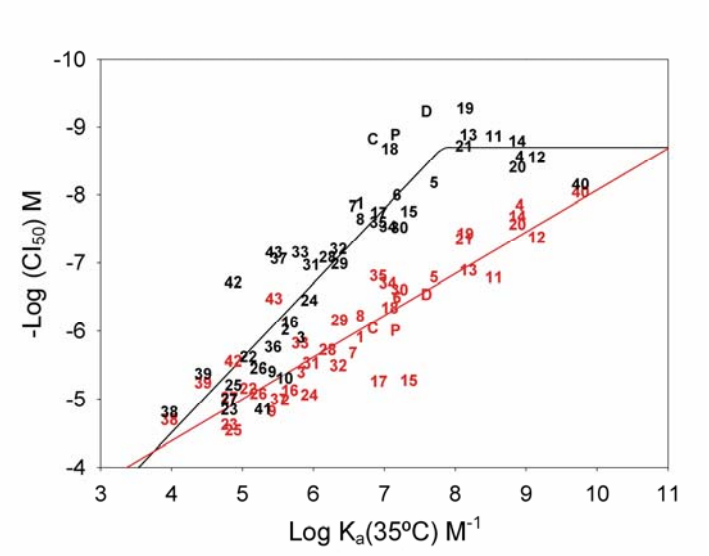

Figura 20. Relación entre afinidad y citotoxicidad de los taxanos en células A2780 (en negro) y A2780AD (en rojo).

Para confirmar que el aumento en la afinidad es una forma de soslayar la resistencia múltiple a drogas conferida por la sobreexpresión de la P-gp y no que sea un caso particular de estas células probamos el efecto del chitax-40 respecto a taxol y docetaxel en la pareja de células LoVo y LoVo-Dox, en este caso células humanas de carcinoma de colon e igualmente que las A2780AD, las LoVo-Dox (seleccionadas por su resistencia a doxorrubicina (Grandi *et al.*, 1986)) sobreexpresan la glucoproteína-P lo que les otorga resistencia múltiple a drogas. De igual forma que se ha observado con las células de carcinoma ovárico, el taxano de alta afinidad es capaz de obviar la presencia de este fenotipo de resistencia múltiple en éstas células (Tabla 7).

Sin embargo las células LoVo necesitan concentraciones mayores de los taxanos de afinidad media utilizados en clínica (taxol y docetaxel) que las A2780 para notar los efectos citotóxicos mientras que se requieren concentraciones muy similares de chitax-40 en los dos tipos celulares para producir estos efectos. Esto podría explicarse fácilmente si los niveles de expresión basales de P-gp en las células LoVo son superiores a los de las A2780. En las dos líneas celulares que sobreexpresan la proteína (LoVo-Dox y A2780AD) las CI_{50} de taxol, docetaxel y chitax-40 son semejantes lo que muestra la resistencia de las células LoVo-Dox también a taxol y docetaxel pero no a chitax-40.

Tabla 7. Comparación de los índices de resistencia en las parejas celulares A2780/A2780AD y LoVo/LoVo-Dox. Datos de las CI_{50} (nM) en cada línea celular y sus índices de resistencia (R/S).

	A2780	A2780AD	R/S	LoVo	LoVo-Dox	R/S
Taxol	0,83 ± 0,02	890 ± 68	1072	155 ± 30	1600 ± 111	10,3
Docetaxel	2,4 ± 0,58	243,8 ± 54	101,5	104 ± 31	596 ± 100	5,7
EpoB	1,37 ± 0,06	0,41 ± 0,1	0,3	1 ± 0,3	1,62 ± 0.02	1,65
Chitax-40	2,63 ± 0,17	1,12 ± 0,55	0,42	6,3 ± 1,5	5.4 ± 1,32	0,85
Chitax-20	4,2 ± 1,3	15,35 ± 5,69	3,65	6,5 ± 0,6	59 ± 2,2	9
EpoA	8,1 ± 0,8	2,4 ± 0,24	0,3	4 ± 0,45	5,9 ± 0,89	1,1

5.2. Citotoxicidad y resistencia en líneas celulares con mutaciones en tubulina.

De igual manera a lo antes mencionado, la batería de compuestos estudiados fue probada frente a otra línea celular procedente de carcinoma de ovario (un clon de la A2780), la 1A9 y a tres mutantes derivados de ésta que presentan mutaciones en β tubulina: las líneas 1A9/PTX10, 1A9/PTX22 y 1A9/A8.

Estas líneas celulares resistentes a taxol se seleccionaron con taxol y verapamilo, un inhibidor de la glucoproteína P, con lo que se evita que la resistencia sea causada por sobreexpresión de esta bomba de membrana (Giannakakou *et al.*, 1997).

Las mutaciones en β tubulina que causan esta resistencia se encuentran en el sitio de taxol: en la línea PTX10 se trata de un cambio de la fenilalanina 270 por una valina, en PTX22 encontramos una treonina en el lugar de la alanina 364 y en las células A8 la mutación transforma la treonina 274 en isoleucina.

De forma muy parecida a lo que pasa en el caso de las células con resistencia múltiple a drogas provocada por la sobreexpresión de P-gp, la resistencia a taxanos es minimizada con los taxanos que muestran constantes de afinidad muy altas (CI_{50} enumeradas en la tabla 8), la relación entre la citotoxicidad y la afinidad tiene sentido únicamente para la línea parental 1A9 que siendo un clon de las células A2780 mantienen la misma relación que la mostrada en la figura 20 para estas células. En el caso de las líneas PTX10, PTX22 y A8 se desconoce la afinidad de los compuestos a sus tubulinas mutantes y por lo tanto no podemos hacer ningún tipo de correlación.

A partir de los índices de resistencia mostrados en la tabla 8 observamos que para las células PTX10 la cadena lateral en C-13 del docetaxel es más favorable respecto a cualquiera de las otras dos (cefalomanina o taxol).

Además la introducción de un grupo polar en la posición meta del anillo en C-2 también parece ofrecer una ventaja para esta mutación en tubulina y los índices de resistencia decrecen considerablemente respecto al parental de esta manera:

-sobre el esqueleto de cefalomanina (R/S = 105) la introducción de un átomo de yodo (chitax-30) reduce el índice de resistencia hasta 18,7; el átomo de cloro (chitax-6) lo lleva a 10,7 y el de bromo (chitax-34) a 8,5; por su parte el grupo metóxido (chitax-13) baja el índice de resistencia hasta 4,6 y la azida hasta 2,2.

-igualmente sobre el patrón de taxol un grupo metóxido (chitax-11) en este mismo lugar vuelve a reducir la resistencia de 64 a 4,2 veces y la azida (chitax-12) a 2,6.

El chitax-40 que combina la cadena lateral en C-13 del docetaxel con un grupo azida en la posición meta del anillo de C-2 presenta un índice de

resistencia de 0,4, lo que indica que es incluso más citotóxico en las células con esta tubulina mutante que en las parentales.

Los resultados indican que los cambios en la "parte norte" de la molécula (C-7 y C-10) son indiferentes para la citotoxicidad en las células PTX10. Así los compuestos deacetilados o propionilados en C-10 no presentan cambios tan pronunciados en sus índices de resitencia, pudiendo llegar, en el mejor de los

Tabla 8. Citotoxicidad de los taxanos en líneas de carcinoma ovárico con tubulinas mutantes en el sitio de taxol. Índices de resistencia (R/S) respecto a la línea parental 1A9.

	1A9	PTX-10		PTX-22		A8	
	CI_{50} (nM)	CI_{50} (nM)	R/S	CI_{50} (nM)	R/S	CI_{50} (nM)	R/S
Taxol	1,37±0,3	88±13	64,2	29±3	21	4,9±1,5	3,6
Docetaxel	0,74±0,3	10,5±4	14,2	2,9±0,2	3,9	1,7±0,1	2,3
Cefalomanina	1±0,09	105±28	105	68±3,3	68	10,3±0,9	10,3
Chitax-1	17±2	900±70	52,9	435±17	25,5	16,2±1,6	0,9
Chitax-2	960±72	14500±3000	15,1	7900±400	8,2	2450±30	2,5
Chitax-3	1500±300	1950±600	1,3	3800±30	2,5	2750±170	1,8
Chitax-4	2,3±0,6	11,6±3,7	5	1,9±0,4	0,83	2±0,04	0,9
Chitax-5	5,7±2	37±5,43	6,5	7,2±1,1	1,26	6,1±0,7	1,1
Chitax-6	9±3	97±23	10,7	51±9,8	5,7	15±4	1,7
Chitax-7	14±3	645±3,5	46	320±14	23	15,2±0,17	1,1
Chitax-8	29,5±4	722±2	24,4	435±17	14,7	20,5±1,41	0,7
Chitax-9	4200±300	>10000		>10000		6750±280	1,6
Chitax-10	6300±800	>20000		>20000		10000±700	1,6
Chitax-11	1,1±0,17	4,6±1,4	4,2	4,45±2,3	4	1,75±0,12	1,6
Chitax-12	2,3±0,2	6±3	2,6	3±0,02	1,3	1,7±0,01	0,7
Chitax-13	1,4 ±0,25	6,4±2,2	4,6	1,9±0,38	1,35	1,5±0,01	1,1
Chitax-14	1,4±0,2	3±0,6	2,2	1,74±0,32	1,24	1,6±0,05	1,1
Chitax-15	17±1,7	242±60	14,3	290±155	17	17,75±0,53	1
Chitax-16	1560±0,3	2730±1450	1,8	3100±980	2	2300±500	1,5
Chitax-17	19,3±0,3	1000±120	51,8	307±150	15,9	25±0,7	1,3
Chitax-18	2,7±0,1	259±28	95,9	52,4±10	19,4	13±2,89	4,8
Chitax-19	0,6±0,08	3,9±1,15	6,5	0,97±0,13	1,6	1,65±0,03	2,7
Chitax-20	4,3±1,6	4,9±0,63	1,1	2±0,6	0,5	1,45±0,3	0,3
Chitax-21	2,1±0,4	20,7±15	9,8	6,3±2	3	1,65±0,17	0,8
Chitax-22	3200±1200	10000±3600	3,1	5300±1000	1,65	7150±30	2,2
Chitax-23	12400±300	28000±6200	2,2	13600±420	1,1	21500±1760	1,7
Chitax-24	342±25	5400±3000	15,8	3500±1600	10,2	497±86	1,4
Chitax-25	5600±1270	23000±6600	4,1	10300±2400	1,8	16500±1760	2,9
Chitax-26	4500±1830	18000±7000	4	9000±1400	2	10000±700	2,2
Chitax-27	9800±1600	9800±2000	1	8000±2000	0,8	13500±3800	1,4
Chitax-28	92±7	3600±140	39,1	2500±50	27,1	147 ± 5,3	1,6
Chitax-29	117±5	3500±170	29,9	2600±150	22,2	170 ± 0,3	1,45
Chitax-30	27±2	505±90	18,7	230±28	8,5	27 ± 2,1	1
Chitax-31	70,5±1	6300±910	69,4	3000±530	42,5	252 ± 8	3,6
Chitax-32	56,5±10	4000±420	70,7	2000±260	35,4	155 ± 10	2,7
Chitax-33	52,5±8	2340±820	44,6	950±30	18,1	27,2 ± 5,5	0,5
Chitax-34	25±0,7	212±30	8,5	160±24	6,4	1,6 ± 0,2	0,64
Chitax-35	24,2±1,2	240±20	9,9	167±10	6,9	7,6 ± 0,28	0,3
Chitax-36	1390±420	>20000		14000±4000	10,1	1800 ± 100	1,3
Chitax-37	68±2,8	8600±950	126,5	4600±670	67,6	610 ± 21	8,9
Chitax-38	14100±2700	20000±2500	1,4	9000±1200	0,6	8100 ± 500	0,6
Chitax-39	4900±100	3500±3800	0,7	4300±2200	0,9	7200 ± 200	1,5
Chitax-40	3,1±0,7	2,4±0,5	0,4	12±1,41	1,9	3,8 ± 0,6	1,2
Chitax-41	15000±2700	>20000		>20000		>20000	
Chitax-42	216±11	3700±490	17,1	5600±560	26	525 ± 3,5	2,4
Chitax-43	52,5±0,3	336±80	6,4	520±50	9,9	76,5 ± 2,4	1,45
Chitax-44	>20000	>20000		>20000		>20000	

casos, a dos veces o cuatro pero no a la mejora de veinte veces que supone la azida en C-2.

En el caso de las células PTX22, y el cambio de la alanina 364 por una treonina en su tubulina, también la cadena lateral de docetaxel en C-13 resulta la más conveniente a la hora de buscar un compuesto que no presente resistencia respecto a las células parentales 1A9 (el docetaxel tiene un índice de resistencia de tan sólo 4).

También de manera parecida los sustituyentes polares en la posición meta del anillo en C-2 reducen los índices de resistencia:

-para la serie de cefalomanina los átomos de yodo, bromo y cloro llevan los índices de resitencia desde 68 para la cefalomanina a 8,5, 6,4 y 5,7 respectivamente y los grupos metóxido y azida hacen desaparecer la resistencia a esta mutación y muestran índices prácticamente inexistentes de 1,4 y 1,2.

-con el taxol (R/S = 21) el grupo metóxido reduce el índice de resistencia a 4 y la azida a 1,3.

Curiosamente en este caso (azida en la posición meta del anillo en C-2) los mejores compuestos son los 20, 4 y 14, todos ellos cefalomaninas lo que hace pensar que los cambios pudieran no ser aditivos.

Igual que para las PTX10 en esta línea celular (PTX22) los cambios en C-7 y C-10 no parecen tener mucha repercusión en cambiar la resistencia de las células por las drogas que los presentan.

El clon de 1A9 denominado A8 se caracteriza por su resistencia a epotilonaA y es sensible a taxol o docetaxel, mostrando baja resistencia a cefalomanina (tabla 8). Estas células se usaron como control para nuestros ensayos en el que no se observan apenas diferencias en los cocientes entre las CI_{50} de estas células y sus parentales para ninguno de los compuestos medidos.

6. UNIÓN A GLUCOPROTEÍNA-P

Vistos los datos de citotoxicidad de la colección de taxanos en células que sobreexpresan la glucoproteína-P es inmediato el preguntarse si los compuestos ante los que no existe esta resistencia tienen dificultad para ser transportados al exterior por la bomba de membrana.

Comprobamos si la expulsión de las drogas estaban dificultadas determinando los valores de la constante de disociación (K_d) del proceso de unión del ligando al transportador.

Para tomar estas medidas se utilizó el apagamiento de la fluorescencia intrínseca del triptófano de la glucoproteína-P (Yang *et al.*, 2007). Los ensayos

fueron realizados en el laboratorio de Frances Sharom en la Universidad de Guelph (Canadá).

Previamente se había demostrado la relación entre el valor de la CI_{50} para la inhibición de la función de la P-gp por una droga y la K_d de su unión (Sharom *et al.*, 1999).

Los resultados mostrados en la tabla 9 sugieren que la P-gp debe tener una habilidad muy parecida para expulsar cada uno de nuestros compuestos ya que sus K_d no son muy dispares. Las K_d de la P-gp se midieron para todas las modificaciones de C-2 disponibles sobre chitax-1 (cefalomanina deacetilada en C-10 y propionilada en C-7; consultar figura 11), además de las moléculas de partida taxol, docetaxel y cefalomanina de manera que resulta fácilmente deducible que las modificaciones en las moléculas con alta afinidad por la tubulina no irán a variar su afinidad por la glucoproteína-P y por tanto serán todas expulsadas al exterior celular de manera similar.

Tabla 9. Constantes de disociación de los taxanos de la glucoproteína-P

	K_d (nM)
Chitax-1	46±2,8
Chitax-4	66±5,2
Chitax-5	54±3,0
Chitax-33	58±6,0
Chitax-36	51±5,0
Chitax-6	66±6,4
Chitax-34	36±4,0
Chitax-30	47±7,0
Chitax-7	88±9,4
Chitax-8	58±5,4
Chitax-32	58±5,0
Chitax-31	53±4,0
Chitax-41	76±11
Chitax-2	39±3,9
Chitax-3	45±5,2
Chitax-9	44±4,0
Chitax-10	41±3,2
Chitax-28	46±5,0
Chitax-29	53±5,0
Chitax-35	46±5,0
Taxol	35±3,0
Cefalomanina	37±3,9
Docetaxel	39±4,0

DISCUSIÓN.

1. INFLUENCIA DE LAS MODIFICACIONES EN LA AFINIDAD DE UNIÓN.

El efecto de las modificaciones de los distintos grupos unidos al esqueleto de bacatina sobre la toxicidad de los compuestos ha sido discutida de forma cualitativa en numerosas revisiones (Kingston y Newman, 2007; Zefirova *et al.*, 2005) pero dado que estos estudios habían sido realizados en diferentes líneas celulares, no era posible relacionar rigurosamente los cambios estructurales de la molécula con los cambios en su citotoxicidad. En el trabajo de Buey *et al.*(2004) se mostró que la afinidad de unión de las epotilonas por su sitio en β tubulina es un parámetro más preciso y objetivo para cuantificar de forma sistemática los efectos de las sustituciones en un set de posiciones específicas y por ello éste ha sido el parámetro empleado en este trabajo para los taxanos.

Una vez determinadas las constantes de unión de todos los compuestos a una temperatura dada (35 ^{o}C) es posible determinar los cambios producidos por cada modificación sencilla de la molécula en la energía libre de unión aparente (Tabla 10) de modo que es factible seleccionar las sustituciones más favorables en cada posición, haciendo posible el diseño de diversos taxanos optimizados.

1.1. Efecto de los cambios en C-2.

Las modificaciones en esta posición han sido descritas como las más efectivas en la modulación de la actividad de los taxanos. El grupo benzoilo resulta esencial y su ausencia (Chen *et al.*, 1993b) o cambio por otras cadenas laterales pequeñas (Nicolaou *et al.*, 1995; Ojima *et al.*, 1994) conduce a una pérdida de actividad prácticamente total en las líneas humanas de cáncer de colon probadas. En cambio alteraciones en la estructura del anillo e incluso su sustitución por anillos no aromáticos o heterocíclicos causan únicamente pérdidas moderadas de la actividad antitumoral (Ojima *et al.*, 1994). La introducción de sustituyentes en el anillo benzóxido confiere ganancia de la actividad cuando se trata de pequeños grupos añadidos en posición meta pero por el contrario provocan caídas de actividad en las otras posiciones (Kingston *et al.*, 1998; Nicolaou *et al.*, 1994; Yang *et al.*, 2007). Los cambios en el enlace entre el anillo y el esqueleto de taxol también producen pérdida de la actividad biológica (Wang *et al.*, 2007).

Los resultados presentados en este trabajo confirman todos estos datos cualitativos, los extienden a otras modificaciones y aportan una caracterización cuantitativa precisa del efecto del cambio en C-2 en la afinidad de unión:

I. Los cambios en la naturaleza de la unión del anillo bencénico suponen una gran pérdida de energía libre de unión. La sustitución del éster por un éter, un tioéter o un grupo amina (chitax-24, 25, 26, 27, 38 y 39) o bien por un tioéster o una amida (chitax-22, 23, 42, 43 y 44) producen pérdidas importantes en la energía libre de unión (de hasta 20 kJ/mol). Esta exigencia tan estricta hace suponer que el ángulo que forma el anillo bencilo con el resto de la mólecula

Tabla 10. Variaciones de las energías libres de unión de los taxanos a microtúbulos dependiendo de sus modificaciones sencillas.

Sitio	Modificación	Compuesto	ΔΔG	Promedio
C2	Benzoilo → bencileter	T→25	13,2	+13,0±0,2
		21→24	12,8	
	benzoilo → sulfobenzoilo	T→27	13,6	+15,9±2,3
		21→26	18,1	
	benzoilo → benzamina	T→38	18,6	+20,1±1,5
		21→39	21,6	
	benzoilo → tiobenzoilo	T→23	19,6	+15,9±3,8
		21→22	12,1	
	benzoilo → benzamida	21→42	19,2	
	Benzamida → 3-metoxi-benzamida	42→43	-3,4	
	Benzamida → 3-Cl-benzamida	42→44	5,3	
	benzoilo → 3 metil- 2 butenoilo	1→2	6,2	
	benzoilo → 3 metil- 3 butenoilo	1→3	4,9	
	benzoilo → 2(E)-butenoilo	1→9	7,3	
	benzoilo → 3-metil- butanoilo	1→10	6,3	
	benzoilo → 2-debenzoilo-1,2-carbonato	C→16	5,8	
	benzoilo → 3-azido benzoilo	1→4	-8	-11,2±1,3
		T→12	-13,9	
		C→14	-12,2	
		18→20	-10,6	
	benzoilo → 3-metoxi-benzoilo	1→5	-6,2	-7,2±0,6
		T→11	-8,3	
		C→13	-8,1	
		18→19	-6,3	
	benzoilo → 3-Cl-benzoilo	1→6	-3,1	
	benzoilo → 3-Br-benzoilo	1→34	-2,3	
	benzoilo → 3-I-benzoilo	1→30	-3,3	
	benzoilo → 3-ciano-benzoilo	1→7	0,6	
	benzoilo → 3-metil-benzoilo	1→8	0	
	benzoilo → 3-hidroximetil-benzoilo	1→36	7,2	
	benzoilo → 3-hidroxi-benzoilo	18→37	9,2	
	3-Cl-benzoilo → 2,4-di-Cl-benzoilo	6→29	4,8	
	benzoilo → 2,4-di-F-benzoilo	1→28	2,7	
	3-metoxi-benzoilo → 2-5-di- metoxi-benzoilo	5→35	4,6	
	benzoilo → 2-tiofeno	1→31	4,1	
	benzoilo → 3-tiofeno	1→32	1,8	
	benzoilo → 6-carboxi-2-piranona	1→41	8,1	
C13	Taxol → Cefalomanina	T→C	1,9	+2,0±0,2
		11→13	1,9	
		12→14	1,6	
		15→17	2,4	
	Taxol → Docetaxel	23→22	-1,7	-3,2±0,9
		25→24	-6,2	
		27→26	-1,3	
		38→39	-2,8	
		T→21	-4,2	
	Cefalomanina → Docetaxel	C→21	-3,8	-5,6±1,1
		17→D	-7,7	
		20→40	-5,2	
C10	acetilo → hidroxilo	T→15	-1,3	-1,7±0,8
		C→17	-0,7	
		21→D	-3,2	
	propionilo → hidroxilo	18→17	0,9	0,9
	acetilo → propionilo	C→18	-1,6	-0,5±0,4
		13→19	0,2	
		14→20	0	
C7	propionilo → hidroxilo	17→1	-1,6	-1,6

tiene que estar bien conservado y que debe existir algún tipo de imposición estérica tal y como se discute para el grupo tiobenzoilo de los compuestos 22 y 23 en (Wang *et al.*, 2007). La importancia de este ángulo se refleja en el hecho de que la disminución de la energía libre causada por la sustitución del grupo benzoilo por un éster alquilo (chitax-2, 3, 9, 10 y 16) es mucho menor (entre 5 y 6 kJ/mol) lo que puede ser explicado por la falta de las interacciones del anillo bencilo con el sitio de unión.

II. La introducción de algunos sustituyentes en la posición meta del benzoilo son favorables para la energía libre de unión del compuesto, los más efectivos son los grupos azida (-11,2 ± 1,1 kJ/mol) y metóxido (-7,2 ± 0,6 kJ/mol) caso de los chitax-4, 5, 11, 12, 13, 14 y 20 y los átomos halógenos como en los compuestos 6, 30 y 34 tienen un efecto menor (-2-3 kJ/mol). Otros grupos de pequeño tamaño como ciano o metilo (chitax-7 y 8) no tienen ningún efecto. Otros grupos igualmente pequeños como hidroxilo e hidroximetilo de los chitax-36 y 37 son desfavorables y la energía libre de unión se ve aumentada entre 7 y 9 kJ/mol.

III. Las dobles sustituciones del mismo anillo en posiciones 2,4 (chitax-28 y 29, átomos de flúor y cloro respectivamente) y 2,5 (chitax-35, sendos grupos metóxido) son desfavorables para la energía libre de unión.

IV. El grupo bencilo puede ser sustituido de manera efectiva por uno tiofenilo (chitax-31 y 32).

En trabajos anteriores (Buey *et al.*, 2004) se muestra que las modificaciones que suponen un aumento en la energía libre de unión llevan parejo un aumento en su citotoxicidad, así que en nuestro caso seleccionamos la sustitución con un grupo azida en la posición meta del anillo benzoilo en el carbono 2 de la molécula para la optimización de su actividad citotóxica.

1.2. Efecto de los cambios en C-13.

Para esta posición evaluamos la influencia de los grupos que se encuentran en los taxanos taxol, docetaxel y cefalomanina.

En la comparación directa con docetaxel se encuentra que su afinidad es casi dos veces mayor que la del taxol (Diaz y Andreu, 1993) con un cambio en la energía libre de -1,6 kJ/mol y a su vez dobla su citotoxicidad en las células 1A9 (Buey *et al.*, 2005). Por otra parte la afinidad y citotoxicidad de la cefalomanina son la mitad que las del docetaxel (Yang *et al.*, 2007). Estos compuestos difieren también del docetaxel en C-7 y C-10 por lo que no podemos conocer la aportación real de la modificación de la cadena lateral en C-13.

En nuestra colección sí que contamos con compuestos que difieren únicamente en esta posición y mantienen idénticas las demás de manera que podemos hacer comparaciones entre los compuestos taxol, cefalomanina, docetaxel y los chitax-11, 12, 13, 14, 15, 17, 20, 21, 22, 23, 24, 25, 26, 27, 38, 39 y 40 (figura 11) y calcular el grupo que mejor contribución tiene en la unión de los taxanos (tabla 10) que es el de la molécula de docetaxel con una disminución en la energía libre de - 3,2 ± 0,9 kJ/mol respecto al grupo del taxol y de -5,6 ± 1,1 kJ/mol sobre el de la cefalomanina.

1.3. Efecto de los cambios en la "parte norte" del anillo de taxano (C-7 y C-10).

Encontramos que las modificaciones en estas posiciones de la molécula tienen un efecto limitado tal y como se podía esperar a partir de sus efectos citotóxicos descritos previamente (Chen *et al.*, 1993a).

En C-10 hemos probado una propionilación además del acetilo original y el hidroxilo propio de la molécula de docetaxel. Esta modificación proporciona una disminución en la energía libre de unión de alrededor de -0,5 kJ/mol respecto a los otros grupos.

Sin embargo esta propionilación en C-7 en lugar del hidroxilo natural aumenta la energía de unión en 1,6 kJ/mol.

Con estos datos la elección de los grupos para la optimización de la molécula será la de un propionilo en C-10 y un hidroxilo en C-7.

2. DISEÑO DE UN TAXANO DE AFINIDAD OPTIMIZADA.

Juntando todos los datos obtenidos para cada posición se puede predecir la composición final de esa molécula óptima buscada: deberá portar la cadena lateral del docetaxel en C-13, un grupo azida en la posición meta del benzoilo en C-2, un propionilo en C-10 y un hidroxilo en C-7.

Con todas las medidas realizadas podemos predecir la energía libre que tendrá este compuesto: nuestro primer compuesto de la serie, chitax-1, tiene una energía libre de -39,4 kJ/mol, la molécula propuesta debería ganar -5,6 kJ/mol por el cambio de la cadena lateral de la cefalomanina por la del docetaxel en C-13, otros -11,2 kJ/mol por la adicción de la azida en la posición meta del benzoilo en C-2, -1,6 kJ/mol del cambio de su propionilo en C-7 por un hidroxilo y -0,9 kJ/mol por la sustitución del hidroxilo en C-10 por un propionilo. Sumando todo esto al taxano diseñado se le predice una ΔG a 35 ^{o}C de -58,7 kJ/mol. Este compuesto fue sintetizado (es el compuesto chitax-40 de nuestra colección) y nuestras medidas de afinidad usando el método de desplazamiento de epoB nos corroboran un afinidad muy similar a la predicha, con valores experimentales de 6,28 ± 0,15 x 10^{9} M^{-1} para su constante de unión a 35 ^{o}C y por tanto -57,7 ± 0,1 kJ/mol para su ΔG.

3. INTERPRETACIÓN ESTRUCTURAL DE LOS DATOS DE UNIÓN.

Teniendo en cuenta los datos de las afinidades de los compuestos por su sitio de unión en tubulina y con los datos estructurales obtenidos computacionalmente de este mismo complejo, es posible diseñar un modelo que cuantifique la aportación de cada grupo incorporado a la molécula en la unión del compuesto a su sitio.

Para explicar el cambio en la afinidad de la molécula debido a las modificaciones en la posición C-2 se han propuesto dos razones: la necesidad de un grupo hidrofóbico en este lugar que mantenga la conformación apropiada del taxano o la interacción directa del anillo bencilo con ciertos residuos de la proteína (Zefirova *et al.*, 2005).

Con los datos de modelado molecular podemos atribuir la mayor afinidad del chitax-40 comparada con la del taxol o el docetaxel (que principalmente viene dada por la azida en el benzoilo de C-2) a dos hechos que mejoran el anclaje del ligando en su sitio de unión en la proteína: el aumento de las interacciones de apilamiento con el imidazol de la His229 y la mejora en las interacciones electrostáticas con Asp26 y Arg369 en el otro lado de la molécula. El mismo razonamiento se puede aplicar al caso de chitax-13 y su grupo metóxido en lugar de la azida y también, en menor medida, a los compuestos con sustituyentes halógenos. Sin embargo la posición más probable de sustituyentes metilo, ciano, hidroxilo o hidroximetilo es expuestos al solvente en lugar de orientados hacia el bolsillo hidrofóbico, de manera que deben contribuir de manera insignificante en la afinidad de la unión como efectivamente se obseva en los datos experimentales.

Igualmente se puede encontrar una explicación estructural a la contribución de la cadena lateral en C-13 en la afinidad del compuesto. La presencia de la cadena del docetaxel frente a la del taxol incrementa la afinidad de la unión porque la fuerza del puente de hidrógeno formado con el carboxilato de Asp26 es mayor cuando se forma con el NH del carbamato (docetaxel, chitax-40) que con el de la amida (taxol) (figura 18).

4. CONFORMACIÓN BIOACTIVA DEL TAXOL.

En nuestras medidas, la señal de TR-NOESY proviene de una molécula de docetaxel libre cuyos protones han sido excitados cuando aún estaba unida a su sitio y se relajan después de la salida del sitio, de tal modo que la señal que obtenemos corresponde a la conformación del compuesto justo en el momento de soltarse de su sitio de unión. Para interpretar los datos estructurales de RMN deberemos, además, tener en cuenta que las drogas estabilizadoras de microtúbulos que se unen al sitio del taxol llegan hasta su localización tras un paso previo de unión al sitio externo en el poro del microtúbulo (Buey *et al.*, 2007; Diaz *et al.*, 2003).

Para poder obtener buenas señales de TR-NOESY, la separación del docetaxel de su sitio en los microtúbulos, después de la excitación, debe ser

rápida, la k_{off} del compuesto ha de estar, en la escala de tiempo de la relajación. Esto en principio parece en discordancia con la baja constante de disociación medida para el taxol en el estudio cinético de (Diaz *et al.*, 2003) (0,091 ± 0,006 s^{-1}). Sin embargo esta constante de disociación no corresponde al proceso de salida de la molécula de su sitio sino al paso limitante de la reacción.

La disociación de los taxanos de los microtúbulos se ha estudiado en profundidad usando los derivados fluorescentes del taxol flutax-1 y flutax-2 que tienen un mecanismo de disociación en dos fases (Diaz *et al.*, 2000). La primera de estas fases es la más lenta (por tanto la que se observa directamente) y tiene una constante de velocidad de 0,022 ± 0,001 s^{-1} (cuatro veces más lenta pues que la del taxol), la segunda, que es la responsable de la liberación del ligando al medio y sólo puede ser medida de forma indirecta a partir de la dependencia de las constantes de velocidad de la concentración, resulta ser cerca de 100 veces más rápida (k_{off} = 1,63 ± 0,18 s^{-1}).

Sin una sonda fluorescente no podemos calcular la constante de velocidad del paso de liberación en la disociación del docetaxel (k_{off}). En los controles que hicimos en los experimentos de RMN con flutax-2 no encontramos ninguna señal de TR-NOESY para este ligando lo que nos indica que su k_{off} no es suficientemente alta para conseguir ofrecer este tipo de señal. En vista de estos resultados podemos concluir que para el docetaxel la velocidad efectiva del paso de liberación en su proceso de disociación tiene que ser mayor que la del flutax-2. Con todo esto y dado que parece razonable pensar que la presencia de la fluoresceína ralentice la disociación de flutax-2 y puesto que las señales de TR-NOESY que aparecen en la medida de la mezcla de docetaxel con microtúbulos desaparecen con la adición de discodermolida (un compuesto con mucha mayor afinidad por el sitio de taxol (Buey *et al.*, 2005)) podemos asumir que las señales de TR-NOESY que obtenemos para el docetaxel corresponden al último paso en su disociación de los microtúbulos que debe estar unido bien al sitio externo o bien a un sitio luminal modificado.

Las características básicas de la conformación derivada de las medidas de RMN se extraen de los picos invertidos de TR-NOESY. Se observan acoplamientos claros entre los protones del terc-butilo y los del benzoilo de C-2 (figura 19B), pero sólo débilmente entre los dos grupos aromáticos, el benzoilo de C-2 y el fenilo de 3' (figura 19D). El acetilo de C-4 también produce NOE con estos dos anillos aromáticos (figura 19B).

Estos datos experimentales descartan la presencia de la conformación polar del docetaxel unido a microtúbulos; la conformación

Figura 21. Superposición de las estructuras de docetaxel con geometría de T-taxol obtenidas en el modelado molecular (en verde) y por RMN (gris).

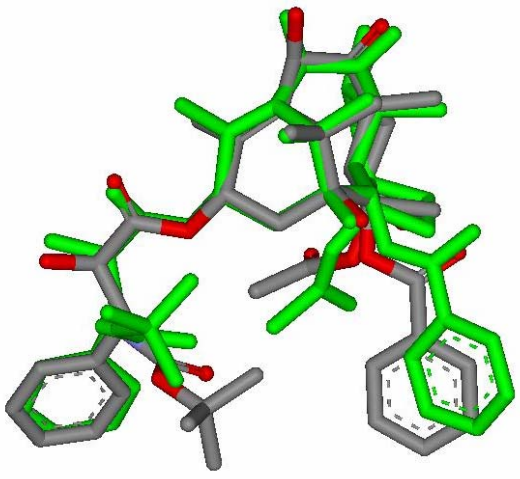

deducida de ellos está básicamente de acuerdo con la derivada del modelado computacional (figura 21).

Aunque la estructura modelada computacionalmente concuerda con la geometría de T-taxol (Snyder *et al.*, 2001), la deducida de los datos de RMN es intermedia entre ésta y la conformación "hidrofóbicamente colapsada" (Vander Velde *et al.*, 1993).

Ya que ambas conformaciones (la calculada computacionalmente y la deducida de los datos de RMN) son tan similares y parecidas a su vez a la de T-taxol podemos intuir que probablemente el paso de pre-liberación no afecta gravemente a la estructura del docetaxel y que la conformación de T-taxol será estable en el entorno de la proteína.

La única diferencia evidente entre las dos estructuras que mostramos se debe a la presencia de la histidina 229; en el modelo la encontramos entre el grupo en C-2 y la cadena lateral de C-13 separándolos, sin embargo las medidas de RMN muestran mayor proximidad entre los protones del benzoilo y el terc-butilo (4-5 Å) que la distancia que sugiere el modelo del complejo docetaxel-β tubulina (5-6 Å).

Con estas restricciones la geometría del docetaxel unido en el estado de pre-liberación deducida de los datos de RMN, que es similar a la de T-taxol, concuerda con la resuelta por el proceso de modelado y recuerda a la descrita para el taxol unido a microtúbulos (Lowe *et al.*, 2001) a pesar de que nuestras condiciones experimentales son considerablemente diferentes.

5. EFECTO DE LAS MODIFICACIONES EN LA ESTRUCTURA DE LOS MICROTÚBULOS.

Los presencia de taxanos afecta al número de protofilamentos que componen un microtúbulo, además este número es diferente dependiendo del taxano presente (los datos para taxol, docetaxel, flutax-1 y flutax-2 aparecen en los trabajos Andreu *et al.*, 1994; Diaz *et al.*, 2000). Disponiendo del abanico de modificaciones que nos ofrece nuestra colección de taxanos quisimos indagar sobre la influencia de las modificaciones sobre el esqueleto de taxol también en el diámetro de los microtúbulos que forman. Desgraciadamente el escaso tiempo de uso del sincrotrón otorgado (ayudado de algún problema técnico con el detector) no fue suficiente para obtener datos de la serie completa de modificaciones individuales -que esperamos poder concluir en nuevas visitas a Grenoble a lo largo del año próximo.

Los datos de los que disponemos hasta el momento nos enseñan que las modificaciones en la "parte norte" de la molécula parecen provocar los mayores cambios sobre el diámetro de los microtúbulos que inducen (consultar tabla 3 y la descripción en el apartado 2.5. de los resultados). Esta zona de la molécula tiene un papel limitado en la unión de la molécula a su sitio en tubulina y en el caso del sitio externo, en particular el sustituyente en C-7, quedan hacia el exterior de los microtúbulos. De algún modo la aparición de un grupo u otro

en estas posiciones modifican el ángulo que pueden formar los protofilamentos entre sí, cambiando por tanto el número de ellos capaz de cerrar el cilindro.

6. RELACIÓN ENTRE AFINIDAD DE UNIÓN, CITOTOXICIDAD Y RESISTENCIA MÚLTIPLE A DROGAS CAUSADA POR LA GLUCOPROTEÍNA P.

La representación doble logarítmica de la citotoxicidad frente a la afinidad de unión por la tubulina de los compuestos (figura 20) muestra claramente que ambas magnitudes guardan una relación al igual que se había observado anteriormente para el caso de las epotilonas y otros ligandos del sitio de taxol, convirtiendo la afinidad de unión en un buen predictor de la citotoxicidad de un ligando.

Aunque la correlación es clara resulta evidente cierta desviación de los datos; parece haber un límite en la citotoxicidad de estos compuestos en las células no-resistentes A2780 (CI_{50} = 1 nM).

La revisión de los datos anteriores del laboratorio (Buey *et al.*, 2004; Buey *et al.*, 2005) saca a la luz que no parece haber ningún MSA con una CI_{50} en estas células por debajo del rango de nanomolar. La discodermolida y muchas epotilonas tienen CI_{50} del orden de 1 nM o mayores a pesar de tener constantes de unión del orden de 10^9 M^{-1}. De hecho el compuesto con mayor afinidad descrito hasta el momento, un derivado de la epotilona (el compuesto 19 en Buey *et al.*, 2004 con una constante de 2,1 x 1010 M-1), es también el más citotóxico (CI_{50} = 0,1 nM) y aunque posee una afinidad de unión tres órdenes de magnitud superior a la del taxol su citotoxicidad mejora únicamente diez veces (Buey *et al.*, 2004).

Estos datos sugieren que para que se produzca la parada del ciclo celular se necesita un porcentaje significativo de tubulina unida al ligando y por tanto la citotoxicidad de las drogas está limitada a la cantidad requerida para alcanzar este porcentaje.

En el rango de concentraciones necesarias para alcanzar la parada del ciclo celular, la cantidad de tubulina con ligando unido supone entre un 2% y un 20% de la proteína celular total (Matesanz *et al.*, 2008).

En experimentos en los que se mide la entrada de las drogas a la célula (de Inés Díaz, 1995; Matesanz *et al.*, 2008) se observa que la cantidad total de compuesto disponible a las concentraciones de CI_{50} es alrededor de un tercio del total de tubulina en la célula. Aunque esto debería ser suficiente, en principio, para unirse a un porcentaje importante de la proteína, los resultados de estos experimentos indican que la cantidad efectiva de ligando disponible para unirse a los sitios de taxol es mucho menor (2-10%).

La explicación de este fenómeno podría ser que aún cuando todos los sitios de unión están dentro del pequeño volumen que ocupan las células, las drogas tienen que atravesar las membranas celulares y alcanzar una concentración celular umbral a la que se oponen las bombas detoxificantes. Si para que un taxano ejerza su citotoxicidad necesita unir un porcentaje

significativo de la tubulina citoplásmica (por ejemplo entre un 2% y un 5%) y la cantidad de ligando disponible para unirse a la proteína es una pequeña parte (2-10%) del total de la concentración de 1 nM (lo que ya supone un tercio de la tubulina celular) se deduce que para un MSA con un mecanismo de acción como el de los taxanos el límite de concentración para su citotoxicidad está en 0,1-1 nM. Esto mismo aplica para una droga de distribución sistémica, para la que la cantidad mínima necesaria para matar las células tumorales dependerá de la cantidad de tubulina disponible para su unión, hecho que impone un límite práctico en las dosis mínimas que podrán ser usadas.

Existiendo este límite el objetivo no se centra en encontrar una droga con la citotoxicidad mayor posible (ninguno de los compuestos nuevos con altas afinidades tienen una citotoxicidad significativamente mayor, en células no resistentes, que las de taxol o docetaxel) sino encontrar aquel que venza el problema principal que surge en los pacientes en tratamiento con MSA (resistencias debidas a la glucoproteína-P) para lo que mejorar la afinidad semeja ser una buena estrategia.

Las células que sobreexpresan la P-gp siguen siendo sensibles a taxanos y se pueden seguir matando con taxol o docetaxel pero a concentraciones mucho más altas. Estas concentraciones tan altas afectan también a las células no tumorales siendo incluso matadas preferentemente, debido a su incapacidad de reducir la concentración intracelular de la droga, en lugar de salvarse de sus efectos gracias a su baja tasa de división.

Los datos de afinidad y citotoxicidad en las células A2780AD guardan la correlación esperada (figura 20) con la salvedad de que la pendiente de la recta es menor, lo que se puede explicar por la capacidad de estas células de reducir la concentración intracelular de las drogas. En esta correlación no se encuentran desviaciones para los valores de CI_{50} más bajos (el menor, 9 nM para chitax-40).

En estas células con resistencias múltiples a drogas los ligandos de alta afinidad son casi cien veces más citotóxicos que los empleados en clínica (taxol y docetaxel) y muestran índices de resistencia muy bajos (tanto como 1,3 para el compuesto de más alta afinidad, chitax-40). Además comprobamos que esto no es un caso extraordinario de esta pareja de células en particular, sino que ocurre también en otras parejas de origen diferente con la P-gp sobreexpresada como en las células de carcinoma de colon LoVo y las resistentes LoVo-Dox (tabla 7).

Si los índices de resistencia de cada compuesto se representan frente a sus afinidades de unión (figura 22) se observa una curva con forma de campana: los índices de resistencia alcanzan un máximo para los taxanos con afinidades por la tubulina y la P-gp similares y decrecen rápidamente a medida que las afinidades por la tubulina se apartan de las de la P-gp ya sea por exceso o por defecto. La excepción a esta norma se encuentra entre los compuestos con un átomo halogenado o un grupo metóxido en la posición meta del anillo aromático de C-2 (chitax-5, 6, 30, 34 y 35) que poseen un índice de resistencia mucho menor que otros compuestos con afinidades equivalentes.

Figura 22. Relación entre la resistencia a células que sobreexpresan la P-gp (A2780AD/A2780) y la afinidad de unión de los compuestos por su sitio en tubulina.

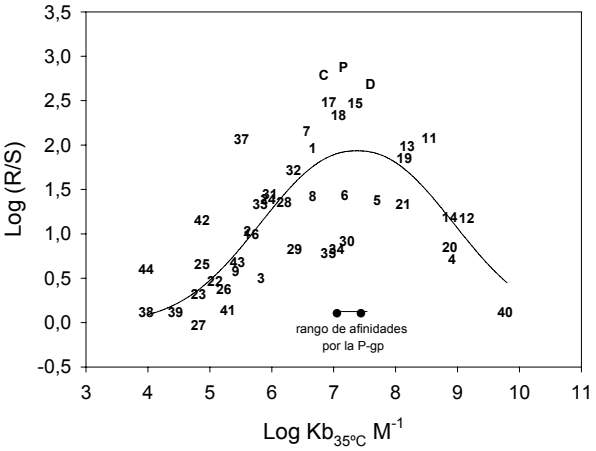

Estos resultados confirman datos previos del laboratorio para otros MSA con alta afinidad o que se unen covalentemente (lo que se podría considerar afinidad infinita), cuyas citotoxicidades no se ven afectadas por la sobreexpresión de la glucoproteína-P (ejemplos son la discodermolida y la cicloestreptina con CI_{50} en A2780/A2780AD de 60/53 nM (Barasoain, sin publicar) y 43,5/51 nM (Buey *et al.*, 2007) respectivamente).

Esto es una clara evidencia de que los ligandos con una alta afinidad de unión al sitio de taxol pueden superar las resistencias múltiples a drogas aparecidas por la sobreexpresión de la glucoproteína-P. El fundamento para este hallazgo es que en estas células la concentración intracelular libre de las drogas con alta afinidad de unión será muy baja.

Para entender mejor el papel de los diferentes parámetros que controlan la entrada y salida de los ligandos en la cantidad de tubulina unida a taxano que podemos encontrar, puede ser de utilidad un modelo simplificado de la unión de los taxanos a la tubulina y la P-gp.

El proceso puede ser descrito esquemáticamente con estas ecuaciones:

$$TX \underset{K_{+1}}{\rightleftarrows} T + X_i + P \underset{K_{+2}}{\rightleftarrows} PX_i \xrightarrow{k_{+3}} PX_e \xrightarrow{k_{+4}} P + X_e \underset{k_{-5}}{\overset{k_{+5}}{\rightleftarrows}} X_i$$

donde T es tubulina, X_i y X_e el taxano intracelular y extracelular respectivamente y P la glucoproteína-P. K_{+1} y K_{+2} son las constantes de unión de los taxanos a tubulina y P-gp, k_{+3} y k_{+4} las constantes cinéticas de los ligandos bombeados al exterior celular y k_{+5} y k_{-5} las constantes cinéticas del flujo pasivo de entrada y salida de los taxanos en la célula. Este sistema se modeló usando el programa kinsim con la idea de estudiar los efectos en los cambios en la relación entre las afinidades de los taxanos por la tubulina y la P-gp.

Para este sistema simplificado se consideró 20 µM la concentración de tubulina, los flujos pasivos de entrada y salida de los taxanos (k_{+5} y k_{-5}) se fijaron en 0,1 s^{-1} (velocidad compatible con el tiempo de equilibrio calculado en las células PtK2 (de Inés Díaz, 1995)). Otorgando una concentración arbitraria de 4 µM a la P-gp presente es obvio que es necesario que la velocidad de salida de la célula facilitada por la bomba (k_{+4}) sea mucho mayor que la pasiva para tener algún efecto. No obstante por encima de cierta razón entre ambas

constantes cinéticas (mayor de 1000:1) no se observa efecto sobre la cantidad de tubulina unida a ligando (figura 23).

El efecto de la sobreexpresión de la glucoproteína-P se muestra en la figura 24. En este modelo simple la cantidad de tubulina con ligando unido decrece muy rápidamente cuando la P-gp es sobreexpresada.

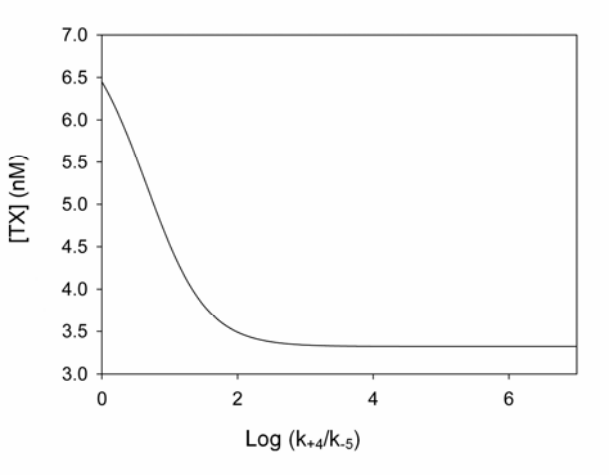

Figura 23. Dependencia de la concentración de ligando unido a tubulina (TX) con la relación entre el flujo pasivo del ligando y la velocidad de salida por bombeo activo. Para esta predicción se fijaron las concentraciones de taxano, tubulina y P-gp en 1, 20 y 4 μM, para K_{+1} y K_{+2} se tomó el valor de 10^7 M^{-1} para cada una de ellas.

Sin embargo, tal y como predecíamos, el incremento en la afinidad del taxano por la tubulina compensa este efecto de la P-gp (figura 25). Aumentando la afinidad de unión del ligando por su diana disminuye consecuentemente la concentración de éste libre, y a la par, el flujo de salida de la célula puesto que la velocidad de expulsión depende de la concentración del ligando intracelular libre. De manera que una concentración teórica de 4 μM de glucoproteína-P reduce 4 veces la cantidad de tubulina con ligando unido pero un aumento en la constante de unión del ligando a la tubulina compensa este efecto y restaura los niveles de tubulina unida al compuesto.

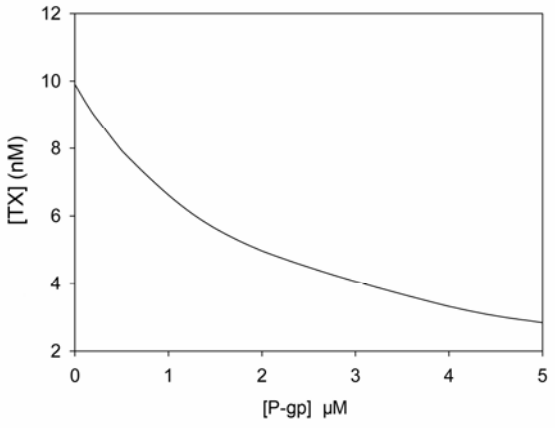

Figura 24. Dependencia de la concentración de ligando unido a tubulina (TX) con la concentración de P-gp. En esta predicción se fijaron las concentraciones de taxano y tubulina en 1 y 20 μM, para K_{+1} y K_{+2} se tomó el valor de 10^7 M^{-1} para cada una de ellas y 10^6 s^{-1} para k_{+3} y k_{+4}.

Está claro que para que un compuesto sea bombeado al exterior de la célula debe unirse antes a la P-gp, asumiendo que esta salida de la droga tenga una cinética con un comportamiento micaeliano el flujo de salida disminuirá si la concentración de ligando libre decrece. Al unirse fuertemente a su diana las concentraciones intracelulares de ligando libre serán del rango de sus constantes de disociación que en el caso de los compuestos de más alta afinidad está muy por debajo de la constante de disociación de la P-gp ($K_{d(tubulina)}$ (chitax-40) = 0,16 nM mientras que la $K_{d(P\text{-}gp)}$ ronda entre 35 nM (taxol) y 88 nM (chitax-7) (tabla 9) (Yang *et al.*, 2007)).

Todo esto implica que a las concentraciones a las que son capaces de ejercer su efecto citotóxico los compuestos de alta afinidad la eficacia de la P-gp

a la hora de bombearlos se ve reducida por un factor de entre 200 y 1000, lo que quiere decir que desde el punto de vista químico y en esta situación la sobreexpresión de la glucoproteína-P es irrelevante.

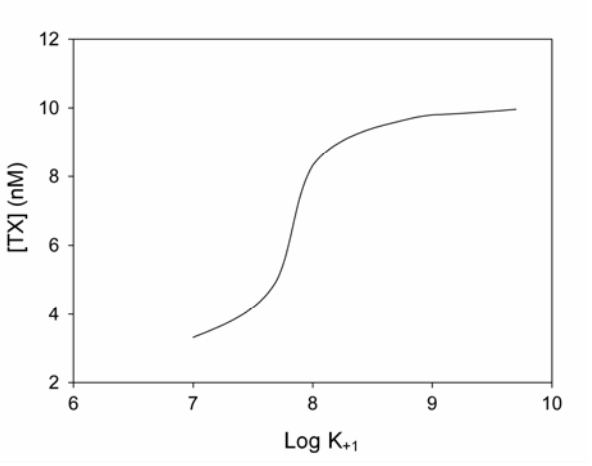

Figura 25. Dependencia de la concentración de ligando unido a tubulina (TX) con la constante de unión a tubulina (K_{+1}). En la predicción se fijaron las concentraciones de taxano, tubulina y P-gp en 1, 20 y 4 μM, para K_{+2} se tomó el valor de 10^7 M^{-1} y 10^6 s^{-1} para k_{+3} y k_{+4}.

Recordemos que los compuestos de baja afinidad también parecen soslayar la sobreexpresión de P-gp. Esto ocurre mediante un mecanismo muy diferente. Para alcanzar sus efectos citotóxicos estas drogas necesitan alcanzar concentraciones muy por encima de las de tubulina o P-gp de manera que la bomba se satura y no puede reducir la concentración intracelular de manera efectiva. Aunque esto sería otro método para evitar la resistencia múltiple a drogas proporcionada por la sobreexpresión de P-gp evidentemente su utilidad en clínica no es muy grande ya que las dosis necesarias para producir efectos citotóxicos serían tan altas que supondrían toda otra serie de efectos nocivos para el paciente.

Los resultados presentados en este trabajo junto con los de los trabajos de (Buey *et al.*, 2004; Buey *et al.*, 2005) apoyan la visión de que la afinidad de unión debería ser la variable primordial objeto de maximización para la mejora en la citotoxicidad de este tipo de compuestos a pesar del límite práctico para este parámetro observado en células no resistentes en una concentración de 1 nM. Además los ligandos de alta afinidad pueden vencer las resitencias múltiples a fármacos ofrecidas por la sobreexpresión de la glucoproteína-P bajando la concentración de ligando libre en la célula que puede ser expulsado por esta bomba.

De manera adicional los compuestos de alta afinidad presentados tendrán la ventaja de disminuir en cierta medida sus efectos secundarios tales como las alergias al surfactante, pues al tener IC_{50} menores que los fármacos usados en clínica (docetaxel y taxol) se podrían utilizar, muy probablemente, dosis menores que las que se usan hasta ahora en clínica con los compuestos mencionados.

7. EFECTO DE LAS MODIFICACIONES EN LA CITOTOXICIDAD DE LOS COMPUESTOS EN CÉLULAS CON TUBULINAS MUTANTES.

Adicionalmente a la resistencia múltiple a drogas conferida por la bomba de membrana anteriormente discutida, se han descrito también resistencias a taxol causadas por mutaciones en la tubulina (Monzo *et al.*, 1999). Aunque la

importancia clínica de este caso ha sido puesta en duda en algunos trabajos (Mesquita *et al.*, 2005), se encuentran, al menos, ejemplos *in vitro* (Giannakakou *et al.*, 1997; Schibler y Cabral, 1986), de modo que la discusión sobre su aparición en pacientes está abierta (se pueden consultar revisiones sobre el tema en (Berrieman *et al.*, 2004; Orr *et al.*, 2003; Pusztai, 2007)) aunque, en cualquier caso, su incidencia no debe ser mayoritaria (Hasegawa *et al.*, 2002).

Nos preguntamos si los mismos taxanos que tan buenos resultados tienen en el aumento de la afinidad por la tubulina y en el mantenimiento de su citotoxicidad sobre células con altos niveles de expresión de la glucoproteína-P son también capaces de conservar su toxicidad en células cuya resitencia a taxol viene dada por la aparición de mutaciones en su tubulina.

Con este objetivo probamos nuestros compuestos en tres clones de 1A9.

Por una parte en las células A8, células que nos servirían de control pues su mutación en β tubulina (Thr274 está sustituida por Ile) les confiere resistencia a epoA (Wang *et al.*, 2005) pero apenas muestran diferencias en su sensibilidad a taxol respecto a la línea celular parental con tubulina silvestre lo que se comprobó con los compuestos de este estudio.

Por otra parte probamos los clones PTX10 y PTX22, líneas celulares resistentes a taxol (Giannakakou *et al.*, 1997). En ambos casos encontramos modificaciones que mejoraban notablemente el índice de resistencia respecto a la molécula patrón e incluso en ciertos casos resultaban en mayores toxicidades sobre las células con las tubulinas mutantes (consultar tabla 8). Sorprende descubrir que estas modificaciones favorables son las mismas para ambos tipos de mutaciones y a su vez el mismo tipo de cambios sobre la molécula de taxol que ayudan a soslayar la resistencia por sobreexpresión de P-gp. Aunque modificaciones similares ayudan a la citotoxicidad en estas líneas celulares y, probablemente, a su afinidad por sus correspondientes tubulinas mutantes (pero aún no la hemos podido medir) la explicación para esto es algo diferente.

Tenemos dos situaciones distintas:

I. En el caso de la tubulina presente en las células PTX10 hay una sustitución en la posición 270 de una fenilalanina, con su voluminosa cadena lateral hidrófoba, por una valina, que tiene una cadena mucho menor, lo que probablemente viene acompañado con un reajuste del empaquetamiento de los residuos que forman el bolsillo y una mayor solvatación de éste (figura 26). Además esta posición está justo en el inicio del lazo M por lo que la mutación le debe conferir mayor movilidad y por ende debe hacer la unión del ligando menos favorable.

II. La mutación en la tubulina de las células PTX22 introduce una treonina donde antes estaba la serina 364 (figura 26) (aunque el aminoácido descrito para esta posición en la tubulina βI humana -isotipo mayoritario en estas células (Giannakakou *et al.*, 1997)- es una alanina, aquí nos referiremos al cambio de una serina, residuo que aparece en la secuencia usada para nuestro

modelado -tubulina βII bovina sobre la que se resuelve la estructura del dímero en Nogales *et al.* (1998)-, sobre el que podemos discutir cómo cambia el entorno en el sitio). Esta serina se encuentra entre el final de un lazo y el comienzo de una lámina beta y parece estar implicada en un puente de hidrógeno con el oxígeno del carbonilo de la metionina 363. Es una zona con un espacio bastante restringido y la introducción de un grupo metilo extra con la treonina puede traer como consecuencia la reorientación del hidroxilo de manera que ya no participe en este puente de hidrógeno y, de manera adicional, el metilo se colocará muy próximo al anillo de la prolina 358. Como consecuencia de esta nueva organización las diferentes prolinas situadas en el lazo al que se unen los taxanos por su cara inferior pueden cambiar su estructura y así modificar la conformación del lazo de manera que disminuya la interacción favorable con este tipo de drogas.

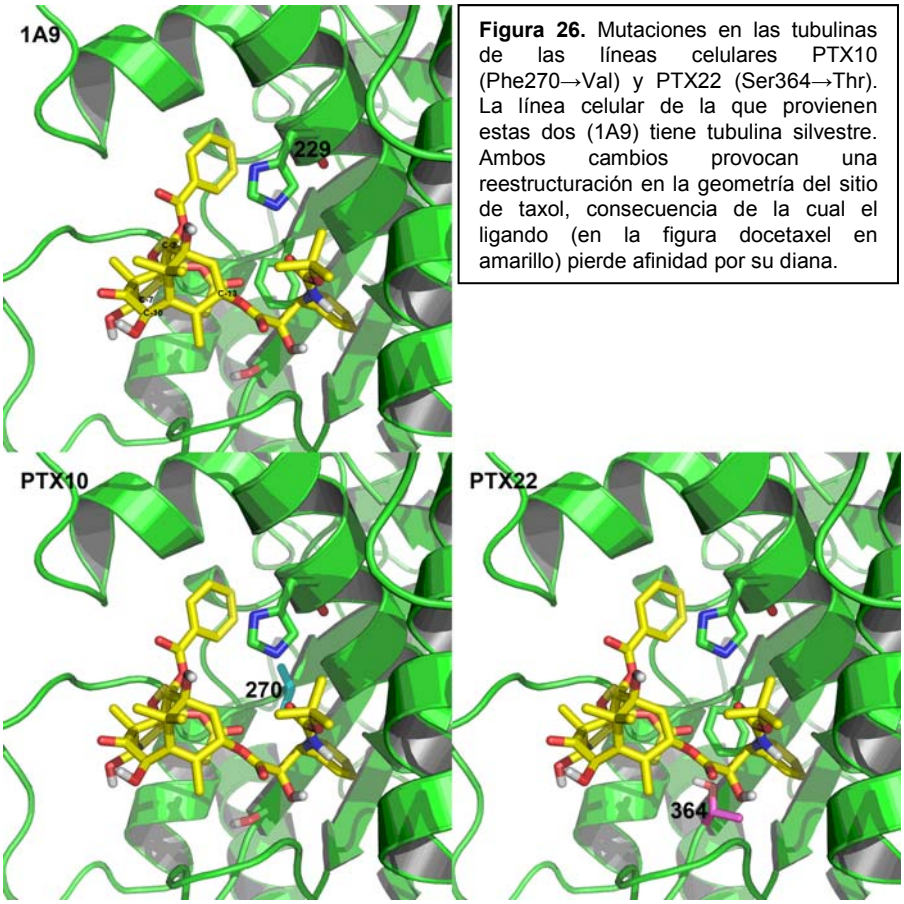

Figura 26. Mutaciones en las tubulinas de las líneas celulares PTX10 (Phe270→Val) y PTX22 (Ser364→Thr). La línea celular de la que provienen estas dos (1A9) tiene tubulina silvestre. Ambos cambios provocan una reestructuración en la geometría del sitio de taxol, consecuencia de la cual el ligando (en la figura docetaxel en amarillo) pierde afinidad por su diana.

Los cambios en la geometría del sitio de taxol provocados por estas mutaciones hacen que los taxanos basen su unión en las interacciones que establezcan con la histidina 229, el aspártico 26 y el bolsillo hidrofóbico en el que se introduce el anillo fenilo en C-2. Por esta razón de las tres moléculas patrón el docetaxel es la que muestra menor resistencia a estas células ya que su terc-butilo en C-13 le confiere mayor afinidad de unión a la tubulina. A su vez cualquier sustitución en C-2 que hace aumentar la afinidad por la tubulina silvestre aumentará también la de estas tubulinas mutantes disminuyendo la

resistencia celular a estos taxanos ya que este anillo no interacciona con ninguna de las zonas afectadas por la reorganización del sitio provocado por cualquiera de estas mutaciones.

CONCLUSIONES.

1.- La afinidad de los taxoles por su sitio de unión está relacionada con su citotoxicidad de forma parecida a como se describe para las epotilonas.

2.- Las modificaciones más efectivas entre las probadas para aumentar la afinidad de los taxanos por su sitio son:

- un grupo terc-butilo en la cadena lateral de C-13

- un grupo propionilo en C-10

- un grupo hidroxilo en C-7

- un grupo azida en la posición meta del anillo benzóxido de C-2

3.- Los sustituyentes en C-13 y C-2 tienen un papel importante en la interacción con la histidina 229 en el bolsillo del taxol lo que les confiere gran influencia sobre la afinidad de la molécula.

4.- Las modificaciones en la "parte norte" influyen en el diámetro de los microtúbulos inducidos por las moléculas que las contienen:
- aumentándolo al aumentar el tamaño del grupo introducido en C-7.
- de manera opuesta en el caso de las modificaciones en C-10.

5.- Los compuestos con afinidades mayores por los microtúbulos, son capaces de evitar la resistencia causada por la sobreexpresión de glucoproteína-P aún cuando su afinidad por ésta no varíe. Esto se debe a que la alta afinidad por la tubulina ejerce de fuerza atractora del compuesto al interior celular y deja una concentración de ligando libre en la célula por debajo de la constante de disociación por la P-gp por lo que ésta no es capaz de bombearlo al exterior.

6.- Los mismos compuestos con altas afinidades son capaces de evitar la resistencia a taxol causada por las mutaciones en tubulina contenidas en las líneas celulares PTX10 y PTX22.

BIBLIOGRAFÍA.

Abramowitz, M. y Stegun, I. A. (1965) Handbook of Mathematical Functions. Dover Publications

Altieri, D. C. (2003) Survivin, versatile modulation of cell division and apoptosis in cancer. Oncogene. 22 (53), 8581-8589

Amos, L. y Klug, A. (1974) Arrangement of subunits in flagellar microtubules. J Cell Sci. 14 (3), 523-549

Anderson, H. J.; Coleman, J. E.; Andersen, R. J. y Roberge, M. (1997) Cytotoxic peptides hemiasterlin, hemiasterlin A and hemiasterlin B induce mitotic arrest and abnormal spindle formation. Cancer Chemother Pharmacol. 39 (3), 223-226

Andreu, J. M.; Gorbunoff, M. J.; Lee, J. C. y Timasheff, S. N. (1984) Interaction of tubulin with bifunctional colchicine analogues: an equilibrium study. Biochemistry. 23 (8), 1742-1752

Andreu, J. M.; Bordas, J.; Diaz, J. F.; Garcia de Ancos, J.; Gil, R.; Medrano, F. J.; Nogales, E.; Pantos, E. y Towns-Andrews, E. (1992) Low resolution structure of microtubules in solution. Synchrotron X-ray scattering and electron microscopy of taxol-induced microtubules assembled from purified tubulin in comparison with glycerol and MAP-induced microtubules. J Mol Biol. 226 (1), 169-184

Andreu, J. M.; Diaz, J. F.; Gil, R.; de Pereda, J. M.; Garcia de Lacoba, M.; Peyrot, V.; Briand, C.; Towns-Andrews, E. y Bordas, J. (1994) Solution structure of Taxotere-induced microtubules to 3-nm resolution. The change in protofilament number is linked to the binding of the taxol side chain. J Biol Chem. 269 (50), 31785-31792

Andreu, J. M. (2007) Large scale purification of brain tubulin with the modified Weisenberg procedure. Methods Mol Med. 137 17-28

Bai, R.; Pettit, G. R. y Hamel, E. (1990) Dolastatin 10, a powerful cytostatic peptide derived from a marine animal. Inhibition of tubulin polymerization mediated through the vinca alkaloid binding domain. Biochem Pharmacol. 39 (12), 1941-1949

Bai, R.; Cichacz, Z. A.; Herald, C. L.; Pettit, G. R. y Hamel, E. (1993) Spongistatin 1, a highly cytotoxic, sponge-derived, marine natural product that inhibits mitosis, microtubule assembly, and the binding of vinblastine to tubulin. Mol Pharmacol. 44 (4), 757-766

Bai, R.; Durso, N. A.; Sackett, D. L. y Hamel, E. (1999) Interactions of the sponge-derived antimitotic tripeptide hemiasterlin with tubulin: comparison with dolastatin 10 and cryptophycin 1. Biochemistry. 38 (43), 14302-14310

Bai, R. L.; Paull, K. D.; Herald, C. L.; Malspeis, L.; Pettit, G. R. y Hamel, E. (1991) Halichondrin B and homohalichondrin B, marine natural products binding in the vinca domain of tubulin. Discovery of tubulin-based mechanism of action by analysis of differential cytotoxicity data. J Biol Chem. 266 (24), 15882-15889

Bai, Ruoli; Pei, Xue-Feng; Boyé, Olivier; Getahun, Zelleka; Grover, Surinder; Bekisz, Joseph; Nguyen, Nga Y.; Brossi, Arnold y Hamel, Ernest (1996) Identification of Cysteine 354 of beta-Tubulin as Part of the Binding Site for the A Ring of Colchicine. J. Biol. Chem. 271 (21), 12639-12645

Bergstralh, D. T. y Ting, J. P. (2006) Microtubule stabilizing agents: their molecular signaling consequences and the potential for enhancement by drug combination. Cancer Treat Rev. 32 (3), 166-179

Berrieman, H. K.; Lind, M. J. y Cawkwell, L. (2004) Do beta-tubulin mutations have a role in resistance to chemotherapy? Lancet Oncol. 5 (3), 158-164

Blagosklonny, M. V. (2007) Mitotic arrest and cell fate: why and how mitotic inhibition of transcription drives mutually exclusive events. Cell Cycle. 6 (1), 70-74

Blangy, A.; Lane, H. A.; d'Herin, P.; Harper, M.; Kress, M. y Nigg, E. A. (1995) Phosphorylation by p34cdc2 regulates spindle association of human Eg5, a kinesin-related motor essential for bipolar spindle formation in vivo. Cell. 83 (7), 1159-1169

Bollag, D. M.; McQueney, P. A.; Zhu, J.; Hensens, O.; Koupal, L.; Liesch, J.; Goetz, M.; Lazarides, E. y Woods, C. M. (1995) Epothilones, a new class of microtubule-stabilizing agents with a taxol-like mechanism of action. Cancer Res. 55 (11), 2325-2333

Borisy, G. G. y Taylor, E. W. (1967a) The mechanism of action of colchicine. Binding of colchincine-3H to cellular protein. J Cell Biol. 34 (2), 525-533

Borisy, G. G. y Taylor, E. W. (1967b) The mechanism of action of colchicine. Colchicine binding to sea urchin eggs and the mitotic apparatus. J Cell Biol. 34 (2), 535-548

Buey, R. M.; Diaz, J. F.; Andreu, J. M.; O'Brate, A.; Giannakakou, P.; Nicolaou, K. C.; Sasmal, P. K.; Ritzen, A. y Namoto, K. (2004) Interaction of epothilone analogs with the paclitaxel binding site: relationship between binding affinity, microtubule stabilization, and cytotoxicity. Chem Biol. 11 (2), 225-236

Buey, R. M.; Barasoain, I.; Jackson, E.; Meyer, A.; Giannakakou, P.; Paterson, I.; Mooberry, S.; Andreu, J. M. y Diaz, J. F. (2005) Microtubule interactions with

chemically diverse stabilizing agents: thermodynamics of binding to the paclitaxel site predicts cytotoxicity. Chem Biol. 12 (12), 1269-1279

Buey, R. M.; Calvo, E.; Barasoain, I.; Pineda, O.; Edler, M. C.; Matesanz, R.; Cerezo, G.; Vanderwal, C. D.; Day, B. W.; Sorensen, E. J.; Lopez, J. A.; Andreu, J. M.; Hamel, E. y Diaz, J. F. (2007) Cyclostreptin binds covalently to microtubule pores and lumenal taxoid binding sites. Nat Chem Biol. 3 (2), 117-125

Castedo, M.; Perfettini, J. L.; Roumier, T.; Andreau, K.; Medema, R. y Kroemer, G. (2004) Cell death by mitotic catastrophe: a molecular definition. Oncogene. 23 (16), 2825-2837

Cornell, Wendy D.; Cieplak, Piotr; Bayly, Christopher I.; Gould, Ian R.; Merz, Kenneth M.; Ferguson, David M.; Spellmeyer, David C.; Fox, Thomas; Caldwell, James W. y Kollman, Peter A. (1995) A Second Generation Force Field for the Simulation of Proteins, Nucleic Acids, and Organic Molecules. J. Am. Chem. Soc. 117 (19), 5179-5197

Cragg, G. M. y Newman, D. J. (2004) A tale of two tumor targets: topoisomerase I and tubulin. The Wall and Wani contribution to cancer chemotherapy. J Nat Prod. 67 (2), 232-244

Cutts, J. H.; Beer, C. T. y Noble, R. L. (1960) Biological properties of Vincaleukoblastine, an alkaloid in Vinca rosea Linn, with reference to its antitumor action. Cancer Res. 20 1023-1031

Chaudhary, A. G.; Rimoldi, J. M. y Kingston, D. G. I. (1993) Modified Taxols. 10. Preparation of 7-Deoxytaxol, a Highly Bioactive Taxol Derivative, and Interconversion of Taxol and 7-epi-Taxol. J Org Chem. 58 3798-3799

Chaudhary, Ashok G. y Kingston, David G. I. (1993) Synthesis of 10-deacetoxytaxol and 10-deoxytaxotere. Tetrahedron Letters. 34 (31), 4921-4924

Chaudhary, Ashok G.; Gharpure, Milind M.; Rimoldi, John M.; Chordia, Mahendra D.; Kingston, David G. I.; Grover, Surinder; Lin, Chii M.; Hamel, Ernest y Gunatilaka, A. A. Leslie (1994) Unexpectedly Facile Hydrolysis of the 2-Benzoate Group of Taxol and Syntheses of Analogs with Increased Activities. J. Am. Chem. Soc. 116 (9), 4097-4098

Checchi, P. M.; Nettles, J. H.; Zhou, J.; Snyder, J. P. y Joshi, H. C. (2003) Microtubule-interacting drugs for cancer treatment. Trends Pharmacol Sci. 24 (7), 361-365

Chen, S. H.; Huang, S.; Kant, J.; Fairchild, C.; Wei, J. y Farina, V. (1993a) Synthesis of 7-Deoxy- and 7,10-Dideoxytaxol via Radical Intermediates. J Org Chem. 58 5028-5029

Chen, Shu-Hui; Wei, Jian-Mei y Farina, Vittorio (1993b) Taxol structure-activity relationships: Synthesis and biological evaluation of 2-deoxytaxol. Tetrahedron Letters. 34 (20), 3205-3206

Chen, W. y Zhang, D. (2004) Kinetochore fibre dynamics outside the context of the spindle during anaphase. Nat Cell Biol. 6 (3), 227-231

Chen, Zhong-liang; Wang, Bao-de y Chen, Min-quin (1987) Steroidal bitter principles from tacca plantaginea structures of taccalonolide A and B. Tetrahedron Letters. 28 (15), 1673-1675

Chordia, Mahendra D.; Chaudhary, Ashok G.; Kingston, David G. I.; Qing Jiang, Yuan y Hamel, Ernest (1994) Synthesis and biological evaluation of 4-deacetoxypaclitaxel. Tetrahedron Letters. 35 (37), 6843-6846

Chretien, D.; Jainosi, I.; Taveau, J. C. y Flyvbjerg, H. (1999) Microtubule's conformational cap. Cell Struct Funct. 24 (5), 299-303

Chu, E.; Callender, M. A.; Farrell, M. P. y Schmitz, J. C. (2003) Thymidylate synthase inhibitors as anticancer agents: from bench to bedside. Cancer Chemother Pharmacol. 52 Suppl 1 S80-89

de Inés Díaz, C. (1995) Interacción de microtúbulos celulares con anticuerpos específicos y con nuevos compuestos antitumorales. Tesis doctoral. Facultad de Ciencias. Universidad Autónoma de Madrid

Denis, Jean Noel; Greene, Andrew E.; Guenard, Daniel; Gueritte-Voegelein, Francoise; Mangatal, Lydie y Potier, Pierre (1988) Highly efficient, practical approach to natural taxol. J. Am. Chem. Soc. 110 (17), 5917-5919

Dervieux, T.; Brenner, T. L.; Hon, Y. Y.; Zhou, Y.; Hancock, M. L.; Sandlund, J. T.; Rivera, G. K.; Ribeiro, R. C.; Boyett, J. M.; Pui, C. H.; Relling, M. V. y Evans, W. E. (2002) De novo purine synthesis inhibition and antileukemic effects of mercaptopurine alone or in combination with methotrexate in vivo. Blood. 100 (4), 1240-1247

Diaz, J. F. y Andreu, J. M. (1993) Assembly of purified GDP-tubulin into microtubules induced by taxol and taxotere: reversibility, ligand stoichiometry, and competition. Biochemistry. 32 (11), 2747-2755

Diaz, J. F.; Menendez, M. y Andreu, J. M. (1993) Thermodynamics of ligand-induced assembly of tubulin. Biochemistry. 32 (38), 10067-10077

Diaz, J. F.; Pantos, E.; Bordas, J. y Andreu, J. M. (1994) Solution structure of GDP-tubulin double rings to 3 nm resolution and comparison with microtubules. J Mol Biol. 238 (2), 214-225

Diaz, J. F.; Strobe, R.; Engelborghs, Y.; Souto, A. A. y Andreu, J. M. (2000) Molecular recognition of taxol by microtubules. Kinetics and thermodynamics of binding of fluorescent taxol derivatives to an exposed site. J Biol Chem. 275 (34), 26265-26276

Diaz, J. F.; Barasoain, I. y Andreu, J. M. (2003) Fast kinetics of Taxol binding to microtubules. Effects of solution variables and microtubule-associated proteins. J Biol Chem. 278 (10), 8407-8419

Diaz, J. F.; Barasoain, I.; Souto, A. A.; Amat-Guerri, F. y Andreu, J. M. (2005) Macromolecular accessibility of fluorescent taxoids bound at a paclitaxel binding site in the microtubule surface. J Biol Chem. 280 (5), 3928-3937

Diaz, J. F. y Buey, R. M. (2007) Characterizing ligand-microtubule binding by competition methods. Methods Mol Med. 137 245-260

Díaz, J.F.; Andreu, J.M. y Jiménez-Barbero, J. (2008) The interaction of microtubules with stabilizers characterized at biochemical and structural levels. . Topics in Current Chemistry. DOI: 10.1007/128_2008_12

Ditchfield, C.; Johnson, V. L.; Tighe, A.; Ellston, R.; Haworth, C.; Johnson, T.; Mortlock, A.; Keen, N. y Taylor, S. S. (2003) Aurora B couples chromosome alignment with anaphase by targeting BubR1, Mad2, and Cenp-E to kinetochores. J Cell Biol. 161 (2), 267-280

Downing, K. H. y Nogales, E. (1999) Crystallographic structure of tubulin: implications for dynamics and drug binding. Cell Struct Funct. 24 (5), 269-275

Dubois, Joëlle; Guénard, Daniel; Guéritte-Voegelein, Françoise; Guedira, Nourredine; Potier, Pierre; Gillet, Brigitte y Beloeil, Jean-Claude (1993) Conformation of Taxotere® and analogues determined by NMR spectroscopy and molecular modeling studies. Tetrahedron. 49 (30), 6533-6544

Duflos, A.; Kruczynski, A. y Barret, J. M. (2002) Novel aspects of natural and modified vinca alkaloids. Curr Med Chem Anticancer Agents. 2 (1), 55-70

Erickson, H. P. y Stoffler, D. (1996) Protofilaments and rings, two conformations of the tubulin family conserved from bacterial FtsZ to alpha/beta and gamma tubulin. J Cell Biol. 135 (1), 5-8

Ganesh, T. (2007) Improved biochemical strategies for targeted delivery of taxoids. Bioorg Med Chem. 15 (11), 3597-3623

Gao, Q. y Chen, S. H. (1996) An unprecedented side chain conformation of paclitaxel (Taxol(R)): Crystal structure of 7-mesylpaclitaxel. Tetrahedron Letters. 37 (20), 3425-3428

Garrett M. Morris, David S. Goodsell Robert S. Halliday Ruth Huey William E. Hart Richard K. Belew Arthur J. Olson (1998) Automated docking using a Lamarckian genetic algorithm and an empirical binding free energy function. Journal of Computational Chemistry. 19 (14), 1639-1662

Gewirtz, D. A. (1999) A critical evaluation of the mechanisms of action proposed for the antitumor effects of the anthracycline antibiotics adriamycin and daunorubicin. Biochem Pharmacol. 57 (7), 727-741

Giannakakou, P.; Sackett, D. L.; Kang, Y. K.; Zhan, Z.; Buters, J. T.; Fojo, T. y Poruchynsky, M. S. (1997) Paclitaxel-resistant human ovarian cancer cells have mutant beta-tubulins that exhibit impaired paclitaxel-driven polymerization. J Biol Chem. 272 (27), 17118-17125

Gidding, C. E.; Kellie, S. J.; Kamps, W. A. y de Graaf, S. S. (1999) Vincristine revisited. Crit Rev Oncol Hematol. 29 (3), 267-287

Gordon, J. C.; Myers, J. B.; Folta, T.; Shoja, V.; Heath, L. S. y Onufriev, A. (2005) H++: a server for estimating pKas and adding missing hydrogens to macromolecules. Nucleic Acids Res. 33 (Web Server issue), W368-371

Grandi, M.; Geroni, C. y Giuliani, F. C. (1986) Isolation and characterization of a human colon adenocarcinoma cell line resistant to doxorubicin. Br J Cancer. 54 (3), 515-518

Guéritte-Voegelein, F., Senilh, V., David, B., Guenard, D., Potier, P. (1986) Chemical studies of 10-deacetyl baccatin III. Hemisynthesis of taxol derivatives. Tetrahedron. 42 4451-4460

Hamel, E. y Lin, C. M. (1983) Interactions of combretastatin, a new plant-derived antimitotic agent, with tubulin. Biochem Pharmacol. 32 (24), 3864-3867

Hamel, E. (1992) Natural products which interact with tubulin in the vinca domain: maytansine, rhizoxin, phomopsin A, dolastatins 10 and 15 and halichondrin B. Pharmacol Ther. 55 (1), 31-51

Hasegawa, S.; Miyoshi, Y.; Egawa, C.; Ishitobi, M.; Tamaki, Y.; Monden, M. y Noguchi, S. (2002) Mutational analysis of the class I beta-tubulin gene in human breast cancer. Int J Cancer. 101 (1), 46-51

Hauf, S.; Cole, R. W.; LaTerra, S.; Zimmer, C.; Schnapp, G.; Walter, R.; Heckel, A.; van Meel, J.; Rieder, C. L. y Peters, J. M. (2003) The small molecule Hesperadin reveals a role for Aurora B in correcting kinetochore-microtubule attachment and in maintaining the spindle assembly checkpoint. J Cell Biol. 161 (2), 281-294

Hayden, J. H.; Bowser, S. S. y Rieder, C. L. (1990) Kinetochores capture astral microtubules during chromosome attachment to the mitotic spindle: direct visualization in live newt lung cells. J Cell Biol. 111 (3), 1039-1045

He, L.; Jagtap, P. G.; Kingston, D. G.; Shen, H. J.; Orr, G. A. y Horwitz, S. B. (2000) A common pharmacophore for Taxol and the epothilones based on the biological activity of a taxane molecule lacking a C-13 side chain. Biochemistry. 39 (14), 3972-3978

Hennessy, M. y Spiers, J. P. (2007) A primer on the mechanics of P-glycoprotein the multidrug transporter. Pharmacol Res. 55 (1), 1-15

Honore, S.; Pasquier, E. y Braguer, D. (2005) Understanding microtubule dynamics for improved cancer therapy. Cell Mol Life Sci. 62 (24), 3039-3056

Hsiang, Y. H.; Hertzberg, R.; Hecht, S. y Liu, L. F. (1985) Camptothecin induces protein-linked DNA breaks via mammalian DNA topoisomerase I. J Biol Chem. 260 (27), 14873-14878

Hsu, J. Y.; Sun, Z. W.; Li, X.; Reuben, M.; Tatchell, K.; Bishop, D. K.; Grushcow, J. M.; Brame, C. J.; Caldwell, J. A.; Hunt, D. F.; Lin, R.; Smith, M. M. y Allis, C. D. (2000) Mitotic phosphorylation of histone H3 is governed by Ipl1/aurora kinase and Glc7/PP1 phosphatase in budding yeast and nematodes. Cell. 102 (3), 279-291

Hung, D. T.; Chen, J. y Schreiber, S. L. (1996) (+)-Discodermolide binds to microtubules in stoichiometric ratio to tubulin dimers, blocks taxol binding and results in mitotic arrest. Chem Biol. 3 (4), 287-293

Jackson, J. R.; Patrick, D. R.; Dar, M. M. y Huang, P. S. (2007) Targeted anti-mitotic therapies: can we improve on tubulin agents? Nat Rev Cancer. 7 (2), 107-117

Jimenez-Barbero, J.; Canales, A.; Northcote, P. T.; Buey, R. M.; Andreu, J. M. y Diaz, J. F. (2006) NMR determination of the bioactive conformation of peloruside A bound to microtubules. J Am Chem Soc. 128 (27), 8757-8765

Johnson, I. S.; Wright, H. F.; Svoboda, G. H. y Vlantis, J. (1960) Antitumor principles derived from Vinca rosea Linn. I. Vincaleukoblastine and leurosine. Cancer Res. 20 1016-1022

Jordan, M. A.; Margolis, R. L.; Himes, R. H. y Wilson, L. (1986) Identification of a distinct class of vinblastine binding sites on microtubules. Journal of Molecular Biology. 187 (1), 61-73

Jordan, M. A.; Thrower, D. y Wilson, L. (1991) Mechanism of inhibition of cell proliferation by Vinca alkaloids. Cancer Res. 51 (8), 2212-2222

Jordan, M. A.; Toso, R. J.; Thrower, D. y Wilson, L. (1993) Mechanism of mitotic block and inhibition of cell proliferation by taxol at low concentrations. Proc Natl Acad Sci U S A. 90 (20), 9552-9556

Jordan, M. A.; Wendell, K.; Gardiner, S.; Derry, W. B.; Copp, H. y Wilson, L. (1996) Mitotic block induced in HeLa cells by low concentrations of paclitaxel (Taxol) results in abnormal mitotic exit and apoptotic cell death. Cancer Res. 56 (4), 816-825

Jordan, M. A. (2002) Mechanism of action of antitumor drugs that interact with microtubules and tubulin. Curr Med Chem Anticancer Agents. 2 (1), 1-17

Jordan, M. A. y Wilson, L. (2004) Microtubules as a target for anticancer drugs. Nat Rev Cancer. 4 (4), 253-265

Kaplan, H. S. (1970) Radiobiology's Contribution to Radiotherapy: Promise or Mirage? Failla Memorial Lecture Radiation Research. 43 (2), 460-476

Kelland, L. (2007) The resurgence of platinum-based cancer chemotherapy. Nat Rev Cancer. 7 (8), 573-584

Kerksiek, K.; Mejillano, M. R.; Schwartz, R. E.; Georg, G. I. y Himes, R. H. (1995) Interaction of cryptophycin 1 with tubulin and microtubules. FEBS Lett. 377 (1), 59-61

Kingston, D. G.; Chaudhary, A. G.; Chordia, M. D.; Gharpure, M.; Gunatilaka, A. A.; Higgs, P. I.; Rimoldi, J. M.; Samala, L.; Jagtap, P. G.; Giannakakou, P.; Jiang, Y. Q.; Lin, C. M.; Hamel, E.; Long, B. H.; Fairchild, C. R. y Johnston, K. A. (1998) Synthesis and biological evaluation of 2-acyl analogues of paclitaxel (Taxol). J Med Chem. 41 (19), 3715-3726

Kingston, D. G.; Bane, S. y Snyder, J. P. (2005) The taxol pharmacophore and the T-taxol bridging principle. Cell Cycle. 4 (2), 279-289

Kingston, D. G. (2007) The shape of things to come: structural and synthetic studies of taxol and related compounds. Phytochemistry. 68 (14), 1844-1854

Kingston, D. G. y Newman, D. J. (2007) Taxoids: cancer-fighting compounds from nature. Curr Opin Drug Discov Devel. 10 (2), 130-144

Kinoshita, K.; Noetzel, T. L.; Pelletier, L.; Mechtler, K.; Drechsel, D. N.; Schwager, A.; Lee, M.; Raff, J. W. y Hyman, A. A. (2005) Aurora A phosphorylation of TACC3/maskin is required for centrosome-dependent microtubule assembly in mitosis. J Cell Biol. 170 (7), 1047-1055

Lakowicz, J R (1999) Principles of fluorescence spectroscopy. Kluwer Academic/ Plenum Publishers

Lee, J. C.; Frigon, R. P. y Timasheff, S. N. (1973) The chemical characterization of calf brain microtubule protein subunits. J Biol Chem. 248 (20), 7253-7262

Ling, Y. H.; Tornos, C. y Perez-Soler, R. (1998) Phosphorylation of Bcl-2 is a marker of M phase events and not a determinant of apoptosis. J Biol Chem. 273 (30), 18984-18991

Liu, Q. y Ruderman, J. V. (2006) Aurora A, mitotic entry, and spindle bipolarity. Proc Natl Acad Sci U S A. 103 (15), 5811-5816

Liu, R.; Siemiarczuk, A. y Sharom, F. J. (2000) Intrinsic fluorescence of the P-glycoprotein multidrug transporter: sensitivity of tryptophan residues to binding of drugs and nucleotides. Biochemistry. 39 (48), 14927-14938

Long, B. H.; Carboni, J. M.; Wasserman, A. J.; Cornell, L. A.; Casazza, A. M.; Jensen, P. R.; Lindel, T.; Fenical, W. y Fairchild, C. R. (1998) Eleutherobin, a novel cytotoxic agent that induces tubulin polymerization, is similar to paclitaxel (Taxol). Cancer Res. 58 (6), 1111-1115

Lowe, J.; Li, H.; Downing, K. H. y Nogales, E. (2001) Refined structure of alpha beta-tubulin at 3.5 A resolution. J Mol Biol. 313 (5), 1045-1057

Mabjeesh, N. J.; Escuin, D.; LaVallee, T. M.; Pribluda, V. S.; Swartz, G. M.; Johnson, M. S.; Willard, M. T.; Zhong, H.; Simons, J. W. y Giannakakou, P. (2003) 2ME2 inhibits tumor growth and angiogenesis by disrupting microtubules and dysregulating HIF. Cancer Cell. 3 (4), 363-375

Margolis, R. L. y Wilson, L. (1978) Opposite end assembly and disassembly of microtubules at steady state in vitro. Cell. 13 (1), 1-8

Markman, M. (2003) Managing taxane toxicities. Support Care Cancer. 11 (3), 144-147

Matalon, S. T.; Ornoy, A. y Lishner, M. (2004) Review of the potential effects of three commonly used antineoplastic and immunosuppressive drugs

(cyclophosphamide, azathioprine, doxorubicin on the embryo and placenta). Reprod Toxicol. 18 (2), 219-230

Matesanz, R.; Barasoain, I.; Yang, C. G.; Wang, L.; Li, X.; de Ines, C.; Coderch, C.; Gago, F.; Barbero, J. J.; Andreu, J. M.; Fang, W. S. y Diaz, J. F. (2008) Optimization of taxane binding to microtubules: binding affinity dissection and incremental construction of a high-affinity analog of paclitaxel. Chem Biol. 15 (6), 573-585

Mesquita, B.; Veiga, I.; Pereira, D.; Tavares, A.; Pinto, I. M.; Pinto, C.; Teixeira, M. R. y Castedo, S. (2005) No significant role for beta tubulin mutations and mismatch repair defects in ovarian cancer resistance to paclitaxel/cisplatin. BMC Cancer. 5 101

Miki, Harukata; Okada, Yasushi y Hirokawa, Nobutaka (2005) Analysis of the kinesin superfamily: insights into structure and function. Trends in Cell Biology. 15 (9), 467-476

Mitchison, T. y Kirschner, M. (1984) Dynamic instability of microtubule growth. Nature. 312 (5991), 237-242

Modok, S.; Mellor, H. R. y Callaghan, R. (2006) Modulation of multidrug resistance efflux pump activity to overcome chemoresistance in cancer. Curr Opin Pharmacol. 6 (4), 350-354

Mollinedo, F. y Gajate, C. (2003) Microtubules, microtubule-interfering agents and apoptosis. Apoptosis. 8 (5), 413-450

Monzo, M.; Rosell, R.; Sanchez, J. J.; Lee, J. S.; O'Brate, A.; Gonzalez-Larriba, J. L.; Alberola, V.; Lorenzo, J. C.; Nunez, L.; Ro, J. Y. y Martin, C. (1999) Paclitaxel resistance in non-small-cell lung cancer associated with beta-tubulin gene mutations. J Clin Oncol. 17 (6), 1786-1793

Mooberry, S. L.; Tien, G.; Hernandez, A. H.; Plubrukarn, A. y Davidson, B. S. (1999) Laulimalide and isolaulimalide, new paclitaxel-like microtubule-stabilizing agents. Cancer Res. 59 (3), 653-660

Neidigh, Kurt A.; Gharpure, Milind M.; Rimoldi, John M.; Kingston, David G. I.; Qing Jiang, Yuan y Hamel, Ernest (1994) Synthesis and biological evaluation of 4-deacetylpaclitaxel. Tetrahedron Letters. 35 (37), 6839-6842

Nicolaou, K. C.; Couladouros, E. A.; Nantermet, P. G.; Renaud, J. ; Guy, R. K. y Wrasidlo, W. (1994) Synthesis of C-2 Taxol Analogues. Angewandte Chemie International Edition in English. 33 (15-16), 1581-1583

Nicolaou, K. C.; Renaud, J.; Nantermet, P. G.; Couladouros, E. A.; Guy, R. K. y Wrasidlo, W. (1995) Chemical Synthesis and Biological Evaluation of C-2 Taxoids. J. Am. Chem. Soc. 117 (9), 2409-2420

Nicolaou, K. C.; Pfefferkorn, J.; Xu, J.; Winssinger, N.; Ohshima, T.; Kim, S.; Hosokawa, S.; Vourloumis, D.; van Delft, F. y Li, T. (1999) Total synthesis and chemical biology of the sarcodictyins. Chem Pharm Bull (Tokyo). 47 (9), 1199-1213

Nogales, E.; Wolf, S. G.; Khan, I. A.; Luduena, R. F. y Downing, K. H. (1995) Structure of tubulin at 6.5 A and location of the taxol-binding site. Nature. 375 (6530), 424-427

Nogales, E.; Wolf, S. G. y Downing, K. H. (1998) Structure of the alpha beta tubulin dimer by electron crystallography. Nature. 391 (6663), 199-203

O'Connor, D. S.; Grossman, D.; Plescia, J.; Li, F.; Zhang, H.; Villa, A.; Tognin, S.; Marchisio, P. C. y Altieri, D. C. (2000) Regulation of apoptosis at cell division by p34cdc2 phosphorylation of survivin. Proc Natl Acad Sci U S A. 97 (24), 13103-13107

Ojima, I.; Duclos, O.; Zucco, M.; Bissery, M. C.; Combeau, C.; Vrignaud, P.; Riou, J. F. y Lavelle, F. (1994) Synthesis and structure-activity relationships of new antitumor taxoids. Effects of cyclohexyl substitution at the C-3' and/or C-2 of taxotere (docetaxel). J Med Chem. 37 (16), 2602-2608

Oosawa, F. y Asakura, S. (1975) Thermodynamics of the polymerization of protein. Academic Press

Orr, G. A.; Verdier-Pinard, P.; McDaid, H. y Horwitz, S. B. (2003) Mechanisms of Taxol resistance related to microtubules. Oncogene. 22 (47), 7280-7295

Ozben, T. (2006) Mechanisms and strategies to overcome multiple drug resistance in cancer. FEBS Lett. 580 (12), 2903-2909

Panda, D.; Miller, H. P. y Wilson, L. (2002) Determination of the size and chemical nature of the stabilizing "cap" at microtubule ends using modulators of polymerization dynamics. Biochemistry. 41 (5), 1609-1617

Pasquier, E.; Honore, S. y Braguer, D. (2006) Microtubule-targeting agents in angiogenesis: where do we stand? Drug Resist Updat. 9 (1-2), 74-86

Pryor, D. E.; O'Brate, A.; Bilcer, G.; Diaz, J. F.; Wang, Y.; Wang, Y.; Kabaki, M.; Jung, M. K.; Andreu, J. M.; Ghosh, A. K.; Giannakakou, P. y Hamel, E. (2002) The microtubule stabilizing agent laulimalide does not bind in the taxoid site,

kills cells resistant to paclitaxel and epothilones, and may not require its epoxide moiety for activity. Biochemistry. 41 (29), 9109-9115

Pusztai, L. (2007) Markers predicting clinical benefit in breast cancer from microtubule-targeting agents. Ann Oncol. 18 Suppl 12 xii15-20

Puthalakath, H.; Huang, D. C.; O'Reilly, L. A.; King, S. M. y Strasser, A. (1999) The proapoptotic activity of the Bcl-2 family member Bim is regulated by interaction with the dynein motor complex. Mol Cell. 3 (3), 287-296

Quasthoff, S. y Hartung, H. P. (2002) Chemotherapy-induced peripheral neuropathy. J Neurol. 249 (1), 9-17

Rai, Sadananda S. y Wolff, J. (1996) Localization of the Vinblastine-binding Site on beta -Tubulin. J. Biol. Chem. 271 (25), 14707-14711

Rao, S.; Krauss, N. E.; Heerding, J. M.; Swindell, C. S.; Ringel, I.; Orr, G. A. y Horwitz, S. B. (1994) 3'-(p-azidobenzamido)taxol photolabels the N-terminal 31 amino acids of beta-tubulin. J. Biol. Chem. 269 (5), 3132-3134

Rao, S.; Orr, G. A.; Chaudhary, A. G.; Kingston, D. G. y Horwitz, S. B. (1995) Characterization of the taxol binding site on the microtubule. 2-(m-Azidobenzoyl)taxol photolabels a peptide (amino acids 217-231) of beta-tubulin. J Biol Chem. 270 (35), 20235-20238

Rao, S.; He, L.; Chakravarty, S.; Ojima, I.; Orr, G. A. y Horwitz, S. B. (1999) Characterization of the Taxol binding site on the microtubule. Identification of Arg(282) in beta-tubulin as the site of photoincorporation of a 7-benzophenone analogue of Taxol. J Biol Chem. 274 (53), 37990-37994

Rappaport, H. P. (1993) Replication of the base pair 6-thioguanine/5-methyl-2-pyrimidine with the large Klenow fragment of Escherichia coli DNA polymerase I. Biochemistry. 32 (12), 3047-3057

Ravelli, R. B.; Gigant, B.; Curmi, P. A.; Jourdain, I.; Lachkar, S.; Sobel, A. y Knossow, M. (2004) Insight into tubulin regulation from a complex with colchicine and a stathmin-like domain. Nature. 428 (6979), 198-202

Rosenberg, B.; Vancamp, L. y Krigas, T. (1965) Inhibition of Cell Division in Escherichia Coli by Electrolysis Products from a Platinum Electrode. Nature. 205 698-699

Rusan, N. M.; Fagerstrom, C. J.; Yvon, A. M. y Wadsworth, P. (2001) Cell cycle-dependent changes in microtubule dynamics in living cells expressing green fluorescent protein-alpha tubulin. Mol Biol Cell. 12 (4), 971-980

Sato, B.; Muramatsu, H.; Miyauchi, M.; Hori, Y.; Takase, S.; Hino, M.; Hashimoto, S. y Terano, H. (2000a) A new antimitotic substance, FR182877. I. Taxonomy, fermentation, isolation, physico-chemical properties and biological activities. J Antibiot (Tokyo). 53 (2), 123-130

Sato, B.; Nakajima, H.; Hori, Y.; Hino, M.; Hashimoto, S. y Terano, H. (2000b) A new antimitotic substance, FR182877. II. The mechanism of action. J Antibiot (Tokyo). 53 (2), 204-206

Scott, R. B. (1970) Cancer chemotherapy--the first twenty-five years. Br Med J. 4 (5730), 259-265

Schibler, M. J. y Cabral, F. (1986) Taxol-dependent mutants of Chinese hamster ovary cells with alterations in alpha- and beta-tubulin. J Cell Biol. 102 (4), 1522-1531

Schiff, P. B.; Fant, J. y Horwitz, S. B. (1979) Promotion of microtubule assembly in vitro by taxol. Nature. 277 (5698), 665-667

Schiff, P. B. y Horwitz, S. B. (1980) Taxol stabilizes microtubules in mouse fibroblast cells. Proc Natl Acad Sci U S A. 77 (3), 1561-1565

Schmidt, M. y Bastians, H. (2007) Mitotic drug targets and the development of novel anti-mitotic anticancer drugs. Drug Resist Updat. 10 (4-5), 162-181

Schwartz, P. S. y Waxman, D. J. (2001) Cyclophosphamide induces caspase 9-dependent apoptosis in 9L tumor cells. Mol Pharmacol. 60 (6), 1268-1279

Shabbits, J. A.; Krishna, R. y Mayer, L. D. (2001) Molecular and pharmacological strategies to overcome multidrug resistance. Expert Rev Anticancer Ther. 1 (4), 585-594

Sharom, F. J.; Liu, R.; Romsicki, Y. y Lu, P. (1999) Insights into the structure and substrate interactions of the P-glycoprotein multidrug transporter from spectroscopic studies. Biochim Biophys Acta. 1461 (2), 327-345

Siddik, Z. H. (2003) Cisplatin: mode of cytotoxic action and molecular basis of resistance. Oncogene. 22 (47), 7265-7279

Skoufias, D. A. y Wilson, L. (1992) Mechanism of inhibition of microtubule polymerization by colchicine: inhibitory potencies of unliganded colchicine and tubulin-colchicine complexes. Biochemistry. 31 (3), 738-746

Skwarczynski, M.; Hayashi, Y. y Kiso, Y. (2006) Paclitaxel prodrugs: toward smarter delivery of anticancer agents. J Med Chem. 49 (25), 7253-7269

Smith, G. F.; Neubauer, B. L.; Sundboom, J. L.; Best, K. L.; Goode, R. L.; Tanzer, L. R.; Merriman, R. L.; Frank, J. D. y Herrmann, R. G. (1988) Correlation of the in vivo anticoagulant, antithrombotic, and antimetastatic efficacy of warfarin in the rat. Thromb Res. 50 (1), 163-174

Snyder, J. P.; Nettles, J. H.; Cornett, B.; Downing, K. H. y Nogales, E. (2001) The binding conformation of Taxol in beta-tubulin: a model based on electron crystallographic density. Proc Natl Acad Sci U S A. 98 (9), 5312-5316

Southam, Chester M. (1963) The Complex Etiology of Cancer. Cancer Res. 23 (8_Part_1), 1105-1115

Spiegelman, B. M.; Penningroth, S. M. y Kirschner, M. W. (1977) Turnover of tubulin and the N site GTP in Chinese hamster ovary cells. Cell. 12 (3), 587-600

Sulkowska, M.; Sulkowski, S.; Skrzydlewska, E. y Farbiszewski, R. (1998) Cyclophosphamide-induced generation of reactive oxygen species. Comparison with morphological changes in type II alveolar epithelial cells and lung capillaries. Exp Toxicol Pathol. 50 (3), 209-220

Tay, B. S.; Lilley, R. M.; Murray, A. W. y Atkinson, M. R. (1969) Inhibition of phosphoribosyl pyrophosphate amidotransferase from Ehrlich ascites-tumour cells by thiopurine nucleotides. Biochem Pharmacol. 18 (4), 936-938

ter Haar, E.; Kowalski, R. J.; Hamel, E.; Lin, C. M.; Longley, R. E.; Gunasekera, S. P.; Rosenkranz, H. S. y Day, B. W. (1996) Discodermolide, a cytotoxic marine agent that stabilizes microtubules more potently than taxol. Biochemistry. 35 (1), 243-250

Terada, Y.; Tatsuka, M.; Suzuki, F.; Yasuda, Y.; Fujita, S. y Otsu, M. (1998) AIM-1: a mammalian midbody-associated protein required for cytokinesis. Embo J. 17 (3), 667-676

Turner, P. F. y Margolis, R. L. (1984) Taxol-induced bundling of brain-derived microtubules. J Cell Biol. 99 (3), 940-946

Uppuluri, S.; Knipling, L.; Sackett, D. L. y Wolff, J. (1993) Localization of the Colchicine-Binding Site of Tubulin. Proceedings of the National Academy of Sciences. 90 (24), 11598-11602

Valiron, O.; Caudron, N. y Job, D. (2001) Microtubule dynamics. Cell Mol Life Sci. 58 (14), 2069-2084

van Vugt, Marcel A. T. M. y Medema, Rene H. (2005) Getting in and out of mitosis with Polo-like kinase-1. 24 (17), 2844-2859

Vander Velde, David G.; Georg, Gunda I.; Grunewald, Gary L.; Gunn, Christopher W. y Mitscher, Lester A. (1993) "Hydrophobic collapse" of taxol and Taxotere solution conformations in mixtures of water and organic solvent. J. Am. Chem. Soc. 115 (24), 11650-11651

Verdier-Pinard, P.; Wang, Z.; Mohanakrishnan, A. K.; Cushman, M. y Hamel, E. (2000) A steroid derivative with paclitaxel-like effects on tubulin polymerization. Mol Pharmacol. 57 (3), 568-575

Wade, R. H. y Hyman, A. A. (1997) Microtubule structure and dynamics. Curr Opin Cell Biol. 9 (1), 12-17

Walker, R. A.; O'Brien, E. T.; Pryer, N. K.; Soboeiro, M. F.; Voter, W. A.; Erickson, H. P. y Salmon, E. D. (1988) Dynamic instability of individual microtubules analyzed by video light microscopy: rate constants and transition frequencies. J Cell Biol. 107 (4), 1437-1448

Wang, L.; Alcaraz, A. A.; Matesanz, R.; Yang, C. G.; Barasoain, I.; Diaz, J. F.; Li, Y. Z.; Snyder, J. P. y Fang, W. S. (2007) Synthesis, biological evaluations, and tubulin binding poses of C-2alpha sulfur linked taxol analogues. Bioorg Med Chem Lett. 17 (11), 3191-3194

Wang, Y.; O'Brate, A.; Zhou, W. y Giannakakou, P. (2005) Resistance to microtubule-stabilizing drugs involves two events: beta-tubulin mutation in one allele followed by loss of the second allele. Cell Cycle. 4 (12), 1847-1853

Wani, M. C.; Taylor, H. L.; Wall, M. E.; Coggon, P. y McPhail, A. T. (1971) Plant antitumor agents. VI. The isolation and structure of taxol, a novel antileukemic and antitumor agent from Taxus brevifolia. J Am Chem Soc. 93 (9), 2325-2327

Weisenberg, R. C.; Borisy, G. G. y Taylor, E. W. (1968) The colchicine-binding protein of mammalian brain and its relation to microtubules. Biochemistry. 7 (12), 4466-4479

Wilson, L.; Panda, D. y Jordan, M. A. (1999) Modulation of microtubule dynamics by drugs: a paradigm for the actions of cellular regulators. Cell Struct Funct. 24 (5), 329-335

Williams, H. J.; Scott, A.I.; Dieden, R.A.; Swindell, C.S.; Chirlian, L.E.; Francl, M.M.; Heerding, J.M. y Krauss, N.E. (1994) NMR and molecular modeling study of active and inactive taxol analogues in aqueous and nonaqueous solution. Canadian Journal of Chemistry. 72 (1), 252-260

Willis, S.; Day, C. L.; Hinds, M. G. y Huang, D. C. (2003) The Bcl-2-regulated apoptotic pathway. J Cell Sci. 116 (Pt 20), 4053-4056

Wood, K. W.; Sakowicz, R.; Goldstein, L. S. y Cleveland, D. W. (1997) CENP-E is a plus end-directed kinetochore motor required for metaphase chromosome alignment. Cell. 91 (3), 357-366

Yan, T.; Berry, S. E.; Desai, A. B. y Kinsella, T. J. (2003) DNA mismatch repair (MMR) mediates 6-thioguanine genotoxicity by introducing single-strand breaks to signal a G2-M arrest in MMR-proficient RKO cells. Clin Cancer Res. 9 (6), 2327-2334

Yang, C. G.; Barasoain, I.; Li, X.; Matesanz, R.; Liu, R.; Sharom, F. J.; Yin, D. L.; Diaz, J. F. y Fang, W. S. (2007) Overcoming Tumor Drug Resistance with High-Affinity Taxanes: A SAR Study of C2-Modified 7-Acyl-10-Deacetyl Cephalomannines. ChemMedChem. 2 (5), 691-701

Yao, X.; Abrieu, A.; Zheng, Y.; Sullivan, K. F. y Cleveland, D. W. (2000) CENP-E forms a link between attachment of spindle microtubules to kinetochores and the mitotic checkpoint. Nat Cell Biol. 2 (8), 484-491

Yvon, A. M.; Wadsworth, P. y Jordan, M. A. (1999) Taxol suppresses dynamics of individual microtubules in living human tumor cells. Mol Biol Cell. 10 (4), 947-959

Zefirova, O. N.; Nurieva, E. V. ; Ryzhov, A. N.; Zyk, N. V. y Zefirov, N. S. (2005) Taxol: Synthesis, Bioactive Conformations, and Structure - Activity Relationships in Its Analogues. ChemInform. 36 (40),

Zhai, Y.; Kronebusch, P. J.; Simon, P. M. y Borisy, G. G. (1996) Microtubule dynamics at the G2/M transition: abrupt breakdown of cytoplasmic microtubules at nuclear envelope breakdown and implications for spindle morphogenesis. J Cell Biol. 135 (1), 201-214

Zhou, J. y Giannakakou, P. (2005) Targeting microtubules for cancer chemotherapy. Curr Med Chem Anticancer Agents. 5 (1), 65-71

ANEXO.

nature chemical biology

ARTICLES

Cyclostreptin binds covalently to microtubule pores and lumenal taxoid binding sites

Rubén M Buey[1,9], Enrique Calvo[2,9], Isabel Barasoain[1], Oriol Pineda[3], Michael C Edler[4], Ruth Matesanz[1], Gemma Cerezo[5], Christopher D Vanderwal[6], Billy W Day[7], Erik J Sorensen[8], Juan Antonio López[2], José Manuel Andreu[1], Ernest Hamel[4] & J Fernando Díaz[1]

Cyclostreptin (1), a natural product from *Streptomyces* sp. 9885, irreversibly stabilizes cellular microtubules, causes cell cycle arrest, evades drug resistance mediated by P-glycoprotein in a tumor cell line and potently inhibits paclitaxel binding to microtubules, yet it only weakly induces tubulin assembly. In trying to understand this paradox, we observed irreversible binding of synthetic cyclostreptin to tubulin. This results from formation of covalent crosslinks to β-tubulin in cellular microtubules and microtubules formed from purified tubulin in a 1:1 total stoichiometry distributed between Thr220 (at the outer surface of a pore in the microtubule wall) and Asn228 (at the lumenal paclitaxel site). Unpolymerized tubulin was only labeled at Thr220. Thus, the pore region of β-tubulin is an undescribed binding site that (i) elucidates the mechanism by which taxoid-site compounds reach the kinetically unfavorable lumenal site and (ii) explains how taxoid-site drugs induce microtubule formation from dimeric and oligomeric tubulin.

The mitotic spindle is an important target in cancer chemotherapy[1]. Spindle function is dependent on microtubule dynamics, which involves stochastic gain and loss of αβ-tubulin heterodimers from microtubule ends. Growth or shortening depends on the activation state of tubulin, which is controlled by the exchangeable nucleotide bound to the β subunit. "Activated" tubulin-GTP adds to microtubule ends, whereas "deactivated" tubulin-GDP dissociates from polymer ends and does not normally polymerize into microtubules.

Compounds that bind to tubulin arrest cells in mitosis and cause apoptosis. These agents interfere with microtubule dynamics even at intracellular concentrations far below the tubulin concentration[2]. Inhibitors of assembly (such as colchicine; 2) inactivate tubulin, thereby preventing microtubule formation. In contrast, microtubule stabilizing agents (MSAs) such as paclitaxel bind preferentially to assembled tubulin, thereby minimizing dissociation of tubulin-GDP from microtubule ends[3]. MSAs also induce assembly of the otherwise inactive tubulin-GDP[4]. In recent years, many structurally diverse taxoid-site MSAs have been discovered, including epothilone B and discodermolide, which are biochemically more potent than paclitaxel[5], and cyclostreptin (FR182877; **Fig. 1a**), which, though apparently less active than paclitaxel, has unusual biochemical properties[6].

Paclitaxel-stabilized, zinc-induced sheets of antiparallel tubulin protofilaments have been used for construction of a model of tubulin with bound paclitaxel[7]. After fitting this model into electron density microtubule maps, investigators concluded that paclitaxel binds to β-tubulin facing the microtubule lumen[8]. This model is supported by tubulin mutation data from cells that are resistant to paclitaxel and epothilones[9].

Two points remain obscure about the biochemical mechanism by which taxoid-site ligands induce tubulin assembly. First, examination of the binding kinetics of paclitaxel[10] yields a high kinetic association constant (k_f = 3.6 × 10^6 M^{-1} s^{-1}), which is inconsistent with a relatively inaccessible lumenal binding site. An exposed site is also supported by microtubule-associated protein (MAP)-mediated reduction in the paclitaxel binding rate[10] and by the binding of antifluorescein antibody to a fluorescein-labeled taxoid bound to microtubules[11]. These findings led us to propose an initial binding site for paclitaxel on the outer microtubule wall near pore type I, which is close to the lumenal site, followed by translocation of the drug to its lumenal site[10]. Because there is 1:1 stoichiometry for paclitaxel binding to αβ-tubulin, the two sites must be mutually exclusive, perhaps with a shared element.

Second, although apparently the paclitaxel site exists only in assembled microtubules[12], taxoid-site drugs can induce microtubule assembly under conditions in which tubulin is normally unable to assemble; thus, no binding sites can be demonstrated. Therefore, given

[1]Centro de Investigaciones Biológicas, Consejo Superior de Investigaciones Científicas, Ramiro de Maeztu 9, Madrid 28040, Spain. [2]Unidad de Proteómica, Centro Nacional de Investigaciones Cardiovasculares, Melchor Fernández Almagro 3, Madrid 28029, Spain. [3]Departament de Química Orgànica, Facultat de Química, Universitat de Barcelona, Av. Diagonal 647, Barcelona 08028, Spain. [4]Toxicology and Pharmacology Branch, Developmental Therapeutics Program, Division of Cancer Treatment and Diagnosis, National Cancer Institute at Frederick, National Institutes of Health, Frederick, Maryland 21702, USA. [5]PharmaMar, S.A. Avda. de los Reyes 1, Colmenar Viejo 28770, Spain. [6]Department of Chemistry, University of California, Irvine, California 92697, USA. [7]Departments of Pharmaceutical Sciences and Chemistry, University of Pittsburgh, Pittsburgh, Pennsylvania 15261, USA. [8]Department of Chemistry, Princeton University, Princeton, New Jersey 08544, USA. [9]These authors contributed equally to this work. Correspondence should be addressed to J.F.D. (fer@cib.csic.es).

Received 20 July 2006; accepted 8 December 2006; published online 7 January 2007; doi:10.1038/nchembio853

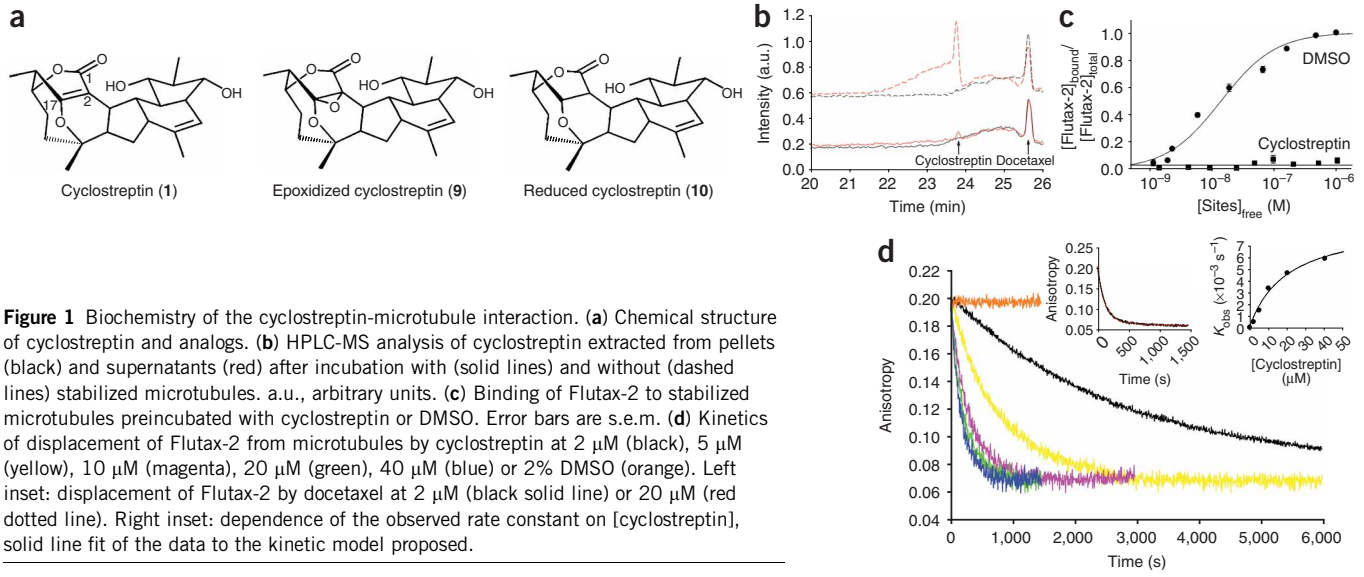

Figure 1 Biochemistry of the cyclostreptin-microtubule interaction. (**a**) Chemical structure of cyclostreptin and analogs. (**b**) HPLC-MS analysis of cyclostreptin extracted from pellets (black) and supernatants (red) after incubation with (solid lines) and without (dashed lines) stabilized microtubules. a.u., arbitrary units. (**c**) Binding of Flutax-2 to stabilized microtubules preincubated with cyclostreptin or DMSO. Error bars are s.e.m. (**d**) Kinetics of displacement of Flutax-2 from microtubules by cyclostreptin at 2 μM (black), 5 μM (yellow), 10 μM (magenta), 20 μM (green), 40 μM (blue) or 2% DMSO (orange). Left inset: displacement of Flutax-2 by docetaxel at 2 μM (black solid line) or 20 μM (red dotted line). Right inset: dependence of the observed rate constant on [cyclostreptin], solid line fit of the data to the kinetic model proposed.

that assembly occurs, we postulated that there is a low-affinity binding site in tubulin dimers or oligomers that cannot be demonstrated because of low paclitaxel solubility[12].

Although cyclostreptin[13] weakly stimulates tubulin assembly, it avidly binds to microtubules, thereby strongly inhibiting the binding of other MSAs to polymer. In addition, cyclostreptin-stabilized microtubules disassemble at 0 °C more slowly than paclitaxel-stabilized microtubules[6]. We have now found that cyclostreptin interacts covalently both *in vitro* and in cells with polymerized tubulin, blocking the binding of even the most potent taxoid-site ligands. Moreover, cyclostreptin is fully active in multidrug-resistant (MDR) ovarian carcinoma (A2780/AD) cells overexpressing P-glycoprotein, which indicates that covalent binding might be a way to overcome MDR. Using HPLC-MS, we found that two amino acid residues, Thr220 and Asn228, are modified in polymerized β-tubulin (Asn228 is near the taxoid site facing the microtubule lumen; Thr220 abuts pore type I), but only Thr220 is modified when cyclostreptin interacts with unpolymerized tubulin.

RESULTS

Cyclostreptin binds irreversibly to microtubules

Because cyclostreptin strongly inhibits binding of taxoid-site ligands to microtubules, we tried to detect microtubule-bound cyclostreptin. We analyzed cyclostreptin-treated microtubules by HPLC-MS. Controls showed that cyclostreptin should have been detectable, but the pellet extracts were devoid of the compound (**Fig. 1b**). Ligand in the supernatant was greatly reduced following incubation of cyclostreptin with microtubules. In the absence of degradation products, cyclostreptin must have reacted irreversibly with the protein.

Cyclostreptin blocks binding of taxoid-site ligands

We examined competition among taxoid-site ligands having different affinities for microtubules (discodermolide (**3**), epothilone B (**4**), epothilone A (**5**), cyclostreptin and paclitaxel (**6**); K_d at 35 °C of 0.18, 1.3, 28, 49 and 70 nM, respectively)[5,6,14]. The competition experiments were performed by adding labeled competitor before or after unlabeled ligand (**Table 1**). All ligands except cyclostreptin behaved as expected if binding reversibly to the same site (order of ligand addition had no effect). With cyclostreptin, the feeble inhibition of discodermolide and epothilone B binding and the strong inhibition of paclitaxel binding without a preincubation became near total inhibition with a preincubation. We also examined the binding to microtubules of 7-*O*-[*N*-(2,7-difluoro-4-fluoresceincarbonyl)-L-alanyl]paclitaxel (Flutax-2; **7**), a fluorescent analog of paclitaxel[15], which bound with an apparent K_d of 14 nM, but not to microtubules preincubated with cyclostreptin (**Fig. 1c**).

Cyclostreptin and taxanes bind by different mechanisms

Cyclostreptin can displace Flutax-2 from stabilized microtubules with an apparent K_a similar to those of paclitaxel and docetaxel (**8**)[6]. To determine whether the same mechanism is involved[15], we compared the effects of docetaxel and cyclostreptin on the kinetics of Flutax-2 dissociation (**Fig. 1d**).

Docetaxel displaces Flutax-2 from microtubules because k_f[docetaxel] >> Flutax-2 dissociation rate constant k_r (ref. 15). With any excess [docetaxel], every empty site is rapidly filled by docetaxel (**Fig. 1d**). The Flutax-2 k_r determined here was $8.9 \pm 0.3 \times 10^{-3}$ s^{-1} at 2 μM and 20 μM docetaxel, which is in agreement with the previously determined value[15] of $7.10 \pm 4 \times 10^{-3}$ s^{-1} (error is s.e.m. for both values).

Cyclostreptin was very different. Although 2–40 μM cyclostreptin fully displaced bound Flutax-2 following monoexponential kinetic curves (**Fig. 1d**), the observed dissociation rate constant (k_{obs}) increased with cyclostreptin concentration until it equaled the k_r of Flutax-2 obtained with docetaxel (**Fig. 1d**). This indicates that the overall reaction is limited by the rate of cyclostreptin binding to microtubules. The explanation that cyclostreptin binds relatively slowly, with rebinding of free Flutax-2, is inconsistent with the monoexponential kinetic curves. These indicate a constant reaction rate, whereas increasing Flutax-2 concentration should cause the apparent k_r to decrease over time.

An alternative explanation is that cyclostreptin binds to the Flutax-2–microtubule complex and induces Flutax-2 dissociation:

$$TF + C \underset{k_{-1}}{\overset{k_1}{\leftrightarrows}} TFC \underset{k_{-2}}{\overset{k_2}{\leftrightarrows}} TC + F$$

where T represents the taxoid site in microtubules, C is cyclostreptin and F is Flutax-2. In this case the observed reaction step would be the second, with monophasic kinetics at steady state (concentration of

Table 1 Dependence on order of ligand addition for the binding of discodermolide, paclitaxel and epothilone B to the taxoid site

	Binding[a] of 2 μM					
	[^{3}H]Discodermolide		[^{14}C]Epothilone B		[^{3}H]Paclitaxel	
	A	B	A	B	A	B
(20 μM)	Percentage of radioactive compound bound[b] ± s.d.					
Cyclostreptin	96 ± 4	19 ± 6	79 ± 10	12 ± 1	60 ± 2	25 ± 2
Epothilone A	95 ± 1	96 ± 5	49 ± 1	49 ± 1	46 ± 3	49 ± 1
Epothilone B	76 ± 1	79 ± 5	9 ± 2	9 ± 1	31 ± 1	33 ± 4
Discodermolide	27 ± 1	31 ± 10	ND	ND	ND	ND

[a]A columns: the radiolabeled ligand was added before the nonradiolabeled competitor. B columns: the nonradiolabeled competitor was added before the radiolabeled ligand. [b]The values represent the amount of radiolabeled compound bound in the presence of the competitor relative to the amount of compound bound in its absence. ND, not determined.

TCF constant during the experiment) and the rate dependent on [cyclostreptin]. Curve fitting[16] to this kinetic model yielded a k_2 value of 0.008 ± 0.002 s^{-1} (which is in agreement with the 0.006 s^{-1} value for Flutax-2 dissociation at 25 °C with docetaxel[15]), a negligible k_{-1} value and a k_1 value of 350 ± 20 M^{-1} s^{-1} (errors are s.e.m.). These values indicate that an irreversible reaction has occurred.

Cellular effects of cyclostreptin

We performed competition experiments between cyclostreptin and Flutax-2 using unfixed cytoskeletons from potoroo kidney (PtK2) cells. When cyclostreptin or paclitaxel was added to cytoskeletons with bound Flutax-2, both compounds displaced Flutax-2. PtK2 cytoskeletons preincubated with paclitaxel, but not those preincubated with cyclostreptin, bound Flutax-2 (**Fig. 2a–c**), thereby demonstrating irreversible binding of cyclostreptin to the cytoskeletons.

Similarly, there were differences in the effects of cyclostreptin and paclitaxel on cellular microtubules. We observed partial recovery of the microtubule network in paclitaxel-treated PtK2 cells, but the effects of cyclostreptin were irreversible. Cells were incubated for 7 h with 2 or 5 μM cyclostreptin or 10 μM paclitaxel, extensively washed and incubated for 16 h or 48 h longer. Untreated cells had typical microtubule networks and normal nuclei after 7 h (**Fig. 2d**). Cells incubated for 7 h with ligand had microtubule bundles (**Fig. 2e**,**f**), and a small percentage of them were micronucleated (4% of the cells) or arrested in mitosis with multiple asters.

After washing and another 16 h in culture, untreated cells had typical microtubule networks (**Fig. 2g**) and normal nuclei, whereas in the treated cells the cyclostreptin effect had progressed: the bundles were unchanged (**Fig. 2h**), and cells with micronucleation or multipolar spindles had increased in number to about 70%. With paclitaxel, microtubules had reverted to a normal appearance (**Fig. 2i**), but

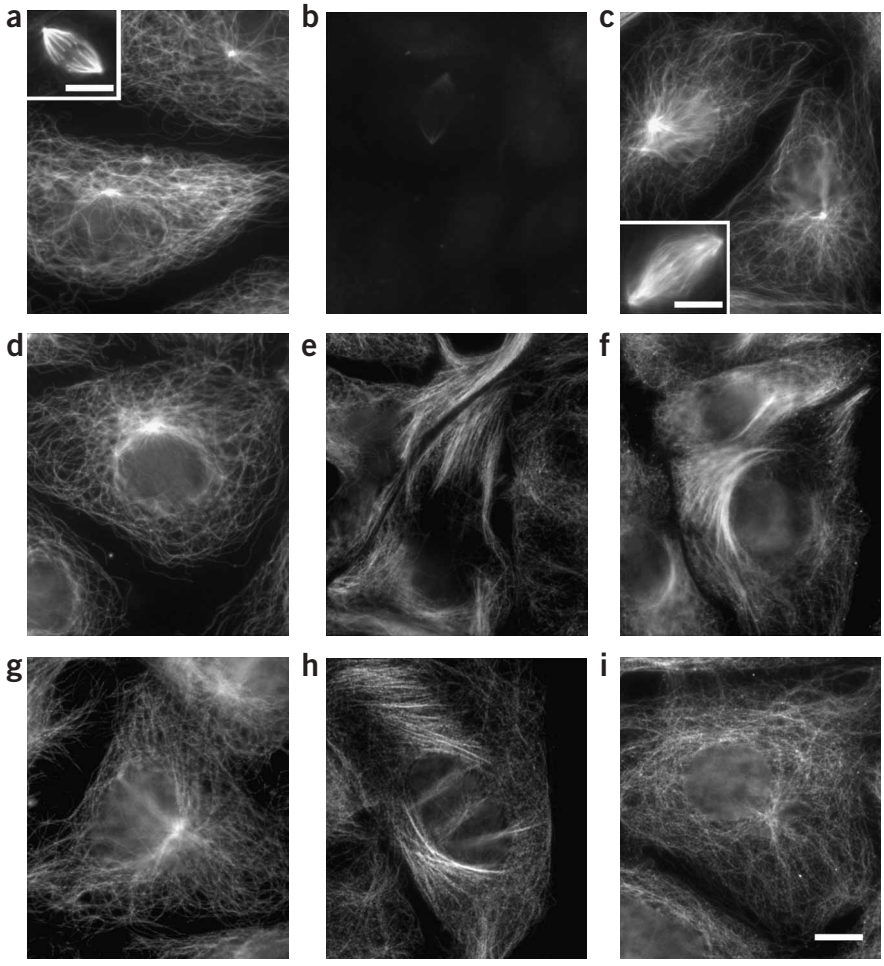

Figure 2 Inhibition of binding of Flutax-2 to PtK2 cytoskeletons by preincubation with cyclostreptin and irreversibility of microtubule effects on PtK2 cells grown in cyclostreptin. (**a**–**c**) Cytoskeletons were preincubated with DMSO (**a**), 10 μM cyclostreptin (**b**) or 10 μM paclitaxel (**c**) and stained with Flutax-2. Insets: Flutax-2–stained mitotic spindles from same cytoskeleton preparations. (**d**–**f**) Cells cultured for 7 h in the presence of DMSO (**d**), 5 μM cyclostreptin (**e**) or 10 μM paclitaxel (**f**) and immunostained. (**g**–**i**) Cells washed after 7 h, left in culture for 16 h and immunostained; shown are the DMSO treatment (**g**), cyclostreptin treatment (**h**) and paclitaxel treatment (**i**). Scale bar represents 10 μm, and all panels and insets have the same magnification.

Table 2 Effects of cyclostreptin compared with paclitaxel and docetaxel on the growth of human carcinoma cells

	IC_{50} (nM) ± s.d.[a]					
	Cell line					
Compound	A2780	A2780/AD	1A9	PTX10	PTX22	A549
Paclitaxel	1.0 ± 0.3	900 ± 200 (900)[b]	1.1 ± 0.2	30 ± 9 (27)	19 ± 5 (17)	3.6 ± 0.4
Docetaxel	0.5 ± 0.1	285 ± 60 (570)	0.6 ± 0.1	ND	ND	7.2 ± 0.3
Cyclostreptin	43.5 ± 4	51 ± 12 (1.2)	44 ± 6	240 ± 50 (5)	58 ± 7 (1.3)	45.5 ± 11
Epoxidized cyclostreptin	Inactive	Inactive	Inactive	Inactive	Inactive	Inactive
Reduced cyclostreptin	Inactive	Inactive	Inactive	Inactive	Inactive	Inactive

[a]IC_{50} (half-maximal inhibitory concentration) values determined in the ovarian carcinoma lines A2780 (parental line), A2780/AD (an MDR line overexpressing P-glycoprotein), 1A9 (a clone of A2780), and PTX10 and PTX22 (paclitaxel-resistant tubulin mutants derived from 1A9), and in the non-small-cell lung carcinoma line A549. IC_{50} values were obtained in at least four independent experiments. [b]The numbers in parentheses are the calculated relative resistance values, obtained by dividing the IC_{50} value of the resistant line by the IC_{50} value of the parental line. ND, not determined. Inactive, no inhibition at 5 μM.

the number of micronucleated cells had increased to about 70%. After a 48-h recovery, cyclostreptin-treated cells had somewhat sparser microtubule bundles but an unchanged number of micronucleated cells. After 48 h without drug, paclitaxel-treated cells continued to recover, with micronucleation reduced to about 40%.

We examined the PtK2 cells for DNA content by flow cytometry (**Supplementary Table 1** online), and these data also indicated a larger recovery after paclitaxel versus cyclostreptin treatment, with a larger population of G2+M cells persisting after cyclostreptin treatment.

We tested the cytotoxicity of cyclostreptin in paclitaxel-resistant and nonresistant carcinoma cell lines (**Table 2**). In the nonresistant line, cyclostreptin was around 40 times less active than paclitaxel. However, PTX10 and PTX22, two lines that are resistant to paclitaxel as a result of tubulin mutations, showed lower relative resistance to cyclostreptin (relative resistance index: 27 and 17 for paclitaxel, respectively, and 5 and 1.3 for cyclostreptin, respectively). Moreover, cyclostreptin was highly active in the MDR line, with a resistance factor of 1.2, as compared with resistance factors of 600–900 for paclitaxel and docetaxel.

We performed cell cycle analysis in PtK2, A549, A2780 and A2780/AD cells incubated for 24 h with paclitaxel or cyclostreptin. The lowest concentrations that gave maximal accumulation of cells in the G2+M phase were 0.5 μM, 20 nM, 15 nM and 1 μM, respectively, for paclitaxel, whereas for cyclostreptin this concentration was 100 nM in each of the four cell lines. Thus, cyclostreptin was more active than paclitaxel in the cell lines that are least sensitive to paclitaxel (PtK2 and A2780/AD) (**Supplementary Table 1**).

Characterization of cyclostreptin binding site by MS

MS chromatograms of digested tubulin samples derived from untreated (**Fig. 3a**) or cyclostreptin-treated (**Fig. 3b**) microtubules showed differential, intense peaks corresponding to tubulin peptides producing a cyclostreptin-derived fragment ion at *m/z* 249.0 (see Methods; peaks 1–2 and 3–7 in the trypsin- and chymotrypsin-digested samples, respectively). These signals were absent in control samples (**Fig. 3a**). MS/MS-based peptide sequencing (**Supplementary Fig. 1** online) of peaks 1–7 demonstrated that all peptide sequences map into β-tubulin$_{219–243}$ (**Fig. 3c**). This sequence contains part of the taxoid site[7]. Peaks 1 and 2 correspond, respectively, to oxidized and nonoxidized cyclostreptin-modified 219-LTTPTYGDLNHLVSATMSG VTTCLR-243. The cyclostreptin-tagged peptide appeared in triply and quadruply charged form in the analyzed mass range. Peaks 3–7 correspond to the sequences indicated (**Fig. 3c**). A comprehensive study of the fragmentation spectrum from the parent ion corresponding to peak 2 revealed β-tubulin$_{219–243}$ to be the binding site for cyclostreptin (**Supplementary Fig. 1**), but the >3 kDa size of this peptide made the precise modification site uncertain. Analysis of the fragmentation spectrum from β-tubulin$_{220–230}$ (peak 5) (**Supplementary Fig. 1**) and β-tubulin$_{220–235}$ (peak 7) revealed that Thr220 forms a covalent bond with cyclostreptin. Analysis of the fragmentation spectra from the ions corresponding to peaks 3, 4 and 6 (**Supplementary Fig. 1**) demonstrated a second modification site: Asn228. No doubly labeled peptides were found, so the covalent reactions with Thr220 and Asn228 are mutually exclusive. Although relative areas measured from chromatographic peaks corresponding to chymotryptic peptides from cyclostreptin-treated samples (**Fig. 3b**) indicate a more extensive reaction with asparagine than with threonine, ionization of chromatographically separated peptides is substantially influenced by the composition of the pool of accompanying peptides eluted at a given retention time. The relative reactivity of the two amino acid residues thus cannot be determined reliably by MS analysis.

However, the chromatographic signal corresponding to 219-LTTPTYGDLNHLVSATMSGVTTCLR-243 showed that there is a 1:1 stoichiometry for the interaction of cyclostreptin with αβ-tubulin in microtubules (**Supplementary Fig. 2** online). In the extracted ion chromatography (EIC) for triply charged ions, this peptide was present in one of two alternative forms. Without cyclostreptin, unmodified 219-LTTPTYGDLNHLVSATMSGVTTCLR-243 (*m/z* 884.4 Da) was observed. When cyclostreptin was included in the reaction mixture, only the corresponding peptide with one cyclostreptin added (*m/z* 1,017.6 Da) was observed. Thus, all β-tubulin subunits in the microtubules were modified by addition of a single cyclostreptin.

We performed similar experiments under nonpolymerizing reaction conditions, in which either the heterodimer or small oligomeric species predominate, depending on the Mg^{2+} concentration. Analysis of precursor ion scanning experiments demonstrated the presence of weak chromatographic peaks 1, 2 and 5, but did not detect peaks 3, 4, 6 and 7. Thus, formation of only small amounts of the Thr220 adduct in nonpolymerized tubulin was detectable (from peak intensity, less than 5% with oligomeric tubulin and less than 0.5% with heterodimeric tubulin). To verify these results and increase sensitivity, we also analyzed samples by multiple reaction monitoring (MRM) scan mode, fixing the Q3 quadrupole for the detection of the diagnostic ion at *m/z* 249.0 Da. Ions at *m/z* 1,017.6, 636.8, 816.4 and 779.4 (at the *m/z* of respective chromatographic peaks 2, 4, 5 and 6) were isolated and fragmented. Only precursors and fragmentation spectra from ions corresponding to peaks 2 and 5 were detected (**Fig. 3b**), which again unambiguously demonstrates the Thr220 modification. We found no

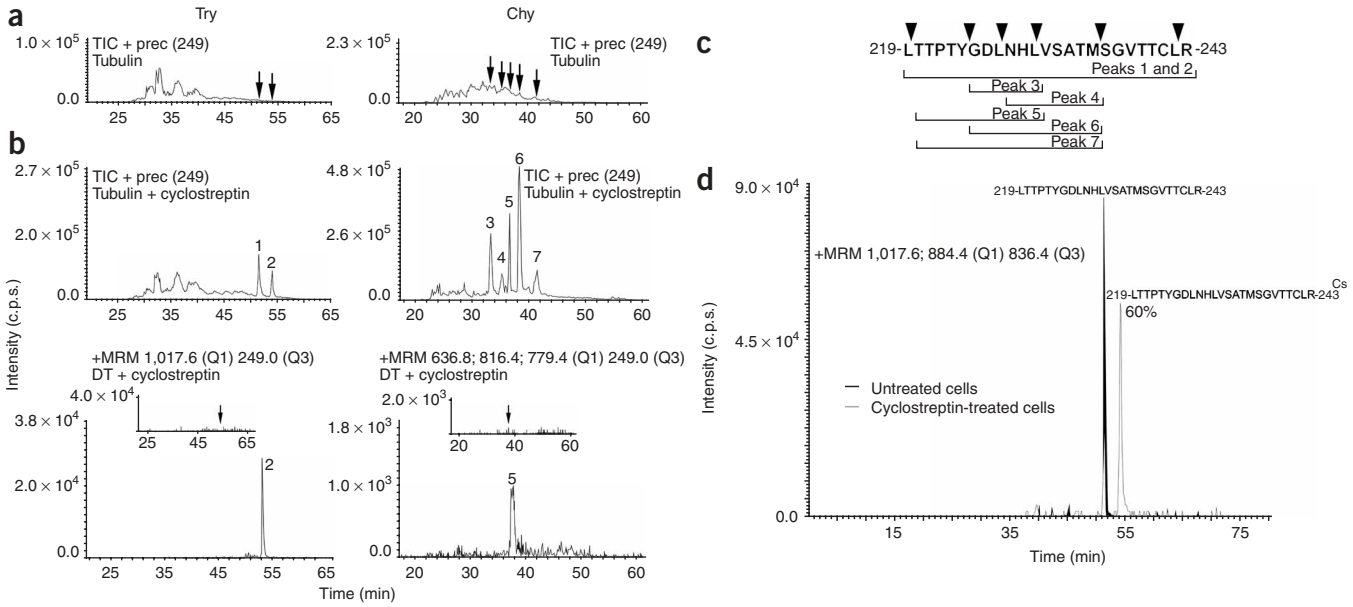

Figure 3 MS analyses of cyclostreptin binding to tubulin. (**a**,**b**) Total ion chromatogram (TIC) of the precursor ion scanning of fragment at *m*/*z* 249.0 from control (**a**) or cyclostreptin-treated (**b**) tubulin samples, digested with trypsin (Try) or chymotrypsin (Chy). The lower panels of **b** show MRM experiments with unassembled, cyclostreptin-treated dimeric tubulin (DT) samples. The upper insets show MRM results for the corresponding dimeric tubulin control samples. Black arrows indicate the retention time expected for signals from peaks 2 (left, trypsin) and 5 (right, chymotrypsin). (**c**) Sequence of β-tubulin$_{219\text{-}243}$ containing the amino acids Thr220 and Asn228 labeled with cyclostreptin (we use the sequence nomenclature of ref. 7, which is used extensively in molecular modeling studies. The two cyclostreptin-modified amino acids are actually Thr218 and Asn226 in β-tubulin[31], and the tryptic peptide actually spans residues 217 to 241). Black triangles indicate the theoretical chymotrypsin cleavage sites within the tryptic peptide. (**d**) MRM experiments with trypsin-digested tubulin extracted from untreated or cyclostreptin-treated cells. Cs, the cyclostreptin tag.

evidence for ions corresponding to peaks 4 and 6, which contain the modified Asn228. The MRM experiments confirmed that the modified peaks are ten-fold more intense in peptides derived from oligomeric versus dimeric tubulin samples.

To verify that the Thr220 modification found in microtubules does not occur in oligomers before microtubule assembly, microtubules stabilized by paclitaxel at a concentration (22 μM paclitaxel; 20 μM tubulin) much greater than the 1 μM drug required to suppress microtubule dynamics[17] were incubated with excess cyclostreptin. This resulted in cyclostreptin displacing paclitaxel from the preformed microtubules. Because paclitaxel binding to microtubules is reversible, cyclostreptin should bind to transiently unoccupied sites, progressively displacing the bound paclitaxel. Therefore, the very same labeling as occurred in the previous experiment when cyclostreptin was added directly to the microtubule assembly mixture is expected, unless the Thr220 modification occurs in oligomers before microtubule assembly, in which case only labeling at Asn228 should be observed. In MRM experiments, ions at *m*/*z* 1,017.6, 636.8, 816.4 and 779.4 (peaks 2, 4, 5 and 6, respectively) were detected, whereas in precursor ion scanning experiments, using the ion at *m*/*z* 249.0 as the diagnostic signal, we also found tubulin-derived peptides corresponding to peaks 3 and 7. Thus, the modifications at Thr220 and Asn228 were unambiguously documented again. We therefore conclude that the Thr220 modification must occur during the binding of cyclostreptin to microtubules.

Cyclostreptin labeling of cellular tubulin

To verify that the tubulin-cyclostreptin adduct is formed in treated cells, we incubated A549 cells for 24 h with 1 μM cyclostreptin or DMSO, isolated their cytoskeletons and digested them with trypsin. We analyzed the digestion mixture by HPLC, with detection by MRM scan mode for the *m*/*z* of the cyclostreptin-labeled form of 219-LTTPTYGDLNHLVSATMSGVTTCLR-243 (not shown). A peak at the expected retention time for the labeled peptide was detected, which indicates formation of the adduct in living cells.

To determine the proportion of cellular tubulin that had reacted with cyclostreptin, we purified tubulin from cyclostreptin-treated and control A549 cells using a one-step ion-exchange procedure. This method yielded tubulin of >90% purity (**Supplementary Fig. 3** online), which is suitable for MS procedures. After treatment with trypsin, the reaction mixture was subjected to HPLC, with analysis in the MRM scan mode with Q1 scanning for the *m*/*z* of unmodified and cyclostreptin-linked 219-LTTPTYGDLNHLVSATMSGVTTCLR-243 (peak 2) and Q3 scanning for a common peptide in the *y*-fragmentation series of both labeled and unlabeled peptide (**Fig. 3d**). Whereas tubulin from control cells showed only one peak, with an *m*/*z* of 884.4 (which corresponds to triply charged unmodified peptide), tubulin from cyclostreptin-treated cells showed two peaks. The major peak, with an *m*/*z* of 1,017.6, corresponded to the triply charged peptide crosslinked to cyclostreptin, and the minor peak was identical to the unmodified peptide from control cells. The areas of the peaks derived from tubulin in control and cyclostreptin-treated cells indicated that about 60% of the tubulin from treated cells contained the adduct. About 60% of tubulin in paclitaxel-treated 1A9 cells forms polymer[18], a proportion that is not very different from the proportion of tubulin that reacts with cyclostreptin in A549 cells. This suggests near total formation of cyclostreptin adduct in the microtubules of treated A549 cells.

Further, we found that both Thr220 and Asn228 were covalently modified in the tubulin we obtained from cyclostreptin-treated cells. We did this by digesting the isolated tubulin with chymotrypsin. The digest was subjected to HPLC, with analysis in the MRM mode with Q1 scanning for signals at *m*/*z* 636.8, 816.4 and 779.4 (corresponding

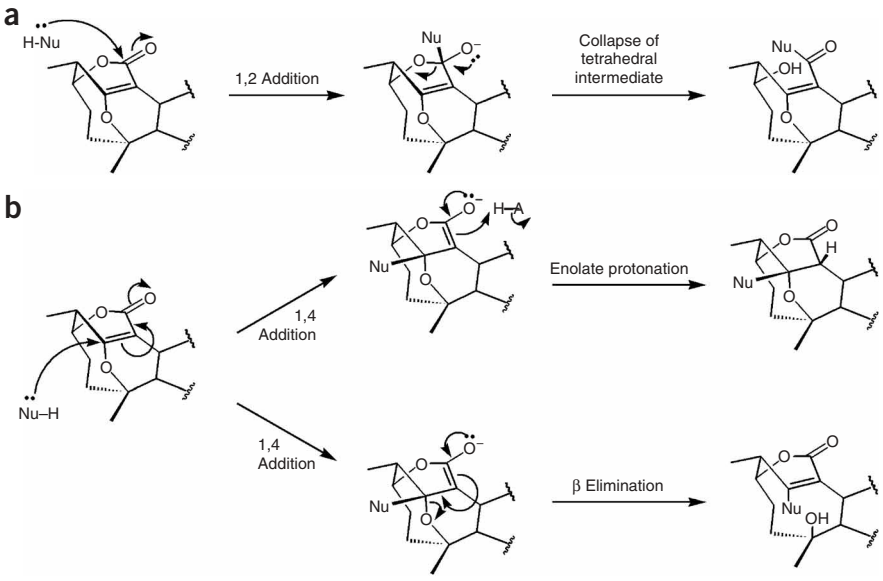

Scheme 1 Possible reaction mechanisms between cyclostreptin and nucleophiles. (**a**) Acylation reaction of the lactone through nucleophilic attack at C1. (**b**) Simple addition of the nucleophile to C17 (top); addition-elimination of the nucleophile at the C2-C17 bond, with formation of a nine-membered ring alcohol (bottom).

respectively to peaks 4, 5 (both containing the Thr220 modification) and 6 (containing the Asn228 modification)) and Q3 scanning for the 249.0 signal, which is diagnostic of the covalent reaction with cyclostreptin (**Supplementary Fig. 3**). The HPLC trace showed the presence of the three peaks, confirming that reactions had occurred with both amino acids.

Cyclostreptin activity requires the strained olefin

The chemical structure of cyclostreptin (**Fig. 1a**) is characterized by a highly strained olefin (C2-C17). C17 and the lactone carbonyl C1 have been proposed as electrophilic sites that could react covalently with proteins[19].

In principle, cyclostreptin could undergo nucleophilic attack at either of these carbons (**Scheme 1**), thereby resulting in an increase in the mass of the peptide that is exactly coincident with the mass of cyclostreptin. Both an acylation reaction of the lactone through nucleophilic attack on C1 (**Scheme 1a**) and a simple addition of nucleophile to C17, with concomitant release of the strain created by the C2-C17 bridgehead alkene, are reasonable modes of covalent bond formation (**Scheme 1b**). A third possibility is an addition-elimination sequence of the nucleophile at the C2-C17 bond. This would result in the formation of a nine-membered ring alcohol (**Scheme 1b**). Modification of other reactive groups of cyclostreptin, with the exception of the unstrained C10-C11 olefin bond, would imply the loss of a water molecule.

An extensive study of the reactivity of the strained olefin of cyclostreptin with model nucleophiles[20] led to the conclusion that the reaction is a simple addition of the nucleophile to C17 driven by strain release. Generally, the reaction was quantitative, as determined by NMR analysis of reaction mixtures, and no evidence for a nine-membered ring product was found. Both the threonine and the asparagine of the peptide have nucleophilic side chains that might attack cyclostreptin at C17 by an analogous addition reaction.

To confirm that the reaction site is the C2-C17 olefin, we prepared two cyclostreptin analogs. First, the double bond was epoxidized (**9**, **Fig. 1a**), yielding an inactive compound[21] (Flutax-2 binding unaltered; no activity against cultured cells (**Table 2**)). Second, the C2-C17 olefin bond was reduced (**10**, **Fig. 1a**), again eliminating the biological activities of cyclostreptin (no effect on cell proliferation (**Table 2**) or Flutax-2 binding; no covalent adduct formed with microtubules as determined by MS). Though the epoxide is potentially electrophilic at C1, C2 and C17, reduced cyclostreptin no longer has the strained olefin; only C1 is a potential electrophile. However, the inactivity of these two analogs buttresses the conclusion that it is the strained olefin of cyclostreptin that reacts with tubulin through a simple addition at C17, as previously demonstrated with model nucleophiles[20].

Molecular modeling

The complex of cyclostreptin with Thr220 was modeled *in silico* by forming a covalent bond with its side chain oxygen (**Supplementary Fig. 4** online). We optimized the resulting adduct with MacroModel (Schrödinger), thereby identifying a possible binding site formed by residues 217–223 and 277–279 from β-tubulin, 323–328 from the adjacent α-tubulin, 95–99 from β-tubulin of a neighboring protofilament, and 128–132 from α-tubulin of a neighboring protofilament (**Supplementary Fig. 4**). Assuming this complex represents that observed experimentally, there are two additional hydrogen bonding interactions that would help stabilize the complex: the hydroxyl group at C15 with Arg278 and the C1 carbonyl group with Thr221. This adduct is further stabilized by hydrophobic contacts with a nonpolar region of the adjacent α-tubulin (Gln128-Leu132).

Cyclostreptin also reacts with Asn228. The atoms of the backbone of this amino acid are located at the lumenal taxoid site, and the side chain forms two strong hydrogen bonds with the exchangeable nucleotide. Therefore, either the position of the Asn228 side chain in microtubules differs from its position in zinc-induced sheets[7,8], or cyclostreptin causes the displacement of the Asn228 side chain by forming a noncovalent precomplex at the paclitaxel site, thereby facilitating a subsequent reaction of cyclostreptin with the Asn228 side chain amide.

DISCUSSION

Cyclostreptin contains two electrophilic functional groups: a strained bridgehead olefin and a lactone carbonyl group. Other natural products containing such moieties react covalently with nucleophilic residues in protein active sites, thereby causing biological effects[22,23].

The biological activities of cyclostreptin overwhelmingly favor microtubules as the target of the compound. However, it is not a classical taxoid-site ligand. Despite strongly displacing taxoid-site ligands from microtubules, it only weakly induces microtubule assembly[5,6,13].

Our results show that cyclostreptin binds covalently to microtubules. Cyclostreptin is the first MSA that has been shown to do so and the first taxoid-site ligand whose binding to dimeric tubulin has been detected. MS analysis showed that in microtubules cyclostreptin forms a covalent bond with either Thr220 or Asn228. We found that in unpolymerized tubulin, only Thr220 forms a bond with

cyclostreptin, and this covalent interaction is much less extensive than the reaction with microtubules. We also demonstrated that both crosslinks to β-tubulin form in cyclostreptin-treated cells. Covalent bond formation explains the unusual biochemical properties of cyclostreptin, such as the distinct requirement for higher temperatures for assembly induction and binding to polymer and the high stability of cyclostreptin polymer to disassembly at 0 °C[6]. Once covalently bound to microtubules, cyclostreptin cannot dissociate and the microtubules cannot disassemble, as they are more stable than untreated control and paclitaxel-induced microtubules.

Similarly, we found that PtK2 cellular microtubule bundles induced by cyclostreptin are more stable than those induced by paclitaxel. Although cyclostreptin is 40-fold less cytotoxic than paclitaxel, it retains its activity in cells that are resistant to paclitaxel by overexpression of P-glycoprotein or by expression of mutant β-tubulins, becoming more potent than paclitaxel in the former case. Therefore, formation of a covalent tubulin adduct can be a mechanism to escape these mechanisms of resistance, at least in cultured cells. Though agents that react covalently with specific targets can be too toxic for use in humans[24], some covalently reactive compounds are successfully used in the clinic. Examples are the antiobesity drug tetrahydrolipstatin, which reacts with pancreatic lipase[25], and the anticancer platinum agents, which react with DNA[26]. In the MDR A2780/AD cells, we found that the covalent adduct of cyclostreptin with tubulin can escape the pump. With the tubulin mutants, cyclostreptin affinity for the altered tubulins might be modified. Alternatively, the longer time frame involved in cell culture studies might still lead to irreversible tubulin inactivation by covalent bond formation, even if the tubulins have reduced affinity for cyclostreptin. In summary, because the formation of the adduct is a kinetically controlled, irreversible process, resistant tumor cells cannot escape the effect of cyclostreptin by reducing its affinity for the target or by enhancing drug efflux, which suggests that the design of ligands that covalently react with the taxoid site or other targets might be an effective way to address drug resistance.

The discovery of the covalent reactions of cyclostreptin with tubulin and microtubules provides new insights into two obscure aspects of the mechanism of ligand binding to the taxoid site. First, modeling of paclitaxel-stabilized zinc sheet protofilaments into a microtubule structure led to the conclusion that the taxoid site is on β-tubulin adjacent to the microtubule lumen[7,8]. In contrast, kinetic measurements, effects of MAPs and antibody binding[10,11,15] indicated an easily accessible site, most logically on the outer microtubule surface. To reconcile these observations, we proposed an exterior taxoid binding site to which ligands bind initially, before transfer to the lumenal site[10]. The two sites could not be occupied simultaneously because of the observed 1:1 binding stoichiometry (similar stoichiometry has been found for discodermolide (M.C.E., unpublished data) and for epothilone A and epothilone B binding[14]). The proposed site was at pore type I, including β-tubulin residues Phe214, Thr220, Thr221 and Pro222 in the H6-H7 loop[10]. We have now shown that the taxoid-site agent cyclostreptin reacts covalently with Thr220 at the proposed pore type I site, and it also reacts with Asn228, a residue at the lumenal site.

The proposed two-step mechanism is consistent with the two-step kinetics of binding of fluorescent taxoids to microtubules[15]. Step one is a bimolecular reaction with a micromolar K_d and a k_f of about 10^6 M^{-1} s^{-1}, which is most consistent with a diffusion-limited reaction involving an exposed site on the microtubule surface, such as the pore type I site containing Thr220. Step two is a monomolecular reaction with a K_{eq} ~20, which indicates that about 5% of the bound ligand remains at the external site. The data obtained with the fluorescent taxoids indicate that the first step involves binding of the taxoid moiety without immobilization of the fluorescein group, as there is no increase in fluorescence anisotropy. This is consistent with the taxoid moiety binding at Thr220, because when the taxoid and fluorescent moieties are separated by a longer linker, the fluorescein moiety is fully accessible to antibodies[11].

The hypothesis that binding at the pore type I site, as manifested by the reaction of cyclostreptin with Thr220, precedes binding of taxoid-site agents to the lumenal site is supported by the fact that covalent binding of cyclostreptin to microtubules abolishes subsequent binding of every taxoid-site agent examined (**Table 1**; **Fig. 1c**). In the Flutax-2 experiment, we incubated 50 nM taxoid with up to 1 μM taxoid sites preincubated with cyclostreptin, and Flutax-2 binding was completely abolished. Even if only 1% of the taxoid sites had been accessible to Flutax-2, a change in the fluorescence anisotropy signal would have been detectable. Cyclostreptin reacts with tubulin in microtubules in a 1:1 proportion, and therefore such microtubules, as the MS data show, would contain αβ dimers with the β-tubulin modified at both Thr220 and Asn228. Though dimers modified at Asn228 would not have bound Flutax-2 because the taxoid site would have been at least partially occupied by the cyclostreptin moiety, one can imagine other routes to the lumenal taxoid site that would be available as a result of modification at Thr220. For example, Flutax-2 might reach the lumen through type II pores or through microtubule ends. The failure to detect even low levels of Flutax-2 binding indicates that an initial interaction at the pore type I site is an obligatory route to the lumenal site.

Second, previous studies[12,27] have shown that paclitaxel binds avidly to microtubules but not to αβ heterodimers. However, paclitaxel and other taxoid-site agents initiate assembly in tubulin solutions in which no microtubules (that is, presumptive binding sites) exist. It has been proposed that paclitaxel might bind to tubulin oligomers[28], thereby leading to assembly under otherwise unfavorable conditions. In the present work, we found a low level of cyclostreptin covalent reactivity with Thr220 in dimeric and oligomeric tubulin, under conditions in which microtubule assembly is prevented by keeping the free Mg^{2+} concentration lower than that required to assemble microtubules with 20 μM tubulin[12]. This demonstrates an MSA binding site in non-assembled tubulin. No reaction with Asn228 was observed, which indicates that the lumenal site is not present without microtubule formation. The binding affinity of MSAs for the site containing Thr220 in αβ heterodimers and oligomers must be very low, but binding to this site might initiate an assembly reaction, with creation of the higher affinity lumenal site and stabilization of nascent polymer. The irreversible covalent reaction of cyclostreptin with Thr220 allows trapping of the binding complex and detection of this evanescent species.

The assembly process might involve transformation of some elements from acting as components of the external site into acting as part of the lumenal site. However, the Thr220 cyclostreptin adduct forms under all reaction conditions examined, including in preformed, paclitaxel-stabilized microtubules following paclitaxel displacement by cyclostreptin. Thus, the external pore type I site must also exist to some extent after assembly. Overall, the data presented here demonstrate the existence of an MSA binding site in unassembled tubulin and support the hypothesis that taxoids reach the lumenal site through transient binding to the pore type I site.

METHODS

Previously described methodologies. Previous papers provide details for preparation of tubulin[29], cyclostreptin[20], epoxidized cyclostreptin[21] and glutaraldehyde-stabilized microtubules, and also for quantitation of the taxoid sites of glutaraldehyde-stabilized microtubules[10,14], electron microscopy, radioactively

labeled ligand binding studies[6], cytotoxicity assays and cell cycle analysis[5], and culture and immunofluorescence analysis of PtK2 potoroo kidney cells[30]. We cultured human ovarian carcinoma 1A9, PTX10 and PTX22[18] and lung carcinoma A549 cells as previously described[5], and we grew A2780 and A2780/AD (P-glycoprotein overexpressing) cells in the same medium supplemented with 0.25 units ml^{-1} of bovine insulin.

Ligands. See **Supplementary Methods** online for preparation of reduced cyclostreptin and information about other ligands.

Binding of cyclostreptin to microtubules. We incubated samples containing crosslinked microtubules (35 μM taxoid sites) and 30 μM cyclostreptin for 30 min at 25 °C in GAB (3.4 M glycerol, 10 mM NaP_i, 1 mM EGTA and 6 mM $MgCl_2$, pH 6.7) plus 0.1 mM GTP. Samples were processed and extracted, with each organic extract residue dissolved in 200 μl of CH_3OH[14]. For uncrosslinked microtubules, samples were prepared using 20 μM tubulin plus 25 μM cyclostreptin in GAB plus 1 mM GTP.

Ligands reversibly bound to pelleted polymer and ligands in the supernatant were detected by HPLC-MS (**Supplementary Methods**).

Inhibition of binding of Flutax-2 to microtubules. We incubated crosslinked microtubules (60 μM) with 66 μM cyclostreptin, epoxidized cyclostreptin, reduced cyclostreptin or 1.3% DMSO overnight at 22 °C in GAB plus 0.1 mM GTP and dialyzed for 5 h against the same solution. Flutax-2 (50 nM) was titrated with these preparations, and K_as for Flutax-2 binding were calculated[14].

We also performed competition of cyclostreptin with Flutax-2 with native PtK2 cytoskeletons stained for 10 min with 0.2 μM Flutax-2, washed (8×) in two wells with 2 ml of 10 mM PIPES, 1 mM EGTA, 1 mM $MgCl_2$, 4% PEG, pH 6.8 and incubated for 15 min with 100 μM cyclostreptin, paclitaxel or 2% DMSO. After washing again, coverslips were mounted and examined. Cytoskeletons were also preincubated with 10 μM cyclostreptin, paclitaxel or 1% DMSO for 10 min, washed, stained with 0.2 μM Flutax-2 and visualized.

Flutax-2 dissociation kinetics. The dissociation kinetics of Flutax-2 from microtubules was measured by fluorescence anisotropy (**Supplementary Methods**).

Purification of tubulin from cells. We incubated five 175-cm^2 flasks with a monolayer of A549 cells for 24 h with 1 μM cyclostreptin or 0.1% DMSO. Cells were removed with phosphate-buffered saline (PBS) and 0.5 mM EDTA, washed with PBS and harvested by centrifugation. The cell pellet (1 ml) was resuspended in 1 ml of 10 mM NaP_i, 1 mM $MgCl_2$, 0.1 mM GTP, 0.24 M sucrose, pH 7.0 and stored in liquid nitrogen. After thawing the cells, DTT and GTP were added to 1 mM, and the cells were hand-homogenized in glass. The homogenate was centrifuged (38,000 r.p.m., 1 h, 4 °C, TLA 100.4 rotor in an Optima TLX ultracentrifuge). The supernatant was adjusted to 0.4 M KCl and loaded onto a HiTrap DEAE Fast Flow 1 ml column in an FPLC system (GE Healthcare) developed at 1 ml min^{-1}. Unbound protein was removed with 5 ml of 10 mM NaP_i, 1 mM $MgCl_2$, 0.1 mM GTP, 0.4 M KCl, pH 7.0. Bound protein was eluted with 0.8 M KCl in the same buffer and desalted into 10 mM NaP_i, 1 mM $MgCl_2$, 0.1 mM GTP, pH 7.0 with a HiTrap desalting column (GE Healthcare). The tubulin was 90% pure, as determined by SDS-PAGE. The tubulin was stored in liquid nitrogen after addition of 0.24 M sucrose.

Protein digestion and sample preparation for MS analysis. We prepared tubulin control, cyclostreptin-treated, and reduced cyclostreptin-treated samples using native microtubules polymerized for 30 min at 37 °C in GAB plus 1 mM GTP (200 μl, 20 μM tubulin with 2.5% DMSO or 25 μM drug). In another sample, 20 μM tubulin in GAB plus 1 mM GTP was assembled with 22 μM paclitaxel for 15 min at 37 °C (>97% assembly[5]) and incubated for another 45 min at 37 °C after addition of 50 μM cyclostreptin to displace bound paclitaxel. Morphology of polymers was always verified to be microtubules. Microtubules were harvested by centrifugation as described above. Pellets were washed twice with water and suspended in 200 μl of 50 mM NH_4HCO_3, 12 mM EDTA, 0.01% SDS, pH 7.6. Unassembled tubulin samples were prepared using 20 μM GTP-tubulin in 10 mM NaP_i, 1 mM EDTA, 0.1 mM GTP, pH 7.0 without (for dimeric tubulin) or with (for oligomeric tubulin) 1.5 mM $MgCl_2$ and 2.5% DMSO or 25 μM cyclostreptin. Samples were centrifuged as described above to remove aggregates, and 20 μl was diluted 1:1 into 50 mM NH_4HCO_3 and digested with trypsin (1 μg sequencing grade, Promega, 2 h, 37 °C) or chymotrypsin (1 μg type VII, TLCK treated, Sigma, 1 h, 25 °C). Reaction mixtures were dried *in vacuo* and, for analysis, dissolved in 5% CH_3CN, 0.5% CH_3COOH.

Nano-HPLC and tandem triple quadrupole MS analysis of peptides. We analyzed peptide solutions from control, cyclostreptin-treated and reduced cyclostreptin-treated samples with a Supelco C18 nanocolumn developed with a CH_3CN gradient. Peptides were eluted into a Protana nanospray ion source and the resulting ions were analyzed on the 4000 Q Trap system (Applied Biosystems) as described in **Supplementary Methods**.

MRM. MRM of selected cyclostreptin-bound peptides derived from unassembled tubulin and tubulin isolated from cells is described in **Supplementary Methods**.

Detection of cyclostreptin labeling of tubulin by nano-HPLC coupled to three-dimensional ion-trap MS. We injected tryptic peptides from control and cyclostreptin-treated microtubules onto a Supelco C18 nanocolumn. A CH_3CN gradient was used to elute peptides to a PicoTip emitter nanospray needle (New Objective) for real-time ionization and peptide fragmentation on an Esquire HCT ion-trap (Bruker Daltoniks) mass spectrometer (**Supplementary Methods** and **Supplementary Fig. 5** online).

MS data analysis. We analyzed all chromatograms and MS/MS spectra from the 4000 Q Trap system with Analyst 1.4.1 (Applied Biosystems). All HPLC-MS/MS experiments were repeated with five independent samples. Chromatographic and MS data from the three-dimensional ion-trap system were processed by DataAnalysis 3.3 (Bruker Daltoniks).

Molecular modeling of cyclostreptin binding to tubulin. We performed the simulations needed to investigate the covalent binding of cyclostreptin with MacroModel 8.5 (Schrödinger) over a model of pore type I that was built from the structure 1JFF in the Protein Data Bank.

Accession codes. Protein Data Bank: the structure 1JFF was used to model pore type I in MacroModel 8.5.

Requests for materials. cdv@uci.edu.

Note: Supplementary information and chemical compound information are available on the Nature Chemical Biology website.

ACKNOWLEDGMENTS

The authors thank J. Vilarrasa for helpful discussions, P. Lastres for his help with flow cytometry, and Matadero Madrid Norte S.A. and José Luis Gancedo S.L. for providing calf brains for tubulin purification. This work was supported in part by grant BFU2004-00358 from Ministerio de Educación y Ciencia and grant 200520M061 from Comunidad Autonoma de Madrid to J.F.D. R.M.B. was supported by a Beca de Formación de Profesorado Universitario del Ministerio de Educación y Ciencia fellowship.

AUTHOR CONTRIBUTIONS

R.M.B. performed research; E.C. performed research; I.B. designed and performed research; O.P. performed research; M.C.E. performed research; R.M. performed research; G.C. performed research; C.D.V. contributed materials and performed research; B.W.D. contributed materials and edited the manuscript; E.J.S. contributed materials; J.A.L. interpreted data; J.M.A. designed research, interpreted data and edited the manuscript; E.H. interpreted data and wrote the paper; J.F.D. designed and performed research, interpreted data and wrote the paper.

COMPETING INTERESTS STATEMENT

The authors declare that they have no competing financial interests.

Published online at http://www.nature.com/naturechemicalbiology
Reprints and permissions information is available online at http://npg.nature.com/reprintsandpermissions

1. Jordan, M.A. & Wilson, L. Microtubules as a target for anticancer drugs. *Nat. Rev. Cancer* **4**, 253–265 (2004).

2. Jordan, M.A., Toso, R.J., Thrower, D. & Wilson, L. Mechanism of mitotic block and inhibition of cell proliferation by taxol at low concentrations. *Proc. Natl. Acad. Sci. USA* **90**, 9552–9556 (1993).
3. Schiff, P.B., Fant, J. & Horwitz, S.B. Promotion of microtubule assembly *in vitro* by taxol. *Nature* **277**, 665–667 (1979).
4. Díaz, J.F. & Andreu, J.M. Assembly of purified GDP-tubulin into microtubules induced by taxol and taxotere: reversibility, ligand stoichiometry, and competition. *Biochemistry* **32**, 2747–2755 (1993).
5. Buey, R.M. *et al.* Microtubule interactions with chemically diverse stabilizing agents: thermodynamics of binding to the paclitaxel site predicts cytotoxicity. *Chem. Biol.* **12**, 1269–1279 (2005).
6. Edler, M.C. *et al.* Cyclostreptin (FR182877), an antitumor tubulin-polymerizing agent deficient in enhancing tubulin assembly despite its high affinity for the taxoid site. *Biochemistry* **44**, 11525–11538 (2005).
7. Nogales, E., Wolf, S.G. & Downing, K.H. Structure of the αβ-tubulin dimer by electron crystallography. *Nature* **391**, 199–203 (1998).
8. Nogales, E., Whittaker, M., Milligan, R.A. & Downing, K.H. High-resolution model of the microtubule. *Cell* **96**, 79–88 (1999).
9. Giannakakou, P. *et al.* A common pharmacophore for epothilone and taxanes: molecular basis for drug resistance conferred by tubulin mutations in human cancer cells. *Proc. Natl. Acad. Sci. USA* **97**, 2904–2909 (2000).
10. Díaz, J.F., Barasoain, I. & Andreu, J.M. Fast kinetics of taxol binding to microtubules. Effects of solution variables and microtubule-associated proteins. *J. Biol. Chem.* **278**, 8407–8419 (2003).
11. Díaz, J.F., Barasoain, I., Souto, A.A., Amat-Guerri, F. & Andreu, J.M. Macromolecular accessibility of fluorescent taxoids bound at a paclitaxel binding site in the microtubule surface. *J. Biol. Chem.* **280**, 3928–3937 (2005).
12. Díaz, J.F., Menendez, M. & Andreu, J.M. Thermodynamics of ligand-induced assembly of tubulin. *Biochemistry* **32**, 10067–10077 (1993).
13. Sato, B. *et al.* A new antimitotic substance, FR182877. I. Taxonomy, fermentation, isolation, physico-chemical properties and biological activities. *J. Antibiot. (Tokyo)* **53**, 123–130 (2000).
14. Buey, R.M. *et al.* Interaction of epothilone analogs with the paclitaxel binding site; relationship between binding affinity, microtubule stabilization, and cytotoxicity. *Chem. Biol.* **11**, 225–236 (2004).
15. Díaz, J.F., Strobe, R., Engelborghs, Y., Souto, A.A. & Andreu, J.M. Molecular recognition of taxol by microtubules. Kinetics and thermodynamics of binding of fluorescent taxol derivatives to an exposed site. *J. Biol. Chem.* **275**, 26265–26276 (2000).
16. Barshop, B.A., Wrenn, R.F. & Frieden, C. Analysis of numerical methods for computer simulation of kinetic processes: development of KINSIM–a flexible, portable system. *Anal. Biochem.* **130**, 134–145 (1983).
17. Derry, W.B., Wilson, L. & Jordan, M.A. Substoichiometric binding of taxol suppresses microtubule dynamics. *Biochemistry* **34**, 2203–2211 (1995).
18. Giannakakou, P. *et al.* Paclitaxel-resistant human ovarian cancer cells have mutant β-tubulins that exhibit impaired paclitaxel-driven polymerization. *J. Biol. Chem.* **272**, 17118–17125 (1997).
19. Adam, G.C., Vanderwal, C.D., Sorensen, E.J. & Cravatt, B.F. (–)-FR182877 is a potent and selective inhibitor of carboxylesterase-1. *Angew. Chem. Int. Edn Engl.* **42**, 5480–5484 (2003).
20. Vanderwal, C.D., Vosburg, D.A., Weiler, S. & Sorensen, E.J. An enantioselective synthesis of FR182877 provides a chemical rationalization of its structure and affords multigram quantities of its direct precursor. *J. Am. Chem. Soc.* **125**, 5393–5407 (2003).
21. Yoshimura, S., Sato, B., Kinoshita, T., Takase, S. & Terano, H. A new antimitotic substance, FR182877. III. Structure determination. *J. Antibiot. (Tokyo)* **53**, 615–622 (2000).
22. Hadvary, P., Sidler, W., Meister, W., Vetter, W. & Wolfer, H. The lipase inhibitor tetrahydrolipstatin binds covalently to the putative active site serine of pancreatic lipase. *J. Biol. Chem.* **266**, 2021–2027 (1991).
23. Liu, S., Widom, J., Kemp, C.W., Crews, C.M. & Clardy, J. Structure of human methionine aminopeptidase-2 complexed with fumagillin. *Science* **282**, 1324–1327 (1998).
24. Evans, D.C., Watt, A.P., Nicoll-Griffith, D.A. & Baillie, T.A. Drug-protein adducts: an industry perspective on minimizing the potential for drug bioactivation in drug discovery and development. *Chem. Res. Toxicol.* **17**, 3–16 (2004).
25. Henness, S. & Perry, C.M. Orlistat: a review of its use in the management of obesity. *Drugs* **66**, 1625–1656 (2006).
26. Brabec, V. & Kasparkova, J. Modifications of DNA by platinum complexes. Relation to resistance of tumors to platinum antitumor drugs. *Drug Resist. Updat.* **8**, 131–146 (2005).
27. Parness, J. & Horwitz, S.B. Taxol binds to polymerized tubulin *in vitro*. *J. Cell Biol.* **91**, 479–487 (1981).
28. Díaz, J.F., Andreu, J.M., Diakun, G., Towns-Andrews, E. & Bordas, J. Structural intermediates in the assembly of taxoid-induced microtubules and GDP-tubulin double rings: time-resolved X-ray scattering. *Biophys. J.* **70**, 2408–2420 (1996).
29. Weisenberg, R.C., Borisy, G.G. & Taylor, E.W. The colchicine-binding protein of mammalian brain and its relation to microtubules. *Biochemistry* **7**, 4466–4479 (1968).
30. Andreu, J.M. & Barasoain, I. The interaction of baccatin III with the taxol binding site of microtubules determined by a homogeneous assay with fluorescent taxoid. *Biochemistry* **40**, 11975–11984 (2001).
31. Krauhs, E. *et al.* Complete amino acid sequence of β-tubulin from porcine brain. *Proc. Natl. Acad. Sci. USA* **78**, 4156–4160 (1981).

DOI: 10.1002/cmdc.200700002

Overcoming Tumor Drug Resistance with High-Affinity Taxanes: A SAR Study of C2-Modified 7-Acyl-10-Deacetyl Cephalomannines

Chun-Gang Yang,[a, b] Isabel Barasoain,[c] Xuan Li,[a] Ruth Matesanz,[c] Ronghua Liu,[d] Frances J. Sharom,[d] Da-Li Yin,[a] J. Fernando Díaz,*[c] and Wei-Shuo Fang*[a, b]

A series of C2-modified 10-deacetyl-7-propionyl cephalomannine derivatives was designed, prepared, and biologically evaluated. Some C2 meta*-substituted benzoate analogues showed potent activity against both drug-sensitive and drug-resistant tumor cells in which resistance is mediated through either P-gp overexpression or β-tubulin mutation mechanisms. The taxoid **15b** and related compounds are of particular interest, as they are much more cytotoxic than paclitaxel, especially against drug-resistant tumor cells; they are able to kill both drug-resistant and drug-sensitive cells (low R/S ratio), and they have high affinity for β-tubulin. Our research results led to an important hypothesis, that is, a taxane with very high binding affinity for β-tubulin is able to counteract drug resistance, which may assist in future taxane-based drug-discovery efforts.*

Introduction

The chemistry and biology of taxanes have been extensively explored since the successful development of paclitaxel (Taxol®, **1a**), a natural taxane originally isolated from *Taxus brevifolia*[1] which is one of the most effective antitumor agents.[2] Although **1a** was found to be effective against tumors resistant to some chemotherapeutic agents, resistance to **1a** itself has also occurred after its use in clinics and has become a serious problem in the failure of chemotherapy with paclitaxel. To overcome this problem, many paclitaxel analogues derived from natural taxanes have been designed and prepared. As a result, several semisynthetic taxanes such as IDN5109 (**2**),[3] DJ-927 (**3**),[4] and BMS-184476 (**4**)[5] (Figure 1) have undergone clinical trials. Most of these compounds were found to exert their activity through counteracting overexpression of the P-glycoprotein (P-gp) multidrug efflux pump and by modulating P-gp functions.[6,7]

Although numerous efforts were made to reveal the structure–activity relationship (SAR) of paclitaxel analogues and related taxoids,[2c] few reports of SARs for taxoids effective against multidrug-resistant (MDR) tumors have appeared. Since the first report of the exceptional efficacy of taxol analogues against MDR tumor cells appeared in 1996,[8] many similar taxoids have been prepared, including those with modifications at C7, C9, and C10 in the northern hemisphere, and C2 in the southern hemisphere of the molecule,[4,5,9–15] as well as in combination with changes at the C13 side chain,[16–18] and compounds with structural modifications at combinations of different sites.[19] Taxoid **5** seems to be one of the most promising agents against MDR tumor cells reported to date because of its high activity (IC_{50} values at nanomolar and sub-nanomolar levels) and equal potency towards both sensitive and resistant tumor cells (R/S ratio derived from IC_{50}(resistant)/IC_{50}(sensitive) is about 1), whereas paclitaxel and docetaxel (Taxotere®, **1c**) are 10- to 1000-fold less potent towards MDR tumor cells.

Whereas most semisynthetic taxoids available to date were found to be effective against MDR cells expressing a high level of P-gp which are derived from continuous treatment with cytotoxic agents, overcoming drug resistance mediated by β-tubulin mutations has not been of primary interest, except for a few reports in which human ovarian carcinoma cell lines 1A9 and 1A9/PTX22 with β-tubulin mutations were employed.[15] Complete effectiveness by C2-modified taxanes was not achieved, although partial sensitivity was realized.

[a] C.-G. Yang, X. Li, Prof. D.-L. Yin, Prof. W.-S. Fang
Department of Medicinal Chemistry, Institute of Materia Medica
Chinese Academy of Medical Sciences
1 Xian Nong Tan Street, Beijing 100050 (China)
Fax: (+86) 10-6301-7757
E-mail: wfang@imm.ac.cn

[b] C.-G. Yang, Prof. W.-S. Fang
Key Laboratory of Bioactive Substances and Resources
Utilization of Chinese Herbal Medicine (Peking Union Medical College)
Ministry of Education, Beijing 100050 (China)

[c] Dr. I. Barasoain, R. Matesanz, Dr. J. F. Díaz
Centro de Investigaciones Biologicas
Consejo Superior de Investigaciones Cientificas
Ramiro de Maeztu 9, 28040 Madrid (Spain)
E-mail: fer@cib.csic.es

[d] Dr. R. Liu, Prof. F. J. Sharom
Department of Molecular and Cellular Biology
University of Guelph, Guelph ON, N1G 2W1 (Canada)

Supporting information for this article is available on the WWW under http://www.chemmedchem.org or from the author.

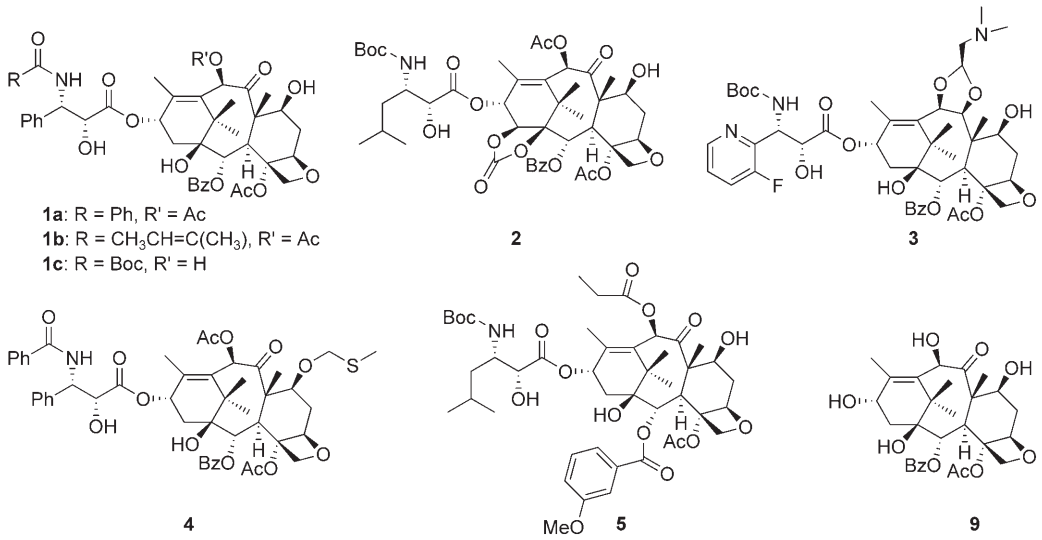

Figure 1. Structures of taxol (**1a**) and its analogues.

Our project aims to design taxoids effective against both drug-sensitive and drug-resistant tumors by counteracting P-gp overexpression and enhancing binding affinity to normal and mutant β-tubulins. We selected cephalomannine (**1b**) as a compound of interest owing to its similarity in both structure and antitumor spectrum to those of **1a** in our primary screen. In addition, it is known that some of the aliphatic 3′-*N*-acyl analogues exhibit slightly greater activity than paclitaxel itself.[2d, 20]

Cephalomannine (**1b**) is a natural congener of paclitaxel, and was isolated in the 1970s from *Taxus wallichiana*, which was erroneously assigned as *Cephalotaxus manii* at the time of its discovery.[21] Its abundance is similar to that of paclitaxel (**1a**) in some *Taxus* spp. Halogenation[22] and epoxidation[23] of the double bond of the 3′-*N*-tigloyl double bond in the C13 side chain of **1b** has led to the preparation of some cephalomannine derivatives with potent cytotoxicity. It was also found that 10-deacetylcephalomannine (**6a**) and 10-deacetoxy-10-oxo-7-*epi*-cephalomannine (**7**) (Figure 2) were less active towards both drug-sensitive MDA-MB 231, and drug-resistant MCF-7/ADR cell lines.[24]

During our initial examination of 7-acylation of cephalomannine, we observed that the antitumor activity of the 7-acyl derivatives decreased with increasing length of the C7 side chain, that is, from acetyl compound **8a** to butyryl compound **8c**, in agreement with previous observations for paclitaxels.[25] Considering that C10 deacetylation in combination with C7 acylation can restore the activity of paclitaxel analogues,[26] we prepared 10-deacetyl-7-acylcephalomannine derivatives and found that 10-deacetyl-7-acetyl and 10-deacetyl-7-propionyl derivatives **6b** and **6c**, respectively, showed improved activity, while 10-deacetyl-7-butyrylcephalomannine (**6d**) exhibited decreased activity. Encouraged by these preliminary results, we set out to prepare C2-modified derivatives of **6c** based on the reasoning that proper structural changes at C7/C10 can counteract P-gp-mediated resistance, and those at C2 may enhance the ability of the compound to bind to wild-type and mutated β-tubulins (because C2 and C4 substitutions are close to the 217–233 and 270–291 sequences of β-tubulin that contain many known mutation sites[27, 28]). The resulting C2-modified 7-propionyl-10-deacetylcephalomannines are expected to exert significant activity against both drug-sensitive and drug-resistant tumors.

Recent pharmacophore studies suggested that the phenyl ring of the 2-benzoate group is close to His 227/His 229 of β-tubulin and is flanked by a "hydrophobic basin" composed of Phe 272, Ala 273, and Ser 374 (the position of this residue is replaced by Ala in the majority of the human β-tubulin isoform) and other residues, thus leading to strong hydrophobic interactions between paclitaxel and β-tubulin.[29] This is in agreement with previous observations that 2-*ortho*- and 2-*para*-substituted benzoates, especially the latter, exhibit much lower ac-

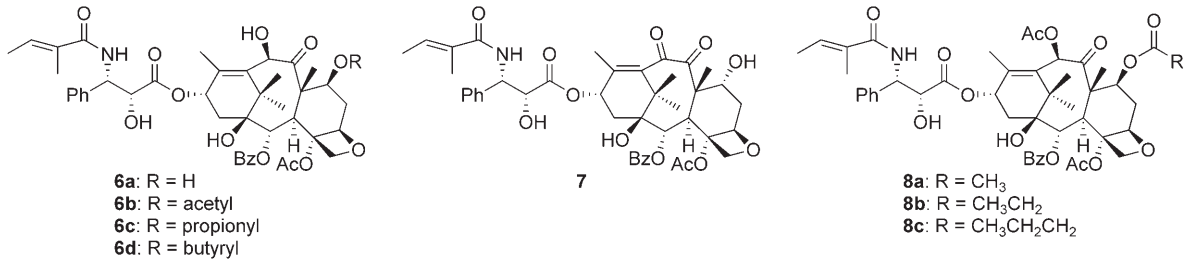

Figure 2. Structures of C7- and C10-modified cephalomannines.

tivity than 2-*meta*-substituted benzoates of paclitaxel.[15,30] The poor activity of 2-*para*-substituted taxanes originates from a steric effect that decreases the hydrophobic interaction between the phenyl ring and adjacent amino acid residues. In addition, some C2-disubstituted benzoates as well as C2 alkanoates or alkenoates also exhibited potent activity.[15,31] Based on this information, we designed and prepared some 2-*meta*-substituted benzoates **15a–j**, heterocyclic carboxylic acid esters **15k–m**, C_{3-4} alkanoates/alkenoates **15n–q**, as well as disubstituted benzoates **15r–t** to examine their SAR at both the cellular (cytotoxicity) and molecular (β-tubulin and P-gp binding ability) levels. Herein we report the syntheses and resulting biological evaluation of these compounds; the SAR of these taxanes and correlations between cellular and binding assays are also discussed.

Results and Discussion

Synthesis

Starting from **1b**, 2′-TBS-10-deacetylcephalomannine **10b** was prepared in >90% yield through protection of the 2′-OH group with *tert*-butyldimethylsilyl chloride (TBSCl) and successive 10-deacetylation by hydrazine hydrate, as previously reported for paclitaxel.[32,33] Selective triethylsilyl (TES) protection of **10b** with *N*,*O*-bis(triethylsilyl)trifluoroacetamide, following a known protocol for selective 10-triethylsilylation of 10-deacetylbaccatin III (**9**),[34] furnished **11**, which was then acylated upon treatment with propanoic anhydride and pyridine (Py) to yield **12** (Scheme 1).

Modification at C2 of **1a** and its derivatives has been realized by several research groups.[30,31,35] Kingston's selective C2 debenzoylation condition (Triton B in CH_2Cl_2) was modified for debenzoylation of **12** to afford taxoid **13** (Scheme 2). To prepare C2-modified taxoids **14** (except **14e**), conjugation of **13** with different acids in the presence of *N*,*N*-dicyclohexylcarbodiimide (DCC) and *N*,*N*-dimethylaminopyridine (DMAP) or pyrrolidinopyridine (PP) was applied, because C2 acylation with 1-(3-dimethylaminopropyl)-3-ethylcarbodiimide hydrochloride (EDC)/DMAP or EDC/PP was extremely slow, and the use of acyl chlorides and LHMDS resulted in very poor yields. Unlike others, taxoid **14e** was prepared with $NaBH_4$ as a reduced product of **14d**. All C2-esterified products were obtained as major products, except in the case of esterification with 3-methylbutenoic acid, for which two products (**14n** and **14o**) were found. Taxoid **14o**, showing two terminal olefin signals around $\delta = 4.9$ ppm as broad singlets, corresponds to a rearranged product of 3-methylbutenoyl taxoid **14n**. All taxoids **14**, without purification, underwent desilylation to furnish final products **15a–t** in satisfactory yields (Scheme 2).

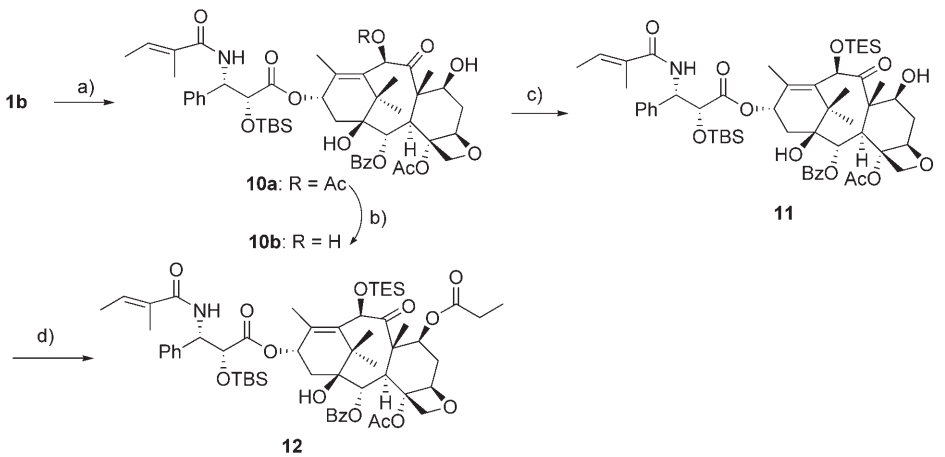

Scheme 1. Reagents and conditions: a) TBSCl, imidazole, DMF, RT, 91.6%; b) 85% $N_2H_4 \cdot H_2O$, ethanol, RT, 91.5%; c) *N*,*O*-bis(triethylsilyl)trifluoroacetamide, LHMDS, THF, −10 °C, 92.9%; d) $(CH_3CH_2CO)_2O$, Py, DMAP, THF, RT, 92.4%.

Cellular and molecular assays

Two groups of tumor cell lines were employed for cytotoxicity assays: human ovarian carcinoma A2780 and A2780/AD10 (MDR overexpressing P-gp), human ovarian carcinoma 1A9 (a subclone of A2780), and mutant lines derived from 1A9, 1A9/PTX10 and 1A9/PTX22. The multidrug-resistant A2780/AD10 tumor cell line is derived from continuous adriamycin treatment of A2780 cells, which induced P-gp overexpression as the major cause of their resistance to cytotoxic agents. The paclitaxel-resistant cell lines 1A9/PTX10 and 1A9/PTX22 are derived from 1A9 by selection with paclitaxel in combination with verapamil.[35] Because P-gp overexpression was inhibited by verapamil, drug resistance in these drug-resistant cells is mediated mainly through β-tubulin mutations. Three taxanes, including the commercially available drugs paclitaxel (**1a**), docetaxel (**1c**), and the starting material cephalomannine (**1b**), were used as reference compounds. From Table 1, it can be observed that **1b** is comparably or slightly less active than paclitaxel (**1a**) in all cellular and molecular assays, whereas docetaxel (**1c**) is usually more active.

Activities against drug-sensitive and drug-resistant tumor cells with P-gp overexpression

All four alkanoates **15n–q** were found to be 2–3 orders of magnitude less active than the three reference taxoids **1a–c** toward drug-sensitive and drug-resistant tumor cell lines. Ojima et al.[31] claimed that C2 benzoate is not an essential group for potent activity of taxoids, as 2-cyclohexanoate or 2-methylbutenoate analogues of docetaxel showed similar cytotoxicity to paclitaxel. They also found that the cytotoxicity of 2-debenzoyl-2-alkyl and 2-alkenyl esters depends on C3′ substitution variations.[31] However, this seems not to be true in our case; all alkyl and alkenyl esters were only weakly active in the parental cell lines 1A9 and A2780, and even the most

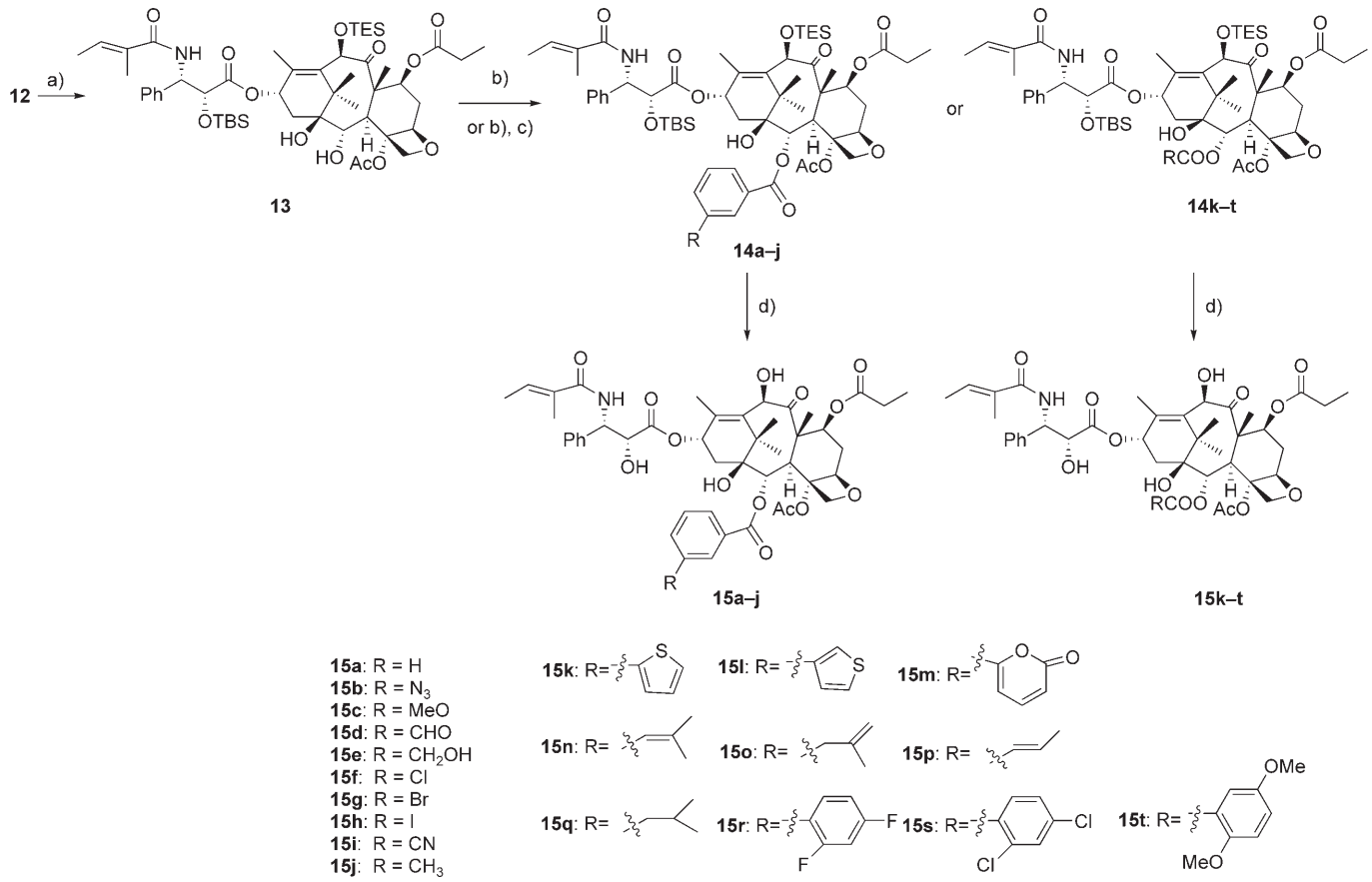

Scheme 2. Reagents and conditions: a) Triton B, CH_2Cl_2, −23 °C, 68.1 %; b) RCOOH, $PhCH_3$, DCC, PP, 65 °C; c) $NaBH_4$, CH_3OH/THF (only for **14e**); d) HF, Py, CH_3CN, RT.

active one (compound **15o**) was much less active than its C2 benzoyl counterpart.

In contrast, C2-*meta*-substituted benzoates were much more potent in cytotoxicity assays. For C2-modified 10-deacetyl-7-propionylcephalomannines **15**, a trend in cytotoxicity[15,30] was observed similar to that of C2-modified paclitaxel analogues: 2-*meta*-OMe and 2-*meta*-N_3 were the most active, and other *meta*-substituted and non-substituted benzoates were less active. It is interesting to note that 2-*meta*-N_3 taxoid **15b** exhibited not only potent activity against A2780 and A2780/AD10 cells, but also a low R/S value, a remarkable characteristic of some of the "advanced second-generation taxoids".[19]

Kingston et al. reported earlier[15,30] that the 2-*meta*-N_3-benzoate of paclitaxel was the most active taxane against HL-60 leukemia and HCT-116 human colon carcinoma cell lines, but less active than 2-*meta*-MeO-benzoate against the 1A9 cell line, and both were more active than paclitaxel. We prepared these two taxanes and found their cytotoxicity matched well with published results, showing superior activity to paclitaxel and even docetaxel, and confirming that 2-*meta*-MeO-benzoate analogues are better than 2-*meta*-N_3 analogues (data not shown). However, in our 10-deacetyl-7-propionyl series, the azido analogue **15b** is more active than the methoxy analogue **15c** in all cases.

We wondered whether the highly potent activity of **15b** originates from covalent binding of its reactive azido group to β-tubulin, so we performed experiments in which the amount of reversibly bound ligand was measured (Figure 3). Bound **15b** can be extracted from the pellets and aqueous solutions with an organic solvent, indicating that it is not irreversibly bound.[36,37] A comparison between the amounts of **15b** recovered from the pellet in the presence of microtubules and from the supernatant in the absence of microtubules showed that under the conditions of the assay **15b** is fully soluble and does not covalently bind to microtubules.

Previous studies demonstrated that neither steric nor electronic nature alone is the dominant factor in the activity of 2-*meta*-substituted benzoates. Although it seems that the polar group (in **15b**, **15c**, and **15f**) may make a positive contribution to the activity in comparison with **15a**, the low activity of **15d** and **15e** suggested the impairing effect of a polar group at the *meta* position of C2 benzoate. Furthermore, similar cytotoxicity among compounds with different halogen substituents **15f**–**h** and their bioisosteres **15i** and **15j** suggested that there is enough room in this region of β-tubulin to accommodate short-length substituents attached to the benzene ring. However, the interchange of C and O atoms from **15c** to **15e** led to a 200-fold loss of cytotoxicity, indicating that a very impor-

Table 1. Cytotoxicity and binding affinity to β-tubulin and P-gp.

Compd	R	IC_{50} [nM][a] A2780	IC_{50} [nM][a] A2780AD	R/S[b]	K_d [nM][c]	ΔG [KJ mol^{-1}][d]	K_d [nM][e]
15a	H	13.2±7	1222±300	92.5	240±40	−39.4±0.56	46±2.8
15b	*m*-N_3	3±1.7	17±4	5.6	1±0.2	−52.6±0.50	66±5.2
15c	*m*-OMe	8.3±2	160±19	19.2	19±4	−45.5±0.59	54±3.0
15d	*m*-CHO	69±77	1500±100	21.7	1449±133	−34.4±0.25	58±6.0
15e	*m*-CH_2OH	1700±120	>20000		>10000	>−30	51±5.0
15f	*m*-Cl	13.2±7.6	274±30	20.7	62±8	−42.4±0.35	66±6.4
15g	*m*-Br	28.7±1.9	196±14	6.8	83±36	−41.7±1.47	36±4.0
15h	*m*-I	30±0.5	246±27	8.2	57±19	−42.6±1.07	47±7.0
15i	*m*-CN	15.3±6.1	2100±660	137.2	256±34	−38.8±0.37	88±9.4
15j	*m*-CH_3	15.5±7	596±105	38.4	203±26	−39.4±0.35	58±5.4
15k	2-thiophene	62±17	3200±250	51.6	417±104	−37.6±0.74	58±5.0
15l	3-thiophene	106±4.2	2950±480	27.8	1020±301	−35.3±0.89	53±4.0
15m	2-chromone	14000±2000	>20000		4762±762	−31.3±0.45	76±11
15n	CH=C$(CH_3)_2$	950±80	10200±1900	10.7	2326±686	−33.2±0.89	39±3.9
15o	$CH_2C(CH_3)$=CH_2	980±70	4000±700	4.1	1389±265	−34.5±0.54	45±5.2
15p	CH=$CHCH_3$	3000±800	15000±3500	5	3571±794	−32.1±0.64	44±4.0
15q	$CH_2CH(CH_3)_2$	4900±600	>20000		2381±381	−33.1±0.45	41±3.2
15r	2,4-difluoro	82±16	1880±200	22.9	571±113	−36.7±0.56	46±5.0
15s	2,4-dichloro	102±8.8	690±60	6.7	402±98	−37.7±0.71	53±5.0
15t	2,5-dimethoxy	25±2	153±39	6.12	114±53	−40.9±1.61	46±5.0
Paclitaxel (**1a**)		1.3±0.4	900±160	692	70±8	−42.1±0.20	35±3.0
Cephalomannine (**1b**)		1.8±0.2	1100±320	611	145±15	−40.3±0.28	37±3.9
Docetaxel (**1c**)		0.3±0.1	290±321	966	25±1	−44.8±0.20	39±4.0

[a] IC_{50} values determined in the parental ovarian carcinoma A2780 line and the MDR P-gp-overexpressing ovarian carcinoma A2780/AD10. IC_{50} values in nM were determined after two days' exposure to drugs using the MTT cell proliferation assay. Data are the mean ±SE of at least four independent experiments. [b] Ratio of IC_{50} (resistant cell line)/IC_{50} (parental cell line). Values are the calculated relative resistance of each mutant cell line obtained by dividing the IC_{50} value of the resistant line by the IC_{50} value of the parental line, A2780. [c] Equilibrium dissociation constants of the ligands to microtubules at 35 °C. [d] Free energy changes derived from equilibrium binding constants of the ligands to microtubules at 35 °C ($-\Delta G_{0app} = RT\ln K_{binding}$). [e] Binding affinity of taxanes for purified P-gp determined by Trp fluorescence quenching.

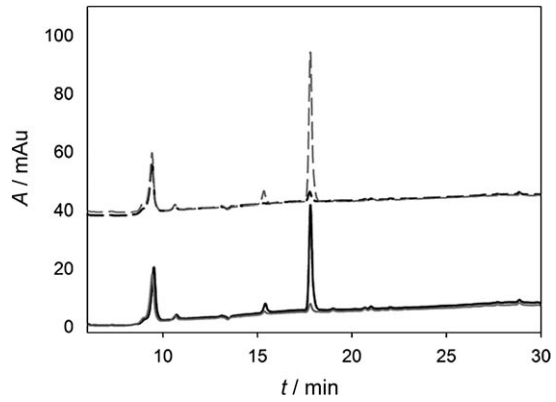

Figure 3. Taxane **15b** is not irreversibly bound to microtubules. Analysis of the **15b** content of microtubule pellets: 5 μM **15b** in GAB was incubated at 37 °C with (——) and without (-----) 10 μM taxoid binding sites in stabilized microtubules. The ligand in the pellets (black line) and supernatants (grey line) was extracted and analyzed as described in the Experimental Section.

tant interaction (such as hydrogen bonding or electrostatic interactions) between β-tubulin and the taxoid was broken in **15e**.

Heterocyclic carboxylic acid esters **15k**–**m**, like their precedent counterparts in the taxol series, were less active than **1a**–**c**. The 2-chromone **15m** is the least active among these analogues. For disubstituted benzoates **15r**–**t**, **15t** was found to show activity similar to that of the *meta*-methoxy taxoid **15c** for both IC_{50} and R/S values, whereas the other two (compounds **15r,s**) were less active.

Binding affinities toward β-tubulin and P-gp

Based on an established protocol,[38,37] we measured the equilibrium binding constants of the different analogues to β-tubulin using a fluorescence-based displacement method, and ΔG was calculated from Gibbs' equation. It was found that ΔG correlated roughly with published cytotoxicity (IC_{50} values) for C2-modified taxol analogues,[15] and also for our C2/C7/C10 taxanes (data not shown). It has been shown that for a group of chemically related taxoid binding site ligands (epothilones) a good correlation can be found between cytotoxicity (IC_{50}) and the free energy of binding to β-tubulin ($r^2 = 0.76$).[38] These findings were apparently unexpected, because it is not possible to know the total equilibrium concentration of the drugs in the cells, the extent of their metabolism, or whether there are any other targets or binding sites for the drugs in intact cells. If −40 to −42 kJ mol^{-1} (for reference taxanes **1a** and **1b**) is set as the standard, we can find only three taxanes that have higher apparent affinity for β-tubulin: docetaxel (**1c**) (−45 kJ mol^{-1}), **15b** (−46 kJ mol^{-1}), and **15c** (< -51 kJ mol^{-1}), all of which have been proven to be more active than **1a** and **1b** in cellular assays. Analogues with lower β-tubulin binding affin-

ity ($\Delta G > -35$ kJ mol^{-1}), including 2-alkanoates and alkenoates (compounds **15n**–**q**) and 2-chromone (**15m**), were found to be about three orders of magnitude less cytotoxic than reference taxanes **1a**–**c**.

To examine the influence of these taxanes on the P-gp drug efflux pump, we determined their K_d values for binding to the transporter by quenching the intrinsic Trp fluorescence of P-gp. A correlation was previously noted between the IC_{50} value for the inhibition of P-gp transport function by a drug, and its K_d value for binding to P-gp, which extended over four orders of magnitude.[39] It was found that the K_d values (Table 1) for all our modified taxanes were similar to those of **1a**–**c** in the assay, suggesting a similar ability of P-gp to pump them out of the cells.

Table 2. Cytotoxicity against parental and drug-resistant tumor cell lines with β-tubulin mutations.

Compd	R	IC_{50} [nM][a]				
		1A9	PTX10	R/S[b]	PTX22	R/S
15a	H	16 ± 2.5	900 ± 70	56.25	435 ± 17	27.1
15b	*m*-N_3	1.9 ± 0.1	11.6 ± 3.7	6.1	1.9 ± 0.4	1
15c	*m*-OMe	5.7 ± 2.6	37 ± 5.43	6.49	7.2 ± 1.1	1.2
15d	*m*-CHO	52.5 ± 8	2340 ± 820	44.5	950 ± 3	18
15e	*m*-CH_2OH	1390 ± 420	> 20000		14000 ± 4000	10
15f	*m*-Cl	6.4 ± 2.9	97 ± 8	15.1	51 ± 9.8	7.9
15g	*m*-Br	25 ± 0.7	212 ± 30	8.5	160 ± 24	6.4
15h	*m*-I	27 ± 2	505 ± 90	18.7	230 ± 2 8	8.5
15i	*m*-CN	12.3 ± 3	645 ± 3.5	52.4	320 ± 14	26
15j	*m*-CH_3	33 ± 4.2	722 ± 2	21.8	435 ± 17	13.1
15k	2-thiophene	56.5 ± 10	4000 ± 420	70.7	2000 ± 260	35.3
15l	3-thiophene	70.5 ± 1	6300 ± 910	89.3	3000 ± 530	42.5
15m	2-chromone	15000 ± 2700	> 20000		> 20000	
15n	$CH{=}C(CH_3)_2$	900 ± 70	15000 ± 2000	16.6	7900 ± 400	8.7
15o	$CH_2C(CH_3){=}CH_2$	1070 ± 50	1950 ± 600	1.8	3800 ± 30	3.5
15p	$CH{=}CHCH_3$	4000 ± 380	> 10000		> 10000	
15q	$CH_2CH(CH_3)_2$	8000 ± 1000	> 20000		> 20000	
15r	2,4-difluoro	92 ± 7	3600 ± 140	39.1	2500 ± 5	27.1
15s	2,4-dichloro	117 ± 5	3500 ± 170	29.9	2600 ± 150	22.2
15t	2,5-dimethoxy	24.2 ± 1.2	240 ± 20	9.9	167 ± 10	6.9
Paclitaxel (**1a**)		0.95 ± 0.5	67 ± 15	70.5	33 ± 4	34.7
Cephalomannine (**1b**)		0.5 ± 0.2	188 ± 10	376	68 ± 3.3	136
Docetaxel (**1c**)		0.7 ± 0.4	10.5 ± 4	15	2.9 ± 0.2	4.1

[a] IC_{50} values determined in parental ovarian carcinoma 1A9 (a clone of A2780), paclitaxel-resistant PTX10, and PTX22 with β-tubulin mutations. IC_{50} values in nM were determined after two days' exposure to drugs using the MTT cell proliferation assay. Data are the mean ± SE of at least four independent experiments. [b] Values are the calculated relative resistance of each mutant cell line obtained by dividing the IC_{50} value of the resistant line by the IC_{50} value of the parental line 1A9.

Activities against drug-sensitive and drug-resistant tumor cells with β-tubulin mutations

PTX10 and PTX22 cells have mutations in the β-tubulin gene at two different positions (Phe 270 → Val in PTX10 and Ala 364 → Thr in PTX22). These two amino acids lie on the floor of the deep hydrophobic pocket surrounding paclitaxel, and changes to them confer paclitaxel resistance.[29] Although these residues do not contact the C2 side chain in the T-Taxol binding conformation model,[29] Phe 270 is in direct contact with the methyl group of C4 of paclitaxel, while Ala 364 forms part of the hydrophobic pocket, but is not in direct contact with the drug molecule. It was previously reported that modifications in the C2 side chain of paclitaxel (*meta*-N_3-paclitaxel)[35] restore at least partially (R/S value of 3) the sensitivity of these cell lines to paclitaxel cytotoxicity. This suggests an interaction between C2 and these hydrophobic pocket residues, prompting us to investigate the effect of the modifications in this region of the molecule on cytotoxicity against cell lines containing β-tubulin mutations.

Similar to the results with P-gp-overexpressing MDR cells, all C2 alkyl analogues were less active than C2 *meta*-substituted benzoyl analogues (Table 2). While **15b** and **15c**/**15t** are the most active compounds, **15m** is still the least active against 1A9 and its drug-resistant counterparts bearing β-tubulin mutations. Full restoration of cytotoxicity was obtained only for compounds **15b** and **15c** with PTX22 cells (R/S values for **15b** and **15c** in 1A9/PTX22 are 1 and 1.2, respectively), and quite good restoration of sensitivity was observed for PTX10 cells (R/S value in 1A9/PTX10 is 6.1 and 6.49, respectively).

Those taxoids with high association constants for binding to β-tubulin, **15b** (-N_3) and **15c** (-OMe), also showed a great improvement in cytotoxicity against cell lines with mutant β-tubulins when compared with paclitaxel. While they were effective in killing the parental 1A9 cell lines (IC_{50} ratios to paclitaxel of 2 and 6, respectively), they were more cytotoxic than paclitaxel in both mutated cell lines (IC_{50} ratios for PTX10 of 0.17 and 0.55, IC_{50} ratios for PTX22 of 0.05 and 0.21, respectively). The fact that the IC_{50} ratios are better in the PTX22 than in the PTX10 cell lines may arise from the fact that a polar residue (Thr) is introduced into β-tubulin in place of a nonpolar residue (Ala), which may facilitate the accommodation of the newly introduced polar groups.

Discussion

Overexpression of P-gp is one of the major reasons for the MDR phenotype in tumors. P-gp is able to pump many hydrophobic molecules, including taxoids, out of the cell. From the high correlation between IC_{50} and ΔG for β-tubulin binding in drug-sensitive cells, it can be deduced that the binding affinity for β-tubulin is the main driving force for entry of taxoids into the cell. In this way, a competition model between P-gp and β-tubulin for the taxoids can be used to explain the results. For our analogues, only small differences are found between the

K_d values for binding of the taxoids to P-gp, whereas differences of 2–3 orders of magnitude are found in the dissociation constants for binding to β-tubulin. The activity of taxoids in cells overexpressing P-gp largely depends on the balance between cell uptake of the drug and pumping of the drug out of the cell. It was shown some time ago that P-gp intercepts drugs at the level of the plasma membrane in intact cells. If P-gp is present and can keep up with the rate of entry of the taxane (in other words, if the taxane concentration is kept well below the IC_{50} value), then the cells are likely not killed. The potent cytotoxic activity of taxanes such as **15b** is probably due to their enhanced β-tubulin binding ability in comparison with paclitaxel, even in P-gp-overexpressing tumor cells. Compound **15b**, which has a very low IC_{50} value (1–2 orders of magnitude lower than paclitaxel in MDR tumor cells), interacts with the P-gp pump in a similar fashion to paclitaxel, but must be retained in cells at a concentration above its IC_{50} value, and is thus able to initiate biochemical cascades leading to cell-cycle arrest and tumor cell killing.

It is logical to suppose that a ligand with a binding affinity for β-tubulin that is orders of magnitude higher than that for binding to P-gp will accumulate inside the cells despite the overexpression of P-gp, and little or no resistance should be observed in this case. Thus an alternative way to combat MDR due to P-gp overexpression is to increase the binding affinity of the drug for its β-tubulin target. According to our data, the affinity of taxoids for binding to P-gp is of the same order of magnitude as that for binding to β-tubulin. This means that a 10-fold increase in P-gp expression can be counteracted by a 10-fold increase in the affinity of the taxoid for β-tubulin, as long as the other parameters that control the flux of taxoids through the membrane and the affinity for P-gp remain constant. To check for the first parameter, the compounds were assayed against drug-sensitive cells, and their cytotoxicity correlated with their binding affinity. Because the two parameters correlated very well, it can be inferred that the modifications made to the taxoid molecules do not affect the parameters (other than β-tubulin binding affinity) that control their entry into cells. The affinity of the ligands for binding to P-gp was measured, and as no significant differences were found between the taxoids as a group, it can be proposed that compounds with very high affinity for binding to β-tubulin will be handled by P-gp in a similar fashion to those with lower affinity. A low resistance index can also be observed for the low-affinity taxanes; low-affinity taxanes should work as taxane-based reversal agents for themselves.[40,41] Owing to the high concentration required to bind tubulin and to be cytotoxic, they should fill all the P-gp sites with a small percentage of the compound available in solution, thus allowing the rest of the compound to enter the cells and kill them.

Although taxoid **15b** exhibits better activity than paclitaxel in A549 xenograft mice (ip doses of 10 and 30 mg kg^{-1}) and shows a C_{max} value of 1.7 mg L^{-1} after ip 30 mg kg^{-1}, it cannot be detected in plasma after oral administration at the same dose (30 mg kg^{-1}). This observation can be explained by the inability of **15b** to effectively penetrate P-gp-expressing cellular barriers in the gastrointestinal tract (in a similar fashion to paclitaxel[42]), also supporting the proposal that the potent activity of **15b** originates from its high β-tubulin binding affinity.

It is important to point out that those taxoids which display high-affinity β-tubulin binding, **15b** and **15c**/**15t**, also show improved activity against cells containing mutant tubulins (PTX10 and PTX22[35]). Our initial thought on mutation-mediated resistance is that it may depend on the position of mutation, that is, whether or not the altered amino acid residues on β-tubulin are close to the site of small-molecule binding. One can postulate that if the mutation in the protein is at a location distant from those regions interacting with the modified groups in the taxoids, a very similar effect would be observed for all ligands. On the other hand, if the mutation is close to those regions interacting with the modified groups in the taxoids, differential effects would be noticed. For our analogues, the differential effects of these taxoids suggests that the C2 modifications are located close to the sites of mutation in 1A9/PTX, such as F270V and A364T, two of six mutants as revealed earlier.[27,28]

In a recent report,[28] the mutation Q292E was identified as being located in helix 9 of β-tubulin, outside the taxoid binding region. The high degree of resistance to epothilones and taxoids exhibited by cells carrying this mutation is mediated through a change in the conformation of β-tubulin so as to hamper the entry of small molecules into the binding region. The high potency of **15b** and **15c** against drug-sensitive 1A9 and drug-resistant 1A9/PTX cell lines may reflect small conformational changes in β-tubulin induced by these mutations, in comparison with wild-type tubulin. However, more studies will be needed to explore this possibility, including assays for binding of **15b** and **15c** to mutant tubulins, as well as computer simulations of their conformations and docking of these molecules into the binding sites of mutant β-tubulin.

The SAR of the taxoids in this study might have been expected to show different patterns of cytotoxicity in drug-sensitive tumor cell lines relative to P-gp-overexpressing cell lines and cell lines with mutated tubulins. To our surprise, a particular compound exhibited a similar potency in all the cell lines. This may be explained by the fact that the ability of the taxoids to bind to β-tubulin varies significantly, whereas their physical properties and their interactions with P-gp are similar. Thus, their cytotoxicities against both drug-sensitive and P-gp-expressing drug-resistant cells are determined mainly by their abilities to bind to β-tubulin. Regarding the activity of the taxoids in the drug-resistant cells with β-tubulin mutations, the similar ability of any taxoid in the C2-modified 10-deacetyl-7-acyl series to bind to mutated tubulins and wild-type β-tubulin provides an explanation for their behavior.

However, it is especially noticeable that the IC_{50} values for many of the compounds are much lower than their dissociation constants (for paclitaxel, $IC_{50} = 1$ nM for 1A9 cells, with $K_d = 100$ nM at 37 °C), which would imply that unless the local drug concentration inside the cell is higher, only a very small fraction of the β-tubulin molecules would contain bound paclitaxel. A possible reason for the cytotoxic effect observed at such a low total drug concentration would be drug accumulation inside the cell due to the high local β-tubulin concentra-

tion, which would make the total intracellular concentration of drug much higher than that found extracellularly. In the case of compounds with similar physicochemical properties, the β-tubulin binding affinity would be the driving force for them to pass through the membrane and the parameter that maximizes the internal concentration of taxoid.

Although a correlation was found between β-tubulin mutations and paclitaxel resistance in non-small-cell lung cancer patients in a clinical report,[43] further work did not support the results from this study. Because all genes obtained in this study were pseudogenes, it has been proposed in a recent review[44] that β-tubulin mutations are unlikely to be induced during chemotherapy. Although there is still a debate on the role of these pseudogenes, high-affinity taxanes are useful in probing ligand–β-tubulin interactions even if their involvement is of lesser clinical relevance.

Conclusions

We have prepared a series of C2-modified 10-deacetyl-7-propionylcephalomannine derivatives, some of which showed potent activity against both drug-sensitive tumor cells and tumor cells with drug resistance arising from both P-gp overexpression and β-tubulin mutation mechanisms. The high potency of some taxoids in this series, such as **15b**, **15c**, and **15t**, is of interest because the superior antitumor activity of **15b** over that of paclitaxel has been proven not only at molecular and cellular levels, but also in tumor-bearing nude mice. Although we speculated from the above data that the cytotoxicity of these compounds against drug-resistant tumor cells is probably due to their high affinity for binding to β-tubulin, the details of their interactions with P-gp and β-tubulin merit further investigations. Overall, our research results led to an important hypothesis, that is, a taxane with very high affinity for binding to β-tubulin ($\Delta G < -50$ kJ mol^{-1}) is able to effectively counteract drug resistance mediated by both P-glycoprotein overexpression and β-tubulin mutations. It was also found recently[45] that some taxanes that are highly active against P-gp-overexpressing tumor cells are not P-gp inhibitors. Thus, we wonder if enhancement of binding affinity to the appropriate receptor could be a generally applicable strategy for the design of MDR-fighting cytotoxic agents.

Experimental Section

General experimental procedures: All chemicals other than anhydrous solvents were obtained from Aldrich and Acros and used without further purification. All anhydrous reactions were performed under N_2, and anhydrous THF was dried over sodium (benzophenone as indicator). All reactions were monitored by TLC (silica gel, GF_{254}) with UV light and H_2SO_4–anisaldehyde spray visualization. All compounds were homogeneous as judged by TLC and were >95% pure by NMR spectroscopy.

2′-*O*-(*tert*-butyldimethylsilyl)cephalomannine (10a): Imidazole (367 mg, 5.34 mmol) and *tert*-butyldimethylsilyl chloride (541 mg, 3.59 mmol) were added successively to a stirred solution of cephalomannine (**1b**; 600 mg, 0.72 mmol) in dried *N*,*N*-dimethylformamide (DMF; 5 mL). The reaction mixture was stirred for 3 h at room temperature and worked up with methanol (2 mL). The crude material was separated over silica gel using EtOAc/petroleum ether (1:3) as eluent to obtain 2′-*O*-(*tert*-butyldimethylsilyl)cephalomannine (**10a**) as a white solid (625 mg, 91.6%); ^{1}H NMR (300 MHz, $CDCl_3$): δ = 8.13 (2H, d, J = 7.2 Hz), 7.60 (1H, t, J = 7.2 Hz), 7.52 (2H, t, J = 7.2 Hz), 7.25–7.50 (5H, m), 6.65 (1H, d, J = 9.0 Hz), 6.45 (1H, q, J = 6.9 Hz), 6.30 (1H, s), 6.29 (1H, overlapped), 5.70 (1H, d, J = 7.2 Hz), 5.59 (1H, d, J = 9.0 Hz), 4.98 (1H, d, J = 7.8 Hz), 4.58 (1H, d, J = 1.8 Hz), 4.44 (1H, dd, J = 6.9, 10.9 Hz), 4.32 (1H, d, J = 8.7 Hz), 4.21 (1H, d, J = 8.4 Hz), 3.82 (1H, d, J = 6.9 Hz), 2.50–2.62 (1H, m, overlapped), 2.54 (3H, s), 2.38 (1H, dd, J = 9.6, 12.3 Hz), 2.24 (3H, s), 2.15 (1H, dd, J = 8.7, 15.3 Hz), 1.85–1.95 (1H, m, overlapped), 1.90 (3H, s), 1.81 (3H, s), 1.72 (3H, d, J = 6.9 Hz), 1.69 (3H, s), 1.29 (3H, s), 1.15 (3H, s), 0.79 (9H, s), −0.07(3H, s), −0.33 ppm (3H, s); ESIMS: m/z $[M+Na]^+$ 968.5, $[M+K]^+$ 989.4.

2′-*O*-(*tert*-butyldimethylsilyl)-10-deacetylcephalomannine (10b): Hydrazine hydrate (2.5 mL, 85% *v*/*v*) was added to a stirred solution of 2′-*O*-(*tert*-butyldimethylsilyl)cephalomannine (**10a**) (380 mg, 0.40 mmol) in anhydrous ethanol (25 mL). The reaction mixture was stirred for 2 h at room temperature and worked up by dilution with EtOAc (500 mL). The solution was washed sequentially with NH_4Cl (aq, 2×200 mL) and brine (2×100 mL), and the organic layer was separated and dried over Na_2SO_4, concentrated in vacuo to yield a crude residue, which was separated over silica gel using EtOAc/petroleum ether (2:3) as eluent to furnish **10b** as a white solid (332 mg, 91.5%); ^{1}H NMR (500 MHz, $CDCl_3$): δ = 8.13 (2H, d, J = 7.5 Hz), 7.60 (1H, t, J = 6.5 Hz), 7.52 (2H, t, J = 7.5 Hz), 7.37 (2H, t, J = 7.5 Hz), 7.24–7.31 (3H, m), 6.68 (1H, d, J = 9.0 Hz), 6.45 (1H, q, J = 7.0 Hz), 6.30 (1H, t, J = 9.0), 5.71 (1H, d, J = 7.5 Hz), 5.58 (1H, d, J = 8.0 Hz), 5.19 (1H, s), 4.97 (1H, d, J = 9.0 Hz), 4.58 (1H, d, J = 1.5 Hz), 4.33 (1H, d, J = 8.5 Hz), 4.26 (1H, overlapped), 4.23 (1H, d, J = 8.5 Hz), 3.94 (1H, d, J = 7.0 Hz), 2.57–2.63 (1H, m), 2.54 (3H, s), 2.36 (1H, dd, J = 10.0, 15.0 Hz), 2.13 (1H, dd, J = 9.0, 15.3 Hz), 1.93 (3H, s), 1.83–1.89 (1H, m), 1.83 (3H, s), 1.82 (3H, s), 1.72 (3H, d, J = 7.5 Hz), 1.26 (3H, s), 1.13 (3H, s), 0.79 (9H, s), −0.05 (3H, s), −0.32 ppm (3H, s); ESIMS: m/z $[M+Na]^+$ 926.6.

2′-*O*-(*tert*-butyldimethylsilyl)-10-*O*-triethylsilyl-10-deacetylcephalomannine (11): *N*,*O*-Bis(triethylsilyl)trifluoroacetamide (907 mg, 2.68 mmol) was added dropwise to a solution of taxane **10b** (300 mg, 0.332 mmol) in freshly distilled THF (10 mL) under N_2 at −10 °C, followed by the addition of lithium bis(trimethylsilyl)amide (3 μL, 0.003 mmol). The reaction mixture was stirred for 10 min at −10 °C and worked up with methanol (1 mL). The crude material was separated over silica gel using EtOAc/petroleum ether (1:2) as eluent to obtain **11** as a white solid (314 mg, 92.9%); ^{1}H NMR (300 MHz, $CDCl_3$): δ = 8.12 (2H, d, J = 6.9 Hz), 7.60 (1H, t, J = 7.2 Hz), 7.51 (2H, t, J = 7.8 Hz), 7.25–7.40 (5H, m), 6.76 (1H, d, J = 8.7 Hz), 6.46 (1H, q, J = 6.3 Hz), 6.22 (1H, t, J = 8.4 Hz), 5.71 (1H, d, J = 7.2 Hz), 5.55 (1H, d, J = 7.8 Hz), 5.21 (1H, s), 4.96 (1H, d, J = 8.4 Hz), 4.75 (1H, d, J = 3.6 Hz), 4.32 (1H, d, J = 8.7 Hz), 4.21 (1H, d, J = 8.4 Hz), 4.20 (1H, overlapped), 3.93 (1H, d, J = 7.2 Hz), 2.58–2.63 (1H, m), 2.52 (3H, s), 2.37 (1H, dd, J = 9.3, 15.6 Hz), 2.16 (1H, dd, J = 9.3, 15.0 Hz), 1.91 (1H, m, overlapped), 1.85 (3H, s), 1.83 (3H, s), 1.73 (3H, d, J = 6.9 Hz), 1.69 (3H, s), 1.21 (6H, s), 0.98 (9H, t, J = 8.4 Hz), 0.80 (9H, s), 0.58–0.68 (6H, m), −0.04 (3H, s), −0.33 ppm (3H, s); ESIMS: m/z $[M+Na]^+$ 1040.5.

2′-*O*-(*tert*-butyldimethylsilyl)-7-propionyl-10-*O*-triethylsilyl-10-deacetylcephalomannine (12): Taxane **11** (322 mg, 0.316 mmol) was dissolved in 5 mL dried THF, followed by the addition of propanoic anhydride (0.40 mL, 3.120 mmol), DMAP (20 mg, 0.164 mmol), and Et_3N (0.8 mL). The mixture was stirred for 20 h at room tempera-

ture, and was worked up by diluting with EtOAc (300 mL). The solution was washed sequentially with $NaHCO_3$ (aq, 2×50 mL) and brine (50 mL), and the aqueous layers were combined and extracted by EtOAc (150 mL). The organic layers were dried over Na_2SO_4 and concentrated under reduced pressure to yield a crude residue, which was separated over silica gel using EtOAc/petroleum ether (1:2) as eluent to obtain **12** (314 mg, 92.4%); ^{1}H NMR (300 MHz, $CDCl_3$): δ = 8.12 (2H, d, J = 7.8 Hz), 7.60 (1H, t, J = 7.8 Hz), 7.51 (2H, t, J = 7.8 Hz), 7.28–7.40 (5H, m), 6.70 (1H, d, J = 8.7 Hz), 6.48 (1H, q, J = 6.9 Hz), 6.20 (1H, t, J = 9.3 Hz), 5.73 (1H, d, J = 6.3 Hz), 5.55 (1H, d, J = 9.3 Hz), 5.47 (1H, dd, J = 7.2, 10.3 Hz), 5.26 (1H, s), 4.94 (1H, d, J = 8.4 Hz), 4.58 (1H, d, J = 2.1 Hz), 4.33 (1H, d, J = 8.4 Hz), 4.22 (1H, d, J = 8.7 Hz), 4.00 (1H, d, J = 7.2 Hz), 2.48–2.56 (1H, m, overlapped), 2.52 (3H, s), 2.37 (1H, dd, J = 10.2, 16.5 Hz), 2.29 (2H, q, J = 7.8 Hz), 2.16 (1H, dd, J = 10.2, 16.5 Hz), 1.92 (3H, s), 1.84 (3H, s), 1.83 (1H, overlapped), 1.81 (3H, s), 1.78 (3H, d, J = 6.9 Hz), 1.21 (6H, s), 1.10 (3H, t, J = 7.2 Hz), 0.97 (9H, t, J = 7.8 Hz), 0.81 (9H, s), 0.53–0.62 (6H, m), −0.03 (3H, s), −0.33 ppm (3H, s); ESIMS: *m/z* $[M+Na]^+$ 1096.5.

2′-*O*-(*tert*-butyldimethylsilyl)-2-debenzoyl-7-propionyl-10-*O*-triethylsilyl-10-deacetyl-cephalomannine (13): Benzyltrimethylammonium hydroxide (40% *w/w* in MeOH, 190.9 μL) was added to a solution of taxane **12** (222.2 mg, 0.21 mmol) in anhydrous CH_2Cl_2 (5 mL) at −23 °C. The reaction mixture was stirred for 10 min and quenched with saturated NH_4Cl (aq, 30 mL). The aqueous layer was extracted with CH_2Cl_2 (3×50 mL), the organic layers were combined, dried over Na_2SO_4, and concentrated under reduced pressure. Silica gel chromatography of the residue (hexane/EtOAc/acetone = 8:3:1) afforded starting material (56.6 mg, 28.2%) and **13** (136.8 mg, 68.1%; 94.9% based on unrecovered starting material); ^{1}H NMR (500 MHz, $CDCl_3$): δ = 7.35 (2H, t, J = 7.0 Hz), 7.29 (1H, d, J = 7.0 Hz), 7.23 (2H, d, J = 7.5 Hz), 6.69 (1H, d, J = 9.0 Hz), 6.47 (1H, q, J = 8.0 Hz), 6.13 (1H, t, J = 8.5 Hz), 5.51 (1H, d, J = 9.5 Hz), 5.44 (1H, dd, J = 7.0, 10.0 Hz), 5.19 (1H, s), 4.94 (1H, d, J = 8.5 Hz), 4.66 (2H, br s), 4.51 (1H, d, J = 1.5 Hz), 3.95 (1H, d, J = 7.0 Hz), 3.64 (1H, d, J = 6.5 Hz), 2.47–2.53 (1H, m), 2.37 (3H, s), 2.27 (2H, q, J = 7.0 Hz), 2.14–2.17 (2H, m), 1.90 (1H, overlapped), 1.87 (3H, s), 1.86 (3H, s), 1.81 (3H, s), 1.77 (3H, d, J = 7.0 Hz), 1.18 (3H, s), 1.08 (3H, t, J = 7.5 Hz), 1.06 (3H, s), 0.95 (9H, t, J = 7.5 Hz), 0.80 (9H, s), 0.51–0.62 (6H, m), −0.07 (3H, s), −0.31 ppm (3H, s); ESIMS: *m/z* $[M+Na]^+$ 992.5.

General procedure for the preparation of 2′-*O*-(*tert*-butyldimethylsilyl)-2-debenzoyl-2-acyl-7-propionyl-10-*O*-triethylsilyl-10-deacetylcephalomannine (14): An appropriate carboxylic acid (0.1 mmol) was dissolved in dried toluene (0.2 mL), and then DCC (20.6 mg, 0.1 mmol) and PP (1.0 mg, 0.007 mmol) were added to the solution. The mixture was stirred at room temperature for 5 min, taxane **13** (9.7 mg, 0.01 mmol) was added, the mixture was stirred at 65 °C until compound **13** was consumed (TLC analysis). The reaction mixture was diluted with EtOAc (10 mL), filtered through a pad of celite, and the celite was washed with EtOAc (10 mL). The filtrate was concentrated in vacuo to dryness. The residue was purified using PTLC (silica gel, hexane/EtOAc/acetone = 8:3:1) to afford **14**. Although it was found that the products were contaminated with dicyclohexylurea by ^{1}H NMR, they were subjected to desilylation without further purification.

General procedure for desilylation of 14: Pyridine (0.533 mL, 6.60 mmol) and HF (aq, 0.293 mL, 6.60 mmol) were added dropwise to a solution of taxane **14** (0.022 mmol) in acetonitrile (1.06 mL) in a 5-mL plastic bottle. The mixture was stirred at room temperature until the starting material was consumed as determined by TLC. The reaction mixture was diluted with EtOAc, washed with saturated $NaHCO_3$ and brine, and the aqueous layers were combined and extracted three times with EtOAc. The organic layer was dried over Na_2SO_4 and concentrated to dryness. Purification of the residue was carried out using PTLC (1:2 EtOAc/petroleum ether) to give homogeneous products.

Analytical data for compounds **15a–t** are given in the Supporting Information.

Tubulin and ligands: Purified calf brain tubulin and chemicals were used as described.[36] Paclitaxel (Taxol®) was provided by the late M. Suffness from the National Cancer Institute (Bethesda, MD, USA). Docetaxel (Taxotere) was kindly provided by Rhône Poulenc Rorer, Aventis (Schiltigheim, France). Taxoids were synthesized by us and characterized on the basis of spectroscopic methods. All the compounds were diluted in dimethyl sulfoxide (DMSO) to a final concentration of 10 mM and stored at −70 °C.

Preparation of stabilized microtubules: Stabilized cross-linked microtubules were prepared by mild cross-linking with 0.2% glutaraldehyde. Excess glutaraldehyde was quenched with $NaBH_4$ (Fluka), and the solution was dialyzed overnight using Slide-A-Lyzer 10K dialysis cassettes (Pierce) against the desired buffer and drop-frozen in liquid nitrogen.[46,47] After this treatment, 90% of the tubulin was found to have incorporated into microtubules, which are stable against dilution and low temperatures. The concentration of paclitaxel binding sites in these cross-linked microtubules was determined as described.[47] 100% of the assembled tubulin dimers were found to bind taxoids immediately after dialysis.

Equilibrium constants for binding of taxoid ligands to microtubules: The equilibrium binding constants of the different ligands to the paclitaxel binding site of assembled microtubules were measured as described.[38,37] Binding constants for compounds reversibly displacing Flutax-2 were calculated using a PC program written by us (Equigra v 5, J. F. Diaz, unpublished software). This program fits the experimental data by least squares to the equilibrium binding constant of the ligand investigated, employing the known values of the reference ligand Flutax-2. The apparent ΔG_0 was calculated from the binding constants using the equation: $-\Delta G_{0app} = RT \ln K_{binding}$

Binding of ligands to microtubules: Samples containing 5 μM compound **15b** and 10 μM taxoid binding sites in stabilized cross-linked microtubules (prepared as described above), were incubated for 30 min at 25 °C in polycarbonate centrifuge tubes (Beckman) in GAB (glycerol assembly buffer; 3.4 M glycerol, 10 mM sodium phosphate, 6 mM magnesium chloride, and 1 mM glycol-bis(2-aminoethylether)-*N,N,N′,N′*-tetraacetic acid (EGTA), pH 6.7) with 0.1 mM GTP (DMSO concentration was always kept under 2%). The samples were then centrifuged at 90000 *g* for 10 min at 25 °C in a Beckman Optima TLX ultracentrifuge with a TLA100 rotor. The supernatants were collected by pipetting, and the pellets were resuspended in 10 mM phosphate (pH 7.0). Both the pellets and supernatants were extracted three times with an equal volume of dichloromethane, dried in vacuo, and dissolved in 60 mL methanol/water (75:25 *v/v*). Ligands reversibly bound to pelleted polymers and free in the supernatant were determined by HPLC. HPLC analysis of the samples was performed in an Agilent 1100 series instrument employing a C18 column (Supercosil, LC18 DB, 250×4.6 mm, 5 μm bead diameter) developed in a gradient from 50–80% (*v/v*) acetonitrile in water at a flow rate of 1 mL min^{-1}, following the absorbance at λ = 220 nm.

Determination of dissociation constants for binding to P-gp by quenching of intrinsic Trp fluorescence: Purified P-gp was isolat-

ed from MDR cells according to established methods.[39] Fluorescence quenching was carried out using 50 μg mL^{-1} purified P-gp in buffer consisting of 2 mM 3-[(3-cholamidopropyl)-dimethylammonio]-1-propanesulfonate (CHAPS), 20 mM *N*-2-hydroxyethylpiperazine-*N*′-2-ethanesulfonic acid (HEPES), 100 mM NaCl, 5 mM $MgCl_2$, pH 7.5, as described previously.[48] Modified taxanes were dissolved in DMSO at 10 mg mL^{-1} as stock solutions, and working solutions (from 1.25–40 μg mL^{-1}) were made by diluting the stock solution with the above buffer. Quenching experiments were performed by successively adding 5-μL aliquots of taxane working solutions to 500 μL P-gp as described previously.[39] The final concentrations of the added taxanes were in the range 0.0125–1.5 μg mL^{-1}. After each addition, the steady-state fluorescence was measured at λ_{ex} = 290 nm and λ_{em} = 330 nm with 2-nm slits. Because the taxanes do not absorb light at the excitation and emission wavelengths, the recorded fluorescence intensities were corrected only for dilution using the following equation:

$$F_{icor} = (F_i - B)(V_i/V_0) \quad (1)$$

for which F_{icor} is the corrected value of the fluorescence intensity at a given point in the titration, F_i is the experimentally measured fluorescence intensity, B is the background fluorescence of the buffer, V_0 is the initial volume of the sample, and V_i is the volume of the sample at a given point in the titration. The data were computer fitted to the following equation:

$$\left(\frac{\Delta F}{F_0} \times 100\right) = \frac{\left(\frac{\Delta F_{max}}{F_0} \times 100\right) \times [S]}{K_d + [S]} \quad (2)$$

in which ($\Delta F/F_0 \times 100$) is the percent quenching (relative to the initial value) following addition of taxane at a concentration [*S*], and the values of dissociation constant (K_d) and maximal percent quenching ($\Delta F_{max}/F_0 \times 100$) were extracted using the Regression Wizard of Sigma Plot (Systat Software, Point Richmond, CA, USA).

Cell culture: Human ovarian carcinoma cell lines 1A9, A2780, A2780/AD (multidrug-resistant, overexpressing P-gp), PTX10, and PTX22 (a gift of P. Giannakakou) were cultured in RPMI-1640 supplemented with 10% fetal calf serum, 2 mM L-glutamine, 40 μg mL^{-1} gentamycin, 100 IU mL^{-1} penicillin, and 100 μg mL^{-1} streptomycin. A2780 and A2780/AD media were supplemented with 0.25 U mL^{-1} bovine insulin.

Cell cytotoxicity assay: Cells were seeded in 96-well plates at a density of 12000 cells in 0.08 mL per well. The next day, cells were exposed to 0.02-mL serial dilutions (0.005 nM to 40 μM) of ligands for 48 h, at which time an MTT (3-(4,5-dimethylthiazol-2-yl)-2,5-diphenyltetrazolium bromide) assay to determine viable cells was performed with some modifications.[49] Briefly, 20 μL of 2.5 mg mL^{-1} MTT was added to each well, incubated for 4 h at 37 °C, then treated with 0.1 mL MTT solubilizer (10% SDS, 45% DMF, pH 5.5). Plates were again incubated overnight at 37 °C to solubilize the blue formazan precipitate before measuring the absorbance at 595/690 nm in an automated Multiscan MC microplate reader. Control wells containing medium without cells were used as blanks. The MTT response is expressed as a percentage of the control (untreated) cells. IC_{50} was calculated from the log dose–response curves and expressed as the mean of at least four independent experiments with standard errors.

Acknowledgements

The authors thank the Foundation for the Author of National Excellent Doctoral Dissertation of P. R. China (Grant No. 199949), the Fok Ying Tong Education Foundation (Grant No. 91037), and the National Natural Science Foundation (Grant No. 20572135) (to W.-S.F.); the Dirección General de Investigación Científica y Tecnológica (DGICYT, Grant BFU2004-00358), the Comunidad Autonoma de Madrid (Grants CAM200520M061 and BIPPED-CM), the Ministerio de Educación y Ciencia of Spain (Grant BFU-2004-0038) (to J.F.D.); and the Canadian Cancer Society (to F.J.S.) for financial support. Thanks to Matadero Madrid Norte S.A. and José Luis Gancedo S.L. for providing the calf brains for tubulin purification and Dr. Jinlan Zhang for performing HRMS experiments. We also appreciate Prof. Jose Andreu for his helpful suggestions.

Keywords: β-tubulin · drug design · drug resistance · P-glycoprotein · structure–activity relationships

[1] M. C. Wani, H. L. Taylor, M. E. Wall, P. Coggon, A. T. McPhail, *J. Am. Chem. Soc.* **1971**, *93*, 2325 – 2327.
[2] For recent reviews, see: a) D. G. I. Kingston, *Chem. Commun.* **2001**, 867 – 880; b) F. Gueritte, *Curr. Pharm. Des.* **2001**, *7*, 1229 – 1249; c) D. G. I. Kingston, P. G. Jagtap, H. Yuan, L. Samala, *Prog. Chem. Org. Nat. Prod.* **2002**, *84*, 53 – 226; d) G. I. Georg, T. C. Boge, Z. S. Cheruvallath, J. S. Clowers, G. C. B. Harriman, M. Hepperle, H. Prak in *Taxol: Sciences and Applications* (Ed.: M. Suffness), CRC, Boca Raton, **1995**, pp. 317 – 386.
[3] M. I. Nicoletti, T. Colombo, C. Rossi, C. Monardo, S. Stura, M. Zucchetti, A. Riva, P. Morazzoni, M. B. Donati, E. Bombardelli, M. D'Incalci, R. Giavazzi, *Cancer Res.* **2000**, *60*, 842 – 846.
[4] Y. Takeda, T. Yoshino, K. Uoto, J. Chiba, T. Ishiyama, M. Iwahana, T. Jimbo, N. Tanaka, H. Terasawa, T. Soga, *Bioorg. Med. Chem. Lett.* **2003**, *13*, 185 – 190.
[5] T. J. Altstadt, C. R. Fairchild, J. Golik, K. A. Johnston, J. F. Kadow, F. Y. Lee, B. H. Long, W. C. Rose, D. M. Vyas, H. Wong, M.-J. Wu, M. D. Wittman, *J. Med. Chem.* **2001**, *44*, 4577 – 4583.
[6] M. R. Vredenburg, I. Ojima, J. Veith, P. Pera, K. Kee, F. Cabral, A. Sharma, P. Kanter, W. R. Greco, R. J. Bernacki, *J. Natl. Cancer Inst.* **2001**, *93*, 1234 – 1245.
[7] M. Shionoya, T. Jimbo, M. Kitagawa, T. Soga, A. Tohgo, *Cancer Sci.* **2003**, *94*, 459 – 466.
[8] I. Ojima, J. C. Slater, E. Michaud, S. D. Kuduk, P.-Y. Bounaud, P. Vrignaud, M.-C. Bissery, J. Veith, P. Pera, R. J. Bernacki, *J. Med. Chem.* **1996**, *39*, 3889 – 3896.
[9] L. Bhat, Y. Liu, S. F. Victory, R. H. Himes, G. I. Georg, *Bioorg. Med. Chem. Lett.* **1998**, *8*, 3181 – 3186.
[10] Y. B. Liu, S. M. Ali, T. C. Boge, G. I. Georg, S. Victory, J. Zygmunt, R. T. Marquez, R. H. Himes, *Comb. Chem. High Throughput Screening* **2002**, *5*, 39 – 48.
[11] J. Kobayashi, H. Hosoyama, X.-X. Wang, H. Shigemori, Y. Koiso, Y. Sudo, T. Tsuruo, *Bioorg. Med. Chem. Lett.* **1998**, *8*, 1555 – 1558.
[12] T. Ishiyama, S. Iimura, S. Ohsuki, K. Uoto, H. Terasawa, T. Soga, *Bioorg. Med. Chem. Lett.* **2002**, *12*, 1083 – 1086.
[13] M. D. Chordia, H. Yuan, P. G. Jagtap, J. F. Kadow, B. H. Long, C. R. Fairchild, K. A. Johnston, D. G. I. Kingston, *Bioorg. Med. Chem.* **2001**, *9*, 171 – 178.
[14] W. S. Fang, Y. Liu, H. Y. Liu, S.-F. Xu, L. Wang, Q.-C. Fang, *Bioorg. Med. Chem. Lett.* **2002**, *12*, 1543 – 1546.
[15] D. G. I. Kingston, A. G. Chaudhary, M. D. Chordia, M. Gharpure, A. A. L. Gunatilaka, P. I. Higgs, J. M. Rimoldi, L. Samala, P. G. Jagtap, *J. Med. Chem.* **1998**, *41*, 3715 – 3726.
[16] I. Ojima, S. Lin, *J. Org. Chem.* **1998**, *63*, 224 – 225.
[17] M. Xue, B. H. Long, C. Fairchild, K. Johnston, W. C. Rose, J. F. Kadow, D. M. Vyas, S.-H. Chen, *Bioorg. Med. Chem. Lett.* **2000**, *10*, 1327 – 1331.

[18] E. J. Roh, D. Kim, C. O. Lee, S. U. Choi, C. E. Song, *Bioorg. Med. Chem.* **2002**, *10*, 3145 – 3151.
[19] I. Ojima, T. Wang, M. L. Miller, S. Lin, C. P. Borella, X. Geng, P. Pera, R. J. Bernacki, *Bioorg. Med. Chem. Lett.* **1999**, *9*, 3423 – 3428.
[20] E. Baloglu, J. M. Hoch, S. K. Chatterjee, R. Ravindra, S. Bane, D. G. I. Kingston, *Bioorg. Med. Chem.* **2003**, *11*, 1557 – 1568.
[21] R. W. Miller, R. G. Powell, C. R. Smith, Jr., E. Arnold, J. Clardy, *J. Org. Chem.* **1981**, *46*, 1469 – 1474.
[22] R. C. Pandey, L. K. Yankov, A. Poulev, R. Nair, S. Caccamese, *J. Nat. Prod.* **1998**, *61*, 57 – 63.
[23] Q. Y. Zheng, C. K. Murray, R. J. Daughenbaugh, US patent 5892063, **1999**.
[24] M. Distefano, G. Scambia, C. Ferlini, D. Gallo, R. De Vincenzo, P. Filippini, A. Riva, E. Bombardelli, S. Mancuso, *Anticancer Drug Des.* **1998**, *13*, 489 – 499.
[25] L. Bhat, Y. Liu, S. F. Victory, R. H. Himes, G. I. Georg, *Bioorg. Med. Chem. Lett.* **1998**, *8*, 3181 – 3186.
[26] R. A. Holton, K.-B. Chai, US patent US 6462208, **2002**.
[27] P. Giannakakou, R. Gussio, E. Nogales, K. H. Downing, D. Zaharevitz, B. Bollbuck, G. Poy, D. Sackett, K. C. Nicolaou, T. Fojo, *Proc. Natl. Acad. Sci. USA* **2000**, *97*, 2904 – 2909.
[28] N. M. Verrills, C. L. Flemming, M. Liu, M. T. Ivery, G. S. Cobon, M. D. Norris, M. Haber, M. Kavallaris, *Chem. Biol.* **2003**, *10*, 597 – 607.
[29] J. P. Snyder, J. N. Nettles, B. Cornett, K. H. Downing, E. Nogales, *Proc. Natl. Acad. Sci. USA* **2001**, *98*, 5312 – 5316.
[30] A. G. Chaudhary, M. M. Gharpure, J. M. Rimoldi, M. D. Chordia, D. G. I. Kingston, S. Grover, C. M. Lin, E. Hamel, A. A. L. Gunatilaka, *J. Am. Chem. Soc.* **1994**, *116*, 4097 – 4098.
[31] I. Ojima, S. D. Kuduk, P. Pera, J. M. Veith, R. J. Bernacki, *J. Med. Chem.* **1997**, *40*, 279 – 285.
[32] M. D. Chordia, D. G. I. Kingston, *J. Org. Chem.* **1996**, *61*, 799 – 801.
[33] A. Datta, M. Hepperle, G. I. Georg, *J. Org. Chem.* **1995**, *60*, 761 – 763.
[34] R. A. Holton, Z. Zhang, P. A. Clarke, H. Nadizadeh, D. J. Procter, *Tetrahedron Lett.* **1998**, *39*, 2883 – 2886.
[35] P. Giannakakou, D. L. Sackett, Y.-K. Kang, Z. Zhan, J. T. M. Buters, T. Fojo, M. S. Poruchynsky, *J. Biol. Chem.* **1997**, *272*, 17118 – 17125.
[36] J. F. Díaz, M. Menéndez, J. M. Andreu, *Biochemistry* **1993**, *32*, 10067 – 10077.
[37] R. M. Buey, I. Barasoain, E. Jackson, A. Meyer, P. Giannakakou, I. Paterson, S. Mooberry, J. M. Andreu, J. F. Díaz, *Chem. Biol.* **2005**, *12*, 1269 – 1279.
[38] R. M. Buey, J. F. Díaz, J. M. Andreu, A. O'Brate, P. Giannakakou, K. C. Nicolaou, P. K. Sasmal, A. Ritzén, K. Namoto, *Chem. Biol.* **2004**, *11*, 225 – 236.
[39] F. J. Sharom, R. Liu, Y. Romsicki, P. Lu, *Biochim. Biophys. Acta* **1999**, *1461*, 327 – 345.
[40] T. A. Brooks, H. Minderman, K. L. O'Loughlin, P. Pera, I. Ojima, M. R. Baer, R. J. Bernacki, *Mol. Cancer Ther.* **2003**, *2*, 1195 – 1205.
[41] T. A. Brooks, D. R. Kennedy, D. J. Gyuol, I. Ojima, M. R. Baer, R. J. Bernacki, *Anticancer Res.* **2004**, *24*, 409 – 415.
[42] A. Sparreboom, J. van Asperen, U. Mayer, A. H. Schinkel, J. W. Smit, D. K. Meijer, P. Borst, W. J. Nooijen, J. H. Beijnen, O. van Tellingen, *Proc. Natl. Acad. Sci. USA* **1997**, *94*, 2031 – 2035.
[43] M. Monzó, R. Rosell, J. J. Sánchez, J. S. Lee, A. O'Brate, J. L. González-Larriba, V. Alberola, J. C. Lorenzo, L. Nuñez, J. Y. Ro, C. Martin, *J. Clin. Oncol.* **1999**, *17*, 1786 – 1793.
[44] H. K. Berrieman, M. J. Lind, L. Cawkwell, *Lancet Oncol.* **2004**, *5*, 158 – 164.
[45] M. Ehrlichova, R. Vaclavikova, R. Vaclavikova, I. Ojima, A. Pepe, L. V. Kuznetsova, C. Jin, J. Truksa, J. Kovar, I. Gut, *Naunyn-Schmiedeberg's Arch. Pharmacol.* **2005**, *372*, 95 – 105.
[46] J. M. Andreu, I. Barasoain, *Biochemistry* **2001**, *40*, 11975 – 11984.
[47] J. F. Díaz, I. Barasoain, J. M. Andreu, *J. Biol. Chem.* **2003**, *278*, 8407 – 8419.
[48] R. Liu, A. Siemiarczuk, F. J. Sharom, *Biochemistry* **2000**, *39*, 14927 – 14938.
[49] T. Mossman, *J. Immunol. Methods* **1983**, 65, 55 – 63.

Received: December 21, 2006
Published online on March 27, 2007

Available online at www.sciencedirect.com
ScienceDirect
Bioorganic & Medicinal Chemistry Letters 17 (2007) 3191–3194
Bioorganic & Medicinal Chemistry Letters

Synthesis, biological evaluations, and tubulin binding poses of C-2α sulfur linked taxol analogues

Lei Wang,[a,e] Ana A. Alcaraz,[c] Ruth Matesanz,[d] Chun-Gang Yang,[a] Isabel Barasoain,[d] J. Fernando Díaz,[d] Ye-Zhi Li,[e] James P. Snyder[c] and Wei-Shuo Fang[a,b,*]

[a]*Institute of Materia Medica, Chinese Academy of Medical Sciences, 1 Xian Nong Tan Street, Beijing 100050, PR China*
[b]*Key Laboratory of Bioactive Substances and Resources Utilization of Chinese Herbal Medicine (Ministry of Education), Peking Union Medical College, Beijing 100050, PR China*
[c]*Department of Chemistry, Emory University, Atlanta, GA 30322, USA*
[d]*Centro de Investigaciones Biologicas, Consejo Superior de Investigaciones Cientificas, Ramiro de Maeztu 9, 28040 Madrid, Spain*
[e]*Department of Chemistry, Jilin University, Changchun, Jilin 130012, PR China*

Received 29 November 2006; revised 6 March 2007; accepted 8 March 2007
Available online 14 March 2007

Abstract—In combination with chemical modifications, bioassays, and computational simulation techniques, C-2 benzoylthio, and benzylthio taxoids were synthesized, biologically evaluated, and their binding conformations rationalized, in order to probe the interaction of taxane molecule with β-tubulin.

Chemical and biological evaluation of the antitumor agent paclitaxel (PTX, Taxol®, **1**) has been a mainstream focus for natural product research since the mid 1990s. The subject remains an active field in the attempt to overcome problems of resistance[1a,b] and toxicity.[1c] Both PTX[2] and its analogue docetaxel **2** (DTX)[3a,b] are currently used clinically for the treatment of ovarian, breast, and non-small lung cancers, especially at the recurrent or metastatic stages.

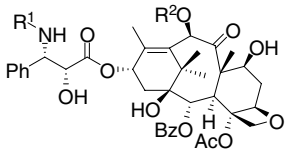

1: R^1 = Bz, R^2 = Ac **2:** R^1 = Boc, R^2 = H

Many other antitubulin agents possessing a similar mechanism of action are also found, including the most widely studied classes such as epothilones, sarcodictyins, eleutherobin, discodermolide, and laulimalide.[4] Compounds that prevent the formation of microtubules but likewise perturb the tubulin-microtubule equilibrium (e.g., colchicine congeners, vinca alkaloids,[5a] hemiasterlins[5b], and noscapine analogues[5c]) have also contributed to the rather large family of tubulin-based antineoplastic agents in recent years.

With respect to PTX, extensive structure-activity relationship (SAR) studies over the past two decades have led to several generalizations. Perhaps the most crucial one concerns three key side chains on the southern hemisphere of the molecule: the C-13 *N*-benzoyl phenylisoserne, the C-2 benzoate, and the C-4 acetate moieties. Both in terms of atomic constitution and molecular conformation, all are critical to taxane tubulin binding and cytotoxicity.[6a,b] At the conformational level, although there are upwards of a dozen different forms of PTX conformers in solution,[7] three extremes have at times been proposed as that bound to β-tubulin: the polar, nonpolar, and T-Taxol conformations.[8] Only the latter has led to the design and synthesis of tethered taxanes that show potency superior to PTX in a combination of microtubule stabilization and cytotoxicity assays.[9]

SAR studies at the C-2 position have shown that both the nature and stereochemistry of the 2-benzoyl group

Keywords: Paclitaxel; Taxol analogues; Binding conformation; SAR studies.
* Corresponding author. Tel.: + 86 10 63165237; fax: + 86 10 63017757; e-mail: wfang@imm.ac.cn

0960-894X/$ - see front matter © 2007 Elsevier Ltd. All rights reserved.
doi:10.1016/j.bmcl.2007.03.026

in PTX derivatives are determinants of activity.[10,11] On the other hand, many paclitaxel analogues with aroyl[12] or alkyl[13] ester groups at the C-2 position have been reported with modest to highly potent cytotoxicity.

We also undertook the preparation of a series of C2 heteroatom-substituted taxoids to probe the PTX C-2 structural requirements. Based on the methodology reported in our first communication,[14a] we were able to develop a cytotoxicity SAR for the 2-amido analogues,[14b] its C-10 modified analogues,[14c] and 2-debenzoyloxy-2α-phenylthio 10-acetyl docetaxel[14d] whose inactivity can be attributed to its shorter chain length at C-2 compared with benzoate.

Although a photoaffinity labeling experiment indicated that C-2 substituents are close to residues 217–231 of β-tubulin[15] and X-ray crystallographic data gave the location of β-tubulin and its taxane ligand,[18] the binding conformation as well as the residues in β-tubulin and functional groups in taxane involved in binding process cannot be determined with precision.

Here we report preparation of the first PTX analogues bearing 2α-benzoylthio and benzylthio moieties designed on the basis of isostere replacement principle, and their initial SARs as well. Their conformations correlated with their binding affinity to β-tubulin are also explored.

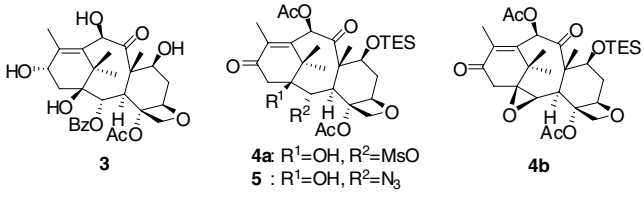

Following a known procedure,[14a] 10-DAB **3** was converted into the key epoxide intermediate **4b**. All reactions proceeded in satisfactory yields from 88–97%. Epoxide **4b** exists as an inseparable mixture containing 2-mesylate **4a** (ca. 2:1). Treatment of the **4a** and **4b** mixture with NaN_3 afforded the double S_N2 product 2-azido baccatin **5** in ca. 85% yield, implying that **4a** was converted to **4b** during the course of the reaction.

Following the same strategy, the mixture of **4a** and **4b** was treated with sodium thiobenzoate to furnish **6a** in 56% yield. The ^1H shifts for H-2 in **6a** are almost identical to the 2-benzoate counterpart, while H-3 is shifted slightly downfield by 0.2 ppm. The latter reflects a modified environment around H-3 arising from changes in the C-2 thioester geometry (bond lengths and angles) by comparison with the corresponding ester. Subsequent reduction of **6a**–**7a** (80%) and incorporation of the C-13 side chains with enantiopureβ-lactams **8a**–**b** afforded products **9aa** and **9ab**, which were then deprotected at C-2′ to the desired 2-PhCOS analogues **10aa** (PTX side chain) and **10ab** (DTX side chain) in 42–44% yields over two steps (Scheme 1). It is interesting to note that the H-13 chemical shifts in **10aa** and **10ab** appear at δ4.9, an upfield shift of 1.2 ppm by comparison with the C-2 benzoates in **1** and **2**. In addition, the quaternary carbons at 198 ppm in the ^{13}C NMR of **10aa** and **10ab** were attributed to C-1′ after careful assignment with 1D and 2D NMR techniques. These observations fall outside expectations since taxoid H-13 and C-1′ resonances (C-13 esters or amides[16]) to date have been observed at 5.5–6.2 ppm and 165–175 ppm, respectively. This should be due to conformational distortion after the introduction of C-2 thioester.

C-2 sulfide baccatin **6b** can also be obtained by treatment of the mixture of **4a** and **4b** with sodium benzylsulfide at room temperature in 83% yield. The most significant changes in the ^1H NMR for **6b** are found at H-2 and H-3. That the protons are shifted upfield by 0.3 and 1.5 ppm, respectively, can be attributed to the loss of the C-2 carbonyl group. Following reduction, coupling of side chains, and deprotection reactions, the final products **10ba** and**10bb** were afforded (Scheme 1).

Next, we determined the free energy changes of binding for all four S-linked taxoids **10aa**–**10bb** at 35 °C as −28 to −30 KJ/mol. This 28–35% reduction in ΔG for binding corresponds to 2000–10000 times loss of binding affinity. The same compounds were subjected to MTT-determined cytotoxicities and found to be much less active in both sensitive and MDR tumor cell lines. In agreement with the potency difference between PTX (**1**) and DTX (**2**), the taxoids **10aa** and **10ba** with a PTX side chain are 3–5 fold less active than **10ab** and **10bb** with the DTX side chain. But there appeared to be no obvious difference in the activity between 2-PhCOS and 2-$PhCH_2S$ series (Table 1).

In order to explain the low activity of those taxanes, the ligand-tubulin interaction was analyzed with molecular dynamics based on T-conformation.

The diminutive binding affinities and cytotoxicities of **10** can be attributed to the alteration of local geometry around the sulfur atoms by comparison with the classic C-2 benzoyl ester. In the latter case, the C-2 phenyl ring of PTX encapsulated by tubulin in the electron crystallographic structure[17] is bounded on three sides in a rather narrow pocket. The opposite faces of the ring are within van der Waals contact of His227 and Leu215, while the *para*-position is in equally short contact with the protein backbone at Asp224. Extension of the C-2 substituent either perpendicular to the faces of the ring or further from the baccatin core can be predicted to create one or more steric clashes. To test the idea that the latter distance increment could cause a steric problem for series **10**, thioester **10aa** was constructed by an O to S modification of T-Taxol, optimized with the MMFF/GBSA force field[18], and docked into β-tubulin by superposing the taxane on the location of the original PTX ligand. To relax the protein-ligand complex, 20 °K molecular dynamics was performed for the thio-PTX ligand and nearby side chains in a 10 Å sphere around the binding site. Once unfavorable steric

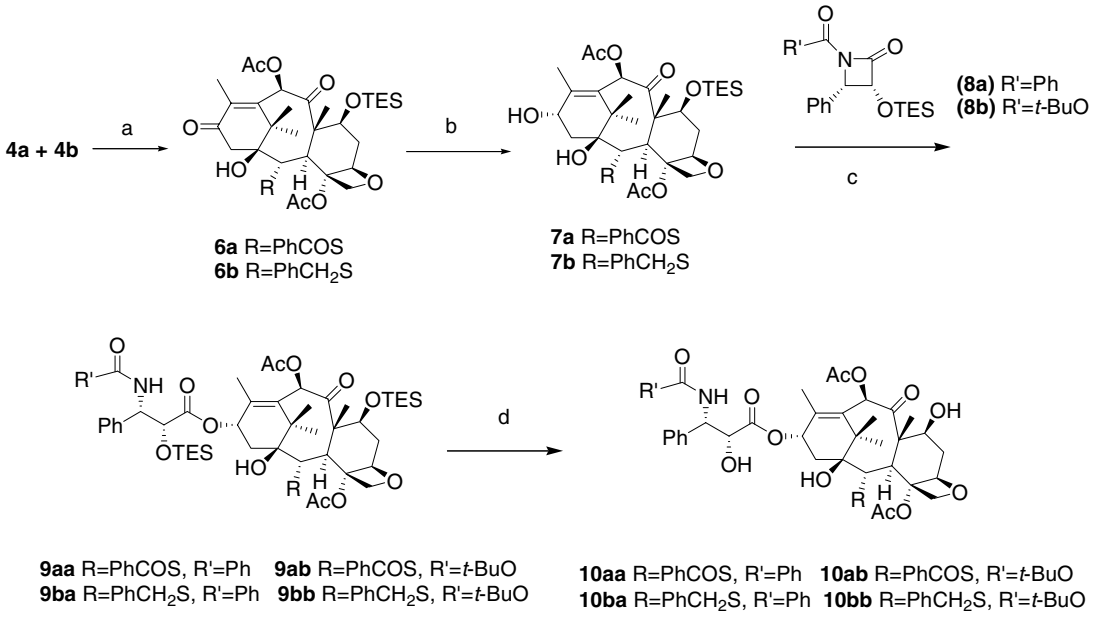

Scheme 1. Synthesis of C2 S-linked taxoids **10aa–bb**. Reagents and conditions: (a) RNa, DMF, r.t; (b) $NaBH_4$, MeOH–THF, −15 °C; (c) LHMDS, THF, −50 → −40 °C; (d) HF–Py, 0 °C → r.t.

Table 1. Cytotoxicity and binding data for taxoids **10**

Compound	R	R′	IC_{50} (μM)[a,b]		ΔG (KJ/mol)[c]
			A2780	A2780/AD	
10ab	PhCOS	Boc	2.4 ± 1.0	6.96 ± 0.67 (2.9)	−30.1 ± 0.6
10aa	PhCOS	Bz	11.7 ± 0.7	27 ± 7 (2.3)	−28.4 ± 1.1
10bb	$PhCH_2S$	Boc	3.5 ± 1.4	8.3 ± 2.7 (2.3)	−29.9 ± 0.7
10ba	$PhCH_2S$	Bz	9.9 ± 1.0	9.4 ± 1.7 (0.94)	−28.6 ± 0.1
PTX(**1**)	PhCOO	Bz	0.0016 ± 0.0002	0.92 ± 0.13 (575)	−42.1 ± 0.2

[a] IC_{50} values in μM were determined after two days exposure to drugs using the MTT cell proliferation assay. Data are means ± SE of four independent experiments.

[b] The numbers in parentheses are the calculated relative resistance obtained by dividing the IC_{50} value of the resistant line by the IC_{50} value of the parental line.

[c] Free energy changes derived from equilibrium binding constants of the ligands to microtubules at 35 °C ($-\Delta G_{0app} = RT\ln K_{(binding)}$).

contacts were removed, the temperature was slowly increased to 300 °K and the system allowed to reach a stable state. At this point, the entire taxane molecule had risen out of the binding site by 1–2 Å, and the terminal C-2 phenyl ring had slipped from the tight His/Leu/Asp sub-pocket to be repositioned in the first water shell around the protein.

A similar set of calculations for thioether **10ba** causes a comparable extrusion of the molecule from the binding pocket. In this case, however, the saturated C-2 side chain deviates from planarity and causes a significant rearrangement of the surrounding residues. Of particular note, the terminal phenyl ring is now perpendicular to His227 and located in a pocket opened by the movement of the Leu217 and Leu215 residues. Figure 1 depicts the final conformation of the C2–S–CH_2–Ph moiety and the displacement of the baccatin core by comparison with PTX.

In conclusion, C2 S-linked paclitaxel analogues are found to be much less active in both tubulin binding ability and cytotoxicity, although for different reasons as revealed by molecular simulations. It is noteworthy

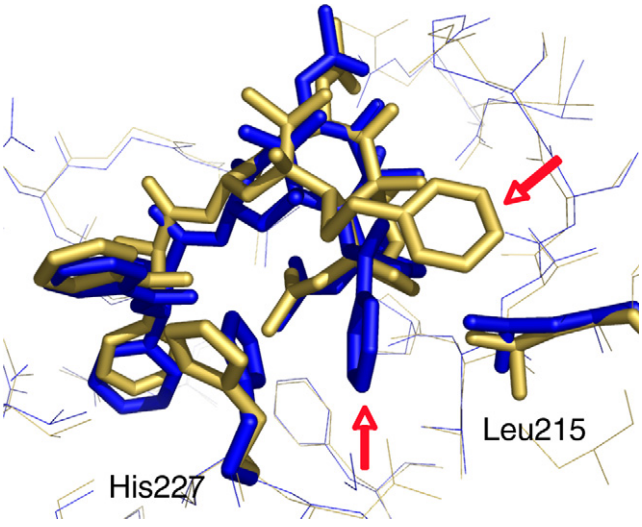

Figure 1. A superposition of PTX (blue) and thioether **10ba** (light gold) in the β-tubulin taxane binding site. For PTX, the C-2 phenyl is sandwiched between His227 and Leu215 (red arrow). Compound **10ba**'s C-2 SCH_2Ph group is predicted to adopt a staggered conformation that relocates the terminal phenyl upward (red arrow) while causing His227 to shift to the left (See text and supplement for computational details).

that T-Taxol conformation has been proven[9,19,20] to be a good predictor for the tubulin binding/bioactivity of taxanes, and here it gives another example for its powerfulness.

Acknowledgments

The authors thank FANEDD (Grant No. 199949), NSFC (Grant No. 20572135), and Fok Ying Tong Education Foundation (Grant No. 91037) (WSF), Comunidad Autonoma de Madrid (BIPPED-CM), Ministerio de Educación y Ciencia of Spain (Grant BFU-2004-0038) (JFD) for financial supports. JPS and AAA are grateful to Professor Dennis Liotta (Emory University) for encouragement and support, JFD thanks Prof. J.M. Andreu for useful discussions and support and Matadero Madrid Norte S.A. and Carnicas Madrid-Canarias S.L. for providing the brains for tubulin purification.

Supplementary data

Supplementary data associated with this article can be found, in the online version, at doi:10.1016/j.bmcl.2007.03.026.

References and notes

1. (a) Orr, G. A.; Verdier-Pinard, P.; McDaid, H.; Horwitz, S. B. *Oncogene* **2003**, *22*, 7280; (b) Gottesman, M. M. *Annu. Rev. Med.* **2002**, *53*, 615; (c) Weiss, R.; Donehower, R. C.; Wiernik, P. H. *J. Clin. Oncol.* **1990**, *8*, 1263.
2. Mekhail, T.; Markman, M. *Expert. Opin. Pharmacother.* **2002**, *3*, 755.
3. (a) Ringel, I.; Horwitz, S. B. *J. Natl. Cancer Inst.* **1991**, *83*, 288; (b) Figgitt, D. P.; Wiseman, L. R. *Drugs* **2000**, *59*, 621.
4. Altmann, K. H. *Curr. Opin. Chem. Biol.* **2001**, *5*, 424.
5. (a) Lobert, S.; Boyd, C. A.; Correia, J. *Biophys. J.* **1997**, *72*, 416; (b) Arif, J. M.; AI-Hazzani, A. A.; Kunhi, M.; AI-Khodairy, F. *J. Biomed. Biotechnol.* **2004**, *2*, 93; (c) Panda, D.; Rathinasamy, K.; Santra, M. K.; Wilson, L. *Proc. Natl. Acad. Sci. U.S.A.* **2005**, *102*, 9878.
6. (a) Kingston, D. G. I. *Chem. Commun.* **2001**, *10*, 867; (b) Gueritte, F. *Curr. Pharm. Des.* **2001**, *7*, 1229.
7. Snyder, J. P.; Nevins, N.; Cicero, D. O.; Jansen, J. *J. Am. Chem. Soc.* **2000**, *122*, 724.
8. (a) Vande Valde, D. G.; Georg, G. I.; Grunewald, G. L.; Gunn, C. W.; Mitscher, L. A. *J. Am. Chem. Soc.* **1993**, *115*, 11650; (b) Dubois, J.; Guenard, D.; Gueritte-Voegelein, F.; Guerida, N.; Potier, P.; Gillet, B.; Beloeil, J.-C. *Tetrahedron* **1993**, *49*, 6533; (c) Paloma, L. G.; Guy, R. K.; Wrasidlo, W.; Nicolaou, K. C. *Chem. Biol.* **1994**, *1*, 107; (d) Wang, M.; Cornett, B.; Nettles, J.; Liotta, D. C.; Snyder, J. P. *J. Org. Chem.* **2000**, *65*, 1059; (e) Ojima, I.; Chadravarty, S.; Inoue, T. *Proc. Natl. Acad. Sci. U.S.A.* **1999**, *96*, 4256.
9. Ganesh, T.; Guza, R. C.; Bane, S.; Ravindra, R.; Shanker, N.; Lakdawala, A. S.; Snyder, J. P.; Kingston, D. G. I. *Proc. Natl. Acad. Sci. U.S.A.* **2004**, *101*, 10006.
10. Chen, S.-H.; Wei, J.-M.; Farina, V. *Tetrahedron Lett.* **1993**, *34*, 3205.
11. Chordia, M. D.; Kingston, D. G. I. *J. Org. Chem.* **1996**, *61*, 799.
12. (a) Chaudhary, A. G.; Gharpure, M. M.; Rimoldi, J. M.; Chordia, M. D.; Gunatilaka, L. A. A.; Kingston, D. G. I. *J. Am. Chem. Soc.* **1994**, *116*, 4097; (b) Nicolaou, K. C.; Renaud, J.; Nantermet, P. G.; Couladouros, E. A.; Guy, R. K.; Wrasidlo, W. *J. Am. Chem. Soc.* **1995**, *117*, 2409.
13. Ojima, I.; Kuduk, S. D.; Pera, P.; Veith, J. M.; Bernacki, R. J. *J. Med. Chem.* **1997**, *40*, 279.
14. (a) Fang, W.-S.; Fang, Q.-C.; Liang, X.-T. *Tetrahedron Lett.* **2001**, *42*, 1331; (b) Fang, W.-S.; Liu, Y.; Liu, H. Y.; Xu, S.-F.; Wang, L.; Fang, Q.-C. *Bioorg. Med. Chem. Lett.* **2002**, *12*, 1543; (c) Fang, W.-S.; Liu, H.-Y.; Fang, Q.-C. *Chin. Chem. Lett.* **2005**, *16*, 38; (d) Fang, W.-S.; Liu, Y.; Fang, Q.-C. *Chin. Chem. Lett.* **2002**, *13*, 708.
15. Rao, S.; Orr, G. A.; Chaudhary, A. G.; Kingston, D. G. I.; Horwitz, S. B. *J. Biol. Chem.* **1995**, *270*, 20235.
16. Chen, S.-H.; Farina, V.; Vyas, D. M.; Doyle, T. W.; Long, B. H.; Fairchild, C. *J. Org. Chem.* **1996**, *61*, 2065.
17. (a) Nogales, E.; Wolf, S. G.; Downing, K. H. *Nature* **1998**, *391*, 199; (b) Lowe, J.; Li, H.; Downing, K. H.; Nogales, E. *J. Mol. Biol.* **2001**, *313*, 1045; (c) Snyder, J. P.; Nettles, J. H.; Cornett, B.; Downing, K. H.; Nogales, E. *Proc. Natl. Acad. Sci. U.S.A.* **2001**, *98*, 5312.
18. See Ref. S9 in supplement materials.
19. Tang, S.; Yang, C.; Brodie, P.; Bane, S.; Ravindra, R.; Sharma, S.; Jiang, Y.; Snyder, J. P.; Kingston, D. G. I. *Org. Lett.* **2006**, *8*, 3983.
20. Ganesh, T.; Yang, C.; Norris, A.; Glass, T.; Bane, S.; Ravindra, R.; Banerjee, A.; Metaferia, B.; Thomas, S. L.; Giannakakou, P.; Alcaraz, A. A.; Lakdawala, A. S.; Snyder, J. P.; Kingston, D. G. I. *J. Med. Chem.* **2007**, *50*, 713.

Arylthioindole Inhibitors of Tubulin Polymerization. 3. Biological Evaluation, Structure−Activity Relationships and Molecular Modeling Studies

Giuseppe La Regina,[†,‡] Michael C. Edler,[§] Andrea Brancale,[∥] Sahar Kandil,[∥] Antonio Coluccia,[†] Francesco Piscitelli,[†] Ernest Hamel,[§] Gabriella De Martino,[†] Ruth Matesanz,[⊥] José Fernando Díaz,[⊥] Anna Ivana Scovassi,[#] Ennio Prosperi,[#] Antonio Lavecchia,[⊗] Ettore Novellino,[⊗] Marino Artico,[†] and Romano Silvestri*[,†]

Istituto Pasteur − Fondazione Cenci Bolognetti, Dipartimento di Studi Farmaceutici, Sapienza Università di Roma, Piazzale Aldo Moro 5, I-00185 Roma, Italy, Welsh School of Pharmacy, Cardiff University, King Edward VII Avenue, Cardiff, CF10 3XF, United Kingdom, Toxicology and Pharmacology Branch, Developmental Therapeutics Program, Division of Cancer Treatment and Diagnosis, National Cancer Institute at Frederick, National Institutes of Health, Frederick, Maryland 21702, Dipartimento di Chimica Farmaceutica e Tossicologica, Università di Napoli "Federico II", Via Domenico Montesano 49, I-80131, Napoli, Italy, Centro de Investigaciones Biológicas, Consejo Superior de Investigaciones Cientificas, C/Ramiro de Maeztu 9, E-28040 Madrid, Spain, and Istituto di Genetica Molecolare − Consiglio Nazionale delle Ricerche, Via Abbiategrasso 207, I-27100 Pavia, Italy

Received December 27, 2006

The new arylthioindole (ATI) derivatives **10**, **14**−**18**, and **21**−**24**, which bear a halogen atom or a small size ether group at position 5 of the indole moiety, were compared with the reference compounds colchicine and combretastatin A-4 for biological activity. Derivatives **10**, **11**, **16**, and **21**−**24** inhibited MCF-7 cell growth with IC_{50} values <50 nM. A halogen atom (**14**−**17**) at position 5 caused a significant reduction in the free energy of binding of compound to tubulin, with a concomitant reduction in cytotoxicity. In contrast, methyl (**21**) and methoxy (**22**) substituents at position 5 caused an increase in cytotoxicity. Compound **16**, the most potent antitubulin agent, led to a large increase (56%) in HeLa cells in the G_2/M phase at 24 h, and at 48 h, 26% of the cells were hyperploid. Molecular modeling studies showed that, despite the absence of the ester moiety present in the previously examined analogues, most of the compounds bind in the colchicine site in the same orientation as the previously studied ATIs. Binding to β-tubulin involved formation of a hydrogen bond between the indole and Thr179 and positioning of the trimethoxy phenyl group in a hydrophobic pocket near Cys241.

Introduction

Microtubules have essential roles in vital cellular functions, such as motility, division, shape maintenance, and intracellular transport. Drugs that interact with tubulin, the protein subunit of microtubules, cause mitotic arrest, interfering with the dynamic equilibrium of these organelles by either inhibiting tubulin polymerization or blocking microtubule disassembly. Inhibitors of tubulin assembly include colchicine (**1**), combretastatin A-4 (CAS4, **2a**), and the *Catharanthus* alkaloids vincristine and vinblastine (Chart 1). At high concentrations, **1** and **2a** interact with α,β-tubulin dimers at the interface between alpha and beta[1] and cause microtubule destabilization and apoptosis. Taxoids and epothilones bind as well to α,β-tubulin to a lumenal site on the β-subunit[2,3] and probably to a recently described microtubule stabilizing agent binding site[4] in the pore on the microtubule surface formed by two different α and β tubulin subunits. Paclitaxel stimulates microtubule polymerization and stabilization at high concentrations, whereas at lower concentrations, the drug inhibits microtubule dynamics with little effect on the proportion of tubulin in polymer.[5,6] Independent of precise mechanism of action, clinical use of antitubulin drugs is associated with problems of drug resistance, toxicity, and bioavailability.[7]

Chart 1. Reference and Arylthioindole Derivatives

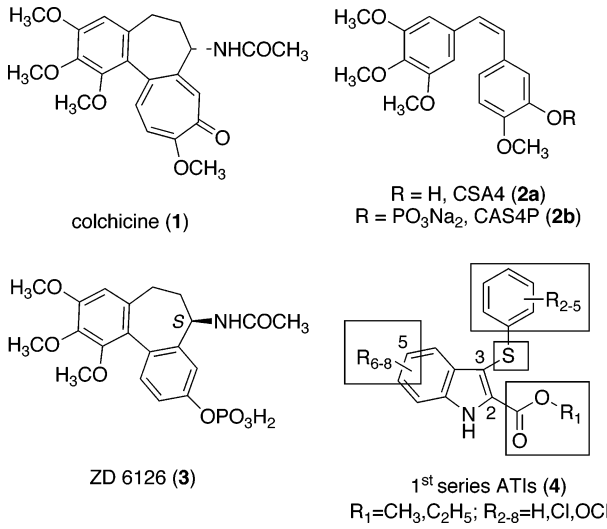

In the past few years, several antitubulin agents that target the colchicine site have been intensively investigated as vascular-disrupting antitumor drugs.[8] For example, combretastatin A-4 phosphate (**2b**) and ZD6126 (**3**) stop blood flow through tumor capillaries, probably caused by rapid disruption of endothelial cell morphology, and consequently, the tumor is starved of nutrients and rapid tumor cell death occurs.[9,10] These vascular-disrupting agents are currently in ongoing clinical trials for either single-drug or multi-drug combination antitumor therapy.[10,11]

Arylthioindoles (ATIs, general structure **4**) are a new class of potent tubulin assembly inhibitors that bind to the colchicine site on β-tubulin close to its interface with α-tubulin.[12]

* To whom correspondence should be addressed. Phone: +39 06 4991 3800. Fax: +39 06 491 491. E-mail: romano.silvestri@uniroma1.it.
† Università di Roma.
‡ Research performed at Cardiff University.
§ National Cancer Institute at Frederick.
∥ Cardiff University.
⊥ Consejo Superior de Investigaciones Cientificas, Madrid.
Consiglio Nazionale delle Ricerche, Pavia.
⊗ Università di Napoli.

10.1021/jm061479u CCC: $37.00
Published on Web 05/12/2007

Chart 2. Design of Arylthioindoles **9**−**28**

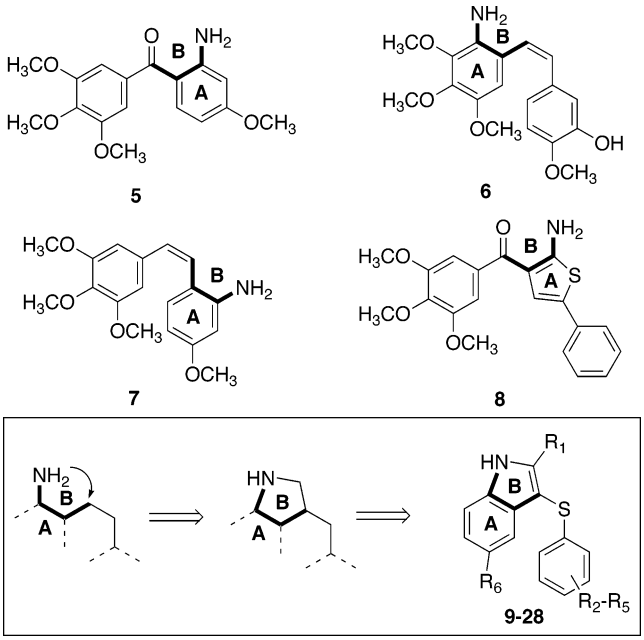

Structure−activity relationship (SAR) analysis clarified structural requirements for good activity in this class of inhibitors. Essential structural features for an active agent have included (A) a small-size ester function at position 2 of the indole, (B) the 3-arylthio group, (C) the sulfur atom bridge, and (D) a substituent at position 5 of the indole (Chart 1).[13] We carried out molecular modeling studies and dynamics simulations that helped explain the experimental data. We therefore used our molecular model in designing and synthesizing new ATI derivatives.[13]

Recent studies have focused on the synthesis of aminoderivatives related to CSA4.[14] The potent antitubulin activity displayed by these analogues (for example **5**,[15] **6**,[16] **7**,[16] and **8**[17], Chart 2) attracted our attention. Compounds **5**−**8** share, as a common structural feature, an amino group located *ortho* to the bridging group (either carbonyl or *cis*-ethenyl group). We hypothesized that this *ortho*-substituted aniline might resemble the indole nucleus of ATI derivatives (see Chart 2), with the indole ring acting as a bioisostere of the *ortho*-substituted aniline. These observations prompted us to design new ATI derivatives **9**−**28**. Predictive docking simulations using our model[13] showed that, despite the absence of the ester moiety at position 2 of the indole ring, most of the compounds should bind in the colchicine site of tubulin in the same orientation as the previously studied ATIs. The new ATI derivatives, like those described previously, were potent inhibitors of tubulin polymerization and of the growth of cancer cells, with activities comparable with those of colchicine and combretastatin A-4. Finally, we should note the recent paper of Hsieh and co-workers,[18] which included a group of 3-aroylthioindoles. These compounds are significantly different from the ATI's we have prepared, because there are major differences in our SAR findings and those of the Hsieh group.

Chemistry

The structures of ATI derivatives **9**−**31** are shown in Table 1. Compounds **10**, **11**, **14**−**26**, and **28** were synthesized by a two-step procedure (Scheme 1). *O*-Ethyl-*S*-(3,4,5-trimethoxyphenyl)carbonodithioate[19] was transformed into 3,4,5-trimethoxythiophenol by heating at 65 °C in aqueous ethanol in the presence of sodium hydroxide. This mixture was made acidic with 6 N HCl and treated at 25 °C with the appropriate indole while adding dropwise an aqueous iodine−potassium iodide

Table 1. Structures of ATIs **9**−**31**

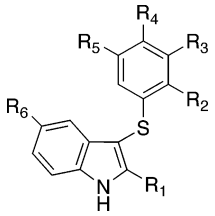

cmpd	R_1	R_2	R_3	R_4	R_5	R_6
9	H	H	H	H	H	H
10	H	H	OCH_3	OCH_3	OCH_3	H
11	CH_3	H	OCH_3	OCH_3	OCH_3	H
12	H	OCH_3	H	H	H	Cl
13	H	H	CH_3	H	CH_3	Cl
14	H	H	OCH_3	OCH_3	OCH_3	Cl
15	CH_3	H	OCH_3	OCH_3	OCH_3	Cl
16	H	H	OCH_3	OCH_3	OCH_3	Br
17	H	H	OCH_3	OCH_3	OCH_3	I
18	H	H	OCH_3	OCH_3	OCH_3	F
19	H	H	OCH_3	OCH_3	OCH_3	NO_2
20	H	H	OCH_3	OCH_3	OCH_3	NH_2
21	H	H	OCH_3	OCH_3	OCH_3	CH_3
22	H	H	OCH_3	OCH_3	OCH_3	OCH_3
23	CH_3	H	OCH_3	OCH_3	OCH_3	OCH_3
24	H	H	OCH_3	OCH_3	OCH_3	OCH_2CH_3
25	H	H	OCH_3	OCH_3	OCH_3	$OCH(CH_3)_2$
26	H	H	OCH_3	OCH_3	OCH_3	OH
27	H	H	OCH_3	OCH_3	OCH_3	OCH_2CH_2OH
28	H	H	OCH_3	OCH_3	OCH_3	$OCH_2CH_2OCH_2Ph$
29	$COOCH_3$	H	OCH_3	OCH_3	OCH_3	H
30	$COOCH_3$	H	OCH_3	OCH_3	OCH_3	Cl
31	$COOCH_3$	H	OCH_3	OCH_3	OCH_3	OCH_3

Scheme 1. Synthesis of Arylthioindole Derivatives **9**−**28**[a]

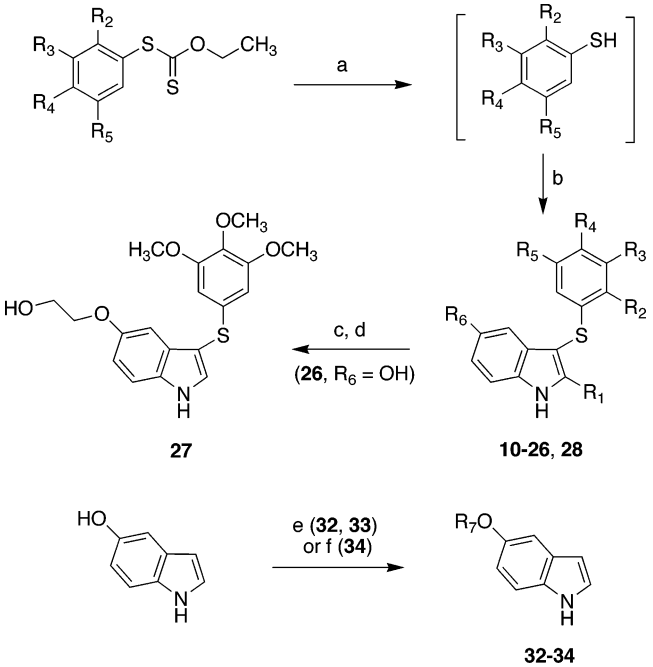

10-26, **28**: R_1= H, CH_3; $R_{2\text{-}5}$ = H, CH_3, OCH_3; R_6 = H, F, Cl, Br, I, NO_2, NH_2, OCH_3,OC_2H_5,$OCH(CH_3)_2$, OH, $OCH_2CH_2OCH_2Ph$. **32**: R_7 = C_2H_5; **33**: R_7 = $OCH(CH_3)_2$; **34**: R_7 = $OCH_2CH_2OCH_2Ph$.

[a] Reagents and reaction conditions: (a) 3 N NaOH, D-(+)-glucose, EtOH, 65 °C, 2 h; (b) appropriate indole, I_2-KI, EtOH−H_2O, 25 °C, 1 h; (c) (2-bromoethoxy)-*tert*-butyldimethylsilane, K_2CO_3, acetone, 24 h, reflux; (d) PTSA, methanol, 25 °C, 30 min; (e) alkyl halide, K_2CO_3, acetone, 24 h, reflux; (f) 2-benzyloxyethanol, DEAD, PPh_3, THF, overnight, reflux.

Table 2. Inhibition of Tubulin Polymerization, Growth of MCF-7 Human Breast Carcinoma Cells, and Colchicine Binding by Compounds **9**−**31**

cmpd	tubulin[a] $IC_{50} \pm SD$ (μM)	MCF-7[b] $IC_{50} \pm SD$ (nM)	inhibition colchicine binding[c] (% ± SD)
9[d]	15 ± 0.7	>2500	nd[e]
10	2.6 ± 0.2	34 ± 9	68 ± 0.8
11	6.8 ± 0.6	46 ± 4	61 ± 4
12	11 ± 2	>2500	nd
13	9.4 ± 0.3	1200 ± 100	33 ± 3
14	2.6 ± 0.2	77 ± 7	51 ± 4
15	2.7 ± 0.5	82 ± 10	59 ± 5
16	1.6 ± 0.3	43 ± 7	65 ± 3
17	2.7 ± 0.3	68 ± 7	61 ± 2
18	3.3 ± 0.3	160 ± 50	39 ± 6
19	16 ± 0.4	560 ± 70	nd
20	13 ± 2	260 ± 30	nd
21	2.7 ± 0.2	16 ± 6	56 ± 3
22	4.1 ± 0.6	22 ± 2	61 ± 4
23	3.3 ± 0.2	18 ± 4	69 ± 0.2
24	2.1 ± 0.1	16 ± 5	76 ± 5
25	19 ± 0.6	1500 ± 700	nd
26	6.3 ± 0.8	190 ± 40	26 ± 0.5
27	6.8 ± 0.8	95 ± 8	31 ± 2
28	>40	260 ± 20	nd
29[d]	2.9 ± 0.1	25 ± 1	74 ± 2
30[d]	2.3 ± 0.3	42 ± 1	57 ± 2
31[d]	2.0 ± 0.2	13 ± 3	90 ± 1
1	3.2 ± 0.4	13 ± 3	
2a	2.2 ± 0.2	17 ± 10	99 ± 1

[a] Inhibition of tubulin polymerization. [b] Inhibition of growth of MCF-7 human breast carcinoma cells.[20] [c] Inhibition of [^{3}H]colchicine binding. Tubulin was at 1 μM, both [^{3}H]colchicine and inhibitor were at 5 μM.[20] [d] Data from lit.[12,13] [e] nd = not determined.

solution. Compounds **12** and **13** were prepared similarly, starting from the corresponding commercially available carbonodithioate. Compound **27** was prepared by treating **26** with (2-bromoethoxy)-*tert*-butyldimethylsilane in the presence of potassium carbonate in boiling acetone; the intermediate silyloxy derivative was stirred with *para*-toluensulfonic acid in methanol at room temperature. The 5-ethoxy- (**32**) and 5-isopropyloxy- (**33**) indoles were obtained by alkylation of 5-hydroxyindole with iodoethane or 2-iodopropane, respectively, in the presence of potassium carbonate. 5-(2-Benzyloxy)ethoxyindole (**34**) was prepared by reaction of 5-hydroxyindole with 2-benzyloxyethanol in the presence of diethyl azodicarboxylate and triphenylphosphine in boiling THF.

Results and Discussion

Biological data for the inhibition of tubulin polymerization, binding of [^{3}H]colchicine to tubulin (more active compounds only), and growth of MCF-7 human breast carcinoma cells by arylthioindoles **9**−**28** in comparison with the reference compounds **1** and **2a** and ATIs **29**−**31**[12,13] are summarized in Table 2.

Replacing the 3-phenylthio of **9** with the 3-(3,4,5-trimethoxyphenyl)thio group (**10**) resulted in a 5.8-fold increase in inhibition of tubulin polymerization. This value (IC_{50} = 2.6 μM) was very close to those of **1** (IC_{50} = 3.2 μM) and **2a** (IC_{50} = 2.2 μM). Most importantly, this chemical modification resulted in great improvement in antiproliferative activity against MCF-7 cells. The IC_{50} obtained with **10** was 34 nM, a value only 2.6- and 2-fold higher than those obtained with reference compounds **1** (IC_{50} = 13 nM) and **2a** (IC_{50} = 17 nM), respectively. The 2-methyl group of **11** caused a 2.6-fold reduction in activity as an inhibitor of tubulin assembly (IC_{50} = 6.8 μM) relative to **10**, while inhibition of MCF-7 cell growth (IC_{50} = 46 nM) was only marginally affected.

Chart 3. Reference Structures for Binding Studies

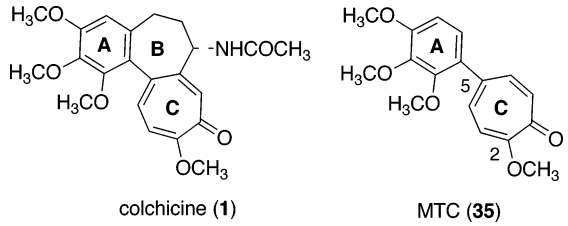

Introduction of a chlorine atom at position 5 of the indole (**14**, IC_{50} = 2.6 μM) did not change the activity of **10** as an inhibitor of assembly, but inhibition of cell growth was reduced greater than 2-fold. When a chlorine atom was introduced into **11** (compound **15**), inhibition of tubulin assembly increased while inhibition of MCF-7 cell growth decreased. (Alternatively, **15** can be viewed as an introduction of a C-2 methyl group into compound **14**, resulting in no change in activity, as compared with the loss of activity when the same methyl group was introduced into **10**.) With the other three halogen atoms (**16**−**18**), a bromine atom (**16**) resulted in a compound more inhibitory than **10** in the tubulin assembly assay and essentially identical to **10** as an inhibitor of MCF-7 cell growth, an iodine atom (**17**) was almost indistinguishable in its effects from the chlorine atom, and a fluorine atom (**18**) resulted in the least active compound in the halogen series, although with the latter compound there was a greater loss in antiproliferative than in antitubulin activity.

Introduction into **10** of a methyl (**21**, IC_{50} = 2.7 μM), a methoxy (**22**, IC_{50} = 4.1 μM; **23**, with a C-2 methyl group also, IC_{50} = 3.3 μM), or an ethoxy (**24**, IC_{50} = 2.1 μM) group at position 5 of the indole resulted in little change in inhibitory effect on tubulin assembly and small increases in antiproliferative activity relative to **10**. These compounds, too, were essentially equipotent with **1** and **2a**, both as inhibitors of tubulin assembly and MCF-7 cell growth. Bulkier ether groups at position 5 of the indole (**25**, **27**, **28**), or even a hydroxyl group at this position (**26**), yielded compounds with reduced activity in both assays.

In the assay measuring inhibition of [^{3}H]colchicine binding, all compounds were examined at 5 μM, with 1 μM tubulin and 5 μM **1**.[20] None of the new compounds approached the standard **2a** as an inhibitor in this assay. With the inhibitors at 1 μM, **2a** inhibited colchicine binding 88%, and the most active of the ATI's, compound **24**, inhibited 42%.

Structure−Affinity−Cytotoxicity Relationships. We also determined binding constants at 20 °C for the colchicine site on tubulin for the new ATIs that were highly active as inhibitors of tubulin polymerization. Inhibition of tubulin polymerization does not directly correlate with binding affinity. On the other hand, binding affinity can be an important parameter involved in cytotoxicity.[21−25]

Compounds **10**, **11**, **14**−**17**, **21**−**23**, **29**, and **30** were compared with **1** and 2-methoxy-5-(2,3,4-trimethoxyphenyl)-2,4,6-cycloheptatrien-1-one (MTC, **35**, Chart 3), an analogue of colchicine lacking the B ring that rapidly reaches an equilibrium in its binding reaction with tubulin (Table 3), while losing part of the free energy of binding due to the entropy contribution needed for the immobilization of the A and C rings in the site.[26] As expected from their cytotoxicities and their activities as inhibitors of [^{3}H]colchicine binding, the compounds bound tightly to the colchicine site of tubulin, as they displaced compound **35** already bound to the colchicine site (Figure 1).

We explored structure−affinity relationships of the substituents at positions 2 and 5 of the indole nucleus. Invariably, the

Table 3. Binding Constants at 20 °C of Compounds **10**, **11**, **14**−**17**, **21**−**23**, **29**, and **30** and the Reference Compounds **1** and **35** for the Colchicine Site on Tubulin

cmpd	binding constant ($\times 10^5$ M^{-1})	ΔG_{app} 20 °C (kJ mol^{-1})
10[a]	52.1 ± 2.8	−37.7 ± 0.1
11[a]	55.0 ± 3.0	−37.8 ± 0.1
14[a]	8.1 ± 0.3	−33.1 ± 0.1
15[a]	20.7 ± 2.4	−35.4 ± 0.3
16[a]	27.6 ± 1.3	−36.1 ± 0.1
17[a]	23.1 ± 2.1	−35.7 ± 0.2
21[a]	19.6 ± 0.5	−35.3 ± 0.1
22[a]	30.5 ± 1.9	−36.4 ± 0.1
23[a]	63.8 ± 1.6	−38.2 ± 0.1
29[b]	5.7 ± 0.4	−32.3 ± 0.2
30[b]	13 ± 2	−34.3 ± 0.3
35[c]	4.7 ± 0.3	−31.8 ± 0.2
1[c]	1600	−46.0

[a] Data obtained measuring compound **35** displacement from the binding site.[27] [b] Data measured using quenching of tubulin fluorescence.[28,29] [c] Data from lit.[28]

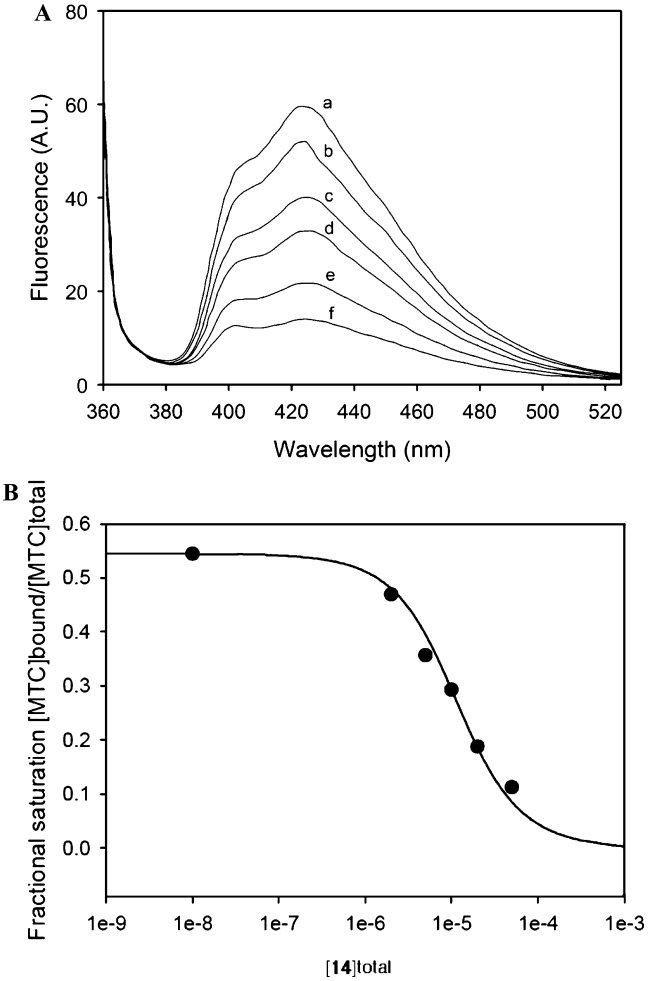

Figure 1. (A) Displacement of **35** from the colchicine site. Fluorescence emission spectra of 10 μM **35** and 10 μM tubulin in 10 mM phosphate−0.1 mM GTP buffer pH 7.0, in the presence of compound **14**: (a) 0 μM, (b) 2 μM, (c) 5 μM, (d) 10 μM, (e) 20 μM, (f) 50 μM. (B) Displacement isotherm at 20 °C of **35** by **14**. The data points were fit to the best value of the binding equilibrium constant of **14**, assuming 0.8 sites per tubulin dimer.[28]

presence of a halogen atom (**14**−**17**) or a methyl (**21**) or methoxy (**22**) group at position 5 resulted in reduction of binding affinity (positive value of $\Delta\Delta G$ 20 °C, Table 4). This reduction was accompanied by a concomitant reduction of cytotoxicity in **14**−**17** relative to **10**, while, in contrast, compounds **21** and **22** were more cytotoxic. The methyl group at position 2 increased binding affinity (negative value of $\Delta\Delta G$ 20 °C, Table 4), but this positive effect was not associated with an increase in cytotoxicity (compare **10** with **11** and **22** with **23**), probably due to a negative effect in solubility of the compound. The 2-methoxycarbonyl group of **29** and **30** caused opposite effects on the binding affinity of **10** and **14**, respectively. However, both **29** and **30** were more cytotoxic.

Table 4. Incremental Thermodynamic Parameters of Binding of Compounds **11**, **14**−**17**, **21**−**23**, **29** and **30** to the Colchicine Site

cmpd	reference cmpd	single group modification[a]	$\Delta\Delta G$ 20 °C (kJ mol^{-1})	MCF-7 ΔIC_{50} (nM)
11	**10**	2-**CH_3**	−0.1 ± 0.2	+12
14	**10**	5-**Cl**	+4.5 ± 0.2	+43
15	**11**	2-CH_3-5-**Cl**	+2.4 ± 0.4	+36
16	**10**	5-**Br**	+1.5 ± 0.2	+9
17	**10**	5-**I**	+1.9 ± 0.3	+34
21	**10**	5-**CH_3**	+2.3 ± 0.2	−18
22	**10**	5-**OCH_3**	+1.2 ± 0.2	−12
23	**22**	2-**CH_3**-5-CH_3O	−1.8 ± 0.2	−4
29	**10**	2-**$COOCH_3$**	+5.3 ± 0.2	−9
30	**14**	2-**$COOCH_3$**-5-Cl	−1.2 ± 0.4	−35
10	**35**		−5.8 ± 0.3	

[a] Single group modification (H → substituent) highlighted in bold on indole nucleus with respect to the indicated reference compound.

These results indicate that cytotoxicity is generally correlated with binding affinity for the colchicine site. However, some results were not fully explained in terms of binding affinity, suggesting that others factors, such as specific effects of the compound on the tubulin molecule,[22] may play a role in the cytotoxic activities of these derivatives.

We also analyzed the data from Table 2, combined with data from our previous studies,[12,13] comparing effects of ATIs on MCF-7 cell proliferation with inhibitory effects on tubulin assembly (Figure 2A) and with inhibitory effects on the binding of [^{3}H]colchicine to tubulin (Figure 2B). As noted above, assembly inhibition correlated poorly with inhibition of the growth of this cell line.

There was much better correlation with inhibition of colchicine binding, which indirectly measures relative affinity of the compounds for the colchicine site. Note, too, that **2a** and two compounds prepared by Flynn et al.[20] (previously cited by us[12]) also fit into the overall pattern generated by the ATIs.

Cell Cycle Analysis. The most potent antitubulin agent **16** was selected for cell cycle studies in HeLa cells. After treatment for 24 h with 0.1, 1.0, and 10 μM **16**, the cells showed a dose-dependent reduction in cell growth. At the highest concentration used, cell growth was reduced about 50% (not shown). Cell cycle analysis (Figure 3 and Table 5) following treatment with 10 μM **16** showed that 56% of the cells were arrested in the G_2/M phase after 24 h. Following replacement of the original medium with medium not containing the drug and incubation for a further 24 h, 53% of the cells remained in G_2/M and an additional 26% of the cells had DNA content >4C. These findings indicate a continuing impairment of cell division, as would be expected following treatment with a tubulin inhibitor.

The morphological features of **16**-treated cells were analyzed by Hoechst staining of cellular DNA. The nuclei of untreated HeLa cells showed the typical diffuse pattern of chromatin distribution, whereas cells treated with **16** became multinucleated as an effect of perturbation of tubulin function (Figure 4A). Although there was a small fraction of cells in the sub-G_1 region (the A_0 compartment in Table 5), other markers of apoptosis were not observed. There was neither a DNA ladder (Figure

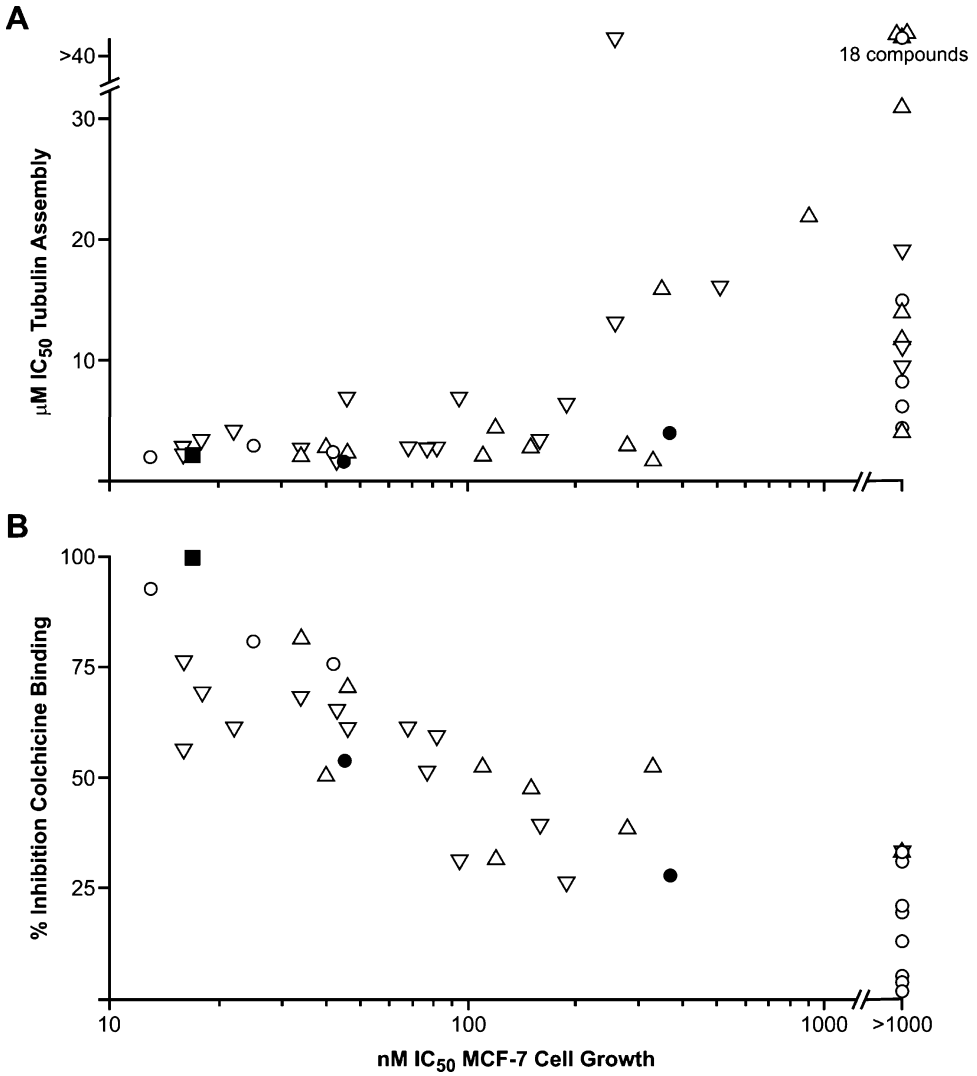

Figure 2. Correlation of MCF-7 cytotoxicity data with inhibition of tubulin assembly (A) and inhibition of colchicine binding (B). Data represented by open inverted triangles are taken from Table 2 of this paper. The open upright triangles represent ATI compounds described in ref 13 and the open circles represent ATI compounds described in ref 12. The solid squares represent data obtained with **2a**. The solid circles represent data obtained with two compounds synthesized by Flynn et al.[20]

4B) nor evidence for PARP-1 proteolysis (Figure 4C), both of which were instead observed following a 3 h treatment with etoposide.

These data suggested that tubulin polymerization inhibition induced in HeLa cells by **16** did not cause apoptosis but rather impaired cell viability through a "mitotic catastrophe".

Molecular Modeling. To investigate the possible binding mode for this new series of compounds, we performed docking simulations, using the FlexX module included in Sybyl 7.2.[30] We previously reported the putative binding for ATIs bearing an ester moiety at position 2 of the indole, describing the main interaction between the inhibitors and the colchicine site of tubulin, which included a hydrogen bond between the carbonyl group of the ester function and a lysine in the binding site.[12,13] With the series reported here, despite the absence of the ester moiety, most of the compounds bind in the same orientation as the previously studied ATIs, forming a hydrogen bond between the indole and Thr179 (residue numbers, as in ref 1, describing the crystal structure we used) and with the trimethoxyphenyl group positioned in a hydrophobic pocket close to Cys241 (Figure 5).

It should be noted that, while most of the compounds in this series dock in a very similar fashion, there are a few exceptions: compounds **9** and **10** showed a slightly different conformation, with the indole buried deeper in the binding pocket, although both compounds still form the interactions described above. In the case of compounds **19** and **28**, on the other hand, the docking simulation did not yield a reasonable pose within the active site. While with compound **28** it is possible to rationalize this observation as being caused by steric hindrance attributable to the substituent at position 5 of the indole, with compound **19**, the best explanation is that electrostatic effects cause a different positioning of the inhibitor in the binding site. If the conformation of compound **19** in the binding site was similar to the poses of the other analogues, its nitro group would be just 3 Å away from the phosphate groups of the nonexchangeable GTP molecule bound to the α-tubulin in the dimer. This GTP site on α-tubulin is near the colchicine site on β-tubulin, and the close proximity of the two ligands would result in an unacceptable electrostatic repulsion between negatively charged groups.

Conclusions

We synthesized new ATI derivatives, many of which strongly inhibited tubulin assembly, with activity in the low micromolar range, comparable to the effects of **1** and **2a**. Derivatives **10**,

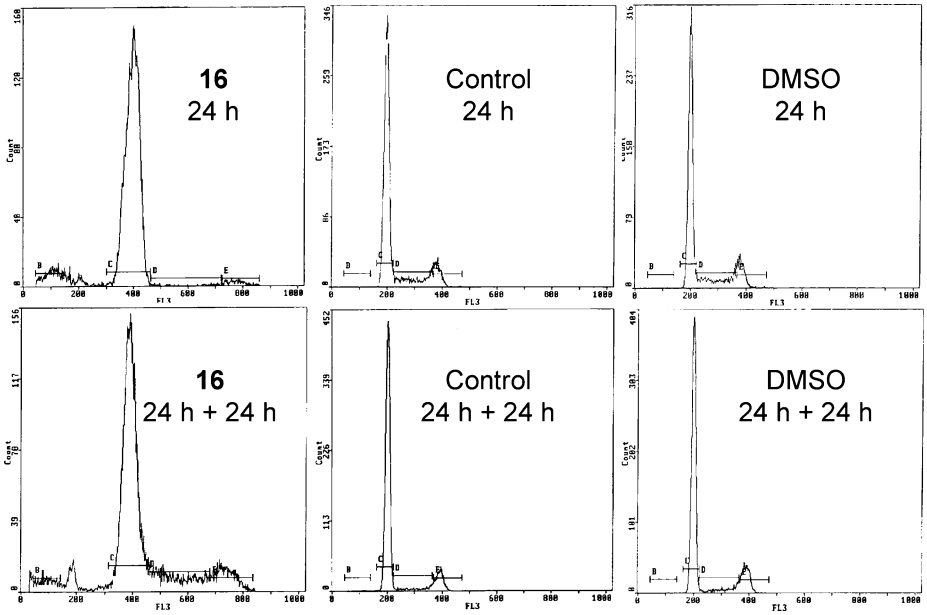

Figure 3. Cell cycle analysis of HeLa cells treated with **16**. A typical experiment is shown. Cells were harvested after treatment with **16** (10 μM) for 24 h and after further recovery in drug-free medium for 24 h (24 h + 24 h). The percentage of cells in each cell cycle phase was quantified (Table 5).

Table 5. Cell Cycle Distribution of **16**-Treated HeLa Cells[a]

cell cycle phase	24 h			24 h + 24 h		
	16[b]	control	DMSO[c]	**16**[d]	control	DMSO
A_0[e]	6.5	0.2	0.1	4.5	0.4	0.2
G_1	1.8	69.6	73.9	3.5	81.4	76.7
S	8.9	17.4	15.2	10.5	6.3	8.1
G_2/M	56.1	12.0	10.1	53.1	11.5	14.4
>4C	4.2	0	0	26.0	0	0

[a] Data are expressed as % of cells in each cell cycle phase. A typical experiment is shown. [b] Cells were treated with **16** at 10 μM for 24 h. [c] Parallel samples incubated with 0.1% DMSO (the same final concentration used with **16** at 10 μM) did not significantly alter cell cycle distribution. [d] Cells were further incubated in drug-free medium for 24 h. [e] Indicates cells with a sub-G_1 DNA content, probably representing a small population of apoptotic cells.

14−**18**, and **21**−**24**, bearing a halogen atom or a small alkyl or ether group at position 5 of the indole, were also potent inhibitors of MCF-7 cell growth. The most active derivatives (**10**, **11**, **16**, and **21**−**24**) inhibited cell growth with IC_{50} values <50 nM. SAR studies indicated reasonable, albeit imperfect, correlation between cytotoxicity and binding affinity for the colchicine site. In particular, a halogen atom at position 5 decreased the free energy of binding of ATIs to tubulin, with concomitant reduction in cytotoxicity. In contrast, methyl (**21**) and methoxy (**22**) substituents at position 5 resulted in more cytotoxic compounds. Compound **16**, the most potent inhibitor of tubulin assembly, induced accumulation of HeLa cells in the G_2/M phase of the cell cycle at 24 h and polyploidization at 48 h. At 24 h, inhibition of tubulin polymerization by **16** had not caused extensive apoptosis, suggesting that impaired cell viability might occur through a "mitotic catastrophe". Molecular modeling studies showed that, despite the absence of the ester moiety, most of the compounds appear to bind in the same orientation as the previously studied ATIs,[12,13] forming a hydrogen bond between the indole and Thr179 and with the trimethoxyphenyl group positioned in a hydrophobic pocket near Cys241. These findings induce us to continue our investigations of the SAR among ATI derivatives in the expectation of developing more potent and selective analogues.

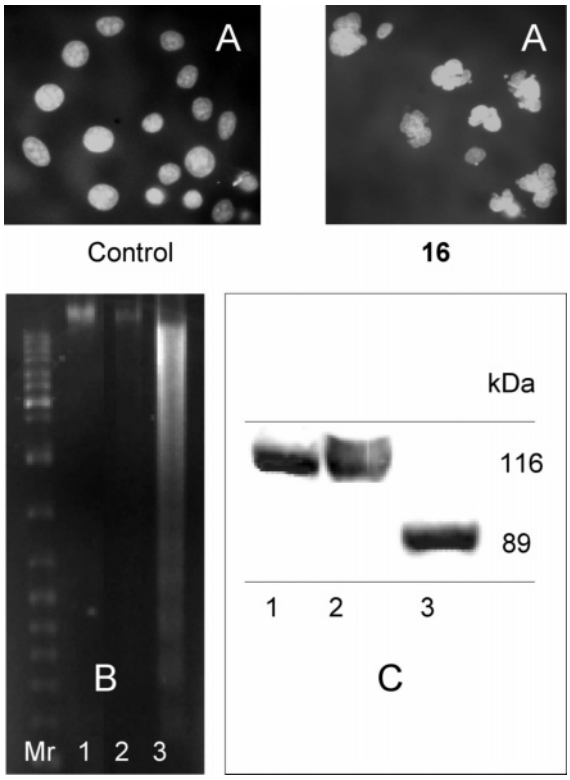

Figure 4. Morphological and biochemical evaluation of apoptotic parameters of HeLa cells treated with **16** and etoposide. (A) Hoechst staining for DNA. (B) Agarose gel electrophoresis; Mr, molecular weight markers; 1, control cells; 2, **16**-treated cells (10 μM, 24 h + 24 h of recovery); 3, etoposide-treated cells (100 μM, 3 h + 24 h of recovery). (C) Western blot for PARP-1; 1, control cells; 2, **16**-treated cells (10 μM, 24 h); 3, etoposide-treated cells (100 μM, 3 h + 24 h of recovery); 116 kDa, intact PARP-1; 89 kDa, caspase-cleaved PARP-1.

Experimental Section

Chemistry. Melting points (mp) were determined on a Büchi 510 apparatus and are uncorrected. Infrared spectra (IR) were run on a SpectrumOne FT spectrophotometer. Band position and absorption ranges are given in cm^{-1}. Proton nuclear magnetic

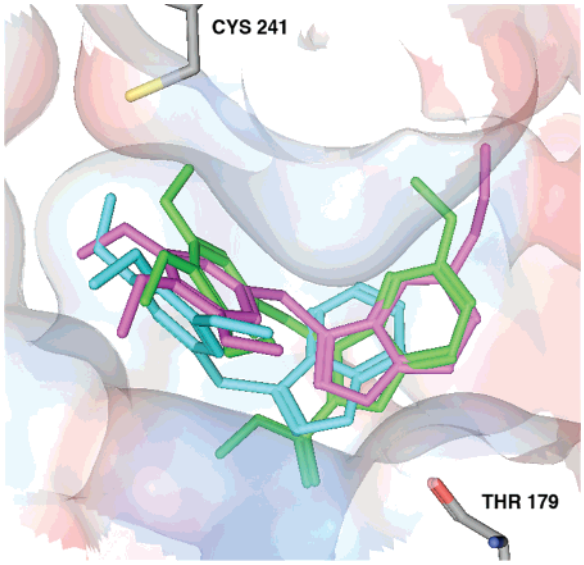

Figure 5. Putative binding mode of different ATIs: compound **31** in green, compound **24** in magenta, compound **10** in cyan.

resonance (^{1}H NMR) spectra were recorded on Bruker 200 and 400 MHz FT spectrometers in the indicated solvent. Chemical shifts are expressed in δ units (ppm) from tetramethylsilane. Mass spetra were recorded on Bruker MicroTOF LC. Column chromatography was performed on columns packed with alumina from Merck (70−230 mesh) or silica gel from Merck (70−230 mesh). Aluminum oxide TLC cards from Fluka (aluminum oxide precoated aluminum cards with fluorescent indicator at 254 nm) and silica gel TLC cards from Fluka (silica gel precoated aluminum cards with fluorescent indicator at 254 nm) were used for thin layer chromatography (TLC). Developed plates were visualized by a Spectroline ENF 260C/F UV apparatus. Organic solutions were dried over anhydrous sodium sulfate. Concentration and evaporation of the solvent after reaction or extraction was carried out on a Büchi Rotavapor rotary evaporator operating at reduced pressure. Elemental analyses were found within ±0.4% of the theoretical values. Compound **9** was synthesized as we previously reported.[12]

Method A. General Procedure for the Synthesis of Compounds 10−26 and 28. Example: 3-[(3,4,5-Trimethoxyphenyl)thio]-1*H*-indole (10). D-(+)-glucose (1.07 g, 0.006 mol) and 3 N NaOH (3.55 mL) were added to a solution of *O*-ethyl-*S*-(3,4,5-trimethoxyphenyl)carbonodithioate[19] (1.54 g, 0.005 mol) in ethanol (20 mL). The reaction mixture was heated at 65 °C for 2 h while stirring. After cooling, water (18 mL) and 6 N HCl (1.58 mL) were poured into the reaction mixture, and indole (0.5 g, 0.0043 mol) was added while stirring. A solution of iodine (1.08 g, 0.0043 mol) and potassium iodide (3.06 g, 0.02 mol) in water (11.5 mL) was dropped into the reaction, and it was stirred at 25 °C for 1 h. Water (20 mL) and a saturated solution of sodium hydrogen carbonate (15 mL) were added, and the mixture was extracted with chloroform. The organic layer was washed with brine, dried, and filtered. Evaporation of the solvent gave **10**, yield 47%, mp 125−128 °C (from ethanol). ^{1}H NMR (DMSO-d_6): δ 3.56 (s, 6H), 3.57 (s, 3H), 6.38 (s, 2H), 7.08 (t, J = 7.44 Hz, 1H), 7.18 (t, J = 7.56 Hz, 1H), 7.45 (d, J = 7.90 Hz, 1H), 7.48 (d, J = 8.07 Hz, 1H), 7.77 (s, 1H), 11.67 ppm (broad s, disappeared on treatment with D_2O, 1H). IR: ν 3356 cm^{-1}. MS: ES$^+$ = 338 (MNa$^+$). Anal. ($C_{17}H_{17}NO_3S$ (315.39)) C, H, N, S.

2-Methyl-3-[(3,4,5-trimethoxyphenyl)thio]-1*H*-indole (11). Compound **11** was synthesized as **10** using 2-methyl-1*H*-indole, yield 53%, mp 135−137 °C (from ethanol/water). ^{1}H NMR (DMSO-d_6): δ 2.44 (s, 3H), 3.57 (s, 9H), 6.29 (s, 2H), 7.03 (t, J = 7.03 Hz, 1H), 7.11 (t, J = 7.27 Hz, 1H), 7.37−7.39 (m, 2H), 11.61 ppm (broad s, disappeared on treatment with D_2O, 1H). IR: ν 3312 cm^{-1}. MS: ES$^+$ = 352 (MNa$^+$). Anal. ($C_{18}H_{19}NO_3S$ (329.42)) C, H, N, S.

5-Chloro-3-[(2-methoxyphenyl)thio]-1*H*-indole (12). Compound **12** was synthesized as **10** using 2-methoxythiophenol, yield 54%, mp 145−148 °C (from ethanol). ^{1}H NMR ($CDCl_3$): δ 3.97 (s, 3H), 6.59 (dd, J = 7.78 and 1.62 Hz, 1H), 6.68−6.72 (m, 1H), 6.86 (dd, J = 8.14 and 1.07 Hz, 1H), 7.05−7.09 (m, 1H), 7.22 (dd, J = 8.64 and 2.04 Hz, 1H), 7.37 (d, J = 8.63 Hz, 1H), 7.50 (d, J = 2.63 Hz, 1H), 7.60 (d, J = 2.02 Hz, 1H), 8.49 ppm (broad s, disappeared on treatment with D_2O, 1H). IR: ν 3433 cm^{-1}. MS: ES$^+$ = 312 (MNa$^+$). Anal. ($C_{15}H_{12}ClNOS$ (289.79)) C, H, Cl, N, S.

5-Chloro-3-[(3,5-dimethylphenyl)thio]-1*H*-indole (13). Compound **13** was synthesized as **10** using 3,5-dimethythiophenol and 5-chloro-1*H*-indole, yield 49%, mp 135−138 °C (from ethanol). ^{1}H NMR (DMSO-d_6): δ 2.12 (s, 6H), 6.66 (s, 2H), 6.70 (s, 1H), 7.18 (dd, J = 8.61 and 2.09 Hz, 1H), 7.35 (d, J = 2.06 Hz, 1H), 7.51 (d, J = 8.14 Hz, 1H), 7.83 (s, 1H), 11.89 ppm (broad s, disappeared on treatment with D_2O, 1H). IR: ν 3357 cm^{-1}. MS: ES$^+$ = 310 (MNa$^+$). Anal. ($C_{16}H_{14}ClNS$ (287.81)) C, H, Cl, N, S.

5-Chloro-3-[(3,4,5-trimethoxyphenyl)thio]-1*H*-indole (14). Compound **14** was synthesized as **10** using 5-chloro-1*H*-indole, yield 59%, mp 135−139 °C (from ethanol). ^{1}H NMR ($CDCl_3$): δ 3.68 (s, 6H), 3.79 (s, 3H), 6.36 (s, 2H), 7.20 (d, J = 8.73 Hz, 1H), 7.35 (d, J = 8.43 Hz, 1H), 7.51 (s, 1H), 7.62 (s, 1H) 8.69 ppm (broad s, disappeared on treatment with D_2O, 1H). IR: ν 3247 cm^{-1}. MS: ES$^+$ = 350 (MH$^+$). Anal. ($C_{17}H_{16}ClNO_3S$ (349.84)) C, H, Cl, N, S.

5-Chloro-2-methyl-3-[(3,4,5-trimethoxyphenyl)thio]-1*H*-indole (15). Compound **15** was synthesized as **10** using 5-chloro-2-methyl-1*H*-indole, yield 54%, mp 178−182 °C (from ethanol). ^{1}H NMR (DMSO-d_6): δ 2.48 (s, 3H), 3.59 (s, 9H), 6.28 (s, 2H), 7.12 (dd, J = 8.53 and 2.00 Hz, 1H), 7.32 (d, J = 4.68 Hz, 1H), 7.40 (d, J = 8.54 Hz, 1H), 11.84 ppm (broad s, disappeared on treatment with D_2O, 1H) IR: ν 3324 cm^{-1}. MS: ES$^+$ = 364 (MH$^+$). Anal. ($C_{18}H_{18}ClNO_3S$ (363.86)) C, H, Cl, N, S.

5-Bromo-3-[(3,4,5-trimethoxyphenyl)thio]-1*H*-indole (16). Compound **16** was synthesized as **10** using 5-bromo-1*H*-indole, yield 59%, mp 154−156 °C (from ethanol). ^{1}H NMR ($CDCl_3$): δ 3.70 (s, 6H), 3.82 (s, 3H), 6.39 (s, 2H), 7.31 (d, J = 8.60 Hz, 1H), 7.35 (dd, J = 8.64 and 1.82 Hz, 1H), 7.50 (d, J = 2.64 Hz, 1H), 7.80 (s, 1H) 8.82 ppm (broad s, disappeared on treatment with D_2O, 1H). IR: ν 3353 cm^{-1}. MS: ES$^+$ = 416, 418 (MNa$^+$). Anal. ($C_{17}H_{16}BrNO_3S$ (394.28)) C, H, Br, N, S.

5-Iodo-3-[(3,4,5-trimethoxyphenyl)thio]-1*H*-indole (17). Compound **17** was synthesized as **10** using 5-iodo-1*H*-indole, yield 60%, mp 178−180 °C (from ethanol). ^{1}H NMR ($CDCl_3$): δ 3.71 (s, 6H), 3.81 (s, 3H), 6.39 (s, 2H), 7.23 (d, J = 8.52 Hz, 1H), 7.47 (d, J = 2.65 Hz, 1H), 7.53 (dd, J = 8.54 and 1.66 Hz, 1H), 8.02 (s, 1H) 8.66 ppm (broad s, disappeared on treatment with D_2O, 1H). IR: ν 3354 cm^{-1}. MS: ES$^+$ = 464 (MNa$^+$). Anal. ($C_{17}H_{16}INO_3S$ (441.29)) C, H, I, N, S.

5-Fluoro-3-[(3,4,5-trimethoxyphenyl)thio]-1*H*-indole (18). Compound **18** was synthesized as **10** using 5-fluoro-1*H*-indole, yield 57%, mp 160−163 °C (from ethanol). ^{1}H NMR ($CDCl_3$): δ 3.68 (s, 6H), 3.78 (s, 3H), 6.37 (s, 2H), 6.98−7.04 (m, 1H), 7.29 (dd, J = 9.16 and 2.51 Hz, 1H), 7.35 (dd, J = 8.83 and 4.21 Hz, 1H), 7.54 (d, J = 2.68 Hz, 1H), 8.52 ppm (broad s, disappeared on treatment with D_2O, 1H). IR: ν 3344 cm^{-1}. MS: ES$^+$ = 356 (MNa$^+$). Anal. ($C_{17}H_{16}FNO_3S$ (333.38)) C, H, F, N, S.

5-Nitro-3-[(3,4,5-trimethoxyphenyl)thio]-1*H*-indole (19). Compound **19** was synthesized as **10** using 5-nitro-1*H*-indole, yield 6%, yellow oil. ^{1}H NMR (DMSO-d_6): δ 3.58 (s, 3H), 3.60 (s, 6H), 6.44 (s, 2H), 7.68 (d, J = 8.54 Hz, 1H), 8.06−8.09 (m, 2H), 8.32 (d, J = 2.33 Hz, 1H), 12.48 ppm (broad s, disappeared on treatment with D_2O, 1H). IR: ν 3284 cm^{-1}. MS: ES$^+$ = 383 (MNa$^+$). Anal. ($C_{17}H_{16}N_2O_5S$ (360.39)) C, H, N, S.

5-Amino-3-[(3,4,5-trimethoxyphenyl)thio]-1*H*-indole (20). Compound **20** was synthesized as **10** using 5-amino-1*H*-indole, yield 17%, mp 128−131 °C (from ethanol). ^{1}H NMR ($CDCl_3$): δ 3.60 (broad s, disappeared on treatment with D_2O, 2H), 3.69 (s, 6H), 3.79 (s, 3H), 6.38 (s, 2H), 6.72 (dd, J = 8.55 and 2.20 Hz, 1H), 6.91 (d, J = 2.17 Hz, 1H), 7.24 (d, J = 8.54 Hz, 1H), 7.42 (d, J =

2.66 Hz, 1H) 8.30 ppm (broad s, disappeared on treatment with D_2O, 1H). IR: ν 3393 cm^{-1}. MS: $ES^+ = 331$ (MH^+). Anal. ($C_{17}H_{18}N_2O_3S$ (330.41)) C, H, N, S.

5-Methyl-3-[(3,4,5-trimethoxyphenyl)thio]-1*H*-indole (21). Compound **21** was synthesized as **10** using 5-methyl-1*H*-indole, yield 45%, oil which solidified on standing, mp 81−84 °C (aqueous ethanol). ^1H NMR ($CDCl_3$): δ 2.45 (s, 3H), 3.69 (s, 6H), 3.83 (s, 3H), 6.40 (s, 2H), 7.10 (d, $J = 7.69$ Hz, 1H), 7.34 (d, $J = 8.24$ Hz, 1H), 7.45 (s, 1H), 7.48 (d, $J = 2.58$ Hz, 1H), 8.38 ppm (broad s, disappeared on treatment with D_2O, 1H). IR: ν 3346 cm^{-1}. MS: $ES^+ = 330$ (MH^+). Anal. ($C_{18}H_{19}NO_3S$ (329.42)) C, H, N, S.

5-Methoxy-3-[(3,4,5-trimethoxyphenyl)thio]-1*H*-indole (22). Compound **22** was synthesized as **10** using 5-methoxy-1*H*-indole, yield 30%, 99−101 °C (from ethanol). ^1H NMR (DMSO-d_6): δ 3.57 (s, 3H), 3.58 (s, 6H), 3.71 (s, 3H), 6.39 (s, 2H), 7.82 (dd, $J =$ 8.76 and 2.43 Hz, 1H), 6.90 (d, $J = 2.38$ Hz, 1H), 7.38 (d, $J =$ 8.76 Hz, 1H), 7.71 (d, $J = 2.70$ Hz, 1H), 11.54 ppm (broad s, disappeared on treatment with D_2O, 1H). IR: ν 3356 cm^{-1}. MS: $ES^+ = 368$ (MNa^+). Anal. ($C_{18}H_{19}NO_4S$ (345.42)) C, H, N, S.

5-Methoxy-2-methyl-3-[(3,4,5-trimethoxyphenyl)thio]-1*H*-indole (23). Compound **23** was synthesized as **10** using 5-methoxy-2-methyl-1*H*-indole, yield 29%, mp 138−142 °C (from ethanol). ^1H NMR (DMSO-d_6): δ 2.44 (s, 3H), 3.58 (s, 9H), 3.71 (s, 3H), 6.30 (s, 2H), 6.74 (dd, $J = 8.66$ and 2.43 Hz, 1H), 6.84 (d, $J =$ 2.20 Hz, 1H), 7.27 (d, $J = 8.68$ Hz, 1H), 11.48 ppm (broad s, disappeared on treatment with D_2O, 1H). IR: ν 3339 cm^{-1}. MS: $ES^+ = 382$ (MNa^+). Anal. ($C_{19}H_{21}NO_4S$ (359.45)) C, H, N, S.

5-Ethoxy-3-[(3,4,5-trimethoxyphenyl)thio]-1*H*-indole (24). Compound **24** was synthesized as **10** using 5-ethoxy-1*H*-indole (**32**), yield 31%, brown oil. ^1H NMR ($CDCl_3$): δ 1.41 (t, $J = 6.98$ Hz, 3H), 3.68 (s, 6H), 3.79 (s, 3H), 4.04 (q, $J = 6.99$ Hz, 2H), 6.38 (s, 2H), 6.92 (dd, $J = 8.79$ and 2.43 Hz, 1H), 7.08 (d, $J = 2.37$ Hz, 1H), 7.33 (d, $J = 8.78$ Hz, 1H), 7.47 (d, $J = 2.68$ Hz, 1H), 8.48 ppm (broad s, disappeared on treatment with D_2O, 1H). IR: ν 3337 cm^{-1}. MS: $ES^+ = 382$ (MNa^+). Anal. ($C_{19}H_{21}NO_4S$ (359.45)) C, H, N, S.

5-Isopropoxy-3-[(3,4,5-trimethoxyphenyl)thio]-1*H*-indole (25). Compound **25** was synthesized as **10** using 5-isopropoxy-1*H*-indole (**33**), yield 31%, brown oil. ^1H NMR (DMSO-d_6): δ 1.20 (d, $J =$ 6.00 Hz, 6H), 3.57 (s, 9H), 4.44−4.48 (m, 1H), 6.39 (s, 2H), 6.79 (dd, $J = 8.75$ and 2.36 Hz, 1H), 6.86 (d, $J = 1.87$ Hz, 1H), 7.36 (d, $J = 8.72$ Hz, 1H), 7.69 (d, $J = 2.66$ Hz, 1H), 11.51 ppm (broad s, disappeared on treatment with D_2O, 1H). IR: ν 3392 cm^{-1}. MS: $ES^+ = 396$ (MNa^+). Anal. ($C_{20}H_{23}NO_4S$ (373.43)) C, H, N, S.

5-Hydroxy-3-[(3,4,5-trimethoxyphenyl)thio]-1*H*-indole (26). Compound **26** was synthesized as **10** using 5-hydroxy-1*H*-indole, yield 28%, 184−186 °C (from ethanol). ^1H NMR ($CDCl_3$): δ 3.34 (s, 9H), 6.35 (s, 2H), 6.67 (dd, $J = 8.62$ and 2.30 Hz, 1H), 6.76 (d, $J = 3.21$ Hz, 1H), 7.27 (d, $J = 8.64$ Hz, 1H), 7.63 (d, $J = 2.70$ Hz, 1H), 8.83 (broad s, disappeared on treatment with D_2O, 1H), 11.37 ppm (broad s, disappeared on treatment with D_2O, 1H). IR: ν 3340, 3279 cm^{-1}. MS: $ES^+ = 354$ (MNa^+). Anal. ($C_{17}H_{17}NO_4S$ (331.39)) C, H, N, S.

5-[2-(Benzyloxy)ethoxy]-3-[(3,4,5-trimethoxyphenyl)thio]-1*H*-indole (28). Compound **28** was synthesized as **10** using 5-(2-(benzyloxy)ethoxy)-1*H*-indole (**34**), yield 35%, brown oil. ^1H NMR ($CDCl_3$): δ 3.68 (s, 6H), 3.79 (s, 3H), 3.85 (t, $J = 4.88$ Hz, 2H), 4.18 (t, $J = 4.83$ Hz, 2H), 4.65 (s, 2H), 6.38 (s, 2H), 6.98 (dd, $J =$ 8.80 and 2.43 Hz, 1H), 7.11 (d, $J = 2.32$ Hz, 1H), 7.30−7.40 (m, 6H), 7.48 (d, $J = 2.67$ Hz, 1H), 8.42 ppm (broad s, disappeared on treatment with D_2O, 1H). IR: ν 3334 cm^{-1}. MS: $ES^+ = 488$ (MNa^+). Anal. ($C_{26}H_{27}NO_5S$ (465.57)) C, H, N, S.

2-[3-[(3,4,5-Trimethoxyphenyl)thio]-1*H*-indol-5-yloxy]ethanol (27). (2-Bromoethoxy)-*tert*-butyldimethylsilane (0.17 g, 0.16 mL, 0.724 mmol) and potassium carbonate (0.1 g, 0.72 mmol) were added to a solution of **26** (0.2 g, 0.603 mmol) in acetonitrile (30 mL). The reaction was refluxed overnight. (2-Bromoethoxy)-*tert*-butyldimethylsilane (0.17 g, 0.16 mL, 0.724 mmol) and potassium carbonate (0.1 g, 0.72 mmol) were added, and the reaction was refluxed for an additional 12 h. After cooling, water (10 mL) was added, and the reaction mixture was extracted with ethyl acetate; the organic layer was washed with brine, dried, and filtered. Evaporation of the solvent gave 5-[2-(*tert*-butyldimethylsilyloxy)-ethoxy]-3-[(3,4,5-trimethoxy phenyl)thio]-1*H*-indole (yield 41% as a brown oil), which was used without further purification. To a solution of the latter compound (0.11 g, 0.225 mol) in methanol (1.13 mL) was added *para*-toluenesulfonic acid monohydrate (0.01 g, 0.05 mmol). The reaction mixture was stirred at 25 °C for 30 min, neutralized with a saturated solution of sodium hydrogen carbonate, and extracted with ethyl acetate; the organic layer was washed with brine, dried, and filtered. Evaporation of the solvent gave a residue that was purified by silica gel column chromatography (ethyl acetate−*n*-hexane 7:1 as eluent) to furnish **27**, yield 22%, as a yellow oil. ^1H NMR ($CDCl_3$): δ 2.19 (broad s, disappeared on treatment with D_2O, 1H), 3.69 (s, 6H), 3.80 (s, 3H), 3.94−3.99 (m, 2H), 4.10 (t, $J = 4.53$ Hz, 2H), 6.39 (s, 2H), 6.94 (dd, $J = 8.79$ and 2.43 Hz, 1H), 7.11 (d, $J = 2.26$ Hz, 1H), 7.33 (d, $J = 8.79$ Hz, 1H), 7.48 (d, $J = 2.68$ Hz, 1H), 8.65 ppm (broad s, disappeared on treatment with D_2O, 1H). IR: ν 3336 cm^{-1}. MS: $ES^+ = 398$ (MNa^+). Anal. ($C_{19}H_{21}NO_5S$ (375.45)) C, H, N, S.

5-Ethoxy-1*H*-indole (32). Iodoethane (1.23 g, 0.63 mL, 0.0079 mol) and potassium carbonate (1.46 g, 0.01 mol) were added to a solution of 5-hydroxy-1*H*-indole (0.7 g, 0.0053 mol) in acetone (49 mL). The reaction mixture was refluxed overnight. Iodoethane (1.23 g, 0.63 mL, 0.0079 mol) and potassium carbonate (1.46 g, 0.01 mol) were added, and the reaction mixture was stirred at the same temperature for an additional 12 h. After cooling, the reaction mixture was filtered, and the resulting solution was diluted with ethyl acetate (30 mL) and washed with 3 N NaOH. The organic layer was washed with brine and dried. Evaporation of the solvent gave a residue that was purified by silica gel column chromatography (chloroform as eluent) to furnish **32**, yield 64%, yellow oil. ^1H NMR ($CDCl_3$): δ 1.49 (t, $J = 6.98$ Hz, 3H), 4.12 (q, $J = 6.98$ Hz, 2H), 6.50−6.52 (m, 1H), 6.91 (dd, $J = 8.78$ and 2.12 Hz, 1H), 7.16−7.18 (m, 2H), 7.28 (d, $J = 8.78$ Hz, 1H), 8.08 ppm (broad s, disappeared on treatment with D_2O, 1H). IR: ν 3409 cm^{-1}.

5-Isopropoxy-1*H*-indole (33). Compound **33** was synthesized as **32** using 2-iodopropane, yield 25%, yellow oil. ^1H NMR ($CDCl_3$): δ 1.38 (d, $J = 6.08$ Hz, 6H), 4.55 (m, 6.00−6.07 Hz, 1H), 6.48−6.50 (m, 1H), 6.88 (dd, $J = 8.75$ and 2.36 Hz, 1H), 7.17−7.19 (m, 2H), 7.28 (d, $J = 8.14$ Hz, 1H), 8.09 ppm (broad s, disappeared on treatment with D_2O, 1H). IR: ν 3412 cm^{-1}.

5-[2-(Benzyloxy)ethoxy]-1*H*-indole (34). A solution of diethyl azodicarboxylate (40% in toluene, 0.64 g, 1.60 mL, 0.0037 mol) was added dropwise to a mixture of 2-benzyloxyethanol (0.56 g, 0.53 mL, 0.0037 mol), 5-hydroxy-1*H*-indole (0.5 g, 0.0037 mol), and anhydrous triphenylphosphine (0.97 g, 0.0037 mol) in anhydrous tetrahydrofuran (23 mL). The reaction mixture was refluxed overnight. After evaporation of the solvent, water (15 mL) and ethyl acetate (15 mL) were added; the organic layer was washed with brine and dried. Removal of the solvent gave a residue that was purified by silica gel column chromatography (chloroform as eluent) to furnish **34**, yield 82%, brown oil. ^1H NMR ($CDCl_3$): δ 3.89 (t, $J = 4.92$ Hz, 2H), 4.23 (t, $J = 4.93$ Hz, 2H), 4.69 (s, 2H), 6.48−6.50 (m, 1H), 6.93 (dd, $J = 8.79$ and 2.44 Hz, 1H), 7.15 (d, $J =$ 2.37 Hz, 1H), 7.18−7.19 (m, 1H), 7.30−7.43 (m, 6H), 8.10 ppm (broad s, disappeared on treatment with D_2O, 1H). IR: ν 3409 cm^{-1}.

Biology. Tubulin Assembly. The reaction mixtures contained 0.8 M monosodium glutamate (pH 6.6 with HCl in 2 M stock solution), 10 μM tubulin, and varying concentrations of drug. Following a 15 min preincubation at 30 °C, samples were chilled on ice, GTP to 0.4 mM was added, and turbidity development was followed at 350 nm in a temperature controlled recording spectrophotometer for 20 min at 30 °C. The extent of the reaction was measured. Full experimental details were previously reported.[31]

[^{3}H]Colchicine Binding Assay. The reaction mixtures contained 1.0 μM tubulin, 5.0 μM [^{3}H]colchicine, and 5.0 μM inhibitor and were incubated 10 min at 37 °C. Complete details were described previously.[32]

MCF-7 Cell Growth. The above paper[32] can also be referenced for methodology of MCF-7 cell growth.

Binding Constants of the Ligands. The binding constants of the ligands were measured at 20 °C either by displacement of compound **35**[27] in a Shimadzu RF540 fluorimeter, with 5 nm excitation and emission slits and with excitation at 350 nm and emission at 422 nm. To check if any fluorescence or inner filter effect could interfere with the assay results, the spectra of all compounds dissolved in ethanol were determined in a Hitachi U-2000 spectrophotometer. Only compound **30** showed absorbance at the excitation wavelength (350 nm) of compound **35**, as well as emission at 422 nm. Therefore, its binding constant was measured by quenching of the intrinsic fluorescence of tubulin.[28,29] The data were analyzed using the software package Equigra v5.[25]

Cell Culture. HeLa cells were grown at 37 °C in a humidified atmosphere containing 5% CO_2 in DMEM (GIBCO BRL, U.K.) supplemented with 10% fetal calf serum (Hyclone, NL), 100 U/mL of penicillin and streptomycin, and 2 mM glutamine (all reagents were from Celbio, Italy). Cells were trypsinized when subconfluent, seeded in T75 flasks at a concentration of 2.5×10^5 cells/mL in complete medium and treated with compound **16** at 0.1−10 μM for 24 h. Cells were harvested either immediately at the end of the treatment or after a further incubation in drug-free medium for 24 h. In some experiments, HeLa cells were treated with 100 μM etoposide for 3 h, followed by a 24 h recovery period.

Viability and Morphology Assays. Viability was assessed by staining cells with trypan blue. Permeable cells were counted in a hemocytometer and considered as nonviable. To evaluate cell morphology, cells grown on glass coverslips were fixed for 10 min in ice-cold 70% ethanol, washed several times with ice-cold PBS, and stained for 10 min at room temperature with 0.1 μg/mL Hoechst 33258 (Sigma). Samples were washed with PBS, mounted on a glass slide in a drop of Mowiol (Calbiochem, Inalco, Italy), and observed by fluorescence microscopy.

Cell Cycle Analysis. Cells were detached by careful trypsinization (to obtain single-cell suspensions to be processed for flow cytometry), then resuspended in cold 0.9% NaCl and fixed with cold 70% (final concentration) ethanol. Cells were stained in a solution of PBS containing 30 μg/mL propidium iodide and 2 mg/mL RNase A (Sigma) and analyzed with an Epics XL flow cytometer (Beckman-Coulter Corp., U.S.A.). At least 10 000 cells/sample were measured.

Evaluation of apoptosis. To investigate DNA degradation, cells were rinsed twice in cold PBS containing 5 mM EDTA. Genomic DNA was extracted from 2.5×10^6 cells and analyzed by agarose gel electrophoresis.[33] PARP-1 proteolysis was used as a marker of caspase activation. Total extracts for western blots were prepared from 2.5×10^6 cells. The western blot analysis was performed as previously reported[33] with the mAb C-2−10 against PARP-1 (Alexis, Vinci-Biochem, Italy). An HRP-conjugated antimouse IgG antibody (Sigma) was used as the secondary antibody. Visualization was performed by the ECL Detection System (Sigma).

Molecular Modeling. All molecular modeling studies were performed on a RM Innovator with Pentium IV 3 GHz processor, running Linux Fedora Core 4 using Molecular Operating Environment (MOE) 2006.08[34] and the FlexX module in Sybyl 7.2.[30] The structure of two tubulin dimers, cocrystalized with a stathmin-like domain and *N*-deacetyl-*N*-(2-mercaptoacetyl)-colchicine (DAMA-colchicine), was downloaded from the PDB data bank (http://www.rcsb.org/pdb/index.html; PDB code: 1SA0).[1] Ligand structures were built with MOE and minimized using the MMFF94x forcefield until a RMSD gradient of 0.05 kcal mol^{-1} $Å^{-1}$ was reached. The partial charges were automatically calculated and the structure was saved as a mol2 file. Docking experiments were carried out using the FlexX docking program of Sybyl 7.2. The DAMA-colchicine present between chain C and chain D of the structure was used to define the binding site, which included all residues within 6.5 Å of the crystallized ligand. The GTP molecule situated at the edge of the binding site on α-tubulin was included as a heteroatom file. DAMA-colchicine was automatically removed from the active site by the software before the docking simulation. The output of FlexX docking was visualized in MOE, and the scoring.svl script[35] was used to identify interaction types between ligand and protein.

Acknowledgment. G. La R. thanks Istituto Pasteur − Fondazione Cenci Bolognetti for his Borsa di Studio per Ricerche all'Estero. G. De M. thanks Italian Miur for her Progetto Mobilità Studiosi Italiani all'Estero. This research was funded by Istituto Pasteur − Fondazione Cenci Bolognetti and Università di Roma "La Sapienza", Ricerche di Ateneo. Authors also thank FIRC (Federazione Italiana per la Ricerca sul Cancro) for its contribution. This work was supported by Grants BFU2004-00358 from the Dirección General de Investigación Científica y Tecnológica (DGICYT) and CAM200520M061 from Comunidad Autonoma de Madrid. This research was also partially supported by a grant of the Fondazione Banca del Monte di Lombardia (Pavia, Italy) to A.I.S. For S.K. we would like to acknowledge the Embassy of the Arab Republic of Egypt for the award of a PhD scholarship.

Supporting Information Available: Elemental analyses of new derivatives **10**−**28**. This material is available free of charge via Internet at http//pubs.acs.org.

References

(1) Ravelli, R. B.; Gigant, B.; Curmi, P. A.; Jourdain, I.; Lachkar, S.; Sobel, A.; Knossow, M. Insight into tubulin regulation from a complex with colchicine and a stathmin-like domain. *Nature* **2004**, *428*, 198−202.
(2) Nogales, E.; Whittaker, M.; Milligan, R. A.; Downing, K. H. High-resolution model of the microtubule. *Cell* **1999**, *96*, 79−88.
(3) Nettles, J. H.; Li, H.; Cornett, B.; Krahn, J. M.; Snyder, J. P.; Downing, K. H. The binding mode of epothilone A on alpha, beta-tubulin by electron crystallography. *Science* **2004**, *305*, 866−869.
(4) Buey, R. M.; Calvo, E.; Barasoain, I.; Pineda, O.; Edler, M. C.; Matesanz, R.; Cerezo, G.; Vanderwal, C. D.; Day, B. W.; Sorensen, E. J.; Lopez, J. A.; Andreu, J. M.; Hamel, E.; Diaz, J. F. Cyclostreptin binds covalently to microtubule pores and lumenal taxoid binding sites. *Nat. Chem. Biol.* **2007**, *3*, 117−125.
(5) Lin, M. C.; Ho, H. H.; Pettit, G. R.; Hamel, E. Antimitotic natural products combretastatin A-4 and combretastatin A-2: Studies on the mechanism of their inhibition of the binding to colchicine to tubulin. *Biochemistry* **1989**, *28*, 6984−6991.
(6) Beckers, T.; Mahboobi, S. Natural, semisynthetic and synthetic microtubule inhibitors for cancer therapy. *Drugs Future* **2003**, *28*, 767−785.
(7) Sridhare, M.; Macapinlac, M. J.; Goel, S.; Verdier-Pinard, D.; Fojo, T.; Rothenberg, M.; Colevas, D. The clinical development of new mitotic inhibitors that stabilize the microtubule. *Anticancer Drugs* **2004**, *15*, 553−555.
(8) Jordan, M. A.; Wilson, L.; Microtubules as a target for anticancer drugs. *Nat. Rev. Cancer* **2004**, *4*, 253−265.
(9) Mealy, N. E.; Balcells, L. M. Drugs under development for the treatment of breast cancer. *Drugs Future* **2006**, *31*, 541−564.
(10) Davis, P. D.; Dougherty, G. J.; Blakey, D. C.; Galbraith, S. M.; Tozer, G. M.; Holder, A. L.; Naylor, M. A.; Nolan, J.; Stratford, M. R. L.; Chaplin, D. J.; Hill, S. A. ZD6126: A novel vascular-targeting agent that causes selective destruction of tumor vasculature. *Cancer Res.* **2002**, *62*, 7247−7253.
(11) Chaplin, D. J.; Horsman, M. R.; Siemann, D. W. Current development status of small-molecule vascular disrupting agents. *Curr. Opin. Invest. Drugs* **2006**, *7*, 522−528.
(12) De Martino, G.; La Regina, G.; Coluccia, A.; Edler, M. C.; Barbera, M. C.; Brancale, A.; Wilcox, E.; Hamel, E.; Artico, M.; Silvestri, R. Arylthioindoles, potent inhibitors of tubulin polymerization. *J. Med. Chem.* **2004**, *47*, 6120−6123.
(13) De Martino, G.; Edler, M. C.; La Regina, G.; Coluccia, A.; Barbera, M. C.; Barrow, D.; Nicholson, R. I.; Chiosis, G.; Brancale, A.; Hamel, E.; Artico, M.; Silvestri, R. Arylthioindoles, potent inhibitors of tubulin polymerization. 2. Structure−activity relationships and molecular modeling studies. *J. Med. Chem.* **2006**, *49*, 947−954.
(14) Tron, G. C.; Pirali, T.; Sorba, G.; Pagliai, F.; Busacca, S.; Genazzani, A. A. Medicinal chemistry of combretastatin A4: Present and future directions. *J. Med. Chem.* **2006**, *49*, 3033−3044.
(15) Liou, J.-P.; Chang, C.-W.; Song, J.-S.; Yang, Y.-N.; Yeh, C.-F.; Tseng, H.-Y.; Lo, Y.-K.; Chang, Y.-L.; Chang, C.-M.; Hsieh, H.-P. Synthesis and structure−activity relationship of 2-aminobenzophenone derivatives as antimitotic agents. *J. Med. Chem.* **2002**, *45*, 2556−2562.

(16) Chang, J.-Y.; Yang, M.-F.; Chang, C.-Y.; Chen, C.-M.; Kuo, C.-C.; Liou, J.-P. 2-Amino and 2′-aminocombretastatin derivatives as potent antimitotic agents. *J. Med. Chem.* **2006**, *49*, 6412−6415.
(17) (a) Romagnoli, R.; Baraldi, P. G.; Pavani, M. G.; Tabrizi, M. A.; Preti, D.; Fruttarolo, F.; Piccagli, L.; Jung, M. K.; Hamel, E.; Borgatti, M.; Gambari, R. Synthesis and biological evaluation of 2-amino-3-(3′,4′,5′-trimethoxybenzoyl)-5-aryl thiophenes as a new class of potent antitubulin agents. *J. Med. Chem.* **2006**, *49*, 3906−3915. (b) Romagnoli, R.; Baraldi, P. G.; Remusat, V.; Carrion, M. D.; Cara, C. L.; Preti, D.; Fruttarolo, F.; Pavani, M. G.; Tabrizi, M. A.; Tolomeo, M.; Grimaudo, S.; Balzarini, J.; Jordan, M. A.; Hamel, E. Synthesis and biological evaluation of 2-(3′,4′,5′-trimethoxybenzoyl)-3-amino 5-aryl thiophenes as a new class of tubulin inhibitors. *J. Med. Chem.* **2006**, *49*, 6425−6428.
(18) Liou, J.-P.; Chang, Y.-L.; Kuo, F.-M.; Chang, C.-W.; Tseng, H.-Y.; Wang, C.-C.; Yang, Y.-N.; Chang, J.-Y.; Lee, S.-J.; Hsieh, H.-P. Concise synthesis and structure−activity relationships of combretastatin A-4 analogues, 1-aroylindoles and 3-aroylindoles, as novel classes of potent antitubulin agents. *J. Med. Chem.* **2004**, *47*, 4247−4257.
(19) Offer, J.; Boddy, C. N. C.; Dawson, P. E. Extending synthetic access to proteins with a removable acyl transfer auxiliary. *J. Am. Chem. Soc.* **2002**, *124*, 4642−4646.
(20) Flynn, B. L.; Flynn, G. P.; Hamel, E.; Jung, M. K. The synthesis and tubulin binding activity of thiophene-based analogues of combretastatin A-4. *Bioorg. Med. Chem. Lett.* **2001**, *11*, 2341−2343.
(21) Perez-Ramirez, B.; Shearwin, K. E.; Timasheff, S. N. The colchicine-induced GTPase activity of tubulin: State of the product. Activation by microtubule-promoting cosolvents. *Biochemistry* **1994**, *33*, 6253−6261.
(22) Perez-Ramirez, B.; Andreu, J. M.; Gorbunoff, M. J.; Timasheff, S. N. Stoichiometric and substoichiometric inhibition of tubulin self-assembly by colchicine analogues. *Biochemistry* **1996**, *35*, 3277−3285.
(23) Barbier, P.; Peyrot, V.; Leynadier, D.; Andreu, J. M. The active GTP- and ground GDP-liganded states of tubulin are distinguished by the binding of chiral isomers of ethyl 5-amino-2-methyl-1,2-dihydro-3-phenylpyrido[3,4-*b*]pyrazin-7-yl carbamate. *Biochemistry* **1998**, *37*, 758−768.
(24) Buey, R. M.; Diaz, J. F.; Andreu, J. M.; O'Brate, A.; Giannakakou, P.; Nicolaou, K. C.; Sasmal, P. K.; Ritzen, A.; Namoto, K. interaction of epothilone analogs with the paclitaxel binding site; relationship between binding affinity, microtubule stabilization, and cytotoxicity. *Chem. Biol.* **2004**, *11*, 225−236.
(25) Buey, R. M.; Barasoain, I.; Jackson, E.; Meyer, A.; Giannakakou, P.; Paterson, I.; Mooberry, S.; Andreu, J. M.; Diaz, J. F. Microtubule interactions with chemically diverse stabilizing agents: Thermodynamics of binding to the paclitaxel site predicts cytotoxicity. *Chem. Biol.* **2005**, *12*, 1269−1279.
(26) Medrano, F. J.; Andreu, J. M.; Gorbunoff, M. J.; Timasheff, S. N. Roles of colchicine rings B and C in the binding process to tubulin. *Biochemistry* **1989**, *28*, 5589−5599.
(27) Medrano, F. J.; Andreu, J. M.; Gorbunoff, M. J.; Timasheff, S. N. Roles of ring C oxygens in the binding of colchicine to tubulin. *Biochemistry* **1991**, *30*, 3770−3777.
(28) Andreu, J. M.; Gorbunoff, M. J.; Lee, J. C.; Timasheff, S. N. Interaction of tubulin with bifunctional colchicine analogues: An equilibrium study. *Biochemistry* **1984**, *23*, 1742−1752.
(29) Andreu, J. M.; Timasheff, S. N. Conformational states of tubulin liganded to colchicine, tropolone methyl ether, and podophyllotoxin. *Biochemistry* **1982**, *21*, 6465−6476.
(30) Tripos, *Sybyl 7.2*; Tripos Inc.: 1699 South Hanley Rd, St. Louis, Missouri 63144, http://www.tripos.com.
(31) Hamel, E. Evaluation of antimitotic agents by quantitative comparisons of their effects on the polymerization of purified tubulin. *Cell Biochem. Biophys.* **2003**, *38*, 1−21.
(32) Verdier-Pinard, P.; Lai, J.-Y.; Yoo, H.-D.; Yu, J.; Marquez, B.; Nagle, D. G.; Nambu, M.; White, J. D.; Falck, J. R.; Gerwick, W. H.; Day, B. W.; Hamel, E. Structure−activity analysis of the interaction of curacin A, the potent colchicine site antimitotic agent, with tubulin and effects of analogs on the growth of MCF-7 breast cancer cells. *Mol. Pharmacol.* **1998**, *53*, 62−76.
(33) Donzelli, M.; Bernardi, R.; Negri, C.; Prosperi, E.; Padovan, L.; Lavialle, C.; Brison, O.; Scovassi, A. I. Apoptosis-prone phenotype of human colon carcinoma cells with a high level amplification of the c-*myc* gene. *Oncogene* **1999**, *18*, 439−448.
(34) Molecular Operating Environment (MOE 2006.08); Chemical Computing Group, Inc.: Montreal, Quebec, Canada, http://www.chemcomp.com.
(35) Code "scoring.svl" obtained from the SLV Exchange website http://svl.chemcomp.com., Chemical Computing Group, Inc., Montreal, Canada.

JM061479U

DOI: 10.1002/chem.200700342

The Total Synthesis and Biological Properties of the Cytotoxic Macrolide FD-891 and Its Non-natural (*Z*)-C12 isomer

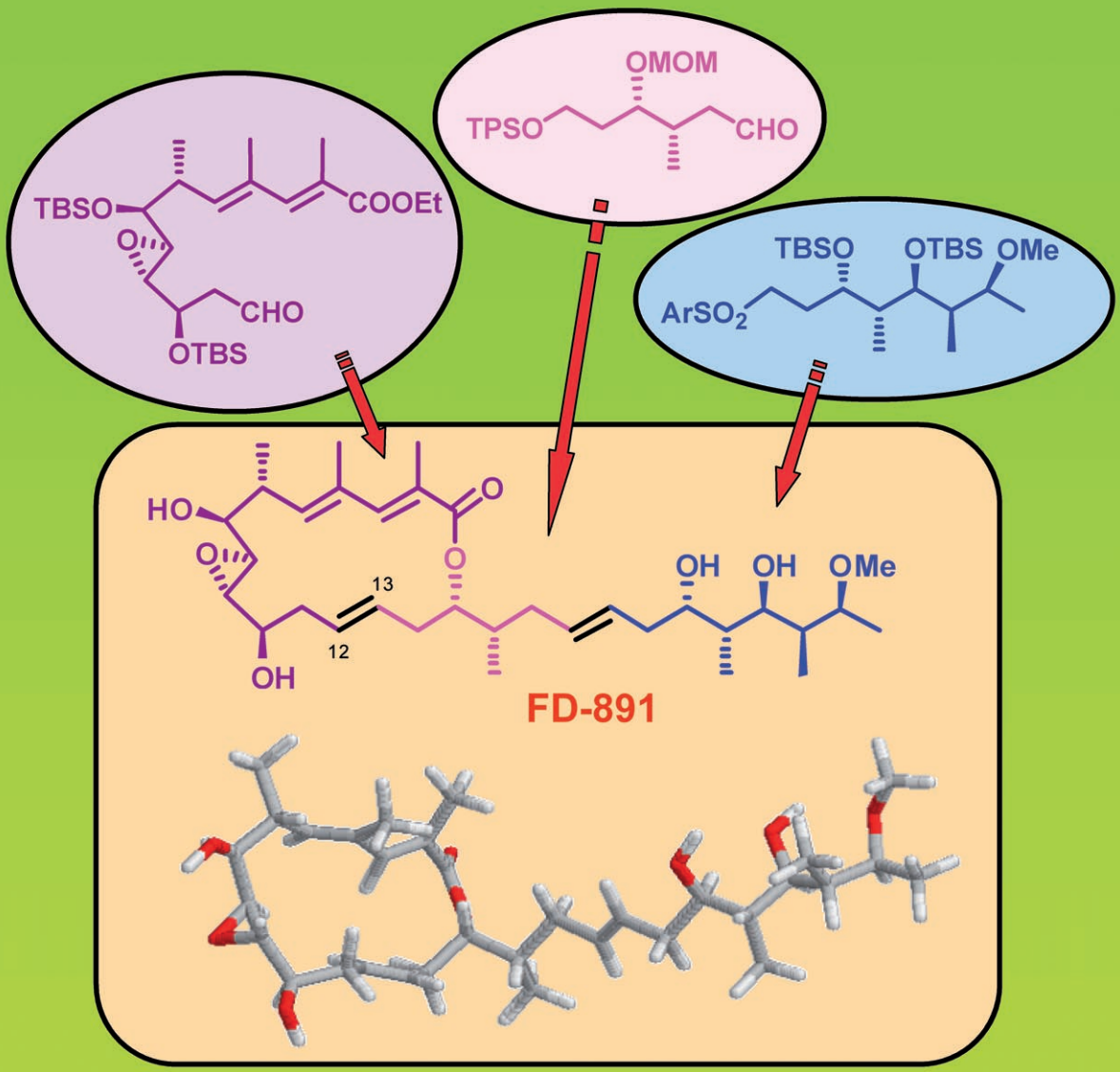

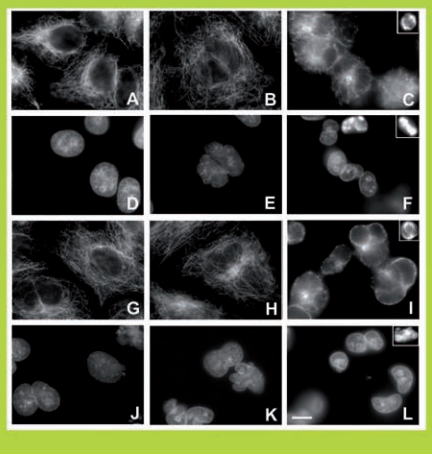

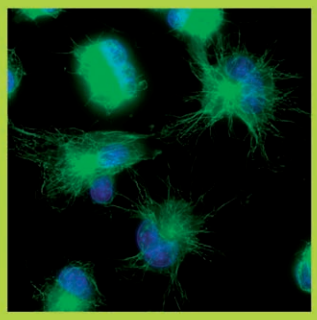

Effect of FD-891 and (*Z*)-FD-891 on a microtubule network

The Total Synthesis and Biological Properties of the Cytotoxic Macrolide FD-891 and Its Non-Natural (*Z*)-C12 Isomer

Jorge García-Fortanet,[a] Juan Murga,[a] Miguel Carda,*[a] J. Alberto Marco,*[b] Ruth Matesanz,[c] J. Fernando Díaz,[c] and Isabel Barasoain*[c]

Dedicated to Professors J. Bosch and M. A. Yus on the occasion of their 60th birthdays and to Professor R. Mestres on his retirement.

Abstract: A total, stereoselective synthesis of the naturally occurring, cytotoxic macrolide FD-891 and of its non-natural (*Z*)-C12 isomer is described. Three fragments of the main carbon chain were stereoselectively prepared by using asymmetric aldol and allylation reactions as the key steps. The molecule was then assembled by using two Julia–Kocienski olefinations to connect the three fragments and a Yamaguchi reaction to close the macrolactone ring. Some specific biological properties (cytotoxicity, binding to tubulin) have been determined for both macrolides. The *E* configuration of the C12–C13 olefinic bond seems to be an important feature in determining the cytotoxicity but the precise biological mechanism of the latter still remains to be cleared.

Keywords: aldol reaction · allylation · antitumor agents · lactones · olefination · tubulin binding

Introduction

Natural products with novel structures and useful pharmacological activities have always constituted main targets for synthetic chemists. Among the former, macrocyclic lactones (macrolides) of polyketide origin with cytotoxic and other similarly valuable biological properties have attracted particular attention in the last three decades. A subclass within these lactones are the so-called plecomacrolides, produced by several *Streptomyces* species and characterized by their ability to specifically inhibit the vacuolar-type H^+-ATPase, that is, to disrupt the acidification of intracellular acidic organelles.[1] This property manifests itself in a range of various biological responses, such as antiviral, antifungal, antibacterial, anticancer and immunosuppressant activities.[2]

Several subtypes of compounds within the plecomacrolide group have been reported.[3] Particularly relevant are the bafilomycins, the hygrolidins and the concanamycins. Members of this group are characterized by displaying 16- or 18-membered lactone rings containing two diene units and a polyoxygenated side chain in which a hemiketal fragment is often present. Their structural complexity and potential pharmacological utility have aroused much interest in the chemical community and therefore given rise to a great deal of synthetic effort.[2] This has included not only the natural macrolides but also analogues thereof with the aim of improving their not always beneficial biological profiles.[4]

Macrolide FD-891, structurally related to the concanamycins even though it lacks a hemiketal moiety, was isolated in 1994 by a Japanese group from the fermentation broth of *S. graminofaciens* A-8890.[5] It shows cytotoxic activity against several tumour cell lines and, in addition, has been found to potently prevent both perforin- and FasL-dependent CTL-mediated killing pathways. In contrast to the structurally related concanamycin A, however, it is unable to inhibit va-

[a] Dr. J. García-Fortanet, Dr. J. Murga, Prof. Dr. M. Carda
Depart. de Q. Inorgánica y Orgánica
Univ. Jaume I, Avda. Sos Baynat s/n
12071 Castellón (Spain)
Fax: (+34) 964-728-214
E-mail: mcarda@qio.uji.es

[b] Prof. Dr. J. A. Marco
Depart. de Q. Orgánica
Univ. de Valencia, c/D. Moliner, 50
46100 Burjassot, Valencia (Spain)
Fax: (+34) 96-354-4328
E-mail: alberto.marco@uv.es

[c] R. Matesanz, Dr. J. F. Díaz, Dr. I. Barasoain
Centro de Investigaciones Biológicas
Consejo Superior de Investigaciones Científicas
c/Ramiro de Maeztu, 9, 28040 Madrid (Spain)
Fax: (+34) 915-360-432
E-mail: fer@cib.csic.es

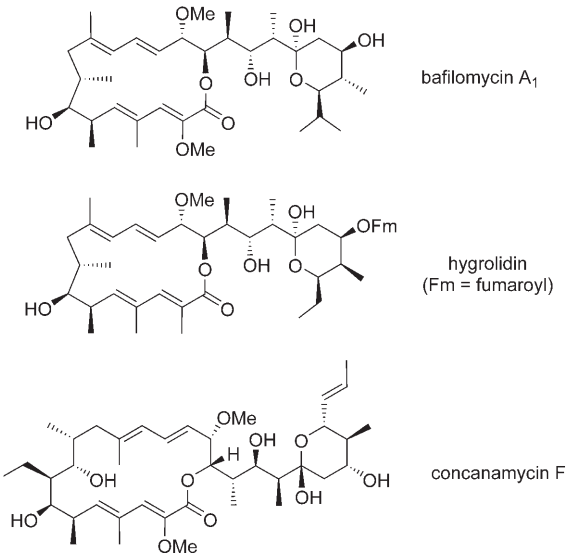

cuolar acidification.[6] More recently, it has been found to be the phytotoxic agent of infections by *Streptomyces* spp. causing potato russet scab.[7] According to the results of chemical degradations and X-ray diffraction analyses of some degradation products, the structure of FD-891 was initially reported in 2002 to be **1**. However, the same group published two years later a correction of its structure, which then turned out to be **2**.[8]

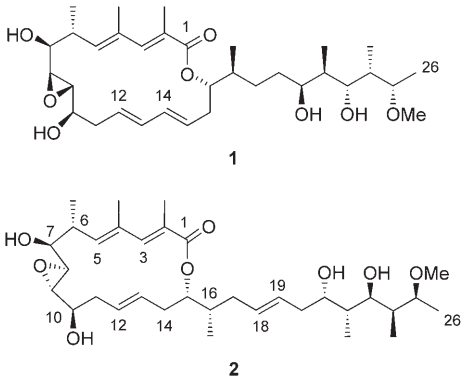

1

2

Results and Discussion

As only structure **1** was known when we started our synthetic work at the end of 2002, we proposed a retrosynthetic disconnection of molecule **1** to fragments **3** (C1–C13, X = Br, I or OSO_2CF_3) and **4** (C14–C26) by means of an esterification and a Heck coupling (Scheme 1). Which one of these two reaction types was to be the final macrocyclisation process would remain an open issue to be decided at a later stage. In any case, both macrolactonisations[9] and intramolecular Heck reactions[10] are amply represented in the literature.

To begin with, we performed a stereoselective synthesis of the whole side chain of molecule **1**. The C14–C26 fragment

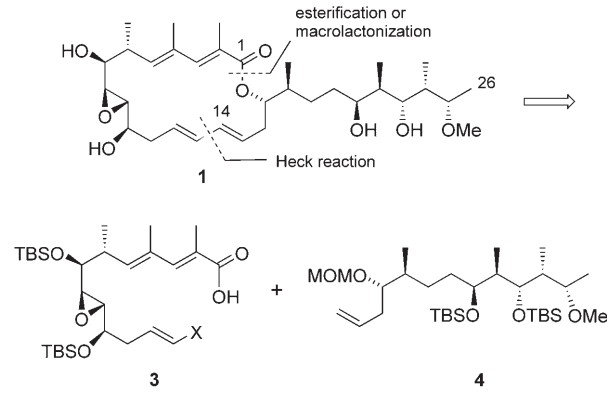

Scheme 1. Retrosynthetic plan for macrolide **1**.

4, which displays seven stereocentres,[11] was retrosynthetically disconnected as depicted in Scheme 2. One key structural transformation in this retrosynthesis (**4**→**5**) is the stereoselective allylation of a chiral α-methyl aldehyde and was planned to be performed in an asymmetric way by using one of Brown's chiral allylboration reagents.[12] The protecting group TPS (*tert*-butyldiphenylsilyl) was selected with the idea of its later selective cleavage in the presence of two TBS (*tert*-butyldimethylsilyl) groups. Two other key retrosynthetic transformations, **6**→**7** and **7**→**8**, are aldol reactions conceived to create the C22–C25 dipropionate segment. In the actual synthesis, both aldol steps were executed with the aid of the chiral oxazolidinones developed by Evans and his group.[13] The ultimate chirality source was the commercially available ester **9**.

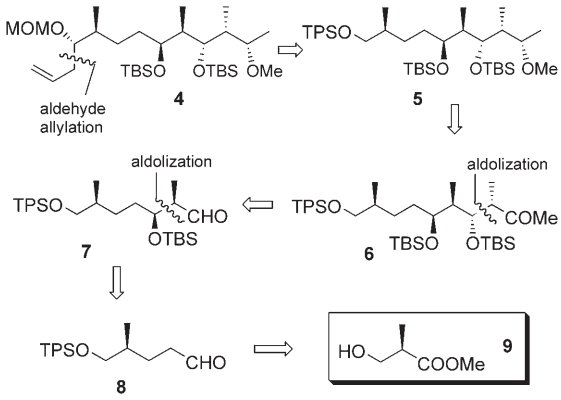

Scheme 2. Retrosynthetic plan for fragment **4**.

Scheme 3 depicts the synthetic sequence which led to **4**. Chiral ester **9** was converted into the known primary alcohol **10** by means of a literature procedure.[14] Swern oxidation of the latter to aldehyde **8** was followed by Evans asymmetric aldolisation by using the *Z* boron enolate of chiral oxazolidinone **21**.[13a] This provided aldol adduct **11** as a single stereoisomer. Conversion of **11** into the Weinreb amide **12**[15] and silylation afforded **13**, which was reduced (DIBAL) to alde-

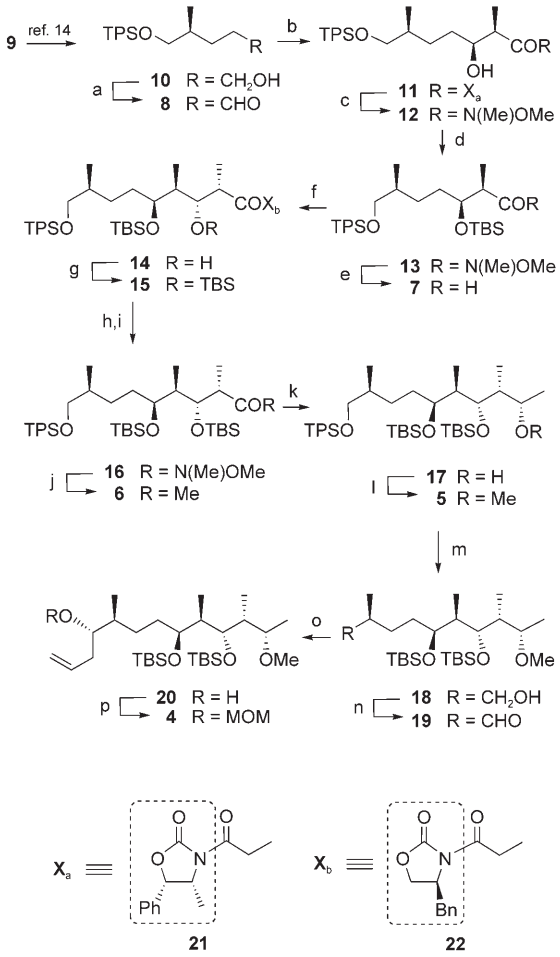

Scheme 3. a) $(COCl)_2$, DMSO, CH_2Cl_2, Et_3N, 1 h, 0 °C; b) **21**, Bu_2BOTf, Et_3N, 0 °C, then **8**, 2.5 h, 0 °C, 89% overall from **10**; c) MeNHOMe·HCl, $AlMe_3$, THF, 3 h, RT, 79%; d) TBSOTf, 2,6-lutidine, CH_2Cl_2, RT, 1 h, 92%; e) DIBAL, THF, −78 °C, 30 min; f) **22**, Bu_2BOTf, Et_3N, 0 °C, then **7**, 3 h, 0 °C, 75% overall from **13**; g) TBSOTf, 2,6-lutidine, CH_2Cl_2, RT, 1 h, 90%; h) 30% H_2O_2, aq LiOH, THF, 0 °C to RT, overnight; i) CDI, MeNHOMe·HCl, CH_2Cl_2, RT, 12 h, 80% overall from **15**; j) MeMgBr, THF, 0 °C, 1 h, 70%; k) Me_2AlCl, Bu_3SnH, CH_2Cl_2, −90 °C, 1 h, 91% (92:8 diastereoisomeric mixture); l) MeOTf, 2,6-di-*tert*-butylpyridine in $CHCl_3$, Δ, 4 h, 84%; m) 10% NaOH, MeOH, Δ, 30 h, 84%; n) $(COCl)_2$, DMSO, CH_2Cl_2, Et_3N, 20 min, 0 °C; o) allylBIpc$_2$ (from (−)-IpcBCl and allylmagnesium bromide), Et_2O, 1 h, −90 °C, 55% overall from **18** as a single stereoisomer; p) MOMCl, iPr_2NEt, CH_2Cl_2, RT, overnight, 79%. DMSO = dimethylsulfoxide, TBS = *tert*-butyldimethylsilyl, TPS = *tert*-butyldiphenylsilyl, DIBAL = diisobutylaluminum hydride, CDI = 1,1′-carbonyl-diimidazole, Tf = trifluoromethanesulfonyl, Ipc = diisopinocampheyl, MOM = methoxymethyl.

hyde **7**. The latter was submitted to a second aldolization with Evans oxazolidinone **22**,[13a] followed by silylation and amidation. This yielded Weinreb amide **16**,[16] which was then converted into methyl ketone **6** by treatment with methylmagnesium bromide. Stereoselective reduction of the carbonyl group of **6** under chelation control[17–20] to alcohol **17** and subsequent *O*-methylation with methyl triflate/2,6-di-*tert*-butylpyridine[21] afforded compound **5**. Selective cleavage of the TPS group in **5** under alkaline conditions[22] provided the primary alcohol **18**, which was oxidized to aldehyde **19**. Asymmetric allylation of the latter[12] afforded secondary alcohol **20** which, through protection of the secondary alcohol group as its MOM derivative,[23] afforded the desired compound **4**.

Just after having published our synthesis of fragment **4**,[11] macrolide FD-891 was reported to have structure **2**, as commented above.[8b] No changes in stereochemistry result from this structural modification, but one olefinic bond has now been moved from inside the ring to the side chain. In view of this, we saw ourselves in the need of carrying out a substantial modification of the initial synthetic plan. Fortunately, most of the ring part of the molecule has remained untouched by the structural amendment and so we have been able to use a part of our previous synthetic concept. For our modified synthesis of FD-891, now having structure **2**, we have chosen the retrosynthetic plan shown in Scheme 4. Ac-

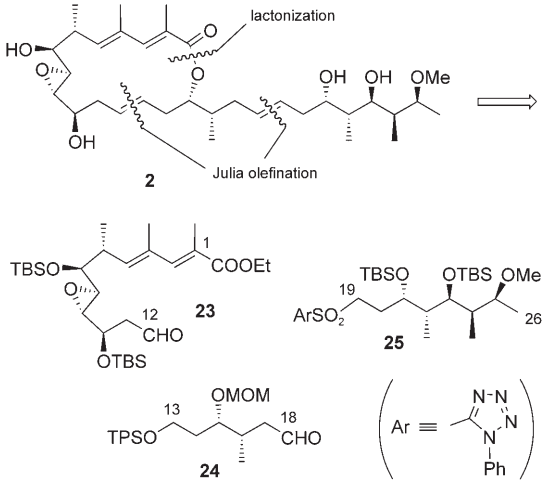

Scheme 4. Retrosynthetic plan for macrolide **2**.

cording to this plan, the molecule of **2** is disconnected to fragments **23** (C1–C12), **24** (C13–C18) and **25** (C19–C26, Ar = 1-phenyl-1*H*-tetrazol-5-yl). The reactions planned to connect these three fragments are a macrolactonisation[9] and two *E*-selective Julia olefinations.[24]

Fragment **23** contains five of the twelve sp^3 stereocentres of the molecule[25] and was retrosynthetically disconnected as shown in Scheme 5. The reactions are basically the same as those we had already ideated for fragment **3** (Scheme 1) of the old structure of FD-891. One key retrotransformation (**26**→**27**) is the stereoselective allylation of an α,β-epoxyaldehyde, while the other (**29**→**30**) is an asymmetric aldol reaction intended to add the Me–C6–C7 propionate segment. The other two propionate segments are added by means of Wittig olefinations (**28**→**29**).

Scheme 6 depicts the synthesis of **23**.[26] The commercially available (*Z*)-2-butene-1,4-diol was first converted into its monoprotected derivative **31**,[27] oxidation of which afforded the (*E*)-2-butenal **30**.[28] The aldol reaction which generates the initial chirality was performed with the aid of Evans

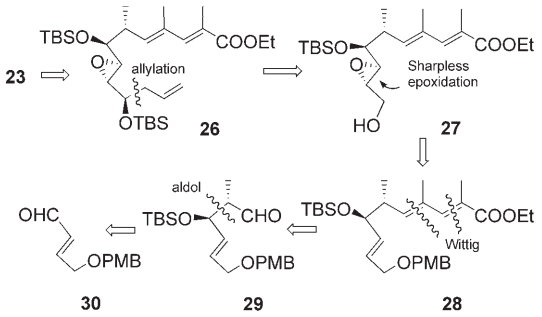

Scheme 5. Retrosynthetic plan for fragment **23**.

chiral oxazolidinone **22** as described in Scheme 3. This yielded aldol **32**, which was converted into Weinreb amide **33** and then silylated to **34**. DIBAL reduction of **34** gave aldehyde **29** which, without chromatographic purification, was taken to the Wittig olefination step to afford the conjugated enoate **35**,[29] subsequently reduced to allylic alcohol **36**. At this stage, we found that the yield of the initial sequence[26] could be markedly improved when the Evans chiral oxazolidinones were replaced by Oppolzer's chiral sultams.[30] Thus, aldehyde **30** was allowed to react with the *Z* boron enolate of chiral sultam **41**. This furnished aldol **37**, which was silylated to **38**. DIBAL reduction of **38** to **29** and subsequent Wittig olefination provided ester **35** with a much better yield than with the previous procedure.[31] Oxidation of **36** to the corresponding aldehyde and Horner–Wadsworth–Emmons olefination yielded the conjugated dienoate **28**. Cleavage of the PMB protecting group with DDQ[32] in wet CH_2Cl_2 to yield **39** was followed by an asymmetric Sharpless epoxidation.[33] The resulting epoxy alcohol **27** was oxidized to the corresponding aldehyde and the latter, in crude form, underwent asymmetric allylation at −110 °C.[12] This procedure provided in 60 % overall yield homoallyl alcohol **40** as a 92:8 mixture of diastereoisomers. Subsequent silylation of the mixture and chromatographic purification gave **26**. Selective oxidative cleavage of the terminal olefinic bond proved problematic due to the presence of the conjugated diene unit. After some experimentation, the problem was solved with the use of Sharpless's reagent AD-mix-β, which permits the dihydroxylation of monosubstituted C=C bonds in the presence of others with a higher substitution degree.[34] This gave a mixture of diastereoisomeric 1,2-diols, which were then oxidatively cleaved with silica-gel-supported $NaIO_4$[35] to yield aldehyde **23**.

Scheme 7 shows the synthesis of fragment **24**.[36] The known aldehyde **42**[37] underwent an asymmetric aldol reaction by using the *Z*-enol borane derived from Oppolzer's chiral propionate equivalent *ent*-**41**.[30] This provided aldol adduct **43** as a single stereoisomer (dr ≥ 98 %, as the minor stereoisomer was not detected by means of high-field $^1H/^{13}C$ NMR spectroscopy). Introduction of the MOM protecting group[23] and functional manipulation gave nitrile **47**, reduction of which afforded aldehyde **24**, which was used directly in crude form in the reaction with **25**.

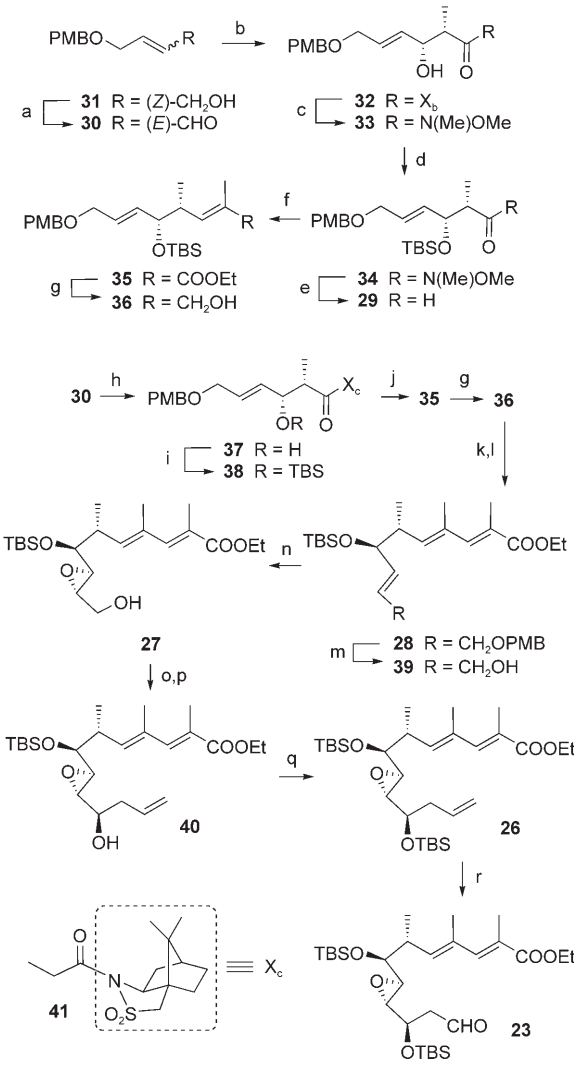

Scheme 6. a) PCC, CH_2Cl_2, RT, 4 d, 52 %. b) **22**, Bu_2BOTf, Et_3N, CH_2Cl_2, −78 °C, 30 min, then **30**, −40 °C, 12 h, 86 %. c) *N*,*O*-dimethylhydroxylamine hydrochloride, Me_3Al, THF, RT, 1 h, then **32**; d) TBSOTf, 2,6-lutidine, CH_2Cl_2, RT, 1 h, 77 % overall yield for the two steps; e) DIBAL, THF, −78 °C, 30 min; f) Ph_3P=C(Me)COOEt, 1,2-dichloroethane, 60 °C, 12 h, 55 % overall yield for the two steps; g) DIBAL, hexane, RT, 1 h, 94 %; h) **41**, Bu_2BOTf, *i*Pr_2NEt, CH_2Cl_2, −5 °C, 30 min, then **30**, −78 °C, 16 h, 95 %; i) TBSOTf, 2,6-lutidine, CH_2Cl_2, RT, 1 h, 88 %; j) DIBAL, CH_2Cl_2, −78 °C, 1 h, then Ph_3P=C(Me)COOEt, 1,2-dichloroethane, 60 °C, 12 h, 88 % overall yield for the two steps; k) MnO_2, CH_2Cl_2, Δ, 2 h; l) $(EtO)_2P(O)CH(Me)COOEt$, *n*BuLi, THF, 0 °C, then addition of the crude aldehyde from step **k**, 16 h, 84 % overall yield for the two steps; m) DDQ, wet CH_2Cl_2, RT, 2 h, 89 %. n) diethyl L-tartrate, Ti(O*i*Pr)$_4$, *t*BuO_2H, powdered 4 Å MS, CH_2Cl_2, −23 °C, 24 h, 90 %; o) Swern oxidation; p) allylBIpc$_2$ (from (+)-Ipc$_2$BCl and allylmagnesium bromide), Et_2O, 1 h, −110 °C, 60 % overall yield for the two steps (dr 92:8); q) TBSOTf, 2,6-lutidine, CH_2Cl_2, RT, 1 h, 95 %; r) 1) AD-mix-β, aq *t*BuOH, RT, 16 h, 81 % based on recovered starting material; 2) $NaIO_4$ on silica gel, CH_2Cl_2, RT, 30 min. PMB = *p*-methoxybenzyl; PCC = pyridinium chlorochromate; DDQ = 2,3-dichloro-5,6-dicyano-1,4-benzoquinone; MS = molecular sieves.

For the synthesis of fragment **25**, depicted in Scheme 8, we made use of much of the chemistry developed for the preparation of fragment **4**[11] of macrolide **1**, the "old" struc-

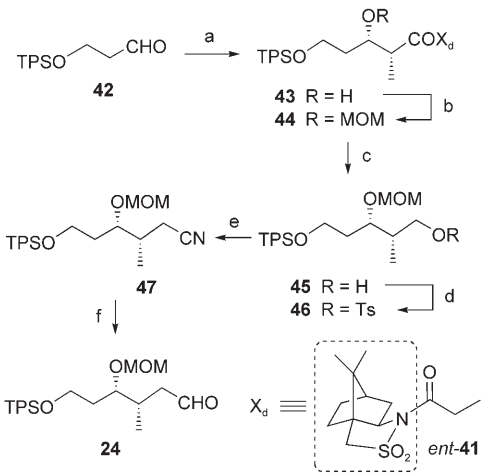

Scheme 7. a) *ent*-**41**, Bu_2BOTf, iPr_2NEt, CH_2Cl_2, −5 °C, 30 min, then **42**, −78 °C, 16 h, 94 %; b) MOMCl, iPr_2NEt, CH_2Cl_2, Δ, 4 h, 91 %; c) $LiAlH_4$, Et_2O, 0 °C, 2 h, 94 %; d) TsCl, Et_3N, CH_2Cl_2, RT, 16 h, 87 %; e) NaCN, DMSO, 80 °C, 2 h, 97 %; f) DIBAL, THF, RT, 3 h. Ts = *p*-toluenesulfonyl.

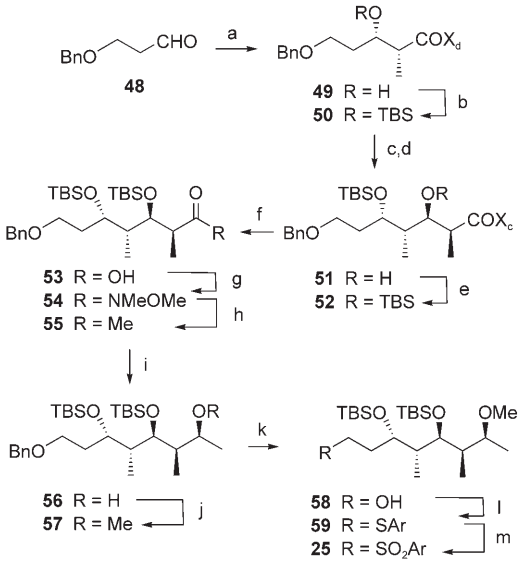

Scheme 8. a) *ent*-**41**, Bu_2BOTf, iPr_2NEt, CH_2Cl_2, −5 °C, 30 min, then **48**, −78 °C, 16 h, 95 %; b) TBSOTf, 2,6-lutidine, CH_2Cl_2, RT, 1 h, 88 %; c) DIBAL, CH_2Cl_2, −78 °C, 1 h; d) **41**, Bu_2BOTf, iPr_2NEt, CH_2Cl_2, −5 °C, 30 min, then aldehyde, −78 °C, 16 h, 80 % overall for the two steps; e) TBSOTf, 2,6-lutidine, CH_2Cl_2, Δ, 1 h; f) aq LiOH, THF, H_2O_2, RT, 1 d; g) MeNHOMe·HCl, CDI, CH_2Cl_2, RT, 16 h, 65 % overall from **51**; h) MeMgBr, THF, 0 °C, 1 h, 78 %; i) Me_2AlCl, Bu_3SnH, CH_2Cl_2, −90 °C, 1 h, 91 % (dr 92:8); j) MeOTf, proton sponge, $CHCl_3$, Δ, 16 h, 85 %; k) H_2, $Pd(OH)_2$, EtOH, RT, 3 h, 98 %; l) 1-phenyl-1*H*-tetrazol-5-thiol, nBu_3P, DIAD, THF, 0 °C, 90 min, 91 %; m) H_2O_2, $Mo_7O_{24}(NH_4)_6$, EtOH, RT, 16 h, 86 %. Bn = benzyl; DIAD = diisopropyl azodicarboxylate; Ar = 1-phenyl-1*H*-tetrazol-5-yl.

ture of FD-891. Thus, the known aldehyde **48**[38] was subjected to an asymmetric aldol reaction with Oppolzer's chiral reagent *ent*-**41**[30,31] to yield aldol **49** as a single stereoisomer. Hydroxyl silylation to **50** followed by reductive cleavage of the chiral auxiliary gave an intermediate aldehyde which was submitted to an asymmetric aldol reaction with **41**.[30] This yielded a single crystalline aldol **51**,[39] which was converted into the silyl derivative **52**. The latter was transformed into methyl ketone **55** by the intermediate acid **53** and the Weinreb[15] amide **54**.[40] Reduction of **55** under chelation control[17] to **56** and *O*-methylation by using methyl triflate and proton sponge[41] stereoselectively afforded **57**. Hydrogenolytic *O*-debenzylation to **58**, introduction of the tetrazolylthio[42] moiety via Mitsunobu reaction by using nBu_3P[43] and Mo(VI)-catalysed sulfide–sulfone oxidation[44] gave rise to the desired aryl sulphone **25**.

With all key fragments in hand, the synthesis proceeded as shown in Scheme 9. Connection between **24** and **25** was performed by using the Julia–Kocienski[24] olefination protocol, which yielded olefin **60** in good yield (75 %, based on recovered **25**) as a single *E* stereoisomer. Selective cleavage of the TPS group[22] gave alcohol **61**, which was converted into aryl sulphone **62** by means of a Mitsunobu reaction (Ph_3P performed better here than nBu_3P) and Mo(VI)-catalyzed oxidation.

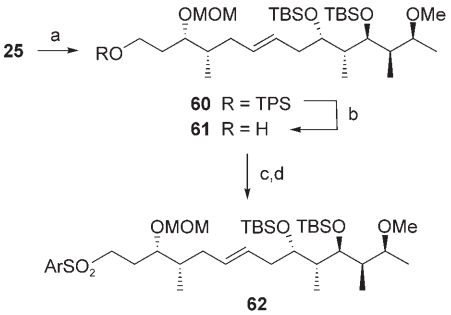

Scheme 9. a) NaHMDS, −78 °C, DME-HMPA 9:1, then addition of freshly prepared **24** (1.5 equiv), 2 h, 75 % (>95 % *E*); b) NaOH, MeOH, Δ, 4 h, 89 %; c) 1-phenyl-1*H*-tetrazol-5-thiol, Ph_3P, DIAD, THF, RT, 1 h, 93 %; d) H_2O_2, $Mo_7O_{24}(NH_4)_6$, EtOH, RT, 16 h, 95 %. NaHMDS = sodium hexamethyldisilazide; DME = 1,2-dimethoxyethane; HMPA, hexamethylphosphoramide.

The final attack towards macrolide **2** was carried out as depicted in Scheme 10. Connection of fragments **23** and **62** was performed as above with the aid of the Julia–Kocienski olefination protocol and gave **63**. The yield was, however, not as high as in Scheme 9 and the reaction was not stereoselective. Changes in various reaction conditions did not lead to improvements.[45] Separation of the *E* and *Z* stereoisomers of **63** was not feasible, but could be done after selective cleavage of the MOM group,[46] which yielded (*E*)-**64** and (*Z*)-**64**.[47] Hydrolysis of the ethyl ester group of (*E*)-**64** was achieved under mild, anhydrous conditions by using TMSOK.[48] The macrolactonisation of the resulting hydroxy acid was performed at high dilution (0.006 M) by using the Yamaguchi procedure[49] and yielded lactone (*E*)-**65**. Cleavage of all silyl groups with TASF[50] finally gave macrolide (*E*)-**2** (FD-891).[51,52] Following the same series of reactions, lactone (*Z*)-**64** was transformed into (*Z*)-**2**, a stereoisomer of the natural macrolide at the C12–C13 double bond.

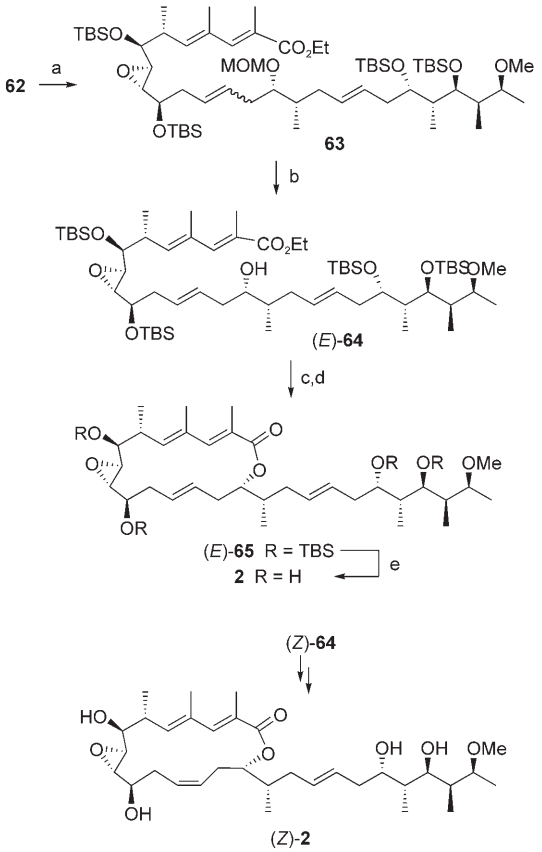

Scheme 10. a) NaHMDS, −78 °C, DME-HMPA 9:1, then addition of freshly prepared **23** (1.5 equiv), 3 h, 60 % (1:1 *E*/*Z* mixture); b) Me_2BBr, CH_2Cl_2, −78 °C, 1 h, 96 %, then isomer separation; c) Me_3SiOK, THF, RT, 10 h; d) 2,4,6-$Cl_3C_6H_2COCl$, *i*Pr_2NEt, CH_2Cl_2, RT, 1 h, 50 % overall for the two steps; e) TASF, DMF, RT, 4 d, 32 %. TASF = tris(dimethylamino) sulfonium difluorotrimethylsilicate.

Biological and biochemical assays: After finishing the total synthesis of the natural macrolide FD-891 ((*E*)-**2**) and its (*Z*)-isomer ((*Z*)-**2**), we investigated some of its biological properties. We first checked the cytotoxicity of compounds (*E*)-**2** and (*Z*)-**2** against two tumoral cell lines. Thus, the IC_{50} values in the case of the ovarian carcinoma A2780 and A2780-AD-MDR (multidrug resistant) cell lines were determined and compared with those of a classical clinical drug, paclitaxel (Table 1).

Table 1. Effect of macrolides (*E*)-**2** and (*Z*)-**2** as compared with paclitaxel on the growth of two human carcinoma cell lines.[a]

Cell line	Paclitaxel[b]	(*E*)-**2**[b]	(*Z*)-**2**[b]
A2780	2.1 ± 0.28	590 ± 174	1916 ± 500
A2780-AD-MDR	660 ± 28 (314)[c]	500 ± 140 (0.85)[c]	2600 ± 450 (1.4)[c]

[a] IC_{50} (50 % inhibition of cell proliferation) of the ligands determined in the parental ovarian carcinoma A2780 cell line and the MDR P-glycoprotein overexpressing ovarian carcinoma A2780 AD. [b] IC_{50} values (nM) are the mean ± standard error of four independent experiments. [c] The numbers in parentheses are the relative resistance of the A2780 AD cell line obtained dividing the IC_{50} of the resistant cell line by the IC_{50} of the parental A2780 cell line.

The results show that the two macrolides were cytotoxic towards both the resistant and the non-resistant cells, even though at a concentration higher than paclitaxel. In addition, (*E*)-**2** appears to be 3–5 times more cytotoxic than (*Z*)-**2**, a fact which suggests that the geometry of the C12−C13 bond plays a relevant role in determining the cytotoxicity. In all likelihood, this is related to the appreciable modification in molecular shape associated to such a stereochemical change. Interestingly, the multidrug-resistant cells showed no resistance to both compounds, indicating that the latter are not substrates for the P-glycoprotein (P-gp) which these cells overexpress in order to pump out the cytotoxic compounds.[53]

In order to study the possible cellular mechanisms that impart cytotoxicity to (*E*)-**2** and (*Z*)-**2**, lung carcinoma A549 cells were treated with either compound at concentrations of 10.0 to 0.2 μM for twenty four hours. Subsequently, their microtubule cytoskeleton and DNA were immunostained. Two hours after addition of the drug, the cells became rounded at the concentrations at which we see the effect. Untreated cells (Figure 1A and D) and cells treated with 0.2 μM of (*Z*)-**2** (G and F) had a typical microtubule cytoskeleton and nucleus. In cells treated with 0.2 μM of (*E*)-**2** (B and E) and 2.5 μM of (*Z*)-**2** (H and K), the microtubule cytoskeleton seems sparser and the nucleus lobulated and in a few cells multinucleated. In cells treated with 1–10 μM of (*E*)-**2** (C and F) and in those treated with 5–10 μM of (*Z*)-**2** (I and L), the cytoplasmic microtubule cytoskeleton is disorganized with fewer and shorter microtubules as compared to PBS-EDTA-treated detached control cells. In some treated cells, the microtubule cytoskeleton is not clearly seen and only a green fluorescence under the cytoplasmic membrane is observed. There is no increase in the number of mitotic cells; most cells have a small nucleus with chromatin that is less dense than that of controls and a few apoptotic cells are observed.

In cell cycle experiments, non-small cell lung carcinoma A549 cells were incubated as before with serial dilutions of the compounds (0.2–10 μM). There is an accumulation in the G2/M phase at 0.2 μM of (*E*)-**2** or at 0.5 μM of (*Z*)-**2** (50 and 55 %, respectively), as compared to 20 % of the control cells. This is accompanied by a reduction of the G0/G1 cells from 64 % in the control cells to 21 and 20 % in the cells treated with (*E*)-**2** and (*Z*)-**2**, respectively. A sub G1 population of 9 and 8 %, respectively, appeared in the treated cells.

In view of the fact that both macrolides showed a visible effect on the cytoplasmic microtubules, we investigated their effect on the in vitro tubulin assembly, as well as the possible binding to microtubules and tubulin. When we checked the influence of the compounds on the in vitro assembly of purified tubulin, however, only negative results were observed, with neither (*E*)-**2** nor (*Z*)-**2** being able to modify the amount of assembled tubulin. To check whether the in vivo effect may be caused through microtubule-associated proteins, we performed similar experiments with microtubular protein, that is, in the presence of microtubule-associated proteins (MAPs). No effect on the amount of polymer pel-

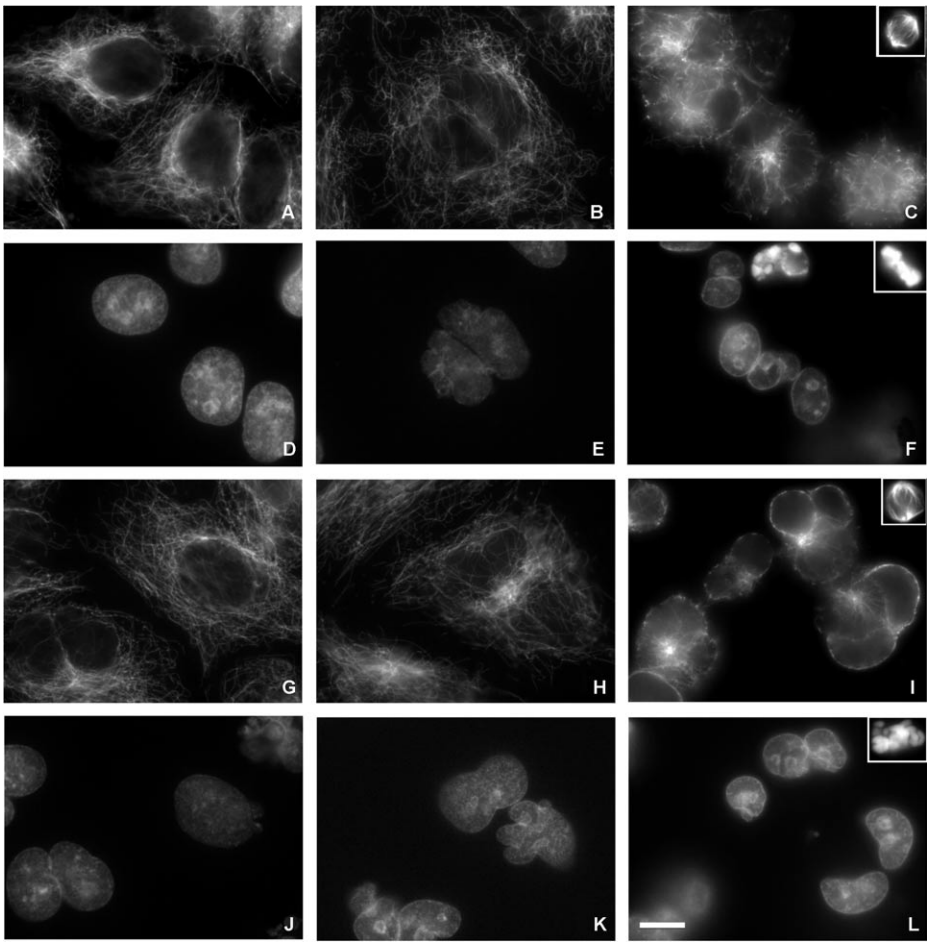

Figure 1. Effect of (*E*)-**2** and (*Z*)-**2** on microtubule network (A–C, G–I) and nucleus morphology (D–F, J–L). A549 cells were incubated for 24 h with DMSO (A,D), (*E*)-**2** 0.2 μM (B,E) or 1 μM (C,F), *Z*-2 0.2 μM (G,J), 2,5 μM (H,K) or 5 μM (I,L). Microtubules were immunostained with α-tubulin monoclonal antibodies and DNA was stained with Hoechst 33342. Insets are mitotic spindles from the same preparation. The scale bar represents 10 μm. All panels and insets have the same magnification.

leted was observed. Electron microscopy was performed on all the polymers and these were normal microtubules.

In order to discard any other possible tubulin-mediated effects, binding of the compounds to polymeric and non-polymeric tubulin was investigated by centrifugation techniques. Native and glutaraldehyde-stabilized microtubules incubated in the presence of the ligand ((*E*)-**2** or (*Z*)-**2**) were pelleted and analysed by means of HPLC. No bound ligand was found in the microtubule pellets, indicating that none of the compounds bind to microtubules with significant affinity.

In order to discard any other site in tubulin that may be occluded by microtubule assembly, non-assembled tubulin was incubated with the ligands and the solution was then centrifuged. All the tubulin was found in the lower part of the tube with none being present in the upper part. HPLC analyses showed no significant differences in compound concentrations between the upper and lower part of the tube indicating that the compounds do not bind with high affinity to tubulin.

From the aforementioned results we can conclude that, at the concentrations at which the drugs produce the effect in cells, they do not significantly bind to tubulin nor do they induce a significant effect in microtubule polymerisation. This indicates that the effects observed in the cellular cytoskeleton take place through other microtubule stabilization/destabilization mechanisms such as, for example, microtubule acetylation/deacetylation,[54] or else through other proteins of the eukaryotic cytoskeleton. This conclusion is further supported by the fact that these drugs do not act in cells as other inhibitors of tubulin polymerisation, such as vinblastin. Thus, while vinblastin does not rapidly affect cell morphology and vinblastin-treated preparations present many mitotic cells, (*E*)-**2** and (*Z*)-**2** exert a rapid effect on cell morphology detaching cells from the plates and show an effect on cytoplasmic microtubules. In contrast, they show no effect on mitotic spindle microtubules at high drug concentrations, as typical with microtubule depolymerisers, and do not give rise to an increase in the number of mitotic cells, even though there is an accumulation on the G2/M phase of the cell cycle.

Experimental Section

General methods: NMR spectra were recorded at 500 (^{1}H NMR spectroscopy) and 125 MHz (^{13}C NMR spectroscopy) in $CDCl_3$ solution at 25 °C. The residual solvent signals were taken as the reference (7.25 ppm for ^{1}H NMR spectroscopy and 77 ppm for ^{13}C NMR spectroscopy). ^{13}C NMR signal multiplicities were determined with the DEPT pulse sequence. Mass spectra were run in the EI (70 eV) or the FAB (*m*-nitrobenzyl alcohol matrix) mode. IR data, which were measured as films on NaCl plates (oils) or as KBr pellets (solids), are given only when relevant functions (C=O, OH, etc.) are present. Optical rotations were measured at 25 °C. Reactions requiring an inert atmosphere (all except those involving water or hydroxylic solvents in the reaction medium) were carried out under dry N_2 with flame-dried glassware. Commercial reagents were used as received. THF and Et_2O were freshly distilled from sodium-benzophenone ketyl. Dichloromethane was freshly distilled from CaH_2. Tertiary amines were freshly distilled from KOH. Unless detailed otherwise, "work-up" means pouring the reaction mixture into brine, followed by extraction with the solvent indicated in parenthesis. If the reaction

medium was acidic (basic), an additional washing with 5% aq $NaHCO_3$ (aq NH_4Cl) was performed, followed by washing with brine, drying over anhydrous $MgSO_4$ and elimination of the solvent under reduced pressure. This was followed by chromatography of the residue on a silica-gel column (60–200 μm) with the indicated solvent. Where solutions were filtered through a Celite pad, the pad was additionally rinsed with the same solvent used and the washing liquids incorporated to the main organic layer.

(4*R*,5*S*)-4-Methyl-5-phenyl-3-[(2*R*,3*S*,6*S*)-7-(*tert*-butyldiphenylsilyloxy)-3-hydroxy-2,6-dimethylheptanoyl]-1,3-oxazolidin-2-one (11): Oxalyl chloride (1.3 mL, 15 mmol) was added dropwise at −78 °C to a solution of DMSO (2.1 mL, 30 mmol) in dry CH_2Cl_2 (30 mL). The mixture was stirred for 5 min at this temperature. A solution of alcohol **10**[14] (4.28 g, 12 mmol) in dry CH_2Cl_2 (10 mL) was then added via syringe. The reaction mixture was stirred for 15 min at −78 °C. After addition of Et_3N (8.4 mL, 60 mmol), the mixture was stirred for 15 min. at −78 °C and then for 1 h at 0 °C. Workup (extraction with CH_2Cl_2) gave crude aldehyde **8** which was used as such in the next reaction.

A solution of oxazolidinone **21** (3.5 g, 15 mmol) in dry CH_2Cl_2 (60 mL) was cooled to −78 °C and treated with nBu$_2$BOTf (1 M solution in CH_2Cl_2, 27 mL, 27 mmol) and Et_3N (4.2 mL, 30 mmol). After stirring for 30 min at −78 °C and then for 1 h at 0 °C, the mixture was treated dropwise with a solution of crude **8** from above in dry CH_2Cl_2 (30 mL). The reaction mixture was stirred at 0 °C for 2.5 h, quenched by addition of a pH 7 buffer solution (60 mL), MeOH (60 mL) and 30% H_2O_2 (30 mL). The resulting mixture was then stirred at room temperature for 30 min. Workup (extraction with CH_2Cl_2) and column chromatography on silica gel (hexane/EtOAc 90:10) afforded aldol **11** as a single diastereoisomer (5.23 g, 89% overall, based on **10**). Colourless oil; $[\alpha]_D = +7.8$ ($c = 1$ in $CHCl_3$); ^{1}H NMR: $\delta = 7.75$–7.70 (m, 4H), 7.45–7.30 (br m, 11H), 5.65 (d, $J = 7.3$ Hz, 1H), 4.80 (quint, $J = 6.8$ Hz, 1H), 3.96 (m, 1H), 3.82 (qd, $J = 7.0$, 2.5 Hz, 1H), 3.58 (dd, $J = 9.8$, 5.8 Hz, 1H), 3.52 (dd, $J = 9.8$, 6.5 Hz, 1H), 3.00 (br s, 1H; OH), 1.73 (m, 1H), 1.65–1.50 (br m, 2H), 1.50–1.35 (br m, 2H), 1.26 (d, $J = 7.0$ Hz, 3H), 1.11 (s, 9H), 0.98 (d, $J = 6.5$ Hz, 3H), 0.90 ppm (d, $J = 7$ Hz, 3H); ^{13}C NMR: $\delta = 177.1$, 152.5, 133.9, 133.8, 133.1, 19.2 (C), 135.5 (×4), 129.4 (×2), 128.7, 128.6 (×2), 127.5 (×4), 125.5 (×2), 78.7, 71.7, 54.6, 42.3, 35.6 (CH), 68.7, 31.4, 29.4 (CH_2), 26.9 (×3), 16.8, 14.2, 10.3 ppm (CH_3); IR: $\tilde{\nu} = 3530$ (br; OH), 1783, 1699 cm^{-1} (C=O); HR-EIMS m/z (%): calcd for $C_{35}H_{45}NO_5Si$–tBu: 530.2362; found: 530.2334 (5) $[M-t\text{Bu}]^+$, 468 (8), 408 (4), 297 (44), 199 (100); elemental analysis: calcd (%) for $C_{35}H_{45}NO_5Si$: C 71.51, H 7.72; found: C 71.39, H 7.60.

(2*R*,3*S*,6*S*)-7-(*tert*-Butyldiphenylsilyloxy)-3-hydroxy-*N*-methoxy-2,6-*N*-trimethylheptanamide (12): A solution of *N*,*O*-dimethylhydroxylamine hydrochloride (2.54 g, 26 mmol) in dry THF (50 mL) was treated dropwise at 0 °C with Me_3Al (2.0 M solution in toluene, 13 mL, 26 mmol). The mixture was stirred for 1 h at room temperature. A solution of aldol **11** from above (5.11 g, 8.7 mmol) in dry THF (15 mL) was then added dropwise by syringe. The reaction mixture was stirred for 3 h at room temperature and then quenched through addition of a saturated aq solution of potassium sodium tartrate (60 mL). Stirring at room temperature for 30 min and workup (extraction with CH_2Cl_2) was followed by column chromatography of the residue on silica gel (hexane/EtOAc 70:30) to yield the Weinreb amide **12** (3.24 g, 79%). Colourless oil; $[\alpha]_D = -12.6$ ($c = 1.2$ in $CHCl_3$); ^{1}H NMR: $\delta = 7.70$–7.65 (m, 4H), 7.45–7.30 (br m, 6H), 3.84 (m, 1H), 3.80 (br s, 1H; OH), 3.68 (s, 3H), 3.54 (dd, $J = 9.8$, 5.8 Hz, 1H), 3.52 (dd, $J = 9.8$, 6.2 Hz, 1H), 3.20 (s, 3H), 2.90 (m, 1H), 1.70 (m, 1H), 1.60 (m, 1H), 1.50 (m, 1H), 1.40–1.25 (br m, 2H), 1.18 (d, $J = 7.0$ Hz, 3H), 1.08 (s, 9H), 0.96 ppm (d, $J = 6.8$ Hz, 3H); ^{13}C NMR: $\delta = 178.3$*, 134.0 (×2), 19.3 (C), 135.5 (×4), 129.4 (×2), 127.5 (×4), 71.7, 38.5, 35.8 (CH), 68.8, 31.4, 29.4 (CH_2), 61.4, 31.8*, 26.9 (×3), 16.8, 10.0 ppm (CH_3) (starred peaks are very low and broad); IR: $\tilde{\nu} = 3460$ (br, OH), 1640 cm^{-1} (C=O); HR-EIMS m/z (%): calcd for $C_{27}H_{41}NO_4Si$–tBu: 414.2100; found: 414.2097 (2) $[M-t\text{Bu}]^+$, 336 (9), 297 (14), 199 (100); elemental analysis: calcd (%) for $C_{27}H_{41}NO_4Si$: C 68.75, H 8.76; found: C 68.68, H 8.61.

(2*R*,3*S*,6*S*)-3-(*tert*-Butyldimethylsilyloxy)-7-(*tert*-butyldiphenylsilyloxy)-*N*-methoxy-2,6-*N*-trimethylheptanamide (13): A solution of alcohol **12** (3.21 g, 6.8 mmol) in dry CH_2Cl_2 (40 mL) was treated dropwise at RT with 2,6-lutidine (1.2 mL, approximately 10.2 mmol) and TBSOTf (2 mL, approximately 8.5 mmol). The mixture was stirred for 1 h at room temperature. Workup (extraction with CH_2Cl_2) was followed by column chromatography of the residue on silica gel (hexane/EtOAc 90:10) to yield **13** (3.66 g, 92%). Colourless oil; $[\alpha]_D = +4.3$ ($c = 0.9$ in $CHCl_3$); ^{1}H NMR: $\delta = 7.70$–7.65 (m, 4H), 7.45–7.35 (br m, 6H), 3.98 (m, 1H), 3.65 (s, 3H), 3.54 (dd, $J = 9.8$, 5.5 Hz, 1H), 3.49 (dd, $J = 9.8$, 6.0 Hz, 1H), 3.17 (s, 3H), 3.00 (m, 1H), 1.70–1.45 (br m, 5H), 1.19 (d, $J = 7.0$ Hz, 3H), 1.09 (s, 9H), 0.95 (d, 3H, overlapped), 0.94 (s, 9H), 0.09 (s, 3H), 0.08 ppm (s, 3H); ^{13}C NMR: $\delta = 176.5$*, 134.0 (×2), 19.3, 18.1 (C), 135.5 (×4), 129.4 (×2), 127.5 (×4), 73.7, 40.4, 36.2 (CH), 69.2, 33.2, 27.7 (CH_2), 61.2, 32.1*, 26.9 (×3), 26.0 (×3), 16.7, 14.4, −4.2, −4.6 ppm (CH_3) (starred peaks are very low and broad); IR: $\tilde{\nu} = 1666$ cm^{-1} (C=O); HR-EIMS m/z (%): calcd for $C_{33}H_{55}NO_4Si_2$–Me: 570.3435; found: 570.3403 (3) $[M-\text{Me}]^+$, 528 (100) $[M-t\text{Bu}]^+$; elemental analysis: calcd (%) for $C_{33}H_{55}NO_4Si_2$: C 67.64, H 9.46; found: C 67.68, H 9.59.

(4*S*)-4-Benzyl-3-[(2*S*,3*R*,4*S*,5*S*,8*S*)-5-(*tert*-butyldimethylsilyloxy)-9-(*tert*-butyldiphenylsilyloxy)-3-hydroxy-2,4,8-trimethylnonanoyl]-1,3-oxazolidin-2-one (14): A solution of **13** (3.63 g, 6.2 mmol) in dry THF (60 mL) was treated dropwise at −78 °C with DIBAL (1 M solution in hexane, 31 mL, 31 mmol). The mixture was stirred for 30 min at the same temperature and quenched through addition of saturated aqueous NH_4Cl (2 mL). The mixture was then stirred at room temperature until formation of a persistent gel. Filtration through Celite (washing with EtOAc) and solvent removal under reduced pressure gave crude aldehyde **7** which was used as such in the next reaction.

A solution of oxazolidinone **22** (1.75 g, 7.5 mmol) in dry CH_2Cl_2 (40 mL) was cooled to −78 °C and treated with nBu$_2$BOTf (1 M solution in CH_2Cl_2, 13.5 mL, 13.5 mmol) and Et_3N (2.1 mL, 15 mmol). After stirring for 30 min at −78 °C and then for 1 h at 0 °C, the mixture was treated dropwise with a solution of crude **7** from above in dry CH_2Cl_2 (15 mL). The reaction mixture was stirred at 0 °C for 3 h, quenched by addition of a pH 7 buffer solution (40 mL), MeOH (40 mL) and 30% H_2O_2 (20 mL) and stirred at room temperature for 30 min Workup (extraction with CH_2Cl_2) and column chromatography on silica gel (hexane/EtOAc 90:10) afforded aldol **14** as a single diastereoisomer (3.53 g, 75% overall from **13**). Colourless oil; $[\alpha]_D = +8.6$ ($c = 1$ in $CHCl_3$); ^{1}H NMR: $\delta = 7.75$–7.70 (m, 4H), 7.45–7.25 (br m, 11H), 4.70 (m, 1H), 4.20–4.15 (m, 2H), 4.00 (br d, $J = 9.7$ Hz, 1H), 3.90–3.85 (m, 2H), 3.50 (2H; AB system), 3.33 (dd, $J = 13.4$, 3.0 Hz, 1H), 2.78 (dd, $J = 13.4$, 9.7 Hz, 1H), 1.80 (m, 1H), 1.70 (br s, 1H; OH), 1.65–1.55 (br m, 2H), 1.50–1.35 (br m, 3H), 1.24 (d, $J = 6.8$ Hz, 3H), 1.07 (s, 9H), 0.92 (d, $J = 6.8$ Hz, 3H), 0.90 (s, 9H), 0.85 (d, $J = 7.0$ Hz, 3H), 0.11 (s, 3H), 0.08 ppm (s, 3H); ^{13}C NMR: $\delta = 176.3$, 153.2, 135.4, 134.0, 133.9, 19.3, 18.0 (C), 135.5 (×4), 129.5 (×2), 129.4, (×2), 128.9 (×2), 127.5 (×4), 127.3, 76.4, 73.0, 55.7, 40.5, 39.6, 35.9 (CH), 68.9, 66.1, 37.8, 30.3, 30.0 (CH_2), 26.9 (×3), 25.9 (×3), 16.8, 11.8, 8.8, −4.4, −4.5 ppm (CH_3); IR: $\tilde{\nu} = 3530$ (br, OH), 1783, 1690, 1680 cm^{-1} (C=O); HR-EIMS m/z (%): calcd. for $C_{44}H_{65}NO_6Si_2$: 759.4350; found: 759.4367 (1) $[M]^+$, 702 (2), 199 (100); elemental analysis: calcd (%) for $C_{44}H_{65}NO_6Si_2$: C 69.52, H 8.62; found: C 69.67, H 8.60.

(4*S*)-4-Benzyl-3-[(2*S*,3*R*,4*R*,5*S*,8*S*)-3,5-bis(*tert*-butyldimethylsilyloxy)-9-(*tert*-butyldiphenylsilyloxy)-2,4,8-trimethylnonanoyl]-1,3-oxazolidin-2-one (15): Alcohol **14** (3.50 g, 4.6 mmol) was dissolved in dry CH_2Cl_2 (30 mL) and treated dropwise at room temperature with 2,6-lutidine (4.8 mL, 41 mmol) and TBSOTf (6.3 mL, approximately 27.6 mmol). The mixture was stirred for 1 h at room temperature. Workup (extraction with CH_2Cl_2) was followed by *careful* column chromatography of the residue on silica gel (hexane/EtOAc 90:10) to yield **15** (3.62 g, 90%). Colourless oil; $[\alpha]_D = +35.4$ ($c = 1.2$ in $CHCl_3$); ^{1}H NMR: $\delta = 7.70$–7.65 (m, 4H), 7.45–7.25 (br m, 11H), 4.60 (m, 1H), 4.20–4.10 (br m, 3H), 4.00 (m, 1H), 3.75 (m, 1H), 3.54 (dd, $J = 9.8$, 5.7 Hz, 1H), 3.50 (dd, $J = 9.8$, 6.3 Hz, 1H), 3.30 (dd, $J = 13.4$, 3.0 Hz, 1H), 2.80 (dd, $J = 13.4$, 9.6 Hz, 1H), 1.75 (m, 1H), 1.65 (m, 1H), 1.60–1.45 (br m, 4H), 1.24 (d, $J = 6.8$ Hz, 3H), 1.09 (s, 9H), 0.95 (br s, 9H, overlapping two methyl doublets), 0.90 (s, 9H), 0.12 (s, 3H), 0.07 (s, 3H), 0.06 (s, 3H), 0.05 ppm (s, 3H); ^{13}C NMR: $\delta = 175.8$, 152.7, 135.4, 134.0, 133.9, 19.3, 18.4, 18.3 (C), 135.6 (×4), 129.5 (×4), 128.9 (×2), 127.6 (×4), 127.3, 73.3, 72.7, 55.7, 43.3, 41.1, 33.2 (CH), 68.9, 65.8, 37.6, 36.3, 28.4 (CH_2), 26.9 (×3), 26.0 (×3), 25.9 (×3), 16.9, 11.7,

10.2, −3.0, −3.4, −3.5, −3.9 ppm (CH_3); IR: $\tilde{\nu}$ = 1786, 1704 cm^{-1} (C=O); HR-EIMS *m/z* (%): calcd for $C_{50}H_{79}NO_6Si_3$–*t*Bu: 816.4611; found: 816.4601 (100) $[M-t\mathrm{Bu}]^+$, 684 (12), 639 (15), 290 (42); elemental analysis: calcd (%) for $C_{50}H_{79}NO_6Si_3$: C 68.68, H 9.11; found: C 68.60, H 9.01.

(2*S*,3*R*,4*R*,5*S*,8*S*)-3,5-bis(*tert*-Butyldimethylsilyloxy)-9-(*tert*-butyldiphenylsilyloxy)-*N*-methoxy-2,4,8-*N*-tetramethylnonanamide (16): A solution of compound **15** (3.59 g, 4.1 mmol) in THF/H_2O 3:1 (20 mL) was cooled to 0 °C and treated with 30% H_2O_2 (2.5 mL, approximately 22 mmol) and LiOH monohydrate (345 mg, 8.2 mmol). The mixture was stirred for 2 h at 0 °C and then overnight at room temperature. After addition of Na_2SO_3 (2.8 g dissolved in 20 mL of water), most of the THF was removed under reduced pressure and the residue was extracted with CH_2Cl_2. This gave a crude acid which was used as such in the next reaction.

A solution of the crude acid from above in dry CH_2Cl_2 (40 mL) was cooled to 0 °C and treated with CDI (650 mg, 4 mmol). After stirring for 30 min at 0 °C, *N*,*O*-dimethylhydroxylamine hydrochloride (780 mg, 8 mmol) was added. The reaction mixture was then stirred overnight at room temperature. Workup (extraction with CH_2Cl_2) and column chromatography on silica gel (hexane/EtOAc 80:20) furnished Weinreb amide **16** (2.49 g, 80% overall from **15**). Colourless oil; $[\alpha]_D = -0.7$ (c = 1.8 in $CHCl_3$); ^{1}H NMR: δ = 7.70–7.65 (m, 4H), 7.45–7.35 (br m, 6H), 4.10 (t, J = 5.3 Hz, 1H), 3.69 (s, 3H), 3.63 (m, 1H), 3.55 (dd, J = 9.8, 5.7 Hz, 1H), 3.48 (dd, J = 9.8, 6.4 Hz, 1H), 3.19 (s, 3H), 3.05 (m, 1H), 1.77 (m, 1H), 1.70–1.55 (br m, 4H), 1.45 (m, 1H), 1.16 (d, J = 7 Hz, 3H), 1.09 (s, 9H), 0.97 (d, J = 6.6 Hz, 3H), 0.94 ppm (br s, 9H, overlapping one methyl doublet), 0.91 (s, 9H), 0.11 (s, 3H), 0.09 (s, 3H), 0.07 (s, 3H), 0.05 ppm (s, 3H); ^{13}C NMR: δ = 176.6*, 134.1, 134.0, 19.3, 18.3, 18.2 (C), 135.6 (×4), 129.5 (×2), 127.6 (×4), 73.2, 72.7, 43.7, 37.8, 36.4 (CH), 69.3, 32.8, 27.7 (CH_2), 61.0, 32.4*, 26.9 (×3), 26.1 (×3), 26.0 (×3), 16.9, 13.4, 11.1, −3.5, −3.8, −4.0, −4.4 ppm (CH_3) (starred peaks are very low and broad); IR: $\tilde{\nu}$ = 1670 cm^{-1} (C=O); HR-EIMS *m/z* (%): calcd for $C_{42}H_{75}NO_5Si_3$–*t*Bu, 700.4248; found: 700.4213 (4) $[M-t\mathrm{Bu}]^+$, 670 (100), 199 (58); elemental analysis: calcd (%) for $C_{42}H_{75}NO_5Si_3$: C 66.52, H 9.97; found: C 66.39, H 9.82.

(3*S*,4*R*,5*R*,6*S*,9*S*)-4,6-Bis(*tert*-butyldimethylsilyloxy)-10-(*tert*-butyldiphenylsilyloxy)-3,5,9-trimethyldecan-2-one (6): A solution of Weinreb amide **16** (2.43 g, 3.2 mmol) in dry THF (30 mL) was cooled under N_2 at −20 °C and treated dropwise with MeMgBr (3 M solution in Et_2O, 3.7 mL, 11.2 mmol). The reaction mixture was then stirred at 0 °C for 1 h and worked up (extraction with CH_2Cl_2). Column chromatography on silica gel (hexane/EtOAc 95:5) afforded ketone **6** (1.6 g, 70%). Colourless oil; $[\alpha]_D = +14.6$ (c = 1.2 in $CHCl_3$); ^{1}H NMR: δ = 7.70–7.65 (m, 4H), 7.45–7.35 (br m, 6H), 4.27 (dd, J = 6.7, 2.3 Hz, 1H), 3.80 (dt, J = 7.2, 4.0 Hz, 1H), 3.52 (dd, J = 9.8, 5.8 Hz, 1H), 3.49 (dd, J = 9.8, 6.0 Hz, 1H), 2.60 (qd, J = 7.0, 2.3 Hz, 1H), 2.17 (s, 3H), 1.70 (m, 1H), 1.65–1.40 (br m, 5H), 1.13 (d, J = 7.0 Hz, 3H), 1.08 (s, 9H), 0.96 (d, J = 6.8 Hz, 3H), 0.90 (s, 9H), 0.89 (s, 9H), 0.87 (d, J = 7.0 Hz, 3H), 0.10 (s, 3H), 0.09 (s, 3H), 0.08 (s, 3H), 0.01 ppm (s, 3H); ^{13}C NMR: δ = 210.8, 134.0 (×2), 19.3, 18.3, 18.2 (C), 135.6 (×4), 129.5 (×2), 127.6 (×4), 73.1, 72.7, 50.2, 43.0, 36.3 (CH), 68.9, 33.3, 28.5 (CH_2), 28.6, 26.9 (×3), 26.1 (×3), 26.0 (×3), 16.9, 10.3, 10.2, −3.3, −3.9, −4.0 (×2) (CH_3); IR: $\tilde{\nu}$ = 1716 cm^{-1} (C=O); HR-EIMS *m/z* (%): calcd for $C_{41}H_{72}O_4Si_3$–*t*Bu, 655.4034; found: 655.4038 (12) $[M-t\mathrm{Bu}]^+$, 483 (27), 469 (33), 199 (44), 135 (73), 73 (100); elemental analysis: calcd (%) for $C_{41}H_{72}O_4Si_3$: C 69.04, H 10.17; found: C 69.19, H 10.00.

(2*S*,3*R*,4*S*,5*R*,6*S*,9*S*)-4,6-Bis(*tert*-butyldimethylsilyloxy)-10-(*tert*-butyldiphenylsilyloxy)-3,5,9-trimethyldecan-2-ol (17): Ketone **6** (1.57 g, 2.2 mmol) was dissolved at −78 °C in dry CH_2Cl_2 (25 mL) and treated with Me_2AlCl (2 M solution in hexane, 5.5 mL, 5.5 mmol). The reaction mixture was stirred for 5 min at −78 °C, then cooled to −90 °C and treated with nBu$_3$SnH (675 μL, 2.5 mmol). After stirring for 1 h at −90 °C, the cooling bath was removed, saturated aq $NaHCO_3$ (10 mL) was added and the mixture was further stirred at room temperature for 30 min. Workup (extraction with CH_2Cl_2) provided a 92:8 mixture of diastereoisomeric alcohols (1.43 g, 91%), which was carefully purified by means of flash column chromatography on silica gel (hexane/EtOAc 95:5) to yield pure **17**. Colourless oil; $[\alpha]_D = -2.6$ (c = 2.2 in $CHCl_3$); ^{1}H NMR: δ = 7.70–7.65 (m, 4H), 7.45–7.35 (br m, 6H), 3.89 (dd, J = 5.5, 1.5 Hz, 1H), 3.84 (quint, $J \approx$ 6.0 Hz, 1H), 3.68 (m, 1H), 3.53 (dd, J = 9.8, 5.7 Hz, 1H), 3.48 (dd, J = 9.8, 6.0 Hz, 1H), 2.20 (br s, 1H; OH), 1.80 (m, 1H), 1.65–1.45 (br m, 6H), 1.18 (d, J = 6.0 Hz, 3H), 1.08 (s, 9H), 0.98 (d, J = 7.0 Hz, 3H), 0.95 (d, J = 6.6 Hz, 3H), 0.93 (s, 9H, overlapping one methyl doublet), 0.90 (s, 9H), 0.11 (s, 3H), 0.10 (s, 3H), 0.06 (s, 3H), 0.05 ppm (s, 3H); ^{13}C NMR: δ = 134.0 (×2), 19.3, 18.3, 18.2 (C), 135.6 (×4), 129.5 (×2), 127.6 (×4), 76.9, 73.8, 72.2, 43.0, 41.6, 36.3 (CH), 69.0, 33.0, 28.2 (CH_2), 26.9 (×3), 26.1
(×3), 26.0 (×3), 21.2, 16.9, 10.6, 8.4, −3.2, −3.3, −4.1 −4.4 ppm (CH_3); IR: $\tilde{\nu}$ = 3450 cm^{-1} (br, OH); HR-EIMS *m/z* (%): calcd for $C_{41}H_{74}O_4Si_3$–*t*Bu: 657.4190; found: 657.4168 (1) $[M-t\mathrm{Bu}]^+$, 525 (2), 469 (7), 199 (14), 135 (18), 73 (100); elemental analysis: calcd (%) for $C_{41}H_{74}O_4Si_3$: C 68.85, H 10.43; found: C 68.98, H 10.25.

(2*S*,3*R*,4*S*,5*R*,6*S*,9*S*)-4,6-Bis(*tert*-butyldimethylsilyloxy)-10-(*tert*-butyldiphenylsilyloxy)-2-methoxy-3,5,9-trimethyldecane (5): A solution of alcohol **17** (1.29 g, 1.8 mmol) in dry $CHCl_3$ (80 mL) was treated at room temperature with 2,6-di-*tert*-butylpyridine (8 mL, 36 mmol) and MeOTf (2 mL, 18 mmol). Both reagents were added in two portions with an interval of 2 h. The reaction mixture was then stirred at reflux until consumption of the starting material (about 2 h, TLC monitoring), and then quenched by addition of methanol (2 mL) and saturated aqueous $NaHCO_3$ (6 mL), followed by further stirring for 30 min at room temperature. Workup (extraction with CH_2Cl_2) and column chromatography on silica gel (hexane/EtOAc 95:5) gave **5** (1.10 g, 84%). Colourless oil; $[\alpha]_D = +4.1$ (c = 1.7 in $CHCl_3$); ^{1}H NMR: δ = 7.70–7.65 (m, 4H), 7.45–7.35 (br m, 6H), 3.82 (br d, J = 6.0 Hz, 1H), 3.74 (m, 1H), 3.53 (dd, J = 9.8, 5.7 Hz, 1H), 3.47 (dd, J = 9.8, 6.2 Hz, 1H), 3.30 (s, 3H), 3.15 (quint, J = 6.5 Hz, 1H), 1.73 (m, 1H), 1.65–1.50 (br m, 5H), 1.45 (m, 1H), 1.13 (d, J = 6.3 Hz, 3H), 1.08 (s, 9H), 0.95 (d, J = 6.5 Hz, 3H), 0.94 (d, J = 6.5 Hz, 3H), 0.91 (s, 9H), 0.90 (s, 9H), 0.86 (d, J = 7.0 Hz, 3H), 0.10 (s, 3H), 0.07 (s, 6H), 0.05 ppm (s, 3H); ^{13}C NMR: δ = 134.1, 134.0, 19.3, 18.5, 18.3 (C), 135.6 (×4), 129.5 (×2), 127.6 (×4), 79.8, 73.3, 72.8, 43.3, 41.4, 36.5 (CH), 69.2, 33.0, 28.1 (CH_2), 56.5, 26.9 (×3), 26.1 (×3), 26.0 (×3), 16.9, 16.5, 11.0, 10.5, −3.2, −3.4, −3.9 −4.0 ppm (CH_3); HR-EIMS *m/z* (%): calcd for $C_{42}H_{76}O_4Si_3$–*t*Bu: 671.4347; found: 671.4293 (7) $[M-t\mathrm{Bu}]^+$, 539 (6), 469 (23), 199 (18), 135 (22), 73 (51), 59 (100); elemental analysis: calcd (%) for $C_{42}H_{76}O_4Si_3$: C 69.17, H 10.50; found: C 69.00, H 10.65.

(2*S*,5*S*,6*R*,7*S*,8*R*,9*S*)-5,7-Bis(*tert*-butyldimethylsilyloxy)-9-methoxy-2,6,8-trimethyldecanol (18): A solution of compound **5** (1.1 g, approximately 1.5 mmol) in 10% NaOH/MeOH (40 mL) was stirred at reflux for 30 h. Workup (extraction with CH_2Cl_2) and column chromatography on silica gel (hexane/EtOAc 90:10) gave **18** (618 mg, 84%). Colourless oil; $[\alpha]_D = +4.9$ (c = 1.7 in $CHCl_3$); ^{1}H NMR: δ = 3.82 (dd, J = 5.8, 1.5 Hz, 1H), 3.68 (br q, $J \approx$ 5.0 Hz, 1H), 3.51 (dd, J = 10.5, 5.8 Hz, 1H), 3.47 (dd, J = 10.5, 6.6 Hz, 1H), 3.30 (s, 3H), 3.14 (quint, J = 6.5 Hz, 1H), 1.73 (m, 1H), 1.70–1.55 (br m, 4H), 1.50–1.45 (m, 2H), 1.40 (br s, 1H; OH), 1.13 (d, J = 6.0 Hz, 3H), 0.94 (d, J = 6.8 Hz, 3H), 0.93 (d, J = 6.5 Hz, 3H), 0.90 (s, 9H), 0.89 (s, 9H), 0.88 (d, J = 7.0 Hz, 3H), 0.09 (s, 3H), 0.07 (s, 3H), 0.06 ppm (s, 6H); ^{13}C NMR: δ = 18.5, 18.3 (C), 80.1, 73.3, 72.4, 43.4, 41.0, 36.2 (CH), 68.2, 32.3, 27.5 (CH_2), 56.5, 26.1 (×3), 26.0 (×3), 16.6, 16.3, 11.3, 10.7, −3.3, −3.6, −4.1 ppm (×2) (CH_3); IR: $\tilde{\nu}$ = 3360 cm^{-1} (br, OH); HR-EIMS *m/z* (%): calcd for $C_{26}H_{58}O_4Si_2$–MeCHOMe: 431.3371; found: 431.3321 (2) $[M-\mathrm{MeCHOMe}]^+$, 231 (48), 75 (100), 59 (65); elemental analysis: calcd (%) for $C_{26}H_{58}O_4Si_2$: C 63.61, H 11.91; found: C 63.74, H 11.75.

(4*S*,5*S*,8*S*,9*R*,10*S*,11*R*,12*S*)-8,10-Bis(*tert*-butyldimethylsilyloxy)-12-methoxy-5,9,11-trimethyltridec-1-en-4-ol (20): Oxalyl chloride (130 μL, 1.5 mmol) was added dropwise at −78 °C to a solution of DMSO (210 μL, 3 mmol) in dry CH_2Cl_2 (3 mL). The mixture was stirred for 5 min at this temperature. A solution of alcohol **18** (614 mg, 1.25 mmol) in dry CH_2Cl_2 (1 mL) was then added via syringe. The reaction mixture was stirred for 15 min at −78 °C. After addition of Et_3N (840 μL, 6 mmol), the mixture was stirred for 15 min at −78 °C and then for 20 min at 0 °C. Workup (extraction with CH_2Cl_2) gave crude aldehyde **19** which was used as such in the next reaction.

Allylmagnesium bromide (commercial 1 M solution in Et_2O, 1.5 mL, 1.5 mmol) was added dropwise at 0 °C via syringe to a solution of (−)-Ipc_2BCl (580 mg, 1.8 mmol) in dry Et_2O (8 mL). The mixture was further stirred for 1 h at 0 °C. The solution was then allowed to stand, which caused precipitation of magnesium chloride. The supernatant solution was then carefully transferred to another flask by means of a cannula. After cooling this flask at −90 °C, a solution of crude **19** from above in dry Et_2O (5 mL) was added dropwise by syringe. The resulting solution was further stirred at the same temperature for 1 h. The reaction mixture was then quenched through addition of phosphate pH 7 buffer solution (8 mL), MeOH (8 mL) and 30% H_2O_2 (4 mL). After stirring for 30 min, the mixture was poured onto saturated aqueous $NaHCO_3$ and worked up (extraction with Et_2O). Careful column chromatography on silica gel (hexane/EtOAc 95:5) afforded **20** (365 mg, 55% overall from **18**). Colourless oil; $[\alpha]_D = +2.7$ ($c = 1.4$ in $CHCl_3$); ^{1}H NMR: $\delta = 5.84$ (m, 1H), 5.15–5.10 (m, 2H), 3.82 (dd, $J = 5.7$, 1.5 Hz, 1H), 3.68 (br q, $J \approx 5.5$ Hz, 1H), 3.52 (dt, $J = 8.8$, 4.2 Hz, 1H), 3.30 (s, 3H), 3.14 (quint, $J = 6.5$ Hz, 1H), 2.30 (m, 1H), 2.17 (dt, $J = 14$, 8.5 Hz, 1H), 1.73 (m, 1H), 1.70–1.60 (br m, 2H), 1.60–1.40 (m, 3H), 1.15 (m, 1H), 1.12 (d, $J = 6.3$ Hz, 3H), 0.93 (d, $J = 6.5$ Hz, 3H), 0.92 (d, $J = 6.5$ Hz, 3H), 0.90 (s, 9H), 0.89 (s, 9H), 0.88 (d, $J = 7.0$ Hz, 3H), 0.09 (s, 3H), 0.07 (s, 3H), 0.06 ppm (s, 6H) (hydroxyl proton not detected); ^{13}C NMR: $\delta = 18.5$, 18.3 (C), 135.5, 80.0, 74.1, 73.4, 72.5, 43.5, 41.1, 38.6 (CH), 117.8, 39.1, 33.0, 27.6 (CH_2), 56.4, 26.1 (×3), 26.0 (×3), 16.4, 14.2, 11.3, 10.7, −3.3, −3.6, −4.1 ppm (×2) (CH_3); IR: $\tilde{\nu} = 3490$ cm^{-1} (br, OH); HR-EIMS *m/z* (%): calcd for $C_{29}H_{62}O_4Si_2-t$Bu: 473.3482; found: 473.3458 (1) $[M-t\text{Bu}]^+$, 455 (3), 271 (22), 253 (43), 231 (55), 139 (54), 59 (100); elemental analysis: calcd (%) for $C_{29}H_{62}O_4Si_2$: C 65.60, H 11.77; found: C 65.49, H 11.60.

(4*S*,5*S*,8*S*,9*R*,10*S*,11*R*,12*S*)-8,10-Bis(*tert*-butyldimethylsilyloxy)-12-methoxy-4-methoxymethoxy-5,9,11-trimethyltridec-1-ene (4): Alcohol **20** (345 mg, 0.65 mmol) was dissolved in dry CH_2Cl_2 (5 mL) and treated with iPr$_2$NEt (350 μL, 2 mmol) and MOMCl (100 μL, 1.3 mmol). The reaction mixture was then stirred overnight at room temperature. Workup (extraction with CH_2Cl_2) and column chromatography on silica gel (hexane/EtOAc 95:5) furnished **4** (295 mg, 79%). Colourless oil; $[\alpha]_D = -3.1$ ($c = 0.9$ in $CHCl_3$); ^{1}H NMR: $\delta = 5.82$ (m, 1H), 5.10 (br dd, $J = 17.0$, 1.5 Hz, 1H), 5.04 (br d, $J = 10.0$ Hz, 1H), 4.65 (d, $J = 7.0$ Hz, 1H), 4.63 (d, $J = 7.0$ Hz, 1H), 3.82 (dd, $J = 5.8$, 1.5 Hz, 1H), 3.70 (br q, $J \approx 5.5$ Hz, 1H), 3.47 (m, 1H), 3.37 (s, 3H), 3.30 (s, 3H), 3.14 (quint, $J = 6.5$ Hz, 1H), 2.35–2.25 (m, 2H), 1.75–1.50 (br m, 6H), 1.40 (m, 1H), 1.12 (d, $J = 6.3$ Hz, 3H), 0.94 (d, $J = 6.8$ Hz, 3H), 0.91 (d, 3H, overlapped), 0.90 (s, 9H), 0.89 (s, 9H), 0.86 (d, $J = 7$ Hz, 3H), 0.09 (s, 3H), 0.07 (s, 3H), 0.06 (s, 3H), 0.05 ppm (s, 3H); ^{13}C NMR: $\delta = 18.5$, 18.3 (C), 135.6, 81.4, 80.0, 73.4, 72.7, 43.5, 41.2, 36.6 (CH), 116.7, 96.1, 36.0, 33.4, 27.2 (CH_2), 56.4, 55.6, 26.1 (×3), 26.0 (×3), 16.4, 14.7, 11.1, 10.6, −3.3, −3.5, −4.0 ppm (×2, CH_3); HR-EIMS *m/z* (%): calcd for $C_{31}H_{66}O_5Si_2-t$Bu: 517.3744; found: 517.3756 (3) $[M-t\text{Bu}]^+$, 283 (22), 253 (6), 231 (55), 139 (34), 59 (100); elemental analysis: calcd for $C_{31}H_{66}O_5Si_2$: C 64.75, H 11.57; found: C 64.54, H 11.63.

(*E*)-4-(4-Methoxybenzyloxy)but-2-enal (30): Alcohol **31**[27] (4.16 g, 20 mmol) was dissolved in dry CH_2Cl_2 (100 mL) and treated with PCC (6.50 g, approximately 30 mmol). The reaction mixture was stirred for four days at room temperature and then filtered through Celite (washing with CH_2Cl_2). After removal of the solvent under reduced pressure, the residue was purified by means of column chromatography on silica gel (hexane/EtOAc 80:20) to yield aldehyde **30** (2.15 g, 52%). Colourless oil; ^{1}H NMR: $\delta = 9.46$ (d, $J = 8.0$ Hz, 1H), 7.20 (m, 2H), 6.82 (m, 2H), 6.74 (dt, $J = 15.5$, 4.0 Hz, 1H), 6.30 (ddt, $J = 15.5$, 8.0, 2.0 Hz, 1H), 4.42 (s, 2H), 4.14 (dd, $J = 4.0$, 2.0 Hz, 2H), 3.70 ppm (s, 3H); ^{13}C NMR: $\delta = 159.0$, 129.2 (C), 192.7, 153.0, 131.1, 128.9 (×2), 113.4 (×2) (CH), 72.1, 67.8 (CH_2), 54.7 ppm (CH_3).

(4*S*)-4-Benzyl-3-[(2*S*,3*R*,4*E*)-3-hydroxy-6-(4-methoxybenzyloxy)-2-methylhex-4-enoyl]-1,3-oxazolidin-2-one (32): A solution of oxazolidinone **22** (700 mg, 3 mmol) in dry CH_2Cl_2 (20 mL) was cooled to 0 °C and treated sequentially with nBu$_2$BOTf (1 M solution in CH_2Cl_2, 5.4 mL, 5.4 mmol) and Et_3N (840 μL, 6 mmol). After stirring for 1 h, the mixture was treated dropwise with a solution of freshly prepared aldehyde **30** (720 mg, 3.5 mmol) in dry CH_2Cl_2 (10 mL). The reaction mixture was stirred at −40 °C for 12 h, quenched by addition of a pH 7 buffer solution (20 mL), MeOH (20 mL) and 30% H_2O_2 (10 mL) and then stirred at room temperature for 30 min. Workup (extraction with EtOAc) and column chromatography on silica gel (hexane/EtOAc 70:30) afforded aldol adduct **32** as a single diastereoisomer (1.13 g, 86% based on **22**). Colourless oil; $[\alpha]_D = +47.6$ ($c = 1.3$ in $CHCl_3$); ^{1}H NMR: $\delta = 7.35$–7.15 (br m, 7H), 6.85 (m, 2H), 5.90 (dt, $J = 15.5$, 5.5 Hz, 1H), 5.78 (dd, $J = 15.5$, 5.5 Hz, 1H), 4.66 (m, 1H), 4.49 (t, $J = 5.5$ Hz, 1H), 4.43 (s, 2H), 4.15–4.10 (m, 2H), 4.00 (d, $J = 5.5$ Hz, 2H), 3.90 (dq, $J = 5.5$, 7.0 Hz, 1H), 3.77 (s, 3H), 3.21 (dd, $J = 13.5$, 3 Hz, 1H), 2.90 (br s, 1H, OH), 2.79 (dd, $J = 13.5$, 9.5 Hz, 1H), 1.26 ppm (d, $J = 7.0$ Hz, 3H); ^{13}C NMR: $\delta = 176.1$, 159.1, 153.0, 135.0, 130.2 (C), 132.1, 129.3 (×2), 129.2 (×2), 128.8 (×2), 128.5, 127.2, 113.7 (×2), 72.1, 55.1, 42.7 (CH), 71.7, 69.6, 66.0, 37.6 (CH_2), 55.0, 11.3 ppm (CH_3); IR: $\tilde{\nu} = 3500$ (br, OH), 1775, 1695 cm^{-1} (C=O); HR-EIMS *m/z* (%): calcd for $C_{25}H_{29}NO_6-H_2O$: 421.1889; found: 421.1881 (1) $[M-H_2O]^+$, 285 (8), 233 (24), 121 (100); elemental analysis: calcd (%) for $C_{25}H_{29}NO_6$: C 68.32, H 6.65; found: C 68.21, H 6.77.

(2*S*,3*R*,4*E*)-3-Hydroxy-*N*-methoxy-6-(4-methoxybenzyloxy)-2-*N*-dimethylhex-4-enamide (33): A solution of *N*,*O*-dimethylhydroxylamine hydrochloride (730 mg, approximately 7.5 mmol) in dry THF (15 mL) was treated dropwise at 0 °C with Me_3Al (2 M solution in toluene, 3.7 mL, approximately 7.5 mmol). The mixture was stirred for 1 h at room temperature. A solution of aldol **32** (1.10 g, 2.5 mmol) in dry THF (6 mL) was then added dropwise via syringe. The reaction mixture was stirred for 3 h at room temperature and then quenched through addition of a saturated aqueous solution of potassium sodium tartrate (50 mL). Stirring at room temperature for 30 min and workup (extraction with CH_2Cl_2) was followed by column chromatography of the residue on silica gel (hexane/EtOAc 1:1) to yield impure **33** (contaminated with the chiral auxiliary), which was used as such in the next step. An aliquot was carefully purified for analytical purposes. Colourless oil; $[\alpha]_D = +12$ ($c = 1$ in $CHCl_3$); ^{1}H NMR: $\delta = 7.26$ (m, 2H), 6.85 (m, 2H), 5.90 (dt, $J = 15.5$, 5.5 Hz, 1H), 5.72 (dd, $J = 15.5$, 5.5 Hz, 1H), 4.45 (m, 1H), 4.44 (s, 2H), 4.01 (d, $J = 5.5$ Hz, 2H), 3.90 (br s, 1H; OH), 3.79 (s, 3H), 3.69 (s, 3H), 3.19 (s, 3H), 2.95 (m, 1H), 1.16 ppm (d, $J = 7$ Hz, 3H); ^{13}C NMR: $\delta = 177.6$*, 159.1, 130.4 (C), 132.2, 129.3 (×2), 128.2, 113.7 (×2), 71.8, 39.5 (CH), 71.7, 69.8 (CH_2), 61.5, 55.2, 31.9*, 10.7 ppm (CH_3) (starred peaks are very low and broad); IR: $\tilde{\nu} = 3440$ (br, OH), 1651 cm^{-1} (C=O); elemental analysis: calcd for $C_{17}H_{25}NO_5$: C 63.14, H 7.79; found: C 63.21, H 7.77.

(2*S*,3*R*,4*E*)-3-(*tert*-Butyldimethylsilyloxy)-*N*-methoxy-6-(4-methoxybenzyloxy)-2-*N*-dimethylhex-4-enamide (34): Weinreb amide **33** from above was dissolved in dry CH_2Cl_2 (20 mL) and treated dropwise at room temperature with 2,6-lutidine (410 μL, 3.5 mmol) and TBSOTf (690 μL, 3 mmol). The mixture was stirred for 1 h at room temperature. Workup (extraction with CH_2Cl_2) was followed by *careful* column chromatography of the residue on silica gel (hexane/EtOAc 70:30) to yield **34** (842 mg, 77% overall yield for the two steps). Colourless oil; $[\alpha]_D = -6.1$ ($c = 1.1$ in $CHCl_3$); ^{1}H NMR: $\delta = 7.26$ (m, 2H), 6.88 (m, 2H), 5.80 (m, 2H), 4.42 (s, 2H), 4.33 (m, 1H), 4.00 (br d, $J \approx 4.5$ Hz, 2H), 3.79 (s, 3H), 3.66 (s, 3H), 3.15 (s, 3H), 3.02 (m, 1H), 1.23 (d, $J = 7$ Hz, 3H), 0.95 (s, 9H), 0.11 (s, 3H), 0.10 ppm (s, 3H); ^{13}C NMR: $\delta = 175.3$*, 158.9, 130.3, 17.9 (C), 134.4, 128.8 (×2), 127.4, 113.4 (×2), 74.6, 42.6 (CH), 71.0, 69.3 (CH_2), 61.0, 54.8, 31.7*, 25.6 (×3), 14.0, −4.4, −5.1 (CH_3) (starred peaks are very low and broad); IR: $\tilde{\nu} = 1657$ cm^{-1} (C=O); HR-EIMS *m/z* (%): calcd for $C_{23}H_{39}NO_5Si-Me$: 422.2362; found: 422.2317 (4) $[M-Me]^+$, 380 (100), 350 (14), 121 (55); elemental analysis: calcd for $C_{23}H_{39}NO_5Si$: C 63.12, H 8.98; found: C 63.24, H 8.79.

(4*R*,5*R*,2*E*,6*E*)-5-(*tert*-Butyldimethylsilyloxy)-8-(4-methoxybenzyloxy)-2,4-dimethylocta-2,6-dienoic acid ethyl ester (35): A solution of Weinreb amide **34** (438 mg, 1 mmol) in dry THF (8 mL) was treated at −78 °C with DIBAL (1 M solution in hexane, 2.5 mL, 2.5 mmol). The reaction was then stirred for 30 min at −78 °C and quenched through addition of saturated aq NH_4Cl (1 mL). The mixture was then stirred at room temperature until formation of a persistent gel. Filtration through Celite (washing with CH_2Cl_2) and solvent removal under reduced pressure gave crude aldehyde **29** which was used as such in the next reaction.

Crude **29** from above was dissolved in dry 1,2-dichloroethane (8 mL) and treated with $Ph_3P{=}C(Me)CO_2Et$ (725 mg, 2 mmol). The reaction was

then heated at 60 °C for 12 h. Removal of all volatiles under reduced pressure and column chromatography of the residue on silica gel (hexane/EtOAc 90:10) furnished conjugated enoate **35** (255 mg, 55 % overall yield for the two steps). Colourless oil; $[\alpha]_D = +6.7$ ($c = 1.1$ in $CHCl_3$); ^{1}H NMR: $\delta = 7.26$ (m, 2H), 6.88 (m, 2H), 6.67 (dq, $J = 10$, 1.5 Hz, 1H), 5.75–5.65 (br m, 2H), 4.42 (s, 2H), 4.17 (m, 2H), 4.05 (br t, $J \approx 5.5$ Hz, 1H), 4.00 (m, 2H), 3.81 (s, 3H), 2.60 (m, 1H), 1.84 (d, $J = 1.5$ Hz, 3H), 1.27 (d, $J = 7$ Hz, 3H), 1.01 (d, $J = 6.8$ Hz, 3H), 0.92 (s, 9H), 0.06 (s, 3H), 0.03 ppm (s, 3H); ^{13}C NMR: $\delta = 168.2$, 159.2, 130.4, 127.2, 18.2 (C), 144.4, 134.4, 129.2 (×2), 127.6, 113.8 (×2), 75.8, 40.3 (CH), 71.4, 69.7, 60.4 (CH_2), 55.3, 25.9 (×3), 14.8, 14.2, 12.7, −4.2, −5.0 ppm (CH_3); IR: $\tilde{\nu} = 1710$ cm^{-1} (C=O); HR-EIMS *m/z* (%): calcd for $C_{26}H_{42}O_5Si-Me$: 447.2567; found: 447.2576 $[M-Me]^+$ (1), 405 (2), 121 (100); elemental analysis: calcd (%) for $C_{26}H_{42}O_5Si$: C 67.49, H 9.15; found: C 67.57, H 9.29.

Sultam 37: A solution of sultam **41** (1.36 g, 5 mmol) in dry CH_2Cl_2 (35 mL) was cooled to −5 °C and treated sequentially with nBu$_2$BOTf (1 M solution in CH_2Cl_2, 5.5 mL, 5.5 mmol) and iPr$_2$NEt (1 mL, approximately 5.5 mmol). After stirring for 30 min at −5 °C, the mixture was cooled to −78 °C and treated dropwise with a solution of aldehyde **30** from above in dry CH_2Cl_2 (5 mL). The reaction mixture was stirred at −78 °C for 16 h, quenched by addition of a pH 7 buffer solution (15 mL) and stirred at room temperature for 30 min. Workup (extraction with CH_2Cl_2) and column chromatography on silica gel (hexane/EtOAc 70:30) afforded aldol adduct **37** as a single diastereoisomer (2.27 g, 95 % based on **41**). White solid, m.p. 97–98 °C; $[\alpha]_D = +85$ ($c = 1.6$ in $CHCl_3$); ^{1}H NMR: $\delta = 7.26$ (m, 2H), 6.88 (m, 2H), 5.92 (dtd, $J = 15.5$, 5.6, 1.3 Hz, 1H), 5.72 (br dd, $J = 15.5$, 5 Hz, 1H), 4.56 (m, 1H), 4.44 (s, 2H), 4.01 (br d, $J = 5.6$ Hz, 2H), 3.88 (t, $J = 6.3$ Hz, 1H), 3.80 (s, 3H), 3.50 (d, $J = 14.0$ Hz, 1H), 3.44 (dd, $J = 14.0$ Hz, 1H), 3.20 (br s, 1H; OH), 3.16 (qd, $J = 7.0$, 3.3 Hz, 1H), 2.05 (m, 2H), 1.95–1.85 (m, 3H), 1.40–1.30 (m, 2H), 1.26 (d, $J = 7.0$ Hz, 3H), 1.15 (s, 3H), 0.97 ppm (s, 3H); ^{13}C NMR: $\delta = 176.5$, 159.2, 130.5, 48.4, 47.8 (C), 131.8, 129.4 (×2), 128.7, 113.8 (×2), 70.7, 65.0, 44.6, 44.4 (CH), 71.7, 69.8, 53.1, 38.3, 32.8, 26.4 (CH_2), 55.3, 20.8, 19.8, 11.8 ppm (CH_3); IR: $\tilde{\nu} = 3520$ (br, OH), 1689 cm^{-1} (br, C=O); HR-FABMS *m/z* (%): calcd for $C_{25}H_{36}NO_6S$: 478.2263; found 478.2215 $[M+H]^+$; elemental analysis: calcd (%) for $C_{25}H_{35}NO_6S$: C 62.89, H 7.44; found: C 62.98, H 7.50.

Sultam 38: Alcohol **37** (2.25 g, 4.7 mmol) was dissolved in dry CH_2Cl_2 (30 mL) and treated dropwise with 2,6-lutidine (815 μL, 7 mmol) and TBSOTf (1.35 mL, 5.9 mmol). The mixture was stirred for 1 h at room temperature. Workup (extraction with CH_2Cl_2) was followed by column chromatography of the residue on silica gel (hexane/EtOAc 90:10) to yield **38** (2.45 g, 88 %). Colourless oil; $[\alpha]_D = +60$ ($c = 4.7$ in $CHCl_3$); ^{1}H NMR: $\delta = 7.26$ (m, 2H), 6.86 (m, 2H), 5.73 (m, 2H), 4.40 (m, 3H), 4.00 (dd, $J = 13.0$, 4.0 Hz, 1H), 3.93 (dd, $J = 13.0$, 4.0 Hz, 1H), 3.78 (s, 3H), 3.73 (m, 1H), 3.44 (d, $J = 14.0$ Hz, 1H), 3.33 (dd, $J = 14.0$ Hz, 1H), 3.19 (quint, $J \approx 7.0$ Hz, 1H), 2.05–2.00 (m, 2H), 1.95–1.85 (m, 3H), 1.30–1.20 (m, 2H), 1.27 (d, $J = 7.0$ Hz, 3H), 1.12 (s, 3H), 0.93 (s, 3H), 0.90 (s, 9H), 0.06 (s, 3H), 0.03 ppm (s, 3H); ^{13}C NMR: $\delta = 173.8$, 159.0, 130.7, 48.1, 47.6, 18.1 (C), 135.1, 129.2 (×2), 128.6, 113.6 (×2), 70.8, 64.8, 47.6, 44.5 (CH), 73.8, 69.8, 53.0, 38.3, 32.6, 26.3 (CH_2), 55.2, 25.8 (×3), 20.7, 19.8, 15.6, −4.2, −4.9 ppm (CH_3); IR: $\tilde{\nu} = 1693$ cm^{-1} (C=O); HR-EIMS *m/z* (%): calcd for $C_{31}H_{49}NO_6SSi-Me$: 576.2815; found: 576.2803 (2) $[M-Me]^+$, 534 (26), 328 (56), 121 (100); elemental analysis: calcd (%) for $C_{31}H_{49}NO_6SSi$: C 62.91, H 8.34; found: C 63.03, H 8.49.

Conversion of sultam 38 into ester 35: A solution of sultam **38** (2.37 g, approximately 4 mmol) in dry CH_2Cl_2 (50 mL) was treated at −78 °C with DIBAL (1 M solution in hexane, 10 mL, 10 mmol). The reaction was then stirred for 30 min at −78 °C and quenched through addition of saturated aqueous NH_4Cl (2 mL). The mixture was then stirred at room temperature until formation of a persistent gel. Filtration through Celite (washing with CH_2Cl_2) and solvent removal under reduced pressure gave crude aldehyde **29**, which was used as such in the next reaction.

Crude **29** from above was dissolved in dry 1,2-dichloroethane (30 mL) and treated with $Ph_3P=C(Me)CO_2Et$ (2.9 g, 8 mmol). The reaction was then heated at 60 °C for 16 h. Removal of all volatiles under reduced pressure and column chromatography of the residue on silica gel (hexane/EtOAc 90:10) furnished conjugated enoate **35** (1.63 g, 88 % overall yield for the two steps).

(4*R*,5*R*,2*E*,6*E*)-5-(*tert*-Butyldimethylsilyloxy)-8-(4-methoxybenzyloxy)-2,4-dimethylocta-2,6-dienol (36): A solution of ethyl ester **35** (1.4 g, approximately 3 mmol) in dry hexane (20 mL) was treated at 0 °C with DIBAL (1 M solution in hexane, 6.5 mL, 6.5 mmol). The reaction was stirred for 1 h at 0 °C and quenched through addition of saturated aqueous NH_4Cl (2 mL). The mixture was then stirred at room temperature until formation of a persistent gel. Filtration through Celite (washing with EtOAc) and solvent removal under reduced pressure, followed by column chromatography of the residue on silica gel (hexane/EtOAc 90:10) afforded alcohol **36** (1.19 g, 94 %). Colourless oil; $[\alpha]_D = -19.4$ ($c = 1.2$ in $CHCl_3$); ^{1}H NMR: $\delta = 7.26$ (m, 2H), 6.88 (m, 2H), 5.65 (m, 2H), 5.25 (br d, $J = 10$ Hz, 1H), 4.42 (s, 2H), 4.00–3.90 (br m, 5H), 3.81 (s, 3H), 2.48 (m, 1H), 1.70 (br s, 1H; OH), 1.66 (br s, 3H), 0.97 (d, $J = 6.8$ Hz, 3H), 0.91 (s, 9H), 0.05 (s, 3H), 0.03 ppm (s, 3H); ^{13}C NMR: $\delta = 159.2$, 134.6, 130.4, 18.2 (C), 135.5, 129.3 (×2), 129.1, 126.9, 113.8 (×2), 77.0, 39.2 (CH), 71.4, 69.9, 69.1 (CH_2), 55.3, 25.9 (×3), 16.3, 14.2, −4.2, −4.9 ppm (CH_3); IR: $\tilde{\nu} = 3450$ cm^{-1} (br, OH); HR-EIMS *m/z* (%): calcd for $C_{24}H_{40}O_4Si$: 420.2696 $[M]^+$; found: 420.2674 (1) $[M]^+$, 402 (1) $[M-H_2O]^+$, 121 (100); elemental analysis: calcd for $C_{24}H_{40}O_4Si$: C 68.53, H 9.58; found: C 68.57, H 9.69.

(6*R*,7*R*,2*E*,4*E*,8*E*)-7-(*tert*-Butyldimethylsilyloxy)-10-(4-methoxybenzyloxy)-2,4,6-trimethyldeca-2,4,8-trienoic acid ethyl ester (28): A solution of alcohol **36** (1.18 g, 2.8 mmol) in dry CH_2Cl_2 (40 mL) was treated with activated MnO_2 (3.5 g, approximately 40 mmol) and heated at reflux for 2 h. Filtration through Celite (washing with CH_2Cl_2) and solvent removal under reduced pressure afforded a crude aldehyde which was used as such in the next step.

An ice-cooled solution of phosphonate $(EtO)_2P(O)CH(Me)COOEt$ (1.2 mL, 5.6 mmol) in dry THF (20 mL) was treated with BuLi (1.6 M solution in hexane, 3 mL, 4.8 mmol). The mixture was stirred for 15 min at 0 °C and treated dropwise with the crude aldehyde from above dissolved in dry THF (20 mL). The stirring was continued for 16 h at 0 °C. Workup (extraction with Et_2O) and column chromatography on silica gel (hexane/EtOAc 80:20) provided **28** (1.18 g, 84 % overall yield for the two steps). Colourless oil; $[\alpha]_D = +26.1$ ($c = 2.2$ in $CHCl_3$); ^{1}H NMR: $\delta = 7.25$ (m, 2H), 7.09 (br s, 1H), 6.86 (m, 2H), 5.69 (m, 2H), 5.43 (br d, $J = 9.8$ Hz, 1H), 4.41 (s, 2H), 4.19 (q, $J = 7$ Hz, 2H), 4.05–3.95 (br m, 3H), 3.79 (s, 3H), 2.59 (m, 1H), 1.97 (br s, 3H), 1.81 (br s, 3H), 1.29 (t, $J = 7.0$ Hz, 3H), 0.99 (d, $J = 6.8$ Hz, 3H), 0.90 (s, 9H), 0.05 (s, 3H), 0.03 ppm (s, 3H); ^{13}C NMR: $\delta = 169.1$, 159.2, 131.7, 130.4, 125.7, 18.2 (C), 142.9, 138.1, 134.6, 129.2 (×2), 127.5, 113.8 (×2), 76.8, 40.1 (CH), 71.4, 69.8, 60.5 (CH_2), 55.2, 25.9 (×3), 16.7, 16.3, 14.3, 14.0, −4.2, −4.9 ppm (CH_3); IR: $\tilde{\nu} = 1703$ cm^{-1} (C=O); HR-EIMS *m/z* (%): calcd for $C_{29}H_{46}O_5Si-t$Bu: 445.2410; found: 445.2392 (1) $[M-t\text{Bu}]^+$, 121 (100); elemental analysis: calcd (%) for $C_{29}H_{46}O_5Si$: C 69.28, H 9.22; found: C 69.20, H 9.34.

(6*R*,7*R*,2*E*,4*E*,8*E*)-7-(*tert*-Butyldimethylsilyloxy)-10-hydroxy-2,4,6-trimethyldeca-2,4,8-trienoic acid ethyl ester (39): A solution of compound **28** (1.16 g, approximately 2.3 mmol) in wet CH_2Cl_2 (30 mL mixed with 1 mL water) was treated with DDQ (570 mg, 2.5 mmol). The mixture was stirred at room temperature until consumption of the starting material (approximately 2 h, TLC monitoring). Workup (extraction with CH_2Cl_2) and column chromatography on silica gel (hexane/EtOAc 95:5) provided **39** (783 mg, 89 %). Colourless oil; $[\alpha]_D = +30.7$ ($c = 1.7$ in $CHCl_3$); ^{1}H NMR: $\delta = 7.08$ (br s, 1H), 5.74 (dt, $J = 15.6$, 5.3 Hz, 1H), 5.67 (dd, $J = 15.6$, 6.2 Hz, 1H), 5.41 (br d, $J = 9.8$ Hz, 1H), 4.19 (q, $J = 7.0$ Hz, 2H), 4.15–4.10 (m, 2H), 3.98 (t, $J = 6.2$ Hz, 1H), 2.58 (m, 1H), 1.96 (br s, 3H), 1.80 (br s, 3H), 1.50 (br s, 1H; OH), 1.29 (t, $J = 7$ Hz, 3H), 0.97 (d, $J = 6.8$ Hz, 3H), 0.89 (s, 9H), 0.03 (s, 3H), 0.00 ppm (s, 3H); ^{13}C NMR: $\delta = 169.2$, 131.7, 125.7, 18.2 (C), 143.0, 138.0, 133.1, 129.9, 76.6, 40.1 (CH), 63.1, 60.5 (CH_2), 25.9 (×3), 16.7, 16.2, 14.3, 14.0, −4.1, −4.9 ppm (CH_3); IR: $\tilde{\nu} = 3460$ (br, OH), 1708 cm^{-1} (C=O); HR-EIMS *m/z* (%): calcd for $C_{21}H_{38}O_4Si$: 382.2539; found: 382.2513 (1) $[M]^+$, 201 (85), 107 (33), 73 (100); elemental analysis: calcd (%) for $C_{21}H_{38}O_4Si$: C 65.92, H 10.01; found: C 66.10, H 10.14.

(6*R*,7*S*,8*R*,9*S*,2*E*,4*E*)-7-(*tert*-Butyldimethylsilyloxy)-8,9-epoxy-10-hydroxy-2,4,6-trimethyldeca-2,4-dienoic acid ethyl ester (27): Powdered 4 Å

MS (100 mg) were suspended in dry CH_2Cl_2 (15 mL) and the suspension was cooled to −23 °C. Then, titanium tetra*iso*propoxide (600 μL, approximately 2 mmol) and diethyl L-(+)-tartrate (343 μL, 2 mmol) were added with stirring, followed by a solution of compound **39** (766 mg, 2 mmol) in dry CH_2Cl_2 (5 mL). The reaction mixture was stirred at −23 °C for 20 min followed by addition of *tert*-butylhydroperoxide (5 mL of a freshly prepared ≈4.1 M solution in toluene, approximately 20 mmol) and further stirring at −23 °C for 24 h. Reaction quenching was performed through addition of water (10 mL), followed by stirring for 30 min at room temperature, addition of 30% aq NaOH (1 mL) and further stirring for 30 min. Workup (extraction with CH_2Cl_2) and column chromatography on silica gel (hexane/EtOAc, first 80:20 then 70:30) provided **27** (718 mg, 90%) as a single stereoisomer. Colourless oil; ^{1}H NMR: δ = 7.06 (brs, 1H), 5.50 (brd, J = 9.8 Hz, 1H), 4.17 (q, J = 7.0 Hz, 2H), 3.90 (brs, 1H, OH), 3.60–3.55 (m, 3H), 3.10 (dt, J = 4.0, 2.0 Hz, 1H), 2.97 (dd, J = 4.0, 2.3 Hz, 1H), 2.67 (m, 1H), 1.95 (brs, 3H), 1.80 (brs, 3H), 1.26 (t, J = 7.0 Hz, 3H), 1.01 (d, J = 6.8 Hz, 3H), 0.85 (s, 9H), 0.01 (s, 3H), 0.00 ppm (s, 3H); ^{13}C NMR: δ = 169.1, 131.9, 125.9, 18.2 (C), 142.6, 137.7, 73,5, 56.5, 55.7, 37.6 (CH), 61.3, 60.6 (CH_2), 25.8 (x 3), 16.5, 15.5, 14.3, 14.0, −4.3, −5.0 ppm (CH_3); IR: $\tilde{\nu}$ = 3450 (br, OH), 1708 cm^{-1} (C=O); elemental analysis: calcd for $C_{21}H_{38}O_5Si$: C 63.28, H 9.61; found: C 63.15, H 9.79.

(6*R*,7*S*,8*R*,9*S*,10*R*,2*E*,4*E*)-7-(*tert*-Butyldimethylsilyloxy)-8,9-epoxy-10-hydroxy-2,4,6-trimethyltrideca-2,4,12-trienoic acid ethyl ester (40): Oxalyl chloride (390 μL, 4.5 mmol) was added dropwise at −78 °C to a solution of DMSO (630 μL, 9 mmol) in dry CH_2Cl_2 (10 mL). The mixture was stirred for 5 min at this temperature. A solution of alcohol **27** (718 mg, 1.8 mmol) in dry CH_2Cl_2 (3 mL) was then added by syringe. The reaction mixture was stirred for 15 min at −78 °C. After addition of Et_3N (2.5 mL, 18 mmol), the mixture was stirred for 15 min at −78 °C and then for 20 min at 0 °C. Workup (extraction with CH_2Cl_2) gave a crude aldehyde which was used as such in the next reaction.

Allylmagnesium bromide (commercial 1 M solution in Et_2O, 2.3 mL, 2.3 mmol) was added dropwise at 0 °C via syringe to a solution of (−)-Ipc_2BCl (870 mg, 2.7 mmol) in dry Et_2O (20 mL). The mixture was further stirred for 1 h at 0 °C. The solution was then allowed to stand, which caused precipitation of magnesium chloride. The supernatant solution was then carefully transferred to another flask via cannula. After cooling this flask at −110 °C, a solution of the crude aldehyde from above in dry Et_2O (10 mL) was added dropwise via syringe. The resulting solution was further stirred at the same temperature for 1 h. The reaction mixture was then quenched through addition of phosphate pH 7 buffer solution (20 mL), MeOH (20 mL) and 30% H_2O_2 (10 mL). After stirring for 30 min, the mixture was poured onto saturated aq $NaHCO_3$ and worked up (extraction with EtOAc). Column chromatography on silica gel (hexane/EtOAc 95:5) afforded **40** as a 92:8 diastereomeric mixture. Repeated column flash chromatography afforded pure **40** (473 mg, 60% overall from **27**). Colourless oil; $[\alpha]_D$ = +9.4 (c = 0.9 in $CHCl_3$); ^{1}H NMR: δ = 7.08 (brs, 1H), 5.84 (ddt, J = 17.5, 10.0, 7.0 Hz, 1H), 5.51 (brd, J = 9.8 Hz, 1H), 5.20–5.10 (m, 2H), 4.18 (q, J = 7.0 Hz, 2H), 3.65 (m, 1H), 3.62 (m, 1H), 3.00 (m, 2H), 2.67 (m, 1H), 2.37 (t, J = 7.0 Hz, 2H), 1.96 (brs, 3H), 1.90 (brd, J = 8.0 Hz, 1H; OH), 1.82 (brs, 3H), 1.27 (t, J = 7.0 Hz, 3H), 1.02 (d, J = 7.0 Hz, 3H), 0.85 (s, 9H), 0.01 (s, 3H), 0.00 ppm (s, 3H); ^{13}C NMR: δ = 169.0, 132.0, 126.0, 18.3 (C), 142.6, 137.7, 133.5, 73.4, 69.0, 57.5, 56.9, 37.6 (CH), 118.4, 60.6, 39.5 (CH_2), 25.9 (×3), 16.6, 15.7, 14.3, 14.0, −4.3, −4.9 ppm (CH_3); IR: $\tilde{\nu}$3490 (br, OH), 1707 cm^{-1} (C=O); HR-FABMS m/z (%): calcd for $C_{24}H_{43}O_5Si$: 439.2879; found: 439.2905 $[M+H]^+$; elemental analysis: calcd (%) for $C_{24}H_{42}O_5Si$: C 65.71, H 9.65; found: C 65.59, H 9.60.

(6*R*,7*S*,8*R*,9*R*,10*R*,2*E*,4*E*)-7,10-Bis(*tert*-butyldimethylsilyloxy)-8,9-epoxy-2,4,6-trimethyltrideca-2,4,12-trienoic acid ethyl ester (26): Alcohol **40** (439 mg, 1 mmol) was dissolved in dry CH_2Cl_2 (6 mL) and treated dropwise with 2,6-lutidine (175 μL, 1.5 mmol) and TBSOTf (290 μL, 1.25 mmol). The mixture was stirred for 1 h at room temperature. Workup (extraction with CH_2Cl_2) was followed by column chromatography of the residue on silica gel (hexane/EtOAc 90:10) to yield **38** (525 mg, 95%). Colourless oil; $[\alpha]_D$ = +11.5 (c = 0.6 in $CHCl_3$); ^{1}H NMR: δ = 7.10 (brs, 1H), 5.84 (ddt, J = 17.5, 10.0, 7.0 Hz, 1H), 5.55 (brd, J = 10.0 Hz, 1H), 5.10–5.05 (m, 2H), 4.19 (q, J = 7.0 Hz, 2H), 3.61 (dd, J = 5.0, 4.0 Hz, 1H), 3.48 (td, J = 6.5, 5.5 Hz, 1H), 2.96 (dd, J = 5.5, 2.2 Hz, 1H), 2.88 (dd, J = 4.0, 2.2 Hz, 1H), 2.68 (ddq, J = 10.0, 5.0, 6.8 Hz, 1H), 2.28 (t, J = 6.5 Hz, 2H), 2.00 (d, J = 1.3 Hz, 3H), 1.85 (d, J = 1.0 Hz, 3H), 1.29 (t, J = 7.0 Hz, 3H), 1.06 (d, J = 6.8 Hz, 3H), 0.89 (s, 9H), 0.88 (s, 9H), 0.07 (s, 3H), 0.04 (s, 6H), 0.01 ppm (s, 3H); ^{13}C NMR: δ = 169.1, 131.9, 125.9, 18.3, 18.2 (C), 142.6, 138.1, 134.5, 73.7, 73.0, 58.5, 57.2, 37.7 (CH), 117.3, 60.6, 39.5 (CH_2), 25.9 (×3), 25.8 (×3), 16.6, 15.7, 14.3, 14.0, −4.2, −4.5, −4.8, −4.9 ppm (CH_3); IR: $\tilde{\nu}$ = 1710 cm^{-1} (C=O); HR-EIMS m/z (%): calcd for $C_{30}H_{56}O_5Si_2$: 552.3666 $[M]^+$; found: 552.3666 (2) $[M]^+$, 511 (10), 371 (26), 107 (63), 73 (100); elemental analysis: calcd (%) for $C_{30}H_{56}O_5Si_2$: C 65.17, H 10.21; found: C 65.29, H 10.02.

The remaining experimental procedures and spectral data can be taken from the supplementary material in reference [36a].

Materials and methods for the biological and biochemical work

Cell culture: Human A549 non-small lung carcinoma cells were continuously maintained in RPMI-1640 supplemented with 10% fetal calf serum, 2 mM L glutamine, 40 μg mL^{-1} gentamycin, 100 IU mL^{-1} penicillin and 100 μg mL^{-1} streptomycin. Human ovarian carcinoma A2780 and A2780AD (MDR overexpressing P-glycoproteins, P-gp) were cultured as above with the addition of 0.25 units/mL of bovine insuline.

Indirect immunofluorescence: A549 cells were plated at a density of 150,000 cells/mL onto 24 well tissue culture plates containing 12 mm round coverslips, cultured overnight and then treated with ligands at different concentrations or with drug vehicle (DMSO) for 24 h. Residual DMSO was less than 0.5%. Attached cells were permeabilised with Triton X100 and fixed with 3.7% formaldehyde, as previously described.[55] Cytoskeletons were incubated with DM1A monoclonal antibody reacting with α-tubulin, washed twice and incubated with FITC goat antimouse immunoglobulins. The coverslips were incubated with 1 μg mL^{-1} Hoechst 33342 in order to stain the chromatin. After washing, the samples were examined and photographed by using a Zeiss Axioplan epifluorescence microscope. The images were recorded with a Hamamatsu 4742–95 cooled CCD camera.

Cytotoxicity assay: Human ovarian carcinomas A2780 and A2780AD were seeded in 96 well plates at a density of 15,000 cells in 0.08 mL per well. The following day, the cells were exposed to 0.02 mL serial dilutions of ligands for 48 h, after which time an MTT assay was performed in order to determine viable cells with some modifications.[56] Briefly, 20 μL of 2.5 mg mL^{-1} of 3-(4,5-dimethylthiazol-2-yl)-2,5-diphenyltetrazolium bromide (MTT) was added to each well, incubated 4 h at 37 °C, then treated with 0.1 mL MTT solubilizer (10% SDS, 45% dimethylformamide pH 5.5). Plates were again incubated overnight at 37 °C in order to solubilise the blue formazan precipitate before measuring the absorbance at 595/690 nm in an automated Multiscan microplate reader. Control wells containing medium without cells were used as blanks. MTT response is expressed as a percentage of the control (untreated) cells. The IC50 was calculated from the log-dose response curves.

Cell cycle analysis: Progression through the cell cycle was assessed by flow cytometry DNA determination with propidium iodide. Cells (150,000 per ml) were incubated with several concentrations of the drugs for 24 h. The cells were fixed with 70% ethanol, treated with RNase and stained with propidium iodide as previously described.[57] The analysis was performed with a Coulter Epics XL flow cytometer.

Effects of ligands on microtubule assembly and stability: The effects of the ligands on tubulin assembly were monitorised by incubating concentrations from 10 to 20 μM tubulin in buffer GAB-1 mM GTP in the presence of 11 or 22 μM ligand. In this buffer tubulin can assemble without ligand with a critical concentration of 3.3 μM.[58] The polymers were sedimented at 90,000 g for 20 min in a TLA 100 rotor, preequilibrated at 37 °C, in a Beckman Optima TLX ultracentrifuge. The supernatants were carefully removed by pipetting, and the pellets resuspended in 10 mM phosphate, 1% SDS, pH 7.0. The pellets and the supernatants were diluted 1:10 in the same buffer, and their concentrations were fluorimetrically measured employing a Fluorolog 3 spectrofluorimeter (excitation wavelength 285 nm, emission wavelength 320 nm using slits of 2 and 5 nm, respectively). Tubulin concentration standard curves were constructed for

each experiment, by using spectrophotometrically measured concentrations of purified tubulin.

The effect of the ligand on polymerisation was also tested in a MAP containing system; microtubular protein (1 mg/mL) was incubated in buffer AB-1 mM GTP, for 30 min at 37 °C in the presence of 11 μM ligand. The polymers were then pelleted at 90,000 g for 20 min in a TLA 100 rotor, preequilibrated at 37 °C, in a Beckman Optima TLX ultracentrifuge. The supernatants were taken, the pellets resuspended in 10 mM sodium phosphate pH 7.0, and the microtubular protein concentrations measured by the method described by Bradford[59] by using BSA (bovine serum albumin) as standard.

Binding of ligands to tubulin microtubules: Samples containing ligand (11 μM) and stabilized crosslinked microtubules (10 μM taxoid binding sites) were prepared as described[60] and incubated in GAB buffer for 30 min at 37 °C in polycarbonate centrifuge tubes (Beckman) (DMSO concentration was always kept under 2%). The samples were then centrifuged at 90,000 g for 10 min at 25 °C in a TLA100 rotor. The supernatants were collected by pipetting and the pellets were resuspended in 10 mM phosphate pH 7.0. Both pellets and supernatants were extracted three times with an excess volume of dichloromethane, dried in vacuum, and dissolved in 25 μL of a methanol/water (v/v 75:25) mixture. Ligands (both bound to pelleted polymers and free in the supernatant), were determined by HPLC. The HPLC analyses of the samples were performed in a C18 column (Supercosil, LC18 DB, 250×4.6 mm, 5 μM bead size) developed in a gradient from 60 to 90% of methanol in water (v/v) at a flow rate of 1 mL min^{-1}.

Samples containing ligand (5 μM) and non-polimerised tubulin (5 μM) were incubated for 30 min at 37 °C in 10 mM phosphate, 1 mM EDTA, 1.5 mM $MgCl_2$, 1 mM GTP, pH 7.0 buffer in polycarbonate centrifuge tubes (Beckman) (DMSO concentration was always kept under 2%). The samples were then centrifuged at 380,000 g for 2 h at 25 °C in a TLA100 rotor. The 100 μL upper and lower fractions of the tube were carefully collected, extracted and analysed as described above.

Acknowledgements

Financial support has been granted (to J.A.M. and M.C.) by the Spanish Ministry of Education and Science (projects BQU2002–00468 and CTQ2005–06688-C02–01/02, including financial support by FEDER funds), and by the Consellería d'Empresa, Universitat i Ciencia de la Generalitat Valenciana (projects GV05/52, ACOMP06/006 and ACOMP06/008). J.G.-F. and J. M. thank the Spanish Ministry of Education and Science for a FPU pre-doctoral fellowship and a Ramón y Cajal contract, respectively. J.A.M. and M.C. further thank Professor T. Eguchi, Department of Chemistry and Material Science, Tokyo Institute of Technology, and Dr. K. Mizoue, from the Taisho Pharmaceutical Company, Saitama (Japan) for the kind sending of an authentic sample of FD-891; and Drs. J. Jiménez-Barbero and M. Bruix, from the CSIC, Madrid (Spain) for their kind help in high-field NMR spectroscopic measurements. I.B. thanks Dr. P. Lastres for his help with flow cytometry. J.F.D. thanks Matadero Madrid Norte S.A. and Carnicas Madrid-Canarias S.L. for providing the pork brains for tubulin isolation. Partial support (to J.F.D) by the Spanish Ministry of Education and Science (project BFU2004–00358) and by CAM (BIPPED project) is also acknowledged.

[1] a) S. Dröse, K. Altendorf, *J. Exp. Biol.* **1997**, *200*, 1–8; b) Further additional mechanisms of action cannot be excluded: J. J. Shacka, B. J. Klocke, K. A. Roth, *Autophagy* **2006**, *2*, 228–230.

[2] a) K. Toshima, *Curr. Org. Chem.* **2004**, *8*, 185–210; b) W.-M. Dai, Y. Guan, J. Jin, *Curr. Med. Chem.* **2005**, *12*, 1947–1993.

[3] a) K. U. Bindseil, A. Zeeck, *J. Org. Chem.* **1993**, *58*, 5487–5492; b) K. U. Bindseil, A. Zeeck, *Liebigs Ann. Chem.* **1994**, 305–312; c) G. Ingenhorst, K. U. Bindseil, C. Boddien, S. Dröse, M. Gassel, K. Altendorf, A. Zeeck, *Eur. J. Org. Chem.* **2001**, 4525–4532.

[4] a) S. Gagliardi, P. A. Gatti, P. Belfiore, A. Zocchetti, G. D. Clarke, C. Farina, *J. Med. Chem.* **1998**, *41*, 1883–1893; b) K. D. Hettiarachchi, P. Z. Zimmet, M. A. Myers, *Cell Biol. Toxicol.* **2006**, *22*, 169–181; c) K. D. Hettiarachchi, P. Z. Zimmet, M. A. Myers, *Food Chem. Toxicol.* **2006**, *44*, 1966–1977.

[5] M. Seki-Asano, Y. Tsuchida, K. Hanada, K. Mizoue, *J. Antibiot.* **1994**, *47*, 1234–1241.

[6] T. Kataoka, A. Yamada, M. Bando, T. Honma, K. Mizoue, K. Nagai, *Immunology* **2000**, *100*, 170–177 (Erratum: Immunology **2000**, 101, 288).

[7] M. Natsume, M. Komiya, F. Koyanagi, N. Tashiro, H. Kawaide, H. Abe, *J. Gen. Plant Pathol.* **2005**, *71*, 364–369.

[8] a) T. Eguchi, K. Kobayashi, H. Uekusa, Y. Ohashi, K. Mizoue, Y. Matsushima, K. Kakinuma, *Org. Lett.* **2002**, *4*, 3383–3386; b) T. Eguchi, K. Yamamoto, K. Mizoue, K. Kakinuma, *J. Antibiot.* **2004**, *57*, 156–157.

[9] a) M. Bartra, F. Urpí, J. Vilarrasa in *Recent Progress in the Chemical Synthesis of Antibiotics and Related Microbial Products* (Ed.: G. Lukacs), Springer Verlag, Berlin, *Vol. 2*, **1993**, pp. 1–65; b) A. Parenty, X. Moreau, J.-M. Campagne, *Chem. Rev.* **2006**, *106*, 911–939.

[10] I. Ojima, M. Tzamarioudaki, Z.-Y. Li, R. J. Donovan, *Chem. Rev.* **1996**, *96*, 635–662.

[11] For a preliminary communication see: J. Murga, J. García-Fortanet, M. Carda, J. A. Marco, *Tetrahedron Lett.* **2004**, *45*, 7499–7501.

[12] a) H. C. Brown, P. V. Ramachandran, *J. Organomet. Chem.* **1995**, *500*, 1–19; b) P. V. Ramachandran, *Aldrichimica Acta* **2002**, *35*, 23–35.

[13] a) D. A. Evans, *Aldrichimica Acta* **1982**, *15*, 23–32; b) B. M. Kim, S. F. Williams, S. Masamune in *Comprehensive Organic Synthesis*, Vol. 2 (Eds.: B. M. Trost, I. Fleming, E. Winterfeldt), Pergamon Press, Oxford, **1993**, pp. 239–276; c) C. J. Cowden, I. Paterson, *Org. React.* **1997**, *51*, 1–200.

[14] K. C. Nicolaou, K. Namoto, A. Ritzén, T. Ulven, M. Shoji, J. Li, G. D'Amico, D. Liotta, C. T. French, M. Wartmann, K. H. Altmann, P. Giannakakou, *J. Am. Chem. Soc.* **2001**, *123*, 9313–9323. However, we have prepared **10** via an adaptation of one route described for the TBS analogue: S. Chandrasekhar, C. R. Reddy, *Tetrahedron: Asymmetry* **2002**, *13*, 261–268.

[15] M. P. Sibi, *Org. Prep. Proced. Int.* **1993**, *25*, 15–40.

[16] Low yields and reaction rates were observed in all attempts at conversion of oxazolidinone **14** into the corresponding Weinreb amide under the standard conditions (MeNHOMe, $AlMe_3$). Therefore, we resorted to the alternative method described in Scheme 3.

[17] D. A. Evans, B. D. Allison, M. G. Yang, C. E. Masse, *J. Am. Chem. Soc.* **2001**, *123*, 10840–10852. See also: T. Ooi, J. Morikawa, D. Uraguchi, K. Maruoka, *Tetrahedron Lett.* **1999**, *40*, 2993–2996.

[18] Prior to the use of Bu_3SnH/Me_2AlCl, we tested reductants such as DIBAL and L-selectride, which have proven useful in closely related instances (D. L. Boger, T. T. Curran, *J. Org. Chem.* **1992**, *57*, 2235–2244). However, they displayed a low stereoselectivity in the present case (dr = about 2:1).

[19] The configuration of the stereocentre created in this step was established by total desilylation of **17** with TBAF and treatment of the resulting tetraol with 2,2-dimethoxypropane and an acid catalyst. This gave a monoacetonide **i** which showed two methyl ^{13}C NMR spectroscopic signals at approximately 30 and 19 ppm. This indicates that it is the acetonide of a *syn*-1,3-diol[20] and can only be that indicated below, as the internal acetonide would necessarily be *anti*.

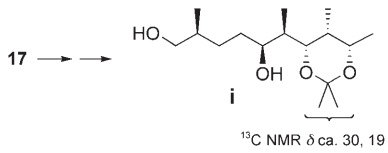

[20] S. D. Rychnovsky, B. N. Rogers, T. I. Richardson, *Acc. Chem. Res.* **1998**, *31*, 9–17.

[21] D. M. Walba, W. N. Thurmes, R. C. Haltiwanger, *J. Org. Chem.* **1988**, *53*, 1046–1056. Meerwein's salt (trimethyloxonium tetrafluoroborate) proved ineffective in the present case.
[22] S. Hatakeyama, H. Irie, T. Shintani, Y. Noguchi, H. Yamada, M. Nishizawa, *Tetrahedron* **1994**, *50*, 13369–13376.
[23] T. W. Greene, P. G. M. Wuts, *Protective Groups in Organic Synthesis*; John Wiley and Sons, New York, 3rd ed., **1999**, pp. 27–33.
[24] P. R. Blakemore, *J. Chem. Soc. Perkin Trans. 1* **2002**, 2563–2585.
[25] For the synthesis of a compound structurally related to fragment **23** see: S.-S. Chng, J. Xu, T.-P. Loh, *Tetrahedron Lett.* **2003**, *44*, 4997–5000.
[26] For a preliminary communication see: J. Murga, J. García-Fortanet, M. Carda, J. A. Marco, *Synlett* **2004**, 2830–2832. Several improvements and optimisations with respect to the published synthesis are reported now.
[27] B. M. Trost, J. D. Chisholm, S. T. Wrobleski, M. Jung, *J. Am. Chem. Soc.* **2002**, *124*, 12420–12421.
[28] This $Z \rightarrow E$ isomerisation during the oxidation with PCC has been reported to occur with the corresponding benzyl derivative: S. J. Danishefsky, E. M. Berman, M. Ciufolini, S. J. Etheredge, B. E. Segmuller, *J. Am. Chem. Soc.* **1985**, *107*, 3891–3898.
[29] This olefination gave a better yield in 1,2-dichloroethane at 60 °C than in toluene at 110 °C, in contrast to that observed in a structurally similar situation: J. A. Marshall, N. D. Adams, *J. Org. Chem.* **2002**, *67*, 733–740.
[30] a) W. Oppolzer, *Tetrahedron* **1987**, *43*, 1969–2004; b) W. Oppolzer, J. Blagg, I. Rodriguez, E. Walther, *J. Am. Chem. Soc.* **1990**, *112*, 2767–2772; c) O. Reiser, *Nachr. Chem. Tech. Lab.* **1996**, *44*, 612–618.
[31] This change of the chiral auxiliary was motivated by the saving of one step, as we were able to directly reduce the silylated aldol adducts to aldehydes, thus circumventing the preparation of Weinreb amides. Furthermore, the first reduction-olefination sequence worked much better with the Oppolzer auxiliary (**38**→**35**, 88% overall yield) than via the Weinreb amide (**34**→**35**, 55% overall yield).
[32] K. Horita, T. Yoshioka, T. Tanaka, Y. Oikawa, O. Yonemitsu, *Tetrahedron* **1986**, *42*, 3021–3028.
[33] T. Katsuki, V. S. Martín, *Org. React.* **1996**, *48*, 1–300.
[34] a) M. B. Andrus, S. D. Lepore, F. A. Sclafani, *Tetrahedron Lett.* **1997**, *38*, 4043–4046; b) M. B. Andrus, T. M. Turner, D. Asgari, W. Li, *J. Org. Chem.* **1999**, *64*, 2978–2979.
[35] Y.-L. Zhong, T. K. M. Shing, *J. Org. Chem.* **1997**, *62*, 2622–2624.
[36] a) Preliminary report on the total synthesis of FD-891: J. García-Fortanet, J. Murga, M. Carda, J. A. Marco, *Org. Lett.* **2006**, *8*, 2695–2698; b) for another recently published synthesis of FD-891 see: M. T. Crimmins, F. Caussanel, *J. Am. Chem. Soc.* **2006**, *128*, 3128–3129.
[37] M. A. Blanchette, M. S. Malamas, M. H. Nantz, J. C. Roberts, P. Somfai, D. C. Whritenour, S. Masamune, *J. Org. Chem.* **1989**, *54*, 2817–2825.
[38] A. P. Kozikowski, P. D. Stein, *J. Org. Chem.* **1984**, *49*, 2301–2309.
[39] The absolute configuration of aldol **51** has been secured by means of X-ray diffraction analysis (see the Supporting Information in reference [36a]).
[40] Silylation of **51** required the use of a considerable excess of silylating agent. Therefore, purification of **52** proved difficult. For this reason, overall yield is given for the three steps **51**→**54**.
[41] P. R. Blakemore, P. J. Kocienski, A. Morley, K. Muir, *J. Chem. Soc. Perkin Trans. 1* **1999**, 955–968.
[42] S. V. Voitekhovich, P. N. Gaponik, G. I. Koldobskii, *Russ. J. Org. Chem.* **2005**, *41*, 1565–1582.
[43] a) O. Mitsunobu, *Synthesis* **1981**, 1–28; b) D. L. Hughes, *Org. React.* **1992**, *42*, 335–656; c) D. H. Valentine Jr, J. H. Hillhouse, *Synthesis* **2003**, 317–334.
[44] T. Masuda, K. Osako, T. Shimizu, T. Nakata, *Org. Lett.* **1999**, *1*, 941–944.
[45] Under the standard conditions for the Julia–Kocienski reaction (KHMDS, THF), we obtained an 80:20 *E*/*Z* mixture but in only 23% yield, even when using a fourfold excess of aldehyde **23**. No improvement in yield or stereoselectivity could be achieved.
[46] a) Y. Guindon, H. E. Morton, C. Yoakim, *Tetrahedron Lett.* **1983**, *24*, 3969–3972; b) Y. Guindon, C. Yoakim, H. E. Morton, *J. Org. Chem.* **1984**, *49*, 3912–3920.
[47] The assignments of configuration to the newly formed olefinic bond in each isomer was difficult because of strong signal overlapping. The problem could be finally solved by NMR spectroscopic measurements at very high field (800 MHz, see acknowledgments).
[48] E. D. Laganis, B. L. Chenard, *Tetrahedron Lett.* **1984**, *25*, 5831–5834.
[49] J. Inanaga, K. Hirata, H. Saeki, T. Katsuki, M. Yamaguchi, *Bull. Chem. Soc. Jpn.* **1979**, *52*, 1989–1993.
[50] K. A. Scheidt, H. Chen, B. C. Follows, S. R. Chemler, D. S. Coffey, W. R. Roush, *J. Org. Chem.* **1998**, *63*, 6436–6437.
[51] The identity of the final desilylation product **2** was confirmed through comparison with an authentic sample of the natural product (see the Acknowledgements).
[52] Cleavage of the silyl groups at C-7 and C-10 takes place with ease. In contrast, those allocated at C-21 and C-23 proved unexpectedly reluctant to cleavage under various mild conditions (too harsh conditions caused decomposition). These two groups are thus responsible for the unsatisfactory yield in the final desilylation step. Such problematic deprotections are not unprecedented: T. B. Durham, N. Blanchard, B. M. Savall, N. A. Powell, W. R. Roush, *J. Am. Chem. Soc.* **2004**, *126*, 9307–9317.
[53] R. J. Kowalski, P. Giannakakou, S. P. Gunasekera, R. E. Longley, B. W. Day, E. Hamel, *Mol. Pharmacol.* **1997**, *52*, 613–622.
[54] A. I. Marcus, A. M. O'Brate, R. M. Buey, J. Zhou, S. Thomas, F. R. Khuri, J. M. Andreu, F. Díaz, and P. Giannakakou, *Cancer Res.* **2006**, *66*, 8838–8846.
[55] C. de Ines, D. Leynadier, I. Barasoain, V. Peyrot, P. Garcia, C. Briand, G. A. Rener, C. Temple, Jr., *Cancer Res.* **1994**, *54*, 75–84.
[56] R. M. Buey, I. Barasoain, E. Jackson, A. Meyer, P. Giannakakou, I. Paterson, S. Mooberry, J. M. Andreu, J. F. Díaz, *Chem. Biol.* **2005**, *12*, 1269–1279.
[57] J. M. Andreu, I. Barasoain, *Biochemistry* **2001**, *40*, 11975–11984.
[58] J. F. Díaz, J. M. Andreu, *Biochemistry* **1993**, *32*, 2747–2755.
[59] M. M. Bradford, *Anal. Biochem.* **1976**, *72*, 248–254.
[60] R. M. Buey, J. F. Díaz, J. M. Andreu, A. O'Brate, P. Giannakakou, K. C. Nicolaou, P. K. Sasmal, A. Ritzén, K. Namoto, *Chem. Biol.* **2004**, *11*, 225–236.

Received: March 1, 2007
Published online: May 22, 2007

DOI: 10.1002/chem.200800039

The Bound Conformation of Microtubule-Stabilizing Agents: NMR Insights into the Bioactive 3D Structure of Discodermolide and Dictyostatin**

Angeles Canales,[a] Ruth Matesanz,[a] Nicola M. Gardner,[b] José Manuel Andreu,[a] Ian Paterson,[b] J. Fernando Díaz,*[a] and Jesús Jiménez-Barbero*[a]

Abstract: A protocol based on a combination of NMR experimental data with molecular mechanics calculations and docking procedures has been employed to determine the microtubule-bound conformation of two microtubule-stabilizing agents, discodermolide (DDM) and dictyostatin (DCT). The data indicate that tubulin in assembled microtubules recognizes DDM through a conformational selection process, with minor changes in the molecular skeleton between the major conformer in water solution and that bound to assembled microtubules. For DCT, the deduced bound geometry presents some key conformation differences around certain torsion angles, with respect to the major conformer in solution, and still displays mobility even when bound. The bound conformer of DCT resembles that of DDM and provides very similar contacts with the receptor. Competition experiments indicate that both molecules compete with the taxane-binding site. A model of the binding mode of DDM and DCT to tubulin is proposed.

Keywords: anticancer agents · conformation analysis · microtubules · molecular modeling · molecular recognition

Introduction

A major challenge of contemporary medicine is in cancer chemotherapy. A cancerous cell is exquisitely well adapted for survival and, although a wide range of drugs targeting the different cell functions necessary for cell division are now available, resistance to chemotherapy is frequently encountered in the clinic.

One of the most commonly used chemotherapeutic agents is paclitaxel and its derivative docetaxel (a semisynthetic analogue).[1,2] These compounds target microtubules, which are essential components of the cytoskeleton, are involved in cell motility, intracellular transport, and maintenance of cell shape, and form part of the mitotic spindle that allows chromosome separation during cell division.[3,4]

In this context, the development of the multidrug-resistance (MDR) phenotype in paclitaxel-treated patients[5,6] has

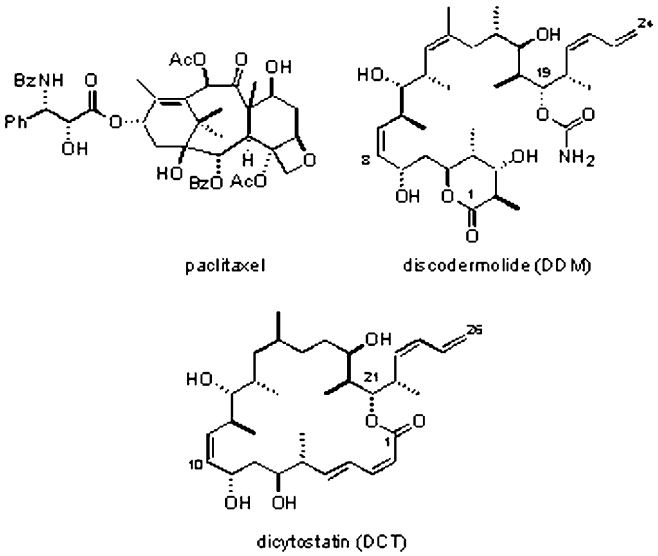

[a] Dr. A. Canales, R. Matesanz, Prof. Dr. J. M. Andreu, Dr. J. F. Díaz, Prof. Dr. J. Jiménez-Barbero
Centro de Investigaciones Biológicas, CSIC
Ramiro de Maeztu 9, 28040 Madrid (Spain)
Fax: (+34) 91-564-4853
E-mail: fer@cib.csic.es
jjbarbero@cib.csic.es

[b] N. M. Gardner, Prof. Dr. I. Paterson
Department of Chemistry, University of Cambridge
Lensfield Road, Cambridge, CB2 1EW (UK)

[**] The Bound Conformation of Microtubule-Stabilizing Agents, Part 2; for Part 1 see: J. Jiménez-Barbero, A. Canales, P. T. Northcote, R. M. Buey, J. M. Andreu, J. F. Díaz, *J. Am. Chem. Soc.* **2006**, *128*, 8757–8765.

Supporting information for this article is available on the WWW under http://www.chemeurj.org/ or from the author.

triggered the search for novel compounds that display the same mechanism of action but are less prone to resistance effects. Indeed, in the last 10 years, many new, structurally unrelated compounds that stabilize microtubules and mimic the activity of paclitaxel/docetaxel have been found from various sources (including corals, marine sponges, bacteria, and plants).[7–15] In a previous study,[16] these microtubule-stabilizing agents (MSA) were classified according to their binding site, either the paclitaxel-binding site or the alternative laulimalide-binding site.[14,15]

From a structural perspective, the paclitaxel-binding site, located in the lumen of the microtubules,[17] is not easily accessible to the paclitaxel molecules in solution. However, it was also shown that paclitaxel binds very quickly to microtubules[18] and that a fluorescent tag attached to paclitaxel bound to microtubules can be recognized by an antibody,[19] which indicates an additional, and external, accessible binding site. This apparent paradox of a hidden but easily accessible luminal binding site was elucidated by the discovery of a new external binding site,[20] to which a covalently binding MSA, cyclostreptin,[12,21] binds before being internalized to the luminal site.

Although paclitaxel and epothilone are known to bind to the luminal site,[17,22] detailed knowledge of where the other paclitaxel mimics bind remains elusive. Since blocking of the external site stops paclitaxel binding,[20] all the known paclitaxel-binding-site ligands should be in competition.

Among the taxoid mimetics, discodermolide (DDM),[10] originally isolated from the deep-sea sponge *Discodermia dissoluta*, displays the highest binding constant to the paclitaxel site.[16] It shows potent antiproliferative activity against a wide range of human cancer cell lines, including P-glycoprotein-overexpressing cell lines.[10,23]

Another potent taxoid mimetic is dictyostatin (DCT), originally isolated from a marine sponge of the *Spongia* genus.[24] Its binding constant for the paclitaxel site is 20 times larger than that of paclitaxel itself.[16] From a structural perspective, there are strong similarities between discodermolide and dictyostatin,[25] which suggests that their bioactive conformations may be similar. Indeed, a hybrid molecule has recently been designed on these grounds.[26]

Despite apparently binding to the same site, the existence of synergy in the effects of paclitaxel and discodermolide on cells and microtubules has been reported.[27–30] These observations could indicate binding to an additional site, such as the recently discovered pore site present in unassembled tubulin, although this is merely speculative.

In elegant recent work by Carlomagno and co-workers,[31] the unassembled-tubulin-bound conformation of discodermolide was reported. Because high-affinity taxane binding does not take place in unassembled tubulin but in assembled microtubules,[20,32] it is uncertain whether the tubulin-bound conformation described therein[31] represents the conformation bound to the luminal taxane-binding site; thus, this requires further exploration.

The knowledge of the bioactive conformation of these molecules is of paramount interest for the rational design of analogues with improved activity. Thus, in this context, we herein report the NMR investigation of the bioactive conformations of both discodermolide and dictyostatin when bound to microtubules. We compare the bound conformations with their geometries in the free state in different solvents,[33,34] as well as with the conformation of discodermolide in the presence of unassembled tubulin reported by Carlomagno and co-workers.[31]

Experimental Section

Protein and chemicals: Purified calf-brain tubulin and chemicals were used as described previously.[35] Discodermolide and dictyostatin were synthesized as reported by Paterson et al.[13,36,37] The compounds were diluted in dimethylsulfoxide (DMSO) solution to give a final concentration of 10 mM and stored at −20 °C.

Preparation of samples for the NMR experiments: The preparation of the samples has been described already.[35] However, we repeat the basic features of the protocol for the sake of clarity. A slowly hydrolyzable nucleotide analogue, guanosine 5′-(α,β-methylenetriphosphate) (GMPCPP),[38] was employed to assemble tubulin. Guanosine 5′-triphosphate (GTP)-bound tubulin in 10 mM sodium phosphate buffer with 6 mM $MgCl_2 \cdot H_2O$ and 1 mM GTP at pH 6.7 was unable to assemble into microtubules at concentrations up to 200 μM.[32] However, when the GTP was substituted by GMPCPP and potassium in the buffer, the critical concentration is very low (4.6 μM at 37 °C). Thus, the protein was equilibrated in a buffer comprising 10 mM potassium phosphate, 6 mM magnesium chloride, and 0.1 mM GMPCPP in D_2O (99.9 %, Merck) at pD 7.0 by a two-step procedure. Sucrose and GTP were removed by a drained centrifuge column of Sephadex G-25 (6×1 cm) equilibrated in a buffer consisting of 10 mM potassium phosphate and 10 μM GTP in D_2O (99.9 %, Merck) at pD 7.3. This was followed by a second chromatography process in a cold Sephadex G-25 column equilibrated in 10 mM potassium phosphate in D_2O (99.9 %, Merck) at pD 7.3, and then 6 mM magnesium chloride and 0.1 mM GMPCPP were added to the solution to give a pD value of 7.0. Immediately before the experiments were performed, the protein concentration was adjusted to 20 μM, the desired amount of target ligand was added to give a final 100–400 μM concentration, and the sample was incubated for 30 minutes at 298 or 310 K (depending on the temperature of the experiment). The sample was found to be completely stable for overnight experiments and only started to slowly degrade after 20 h. Under these conditions, the critical concentration of tubulin is 1.5 μM at 298 K and 0.9 μM at 310 K. This means that either 92.5 or 95.5 % of the sample (at 298 or 310 K, respectively) is assembled into microtubules. A portion of the formed polymers was adsorbed onto formvar/carbon-coated 300 mesh copper grids, negatively stained with 1 % uranyl acetate, observed with a Jeol 1230 transmission electron microscope (JEOL, Tokyo, Japan), and found to consist of microtubules.

Computational methods

Conformational searching and dynamics: Molecular mechanics calculations on DDM and DCT were performed by using the Maestro 7.5 package[39] and the MM3* force field.[40] Bulk-water solvation was simulated by using the generalized Born/surface area (GB/SA) continuum solvent model.[41] The conformational searches were carried out with 20 000 steps of the usage-directed Monte Carlo/energy minimization (MC/EM) procedure. Extended nonbonded cutoff distances (a van der Waals cutoff of 8.0 Å and an electrostatic cutoff of 20.0 Å) were used.

For the Monte Carlo/stochastic dynamics (MC/SD) simulations, van der Waals and electrostatic cutoffs of 25 Å, together with a hydrogen-bond cutoff of 15 Å, were used. The dynamic simulations were run by using the MM3* force field. Charges were taken from the force field. The same degrees of freedom of the MC/EM searches were used in the MC/SD runs. All simulations were performed at 300 K, with a dynamic time step of 1 fs and a frictional coefficient of 0.1 ps^{-1}. Two runs of 10 ns each were performed by starting from the major conformations of the substrates, se-

lected from the MC/EM outputs. The Monte Carlo acceptance ratio was about 2%; each accepted MC step was followed by an SD step. Structures were sampled every 1 ps and saved for later evaluation. Monitoring of both energetic and geometrical parameters checked the convergence.

Molecular dynamics simulations and docking calculations: Docking of discodermolide and dictyostatin was performed by using the AutoDock 3.0 program.[42] During an AutoDock 3.0 simulation, multiple Lamarckian genetic algorithm runs occurred, with each one providing a predicted binding mode, and cluster analysis was performed at the end of the simulation. Atomic coordinates for the different conformers were obtained from molecular mechanics calculations (see above). The α/β-tubulin dimer coordinates (PDB code 1JFF)[43] were taken from the Protein Data Bank[44] and used as described.[35]

Grids of probe-atom interaction energies and electrostatic potentials were generated by the AutoGrid program present in the AutoDock 3.0 package. Grid spacings of 0.6 and 0.375 Å were used for the global and local searches, respectively. For each calculation, 1 job of 100 docking runs was performed by using a population of 200 individuals and an energy evaluation number of 3×10^6.

NMR experiments: NMR spectra were recorded at 298–313 K in D_2O on Bruker AVANCE 500 and 700 MHz spectrometers. For the experiments with the free ligands, the compounds were dissolved in D_2O and argon was passed through to degas the solution. TOCSY[45] and HSQC[46] experiments were performed by using the standard sequences. 2D transverse-ROESY (T-ROESY) experiments[47] were performed with mixing times of 300, 400, 500, and 600 ms. The 500 MHz NOESY[48] cross-peaks were basically zero at room temperature and moderately positive at 313 K. The strength of the 180° pulses during the T-ROESY spin-lock period was attenuated four times with respect to that of the 90° hard pulses (between 7.2 and 7.5 μs). To deduce the interproton distances, relaxation-matrix calculations were performed by using software written in house, which is available from the authors upon request.[49]

For the bound ligands, TR-NOE experiments were performed as previously described with a freshly prepared ligand/microtubule solution.[35] TR-NOESY experiments were then performed with mixing times of 50, 100, 200, 250, and 300 ms, for molar ratios of ligand/protein from 5:1 to 20:1. No purging spin-lock period to remove the NMR signals of the macromolecule background was employed, since they were basically not observable due to the huge size of the receptor. First, line broadening of the ligand protons was monitored after addition of the ligand. Strong negative NOE cross-peaks were observed, in contrast to the results for ligands in the free state; these cross-peaks indicated binding of both molecules to the microtubule preparation. The theoretical analysis of the TR-NOEs of the ligand protons was performed according to the CORCEMA program[50,51] by using a relaxation matrix with exchange, as previously described.[35] Different exchange-rate constants were employed to obtain the optimal match between the experimental and theoretical results of the intraresidue cross-peaks of the protons belonging to the *Z* double bonds of discodermolide (H8, H9) and dictyostatin (H10, H11), which have a relatively fixed geometry for any given protein/ligand ratio. The overall correlation time, τ_c, for the free state was always set to 0.35 ns, since NOESY cross-peaks for the free molecule were basically zero at room temperature and 500 MHz. The τ_c value for the bound state was set to 100 ns. To fit the experimental TR-NOE intensities, off-rate constants, k_{off}, between 50 and 500 s^{-1} were tested. Optimal agreement was achieved for $k_{off}=150\ s^{-1}$.

T-ROESY experiments were also carried out to exclude spin-diffusion effects. A continuous-wave spin-lock pulse was used during the 250 ms mixing time. Key NOEs were shown to be direct cross-peaks, since they showed different signs to the diagonal peaks.[52,53]

Results and Discussion

The conformation of free discodermolide in water solution: The conformational behavior of free discodermolide in the unbound state has been previously explored both in the solid state and in two different solvents, DMSO and acetonitrile.[33,34] The conclusions are strikingly different. Discodermolide in DMSO seems to be a very flexible molecule with over ten conformers contributing to the conformational equilibrium.[34] Curiously, the form observed by X-ray crystallography is claimed to represent less than 1% of the population in this solvent. By contrast, the major conformation deduced in acetonitrile solution,[33] which arises from minimization of $A^{1,3}$ strain and *syn*-pentane nonbonded interactions, was in good agreement with the solid-state conformation, except for the orientation of the δ-lactone. Subtle differences in the overall shape of the six-membered lactone ring were also evident in the three studies. In principle, two types of conformers were proposed: the chair conformer with two axially and equatorially oriented substituents, somewhat distorted towards a $^3H_4$ half-chair form (in acetonitrile, in the solid state, and partially in DMSO), or a $^3S_1$ skew-boat form. The different possibilities, along with their structural features, are given in Tables 1 and 2, and Table S3 and Figures S1, and S11 in the Supporting Information.

In this work, the conformation of discodermolide in water solution (D_2O) was explored. The 500 MHz NOESY cross-peaks were basically zero at room temperature and moderately positive at 313 K. Thus, T-ROESY experiments were used to access the key conformational information. A complete assignment of the ^1H NMR resonance signals of discodermolide was achieved on the basis of TOCSY, HSQC, and T-ROESY experiments. The difference in chemical shifts and coupling constants (Figure S11 in the Supporting Information) between the reported data in acetonitrile and those measured in water are given in Table S1 in the Supporting Information. Some noticeable differences are observed for the chemical shifts, which are similar for the H12 to H16 region, including the corresponding methyl groups, and rather different for the other parts of the molecule, especially for the lactone moiety and from C17 to the C24 tail.

The analysis of the vicinal proton–proton coupling constants for the six-membered ring permitted its conformation to be assessed. Generally speaking, no major changes were deduced for the coupling constants between the available dimethylsulfoxide and acetonitrile values and those recorded in water. A clear difference is only observed for the $^3J_{H4,H5}$ coupling between water and DMSO on the one hand and acetonitrile on the other, but this is likely to be a typographic mistake in the latter publication.

To assess the conformational distribution in water, the *J* data were complemented by NOE experiments. The relationship between NOE signals and proton–proton distances is well established and can be worked out at least semiquantitatively by using a full relaxation-matrix approach.[54] The NOE intensities reflect the conformer populations, and therefore information on the population distributions in free solution can be obtained by focusing on the key NOEs that characterize the different possible conformations.

At 500 MHz and room temperature, all of the cross-peaks observed in the NOE spectra of discodermolide in water so-

Table 1. Analysis of the estimated interproton distances for discodermolide in the free and tubulin-bound states. For the bound state, the experimental distances, r [Å], are estimated according to a full matrix-relaxation approach from a CORCEMA-based[46] analysis of the TR-NOESY data. The H8–H9 and H21–H22 distances (2.2 Å) were taken as internal references. The estimated experimental errors are considered to be around ±10%. The reported data for the free state in acetonitrile[31] or dimethylsulfoxide[32] are also given. The best fits between our data in the free state and those reported in references [31] or [32] are underlined. Key NOEs that further support this conclusion are in bold.

Proton pair	Predicted for the major conformer in the skew form (MM3*)	Predicted for the major conformer in the half-chair form (MM3*)	Reported for the free state in CD_3CN[a]	Reported for the free state in DMSO[b]	From the experiment: T-ROESY build up curve for the free state (error: ±10%)	From the experiment: NOESY build up curve for the bound state (error: ±10%)
H2–H3	2.9	2.6	2.6	–	2.8	2.6
H2–H5	2.8	4.1	4.1	2.6	3.4	>3.7
H3–H4	2.4	2.4	2.5	2.3	2.5	2.5
H3–$CH_3$25	2.5	2.4	3.0	3.1	2.4	2.4
H3–$CH_3$26	2.7	2.0	3.1	3.1	2.5	2.2
H4–H18	2.8	2.8	–	–	2.8	2.8
H4–$CH_3$25	3.7	2.4	2.8	–	2.8	2.5
H5–H7	3.1	3.1	3.2	3.4	overlap	overlap
H5–$CH_3$26	2.7	2.5	3.1	3.1	2.6	2.5
H6R–H8	3.0	3.0	3.1	–	2.7	3.1
H6R–H15	2.1	2.3	–	–	2.3	2.3
H6S–$CH_3$26	2.3	2.2	2.7	--	2.2	2.2
H7–H9	3.7	3.6	**3.8**	2.4	not observed	not observed
H7–H10	2.1	2.2	2.1	2.2	2.0	2.3
H7–$CH_3$27	3.0	2.8	3.2	3.4	2.8	2.9
H8–H12	4.0	3.6	**4.2**	2.9	not observed	not observed
H8–H22	2.9	2.7	–	–	2.7	2.8
H9–H11	3.7	3.6	**3.8**	2.7	not observed	not observed
H9–H12	2.8	2.8	2.9	2.8	2.6	2.9
H10–H11	2.5	2.3	2.5	–	2.3	2.4
H10–H13	2.8	2.9	3.0	2.8	2.8	2.9
H10–$CH_3$27	2.5	2.4	2.9	–	2.4	2.4
H11–H12	3.1	2.9	3.1	3.0	3.1	3.0
H11–H13	2.5	2.4	2.4	2.4	2.3	2.5
H11–$CH_3$27	2.5	2.4	3.0	3.0	2.4	2.4
H11–$CH_3$28	2.6	2.6	3.2	3.1	2.5	2.5
H12–H15R	2.0	2.1	2.0	2.2	2.0	2.1
H12–$CH_3$30	3.4	3.3	**3.7**	4.3	**3.2**	3.2
H13–$CH_3$28	2.8	2.7	3.2	3.1	2.6	2.6
H15B–$CH_3$31	2.7	2.7	3.2	–	2.6	2.6
H16–$CH_3$29	2.4	2.3	–	–	2.2	2.4
H16–$CH_3$31	2.2	2.2	–	–	2.0	2.3
H17–H18	2.5	2.3	2.5	2.3	2.4	2.4
H17–H19	3.1	2.9	3.1	2.9	3.0	3.0
H17–H20	2.1	2.1	2.1	–	2.1	2.3
H17–H23	2.4	2.5	2.5	2.5	2.5	2.6
H17–$CH_3$30	2.5	2.5	3.0	2.6	2.5	2.5
H18–H21	2.9	2.9	2.7	2.6	2.8	3.0
H18–H20	3.1	3.1	–	–	3.0	3.1
H18–H19	3.1	2.9	3.1	–	2.9	2.8
H18–H21	2.9	2.9	–	–	2.9	2.9
H19–H20	2.5	2.4	2.4	–	2.4	2.4
H19–H21	3.8	3.7	–	3.0	not observed	not observed
H19–$CH_3$31	2.6	2.6	**2.6**	3.1	**2.6**	2.6
H19–$CH_3$32	2.5	2.5	**2.5**	2.9	**2.5**	2.5
H20–H21	3.1	3.1	–	–	3.1	3.1
H20–H23	2.1	2.1	2.1	2.2	2.1	2.2
H21–$CH_3$32	2.6	2.6	3.3	3.0	2.6	2.5
H22–H24	2.5	2.5	2.5	2.2	2.4	2.5

[a] See reference [31]. [b] See reference [32].

lution were very weak, almost close to zero. The $\omega\tau_c$ value is close to 1.1 and provides an almost zero longitudinal NOE.[54] Thus, the basic information was derived from T-ROESY experiments,[47] which provided the crucial cross-peaks that are reported in Table 1. The spectrum is shown in Figure S2 in the Supporting Information. By comparing these NOE parameters, it could be deduced (see Table 1) that the observed values in water are more similar to those available in acetonitrile than to those reported in DMSO.

Table 2. Comparison between the experimental values of *J* couplings in water solution (this work) and those reported for discodermolide in dimethylsulfoxide and acetonitrile solutions.[31,32] The two values between brackets in the *J* exp water column correspond to the expected values for the skew-boat and chair conformers, respectively. The couplings for the six-membered ring are in agreement with a percentage of skew boat of around 60–75%. The couplings for the lateral chains are in agreement with a major conformation for most of the linkages (see percentages). For each linkage, the major conformer is given.

Torsion angle	*J* exp DMSO[a]	*J* exp MeCN[b]	*J* exp H_2O (this work)	Estimated chair/skewboat equilibrium	Estimated % of a major conformer around the corresponding linkage
H2–H3	not reported	4.2	3.6 (1.2, 5.2)	40:60	
H3–H4	not reported	4.2	3.5 (1.2, 4.2)	25:75	
H4–H5	10	2* (typographic mistake)	10.1 (10.7, 10.2)		
H5–H6*S*	<1	<1	1.8		>90
H5–H6*R*	10	10.0	9.5		>80 (*anti* type)
H6*S*–H7	9.5	10.8	9.9		>85 (*anti* type)
H6*R*–H7	<1	2.4	1.8		>90
H7–H8	9.5	9.1	9.0		>80 (*anti* type)
H9–H10	10	10.1	10.5		>95 (*anti* type)
H10–H11	2.2	not given	2.4		>85 (*syn* type)
H11–H12	8.8	6.6	9.8		>90 (*anti* type)
H12–H13	10	10.0	10.1		>95 (*anti* type)
H16–H17	7.8	6.2	7.3		>60 (equilibrium)
H17–H18	2.3	3.5	2.8		>80 (*syn* type)
H18–H19	9.1	8.0	9.5		>90 (*anti* type)
H19–H20	2.8	4.1	3.4		>80 (*syn* type)
H20–H21	10	10.6	10.7		>95 (*anti* type)
H22–H23	not reported	10.7	11.3		>95 (*anti* type)

[a] See reference [32]. [b] See reference [31].

The conformation of the six-membered lactone ring was first addressed. The coupling constants (Table 2a) are in between those expected for the half chair and the skew boat.

With regard to the NOE values (Table 1), the key H2–H3 NOE (corresponding distance 2.8 Å) is always (at all mixing times) significantly weaker than the H3–H4 NOE (2.5 Å). This fact, together with the observation of a weak H2–H5 cross-peak, is in agreement with the presence of a certain population of the skew-boat form (Table 1). The stronger H3–$CH_3$25 NOE (medium, 2.4 Å) with respect to that of H3–$CH_3$26 (medium, 2.5 Å) also supports the existence of an equilibrium between the $^3S_1$ skew-boat form and the half-chair conformer. The energy difference between both forms is indeed small (less than 2 kcal mol^{-1}) according to MM3* calculations, and this supports the existence of both geometries in solution.

For the rest of the molecule, close inspection of the *J* values indicates the presence of conformational averaging, especially around C16–C17 ($J_{H16,H17}$ = 7.3 Hz). No *J* information is available for the C14–C15 fragment. For most of the C–C linkages, the vicinal H–H couplings are either equal or larger than 9 Hz or smaller than 3.5 Hz, thereby indicating the presence of a major geometry around the different linkages (>85%), especially around C9–C10, C12–C13, C20–C21, and C22–C23 (*J* = 10 Hz or larger, with more than 90% for a given geometry). Values of around 9.0–9.8 Hz are observed for the C5–C6, C6–C7, C7–C8, C11–C12, and C18–C19 bonds. Therefore, a major conformation is also present for these linkages (80–90%), although minor contributions from alternative orientations are possibly taking place. Different geometries for rotation around these linkages are given in the Supporting Information.

Nevertheless, the global minimum found in the MM3* calculations provides the best fit between the expected and observed NMR spectroscopic data. This conformation, with skew-boat geometry for the lactone ring, is depicted in Figure 1. Additional possible conformations found around the C11–C12, C16–C17, and C18–C19 linkages are depicted in Figure S3 in the Supporting Information.

There are several NOEs that define the topology of the chain. As mentioned before, no couplings are available for the C14–C15 linkage. However, the H12–H15R and the $CH_3$28–$CH_3$30 NOEs are sensitive to the corresponding C12–C13, C14–C15, and C15–C16

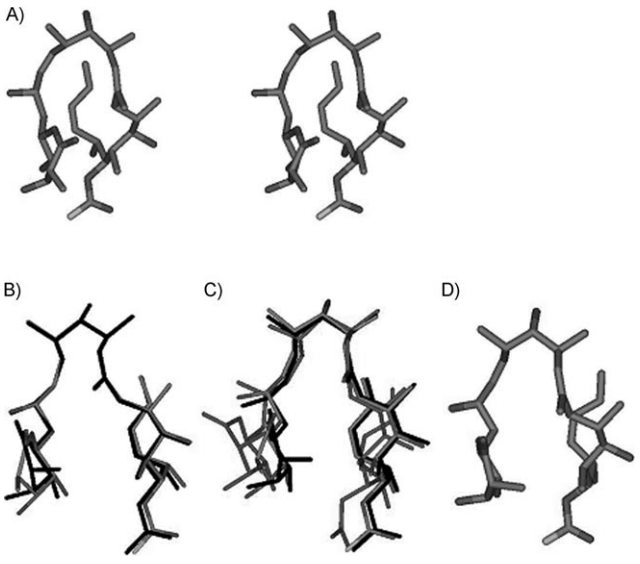

Figure 1. Conformation analysis of discodermolide. A) Stereoscopic view of the global minimum of DDM in water solution. B) Superimposition of the half-chair and skew-boat conformers of discodermolide showing the major conformer around the C5–C24 chain. C) Superimposition of these two forms with that deduced by Carlomagno and co-workers for DDM bound to soluble tubulin.[31] Some differences in the orientation and shape of the six-membered ring can be appreciated. D) The bound conformer to assembled microtubules, as deduced by TR-NOESY experiments (see text).

torsions. The average experimental H12–H15R distance is 2.1 Å, whereas the $CH_3$28–$CH_3$30 distance is around 2.6 Å; these results indicate a very major conformation (close to the MM3* global minimum) in this region. Moreover, the H4–$CH_3$31 (2.8 Å) and H8–H22 NOEs (2.7 Å) indicate a major orientation between the six-membered ring and the C13–C19 side chain and between the C5–C13 and C19–C22 side chains, respectively, in agreement with the predicted MM3* global minimum (Figure S9 in the Supporting Information). Nevertheless, some of the expected NOEs for short to moderate distances are missing, thereby indicating the presence of conformational averaging. With all of these *J* and NOE data simultaneously observed, it can be safely assumed that, although there is a major global conformation in water solution, there is conformational heterogeneity especially at the lactone moiety and at the C16–C17 linkage. The fact that there is conformational mobility is evident by the lack of the H21–$CH_3$26 NOE, which is at a relatively short distance for both the skew (2.6 Å) and the chair (2.9 Å) forms, and of the H12–H24 NOE (at a moderate distance of 3.1–3.2 Å). Nevertheless, the conformational rigidity of discodermolide in water is significantly higher than in the organic solvents previously studied.[33,34] The hairpinlike shape of the molecule in its major conformation (Figure S9 in the Supporting Information) makes possible the presentation of all of its polar groups at the periphery, thus favoring their interaction with the solvent molecules and minimizing the lipophilic surface for interaction with water.

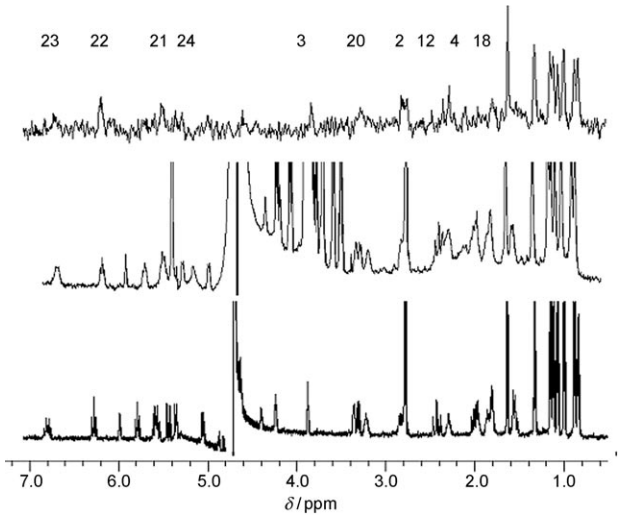

Figure 2. ^{1}H NMR spectra (500 MHz) of DDM in water solution with different experimental conditions at 298 K. Bottom trace: DDM in the free state. Middle trace: DDM in the presence of microtubules (D_2O, 298 K), with a DDM/tubulin molar ratio of 20:1. The large signals of the nucleotide employed to stabilize the microtubules are evident. Top trace: STD spectrum (saturation time: 2 s) of DDM in the presence of microtubules, with a DDM/tubulin molar ratio of 20:1. Apart from the methyl groups, which show clear intensities, the most significant STD signals are marked with the number of the corresponding proton resonances. The signals of the nucleotide do not appear in the STD spectrum (huge nucleotide/tubulin ratio).

NMR TR-NOESY studies of discodermolide and dictyostatin in the presence of microtubules

Discodermolide: The key point in trying to understand the properties of DDM is to deduce the bioactive conformation bound to microtubules.[55] As previously shown, for ligands that are not bound tightly and that exchange between the free and bound states at a reasonably fast rate, the transferred nuclear Overhauser enhancement spectroscopy experiment (TR-NOESY) provides an adequate means to determine the conformation of the bound ligand.[35,56] As previously described,[35] and to work with biochemical conditions in which microtubules are stable, native tubulin was assembled with GMPCPP (see reference [35] and also the Experimental Section).

The addition of the microtubule solution to an NMR tube containing discodermolide induced broadening of the resonance signals in the ^{1}H NMR spectrum, which indicates that binding occurs (Figure 2).

TR-NOESY experiments (Figure 3 and Figures S4 and S7 in the Supporting Information) were then performed on the ligand/microtubule sample at different mixing times. Negative cross-peaks were clearly observed at 303 K, as expected for ligand binding and in contrast with the observations for the free ligand, for which no NOEs were observed (zero crossing in the NOE curve).

For the 10:1 to 20:1 ligand/protein molar ratios employed, obviously the coupling constants are basically defined by the couplings in the free state, thus the bound geometry has to be defined by the TR-NOE data. The observed NOE data for the bound state are very similar to those described above for discodermolide in water. Now, however, the NOE data are in agreement with a half-chair conformation for the

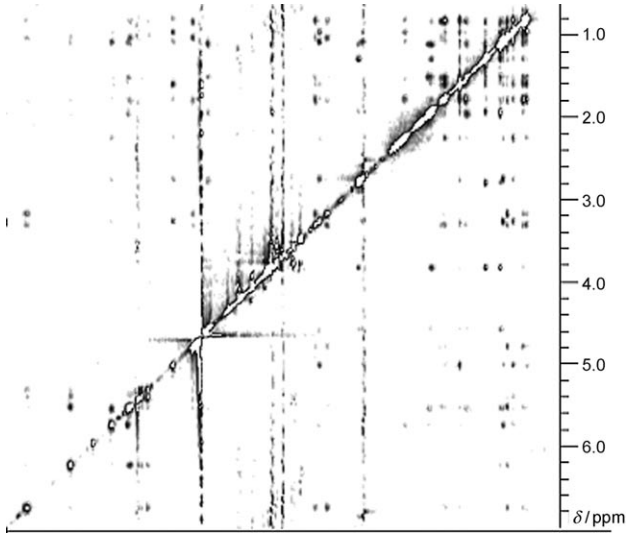

Figure 3. TR-NOESY spectrum (mixing time: 100 ms) of discodermolide (DDM) in the presence of microtubules (D_2O, 298 K), with a tubulin/DDM molar ratio of 20:1. Negative cross-peaks are observed, which indicates that the bioactive conformation can be extracted from the quantitative analysis of these peaks.

six-membered ring orientation, due to the weakness of the H2–H5 cross-peak, as well as the relative changes in the intensities of the key NOEs from the $CH_3$25 and $CH_3$26 signals. Thus, there is a conformational selection process regarding the shape of the six-membered ring. Nevertheless, despite this conformational selection for the lactone ring, the orientation of the six-membered ring moiety relative to the backbone is almost identical to that observed in the free state, as shown by the key short contacts mentioned above (Table 1). Also, the analysis of the TR-NOESY cross-peaks, by using a full relaxation-matrix approach, with the help of the CORCEMA program, permitted us to deduce that the relative orientation of the C5–C24 hydrocarbon chain remains basically unaltered upon binding.

T-ROESY experiments allowed the exclusion of spin-diffusion effects for the key cross-peaks. Thus, the observed pattern is that expected for a conformer with no significant distortion by the microtubules in the area of C5–C24 from the global shape of the major conformer deduced in water. On the other hand, the observed cross-peaks are in agreement with the existence of a conformational selection process for the lactone. Therefore, while distinct flexibility appears for the different torsional degrees of freedom of discodermolide in acetonitrile or dimethylsulfoxide,[33,34] the orientation of the C5–C24 chain is highly preorganized in water solution with respect to that bound by tubulin, probably to minimize entropic penalties. A preorganized conformation of discodermolide in water solution is supported by a favorable entropy change upon its binding to microtubules of 80 $J\,mol^{-1}\,K^{-1}$, which is reduced to 10 $J\,mol^{-1}\,K^{-1}$ in DCT (see below) and which changes sign for other MSAs (taxanes and epothilones).[18] Views of the polar and nonpolar surfaces of the major conformer are shown in Figure 4.

There are some slight changes in the deduced bound conformation with respect to that described by Carlomagno and co-workers with unassembled tubulin.[31] A superimposition is shown in Figure 1. Although the structure provided by Carlomagno and co-workers[31] shows a chair for the six-membered ring and its orientation is somewhat different with respect to the rest of the chain, the presentation of the molecule is remarkably similar, despite the change in the mode of preparation of tubulin in both cases.

Further insights into the mode of binding of DDM were deduced from saturation transfer difference (STD) experiments.[57] First, the interaction was demonstrated to be specific by using competitive STD experiments.[58] Thus, baccatin, the core skeleton of paclitaxel and docetaxel, was employed as a model ligand. Baccatin binds to microtubules and competes with paclitaxel, although with 100-times-lower affinity ($1.5\times10^5\,M^{-1}$ for Baccatin III as compared with $3.7\times10^7\,M^{-1}$ for paclitaxel). Clear STD (Figure 5) and TR-NOE signals were obtained for baccatin when it was added to a solution containing microtubules. The STD (Figure 5) and TR-NOE signals (data not shown) were completely removed from the corresponding spectra when discodermolide or dictyostatin were added to the same NMR tube, thus indicating that these compounds compete for the taxane-binding site in microtubules, as already described, and both have a much higher affinity than baccatin III.

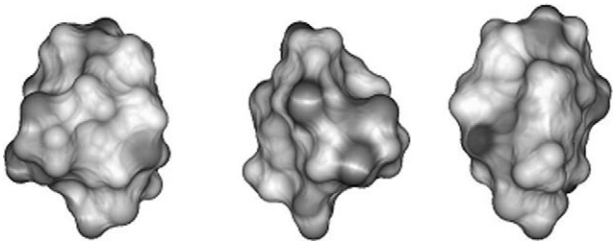

Figure 4. Different perspectives of the representation of the polar and nonpolar areas of the conformer of discodermolide bound by microtubules. This conformer seems to have a well-defined patch of polar and nonpolar areas.

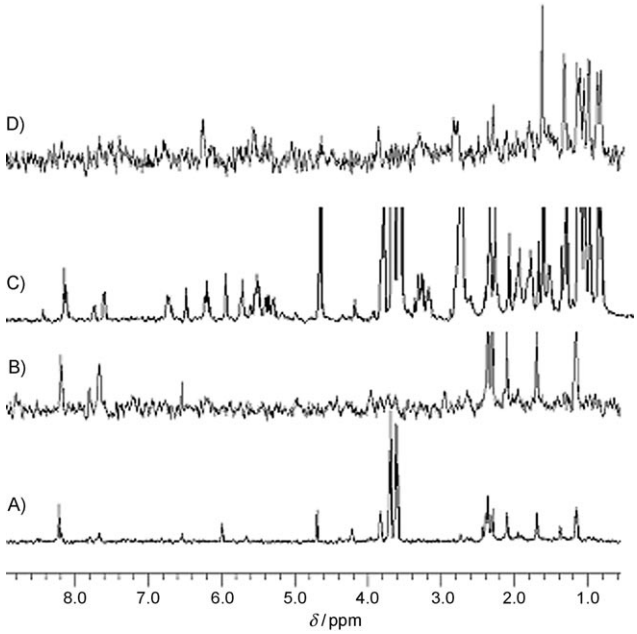

Figure 5. A) ^{1}H NMR (500 MHz) spectrum of baccatin in the presence of microtubules (D_2O, 298 K), with a baccatin/tubulin molar ratio of 15:1. B) STD spectrum of this sample. The signals of baccatin are evident. C) ^{1}H NMR spectrum of DDM and baccatin in the presence of microtubules (D_2O, 298 K), with a baccatin/DDM/tubulin molar ratio of 10:10:1. D) STD spectrum (saturation time: 2 s) of this last sample. The STD spectrum corresponds to that observed for DDM (Figure 2). Thus, the signals of baccatin are removed, which indicates competitive binding. Similar effects were observed when dictyostatin was added to the NMR tube containing baccatin.

Moreover, when the amount of DDM or DCT was increased, the TR-NOE spectra depicted in Figure 3 and in Figure S4 in the Supporting Information were again obtained, as well as the corresponding STD spectra for these molecules (Figure 5).

STD experiments were performed on the same TR-NOESY samples mentioned above. Although the beneficial accumulation effect of STD experiments in terms of the signal/noise ratio makes preferable the use of high ligand/receptor ratios, the limited solubility of both DDM and DCT

in water solution only permitted the use of the 10:1 or 20:1 molar ratio samples described above. The corresponding STD spectrum for DDM is shown in Figure 2. For discodermolide, the STD spectrum provided clear enhancements for the methyl groups at the periphery of the backbone, and for certain signals, especially those belonging to the lactone ring (H2–H4), H12, and the C18–C24 portion of the chain. Notably, H2 and H22 gave the most significant STD enhancements. The STD pattern was semiquantitatively explained by means of the CORCEMA-STD[50,51] program by using the docked structure of DDM in the tubulin-binding site (see below). A fair agreement was obtained between the experimental and modeled STD data, with an *R* factor of 0.14, more than reasonable for this molecular system.

Dictyostatin: As mentioned in the introduction, dictyostatin is a microtubule-stabilizing macrolide that is structurally related to discodermolide. Indeed, the configurations of the stereocenters of both molecules are remarkably homologous and consistent with a common biogenesis.[25] The conformational behavior of this molecule has been elucidated in methanol solution by using NMR spectroscopy and molecular mechanics calculations.[25] This analysis indicated the presence of an equilibrium between two major forms (Figure 6), the s-*trans* (major) and the s-*cis* (minor) forms, which basically differ in the conformation around C1–C2. The characteristic torsion angles for both forms are given in Table S3 in the Supporting Information, whereas the corresponding short distances, which can be correlated with experimental NOEs, are gathered in Table 3. The observed *J* couplings in methanol[25] were basically identical to those deduced in water solution (see Figure S5 in the Supporting Information) and, thus, indicate a similar conformational behavior in both polar solvents (see Table S2 and Figure S10 in the Supporting Information).

The bioactive conformation of DCT bound to microtubules was deduced by using TR-NOESY experiments and by following the protocol described above for DDM (see Figures S6 and S8 in the Supporting Information). Also in this case, strong negative cross-peaks were observed at 303 K, as expected for ligand binding (Figure 7). For DCT,

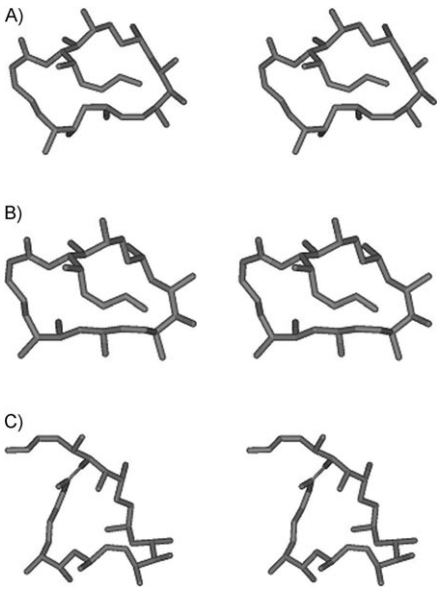

Figure 6. Conformation analysis of dictyostatin. A) Stereoscopic view of the s-*trans* global minimum. B) Stereoscopic view of the bound conformer. C) Stereoscopic view of the s-*cis* local minimum.

Table 3. Analysis of the estimated interproton distances for dictyostatin in the microtubule-bound state. The experimental distances, *r* [Å] (± 10%), are estimated according to a full matrix-relaxation approach from a CORCEMA-based analysis of the TR-NOESY data. The H10–H11 and H21–H22 distances were taken as internal references. The reported data for the free-state conformations (regular s-*trans* and s-*cis* conformers) are also given. The best-fit conformer is a secondary minimum (approximately 4.5 Kcal mol^{-1}) deduced from the MM3* calculations for dictyostatin. This minimum displays an s-*trans* geometry. Also, it is necessary to consider different rotamers around C20–C21 to quantitatively explain all of the NOEs involving the lateral chain. The data supporting these conclusions are in bold.

Proton pair	Global minimum of s-*trans* [Å]	Local minimum of s-*cis* [Å] C22−C26	Bound conformer [Å] of C22−C26[a]	Distance from experiment [Å] (error: ±10%)
H2–H3	2.4	2.4	2.3	2.3
H2–H4	3.9	3.9	3.9	**>3.5**
H3–H4	3.1	3.1	3.1	3.1
H3–H5	2.6	2.5	2.5	2.5
H4–H5	3.1	3.1	3.1	3.1
H4–H6	2.3	2.3	2.4	2.4
H4–H8b	3.4	2.8	3.1	3.2
H4–H23	**2.4**	**8.4, 3.0, 6.6**	2.6**, 4.2, 7.8**	**>3.5**
H4–Me20	3.1	3.5	3.6	2.9
H4–Me22	**2.8**	**6.7, 6.1, 3.2**	**3.8, 2.6,** 7.0	**3.4**
H5–H6	3.1	3.1	3.1	3.1
H5–H7	3.7	3.9	3.8	3.5
H5–H8a	2.9	3.2	3.7	3.4
H6–H7	2.4	2.4	2.6	2.5
H6–H8b	2.5	2.5	2.8	2.7
H7–H10	**2.3**	**4.6**	**4.4**	**>3.5**
H8b–H10	2.5	2.7	2.7	2.7
H8b–H24	**2.7**	**8.0, 4.5, 8.7**	**3.1, 6.0, 7.0**	**3.5**
H10–H11	2.3	2.3	2.3	2.3
H10–H24	**2.6**	**8.9, 5.1, 8.0**	**2.3, 4.7, 7.0**	**>3.5**
H11–H13	3.8	3.8	3.8	3.5
H11–H14	**3.1**	**2.5**	**2.5**	**2.6**
H12–H13	2.5	2.4	2.4	**2.5**
H12–H15a	2.1	2.3	2.1	2.3
H17b–H20	**2.3**	**4.7**	**3.1**	**3.4**
H19–H20	2.5	2.3	2.4	2.4
H19–H21	3.3	3.6	3.2	3.3
H19–H22	2.1	5.0, 4.9, 5.6	2.2, 3.9, 3.0	2.4
H19–H25	**2.4**	**7.1, 6.6, 7.5**	**2.5, 5.0, 5.0**	**2.8**
H20–H21	3.0	2.3	3.1	2.6
H20–H23	3.1	4.6, 4.0, 5.4	**3.0**, 5.3, 4.8	3.2
H21–H22	2.4	3.1, 2.5, 2.5	3.1, 2.5, 2.5	2.7
H21–H23	2.9	2.5, 3.7, 2.9	3.8, 4.4, 2.6	2.8
H22–H24	3.8	3.8	3.8	>3.5
H22–H25	2.1	2.1	2.1	2.1
H24–H25	3.2	3.2	3.2	3.2
H24–H26a	3.8	3.8	3.8	>3.5
H24–H26b	2.5	2.5	2.5	2.4

[a] Rotamers: H21/H22 171, −60, 60.

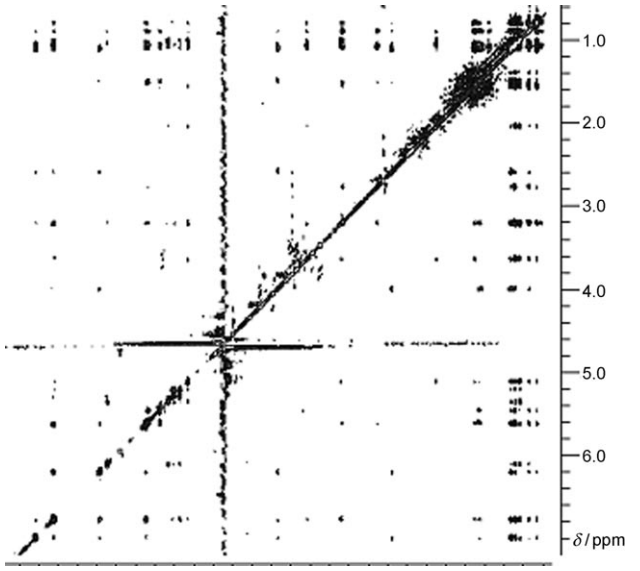

Figure 7. TR-NOESY spectrum (mixing time: 100 ms) of dictyostatin in the presence of microtubules (D_2O, 298 K), from which the bioactive conformation of the macrocycle is deduced. Other experiments were recorded with mixing times of 50, 150, and 200 ms.

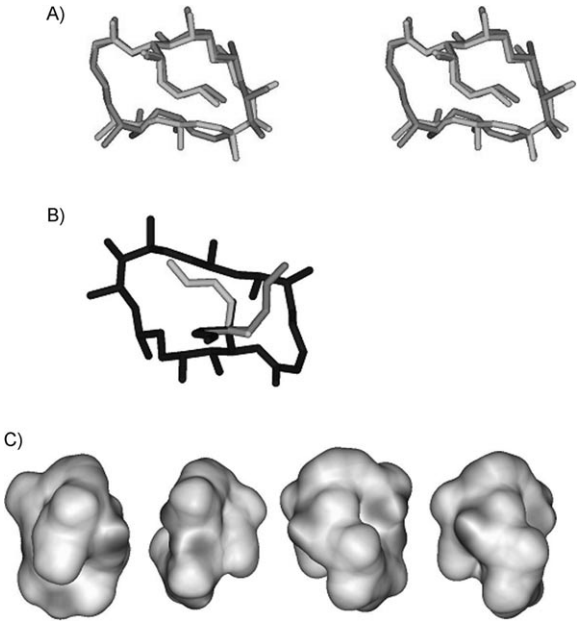

Figure 8. Conformation analysis of dictyostatin when bound to microtubules. A) Stereoscopic view of the superimposition of the major conformer found in free solution (light print) with that bound (dark print) to microtubules. The major changes affect the C8–C9 torsion angle and the corresponding adjustments. B) Superimposition of the three possible rotamers around the lateral C21–C22 linkage. C) Different perspectives of the polar and nonpolar patches of the bound conformer of dictyostatin.

no NOEs were observed in the free state (zero crossing in the NOE curve).

The observed TR-NOE cross-peaks (Figure 7 and Table 3, and Figure S8 in the Supporting Information) were translated into distances with the assistance of the CORCEMA program[50] by using the two more stable s-*cis* and s-*trans* geometries. Upon comparison of the experimental and expected values for both conformers, in this case, and contrary to the observations for DDM, no simultaneous fitting of all the NOE data could be obtained by using either individual conformer. For instance, the estimated experimental long distances for the H7–H10 and H17–H20 proton pairs (lack of these key NOEs, bold in Table 3), which are at very short distances in the regular s-*trans* geometry, together with the observation of relatively short distances for the H11–H14 and H4–$CH_3$20 pairs, clearly indicate that the global minimum, the s-*trans* form, is not bound to the microtubules (Table 3).

On the other hand, the s-*cis* geometry also fails to describe some of the observed NOEs, especially those involving the C22–C26 tail. A rotation around the C21–C22 bond, maintaining the *s-cis* form, still does not permit an explanation of the above-mentioned experimental NOEs, which are underlined in Table 3.

Thus, there is a significant conformational change in the DCT conformation upon binding to microtubules. By using the MM3*-based calculated secondary minima for DCT, the best agreement was found when a third local minimum was considered (see Table 3). This conformer displays similar torsion angles to the s-*trans* form but shows a major torsional change around the C8–C9 linkage, and minor adjustments around the entire skeleton (Figure 8). According to the MM3* calculations, the energy difference between the s-*trans* conformer and this conformer amounts to 4.7 kcal mol^{-1}. In addition, to fit the NOEs for the lateral diene chain, consideration of an equilibrium between at least two (probably three) rotamers around C21–C22 should be considered (Figure 8). Thus, now, it is possible to fit almost quantitatively all of the observed NOEs. Hence, there is a conformational variation process regarding the shape of the macrolide ring. Therefore, whereas DDM seems to show a preorganized conformation in water solution to interact with microtubules, this is not the case for DCT. Views of the polar and nonpolar surfaces of the bound DCT conformer are also shown in Figure 8.

The bound conformer of DCT resembles that of bound DDM (Figure 9). In fact, they display similar polar and nonpolar surfaces that allow them to interact with the corresponding receptor. Modification of the orientation of the lateral diene chain of DCT does not substantially modify the good match between both molecules.

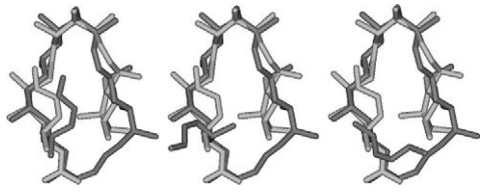

Figure 9. Superimposition of the bound conformer of discodermolide (light print) with the three possible rotamers around the lateral C21–C22 linkage of the bound conformer of dictyostatin (dark print). The degree of adjustment is more than satisfactory.

STD experiments were also performed on the sample of DCT in the presence of assembled microtubules (Figure 10). The experiment indicated the existence of ligand binding to the microtubules, with most of the ^{1}H NMR spectroscopic signals providing clear STD enhancements, although with different intensities. The obtained enhancements and the bound conformation docked into tubulin (see below) were considered for the simulation of the STD data with the CORCEMA-STD program. A satisfactory match between the experimental and observed data was obtained, thus providing further evidence for the goodness of the TR-NOESY/STD-docking approach employed herein (see below).

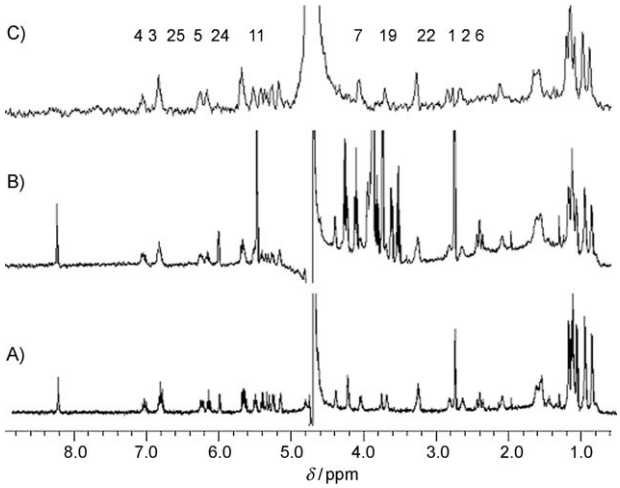

Figure 10. A) ^{1}H NMR (500 MHz) spectrum of free dictyostatin (D_2O, 298 K), with a baccatin/tubulin molar ratio of 15:1. B) ^{1}H NMR spectrum of dictyostatin in the presence of microtubules (D_2O, 298 K), with a molar ratio of 20:1. C) STD spectrum (saturation time: 2 s) of this last sample. Clear enhancements are observed for most of the dictyostatin signals, whereas those of the nucleotide employed for stabilizing the microtubules are not observed (huge nucleotide/tubulin molar ratio).

The interactions of DDM and DCT with tubulin as revealed by the docking procedure: As mentioned above, the experimentally derived NMR conformation of DDM was docked onto β-tubulin[43] (PDB code: 1JFF) as already described[35] and as explained in the Experimental Section, by using the AUTODOCK program.[42]

However, it has to be noted that two binding sites have been described for taxanes, the final luminal binding site, which has been experimentally proved for paclitaxel and epothilone, and an external transient binding site of unknown structure, that has been experimentally proved for cyclostreptin. Since it is not proved that dictyostatin and discodermolide reach the final internal luminal site, they might compete with paclitaxel by just binding to the free external site. Thus, the docking results have to be taken with caution. Indeed, the determined bound conformation is very similar to that described by Carlomagno and co-workers[31] with tubulin in a nonmicrotubule form, for which the luminal site might not be fully present or structured.

First, a global search for binding sites in the α/β-tubulin dimer was carried out, with a grid spacing of 0.6 Å. Because all of the binding modes obtained in this calculation were located at the region of β-tubulin that faces inside the microtubule, the second step involved a local search for the β-tubulin monomer, with a grid spacing of 0.375 Å.

The local docking for β-tubulin suggested that there is a preferred DDM-binding region within this monomer, since most of the 100 structures could be gathered in the lowest energy cluster. In fact, this binding site corresponds to the taxane-binding site[59] involving the α helices 6 and 7 and the β strands 8–10 with their corresponding loops (Figure 11). This model predicts no evident contacts with either helix 1 or 5.

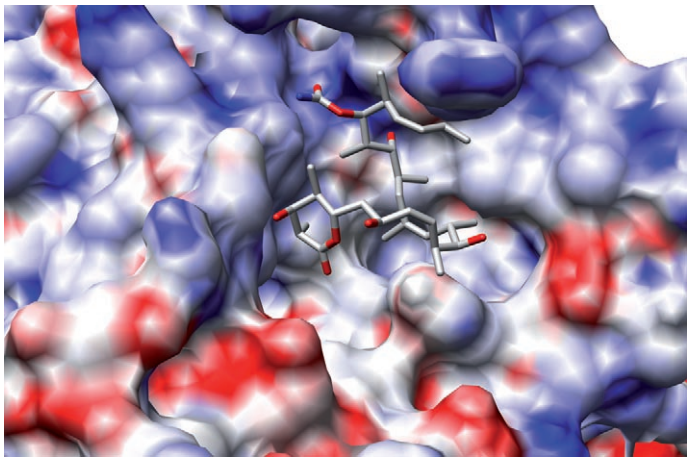

Figure 11. The interaction of DDM with β-tubulin, as deduced by AUTODOCK. The NMR-derived bound conformation of DDM was used with the refined coordinates of tubulin from PDB file 1JFF. The binding site perfectly correlates with the taxane-binding site. The charges at the protein surface were estimated by using Poisson–Boltzmann electrostatic calculations with the PDB2PQR program.[62,63]

There are a variety of nonpolar intermolecular contacts between DDM and tubulin. According to this binding mode, there are polar contacts of the ligand with His229 (helix 7), several residues at the M loop (Pro274, Thr276, Ser277, and Gln282), and Gly370. His229 is a key residue in the middle of helix 7. Stabilizing van der Waals interactions (within 5 Å of DDM) are also found, especially with Leu217, Leu275, Pro360, and Leu371 (the coordinates of the modeled DDM–tubulin complex are available from the authors upon request). It has been reported[31,60] that, in contrast to paclitaxel, DDM conserves full activity on cell lines presenting the F270V and A364T mutations. Indeed, no major contacts are found between DDM and these residues in our complex.

It is possible to speculate how this MSA exerts its function. Interestingly, in our model, DDM (and DCT, see below) directly contacts with the M loop. This M loop has been shown to be a key element of the lateral interactions

between microtubule protofilaments.[59,60] This evidence suggests the possibility that DDM stabilizes microtubules by stabilizing lateral contacts between protofilaments, as has been previously proposed for taxol.

The docking analysis was also performed for DCT by following the same methodology described for DDM. Indeed, an identical binding site was also deduced, which can fit the deduced NMR-bound conformer of DCT and that of DDM (Figure 12). DCT interacts with polar contacts again with

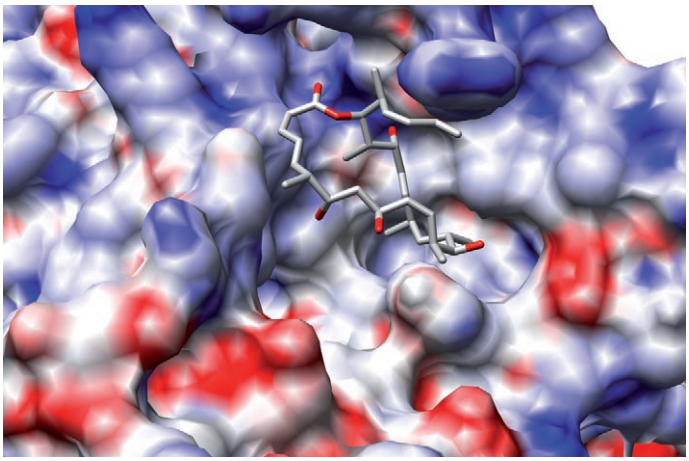

Figure 12. The interaction of DCT with β-tubulin, as deduced by AUTODOCK. The NMR-derived bound conformation of DCT was used with the refined coordinates of tubulin from PDB file 1JFF. The binding site perfectly correlates with the taxane-binding site. The charges at the protein surface were estimated by using Poisson–Boltzmann electrostatic calculations with the PDB2PQR program.[62,63]

His229, Pro274 (at the M loop), Thr276, Arg278, Gln282, and Gly370. For this macrocyclic molecule, which has a larger hydrophobic chain than DDM, a higher number of van der Waals interactions take place, namely with Leu217, Leu219, Leu230, Ala233 at helix 7, Leu275, and Leu371, with those residues providing the more important nonpolar contacts (within 5 Å of DCT). Thus, for both DDM and DCT, the two independently NMR-derived conformations for the assembled microtubule-bound state perfectly fit within the same binding site, as can be observed in Figure S12 in the Supporting Information. The intermolecular contacts observed for DCT with tubulin were indeed very similar to those described above for DDM, as can be observed from the superimposition of both molecules at the binding site.

Nevertheless, despite the fact that according to the combination of experimental and AUTODOCK data, both molecules target the taxane-binding site, the paclitaxel-binding pocket is not completely occupied by DDM or DCT. Superpositions of the three bound ligands are presented in Figure 13 and in the graphical abstract; these show that DDM and DCT roughly overlap the taxane skeleton but do not make the additional contacts provided by the docetaxel side chain, specifically with helix 1 and the other side of

Figure 13. Superimposition of the NMR-derived bound conformers of DDM and DCT, as deduced by AUTODOCK, with paclitaxel, as described in the coordinates of the PDB file 1JFF for the β-tubulin complex. In this case, the protein has been removed for the sake of clarity. There are still possibilities for the extension of DDM and DCT to provide additional contacts with the target receptor.

His229. It may be speculated that, if this model were correct, addition of a proper paclitaxel or docetaxel side chain to DCM or DCT might further stabilize their binding by about -3 kcal mol^{-1} (from a comparison of the affinities of baccatin and paclitaxel, see reference [61]).

Conclusion

A variety of NMR spectroscopic data, including TR-NOESY/STD, qualitative line-broadening analysis, and NMR competition experiments, assisted by molecular mechanics calculations, has been employed to deduce the microtubule-bound conformation of two MSAs, DDM, and DCT. The data indicate that tubulin in assembled microtubules recognizes DDM through a conformational selection process, in which the half-chair conformer (and not the skew-boat form that is predominant in solution) of the lactone moiety is bound by the receptor. There are very minor changes in the rest of the molecular skeleton between the major conformer in water solution and that bound to assembled microtubules. Indeed, despite the many torsional degrees of freedom of DDM, intramolecular interactions within the molecule and hydration strongly affect its conformational features, and it only shows conformational mobility around a fairly narrow part of the molecule. This evidence strongly contrasts with the observations in other solvents. Yet, this feature serves to modulate the presentation of polar and nonpolar surfaces to interact with the binding site of tubulin. With regard to DCT, its microtubule-bound conformation has also been derived by using the same combined protocol of NMR spectroscopy and molecular docking. The deduced bound geometry presents some key conformational differences, with respect to the major one existing in solution, around certain torsion angles and additionally displays mobility (even when bound) along the lateral C22–C26 diene chain. In any case, the bound conformer of DCT resembles that of DDM and provides very similar contacts with the receptor. Competition experiments have indicated that both molecules compete with the taxane-binding site, thereby providing further support to previously described biochemical data.

A model of the binding mode of both MSAs to tubulin, involving the taxane-binding site of tubulin, has been postulated. A hypothesis for both the major polar and nonpolar interactions between both MSA compounds (DDM and DCT) and the receptor has also been proposed.

The employed approach should be of general use within this field. Moreover, this experimental determination of the conformation of a microtubule-stabilizing agent when bound to microtubules in solution should be helpful for the design of analogues with improved activity.

Acknowledgement

We thank the Ministery of Education and Science of Spain and Comunidad Autonoma de Madrid for funding (grant nos. CTQ2006-10874-C02-01 to J.J.-B., BIO2007-61336 to J.F.D., and BIPPED S-BIO-0214-2006 to J.M.A., J.F.D., and J.J.-B.). Dr. R. Campos provided generous access to the Bruker AVANCE 700 MHz spectrometer of CNIO (Madrid, Spain). We thank Prof. N. R. Krishna (University of Birmingham, AL, USA) for the use of the CORCEMA program for TR-NOESY and STD analysis and Dr. A. Olson (Scripps Research Institute, CA, USA) for providing AutoDock and auxiliary programs. I.P. thanks the Engineering and Physical Sciences Research Council and AstraZeneca (CASE studentship to N.M.G.) for funding.

[1] P. B. Schiff, J. Fant, S. B. Horwitz, *Nature* **1979**, *277*, 665–667.
[2] F. Gueritte-Voegelein, D. Guenard, F. Lavelle, M. T. Le Goff, L. Mangatal, P. Potier, *J. Med. Chem.* **1991**, *34*, 992–998.
[3] T. Mitchison, M. Kirschner, *Nature* **1984**, *312*, 237–242.
[4] M. A. Jordan, L. Wilson, *Nat. Rev. Cancer* **2004**, *4*, 253–265.
[5] B. Tan, D. Piwnica-Worms, L. Ratner, *Curr. Opin. Oncol.* **2000**, *12*, 450–458.
[6] J. A. Shabbits, R. Krishna, L. D. Mayer, *Expert Rev. Anticancer Ther.* **2001**, *1*, 585–594.
[7] L. He, G. A. Orr, S. B. Horwitz, *Drug Discovery Today* **2001**, *6*, 1153–1164.
[8] D. M. Bollag, P. A. McQueney, J. Zhu, O. Hensens, L. Koupal, J. Liesch, M. Goetz, E. Lazarides, C. M. Woods, *Cancer Res.* **1995**, *55*, 2325–2333.
[9] E. Hamel, D. L. Sackett, D. Vourloumis, K. C. Nicolaou, *Biochemistry* **1999**, *38*, 5490–5498.
[10] R. J. Kowalski, P. Giannakakou, S. P. Gunasekera, R. E. Longley, B. W. Day, E. Hamel, *Mol. Pharmacol.* **1997**, *52*, 613–622.
[11] Z. Wang, D. Yang, A. K. Mohanakrishnan, P. E. Fanwick, P. Nampoothiri, E. Hamel, M. Cushman, *J. Med. Chem.* **2000**, *43*, 2419–2429.
[12] M. C. Edler, R. M. Buey, R. Gussio, A. I. Marcus, C. D. Vanderwal, E. J. Sorensen, J. F. Díaz, P. Giannakakou, E. Hamel, *Biochemistry* **2005**, *44*, 11525–11538.
[13] I. Paterson, R. Britton, O. Delgado, A. Meyer, K. G. Poullennec, *Angew. Chem.* **2004**, *116*, 4729–4733; *Angew. Chem. Int. Ed.* **2004**, *43*, 4629–4633.
[14] D. E. Pryor, A. O'Brate, G. Bilcer, J. F. Díaz, Y. Wang, M. Kabaki, M. K. Jung, J. M. Andreu, A. K. Ghosh, P. Giannakakou, E. Hamel, *Biochemistry* **2002**, *41*, 9109–9115.
[15] T. N. Gaitanos, R. M. Buey, J. F. Díaz, P. T. Northcote, P. Teesdale-Spittle, J. M. Andreu, J. H. Miller, *Cancer Res.* **2004**, *64*, 5063–5067.
[16] R. M. Buey, I. Barasoain, E. Jackson, A. Meyer, P. Giannakakou, I. Paterson, S. Mooberry, J. M. Andreu, J. F. Díaz, *Chem. Biol.* **2005**, *12*, 1269–1279.
[17] E. Nogales, M. Whittaker, R. A. Milligan, K. H. Downing, *Cell* **1999**, *96*, 79–88.
[18] J. F. Díaz, I. Barasoain, J. M. Andreu, *J. Biol. Chem.* **2003**, *278*, 8407–8419.
[19] J. F. Díaz, I. Barasoain, A. A. Souto, F. Amat-Guerri, J. M. Andreu, *J. Biol. Chem.* **2005**, *280*, 3928–3937.
[20] R. M. Buey, E. Calvo, I. Barasoain, O. Pineda, M. C. Edler, R. Matesanz, G. Cerezo, C. D. Vanderwal, B. W. Day, E. J. Sorensen, J. A. Lopez, J. M. Andreu, E. Hamel, J. F. Díaz, *Nat. Chem. Biol.* **2007**, *3*, 117–125.
[21] B. Sato, H. Nakajima, Y. Hori, M. Hino, S. Hashimoto, H. Terano, *Jpn. J. Antibiot.* **2000**, *53*, 204–206.
[22] J. H. Nettles, H. Li, B. Cornett, J. M. Krahn, J. P. Snyder, K. H. Downing, *Science* **2004**, *305*, 866–869.
[23] E. ter Haar, R. J. Kowalski, E. Hamel, C. M. Lin, R. E. Longley, S. P. Gunasekera, H. S. Rosenkranz, B. W. Day, *Biochemistry* **1996**, *35*, 243–250.
[24] G. Pettit, Z. Cichacz, F. Gao, M. Boyd, J. Schmidt, *J. Chem. Soc. Chem. Commun.* **1994**, 1111–1112.
[25] I. Paterson, R. Britton, O. Delgado, A. E. Wright, *Chem. Commun.* **2004**, 632–633.
[26] I. Paterson, N. M. Gardner, *Chem. Commun.* **2007**, 49–51.
[27] L. A. Martello, M. J. LaMarche, L. He, T. J. Beauchamp, A. B. Smith, S. B. Horwitz, *Chem. Biol.* **2001**, *8*, 843–855.
[28] L. A. Martello, H. M. McDaid, D. L. Regl, C. P. Yang, D. Meng, T. R. Pettus, M. D. Kaufman, H. Arimoto, S. J. Danishefsky, A. B. Smith III, S. B. Horwitz, *Clin. Cancer Res.* **2000**, *6*, 1978–1987.
[29] S. Honore, K. Kamath, D. Braguer, S. B. Horwitz, L. Wilson, C. Briand, M. A. Jordan, *Cancer Res.* **2004**, *64*, 4957–4964.
[30] S. Honore, K. Kamath, D. Braguer, L. Wilson, C. Briand, M. A. Jordan, *Mol. Cancer Ther.* **2003**, *2*, 1303–1311.
[31] V. M. Sanchez-Pedregal, K. Kubicek, J. Meiler, I. Lyothier, I. Paterson, T. Carlomagno, *Angew. Chem.* **2006**, *118*, 7443–7447; *Angew. Chem. Int. Ed.* **2006**, *45*, 7388–7394.
[32] J. F. Díaz, M. Menéndez, J. M. Andreu, *Biochemistry* **1993**, *32*, 10067–10077.
[33] A. B. Smith III, M. J. LaMarche, M. Falcone-Hindley, *Org. Lett.* **2001**, *3*, 695–698.
[34] E. Monteagudo, D. O. Cicero, B. Cornett, D. C. Myles, J. P. Snyder, *J. Am. Chem. Soc.* **2001**, *123*, 6929–6930.
[35] J. Jiménez-Barbero, A. Canales, P. T. Northcote, R. M. Buey, J. M. Andreu, J. F. Díaz, *J. Am. Chem. Soc.* **2006**, *128*, 8757–8765.
[36] I. Paterson, G. J. Florence, K. Gerlach, J. Scott, N. Sereinig, *J. Am. Chem. Soc.* **2001**, *123*, 9535–9544.
[37] I. Paterson, O. Delgado, G. J. Florence, I. Lyothier, M. O'Brien, J. P. Scott, N. Sereinig, *J. Org. Chem.* **2005**, *70*, 150–160.
[38] A. A. Hyman, S. Salser, D. N. Drechsel, N. Unwin, T. J. Mitchison, *Mol. Biol. Cell* **1992**, *3*, 1155–1167.
[39] Macromodel, Version 9.1, Schrödinger, LLC, New York, NY, **2005**.
[40] N. L. Allinger, Y. H. Yuh, J. H. Lii, *J. Am. Chem. Soc.* **1989**, *111*, 8551–8566.
[41] W. C. Still, A. Tempczyk, R. C. Hawley, T. Hendrickson, *J. Am. Chem. Soc.* **1990**, *112*, 6127–6129.
[42] G. M. Morris, D. S. Goodsell, R. S. Halliday, R. Huey, W. E. Hart, R. K. Belew, A. J. Olson, *J. Comput. Chem.* **1998**, *19*, 1639–1662.
[43] J. Lowe, H. Li, K. H. Downing, E. Nogales, *J. Mol. Biol.* **2001**, *313*, 1045–1057.
[44] H. M. Berman, J. Westbrook, Z. Feng, G. Gilliland, T. N. Bhat, H. Weissig, I. N. Shindyalov, P. E. Bourne, *Nucleic Acids Res.* **2000**, *28*, 235–242.
[45] A. Bax, D. G. Davis, *J. Magn. Reson.* **1985**, *65*, 355–360.
[46] G. Bodenhausen, D. J. Ruben, *Chem. Phys. Lett.* **1980**, *69*, 185–189.
[47] T. L. Hwang, A. J. Shaka, *J. Am. Chem. Soc.* **1992**, *114*, 3157–3159.
[48] A. Kumar, R. R. Ernst, K. Wuthrich, *Biochem. Biophys. Res. Commun.* **1980**, *95*, 1–6.
[49] A. Poveda, J. L. Asensio, M. Martín-Pastor, J. Jiménez-Barbero, *J. Biomol. NMR* **1997**, *10*, 29–43.
[50] H. N. B. Moseley, E. V. Curto, N. R. Krishna, *J. Magn. Reson. Ser. B* **1995**, *108*, 243–261.
[51] V. Jayalakshmi, T. Biet, T. Peters, N. R. Krishna, *J. Am. Chem. Soc.* **2004**, *126*, 8610–8611.
[52] S. R. Arepalli, C. P. J. Glaudemans, G. D. Daves, P. Kovac, A. Bax, *J. Magn. Reson. Ser. B* **1995**, *106*, 195–198.

[53] J. L. Asensio, J. F. Espinosa, H. Dietrich, F. J. Cañada, R. R. Schmidt, M. Martín-Lomas, S. Andre, H. J. Gabius, J. Jiménez-Barbero, *J. Am. Chem. Soc.* **1999**, *121*, 8995–9000.
[54] B. Neuhaus, M. P. Williamson, *The Nuclear Overhauser Effect in Structural and Conformational Analysis*, VCH, New York, **1989**.
[55] J. Jiménez-Barbero, F. Amat-Guerri, J. P. Snyder, *Curr. Med. Chem. Anti-Cancer Agents* **2002**, *2*, 91–122.
[56] F. Ni, *Progr. NMR Spectrosc.* **1994**, *26*, 517–606.
[57] M. Mayer, B. Meyer, *J. Am. Chem. Soc.* **2001**, *123*, 6108–6117.
[58] B. Meyer, T. Peters, *Angew. Chem.* **2003**, *115*, 890–918; *Angew. Chem. Int. Ed.* **2003**, *42*, 864–890.
[59] J. P. Snyder, J. H. Nettles, B. Cornett, K. H. Downing, E. Nogales, *Proc. Natl. Acad. Sci. U.S.A.* **2001**, *98*, 5312–5316.
[60] H. Li, D. J. DeRosier, W. V. Nicholson, E. Nogales, K. H. Downing, *Structure* **2002**, *10*, 1317–1328.
[61] I. Barasoain, J. M. Andreu, *Biochemistry* **2001**, *40*, 11975–11984.
[62] N. A. Baker, D. Sept, S. Joseph, M. J. Holst, A. McCammon, *Proc. Natl. Acad. Sci. U.S.A.* **2001**, *98*, 10037–10041.
[63] T. J. Dolinsky, J. E. Nielsen, J. A. McCammon, N. A. Baker, *Nucleic Acids Res.* **2004**, *32*, 665–667.

Received: January 9, 2008
Published online: April 30, 2008

Chemistry & Biology
Article

Optimization of Taxane Binding to Microtubules: Binding Affinity Dissection and Incremental Construction of a High-Affinity Analog of Paclitaxel

Ruth Matesanz,[1,5] Isabel Barasoain,[1,5] Chun-Gang Yang,[2,3] Lei Wang,[2,6] Xuan Li,[2] Concepción de Inés,[1] Claire Coderch,[4] Federico Gago,[4] Jesús Jiménez Barbero,[1] José Manuel Andreu,[1] Wei-Shuo Fang,[2,3,7,*] and José Fernando Díaz[1,7,*]
[1]Centro de Investigaciones Biológicas, Consejo Superior de Investigaciones Científicas, Ramiro de Maeztu 9, 28040 Madrid, Spain
[2]Institute of Materia Medica, Chinese Academy of Medical Sciences, 1 Xian Nong Tan Street, Beijing 100050, China
[3]Key Laboratory of Bioactive Substances and Resources Utilization of Chinese Herbal Medicine, Peking Union Medical College (Ministry of Education), Beijing 100050, China
[4]Department of Pharmacology, University of Alcalá, 28871 Alcalá de Henares, Spain
[5]These authors contributed equally to this work
[6]Present address: College of Life Sciences, Jilin University, Changchun, Jilin 130012, China
[7]This article is dedicated to the memory of our late colleague, Dr. Ángel R. Ortiz
*Correspondence: wfang@imm.ac.cn (W.-S.F.), fer@cib.csic.es (J.F.D.)
DOI 10.1016/j.chembiol.2008.05.008

SUMMARY

The microtubule binding affinities of a series of synthetic taxanes have been measured with the aims of dissecting individual group contributions and obtaining a rationale for the design of novel compounds with the ability to overcome drug resistance. As previously observed for epothilones, the positive and negative contributions of the different substituents to the binding free energies are cumulative. By combining the most favorable substitutions we increased the binding affinity of paclitaxel 500-fold. Insight into the structural basis for this improvement was gained with molecular modeling and NMR data obtained for microtubule-bound docetaxel. Taxanes with affinities for microtubules well above their affinities for P-glycoprotein are shown not to be affected by multidrug resistance. This finding strongly indicates that optimization of the ligand-target interaction is a good strategy to overcome multidrug resistance mediated by efflux pumps.

INTRODUCTION

Cancer is one of the major causes of premature death in humans, and multidrug resistance (MDR) of neoplastic tissues is a major obstacle in cancer chemotherapy. Though many tumors initially respond favorably to chemotherapeutic treatment, effectiveness at tumor regression is limited by the development of resistance. Although several primary reasons account for MDR, the predominant cause is the overexpression and drug efflux activity of several transmembrane proteins, as best exemplified by P-glycoprotein (P-gp) (Shabbits et al., 2001).

P-gp is a member of the ATP binding cassette (ABC) family, with broad substrate specificity for substances, including anticancer drugs, peptides, and HIV protease inhibitors. It has been shown that the extent of drug resistance in human tumors correlates well with P-gp expression (Tan et al., 2000).

In a previous work with a small group of C-2 substituted cephalomannines (CPHs) (Yang et al., 2007), we noticed that the resistance indexes for high-affinity taxanes in MDR cells are much lower than those for the medium-affinity taxanes, paclitaxel (TXL) and docetaxel (DXL), used in clinical practice. These results suggest that increasing the binding affinity of these compounds might be an alternative to overcome MDR, the rationale for this being that affinity for tubulin is the main force driving the entrance of the ligand into cells.

When MDR cells are exposed to taxanes, two opposite forces control ligand uptake: (1) binding to P-gp, which pumps the ligand out of the cell, and (2) binding to tubulin, which reduces the intracellular concentration of the ligand and keeps it bound inside the cell. Thus, the higher the binding affinity of the ligand for tubulin, the lower the intracellular concentration of free ligand. Because efflux relies on drug binding to P-gp, which in turn depends on free ligand concentration, at intracellular ligand concentrations far below its dissociation constant from P-gp, the efflux will be strongly decreased. In the most extreme case of a ligand that binds covalently to the taxane site, such as the natural product cyclostreptin, every molecule entering the cell will be finally trapped by tubulin, and the tumor cell's MDR phenotype will be completely circumvented (Buey et al., 2007).

Although numerous chemical and biological qualitative studies of the structure-activity relationships of taxanes have been performed (Zefirova et al., 2005; Kingston and Newman, 2007), an in-depth study of the contributions of the different substituents to the binding thermodynamics has not been conducted. We have previously shown that for epothilone (EPO) derivatives (Buey et al., 2004), the thermodynamic contributions of the substituents are accumulative, that is, the same substitution on different ligands produces a similar change on the binding affinity. The effect of a single modification can thus be quantified, and both favorable and unfavorable contributions can be combined to build tailor-made ligands with the desired affinities.

We now report on the thermodynamics of binding of a set of 44 taxanes (called Chitax [CTX]), plus the three reference compounds, TXL, DXL, and CPH (Figure 1), to crosslinked stabilized

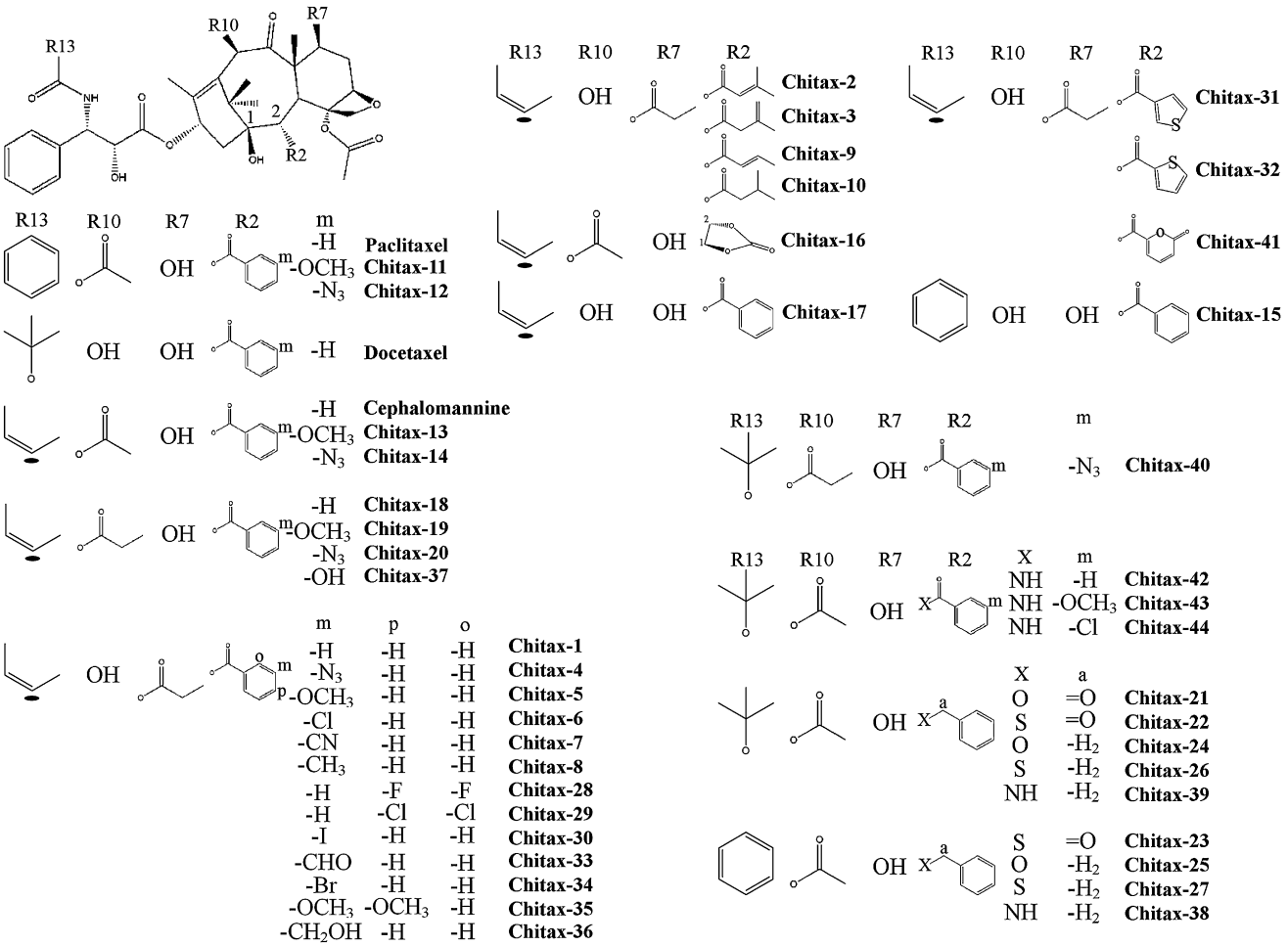

Figure 1. Chemical Structure of the Taxanes Employed in This Study

microtubules (MT) in order to quantify the contributions of single modifications at four specific locations of the taxane scaffold: two of them, C2, in the southern part of the molecule, and C13, where side chains have been described as essential for taxane activity (Chen et al., 1993b), and another two, C7 and C10, in the northern part of the molecule, where substituents have been shown as nonessential for taxane activity (Chen et al., 1993a). It is known that the side chains at these positions accept modifications that modulate the activity, favorably and unfavorably (Ojima et al., 1997; Kingston et al., 1998; Yang et al., 2007). The activity of these taxanes was investigated against the parental (A2780) and MDR P-gp-overexpressing (A2780AD) human ovarian carcinoma cell lines (Rogan et al., 1984). We were able to correlate the binding affinity of these tubulin ligands to their cytotoxicity in the resistant cells. Moreover, the resulting thermodynamic data was used to design novel high-affinity taxanes with the ability to overcome P-gp-related resistance. The higher affinity of these newly designed compounds has been rationalized by experimentally determining the tubulin bound conformation of DXL and by modeling the complexes of β-tubulin with DXL, TXL, and the best of the designed taxanes.

RESULTS

Thermodynamics of Binding of TXL Analogs to Stabilized MTs

All the compounds were first shown to be TXL-like MT-stabilizing agents (MSA) (see Table S1 available online). Then, their affinity for the taxane-binding site was measured using the competition method previously employed (Buey et al., 2004; Table 1 and Table S2). Every compound was initially measured using Flutax-2 as the competitor. Compounds 4, 11, 12, 13, 14, 19, 20, and 21 displayed very high affinities, completely displacing Flutax-2 at equimolar concentrations (Figure 2A). This indicated that they were in the limit of the range of measurement allowed by the previously employed test (Díaz and Buey, 2007).

To measure the binding affinity of these compounds more precisely, we used a direct competition experiment with a higher-affinity compound, EPO-B, whose binding affinity (7.5×10^8 M^{-1} at 35°C) has been previously determined (Buey et al., 2005; Figure 2B). This allowed the precise determination of the binding affinities of compounds 4, 11, 12, 13, 14, 19, 20, and 21, whose values range between 1.42×10^8 M^{-1} for the compound with the lowest affinity, CTX-21, and 1.51×10^9 M^{-1} for

Table 1. Apparent Binding Affinities, Thermodynamic Parameters of Binding of Taxanes for the TXL site, 10^7 M^{-1}, and Cytotoxicity of the Compounds to Nonresistant and Resistant Ovarian Carcinoma Cells

Compound	Kb 35°C	ΔG 35°C kJ/mol	ΔH kJ/mol	ΔS J/mol	IC_{50} A2780 nM	IC_{50} A2780AD nM	R/S
TXL[a]	1.43 ± 0.17	−42.1 ± 0.3	−51 ± 4	−29 ± 13	1.3 ± 0.4	980 ± 149	753
DXL[a]	3.93 ± 0.27	−44.8 ± 0.2	−53 ± 2	−26 ± 8	0.6 ± 0.2	290 ± 16	483
CPH	0.69 ± 0.08	−40.3 ± 0.3	−39 ± 6	−6 ± 18	1.5 ± 0.2	910 ± 285	606
CTX-1	0.49 ± 0.12	−39.4 ± 0.6	−56 ± 12	−56 ± 39	13.2 ± 7	1222 ± 300	92.5
CTX-2	0.043 ± 0.018	−33.2 ± 0.9	−66 ± 18	−109 ± 38	950 ± 80	10,200 ± 1900	10.7
CTX-3	0.072 ± 0.017	−34.5 ± 0.5	−32 ± 9	10 ± 29	1250 ± 200	4000 ± 700	3.2
CTX 4[b]	87 ± 19	−52.7 ± 0.5	−46 ± 13	19 ± 44	2.7 ± 0.6	14 ± 3.8	5.2
CTX-5	5.37 ± 1.39	−45.6 ± 0.6	−40 ± 4	19 ± 14	6.6 ± 1.8	160 ± 19	24.2
CTX-6	1.62 ± 0.24	−42.5 ± 0.4	−39 ± 2	13 ± 7	10 ± 2.4	274 ± 30	27.4
CTX-7	0.39 ± 0.06	−38.8 ± 0.4	−38 ± 5	4 ± 17	14.5 ± 2.9	2100 ± 660	145
CTX-8	0.492 ± 0.073	−39.4 ± 0.3	−28 ± 3	39 ± 10	22.5 ± 5	596 ± 105	26.4
CTX-9	0.028 ± 0.008	−32.1 ± 0.6	−15 ± 4	56 ± 12	3900 ± 370	15,000 ± 3500	3.8
CTX-10	0.042 ± 0.008	−33.1 ± 0.4	−12 ± 5	68 ± 18	4900 ± 600	>20000	>4
CTX 11[b]	38 ± 10	−50.5 ± 0.6	−14 ± 20	117 ± 65	1.36 ± 0.2	163 ± 37	120
CTX 12[b]	151 ± 3	−54.1 ± 0.1	−29 ± 9	84 ± 29	2.8 ± 0.38	42 ± 13	15
CTX 13[b]	16.5 ± 2.8	−48.4 ± 0.4	−28 ± 1	66 ± 1	1.3 ± 0.2	128 ± 17	98.4
CTX 14[b]	80.0 ± 2.9	−52.5 ± 0.1	−46 ± 6	21 ± 19	1.6 ± 0.3	25 ± 10	15.6
CTX-15	2.384 ± 0.53	−43.5 ± 0.5	−18 ± 11	80 ± 35	17.5 ± 2.7	5250 ± 1000	300
CTX-16	0.050 ± 0.030	−33.6 ± 1.2	−18 ± 9	49 ± 30	740 ± 100	7360 ± 750	9.9
CTX-17	0.902 ± 0.37	−41.0 ± 0.9	−24 ± 3	55 ± 10	18 ± 5.6	5412 ± 1200	301
CTX-18	1.281 ± 0.27	−41.9 ± 0.5	−22 ± 4	64 ± 14	2.1 ± 0.8	452 ± 36	215.2
CTX 19[b]	14.8 ± 0.2	−48.2 ± 0.1	−48 ± 3	0 ± 9	0.54 ± 0.07	39 ± 11	72.2
CTX 20[b]	80.6 ± 5.1	−52.5 ± 0.2	−92 ± 19	−124 ± 64	3.9 ± 1.2	27.4 ± 4	7
CTX 21[b]	14.2 ± 1.6	−48.0 ± 0.3	−26 ± 5	72 ± 16	1.9 ± 0.3	41 ± 11	21.5
CTX-22	0.013 ± 0.00	−30.1 ± 0.0	−46 ± 7	−151 ± 23	2400 ± 1000	6960 ± 670	2.9
CTX-23	0.007 ± 0.00	−28.6 ± 0.0	−37 ± 7	−123 ± 22	11,500 ± 1000	23,800 ± 2200	2.1
CTX-24	0.094 ± 0.01	−35.2 ± 0.3	−65 ± 10	−95 ± 33	353 ± 19	8600 ± 3800	24.3
CTX-25	0.008 ± 0.00	−28.9 ± 0.0	−47 ± 7	−154 ± 24	6200 ± 2600	28,500 ± 5300	4.6
CTX-26	0.018 ± 0.00	−31.0 ± 0.0	−73 ± 11	−77 ± 137	3500 ± 1400	8300 ± 2700	2.4
CTX-27	0.007 ± 0.00	−28.6 ± 0.0	−42 ± 6	−138 ± 21	10,000 ± 740	9400 ± 1700	0.94
CTX-28	0.17 ± 0.04	−36.7 ± 0.5	−17 ± 8	62 ± 25	82 ± 16	1880 ± 200	22.9
CTX-29	0.25 ± 0.08	−37.7 ± 0.7	−52 ± 9	−48 ± 30	102 ± 8.8	690 ± 60	6.8
CTX-30	1.76 ± 0.91	−42.7 ± 1.1	−11 ± 15	92 ± 49	30 ± 0.5	246 ± 27	8.2
CTX-31	0.10 ± 0.04	−35.4 ± 0.9	−44 ± 11	−30 ± 36	106 ± 4.2	2950 ± 480	27.8
CTX-32	0.24 ± 0.08	−37.6 ± 0.7	−7 ± 16	87 ± 55	62 ± 17	3200 ± 250	51.6
CTX-33	0.07 ± 0.01	−34.4 ± 0.3	−81 ± 12	−152 ± 39	69 ± 77	1500 ± 100	21.7
CTX-34	1.20 ± 0.93	−41.7 ± 1.5	−38 ± 28	14 ± 94	28.7 ± 1.9	196 ± 14	6.8
CTX 35	0.88 ± 0.77	−40.9 ± 1.6	−29 ± 33	13 ± 112	25 ± 2	153 ± 39	6.12
CTX 36	0.029 ± 0.020	−32.2 ± 1.3	−48 ± 6	−63 ± 18	1700 ± 120	>20000	>11.7
CTX 37	0.035 ± 0.010	−32.7 ± 0.6	−91 ± 7	−207 ± 24	86 ± 9.8	10,000 ± 1000	116.2
CTX 38	0.001 ± 0.001	−23.6 ± 1.8	−44 ± 9	−70 ± 34	15,400 ± 3200	20,000 ± 3000	1.3
CTX 39	0.003 ± 0.001	−26.4 ± 0.7	−157 ± 10	−461 ± 28	4200 ± 100	5700 ± 300	1.3
CTX 40[b]	628 ± 15	−57.7 ± 0.1	−26 ± 24	99 ± 80	7 ± 1	9.1 ± 0.45	1.3
CTX 41	0.021 ± 0.004	−31.4 ± 0.4	−94 ± 9	−202 ± 28	14,000 ± 2000	>20000	1.4
CTX 42	0.008 ± 0.003	−28.9 ± 0.8	−106 ± 13	−250 ± 43	192 ± 20	2750 ± 430	14.3
CTX 43	0.030 ± 0.008	−32.3 ± 0.6	−85 ± 20	−169 ± 66	69.5 ± 3.8	331 ± 70	4.8
CTX 44	0.001 ± 0.001	−23.6 ± 1.8	−177 ± 23	−493 ± 75	>20,000	>20,000	

Errors are standard errors of the mean.
[a] Binding affinity and thermodynamic parameters data are from Buey et al. (2004).
[b] Compounds measured with the EPO-B displacing method.

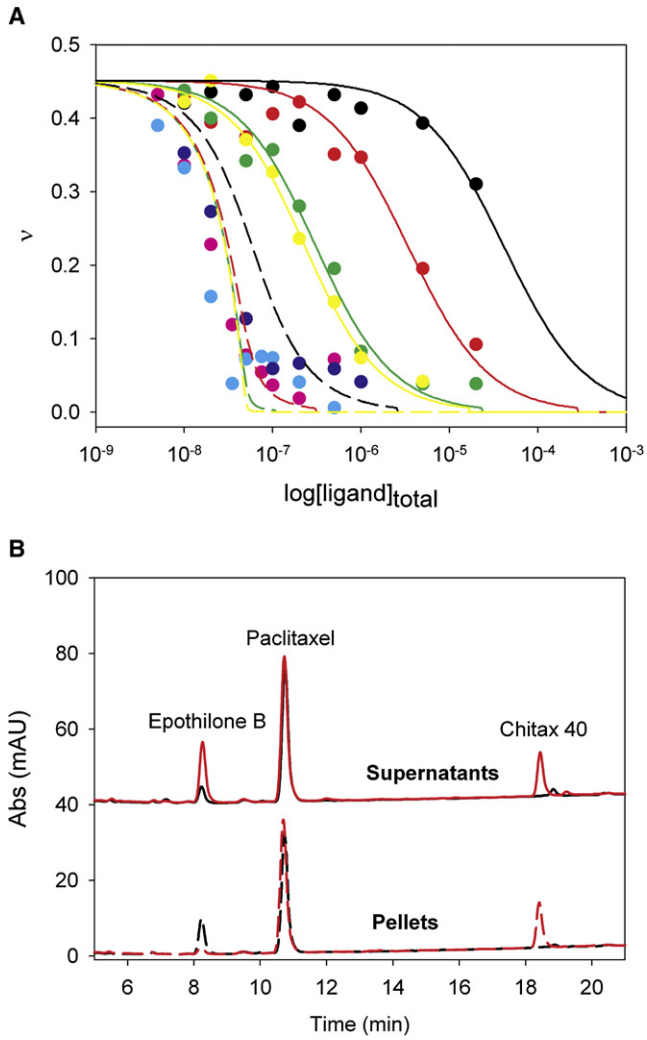

Figure 2. Binding of the Ligands to the Paclitaxel Site

(A) Displacement of the fluorescent taxane Flutax-2 bound to MT sites (50 nM) by taxanes at 35°C. The solid lines were generated with the best-fit value of the binding equilibrium constant of the competitors with binding affinities lower to 10^7 M^{-1}, assuming a one-to-one binding to the same site. Additional lines (dashed) show the expected displacement for ligands with binding constants of 10^8 M^{-1} (black), 10^9 M^{-1} (red), 10^{10} M^{-1} (green), and 10^{11} M^{-1} (yellow). Ligands binding data are as follows: green CPH, red CTX-2, yellow CTX-6, dark blue CTX-11, magenta CTX-12, light blue CTX-14, black CTX-27.

(B) Displacement of EPO-B bound to MT sites (10 μM) by CTX-40 at 35°C. One micromolar TXL-binding sites were incubated with 1.1 μM EPO-B (black lines) or with 1.1 μM EPO-B and 1.1 μM CTX-40 (red lines), MTs were harvested by sedimentation, ligands extracted from supernatants (solid lines) and pellets (dashed lines), and HPLC analyzed. One micromolar TXL was used as the internal standard. Supernatant traces were displaced 40 mAU for presentation purposes.

the highest-affinity compound, CTX-12. This method was validated when the binding affinities of compounds 11, 13, 19, and 21 (those in the range of 10^8 M^{-1}) were shown to be similar using either EPO-B or Flutax-2 (see the Supplemental Data).

To confirm that the high affinity of compounds containing 3-N_3 benzoyl at C2 does not originate from covalent binding of its reactive azido group to β-tubulin, we performed experiments in which the amounts of reversibly bound compounds 4, 12, and 14 were measured. The bound compounds could be extracted from the pellets and aqueous solutions with the aid of an organic solvent, indicating that they are not irreversibly bound.

Molecular Modeling

One conspicuous characteristic of the taxane-binding site in β-tubulin (Lowe et al., 2001) is the presence of the highly exposed side chain of His229 (located in the middle of helix 7 and positionally equivalent to Arg229 in α-tubulin) that splits the cavity into two major pockets. Because continuum electrostatic calculations predicted the imidazole ring of this residue to be doubly protonated at pH 6.5 (pK_{His229} = 7.2), this ionization state was used in subsequent work.

Molecular dynamics (MD) studies of TXL, DXL, and CTX-40 in aqueous solution provided us with a range of different conformers, the most abundant of which (Figure S1) were independently studied in a first rigid-body approach by the automated docking program. The conformation previously reported for TXL (Lowe et al., 2001; Snyder et al., 2001) using either DOCK or FlexX was also found by AutoDock among the best scoring solutions. Because similar poses were found for DXL (Figure S2) and CTX-40 as well, this common disposition of the taxane in the binding site of β-tubulin was used in the modeling of all the complexes. Noteworthy is that these conformations are not the most populated in aqueous solution (data not shown) although they are sporadically observed in the course of transitions toward other more stable and "hydrophobically collapsed" conformations. The proposed docked conformation for TXL is then coincident with that previously found in crystals of 7-mesyl-paclitaxel, which was reportedly induced by specific interactions of the side chain at C13 with solvent (Gao and Chen, 1996).

The feasibility of the resulting modeled complexes was assessed by subjecting each of them to a 10 ns MD simulation followed by a simulated annealing procedure that provided us with a set of representative complex structures for further analysis and energy decomposition. In all cases, the ligand adopts a conformation in good agreement with the T-taxol geometry (Snyder et al., 2001; Figure 3) and is anchored in the binding site through a common set of well-defined interactions. Thus, the oxetane oxygen of the taxane is engaged in a good hydrogen bond with the NH of Thr276, whereas another hydrogen bond is established between the amide or carbamate carbonyl oxygen on the C13 substituent and the Nε of His229. The common phenyl ring at C13 (3′-Ph) establishes close van der Waals contacts with the hydrophobic side chains of Val23 and Ala233, whereas the benzoyl phenyl ring at C2 (2-OBz) gets lodged into another hydrophobic cavity, on the other side of His229, made up of the side chains of Leu217, Leu219, and Leu275. The offset stacking interaction of this latter phenyl with the imidazole ring of His229 (Figure S3) is improved by the substituent at the meta position whose 1,2- (methoxy, CTX-13) or 1,3-dipole (azide, CTX-40) additionally establishes a favorable electrostatic interaction with the amide dipole of the backbone peptide bond between His229 and Leu230 (Figure 3). Of the three hydroxyl groups that are common to the four ligands studied, that present on the C13 substituent is consistently engaged in a hydrogen bonding interaction with the carboxylate of Asp26 in helix 1 and the backbone nitrogen of Arg369, whereas that at C7 can

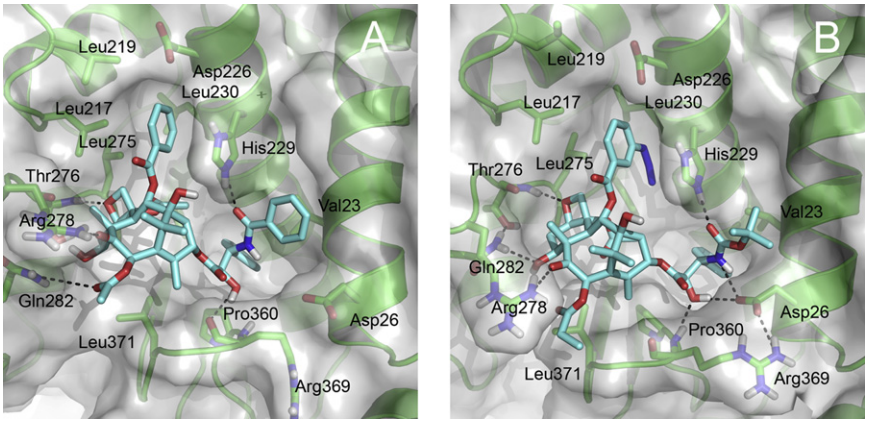

Figure 3. Model of the Ligands Bound to the Paclitaxel Site

(A) TXL and (B) CTX-40 in the binding site of β-tubulin at the end of the simulated annealing procedure. Note that the doubly protonated imidazole ring of His229 participates in (1) a hydrogen bonding interaction with the amide or carbamate carbonyl oxygen on the C13 substituent through the Nε, and (2) an offset stacking interaction with the phenyl ring on the C2 substituent.

establish transient hydrogen bonds with the carboxamide group of Gln282. The hydroxyl at C1 is permanently exposed to the solvent.

The four complexes yielded very low RMS deviations for the protein atoms with respect to the refined β-tubulin-TXL structure 1JFF (~1.3 Å on average for 400 atoms). The major differences when compared with this particular complex are the presence of a different rotameric state for His229, which we propose is protonated at physiological pH, and improved stacking and hydrogen bonding interactions between the ligand and the protein as a consequence of the mutual adaptation resulting from the simulated annealing procedure.

NMR Characterization of Bound Docetaxel

As a further step, and to provide empirical support for the modeling-derived conformations that formed the basis for the quest of the structure-activity relationship, the MT-bound conformation of DXL was elucidated, under the experimental conditions used for determining the binding constants (see the Supplemental Data file DXLNMR.pdb).

As previously shown, the transferred nuclear Overhauser enhancement (TR-NOESY) technique provides an adequate means to determine the bound conformation of ligands that exchange between free and bound states at a reasonably fast rate. TR-NOESY experiments were then performed on the DXL:MT sample at different mixing times. Negative crosspeaks were clearly observed at 310 K (Figures 4A and 4B), as expected for a ligand that binds to the assembled MTs preparation, in contrast with the lack of NOEs detected in the free state (Figure 4C).

Two control experiments were performed employing either Flutax-2 instead of DXL (the effective k_{off} of Flutax-2 release from MTs is 1.63 ± 0.18 s^{-1} (Diaz et al., 2000) or both DXL and discodermolide (DDM) at equimolecular concentrations. No TR-NOESY signals were observed in the presence of Flutax-2, indicating that the effective k_{off} of DXL is higher than that previously measured for Flutax-2, and the DXL signals were cancelled out by DDM (whose affinity for the TXL-binding site is 100× higher), indicating that DXL is effectively bound to the TXL site (Buey et al., 2005).

Cytotoxicity in Resistant and Nonresistant Tumor Cells

To check the effects of the studied modifications on the cytotoxicities of the compounds and to validate the binding affinity approach as a tool to be used in ligand optimization, we performed IC_{50} tests in A2780 human ovarian carcinoma cells and their MDR A2780AD counterparts (Table 1 and Figure 5A).

The cytotoxicities of the ligands in non-P-gp-overexpressing A2780 cells show a linear relationship (r = 0.81) with their binding affinities, but only for those compounds with a ΔG at 35°C higher than −47.5 kJ/mol^{-1} (K_b at 35°C higher than 10^8 M^{-1}), which points to a limit in the cytotoxicity that can be achieved. Thus, despite the increase in affinity of three orders of magnitude between CPH and CTX-40, the IC_{50} remained in the order of nanomolar.

In the case of the MDR A2780AD cells, a good linear relationship (r = 0.80) between cytotoxicities and binding affinities is observed for the full set of ligands, strongly suggesting that for these P-gp-overexpressing cells, tubulin binding is the main force competing with P-gp-mediated extrusion.

The best regression lines have slopes of 1.10 for A2780 cells and 0.61 for A2780AD cells, which indicates that P-gp-overexpression effectively reduces the intracellular drug concentration, thus making it necessary to increase the load to exert a cytotoxic effect.

Intake of Taxanes by Tumor Cells

The amount of compound made available for binding to the tubulin site was measured by employing radioactively labeled DXL and TXL at the concentrations needed to stop the cell cycle in G_2/M, in two leukemic cell lines (U937 and K562) and the kidney epithelial nontumor cell line PtK2 from *Potorus tridactylis*. In these conditions, the intracellular drug concentration, which ranges from 0.3 to 2.8 μM and represents a small percentage of the total drug and the cell tubulin concentrations (Table S3), increases with the total drug concentration and reaches a maximum in PtK2 cells at 300 nM DXL and 600 nM TXL. The equilibration of the ligand inside the cells is fast, with a half-life of 3 min for ^{14}C-DXL and 10 min for ^{3}H-TXL at a drug concentration of 1 μM. The drug inside the cell was found to be in the cytoplasm, with only a small fraction bound to the nucleus, as expected.

Because the total intracellular drug concentration is more than one order of magnitude above its MT dissociation constant and much lower than the total tubulin concentration (which was considered to be ~5% of the total protein measured), the mass action law dictates that most of the compound inside the cells is essentially bound to tubulin and the intracellular concentration

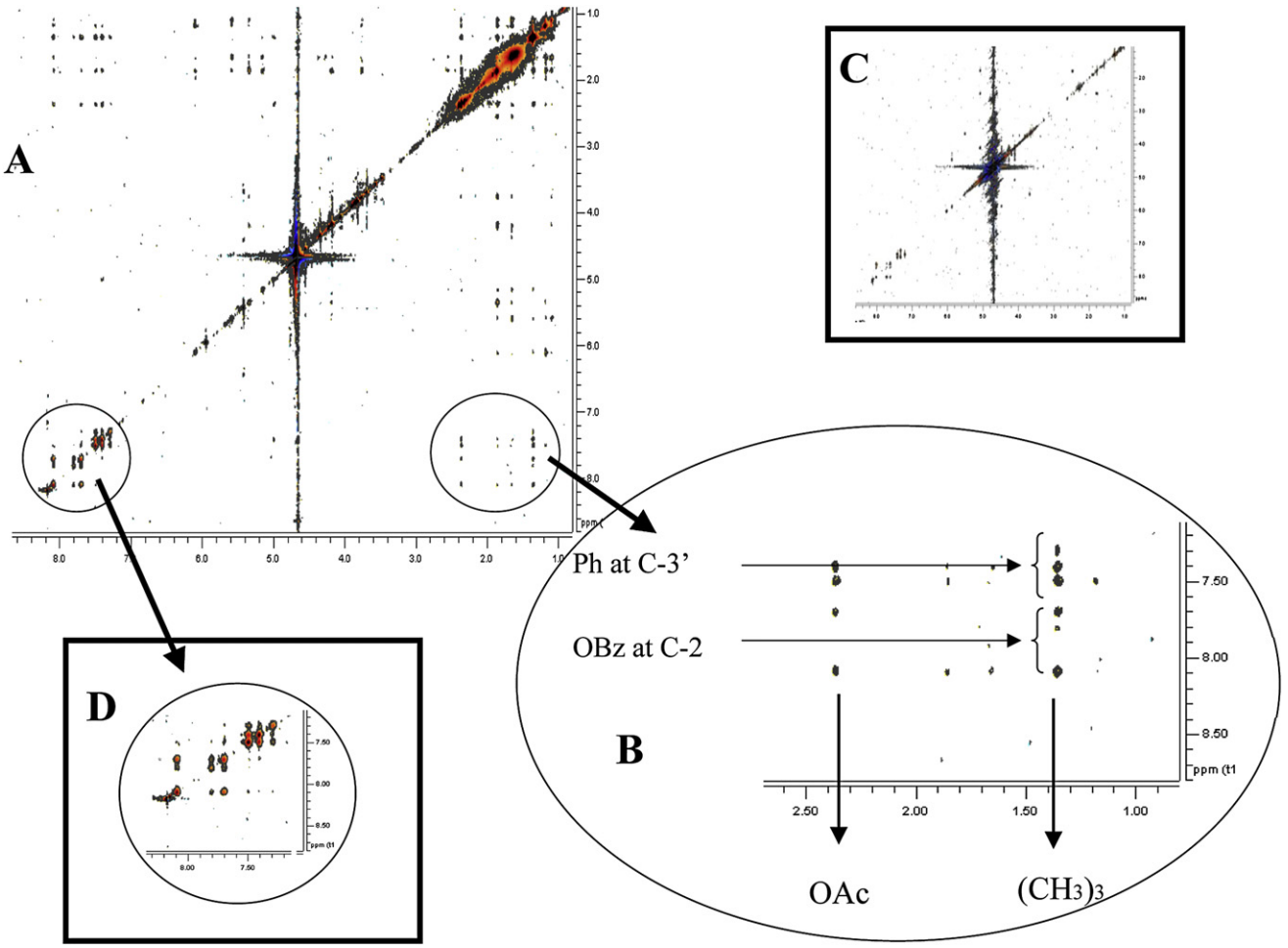

Figure 4. NMR Characterization of the Prerelease Conformation of Bound Docetaxel

(A) The 500 MHz TR-NOESY (mixing 200 ms, 310 K) spectrum of DXL in buffered water solution in the presence of MTs (20:1 molar ratio).

(B) Expansion showing the key TR-NOESY region: close contacts between the tert-butyl chain and the aromatic 2-OBz ring (besides the trivial crosspeaks with the vicinal 3′-Ph moiety).

(C) The NOESY experiment under the same experimental conditions (200 ms) in the absence of MTs did not show any crosspeak. (D) Expansion of the aromatic region in the TR-NOESY spectrum; no NOEs between the two aromatic 3′-Ph and 2-OBz moieties are observed.

of free drug is close to the dissociation constant (i.e., 70 nM for TXL and 25 nM for DXL).

DISCUSSION

The effects of modifications on the substituents attached to the baccatin scaffold on the cytotoxicity of taxanes have been qualitatively discussed in several reviews (Zefirova et al., 2005; Kingston and Newman, 2007). However, the fact that these studies were performed in different cell lines precludes a rigorous evaluation of the relationship between structural changes and cytotoxicity. To quantify the effects of substitutions at a set of specific positions in a systematic way, the binding affinity for the taxane-binding site on β-tubulin has proved to be a more precise and objective parameter (Buey et al., 2004).

With all the binding constants determined at a given temperature (35°C), it has been possible to determine the changes in apparent binding free energy caused by single-group modifications (Table 2) and to select the most favorable substituents at the positions chosen for optimization. Once this knowledge was obtained, it became feasible to design several optimized taxanes.

Effect on Binding Affinity of Changes at the C2 Position

C2 modifications have proven to be the most effective in modulating the activity of taxanes. Thus, the 2-OBz is essential as its removal (Chen et al., 1993b) or replacement with other small side chains (Ojima et al., 1994; Nicolaou et al., 1995) results in almost total loss of activity in the human colon cancer cell line tested. In contrast, changes in the structure of the ring, including its replacement with nonaromatic or heterocyclic rings, result in only moderate losses of antitumor activity (Ojima et al., 1994). Introduction of substituents on the 2-OBz ring, (Nicolaou et al., 1994; Kingston et al., 1998; Yang et al., 2007) results in increases of activity for small groups at the meta position but loss of activity

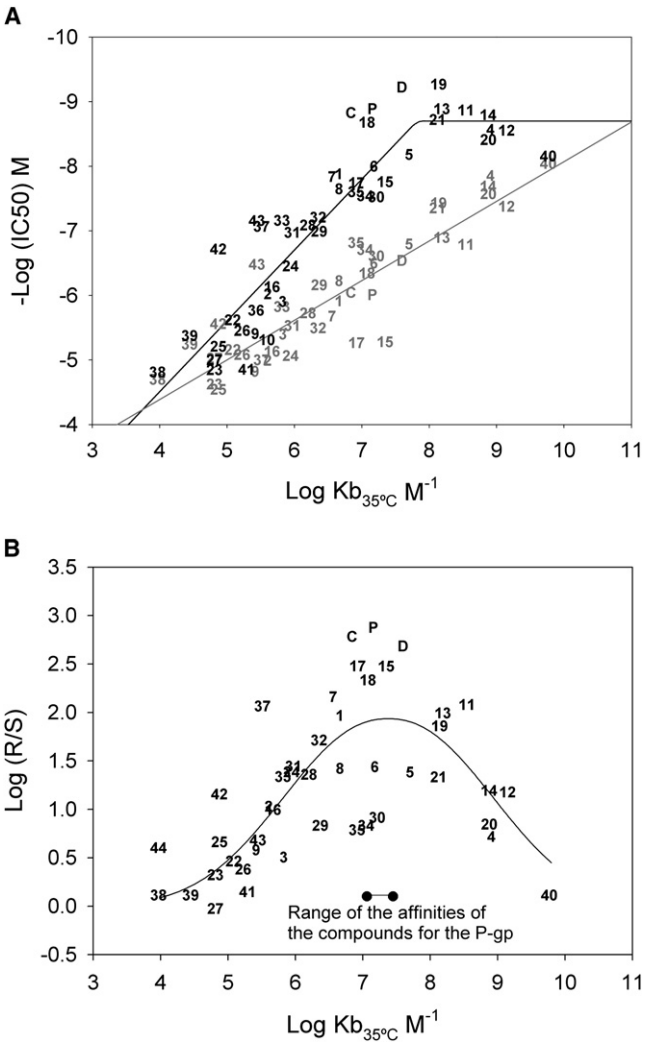

Figure 5. Comparison between Binding Affinity and Cytotoxicity in A2780 and A2780AD Cells

(A) Dependence of the IC_{50} of the ligands against A2780 (black) and A2780AD (gray) human ovarian carcinoma cells on the affinity for the TXL-binding site in MTs (binding constant, K_b). The black line represents the best fit of IC_{50} against A2780 cells versus binding affinity for ligands with binding affinity under $5 \times 10^8\ M^{-1}$. The gray line represents the best fit of IC_{50} against A2780AD cells versus binding affinity.

(B) Dependence of the resistance index of the A2780AD MDR cells on the affinity of the compounds for the taxane binding site. The range of binding affinities of taxanes for P-gp was taken from Yang et al. (2007).

for the other positions. Changes in the linker connecting the benzene ring to the taxane core also result in decreased biological activity (Wang et al., 2007).

Our results confirm and extend the qualitative data summarized above and provide a precise quantitative characterization of the effects of C2 modifications on binding affinity:

(a) Changing the nature of the linker between the benzene ring and the taxane scaffold results in a large loss of binding free energy. Thus, the replacement of the ester by an ether, thioether, or amine moiety (compounds 24, 25, 26, 27, 38, and 39) or by a thioester or an amide (compounds 22, 23, 42, 43, and 44) results in a heavy loss of binding free energy (up to 20 kJ/mol^{-1}). This stringent requirement indicates that the angle between the benzyl ring and the taxane core has to be strictly preserved and must be related to steric hindrance, as previously discussed for the thiobenzoyl compounds 22 and 23 (Wang et al., 2007), because the analogs in which the benzyl group is replaced by an alkyl ester (compounds 2, 3, 9, 10, and 16) only display a moderate loss of binding free energy (5–6 kJ/mol^{-1}), which can be assigned to the loss of interactions between the benzyl ring and the binding site.

(b) Modification of the meta substituents on the benzyl ring leads to gains of binding free energy that are the largest for $-N_3$ (-11.2 ± 1.1 kJ/mol^{-1}) and $-OCH_3$ (-7.2 ± 0.6 kJ/mol^{-1}) groups (compounds 4, 5, 11, 12, 13, 14, 20) and much smaller (-2–3 kJ/mol^{-1}) for halogen atoms (compounds 6, 30, and 34), whereas other small groups ($-$CN and $-CH_3$) have no effect (compounds 7 and 8). Other similarly small substitutions ($-$OH and $-CH_2OH$; compounds 36 and 37) are detrimental, resulting in a loss of 7–9 kJ/mol^{-1} of binding free energy.

(c) Introduction of double substituents at the 2,4 (compounds 28, 29) and 2,5 (35) positions results in loss of binding affinity.

(d) The thienoyl moiety (compounds 31 and 32) can effectively replace the benzoyl group.

Because previous work from our group (Buey et al., 2004) has shown that substitutions leading to gains in binding free energy also give rise to increased cytotoxicity, the $-N_3$ substituent at the meta position of 2-OBz was selected as the most suitable for molecule optimization.

Effect on Binding Affinity of Changes at the C13 Position

The side chains present at position C13 in one semisynthetic (DXL) and two natural taxanes (CPH and TXL) were evaluated to choose the optimal one for binding. Although from the direct comparison of TXL and DXL alone (Diaz and Andreu, 1993) it is not possible to assess the effect of the C13 side chain on the binding free energy due to the presence of additional differences in the substituents at C7 and C10, DXL showed a 1.9-fold larger binding affinity relative to TXL, which corresponds to a change of -1.6 kJ/mol^{-1} in free energy of binding. A similar difference (2×) was observed in the cytotoxicity on 1A9 cells (Buey et al., 2005). In contrast, the tubulin binding affinity and the cytotoxicity of CPH are about 2× lower than those of DXL (Yang et al., 2007).

In our series, by comparing compounds TXL, DXL, CPH, 11, 12, 13, 14, 15, 17, 20, 21, 22, 23, 24, 25, 26, 27, 38, 39, and 40, differing only in the side chain at C13 present in the reference molecules, we can now establish that, of the three side chains, DXL provides the largest contribution to the binding free energy, ($\Delta\Delta G$ C13-DXL$-$C13-TXL $= -3.2 \pm 0.9$ kJ/mol^{-1}, $\Delta\Delta G$ C13-CPH$-$C13-DXL $= -5.6 \pm 1.1$ kJ/mol^{-1}).

Effect on Binding Affinity of the Substituents Present in the Northern Side of the Taxane Ring (C7 and C10)

Modifications on the northern face of TXL at positions C7 and C10 have little effect on tubulin binding, as expected from the previously described effects on cytotoxicity (Chen et al., 1993a). From all the substituents tested at C10, the best one turns out to be the propionyl group, which provides an

Table 2. Incremental Free Energy of Binding of TXL Analogs to MTs Due to Single Group Modifications

Modification Type	Modification	Compounds	ΔΔG	Avg (Std Err)
C2	Benzoyl → benzylether	T → 25	+13.2	+13.0 ± 0.2
		21 → 24	+12.8	
	Benzoyl → benzylsulphur	T → 27	+13.6	+15.9 ± 2.3
		21 → 26	+18.1	
	Benzoyl → benzylamine	T → 38	+18.6	+20.1 ± 1.5
		21 → 39	+21.6	
	Benzoyl → thiobenzoyl	T → 23	+19.6	+15.9 ± 3.8
		21 → 22	+12.1	
	Benzoyl → benzamide	21 → 42	+19.2	
	Benzamide → 3-OCH_3-benzamide	42 → 43	−3.4	
	Benzamide → 3-Cl^-benzamide	42 → 44	+5.3	
	Benzoyl → 3-methyl- 2 butenoyl	1 → 2	+6.2	
	Benzoyl → 3-methyl- 3 butenoyl	1 → 3	+4.9	
	Benzoyl → 2(E)-butenoyl	1 → 9	+7.3	
	Benzoyl → 3-methyl- butanoyl	1 → 10	+6.3	
	Benzoyl → 2-debenzoyl-1,2-carbonate	C → 16	+5.8	
	Benzoyl → 3-N_3 Benzoyl	1 → 4	−8.0	−11.2 ± 1.3
		T → 12	−13.9	
		C → 14	−12.2	
		18 → 20	−10.6	
	Benzoyl → 3-OCH_3-benzoyl	1 → 5	−6.2	−7.2 ± 0.6
		T → 11	−8.3	
		C → 13	−8.1	
		18 → 19	−6.3	
	Benzoyl → 3-Cl^-benzoyl	1 → 6	−3.1	
	Benzoyl → 3-Br-benzoyl	1 → 34	−2.3	
	Benzoyl → 3-I-benzoyl	1 → 30	−3.3	
	Benzoyl → 3-NC-benzoyl	1 → 7	+0.6	
	Benzoyl → 3-CH3-benzoyl	1 → 8	0.0	
	Benzoyl → 3-CH_2OH-benzoyl	1 → 36	+7.2	
	Benzoyl → 3-OH-benzoyl	18 → 37	+9.2	
	3-Cl^-Benzoyl → 2,4-di-Cl^-benzoyl	6 → 29	+4.8	
	Benzoyl → 2,4-di-F-benzoyl	1 → 28	+2.7	
	3-OCH_3-Benzoyl → 2-5-di- OCH_3-benzoyl	5 → 35	+4.6	
	Benzoyl → 2-thienoyl	1 → 31	+4.1	
	Benzoyl → 3-thienoyl	1 → 32	+1.8	
	Benzoyl → 6-carboxy-pyran-2-one	1 → 41	+8.1	
C13 Side Chain	TXL → CPH	T → C	+1.9	+2.0 ± 0.2
		11 → 13	+1.9	
		12 → 14	+1.6	
		15 → 17	+2.4	
	TXL → DXL	23 → 22	−1.7	−3.2 ± 0.9
		25 → 24	−6.2	
		27 → 26	−1.3	
		38 → 39	−2.8	
		T → 21	−4.2	
	CPH → DXL	C → 21	−3.8	−5.6 ± 1.1
		17 → D	−7.7	
		20 → 40	−5.2	
C10	Acetyl → –OH	T → 15	−1.3	−1.7 ± 0.8

198

Table 2. *Continued*

Modification Type	Modification	Compounds	ΔΔG	Avg (Std Err)
		C → 17	−0.7	
		21 → D	−3.2	
	Propionyl → –OH	18 → 17	+0.9	+0.9
	Acetyl → propionyl	C → 18	−1.6	−0.5 ± 0.4
		13 → 19	+0.2	
		14 → 20	0.0	
C7	Propionyl → –OH	17 → 1	−1.6	−1.6

Errors are standard errors of the mean.

incremental free energy change of around −0.5 kJ/mol^{-1} over the natural C10 acetyl. In contrast, introduction of the same group at position C7 brings about a loss of 1.6 kJ/mol^{-1} of binding free energy relative to the −OH present in TXL. For this reason, a propionyl at C10 and a hydroxyl at C7 were selected as optimal substituents at these positions.

Optimal Taxane

According to the data measured, the optimal taxane should have DXL's side chain at C13, an *m*-N_3-benzoyl at C2, a propionyl at C10, and a hydroxyl at C7. Starting from compound 1, the first one in the series, with an apparent binding affinity of −39.4 kJ/mol^{-1}, the resulting molecule should gain −5.6 kJ/mol^{-1} from the replacement of the CPH side chain with that of DXL, −11.2 kJ/mol^{-1} from the substitution of *m*-N_3-benzoyl for benzoyl at C2, −1.6 kJ/mol^{-1} from the change of a propionyl at C7 to a hydroxyl, and −0.9 kJ/mol^{-1} from the change of a hydroxyl at C10 to a propionyl. Taking all of these changes together, the optimal taxane would have a predicted ΔG at 35°C of −58.7 kJ/mol^{-1}. When the compound was synthesized (CTX-40) and its binding affinity was measured using the EPO-B displacement method (K_b 35°C = 6.28 ± 0.15 × 10^9 M^{-1}; ΔG = −57.7 ± 0.1 kJ/mol^{-1}), the experimental value was found to be in good correspondence with the predicted value.

Structural Interpretation of the Binding Data

Two different reasons have been proposed for the changes in activity due to modifications at C2: (1) the need for a hydrophobic group to maintain the proper taxane conformation or (2) direct interactions of the benzoyl with hydrophobic side chains of the protein (Zefirova et al., 2005). The modeling data support the view that the higher affinity of CTX-40 relative to TXL and DXL, which is mostly conferred by the phenylazide substituent present at C2, may largely stem from the simultaneous improvement of the stacking interactions with the imidazole ring of His229(+) and a better electrostatic interaction with Asp26 and Arg369 on the opposite side of the molecule, resulting from a better anchoring of the ligand in the binding site. The same rationale applies to CTX-13, which has a methoxy substituent in place of the azide, and to a lesser extent to the derivatives containing halogen atoms. As regards the methyl, cyano, hydroxyl, or hydroxymethyl substituents, they are likely to be found facing the solvent rather than orientated toward the binding pocket, thus contributing negligibly to the binding affinity, in good accord with the experimental evidence.

Likewise, the enhanced affinity contribution of the DXL and CTX-40 side-chain at C13 relative to that of TXL arises from an improved hydrogen-bonding interaction of the carbamate NH relative to the amide NH with the carboxylate of Asp26.

Prerelease Conformation of Bound Docetaxel

Transferred NOESY signals arise from a free DXL molecule whose protons have been excited when still bound to the protein but relaxed after release from the binding site. Thus, the conformation deduced from these signals corresponds to a prerelease state of the ligand. It has been described that MT-stabilizing agents binding to the TXL site reach their luminal final location through prior transient binding to a site located in the MT pore (Diaz et al., 2003; Buey et al., 2007). Therefore the NMR structural data have to be interpreted with this caution.

Because DXT release from MT following excitation has to be fast in order to get trNOESY signals, the K_{off} of the ligand should be fast in the relaxation time scale. This is apparently in contradiction with the slow dissociation constant measured for TXL in a kinetic study, 0.091 ± 0.006 s^{-1} (Diaz et al., 2003). This observed dissociation constant does not correspond to the release step but to the rate-limiting step of the reaction. The dissociation of taxanes from MT has been studied in detail using the fluorescent taxane derivatives Flutax-1 and Flutax-2, which dissociate from MT following a two-step mechanism (Diaz et al., 2000). The first step, which is the slower one (thus the one directly observed), has a kinetic rate constant of 0.022 ± 0.001 s^{-1} (4-fold slower than that of TXL), whereas the second one (responsible for the release of the ligand to the medium and which can be measured only indirectly from the dependence of the kinetic rate constants on concentration) is nearly 100 times faster (k_{off} = 1.63 ± 0.18 s^{-1}).

In the absence of the fluorescent probe it is not possible to calculate the value of the kinetic rate constant of the release step of DXL dissociation (k_{off}). Control experiments with Flutax-2 performed in the same conditions did not show any trNOESY signal from this ligand, which indicates that its k_{off} value is not large enough to provide good trNOESY signals. Therefore, the effective kinetic rate of the release step of the dissociation process of DXL has to be higher. Because it is not unreasonable to think that the presence of the fluorescein moiety slows down the dissociation of Flutax-2 and the observed trNOESY crosspeaks for the DXL:MT ensemble are cancelled out by addition of DDM (a TXL-binding site ligand with a much higher affinity (Buey et al., 2005), it can be assumed that the detected signals arise

from DXL in the last step of dissociation from MT, which may be bound to either the external site or to a modified luminal site.

The basic features of the NMR-derived conformation might be extracted from the trNOESY crosspeaks. Clear NOEs are observed between the t-butyl protons and the 2-OBz protons (Figure 4B), whereas only extremely weak NOEs are observed between both aromatic (2-OBz and 3′-Ph) moieties (Figure 4D). The OAc-4 group also provides NOEs with both aromatic rings (Figure 4B). These experimental observations allow us to discard the presence of the so-called "polar conformation" for DXL when this molecule is bound to MT. The NMR-derived conformation is thus basically in agreement with the conformation derived from the modeling approach (see Figure S4). And though the modeled structure is in agreement with the so-called "T-taxol geometry" (Snyder et al., 2001), the NMR-derived conformation is intermediate between this one and that dubbed collapsed geometry (Vandervelde et al., 1993). That both conformations are fairly similar and resemble the T-taxol conformation possibly indicates that the prerelease step does not largely affect the conformation of DXL, and that the T-taxol conformation is stable in the protein environment. The only observed difference is likely due to the presence of His229, which in the modeled structure is found between the 2-OBz and the C13 side chain, thus further separating these two moieties. The NMR observations are in agreement with a closer proximity between the OBz and the t-Bu protons (~4–5 Å) than that suggested by the modeled DXL-β-tubulin complex (~5–6 Å). Under these constraints, the NMR-deduced prerelease bound geometry for DXL, which is close to that of T-taxol, is in agreement with that derived by the modeling procedure and resembles that described for the tubulin-bound conformation of TXL (Lowe et al., 2001), though the experimental conditions herein are markedly different.

Binding Affinity, Cytotoxicity and P-gp-Overexpression-Mediated Multidrug Resistance

The double-log plots representing cytotoxicity versus tubulin binding affinity (Figure 5A) clearly indicate that, as in the case of EPOs and other taxane-binding site ligands, both magnitudes are related, with the binding affinity behaving as a good predictor of cytotoxicity. However, a deviation from the predicted behavior can be noted from this data. There is an apparent cytotoxicity limit (IC_{50} = 1 nM) for these compounds against the non–P-gp-overexpressing cells. A review of the results from our earlier work (Buey et al., 2004, 2005) indicates that there are no MSA with an IC_{50} below nM in these cells. Despite having binding constants of the order of 10^9 M^{-1}, DDM and several EPOs have IC_{50}s in the order of 1 nM or higher. In fact, cis-CP-tmt-EPO-B (compound 19 in Buey et al. [2004]), the compound with the highest affinity for the TXL-binding site so far described (2.1×10^{10} M^{-1}), and also the most cytotoxic (IC_{50} = 0.1 nM), displays a binding affinity three orders of magnitude above that of TXL but only a 10-fold increase in cytotoxicity (Buey et al., 2004). These data suggest that a significant percentage of tubulin within the cell has to be bound to stop the cell cycle; cytotoxicity is thereby limited by the amount of compound that is needed to achieve this goal.

At the drug concentrations required to stop cell-cycle progression, the percentage of tubulin bound by the ligand is in the range of 2%–20% of the whole available protein. In the drug intake experiments, the total amount of compound available at the concentrations needed to stop the cell cycle (or at the IC_{50}) is around one-third (comparable) of the total amount of tubulin. Although this should be enough, in principle, for binding to a significant percentage of the protein, the results indicate that the amount of ligand available for binding to the sites is effectively much smaller (2%–10%). The reason for this might be that though all the binding sites are inside the small volume occupied by the cells, the drugs have to pass through the cell membranes and reach a threshold intracellular concentration that is opposed by the detoxification pumps. If a significant percentage (say 2%–5%) of cytoplasmic tubulin has to be bound for the taxane to exert its cytotoxicity, and the amount of ligand available for protein binding is a small percentage (2%–10%) of the total 1 nM concentrations—which is already one-third of the total amount of tubulin in the cells—it follows that for the MSA with a taxane way of action the 0.1–1 nM concentration is a limit for its cytotoxicity in cells. The same reasoning can be applied to a systemically distributed drug for which the minimal amount needed to kill the tumor cells is related to the amount of tubulin available for binding, which imposes a practical limit on the lowest dose that can be used.

However, if the goal is not to find a drug with the highest cytotoxicity possible (none of the newly synthesized high-affinity compounds has a remarkably better cytotoxicity on nonresistant cells than TXL and DXL) but rather to find one with the ability to overcome the main problem appearing in patients undergoing treatment with MSA—namely P-gp-mediated resistance—attempts to increase the affinity would seem to be steps in the right direction. Cells overexpressing P-gp are still sensitive to taxanes because they can still be killed by higher concentrations of either TXL or DXL. These very high concentrations affect normal nontumor cells as well, causing them to be differentially killed because of their inability to reduce the intracellular drug concentration, rather than differentially spared because of their lower division rate.

The data with A2780AD cells shows the expected correlation (although with a lower slope arising from their ability to reduce the intracellular drug concentration) between affinity and cytotoxicity that was previously observed for chemically related compounds (Buey et al., 2004) with no deviations being noted at the highest cytotoxicity values (9 nM for CTX-40). In this type of MDR cells the high-affinity drugs are nearly 100-fold more cytotoxic than the clinically employed taxanes (TXL and DXL) and display very low resistance indexes (as low as 1.3 for the highest-affinity derivative, CTX-40). This result was confirmed with LoVo human colon carcinoma cells and their MDR LoVo-Dox counterparts (Grandi et al., 1986; see the Supplemental Data).

When the resistance indexes of the compounds are represented against their binding affinities (Figure 5B), a bell-shaped curve is observed: the resistance index shows a maximum for taxanes displaying similar affinities for tubulin and P-gp, and then rapidly decreases when the affinity of the compound for tubulin either increases or decreases. An exception to this rule is found for compounds having a halogen atom (or a methoxy group) at the meta position of 2-OBz (CTX-5, 6, 30, 34, and 35) as they exhibit a much lower resistance index than that of other compounds with equivalent affinity.

The results confirm our previous data with other high-affinity ligands or with covalent binders (which can be considered to have infinite affinity) whose cytotoxicity is unaffected by P-gp overexpression (e.g., DDM: IC_{50} values of 60 nM and 53 nM [I. Barasoain, unpublished data] or cyclostreptin: IC_{50} values of 43.5 nM and 51 nM [Buey et al., 2007]) against A2780 and A2780AD cells, respectively, which is a clear indication that ligands with high affinity for the taxane-binding site can overcome the P-gp-mediated MDR phenotype. The rationale for this finding is that, in these cells, the intracellular free concentration of the high-affinity binding drugs will be low (see Figures S5–S7 for a detailed mathematical model). It is clear that for the ligand to be pumped out it first has to bind to P-gp, and assuming that the kinetics of drug efflux follows a Michaelis-Menten behavior, the ligand outflow will decrease with lower free ligand concentration. Because these ligands are tightly bound to tubulin, their intracellular free concentrations are of the order of their dissociation constants, which in the case of the high-affinity compounds (K_d of CTX-40 = 0.16 nM at 35°C) are far below their dissociation constants from P-gp (which range between 35 nM for TXL and 88 nM for CTX-7; Yang et al., 2007). This implies that, at concentrations able to exert cytotoxicity, the efficacy of P-gp to pump out the high-affinity compounds will be reduced by a factor between 200 and 1,000 (see the Supplemental Data). From a chemical standpoint, P-gp overexpression is irrelevant.

However, the low-affinity tubulin-binding ligands may escape the effect of the pump through a different mechanism. Because they need to reach concentrations that are much higher than those of either tubulin or P-gp to bind their target and thereby exert their cytotoxicity, the pump gets overloaded (saturated) and cannot effectively reduce the intracellular drug concentration. For this reason, these ligands act as MDR reversal agents by themselves (Brooks et al., 2003).

The present findings support the view (Buey et al., 2004, 2005) that binding affinity is the main variable to be maximized in attempts to increase the cytotoxicity of this type of compound (although on nonresistant cells a practical limit is observed at around 1 nM concentration). Additionally, high-affinity compounds can escape MDR due to P-gp overexpression by lowering the concentration of free ligand that can be pumped out by P-gp.

SIGNIFICANCE

The binding affinities of a series of synthetic taxanes for MTs have been measured with the aims of dissecting individual group contributions and obtaining a rationale for the design of novel compounds with the ability to overcome drug resistance. As previously observed for EPOs, the positive and negative contributions of the different substituents to the binding free energy are cumulative. By combining the most favorable substitutions in a single analog, the binding affinity was increased 500-fold over that of TXL. Insight into the structural basis for this improvement was gained when models were built that assigned an important role to the interactions of C2 and C13 substituents with the protonated side chain of His229. The relative orientation of these groups was found to be in agreement with NMR data obtained for MT-bound DXL.

The cytotoxicities of the compounds in ovarian carcinoma A2780 cells were found to correlate with their affinities, with an apparent cytotoxicity limit in the nanomolar range. A bell-shaped curve was obtained when the taxane resistance index was plotted versus the binding affinity showing that the P-gp-overexpressing multidrug-resistant A2780AD cells are sensitive to the highest and lowest affinity compounds, whereas resistance indexes in the range of 100 to 1,000 were obtained for those whose binding affinities for tubulin and P-gp are similar.

The finding that taxanes with affinities for MTs well above their affinities for P-gp are not affected by multidrug resistance strongly indicates that for a series of compounds with similar pharmacokinetic and bioavailability properties, optimization of the ligand-target interaction is a good strategy to overcome multidrug resistance mediated by efflux pumps.

EXPERIMENTAL PROCEDURES

Proteins and Ligands

Purified calf brain tubulin and chemicals were as described (Diaz and Andreu, 1993). Full details of the synthesis and characterization of the ligands employed can be found in the Supplemental Data.

Ligand-Induced Tubulin Assembly

Critical concentrations of ligand-induced tubulin assembly were measured as described (Buey et al., 2005).

Equilibrium Binding Constants of the Ligands to MTs and Tubulin

The binding constants of the ligands with apparent binding affinities below 10^8 M^{-1} for the TXL-binding site were measured as described (Buey et al., 2004). For the EPO-B method, samples of 1 ml containing 1 μM sites in glutaraldehyde-stabilized MTs, 1.1 μM EPO-B and 1.1 μM of the test compound in GAB (glycerol assembly buffer; 3.4 M glycerol, 10 mM sodium phosphate, 6 mM $MgCl_2$, and 1 mM EGTA [pH 6.7]) with 0.1 mM GTP were incubated for 30 min at 35°C in polycarbonate centrifuge tubes (Beckman Coulter, Inc., Fullerton, CA). The samples were then centrifuged at 90,000 × g for 20 min at 35°C in a TLA-100.2 rotor employing a Beckman Optima TLX ultracentrifuge. The supernatants were collected by pipetting, and the pellets were resuspended in 10 mM phosphate buffer (pH 7.0). One micromolar TXL was added as the internal standard, except for the experiments with CTX-13 in which 1 μM DXL was used instead. Both the pellets and the supernatants were extracted three times with an excess volume of dichloromethane, dried in vacuum, and dissolved in 35 μl of methanol. The samples were analyzed by HPLC.

Reversibility of binding was checked by incubating samples containing 5 μM compounds 4, 12, or 14, and 10 μM taxoid binding sites in stabilized crosslinked MT for 30 min at 25°C in polycarbonate centrifuge tubes (Beckman) in GAB with 0.1 mM GTP (DMSO concentration was always kept under 2%). The samples were then centrifuged at 90,000 g for 10 min at 25°C in a Beckman Optima TLX ultracentrifuge with a TLA100 rotor, processed, and analyzed as described.

Binding constants for compounds reversibly displacing Flutax-2 or EPO-B were calculated using Equigra v5 (Díaz and Buey, 2007). The thermodynamic parameters (apparent ΔG_0, ΔH_0, and ΔS_0) were calculated as described (Buey et al., 2005).

Binding of the compounds to unassembled dimeric tubulin was measured by centrifugation. Two hundred microliter samples containing 20 μM tubulin and 25 μM compound in 10 mM phosphate, 1 mM EDTA (pH 7.0) buffer (PEDTA) containing 1 mM GDP were incubated for 1 hr at 35°C in polycarbonate centrifuge tubes (Beckman). The samples were then centrifuged at 386,000 × g for 1 hr at 35°C in a TLA100 rotor employing a Beckman Optima TLX ultracentrifuge. The upper and lower 100 μl of the solution were carefully collected by pipetting, and the pellets were resuspended in 10 mM phosphate buffer (pH 7.0). The tubulin concentrations in the three samples were

measured by the Bradford assay, and 5 μM DXL was added as the internal standard. The samples were extracted and analyzed as described.

HPLC analysis of all samples was performed in an Agilent 1100 series instrument employing a Supercosil, LC18 DB, 250 × 4.6 mm, 5 mm bead diameter column developed in a gradient from 50% to 80% (v/v) acetonitrile in water at a flow rate of 1 ml/min^{-1}, following the absorbance at λ = 220 nm.

Cell Biology Studies

PtK2 (kidney epitelial cell from *Potorus tridactylis*), U937 (monocytic human leukemia), K562 (myelocytic human leukemia), A2780, P-gp-overexpressing A2780AD (ovarian carcinoma) cells were cultured as described previously (Buey et al., 2005). Cytotoxicity assays were performed with the MTT assay modified as described in Yang et al. (2007).

Cell intake of ^{3}H-TXL and ^{14}C-DXL were measured as reported (Manfredi et al., 1982) with modifications, using PtK2, U937, and K562 cells. These cells, and especially the PtK2 cells, were used because they are more resistant to taxanes, and more reproducible results could be obtained. Cells were grown in 24-well plates at a density of 500,000 cells/ml (PtK2) or 300,000 cells/ml (leukemic cell lines) and were incubated in 1 ml of medium with the desired drug concentration. Supernatants were collected, and cells were washed three times with 1 ml of cold PBS and incubated overnight with 0.25 ml of NaOH 0.1M, and then neutralized with 0.25 ml of HCl 0.1 M. The total protein concentration was determined by the Lowry method and the drug (both in the supernatants and incorporated into cells) was measured by liquid scintillation counting in a LKB 1219 spectrometer (GE Healthcare Bio-Sciences, Uppsala, Sweden). The correction for unspecific binding was determined by measuring the amount incorporated in cells preincubated with 10 μM colchicine for 4 hr at 37°C and washed three times prior to the incubation with ^{3}H-TXL or ^{14}C-DXL. Cell volume was calculated from the volume occupied by the pellets and found to be 2.5 ± 0.2, 3.96 ± 0.05, and 4.3 ± 0.9 μL/10^{6} cells for U937, K562, and PtK2, respectively.

The amounts of drugs bound to the nucleus and cytoplasm of the cells were determined as described in Simpson et al. (1987).

Molecular Modeling

The refined structure of the α,β-tubulin dimer at 3.5 Å resolution (Lowe et al., 2001; Protein Data Bank code: 1JFF) was used for molecular modeling and ligand docking. Addition of missing hydrogen atoms and computation of the protonation state of ionizable groups in β-tubulin at pH 6.5 were carried out using the H^{++} Web server (Gordon et al., 2005), which relies on AMBER (Cornell et al., 1995) force-field parameters and finite difference solutions to the Poisson-Boltzmann equation. The molecular graphics program PyMOL (DeLano Scientific, LLC, Palo Alto, CA) was employed for molecular visualization and representation. The charge distribution for the ligands studied was obtained by fitting the quantum mechanically calculated (RHF 6-31G*\\3-21G*) molecular electrostatic potential (MEP) to a point charge model, as implemented in Gaussian 03 (Gaussian, Inc., Wallingford, CT). Consistent bonded and nonbonded AMBER parameters were assigned to ligand atoms in the taxanes by analogy or through interpolation from those already present in the AMBER database (ff03).

The Lamarckian genetic algorithm implemented in AutoDock 3.0.5 (Morris et al., 1998) was used to generate automated docked poses of TXL, DXL, CTX-13, and CTX-40 within the taxane-binding site by randomly changing the overall orientation of conformers from the MD ensembles that were representative of the major populations, as well as the torsion angle involving the 2-OBz.

NMR Experiments

The NMR experiments were performed at 310 K in D_2O as described (Jimenez-Barbero et al., 2006), with modifications described in the Supplemental Data, on a Bruker AVANCE 500 spectrometer (Bruker, Bruker BioSpin GmbH, Rheinstetten, Germany).

SUPPLEMENTAL DATA

Supplemental Data include seven figures, three tables, Supplemental Experimental Procedures, Supplemental References, and two additional Supplemental Data files and can be found with this article online at http://www.chembiol.com/cgi/content/full/15/6/573/DC1/.

ACKNOWLEDGMENTS

We thank F. Amat-Guerri for Flutax-2, K.C. Nicolaou for EPO-B, the late M. Suffness for TXL, Rhône Poulenc Rorer Aventis for DXL, and José J. Ramírez and Tulsi Pindolia for their help in the early stages of the molecular modeling work. We also thank Carne Sierra Madrid S.A. (CIF: A78074168) for providing the calf brains for tubulin purification. This work was supported in part by grant BIO2007-61336 from M.E.C. to J.F.D., BIPPED-CM from Comunidad de Madrid to F.G., J.F.D., J.J.B., and J.M.A., and grants NSFC 20572135 and MOST 2006DFA31490 to W.S.F.

Received: November 15, 2007
Revised: May 4, 2008
Accepted: May 7, 2008
Published: June 20, 2008

REFERENCES

Brooks, T., Minderman, H., O'Loughlin, K.L., Pera, P., Ojima, I., Baer, M.R., and Bernacki, R.J. (2003). Taxane-based reversal agents modulate drug resistance mediated by P-glycoprotein, multidrug resistance protein, and breast cancer resistance protein. Mol. Cancer Ther. *2*, 1195–1205.

Buey, R.M., Diaz, J.F., Andreu, J.M., O'Brate, A., Giannakakou, P., Nicolaou, K.C., Sasmal, P.K., Ritzen, A., and Namoto, K. (2004). Interaction of epothilone analogs with the paclitaxel binding site: relationship between binding affinity, microtubule stabilization, and cytotoxicity. Chem. Biol. *11*, 225–236.

Buey, R.M., Barasoain, I., Jackson, E., Meyer, A., Giannakakou, P., Paterson, I., Mooberry, S., Andreu, J.M., and Diaz, J.F. (2005). Microtubule interactions with chemically diverse stabilizing agents: thermodynamics of binding to the paclitaxel site predicts cytotoxicity. Chem. Biol. *12*, 1269–1279.

Buey, R.M., Calvo, E., Barasoain, I., Pineda, O., Edler, M.C., Matesanz, R., Cerezo, G., Vanderwal, C.D., Day, B.W., Sorensen, E.J., et al. (2007). Cyclostreptin binds covalently to microtubule pores and lumenal taxoid binding sites. Nat. Chem. Biol. *3*, 117–125.

Chen, S.H., Huang, S., Kant, J., Fairchild, C., Wei, J.M., and Farina, V. (1993a). Synthesis of 7-deoxytaxol and 7,10-dideoxytaxol via radical intermediates. J. Org. Chem. *58*, 5028–5029.

Chen, S.H., Wei, J.M., and Farina, V. (1993b). Taxol structure-activity relationships: synthesis and biological evaluation of 2-deoxytaxol. Tetrahedron Lett. *34*, 3205–3206.

Cornell, W.D., Cieplak, P., Bayly, C.I., Gould, I.R., Merz, K.M., Ferguson, D.M., Spellmeyer, D.C., Fox, T., Caldwell, J.W., and Kollman, P.A. (1995). A second generation force field for the simulation of proteins, nucleic acids, and organic molecules. J. Am. Chem. Soc. *117*, 5179–5197.

Diaz, J.F., and Andreu, J.M. (1993). Assembly of purified GDP-tubulin into microtubules induced by taxol and taxotere: reversibility, ligand stoichiometry, and competition. Biochemistry *32*, 2747–2755.

Díaz, J.F., and Buey, R.M. (2007). Characterizing ligand-microtubule binding by competition methods. Methods Mol. Med. *137*, 245–260.

Diaz, J.F., Strobe, R., Engelborghs, Y., Souto, A.A., and Andreu, J.M. (2000). Molecular recognition of taxol by microtubules. Kinetics and thermodynamics of binding of fluorescent taxol derivatives to an exposed site. J. Biol. Chem. *275*, 26265–26276.

Diaz, J.F., Barasoain, I., and Andreu, J.M. (2003). Fast kinetics of Taxol binding to microtubules. Effects of solution variables and microtubule-associated proteins. J. Biol. Chem. *278*, 8407–8419.

Gao, Q., and Chen, S.H. (1996). An unprecedented side chain conformation of paclitaxel (Taxol$^{(R)}$): crystal structure of 7-mesylpaclitaxel. Tetrahedron Lett. *37*, 3425–3428.

Gordon, J.C., Myers, J.B., Folta, T., Shoja, V., Heath, L.S., and Onufriev, A. (2005). H^{++}: a server for estimating pKas and adding missing hydrogens to macromolecules. Nucleic Acids Res. *33*, W368–371.

Grandi, M., Geroni, C., and Giuliani, F.C. (1986). Isolation and characterization of a human colon adenocarcinoma cell-line resistant to doxorubicin. Br. J. Cancer *54*, 515–518.

Jimenez-Barbero, J., Canales, A., Northcote, P.T., Buey, R.M., Andreu, J.M., and Diaz, J.F. (2006). NMR determination of the bioactive conformation of peloruside a bound to microtubules. J. Am. Chem. Soc. *128*, 8757–8765.

Kingston, D.G., and Newman, D.J. (2007). Taxoids: cancer-fighting compounds from nature. Curr. Opin. Drug Discov. Devel. *10*, 130–144.

Kingston, D.G.I., Chaudhary, A.G., Chordia, M.D., Gharpure, M., Gunatilaka, A.A.L., Higgs, P.I., Rimoldi, J.M., Samala, L., Jagtap, P.G., Giannakakou, P., et al. (1998). Synthesis and biological evaluation of 2-acyl analogues of paclitaxel (Taxol). J. Med. Chem. *41*, 3715–3726.

Lowe, J., Li, H., Downing, K.H., and Nogales, E. (2001). Refined structure of αβ-tubulin at 3.5 A resolution. J. Mol. Biol. *313*, 1045–1057.

Manfredi, J.J., Parness, J., and Horwitz, S.B. (1982). Taxol binds to cellular microtubules. J. Cell Biol. *94*, 688–696.

Morris, G.M., Goodsell, D.S., Halliday, R.S., Huey, R., Hart, W.E., Belew, R.K., and Olson, A.J. (1998). Automated docking using a Lamarckian genetic algorithm and an empirical binding free energy function. J. Comput. Chem. *19*, 1639–1662.

Nicolaou, K.C., Couladouros, E.A., Nantermet, P.G., Renaud, J., Guy, R.K., and Wrasidlo, W. (1994). Synthesis of C-2 Taxol analogs. Angew. Chem. Int. Ed. Engl. *33*, 1581–1583.

Nicolaou, K.C., Renaud, J., Nantermet, P.G., Couladouros, E.A., Guy, R.K., and Wrasidlo, W. (1995). Chemical synthesis and biological evaluation of C-2 taxoids. J. Am. Chem. Soc. *117*, 2409–2420.

Ojima, I., Duclos, O., Zucco, M., Bissery, M.C., Combeau, C., Vrignaud, P., Riou, J.F., and Lavelle, F. (1994). Synthesis and structure-activity-relationships of new antitumor taxoids. Effects of cyclohexyl substitution at the C-3′ and/or C-2 of taxotere (Docetaxel). J. Med. Chem. *37*, 2602–2608.

Ojima, I., Kuduk, S.D., Pera, P., Veith, J.M., and Bernacki, R.J. (1997). Synthesis and structure-activity relationships of nonaromatic taxoids: effects of alkyl and alkenyl ester groups on cytotoxicity. J. Med. Chem. *40*, 279–285.

Rogan, A.M., Hamilton, T.C., Young, R.C., Klecker, R.W., and Ozols, R.F. (1984). Reversal of adriamycin resistance by verapamil in human ovarian cancer. Science *224*, 994–996.

Shabbits, J.A., Krishna, R., and Mayer, L.D. (2001). Molecular and pharmacological strategies to overcome multidrug resistance. Expert Rev. Anticancer Ther. *1*, 585–594.

Simpson, R.U., Hsu, T., Begley, D.A., Mitchell, B.S., and Alizadeh, B.N. (1987). Transcriptional regulation of the C-Myc protooncogene by 1,25-dihydroxyvitamin-D3 in Hl-60 promyelocytic leukemia cells. J. Biol. Chem. *262*, 4104–4108.

Snyder, J.P., Nettles, J.H., Cornett, B., Downing, K.H., and Nogales, E. (2001). The binding conformation of Taxol in β-tubulin: a model based on electron crystallographic density. Proc. Natl. Acad. Sci. USA *98*, 5312–5316.

Tan, B., Piwnica-Worms, D., and Ratner, L. (2000). Multidrug resistance transporters and modulation. Curr. Opin. Oncol. *12*, 450–458.

Vandervelde, D.G., Georg, G.I., Grunewald, G.L., Gunn, G.W., and Mitscher, L.A. (1993). "Hydrophobic collapse" of taxol and taxotere solution conformations in mixtures of water and organic solvent. J. Am. Chem. Soc. *115*, 11650–11651.

Wang, L., Alcaraz, A.A., Matesanz, R., Yang, C.G., Barasoain, I., Díaz, J.F., Li, Y.Z., Snyder, J.P., and Fang, W.S. (2007). Synthesys, biological evaluation, and tubulin binding poses of C-2a sulfur linked taxol analogues. Bioorg. Med. Chem. Lett. *17*, 3191–3194.

Yang, C.G., Barasoain, I., Li, X., Matesanz, R., Liu, R., Sharom, F.J., Diaz, J.F., and Fang, W. (2007). Overcoming tumor drug resistance mediated by P-glycoprotein overexpression with high affinity taxanes: a SAR study of C-2 modified 7-acyl-10-deacetil cephalomannines. ChemMedChem *2*, 691–701.

Zefirova, O.N., Nurieva, E.V., Ryzhov, A.N., Zyk, N.V., and Zefirov, N.S. (2005). Taxol: synthesis, bioactive conformations, and structure-activity relationships in its analogs. Russ. J. Org. Chem. *41*, 315–351.

Bioorganic & Medicinal Chemistry Letters xxx (2008) xxx–xxx

Contents lists available at ScienceDirect

Bioorganic & Medicinal Chemistry Letters

journal homepage: www.elsevier.com/locate/bmcl

Synthesis and biological activities of high affinity taxane-based fluorescent probes

Xuan Li [a,b], Isabel Barasoain [c], Ruth Matesanz [c], J. Fernando Díaz [c], Wei-Shuo Fang [a,b,*]

[a] Key Lab of Bioactive Substances and Resources Utilization of Chinese Herbal Medicine (PUMC), Ministry of Education, Beijing 100050, China
[b] Institute of Materia Medica, Chinese Academy of Medical Science, 1 Xian Nong Tan Street, Beijing 100050, China
[c] Centro de Investigaciones Biológicas, Consejo Superior de Investigaciones Científicas, Ramiro de Maeztu 9, 28040 Madrid, Spain

ARTICLE INFO

Article history:
Received 8 August 2008
Revised 21 November 2008
Accepted 5 December 2008
Available online xxxx

Keywords:
Paclitaxel
Cephalomannine
High affinity taxanes
Fluorescence
Fluorescein
Difluorescein

ABSTRACT

Three fluorescent probes **3a, 3b**, and **4** have been synthesized through conjugation of fluorescein and difluorescein groups to the 7-OH of C-2 modified paclitaxel and cephalomannine derivatives with very high affinity to microtubules. All these probes exhibited potent tubulin assembly promotion and tumor cell killing activities, thus may be useful as tools for the determination of thermodynamic parameters and exploration of ligand–microtubule interactions.

The plant-derived natural product paclitaxel (**1a**), exerting its mechanism through disruption of dynamics of tubulin/microtubule polymerization–depolymerization process,[1] has been widely used for the treatment of various solid tumors.[2] In order to study the interaction of **1a** with tubulin/microtubule system and visualize the microtubule dynamics in the presence of **1a**, various spectroscopic methods have been applied. One of the most useful techniques to explore such interactions is fluorescence spectroscopy,[3–5] in which various probes derived from **1a** or its derivatives with fluorophore tags at different positions of taxanes are often used.[6–12]

Most of taxane-based fluorescent probes are prepared from **1a**, by the introduction of a fluorophore at C-7 position through proper linkage. Because C-7 and other "northern hemisphere" substituents in **1a** are known not to interact with tubulin significantly, so these probes are believed to minimize the interference of large fluorescent groups such as fluorescein and rhodamine in the binding pocket. With the fluorescein and difluorescein-tagged **1a**, Flutax-1 (**2a**), and -2 (**2b**), it is possible to determine the thermodynamic and kinetic parameters for the taxane–tubulin binding process,[13–15] analyze the ligand's conformation in D_2O/DMSO-d_6,[16] and locate the centrosome and spindle pole microtubules as the main targets for taxanes to induce cell death.[11]

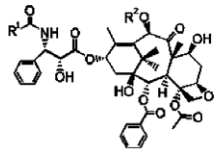

1a R^1=Ph, R^2=Ac
1b R^1=*t*-BuO, R^2=H

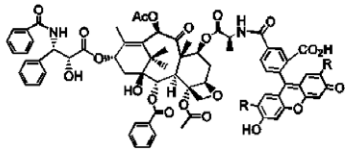

2a R=H
2b R=F

It has been found that precise determinations of thermodynamic parameters for ligand–tubulin binding is critical to quantify the enthalpic and entropic contributions to the binding process, thus predict the cytotoxicity of the ligands and help the design of high affinity ligands (i.e. taxanes) through the binding affinity dissection.[17–19] During the process of the determination of thermodynamic parameters by the competitive displacement method, fluorescent probes with binding affinity within three orders of magnitudes to the targeted ligands are usually applied. However, displacement methods cannot distinguish ligands with affinities much higher than probes (e.g. **2a** or **2b** in our case) thus it is not possible to determine the binding affinity or thermodynamic parameters precisely.[20] The thermodynamic parameter of binding of compounds with high affinity for the taxane site have been determined by displacement of a non-fluorescent compound, Epothilone B, with high affinity (K_a 7.5×10^8 M^{-1} at 35 °C) for the paclitaxel site.[17,19] In this method, the Epothilone B concentrations in supernatants and pellets required to measure the binding constant of the

* Corresponding author. Tel.: +86 10 63165237; fax: +86 10 63017757.
E-mail addresses: fer@cib.csic.es (J. Fernando Díaz), wfang@imm.ac.cn (W.-S. Fang).

0960-894X/$ - see front matter © 2008 Published by Elsevier Ltd.
doi:10.1016/j.bmcl.2008.12.018

competitor have to be determined employing HPLC, thus the method has a low throughput and is time consuming. Hence, a high affinity fluorescent taxane is desirable for the parameter determination by fluorescence spectroscopy during the optimization of the binding affinity of taxanes to tubulin.

The introduction of methoxy or azido group to the *meta* position of C-2 benzoate phenyl in **1a** and its analogs has been proved to enhance the tubulin polymerization promotion ability and cytotoxicity significantly.[22,23] It was also known that the binding affinity of taxanes to tubulin/microtubule can be potentiated by such a modification.[15,19] So, we prepared fluorescent probes **3** and **4** from 2-(*m*-MeO)-benzoyl paclitaxel and 2-(*m*-N_3)-benzoyl cephalomannine which are higher affinity tubulin binders than **1** and **2**, and investigated their fluorescence properties and biological activities.

Chemical syntheses. The synthesis of **3** was performed in a similar way to that of 2-modified taxanes,[19,21] except the 7-TES group was replaced with 7-alanine (7-Ala).

Paclitaxel (**1a**) was first protected at 2′-OH and then conjugated with Boc-Ala-OH at 7-OH to afford **5**. Compound **5**, upon 2-debenzoylation and subsequent acylation, was converted to 2-(*m*-MeO-Bz)-paclitaxel analog **6**. Deprotection of 2′-*O*-*tert*-butyldimethylsilyl and *N*-*tert*-butyloxycarbonyl groups under mild conditions furnished 7-Ala-2-modified paclitaxel analog **7**, with free amino group ready for the conjugation of fluorescent groups. Coupling of **7** with 5-fluorescein succinimidyl ester (5-FAM SE) or 5-difluorescein succinimidyl ester (OG 488 SE) in sodium carbonate–dicarbonate buffer (pH 9.0) furnished the desired conjugates **3a** (20% yield) and **3b** (60% yield) (Scheme 1).

The fluorescent probe **4** was also prepared from cephalomannine similarly in 14% overall yield for seven steps.

The final products **3**[25,26] and **4**,[27] after chromatographic separations, are still contaminated by ca. 20–55% weight of NaOAc (ca. 1:20–1:4 taxane–NaOAc peak ratios in the corresponding NMR spectra). Since these impurities do not interfere with the parameter determination, the probes are not subjected to further purifications.

Binding to the paclitaxel site in microtubules. The compounds were tested for their ability to bind tubulin in the paclitaxel site. All of them, upon binding to the paclitaxel site, underwent a large increase in the anisotropy of their fluorescence as is the case for other fluorescent derivatives of paclitaxel[13] (Table 1).

As expected for the introduction of binding enhancement groups[15,19] in **1a**, docetaxel (**1b**) does not displace them from the crosslinked microtubules (no decrease in the anisotropy of binding is observed after addition of 10 μM docetaxel) as in the case for

Table 1
Anisotropy of the fluorescence emission of the fluorescent taxoids in different status[a]

Ligands	Free	Bound[b]	Displaced[b]
2a[c]	0.05 ± 0.02	0.24 ± 0.02	0.05 ± 0.02
2b[c]	0.04 ± 0.01	0.26 ± 0.02	0.08 ± 0.01
3a	0.046 ± 0.003	0.168 ± 0.007	0.052 ± 0.008
3b	0.046 ± 0.001	0.202 ± 0.031	0.068 ± 0.010
4	0.059 ± 0.010	0.291 ± 0.020	0.077 ± 0.010

[a] Determined with fluorescent ligands (50 nM) in GAB buffer at 25 °C. Excitation and emission wavelengths for **3a** and **3b** are 492 and 524 nm, and for **4** 493 and 521 nm, respectively.
[b] Bound to 1 μM of paclitaxel binding sites in stabilized microtubules by crosslinking, and further displaced by the addition of 10 μM discodermolide.
[c] Data from Ref. 13. Bound to microtubules assembled from 20 μM pure tubulin in GAB, and further displaced by the addition of 50 μM docetaxel.

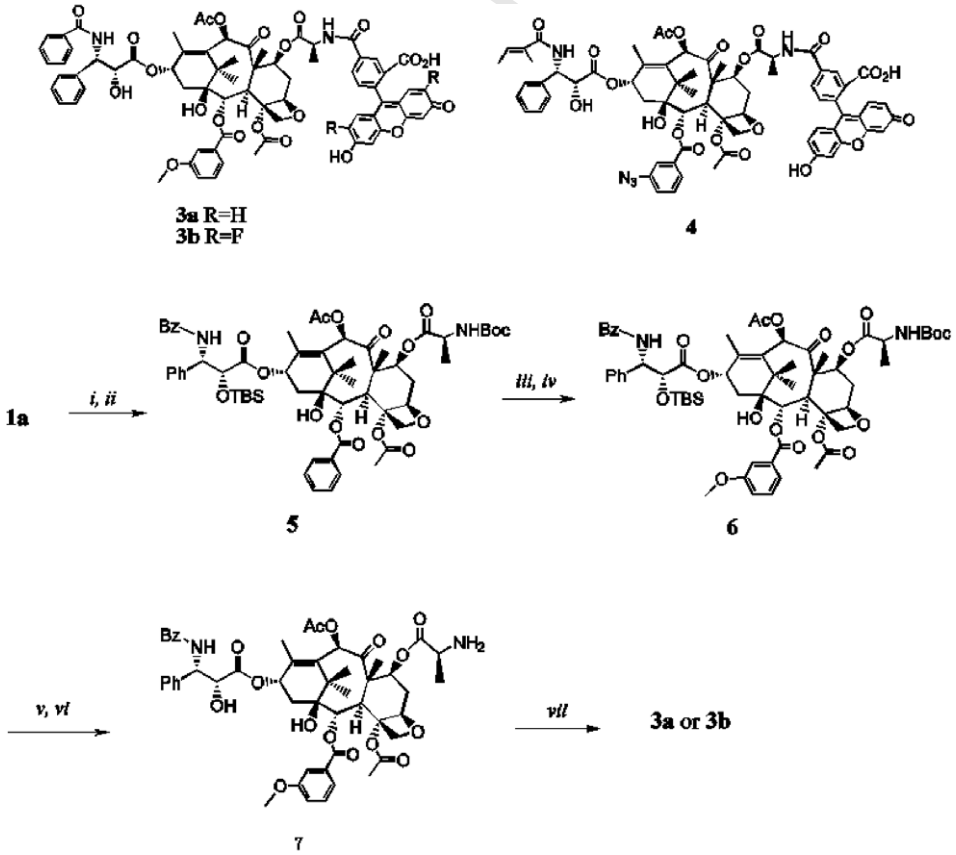

Scheme 1. Reagents and conditions: (i) TBSCl, imidazole, DMF, 70 °C, 97%; (ii) Boc-Ala-OH, DCC, DMAP, toluene, 35 °C, 86%; (iii) Triton B, CH_2Cl_2, −20 °C, 77%; (iv) *m*-methoxy benzoic acid, DCC, 4-PP, 65 °C, 73%; (v) 40% aq HF, Py, CH_3CN, 35 °C, 97%; (vi) CF_3COOH, $PhSCH_3$, CH_2Cl_2, 0 °C, 61%; (vii) 5-FAM SE or OG 488 SE, DMF, sodium carbonate–dicarbonate buffer (pH 9.0), rt, 20% for **3a**, 60% for **3b**.

Please cite this article in press as: Li, X. et al., *Bioorg. Med. Chem. Lett.* (2008), doi:10.1016/j.bmcl.2008.12.018

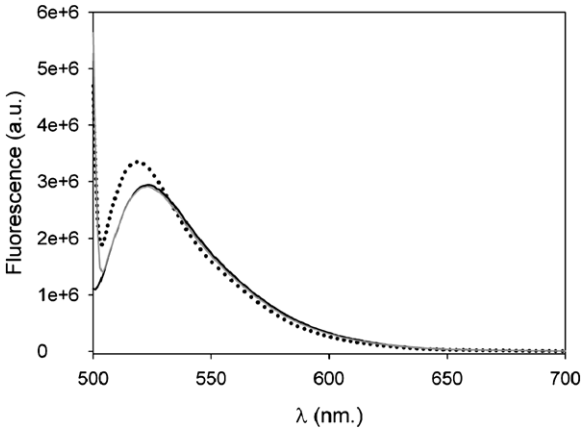

Figure 1. Fluorescence spectra of **4** (50 nM) black line, **4** plus microtubules (1 μM), dotted line and **4**, microtubules plus discodermolide (10 μM), gray line in GAB buffer.

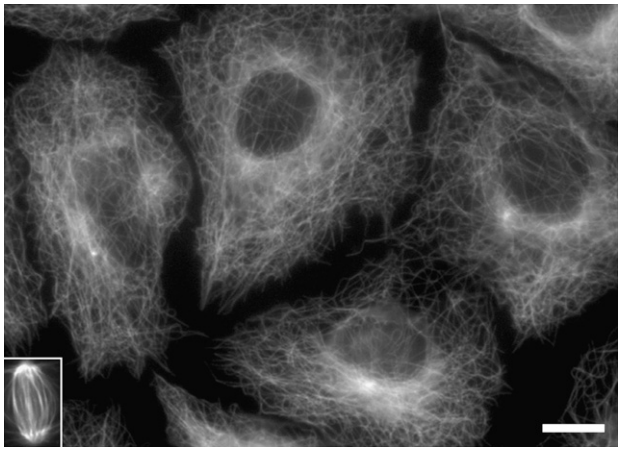

Figure 2. Visualization of microtubules with **4** in A549 human lung carcinoma cells. A549 unfixed microtubule cytoskeletons were incubated with 1 μM **4** for 5 min. Inset: **4** stained mitotic spindle from the same preparations. Scale bar represents 10 μm for both images.

Flutax-1 (**2a**) and Flutax-2 (**2b**).[13] Their binding constants to microtubules were also measured, and found to be $4.4 \pm 1.9 \times 10^8$, $6.8 \pm 1.7 \times 10^8$, and $12 \pm 4 \times 10^8$ M^{-1} for **3a**, **3b**, and **4**, respectively. All these facts indicate that their binding affinities are much higher than that of docetaxel. The specificity of the binding was checked by adding 10 μM discodermolide, the natural paclitaxel binding site ligand with the highest affinity known to date, to the samples containing the fluorescent taxanes bound to stabilized microtubules. Discodermolide displaces the bound taxane, resulting in a decrease of the anisotropy of the fluorescence of the sample to the values observed for the free compound. The same effect can be shown by fluorescence intensity (Fig. 1). Addition of microtubules to the solution of **4** led to the change of its fluorescence spectra, with a small increase in fluorescence intensity, while addition of discodermolide to this solution restored the spectra, due to the displacement of fluorescent probe 4 from its binding site in microtubule.

Microtubule assembly induction. The compounds were then tested for their ability to induce microtubule assembly in conditions which tubulin do not assemble.[24] The compounds were able to induce assembly of GTP-tubulin into microtubules, indicating that the introduction of the fluorescent group does not perturb their tubulin promotion activity (for the critical concentration data, see Table 2). All three high affinity taxane-based fluorescent probes were found to be tubulin assembly promoters comparable with the more potent taxanes (including the clinically used taxanes, paclitaxel, and docetaxel, as well as two fluorescent taxanes (**2a** and **2b**) previously employed[12,20] (supplementary information of Ref. 19). Among the three probes, **3b** is the more active one, although the differences are in within the experimental errors of the docetaxel measurement.

Ligand binding to cellular microtubules and cytotoxicity. To test if these fluorescent probes can bind to native cellular microtubules, we incubated unfixed A549 human lung carcinoma cytoskeletons with them and imaged by fluorescence microscopy as with other fluorescent taxanes[12] (Fig. 2). It was found that they readily and brightly stained interphasic cellular microtubules as well as mitotic spindles, centrosomes and the central part of the midbody in cytokinesis.

Cytotoxicities were tested on A2780 ovarian carcinoma cells and their P-gp overexpressing counterpart A2780AD cells. All three newly synthesized compounds were able to kill the non-resistant cells (Table 3). However, despite having higher affinity to microtubules than paclitaxel (they cannot be displaced from crosslinked stabilized microtubules by a 200 times excess of docetaxel), their cytotoxicity is much lower than paclitaxel and docetaxel (Table 3) and their unlabeled partners,[19] indicating that the polar fluorescent moiety impedes their cell permeability. The poor cytotoxicity for **4**, **2a**, and **2b** in P-glycoprotein overexpressing A2780AD cells (which is not the case for their unlabeled partners[19]) may suggested that the introduction of the fluorescent moiety usually makes them better substrates for membrane transporter proteins such as P-glycoprotein. However, Fx-2 (**3a**) and Fchitax-3 (**3b**) are more active in resistant cells (*R*/*S* index of 36 and 26, respectively), than their parent compound Chitax-11 (*R*/*S* index 120). It is also interesting to note that cytotoxicities of the difluorescein bearing probes (**2b and 3b**) are less active than fluorescein bearing ones (**2a and 3a**), although the former are slightly more potent tubulin polymerization promoters.

In conclusion, all three fluorescent probes can be applied to the determination of binding affinity or thermodynamic parameters for taxanes with much higher affinity than **1**. In addition, **3a** and

Table 2
Critical concentrations of the ligand-induced assembly reactions[a]

Ligands	Critical concentrations (μM)	Ligands	Critical concentrations (μM)
4	2.45 ± 0.41	**1a**[b]	4.23 ± 0.68
3a	2.26 ± 0.40	**1b**[b]	2.50 ± 0.37
3b	2.17 ± 0.39	**2a**	3.84 ± 0.56
		2b	3.22 ± 0.46

[a] Determined in the presence of a 10% excess of ligand in 10 mM phosphate, 1 mM EDTA, 4 mM $MgCl_2$, pH 6.7 solution in the presence of 1 mM GTP.[17]
[b] Data from Ref. 17.

Table 3
Cytotoxicity of the compounds against drug-sensitive and -resistant cells

Ligands	A2780[a] (nM)	A2780AD	*R*/*S*[b]
4	220 ± 15	>20,000	>91
3a	19.5 ± 0.35	716 ± 120	36.7
3b	272 ± 12	7200 ± 200	26.4
1a	1.3 ± 0.4	980 ± 149	753
1b	0.6 ± 0.2	290 ± 16	483
2a	256 ± 17	>20,000	>78
2b	800 ± 28	>20,000	>25

[a] IC_{50} values were determined in parental ovarian carcinoma A2780 cells and its drug resistant counterpart A2780AD cells after 48 h incubation in the presence of the drugs using an MTT cell proliferation assay.[15]
[b] The resistance factor is calculated dividing the IC_{50} of the resistant cell line by the IC_{50} of the drug sensitive cell line.

Please cite this article in press as: Li, X. et al., *Bioorg. Med. Chem. Lett.* (2008), doi:10.1016/j.bmcl.2008.12.018

3b may also be useful in the exploration of ligand–microtubule interactions at cellular level.

Acknowledgments

We thank Carne Sierra Madrid S.A. (CIF: A78074168) for providing the calf brains for tubulin purification, and Dr. Ying Zhao and Ms. Xuan Xiao for their assistance in the manuscript preparation. This work was supported by NSFC (20572135 and 30630069), MOST grants (2006DFA31490) to W.S.F., and BIO2007-61336 from MEC and BIPPED-CM (S2006/BIO-0214) grants to J.F.D.

References and notes

1. Jordan, M. A.; Wilson, L. *Nat. Rev. Cancer* **2004**, *4*, 253.
2. *TAXOL Science and Applications*; Suffness, M., Ed.; CRC Press Inc.: Boca Raton, FL, 1995; pp 1–448.
3. Sengupta, S.; Boge, T. C.; Liu, Y.; Hepperle, M.; Georg, G. I.; Himes, R. H. *Biochemistry* **1997**, *36*, 5179.
4. Li, Y.; Poliks; Cegelski, L.; Poliks, M.; Gryczynski, Z.; Piszczek, G.; Jagtap, P. G.; Studelska, D. R.; Kingston, D. G. I.; Schaefer, J.; Bane, S. *Biochemistry* **2000**, *39*, 281.
5. Shanker, N.; Kingston, D. G. I.; Ganesh, T.; Yang, C.; Alcaraz, A. A.; Geballe, M. T.; Banerjee, A.; McGee, D.; Snyder, J. P.; Bane, S. *Biochemistry* **2007**, *46*, 11514.
6. Dubois, J.; Le, G. M. T.; Gueritt-Voegelein, F.; Guenard, D.; Tollon, Y.; Wright, M. *Bioorg. Med. Chem.* **1995**, *3*, 1357.
7. Souto, A. A.; Acuna, A. U.; Andreu, J. M.; Barasoain, I.; Abal, M.; Amat-Guerri, F. *Angew. Chem. Int. Ed. Engl.* **1995**, *34*, 2710.
8. Guy, R.; Scott, Z.; Sloboda, R.; Nicolaou, K. C. *Chem. Biol.* **1996**, *3*, 1021.
9. Rao, C. S.; Chu, J. J.; Liu, R. S.; Lai, Y. K. *Bioorg. Med. Chem.* **1998**, *6*, 2193.
10. Baloglu, E.; Kingston, D. G. I.; Patel, P.; Chatterjee, S. K.; Bane, S. L. *Bioorg. Med. Chem.* **2001**, *11*, 2249.
11. Abal, M.; Souto, A. A.; Amat-Guerri, F.; Acuña, A. U.; Andreu, J. M.; Barasoain, I. *Cell Motil. Cytoskeleton* **2001**, *49*, 1.
12. Evangelio, J. A.; Abal, M.; Barasoain, I.; Souto, A. A.; Lillo, M. P.; Acuna, A. U.; Amat-Guerri, F.; Andreu, J. M. *Cell Motil. Cytoskeleton* **1998**, *39*, 73.
13. Díaz, J. F.; Strobe, R.; Engelborghs, Y.; Souto, A. A.; Andreu, J. M. *J. Biol. Chem.* **2000**, *275*, 26265.
14. Díaz, J. F.; Barasoain, I.; Andreu, J. M. *J. Biol. Chem.* **2003**, *278*, 8407.
15. Yang, C. G.; Barasoain, I.; Li, X.; Matesanz, R.; Liu, R.; Sharom, F. J.; Yin, D.-L.; Díaz, J. F.; Fang, W.-S. *ChemMedChem* **2007**, *2*, 691.
16. Jiménez-Barbero, J.; Souto, A. A.; Abal, M.; Barasoain, I.; Evangelio, J. A.; Acuña, A. U.; Andreu, J. M.; Amat-Guerri, F. *Bioorg. Med. Chem.* **1998**, *6*, 1857.
17. Buey, R. M.; Barasoain, I.; Jackson, E.; Meyer, A.; Ginnakakou, P.; Paterson, I.; Mooberry, S.; Andreu, J. M.; Díaz, J. F. *Chem. Biol.* **2005**, *12*, 1269.
18. Buey, R. M.; Díaz, J. F.; Andreu, J. M.; O'Brate, A.; Ginnakakou, P.; Nicolaou, K. C.; Sasmal, P. K.; Ritzen, A.; Namoto, K. *Chem. Biol.* **2004**, *11*, 225.
19. Matesanz, R.; Barasoain, I.; Yang, C.-G.; Lei Wang, L.; Li, X.; de Inés, C.; Coderch, C.; Gago, F.; Jiménez-Barbero, J.; Andreu, J. M.; Fang, W.-S.; Díaz, J. F. *Chem. Biol.* **2008**, *15*, 573.
20. Diaz, J. F.; Andreu, J. M. *Biochemistry* **1993**, *32*, 2747–2755.
21. Yang, C.-G. Ph.D. Thesis, Peking Union Medical College, June 2007.
22. Chaudhary, A. G.; Gharpure, M. M.; Rimoldi, J. M.; Chordia, M. D.; Gunatilaka, A. A. L.; Kingston, D. G. I.; Grover, S.; Lin, C. M.; Hamel, E. *J. Am. Chem. Soc.* **1994**, *116*, 4097.
23. Kingston, D. G. I.; Chaudhary, A. G.; Chordia, M. D.; Gharpure, M.; Gunatilaka, A. A. L.; Higgs, P. I.; Rimoldi, J. M.; Samala, L.; Jagtap, P. G.; Giannakakou, P.; Jiang, Y. Q.; Lin, C. M.; Hamel, E.; Long, B. H.; Fairchild, C. R.; Johnston, K. A. *J. Med. Chem.* **1998**, *41*, 3175.
24. Díaz, J. F.; Buey, R. M. Microtubule Protocols. In Zhou, J., Ed.; Humana Press Inc.: Totowa, NJ, 2007; pp 245–260.
25. *Spectral data for* ***3a***. ^{1}H NMR (500 MHz, CD_3OD): δ 8.41 (1H, d, J = 2.0 Hz), 7.96 (1H, dd, J = 1.5, 7.5 Hz), 7.80 (2H, m), 7.62 (1H, m), 7.59 (1H, m), 7.50–7.16 (11H, m), 6.96 (2H, dd, J = 2.0, 9.0 Hz), 6.47 (2H, dd, J = 2.0, 9.0 Hz), 6.44 (2H, m), 6.31 (1H, s), 6.09 (1H, t, J = 9.0 Hz), 5.62 (1H, dd, J = 7.5, 11.0 Hz), 5.60 (1H, d, J = 7.0 Hz), 5.56 (1H, d, J = 5.5 Hz), 4.96 (1H, d, J = 10.0 Hz), 4.71 (1H, d, J = 6.0 Hz), 4.59 (1H, q, J = 7.5 Hz), 4.20 (1H, d, J = 8.5 Hz), 4.14 (1H, d, J = 8.0 Hz), 3.87 (1H, d, J = 7.0 Hz), 3.85 (3H, s), 2.56 (1 H, ddd, J = 5.5, 8.0, 15.0 Hz), 2.30 (3H, s), 2.17 (1H, dd, J = 9.5, 15.5 Hz), 2.13 (3H, s), 1.93 (1H, dd, J = 9.5, 15.5 Hz), 1.86 (3H, s), 1.79 (1H, overlapped), 1.76 (3H, s), 1.38 (3H, d, J = 7.0 Hz), 1.10 (3H, s), 1.07 (3H, s). ESI-HRMS: m/z $[M+H]^+$ 1313.42439 (found), 1313.43419 (calcd).
26. *Spectral data for* ***3b***. ^{1}H NMR (500 MHz, CD_3OD): δ 8.45 (1H, d, J = 1.5 Hz), 8.00 (1H, dd, J = 2.0, 8.0 Hz), 7.80 (2H, m), 7.63 (1H, m), 7.58 (1H, m), 7.48–7.16 (11H, m), 6.66 (2H, dd, J = 3.5, 6.5 Hz), 6.58 (2H, d, J = 7.5 Hz), 6.31 (1H, s), 6.07 (1H, t, J = 8.5 Hz), 5.61 (1H, dd, J = 7.5, 10.5 Hz), 5.59 (1H, d, J = 7.0 Hz), 5.55 (1H, d, J = 5.5 Hz), 4.96 (1H, d, J = 9.0 Hz), 4.72 (1H, d, J = 6.0 Hz), 4.61 (1H, q, J = 7.0 Hz), 4.20 (1H, d, J = 8.0 Hz), 4.14 (1H, d, J = 8.0 Hz), 3.87 (1H, d, J = 7.0 Hz), 3.84 (3H, s), 2.57 (1H, ddd, J = 5.5, 8.0, 15.0 Hz), 2.29 (3H, s), 2.15 (1H, dd, J = 9.5, 15.5 Hz), 2.12 (3H, s), 1.90 (1H, dd, J = 9.5, 15.5 Hz), 1.87 (3H, s), 1.79 (1H, overlapped), 1.77 (3H, s), 1.39 (3H, d, J = 7.5 Hz), 1.10 (3H, s), 1.07 (3H, s). ESI-HRMS: m/z $[M+H]^+$ 1349.40696 (found), 1349.41535 (calcd).
27. *Spectral data for* ***4***. ^{1}H NMR (500 MHz, CD_3OD): δ 8.44 (1H, s), 8.08 (1H, dd, J = 2.0, 8.0 Hz), 7.84 (1H, d, J = 7.5 Hz), 7.73 (1H, m), 7.52 (1H, t, J = 8.0 Hz), 7.37–7.19 (7H, m), 6.79 (2H, d, J = 9.0 Hz), 6.62 (2H, d, J = 2.0 Hz), 6.53 (2H, dd, J = 2.0, 9.0 Hz), 6.38 (1H, q, J = 7.0 Hz), 6.32 (1H, s), 6.06 (1H, t, J = 9.0 Hz), 5.62 (1H, d, J = 7.0 Hz), 5.61 (1H, dd, J = 6.5, 11.0 Hz), 5.42 (1H, d, J = 4.5 Hz), 4.96 (1H, d, J = 9.0 Hz), 4.61 (1H, d, J = 4.5 Hz), 4.58 (1H, q, J = 7.0 Hz), 4.19 (1H, d, J = 8.0 Hz), 4.13 (1H, d, J = 8.0 Hz), 3.88 (1H, d, J = 7.0 Hz), 2.56 (1H, ddd, J = 5.5 7.5, 14.5 Hz), 2.32 (3H, s), 2.21 (1H, dd, J = 9.5, 15.5 Hz), 2.13 (3H, s), 2.00 (1H, dd, J = 9.5, 15.5 Hz), 1.86 (3H, s), 1.79 (1H, overlapped), 1.78 (3H, s), 1.76 (3H, s), 1.71 (3H, d, J = 7.0 Hz), 1.38 (3H, d, J = 7.0 Hz), 1.12 (3H, s), 1.08 (3H, s). ESI-HRMS: m/z $[M+H]^+$ 1302.44347 (found), 1302.44068 (calcd).

Please cite this article in press as: Li, X. et al., *Bioorg. Med. Chem. Lett.* (2008), doi:10.1016/j.bmcl.2008.12.018